



6-2012

## Integrating Depositional Facies and Stratigraphy in Characterizing Hydrothermal Dolomite Reservoirs: Trenton Group of the Albion-Scipio Trend, Michigan

Marcel R. Robinson  
*Western Michigan University*

Follow this and additional works at: [https://scholarworks.wmich.edu/masters\\_theses](https://scholarworks.wmich.edu/masters_theses)



Part of the Geology Commons, and the Hydrology Commons

---

### Recommended Citation

Robinson, Marcel R., "Integrating Depositional Facies and Stratigraphy in Characterizing Hydrothermal Dolomite Reservoirs: Trenton Group of the Albion-Scipio Trend, Michigan" (2012). *Masters Theses*. 18. [https://scholarworks.wmich.edu/masters\\_theses/18](https://scholarworks.wmich.edu/masters_theses/18)

This Masters Thesis-Open Access is brought to you for free and open access by the Graduate College at ScholarWorks at WMU. It has been accepted for inclusion in Masters Theses by an authorized administrator of ScholarWorks at WMU. For more information, please contact [wmu-scholarworks@wmich.edu](mailto:wmu-scholarworks@wmich.edu).



INTEGRATING DEPOSITIONAL FACIES AND STRATIGRAPHY IN  
CHARACTERIZING HYDROTHERMAL DOLOMITE RESERVOIRS:  
TRENTON GROUP OF THE ALBION-SCIPIO TREND,  
MICHIGAN BASIN

by

Marcel R. Robinson

A Thesis  
Submitted to the  
Faculty of The Graduate College  
in partial fulfillment of the  
requirements for the  
Degree of Master of Science  
Department of Geosciences  
Advisor: G. Michael Grammer, Ph.D.

Western Michigan University  
Kalamazoo, Michigan  
August 2012



THE GRADUATE COLLEGE  
WESTERN MICHIGAN UNIVERSITY  
KALAMAZOO, MICHIGAN

Date March 20, 2012

WE HEREBY APPROVE THE THESIS SUBMITTED BY

Marcel R. Robinson

ENTITLED Integrating Depositional Facies and Stratigraphy in Characterizing  
Hydrothermal Dolomite Reservoirs: Trenton Group of the Albion-Scipio Trend, Michigan  
Basin

AS PARTIAL FULFILLMENT OF THE REQUIREMENTS FOR THE


DEGREE OF Master of Science

Geosciences  
(Department)

  
G. Michael Grammer, Ph.D.  
Thesis Committee Chair

Geology  
(Program)

  
William B. Harrison III, Ph.D.  
Thesis Committee Member

  
Michelle A. Kominz, Ph.D.  
Thesis Committee Member

APPROVED

  
Dean of The Graduate College

Date June 2012

INTEGRATING DEPOSITIONAL FACIES AND STRATIGRAPHY IN  
CHARACTERIZING HYDROTHERMAL DOLOMITE RESERVOIRS:  
TRENTON GROUP OF THE ALBION-SCIPIO TREND,  
MICHIGAN BASIN

Marcel R. Robinson, M.S

Western Michigan University, 2012

Reservoir characterization of carbonate rocks requires understanding the role of depositional and diagenetic parameters in reservoir distribution. This is especially true for the diagenetically-altered and structurally-influenced Trenton-Black River reservoirs of the Michigan Basin. Evaluating the depositional evolution and reservoir characteristics of component depositional facies through modeling and stratigraphic reconstruction would aid in exploration and characterization through providing a prediction tool for reservoir distribution, both within and outside of the Michigan Basin.

Results indicate that reservoir development is controlled by primary rock fabric related to depositional facies. Depositional and stratigraphic reconstructions show facies distribution trends occur consistently and therefore predictably away from data controls.

Integrating depositional and stratigraphic reconstructions from core with modern borehole imaging technology and geophysical survey techniques may increase the predictability of reservoir quality and distribution within hydrothermal dolomite reservoirs.

Copyright by  
Marcel R. Robinson  
2012

## ACKNOWLEDGMENTS

First and foremost, I would like to thank my thesis advisor, Dr. G. Michael Grammer, and my committee members, Drs. William B. Harrison III and Michelle A. Kominz. The support that I received from them not only in the completion of this manuscript, but also in the advancement my education has proven invaluable.

I would like to thank for financial support during this research the Michigan Geological Repository for Research and Education, the Department of Geosciences at Western Michigan University, the Michigan Basin Geological Society, and the Research Partnership to Secure Energy for America, and the Eastern Section of American Association of Petroleum Geologists. I would also like to thank the staff and faculty at the Michigan Geological Repository for Research and Education and the Department of Geosciences for their assistance with a spectrum of academic and procedural matters during my graduate education.

I would like to thank my friends for having provided insightful discussion, support, and camaraderie.

I am deeply indebted to my family for support and love that they provided me throughout my academic and non-academic endeavors. I would like to offer my deepest appreciation to my parents, Rand M.R. Robinson and Marcia G. Robinson, for their unwavering love and support, and instilling in me the value of a curious and an inquisitive disposition toward the world. I thank my sons, Miles and Levi, with all of a father's love and admiration for their inspiration and their exceptional talents in helping my own understanding by simply asking—"why?" Lastly, but certainly

## ACKNOWLEDGMENTS – CONTINUED

not the least, I thank Johna, and express my appreciation for her devotion, understanding, and love. Our family and my achievements are anchored with her, and the unending love and support she gives us.

Marcel R. Robinson

## TABLE OF CONTENTS

ACKNOWLEDGMENTS .....	ii
TABLE OF CONTENTS.....	iv
LIST OF TABLES .....	x
LIST OF FIGURES .....	xi
Introduction.....	1
Summary of the Problem .....	1
Preliminary Hypotheses.....	2
Objectives and Goals .....	4
Geologic Background .....	5
Regional Geology .....	5
Middle Ordovician.....	7
Stratigraphy.....	9
Sea Level.....	11
Potassium (K)-Bentonites in the Ordovician .....	16
Structure.....	18
Previous Studies.....	20
Depositional Fabrics and Interpretations .....	20
Albion-Scipio Trend and Associated TBR Reservoirs .....	25

Table of Contents—Continued

Discovery and Development.....	25
Albion-Scipio and Stoney Point Reservoirs .....	27
Dolomite and Dolomitization .....	31
Controls on the Lateral Distribution of HTD.....	35
Methodology.....	37
Core Data .....	37
Core Description .....	37
Bioturbation Index .....	40
Grain-bed Indexes.....	43
Whole Core Analysis .....	43
Wire-line Logs .....	45
Data Limitations .....	46
Depositional System Reconstruction .....	48
Facies Associations.....	49

Table of Contents—Continued

Deeper Platform Environment .....	50
Facies 1: Mudstone to Wackestones .....	50
Facies 2: Biotubated Peloidal-bioclastic Wackestone .....	52
Shallower Platform Environment .....	57
Facies 3: Bioturbated Bioclastic Packstone-grainstone .....	57
Facies 4: Grainstone Shoal .....	61
Facies 5: Mottled Packstone-wackestone .....	65
Facies 6: Oxidized Fenestral Packstones .....	72
Ramp-Platform Independent Deposits .....	76
Facies 7: Volcanic Tephra .....	76
K-Bentonite Chronostratigraphy .....	78
Black River Shale .....	81
Facies Reconstruction: Black River Shale .....	82
E-Shale .....	84
Facies Reconstruction: E-Shale .....	85
Facies and Sequence Stacking Patterns .....	85



Table of Contents—Continued

Approach.....	85
Sequence and Cyclostratigraphy.....	87
The TBR Approach.....	88
Stacking Pattern Hierarchy.....	91
Large-scale Sequences.....	91
HFSs and HFCs.....	94
Implications of Stacking Patterns.....	97
Issues with Stacking Pattern Causal Mechanisms.....	99
Autogenic Facies Controls.....	99
Sedimentation Rates.....	100
Sediment Compaction.....	101
Storm Activity.....	102
Tectonics.....	103
Depositional Analogs.....	104

Table of Contents—Continued

The Persian (Arabian) Gulf and the Great Pearl Bank Barrier (GPB)....	106
Problems with the Persian Gulf as a TBR Analog.....	111
Comparable TBR Deposits in the Persian Gulf.....	112
Great Bahama Bank (GBB) .....	114
Problems with the GBB as a TBR Analog.....	118
Comparable TBR Deposits on the GBB .....	118
Analog Synthesis .....	120
Development of the Facies Mosaic.....	120
Summary of Depositional Reconstruction.....	124
Reservoir Aspects .....	125
Reservoir Type.....	125
Comparison of Reservoir and Depositional Aspects .....	128
Depositional Facies vs. Reservoir Attributes and Type.....	129
Primary and Secondary Reservoir .....	131
Reservoir Roles of Other Depositional Facies.....	132
Reservoir Roles of Other Depositional Facies.....	134
NF Reservoir-type vs. T-R Trends in Facies Stacking Patterns .....	136
Facies and Stacking Pattern Controls on Reservoir Quality Distribution .....	139
Controls on Reservoir Quality Distribution.....	141
Facies 2 .....	141
Facies 3 .....	142
Summary of Reservoir Aspects .....	143

Table of Contents—Continued

Summary and conclusions .....	144
Considerations for Future Work .....	148
MTDs .....	148
Additional Future Considerations .....	152
Bibliography .....	155
APPENDICES	
A – Core Descriptions.....	173
B – Core Plates .....	249
C – Core Log-Graphical Core Description .....	322
D – Photomicrographs and Descriptions .....	385
E – Reservoir Aspects.....	478

## LIST OF TABLES

1. Information for cores used in this study .....	38
2. Bioturbation Index used to visually describe and classify the percentage of sediment, primary bedding, reworking of sedimentary structures, and burrow preservation, density and overlap.....	42
3. Diagnostic attributes of depositional facies .....	49
4. Individual reservoir types defined with minimum and maximum permeability values .....	126
5. Summary of reservoir attributes and reservoir-types compared with depositional facies.....	127

## LIST OF FIGURES

1. Map outlining Michigan Basin structures and the distribution of sub-crop/outcrop locations.....	6
2. Map showing paleogeographic position of Laurentia and the Michigan Basin in the Middle Ordovician.....	8
3. Stratigraphic column, Trenton-Black River type-log, and regional depositional trends for the Middle Ordovician.....	12
4. Trenton and Black River Group isopachs in southern Michigan.....	13
5. Extent of Mohawkian K-bentonites in North America and isopach of the Deicke (Black River Shale) K-bentonite.....	15
6. Map showing Michigan Basin and TBR structural features.....	19
7. Burrow ( <i>Callianasa</i> ) mold; Photo of modern <i>Callianasa</i> burrow excavation mounds; and schematic showing the development of grain filled burrow galleries.....	24
8. Regional map showing TBR oil and gas fields and distribution of formation lithologies.....	26
9. Core slab photographs and thin-section photomicrographs showing characteristic TBR HTD textures.....	30
10. Schematic cross-sections of Albion-Scipio and Stoney Point reservoirs ..	32
11. Schematic diagram showing the structurally-controlled hydrothermal dolomite model.....	34
12. Distribution of core used in this study in relationship to the Albion-Scipio trend and Stoney Point field.....	39
13. Example of graphical core description log.....	41
14. Core photos and interpretive outlines illustrating a variety of grain-bed characteristics.....	44

List of Figures—Continued

15.	Schematic overview of the TBR depositional profile.....	51
16.	Facies 1- Core photograph showing very dark gray-black mudstone to sparse skeletal .....	52
17.	Facies 1- Thin section photomicrographs .....	55
18.	Facies 2- Core photograph showing moderately bioturbated wackestone to mudstone textures .....	56
19.	Facies 2- Thin section photomicrograph .....	57
20.	Facies 3- Core photographs .....	60
21.	Facies 3- Thin section photomicrographs .....	62
22.	Core photograph showing a grain-bed with characteristics found in Facies 3 .....	63
23.	Facies 4- Core photograph showing high-angle cross-bedded grainstone .....	64
24.	Facies 4- Thin section photomicrographs and example of white card observation technique .....	67
25.	Facies 5- Core photographs .....	69
26.	Facies 5- Thin section photomicrographs .....	71
27.	Facies 6- Core photographs .....	73
28.	Facies 6- Thin section photomicrograph .....	74
29.	Facies 7- Core photographs (Black River Shale).....	77
30.	Facies 7- Core photographs (E-Shale).....	79
31.	Wire-line log cross-section showing regional continuity of K-bentonites in the Michigan Basin TBR interval.....	80
32.	Facies cross-sections showing strike and dip orientations in the in the Albion-Scipio and Stoney Point study area .....	83
33.	K-bentonite constrained facies distributions .....	86
34.	Idealized vertical succession of TBR depositional facies over a transgressive-regressive cycle of relative sea level change .....	90

List of Figures—Continued

35. Stratigraphic framework synthesis: detailed core-log view.....	93
36. Stratigraphic framework synthesis: detailed facies view.....	95
37. Comparison of Mohawkian changes in relative sea level on the Laurentian craton .....	98
38. Maps showing facies type and generalized texture in the southern Persian Gulf .....	107
39. Satellite image showing the Great Pearl Bank Barrier and Khor al Bazam at the Persian Gulf Trucial Coast (U.A.E.).....	108
40. Satellite image showing the Great Bahama Bank and general facies map of the Great Bahama Bank.....	115
41. Maps showing detailed facies (A.) and carbonate mud distribution (B.) in the GBB interior lagoon.....	117
42. Plot showing the porosity-permeability relationships for GR and NF reservoir-types .....	128
43. Porosity vs. permeability cross-plots showing NF reservoir data for individual depositional facies .....	130
44. Thin-section photomicrographs showing intercrystalline porosity occurring in association with burrows in Facies 3.....	133
45. Thin-section photomicrograph showing isolated vug porosity occurring in dolomitized Facies 2 .....	134
46. Plots showing average and median NF porosity variability with position in T and R trends and large and HFS sequence hierarchy.....	138
47. Plots showing average and median NF permeability variability with position in T and R trends and large and HFS sequence hierarchy .....	140
48. Depositional platform morphologies reconstructed to represent time- slices at the isochronous K-bentonite surfaces—compatible with facies, cross-section, and modern analog analysis.....	147
49. MTD- Core photograph showing debris flow breccia .....	150

## INTRODUCTION

### Summary of the Problem

Middle Ordovician Trenton and Black River Group (TBR) carbonates are regionally extensive and locally host prolific hydrocarbon reservoirs. Trenton and Black River Group reservoirs in the Albion-Scipio trend and Stoney Point field of the southern Michigan Basin are considered examples of hydrothermal dolomite (HTD) reservoirs (Hurley and Budros, 1990; Davies and Smith, 2006). In these reservoirs, impermeable limestones host laterally discontinuous, high-porosity, and high-permeability dolomite bodies that are found in association with major fault/fracture surfaces (i.e. fault and joint surfaces). The HTD origin of these reservoirs is well documented (Prouty 1989; Hurley and Budros, 1990; Allen and Wiggins, 1993; Wilson *et al.*, 2001; Smith, 2006; Grammer *et al.*, 2007).

Current modeling of the processes of reservoir formation focuses on structurally coincident reservoir distribution and HTD fluid origin (Davies and Smith, 2006). However, these 1-10's of kilometer-scale structural HTD reservoir models are inadequate in addressing recognized 10-100's of meter-scale lateral HTD reservoir extensions away from major fault/fracture surfaces, which result in local vertical and horizontal compartmentalization of the reservoir quality (Hurley and Budros, 1990). The lateral extension of HTD zones away from faults are observable as discrete packages, oriented similarly to stratigraphic contacts.

Previous studies of the Albion-Scipio trend have not addressed reservoir-scale depositional modeling of facies character, geometries, or distribution in the Trenton Group depositional system. Thus, little is understood regarding how rock fabrics,



which are controlled by depositional facies, influenced HTD fluid-flow patterns during dolomitization and the resulting reservoir quality distribution in the Trenton Group. Developing an understanding of HTD reservoir distribution at a depositional facies-scale better defines the controls on reservoir quality occurrence and mitigates the drilling of unproductive wells.

The significance in addressing and understanding facies controls on HTD reservoir development in the Albion-Scipio and Stoney Point fields is key when considering not only the potential for establishing best practices in developing these specific reservoirs, but also recognizing the global distribution of HDT reservoirs (Davies and Smith, 2006). The world-wide economic implications of an increased understanding of the controls on hydrothermal dolomitization are profound, as the process commonly results in hydrocarbon reservoirs and desirable ore mineral emplacements (i.e. Pb and Zn). Likewise, the development of a well-constrained facies distribution and depositional model is important to the understanding of regional epeiric carbonate sedimentation dynamics, both in the Michigan Basin and throughout the sedimentary rock record. Intracratonic strata, such as the Michigan Basin TBR interval, constitute a significant volume of the rock record (Pratt and Holmden, 2008). While they hold an estimated quarter of the world hydrocarbon reserves (Leighton, 1991), they commonly have no actualistic modern analog. The increase of knowledge of Michigan Basin regional TBR deposition also translates to a better understanding of globally distributed epeiric sedimentation through geologic time.

### Preliminary Hypotheses

The fundamental hypothesis of this investigation is that the primary rock

fabric of the host limestone and the fault/fracture fluid conduits control HTD fluid pathways. The relatively higher permeability of a given depositional fabric affords a preferential HTD fluid migration path when intersecting structural conduits. The distribution of primary rock fabrics in three dimensions is a function of depositional environment and facies geometries, which then controls HTD distribution away from fault zones. The construction of a constrained depositional model of the Trenton Group, including the Albion-Scipio trend, improves the understanding of the relationship between strati-form HTD development away from faults and its genetic controls (i.e. depositional geometries, stacking patterns, and primary rock fabrics). Although some workers have attributed the lateral extension of HTD away from the Albion-Scipio fault zone exclusively to the local rock mechanic-controlled structure (Wilson *et al.*, 2001), facies controlled strati-form HTD distribution is documented in similar HTD emplacements in Italy (Wilson *et al.*, 1990), the southern Canadian Rockies (Yao and Demicco, 1997), China (Chen *et al.*, 2004), Saudi Arabia (Lindsay *et al.*, 2006), and Iran (Sharp *et al.*, 2010). Recent research focused on the Black River Group shows primary depositional facies are a control on the lateral variability in HTD reservoir distribution (Schulz, 2011; Thornton, 2011). This study tests the depositional facies control on reservoir development with a focus on the Upper Black River Group (uppermost 70 feet, 21 meters) and the Trenton Group.

A secondary hypothesis of this study is that regional volcanic ash deposits in the TBR carbonates provide isochronous surfaces, from which a chronostratigraphic framework can be constructed. This framework provides the foundation for a well-constrained reconstruction of the distribution of depositional facies immediately preceding, and subsequent to, the ash (K-bentonite) deposit. Then the chronostratigraphically-derived depositional model serves as a constrained basis for

interpretation of depositional facies stacking patterns in core. Facies stacking patterns in turn constrain the stratigraphic framework for a robust depositional model of the TBR.

### Objectives and Goals

This study constructs constrained depositional facies models of Upper Black River Group and Trenton Group carbonate deposits in the vicinity of the Michigan Basin Albion-Scipio and Stoney Point hydrothermal dolomite reservoirs. The constrained paleogeographic reconstructions are the basis of subsequent interpretations of facies distributions and the comparison of depositional facies to HTD-reservoir quality. It utilizes core, core analyses, and wire-line logs within stratigraphic frameworks to understand the incidence of reservoir facies and any relationship to depositional facies, serving to better predict the distribution of each facies type where rock data is limited or not available.

The primary goals of this research were to:

1. Construct a chronostratigraphically constrained, regional depositional facies model of the upper Black River Group and Trenton Group carbonates in the study area.
2. Better understand the role of depositional facies in the development of HTD reservoir quality laterally away from primary faults and fractures, thereby increasing predictability in reservoir facies away from the main structure.

These goals are addressed through description of fourteen conventional cores, interpreting core observations and developing sedimentological models within stratigraphic frameworks, and integrating these results with rock physical property

measurements to compare sedimentological, stratigraphic, and reservoir parameters.

## GEOLOGIC BACKGROUND

### Regional Geology

The Michigan Basin (Figure 1) is centered in the southern peninsula of Michigan and occupies 80,000 mi<sup>2</sup> (207,000 km<sup>2</sup>) (Catacosinos *et al.*, 1990). The Basin extends into portions of eastern Wisconsin, southwestern Ontario, northern Ohio, Indiana, and Illinois, and the eastern portion of Michigan's northern peninsula. The Michigan Basin is bordered to the north by the Canadian Shield, to the west by the Wisconsin Arch and Wisconsin Dome, to the east by the Algonquin Arch, to the southwest by the Kankakee Arch, and to the southeast by the Findlay Arch (Figure 1). Crystalline basement rocks in the Michigan Basin are composed of the igneous Central and Penokean Provinces in the southwest and north, respectively, and the metamorphic Grenville Province in the east. The Basin is cut by the failed northwest trending Precambrian Keweenaw Rift and associated rift sequence emplacements and deposits (Fowler and Kuenzi, 1978; Hurley and Budros, 1990).

Paleozoic sediments deposited in Cambrian to Pennsylvanian Periods dominate basin fill, which is measured at a maximum of 16,000 ft (5000 m) thick at the basin center. Paleozoic and Mesozoic sedimentary rocks in the Michigan Basin are overlain by Quaternary glacial deposits up to 1,200 ft (366 m) thick (Catacosinos *et al.*, 1990). Active basin subsidence began in the Cambrian Period and continued through the Mississippian Period (Hurley and Budros, 1990).

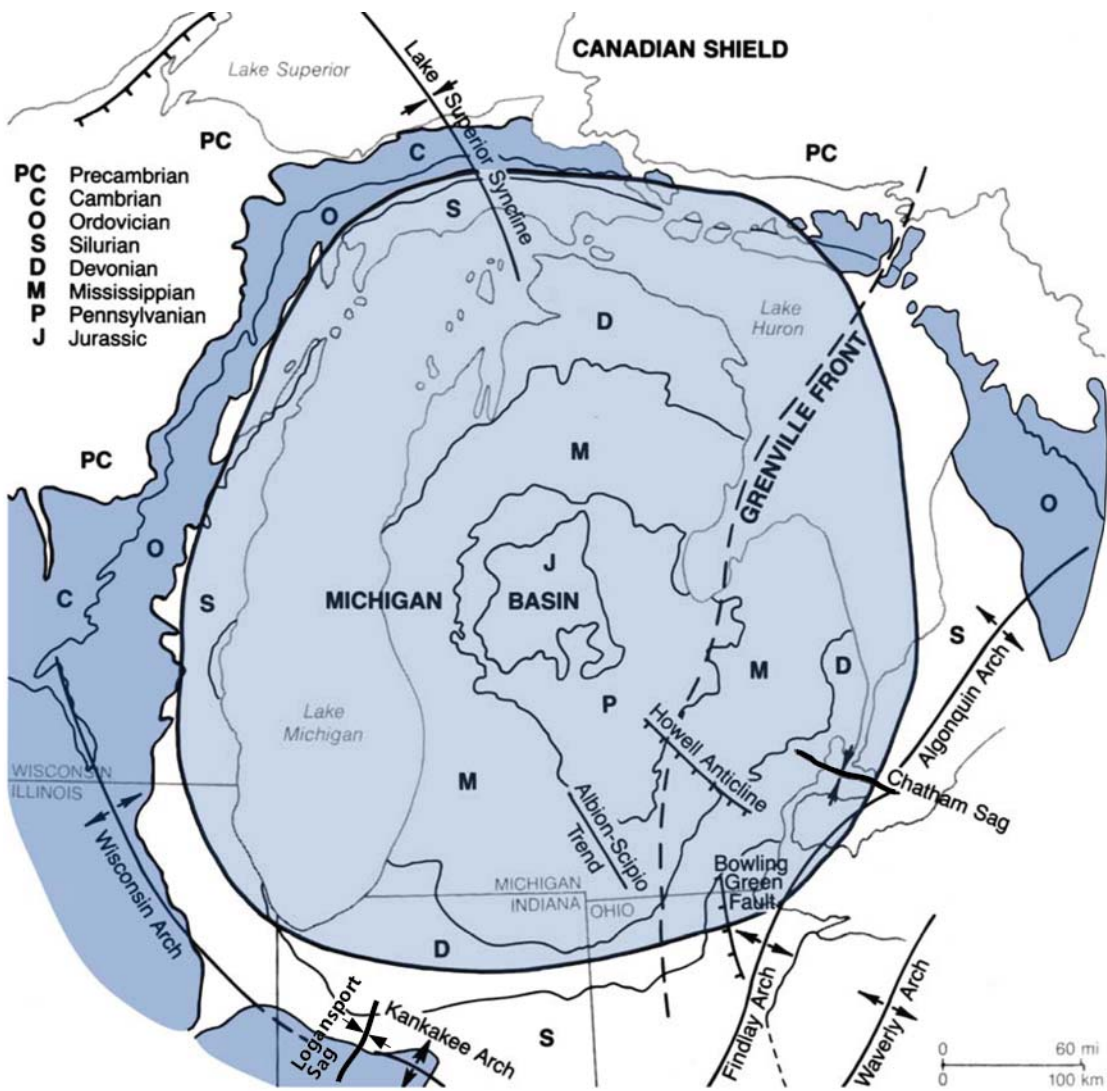


Figure 1. Map outlining Michigan Basin structures and the distribution of sub-crop/outcrop locations. The Albion-Scipio structural trend coincides with prolific hydrocarbon production. Ordovician and Cambrian sub-crop/outcrop locations highlighted in dark blue. Note regional arches intersected by local “sags” at basin flanks. (Modified from Ives, 1960; and Catacosinos *et al.*, 1990).

## Middle Ordovician

The Michigan Basin is an intracratonic basin and was located at approximately 20-25° S Latitude during Late-Middle Ordovician (Mohawkian) time (McKerrow *et al.*, 1991) (Figure 2). During the Mohawkian, the Michigan Basin was located in a tropical/sub-tropical climate similar to that found in modern Florida (Morrow, 1978), and was part of an epeiric sedimentary platform that dominated the Laurentian craton (Keith, 1989). By comparison with modern global atmospheric circulation patterns, paleogeographic reconstructions for the Middle Ordovician suggest that the Michigan Basin was traversed by southeasterly trade-winds (McKerrow *et al.*, 1991; Ettensohn *et al.*, 2002). Assuming consistent global atmospheric circulation patterns through time, the southeast trade-winds result in a dominant southwestern surface water transport direction (net Ekman transport 90° to prevailing winds) during TBR deposition (south-southwestern direction in present basin orientation) (Kennett, 1982; Ettensohn *et al.*, 2002) (Figure 2).

Basin and craton scale tectonic activity influenced the evolution of the Michigan Basin TBR depositional system, while craton activity affected time-equivalent regional sedimentation and the study area. Geodynamic modeling shows that dynamic tilting of the Laurentian craton during the Mohawkian was directed toward the Taconic Orogen to the East (Coakley and Gurnis, 1995). Howell and van der Pluijm (1999) conclude that little Michigan Basin centered subsidence occurred during the accumulation of the TBR. Recognition of the local Basin and regional craton tectonic activity constrains controls influencing TBR deposition in the study area, and also placement of the TBR system reconstruction into the broader craton depositional context.

Outcrop and core studies show that the Michigan Basin was strongly

influenced by storm activity during TBR deposition. Brett and Brookfield (1984) and Brookfield and Brett (1988), through Trenton outcrop studies at the basin margin,

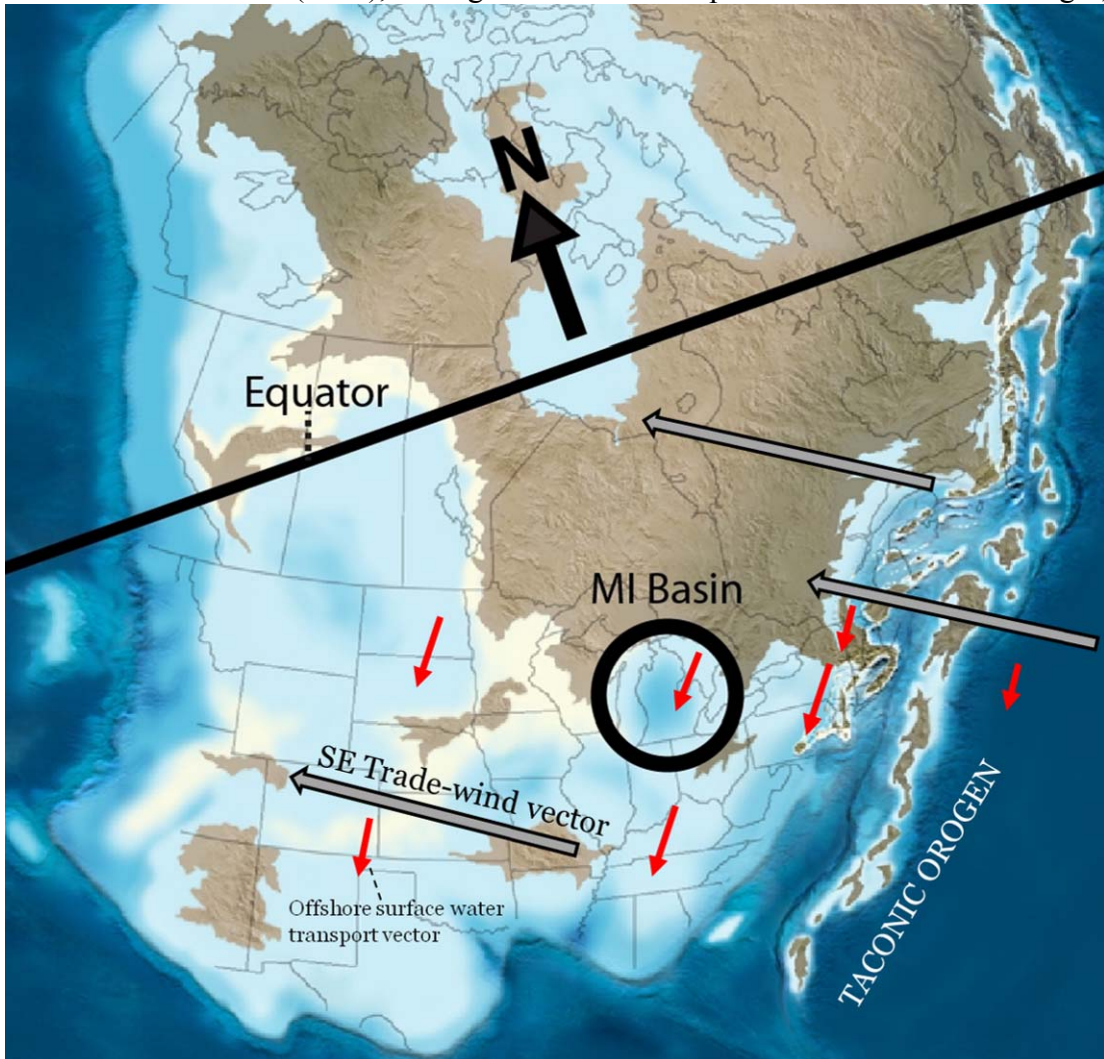


Figure 2. Map showing paleogeographic position of Laurentia and the Michigan Basin in the Middle Ordovician. The Michigan Basin (circled) was characterized by widespread shallow carbonate deposition during the Mohawkian time interval. Paleogeography indicates that southeastern trade-winds (gray arrows) yielded a net southwestern direction of surface water transportation (red arrows). Water depth interpreted in shades of blue (white=shallow, dark blue=deep). Figure adapted from McKerrow *et al.* (1991); Blakey ([www4.nau.edu/blakey.html](http://www4.nau.edu/blakey.html), 6-2010); and Ettensohn *et al.* (2002).

show that episodic high-energy storm activity is recorded throughout this interval. Hurley and Budros (1990) attribute depositional textures in Albion-Scipio TBR core to “storm winnowing.” Strong storm influence is well documented in TBR correlative strata of Ohio and Kentucky (Jennette and Pryor, 1993), Tennessee (Brett et al., 2004), and the Virginia-Appalachian Basin (Kreisa, 1981). Based on bedding criteria outlined by Kreisa (1981) and Aigner (1985), and preservation of storm deposits related to biologic activity (Wanless et al., 1988), recent studies of Albion-Scipio TBR core further document characteristics of storm deposition (Schulz, 2011; Thornton, 2011; and this study). Through description and analysis of these storm influences throughout the TBR at Albion-Scipio and Stoney Point, aspects of the depositional system can be better understood and aid system reconstruction.

### Stratigraphy

The TBR of the Michigan Basin is Middle Ordovician (Mohawkian) in age, and sedimentation was a component of widespread shallow-water carbonate accumulation in the Laurentian epeiric seas (Wilson *et al.*, 2001). Michigan Basin TBR carbonates are time equivalent to the Galena-Decorah-Platteville deposits in Wisconsin, Illinois, and Iowa; the Trenton and Black River Formations in Ohio; the Trenton and Black River Groups in Indiana, New York, and Ontario; and the Lexington-Black River deposits in Kentucky (Budai and Wilson, 1991; Wilson *et al.*, 2001). Keith (1985) combines portions of the Michigan Basin TBR and Galena-Decorah-Platteville deposits to the west, into the continuous Galena Shelf, which merges with the mixed carbonate-siliciclastic Trenton Platform along the eastern flank of the Michigan Basin. These time-equivalent deposits have been studied in detail at outcrop and therefore may offer insight into the reservoir-scale TBR



depositional system, which is significant because no detailed investigation has previously been completed in the study area.

Peer reviewed literature lacks a clear standardization of stratigraphic nomenclature for Michigan Basin Mohawkian-age carbonates. This study therefore chooses to adopt group divisions in the TBR interval (Trenton Group, Black River Group) (Figure 3).

Dependent upon location within the Michigan Basin, the Black River Group unconformably overlies the Glenwood Formation, the St. Peter Sandstone, or the Early Ordovician Prairie du Chien Group (Catacosinos *et al.*, 2000; Nadon *et al.*, 2000). In the vicinity of the Albion-Scipio trend the Black River Group overlies the Glenwood Formation (Hurley and Budros, 1990). The Trenton Group conformably overlies the Black River Group. The TBR measures 600 ft (183 m) thick immediately adjacent to the structure of the Albion-Scipio trend, where solution collapse/dolomitization features reduce the total thickness in the trend (Hurley and Budros, 1990) (Figure 4). The Upper Ordovician (Cincinnatian) Utica Shale overlies the Trenton Group, with the Collingwood Member absent from the top of the Trenton Group throughout the southern Michigan Lower Peninsula. Some authors have argued that sub-aerial exposure has resulted in a karst unconformity at the Trenton/Utica contact (Rooney, 1966; DeHaas and Jones, 1989), while others argue that the contact represents a low sedimentation rate condensed section yielding a marine hardground (Fara and Keith, 1984; Keith, 1985). The debate over the nature of the Trenton/Utica contact is further discussed in the Previous Studies section.

Consideration of the stratigraphic and depositional relationships, both within the Michigan Basin, and in time-equivalent deposits external to the Basin, aids in depositional reconstruction of the TBR in the study area. These relationships offer

insight into the controls on deposition at multiple scales. Because the TBR reservoir-scale depositional system existed as a component of the Michigan Basin, and also the larger Mohawkian system, a review of the regional system as a whole allows for characteristics common to multiple locations (e.g. allogenic relative sea level changes) or local phenomenon (autogenic facies transitions) to be identified. The identification and recognition of regional and local characteristics (and possibly causal mechanisms) works to constrain the reconstruction of the TBR depositional system in the study area.

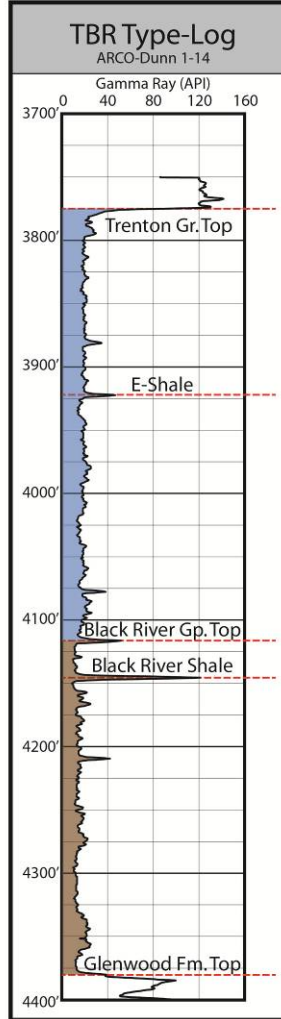
### Sea Level

Shallow-water marine carbonate sedimentary systems are fundamentally influenced by water depth, and so the character of the system is in part dependent on sea level. Local or relative sea level changes are controlled by the sum of externally derived (allogenic) tectonic activity and eustatic (global) sea level, locally sourced sedimentation rates and changes in sedimentary system dynamics and processes (autogenic), and various other factors (e.g. restriction and decoupling of isolated basin waters from the global ocean, compaction/differential compaction of sediment effecting subsidence). Eustatic sea level fluctuations are attributed generally to changes in the volume of water in the global ocean, or changes in global basin dimensions affecting the volume of water contained or displaced (Plint et al., 1992). This study focuses on periodicities in relative sea level change comparable to the allogenic third-order cyclicity reviewed by Plint et al. (1992) and Read (1995). The third-order scale cyclicity (1-10 million years) in this study is possibly composed of higher order packages, or fourth- and fifth-order, or high-frequency cyclicity (HFC) (10,000-100,000 year) in relative sea level change (Plint et al., 1992; and Read,

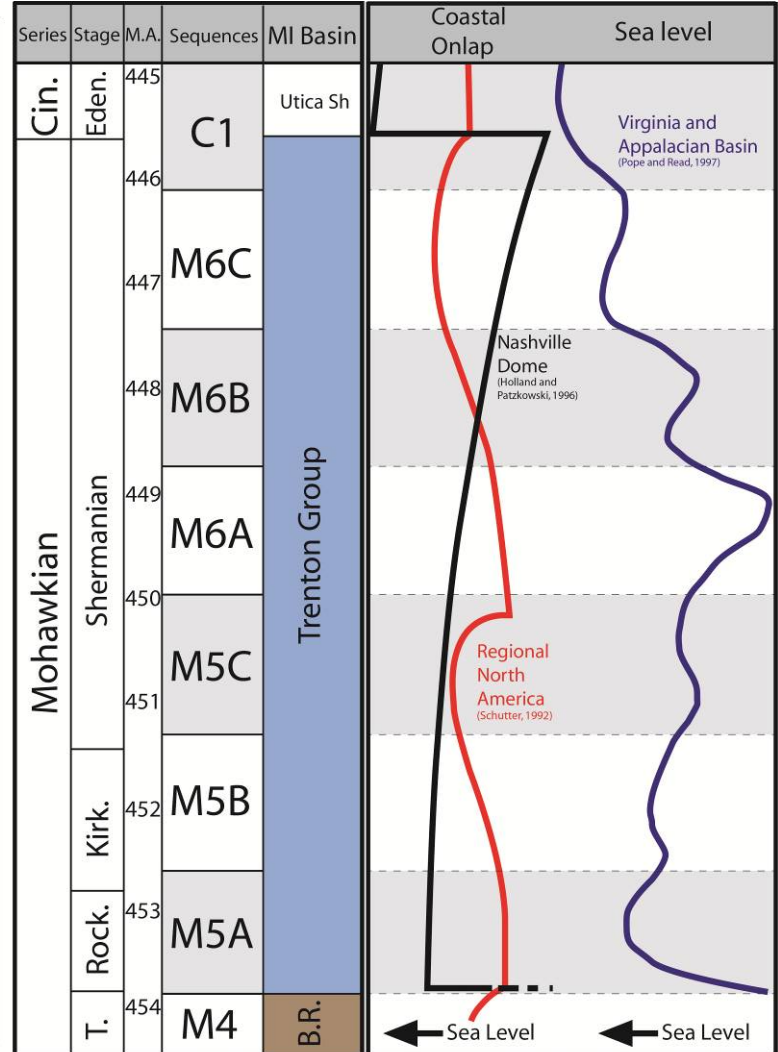
Period	Epoch	North American Series	Subsurface Nomenclature
ORDOVICIAN	Late	Cincinnatian	Utica Shale
			Collingwood Shale
	Middle	Mohawkian	Trenton Group
			Black River Group
			Glenwood Fm.
Chazyan	St. Peter Ss.		

Modified from Catocinos *et al.*, 2000

A.



B.



Modified from Brett *et al.*, 2004

Modified from Pope and Read, 1997

C.

Figure 3. Stratigraphic column, Trenton-Black River type-log, and regional depositional trends for the Middle Ordovician. Charts showing (A.) Middle-Late Ordovician stratigraphy in the Michigan Basin; (B.) Gamma Ray type-log for the TBR interval, outlining group divisions and K-bentonites (Black River Shale, E-Shale) used in this study; and (C.) Mohawkian depositional cyclicity (named sequences M5A through C1), water depth (black curve (Holland and Patzkowski, 1996)), North American regional costal onlap (red curve (Schutter, 1992)), and relative sea level interpretations (blue curve (Pope and Read, 1997)). The Trenton Group interval is highlighted in blue, and the Black River Group in brown. Likely 3<sup>rd</sup> order depositional cyclicity and sea level fluctuation is documented in Trenton-time equivalent Eastern North American deposits (C) (Pope and Read, 1997; Brett *et al.*, 2004). The Collingwood Member (A) of the Trenton Group does not extend into the southern half of the Michigan Basin, and so will not be further considered in this study. T. = Turinian, Rock. = Rocklandian, Kirk.= Kirkfieldian, Eden. = Edenian, Cin. = Cincinnati. (A. modified from Catacosinos *et al.*, 2000; C. modified from Pope and Read, 1997; Brett *et al.*, 2004).

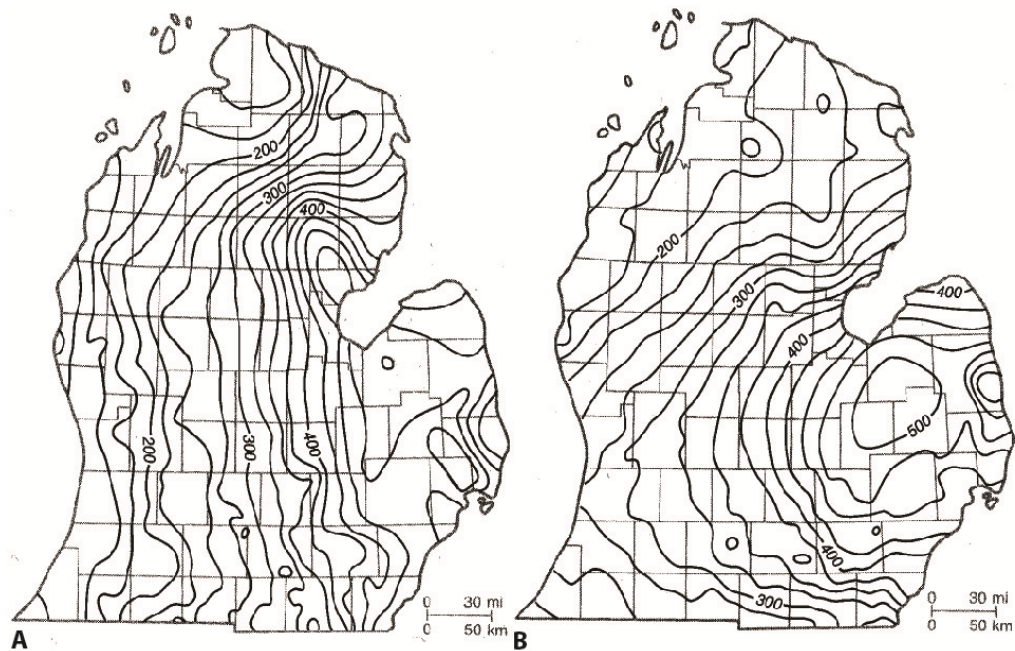


Figure 4. Trenton and Black River Group isopachs in southern Michigan. Maps illustrate thickening of both Black River Group (A) and Trenton Group (B) to the east showing differences in sediment accumulation geometries, suggesting that a basin centered subsidence resumed in the Trenton Group deposition. This is relative to Black River Group

sediment deposits during a period of quiescence in basin subsidence and eastern tilting of the Laurentia continent. C.I.= 25 feet (thickness). (From Catacosinos *et al.*, 1990).

1995).

Changes in sea level recorded in Middle Ordovician deposits outside of the Michigan Basin give insight into patterns of sedimentation observed in the Trenton Group. The long term (first-order) eustatic sea level trend during Middle Ordovician deposition was positioned approximately 500-675 ft (152-206 m) elevated relative to present day sea level (Read, 1995; Haq and Schutter, 2008), resulting in widespread cratonic inundation. Fourth- and fifth-order Milankovitch-scale cyclicity is documented during the Middle Ordovician as inter-cratonic correlative meter-scale transgressive and regressive sedimentary packages superimposed on the long-term or lower order trends (Ross and Ross, 1992).

Work by Holland and Patzkowski (1996), Pope and Read (1997, 1998), and Brett *et al.*, (2004) divides the Trenton Group interval into six depositional sequences at third-order scales (c.a. 1.3 My, average), through correlation across the differing tectonic regimes of the Nashville Dome (tectonic fore-bulge) and Trenton Shelf carbonates (tectonic foreland ramp, *sensu* Keith, 1986) (Figure 3 and 5). Brookfield (1982) proposes that depositional cyclicity in Ontario Michigan Basin TBR tidal deposits can be attributed to glacio-eustatic (i.e. HFC) influences, and Brett and Brookfield (1984) agree with this speculation as mechanisms of cycle development at Basin flanks. The time-equivalent meter-scale sequences correlated external to the Michigan Basin, along with Milankovitch-scale cyclicity documented in Basin margin deposits, strengthens comparison of documented assumed allogenic sea level signals with changes in relative sea level interpreted in this study of the TBR deposits in Albion-Scipio and Stoney Point locations.

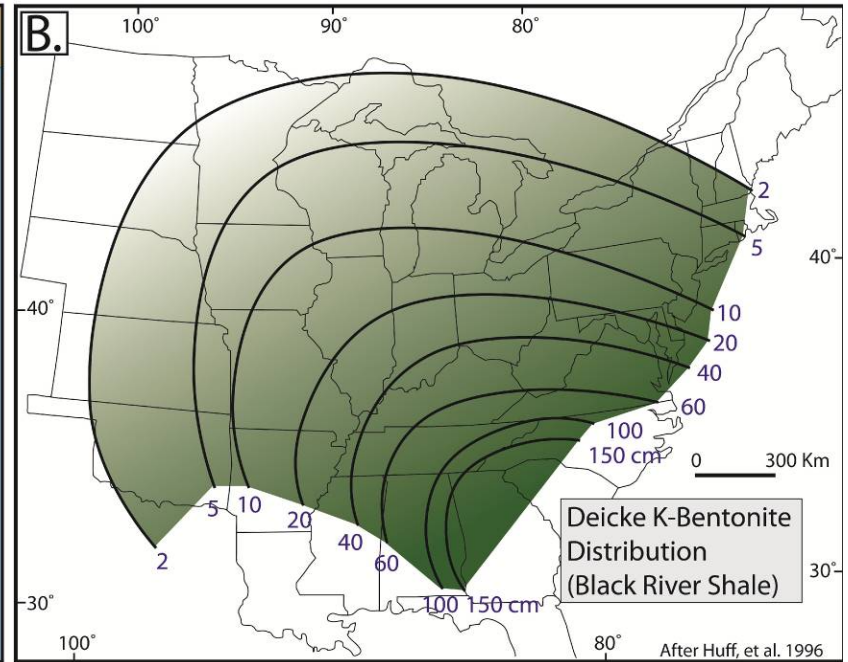
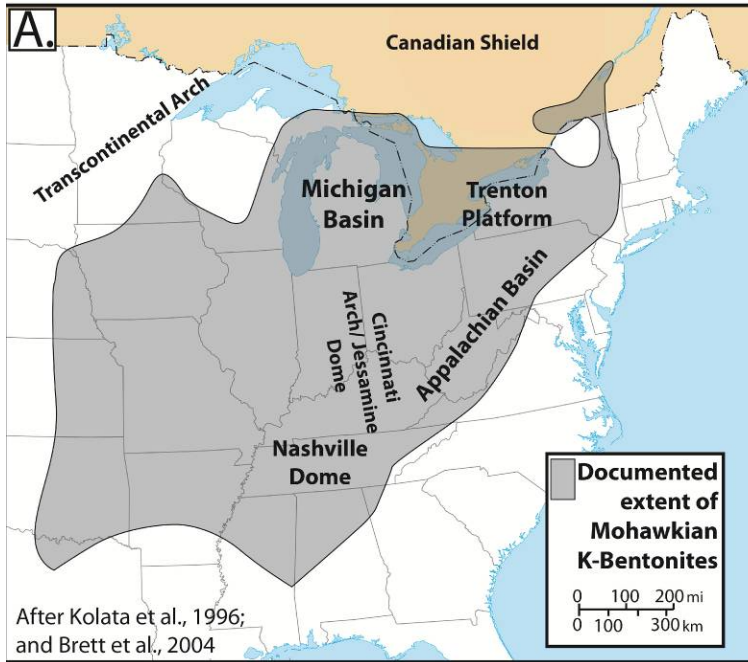


Figure 5. Extent of Mohawkian K-bentonites in North America and isopach of the Deicke (Black River Shale) K-bentonite. Map showing the extent of Mohawkian K-bentonite deposits and locations of correlated Trenton Group equivalent deposits (A.), and isopach (scale is in cm, non-linear) of the regionally correlated Deicke K-bentonite (the Michigan Basin's Black River Shale) (B.). Deicke distribution shows that ash sourced from Taconic Orogen related volcanism was transported inboard by southeastern trade-winds. The K-bentonites represent an assemblage of regional volcanic ash deposits that are powerful stratigraphic correlation tools, in that each captures an isochronous surface in the depositional record. The isochronous nature of these beds allows for well-constrained reconstruction of depositional facies distributions at multiple horizons throughout the TBR interval. (Figures modified after Kolata *et al.*, 1996 and Brett *et al.*, 2004 (A.) and Huff *et al.*, 1996 (B.))

### Potassium (K)-Bentonites in the Ordovician

Active Taconic volcanism during the Middle Ordovician episodically supplied ash deposits to the Laurentian craton, including the Michigan Basin (Huff *et al.*, 1992; Kolata *et al.*, 1996) (Figure 5). The volcanic ash beds, presently observed as K-bentonites, represent chronostratigraphically significant strata that capture time-slices of facies distributions at multiple times in the TBR depositional system. These deposits are used in this study as datums to evaluate intervening depositional system dynamics. The chronostratigraphically significant nature of K-bentonite beds provide constrained facies distributions and geometries at instants in geologic time and aid in the construction of paleogeography and stratigraphic frameworks.

The two specific K-bentonites used as chronostratigraphic surfaces in this study are informally referred to in the Michigan Basin subsurface nomenclature as the Black River Shale and E-Shale marker beds (Hurley and Budros, 1990). These marker beds are located approximately 30 ft (9 m) below the top of the Black River Group and 150 ft (45 m) below the top of the Trenton Group, respectively (Figure 3).

On the basis of chemical analyses and stratigraphic position, Kolata et al. (1996) determined that the Black River Shale is equivalent to the extensive (230,000 mi<sup>2</sup>, 600,000 km<sup>2</sup>; Huff and Kolata, 1990) Deicke K-bentonite bed (Figure 5b). Variable dating methods of the Diecke have yielded a number of dates (e.g, 457.1 ± 1.0 Ma, apatite Nd and Sr isotopes TN, USA, Samson, et al., 1989; 454.5 ± 0.5 Ma, zircon <sup>238</sup>U/<sup>206</sup>Pb, NL, CA, Tucker and McKerrow, 1995; 449.8 ± 2.3 Ma, biotite <sup>40</sup>Ar/<sup>39</sup>Ar from, KY, USA, Min, et al. 2001), however 454 to 455 Ma is commonly cited in recent literature.

Chemical fingerprinting of the E-Shale has not conclusively identified this bed as a volcanic tephra deposit. However, this bed has been correlated to an unnamed K-bentonite in Basin margin Trenton outcrop in southwest Ontario by Trevail (1990) and correlates to the Dygerts K-bentonite correlated into the Basin by Kolata *et al.* (1996) Furthermore, the E-Shale is mineralogically identified as volcanic in origin with x-ray diffraction in Albion-Scipio trend cores (Feutz, 2012). Because of the consistency in stratigraphic/wire-line log position, correlation with the established Dygerts K-bentonite, and a mineralogical composition consistent with a volcanic origin, the E-shale is considered to represent a single ash fall event deposit in this study.

These K-bentonites are prominently expressed on wire-line logs. Concentrations of radiogenic elements (K, Th, U) in the K-bentonites result in strong positive gamma-ray wire-line log (GR) excursions relative to the clean carbonate in the TBR interval. The Black River Shale and E-Shale are readily identifiable in the context of the TBR bentonites as a whole because of high GR measurements relative to other bentonites or marine shales containing radiogenic material, and distinct log patterns and stratigraphic positioning (Figure 3).



## Structure

The Michigan Basin structural homocline dips  $0.5^\circ$  toward N15°E, with the top of the Trenton Group at 3,340 ft (1018 m) in the south, and maximum depths in Albion-Scipio and Stoney Point locations of 4,300 ft (1311 m) (Hurley and Budros, 1990) (Figure 6). Movement along north-northwest trending faults in the Michigan Basin (Ells, 1962; Fisher, 1988) related to Taconic and Acadian orogenic activity likely occurred episodically until ending in the Early Devonian (Hurley and Budros 1990). Structural modeling (Harding, 1974) and seismic data (Smith, 2006) show that left-lateral dilatational stress caused the development of negative flower structures that are associated with the Albion-Scipio structural-sag (20-60 ft, 6-18 m relief), and associated right-stepping *en echelon* lineaments (Figure 6) (Ells, 1966; Hurley and Budros 1990). Faulting during early burial supports the possibility of HTD fluid migration into primary porosity of coarse-grained Trenton Group rocks, based on recent studies of porosity/permeability relationships with depth in carbonates (Melzer and Budd, 2008) and mechanical parameters necessary for TBR HTD fabric development (Davies and Smith, 2006; Langhorne (Taury) Smith, personal communication, 2009). The recognition of similar structural trends in the Michigan Basin suggest that additional undiscovered Albion-Scipio-type HTD reservoirs may have formed elsewhere in this carbonate interval, as evidenced by the discovery of the linear TBR Napoleon field in 2009 (located 20 mi due east of the midpoint of Albion-Scipio trend) (Figure 6).

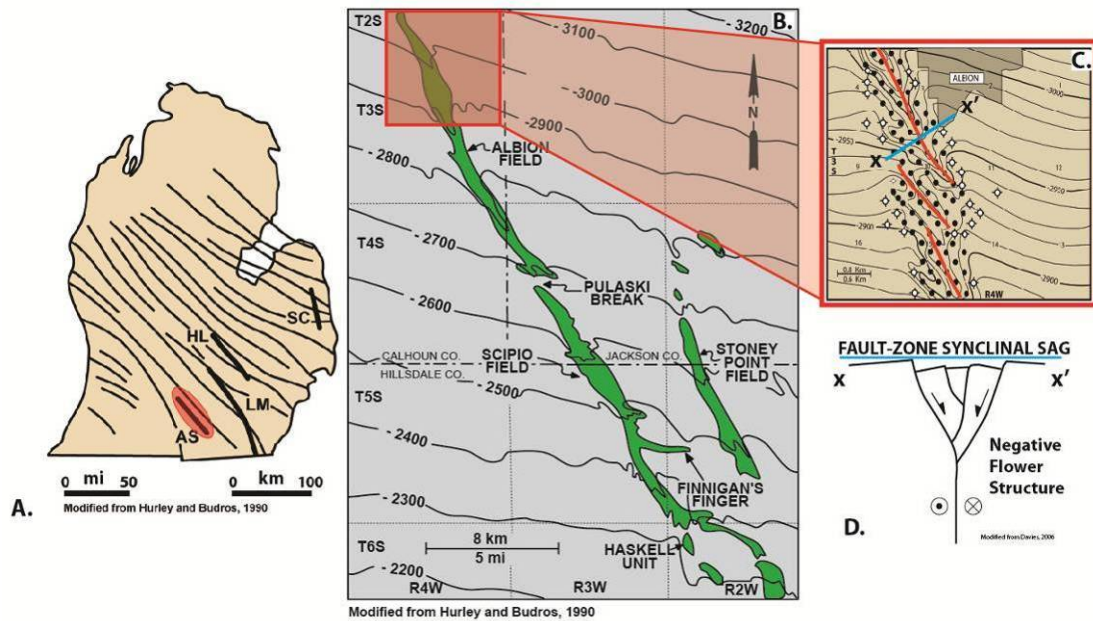


Figure 6. Map showing Michigan Basin and TBR structural features. **A.)** Structural grain of the Michigan Basin and major faults: SC=Sanilac, HL= Howell, LM= Lucas-Monroe, AS= Albion-Scipio (red circle) **B.)** Regional dip of the Michigan Basin and structural sags of the Albion-Scipio trend and Stoney Point Field [contours map the depth (sub-sea level, ft) to top of the Trenton Group, C.I.= 100 ft]; **C.)** Enlarged view showing the field structure. Note productive trend wells (black circles) outlined by adjacent dry holes (white circles). Field [contours map the depth (sub-sea level, ft) to top of the Trenton Group, C.I.= 10 ft]; **D.)** Schematic cross section showing mechanics of the formation of negative flower structures. Blue line approximates the blue line in C. (**A.**, **B.**, and **C.** Modified from Hurley and Budros, 1990; **D.** Modified from Davies, 2006)

## PREVIOUS STUDIES

### Depositional Fabrics and Interpretations

Early study of the TBR rocks in the Michigan Basin was generalized in nature and limited in descriptive detail. Cohee (1948) discussed the Black River and Trenton Groups in very general terms, describing the Black River as fine-grained dark-gray to black limestone and shale at the base, and the upper section as light brown/gray fossiliferous dense-to-crystalline limestone and dolomite. In reference to the Trenton Group, Cohee (1948, p. 1432) states, “its lithologic character is similar to that of the Black River limestone.” This limited description offers very little toward environmental interpretation.

Later studies of core in the Albion-Scipio trend area give higher detailed descriptions of fabric and interpretations regarding TBR deposition, although they remain limited in depositional facies description. Taylor and Sibley (1986) more thoroughly characterize skeletal components in the TBR as a diverse assemblage of echinoderm, brachiopod, trilobite, ostracod, mollusk, bryozoan, sponge, and crinoid fragments. They also identify a brown-gray nodular mudstone distributed through the TBR, interpreting it to represent deep water depositional environments similar to Cretaceous chinks (although indicating no value for “deep”, and additionally interpreting them to compose storm rip-up clasts). Hurley and Budros (1990) distinguish the Trenton Group from the Black River Group on the basis of depositional texture, where the Trenton is characterized by mudstones, crinoidal wackestones, and storm-winnowed laminated crinoidal packstones. Hurley and Budros (1990) state that, in general, chert nodules, peloidal grainstones, and fewer fossil allochems are present in the Black River Group. Hurley and Budros (1990) do

not note a change in faunal diversity between the Black River and Trenton groups at Albion-Scipio and Stoney Point locations. These TBR descriptions in the study area lack identification of individual depositional facies as a tool for sedimentological reconstruction, and thus perpetuate the “layer cake stratigraphy” concept of shallow water carbonate accumulation.

Additional regional (Keith, 1985, 1989), basin-margin outcrop (Brett and Brookfield, 1984; Brookfield and Brett, 1988) and study area (Schulz, 2011; and Thornton, 2011) TBR studies indicate that these sediments were deposited in normal marine waters on a storm dominated carbonate ramp. The TBR package was deposited in normal marine sub-tidal conditions, and shows a general increase in high-energy deposits in proximal positions to regional arch features (Keith, 1989). Regional facies analysis of the Galena Platform deposits (*sensu* Keith, 1985) shows high-energy shoal facies distant from landmasses (Fara and Keith, 1989). This relationship, in conjunction with depositional surface slope of  $<1^\circ$  and water depths of 10-300 ft (3-91 m), agrees well with carbonate ramp depositional models described by Irwin (1965), Ahr (1973), Read (1985, 1998), and Burchette and Wright (2000).

The Michigan Basin was protected from open ocean conditions during TBR deposition, owing to the paleogeographic setting. This protection can be attributed to the interior location on a craton-scale shallow sea, partial isolation by the sub-aerially exposed Canadian Shield, and surrounding bathymetric highs associated with regional arches (Ives, 1960; Catacosinos et al., 1990; and Kolata et al., 1998) (Figures 1, 2). Tidal and fair-weather wave energy was likely dissipated through frictional dampening over these surrounding bathymetric barriers and shallow cratonic seas (Keulegan, and Krumbein, 1949; Irwin, 1965; Beyer *et al.*, 2008). As a result of the absorption of these hydraulic energies, lower ambient energy conditions predominate

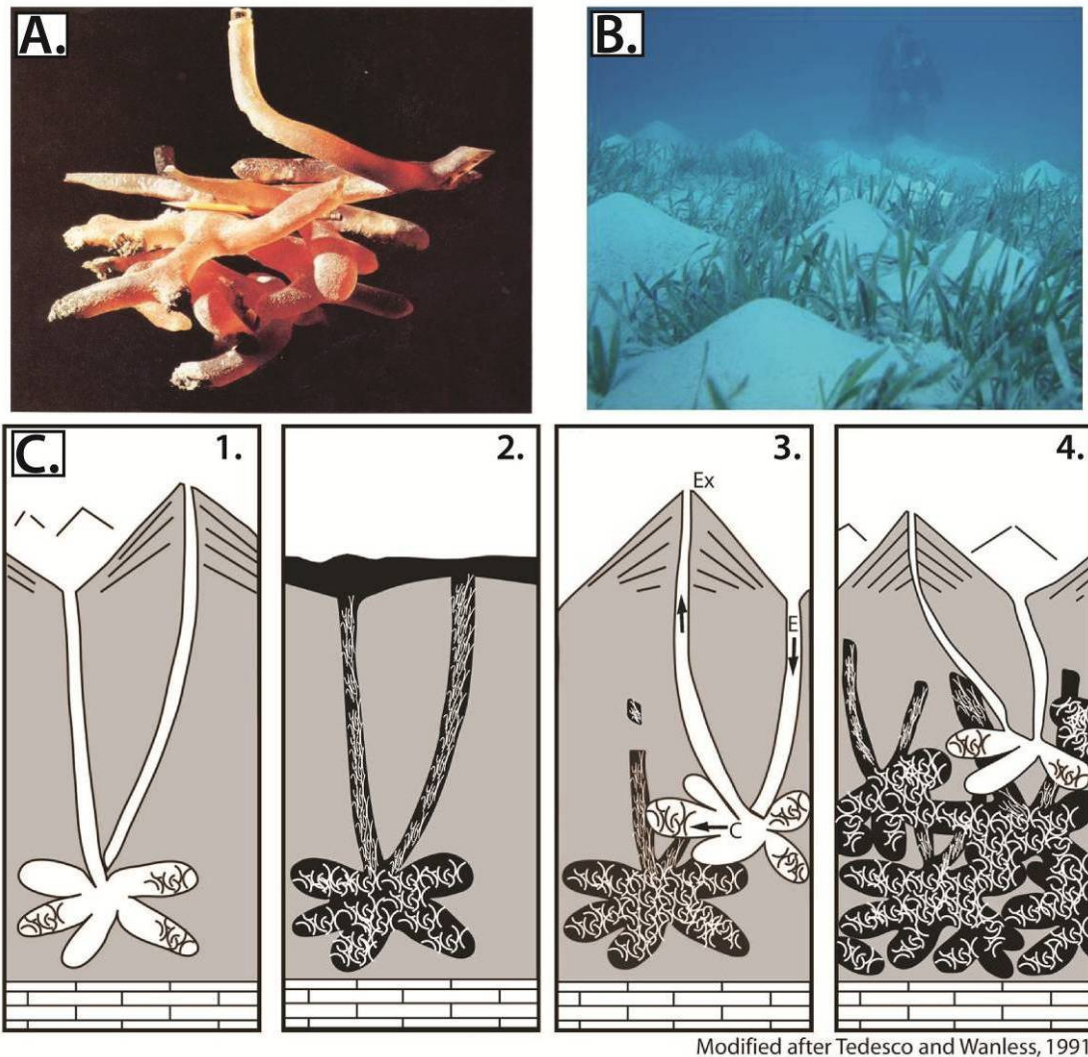
on the TBR platform relative to similar carbonate platforms situated adjacent to deep ocean waters (i.e. the modern Florida Shelf, eastern margin of the Great Bahama Bank). Storm domination of TBR deposits may have also indirectly resulted from the reduced tidal and fair-weather wave influences.

Normal marine salinities and circulation dominated TBR deposition, although a degree of isolation affected the energy conditions. Abundant stenohaline and filter feeding organisms (crinoid and bryozoan) in TBR deposits give evidence of these conditions (Kammer and Ausich, 2004). The Chatham and Logansport Sags constituted circulation bypasses as bathymetric lows intersecting basin-peripheral arches, and likely afforded connectivity and circulation with the open epicontinental portion of the Laurentian Sea (Ives, 1960; Figure 1). The net result of this regional paleogeographic setting was storm-dominated, well circulated waters containing sufficient nutrients to support filter feeding organisms in the study area.

In a recent study of the Black River Group, Schulz (2011) notes the presence of pervasive bioturbation and burrow mottling in cores taken in and around Albion-Scipio and Stoney Point reservoirs. Schulz (2011) concludes that *Thalassinoides* burrows are filled with coarse-grain sediments relative to the burrowed matrix. Schulz suggests that the coarse-grain burrow fills are likely deposits winnowed and injected during high energy storms (i.e. “tubular tempestites” of Wanless *et al*, 1988) or by bottom currents. In settings similar to the TBR, Wanless *et al*, (1988) suggest that the selective expulsion of fines by burrowing organisms may also contribute to a relatively coarse-grained burrow fill.

Modern carbonate depositional settings show that the burrowing shrimp *Callianassa*, typically described as a modern analog for *Thalassinoides*, generate burrow galleries hundreds-to-thousands of square-meters in area, creating an

interconnected burrow network up to two meters below the sediment surface (Tedesco and Wanless, 1991) (Figure 7). The pervasive burrowing of sub-tidal deposits, and the subsequent filling of burrow voids by coarse grains, potentially develops zones of laterally extensive, relatively high porosity and permeability “plumbing” systems within the strata. Examples of preferential dolomitization of burrow networks through HTD processes are documented in carbonate outcrop studies of Late Jurassic deposits in Saudi Arabia (Lindsay *et al.*, 2006) and Lebanon (Nader *et al.*, 2007), and Cretaceous deposits in Iran (Sharp *et al.*, 2010). This study’s evaluation of the distribution of such high permeability burrowed facies, in the context of associated depositional facies and a constrained stratigraphic framework, helps to better understand the role of burrowing in HTD reservoir quality development and distribution in the Albion-Scipio trend.



Modified after Tedesco and Wanless, 1991

Figure 7. Burrow (*Callianasa*) mold; Photo of modern *Callianasa* burrow excavation mounds; and schematic showing the development of grain filled burrow galleries. The *Callianasa* burrowing crustacean offers insight as a modern analog to the development of ancient *Thalassinoides* high-permeability burrow galleries observed in the TBR interval. *Callianasa* burrow branches extend into three-dimensions in the subsurface (resin mold in A., pencil for scale). High burrow density at a given time (note density of excavation mounds in B., diver in background for scale) and multiple generations of burrowing in storm-influenced environments result in the sequence outlined in (C.): 1.) excavation of a burrow, concentrating grains too large for the organism to expel; 2.) a storm event winnows fine grains from surface sediments and infills the burrow with coarser grains than burrowed substrate; 3.) post-storm excavation

of burrows commonly intersect portions of earlier burrow generation in the subsurface; 4.) multiple generations of burrow-infill sequences obliterate original depositional facies fabric while developing a coarse grain filled burrow network, or gallery. (Figure (A.) from Enos et al., 1983; (B.) courtesy of W.B. Harrison, III; and (C.) modified from Tedesco and Wanless, 1991.)

## Albion-Scipio Trend and Associated TBR Reservoirs

### Discovery and Development

Production of hydrocarbons from TBR reservoirs began with the discovery of oil at the Findlay-Kankakee arch in 1884 (Keith, 1986), with subsequent discoveries of the Indiana-Lima trend and Bowling Green fault-zone, all contributing to total production of approximately 500 million barrels of oil (80 million m<sup>3</sup>) (Keith, 1986) (Figure 8). The discovery well for the Albion-Scipio trend in June of 1957 resulted from a prediction from a fortuneteller locating the well in Scipio Township, MI (Buehner and Davis, 1968). In 1958, a discovery well locating the Albion Field 12 mi (19 km) northwest of the Scipio discovery was completed. The initial Albion-Scipio trend development strategy was limited to interpolation between the discovery wells and extrapolation or step-outs from the line connecting discovery wells (parallel and perpendicular). The increase in well data resulting from additional drilling at the trend made available wire-line logs as a primary exploration tool. Although field-scale geophysical exploration tools were not used during the high frequency drilling of the 1960s (Buehner and Davis, 1968), the trend was further developed during this time with a strategy of targeting new wells in the linear structural sag. This field development strategy focused on the sag identification in wire-line log cross-sections and contour mapping of the Trenton Group top. The step-out, or extrapolative,



drilling strategies away from the linear trend commonly resulted in dry holes (non-productive wells) that are often within 0.25 mi (0.4 km) of productive wells (Figure 6).

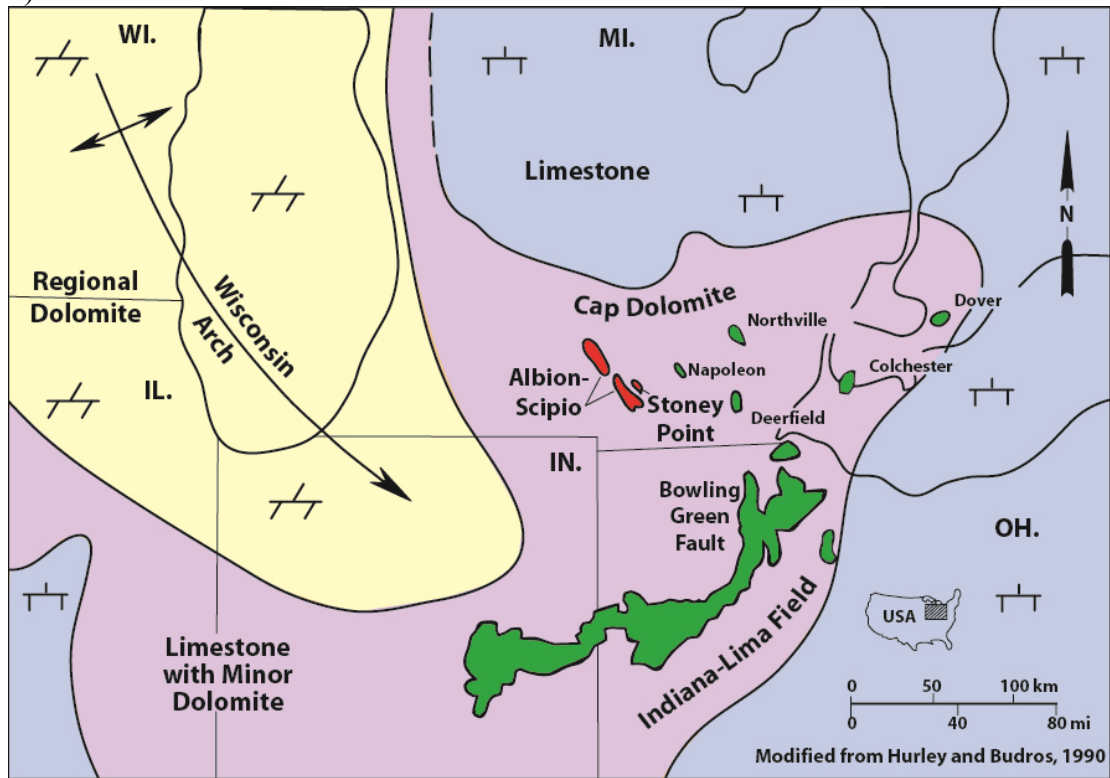


Figure 8. Regional map showing TBR oil and gas fields and distribution of formation lithologies. Albion-Scipio trend shown in red. Napoleon field is an HTD reservoir discovered in 2009 located east of the Albion-Scipio trend. Note coincidence of HTD field locations and cap dolomite distribution. (Modified from Hurley and Budros, 1990; Bellinger, 2009)

Aside from minor TBR production from fields located in southern Michigan and southeastern Ontario—such as the Northville, Deerfield, and Dover fields—the only subsequent major discoveries in southern Michigan Basin locations are the Stoney Point and Napoleon fields (Figures 6 and 8).

The Stoney Point field is located approximately 5 mi (8 km) east of and sub-parallel to the main Albion-Scipio fairway (Figure 6). The Stoney Point discovery

well was drilled primarily on the basis of soil-gas geochemical analysis in December 1982 (Hurley and Budros, 1990). The present geometries of the Albion-Scipio trend and Stoney Point field are each approximately 1 mi (1.6 km) wide and 30 mi (50 km) and 7 mi (11.2 km) in length, respectively.

Renewed exploration in Albion-Scipio-type reservoirs, such as the recently discovered Napoleon field (Figure 8), requires a better understanding of reservoir formation processes in order to establish best practices for reservoir development and avoid the close step-out dry holes that were encountered previously in the development of these HTD reservoirs. The right-stepping (basin-ward) *en echelon* trend of the Napoleon field first reported production in July 2009 (Michigan Department of Natural Resources and Environment), and shows a similar orientation to Albion-Scipio trend and Stoney Point field. Presently, Napoleon field has approximately the same dimensions as Stoney Point, although delimiting of the reservoir(s) is currently incomplete. Given the similarities in apparent reservoir geometry, the Napoleon field likely developed through HTD processes similar to the Albion-Scipio and Stoney Point reservoirs.

#### Albion-Scipio and Stoney Point Reservoirs

Hurley and Budros (1990) compiled the most detailed study to-date on the Albion-Scipio and Stoney Point fields from a hydrocarbon reservoir perspective, and that work is summarized below.

Reservoir facies are exclusively dolomite in composition and are generally characterized by vuggy, cavernous and inter-crystalline (sucrosic) porosity (*sensu* Choquette and Pray, 1971). Comparisons of porosity vs. permeability show no uniform relationship in these reservoirs. Whole-core analyses report median

porosities of 2 to 5% with permeabilities ranging from 0.01 to 8,000 mD, but generally (85%) less than 10 mD. The reservoir is sealed laterally by impermeable host limestone and vertically by a regional, ferroan cap dolomite. Correlation of low permeability shale/K-bentonites and preferentially dolomitized rock bodies located immediately below the low permeability beds suggests that HTD fluids migrated upward along structural surfaces and pooled at beds where fluid flow was impeded (also, Feutz, 2012) (i.e. pooling of the vertically migrating HTD-fluid at these baffles or seals likely caused extensive dolomitization below the shale/K-bentonite).

Reservoirs in the Albion-Scipio trend and Stoney Point field are compartmentalized at an inter-well and reservoir-scale. The Albion-Scipio trend is divided into three reservoir-scale compartments and Stoney Point into four. On the basis of produced gas-oil ratios, bottom-hole pressures, and gas-oil and oil-water contact levels, these reservoir-scale compartments are oriented/distributed along the long axes of the fields (compartments ranging in length from approximately 2-12 mi (3-39 km) in Albion-Scipio trend, and 8 mi (13 km) in Stoney Point). Inter-well heterogeneity is likely related to the heterogeneous depositional geometries and fabrics detailed as a primary focus of the current study, as well as to complex negative flower-structural geometries and *en echelon* lineament distribution noted by Hurley and Budros (1990).

Dolomite fabric and distribution controlled by HTD reservoir development processes are likely related to both structure and the primary rock fabric. Hurley and Budros (1990) recognize a high variability in measured TBR porosity and permeability. It is reasonable to assume then that variable porosity and permeability measurements relate to the reported reservoir rock fabrics (e.g. Anselmetti and Eberli, 1999 and Grammer *et al.* 2004). These variations may be manifested as follows:

moldic porosity lacking communication in low-permeability matrix; very high-permeability or open/solution-enhanced fractures exhibiting low bulk porosity; connected vug/cavern networks measuring high porosity and permeability; and high-permeability sucrosic inter-crystalline porosity juxtaposed against low porosity and permeability matrix (Figure 9).

Schulz (2011) proposes, and Thornton (2011) establishes that interconnected burrow networks filled with coarse-grain sediments acted as preferential HTD fluid conduits away from faults in the Black River Group. The commonly resulting reservoir type in these burrow networks is the high-permeability sucrosic inter-crystalline fabric discussed above (Thornton, 2011). Fabric selective dolomitization of burrowed facies offers an explanation for the observed vertical reservoir compartmentalization away from structural trends (i.e. strati-form dolomite) with no observed shale aquitard at an inter-well scale.

As discussed, the Michigan Basin TBR HTD reservoirs show complex relationships between internal reservoir structures and the reservoir structure as a whole. The complexity of reservoir development through HTD processes and resulting reservoir heterogeneity and distributions are likely controlled by structural deformation as well as primary rock fabrics. Because of the hypothesis of this relationship, depositional processes and the HTD reservoir formation process must be investigated and reviewed, respectively.

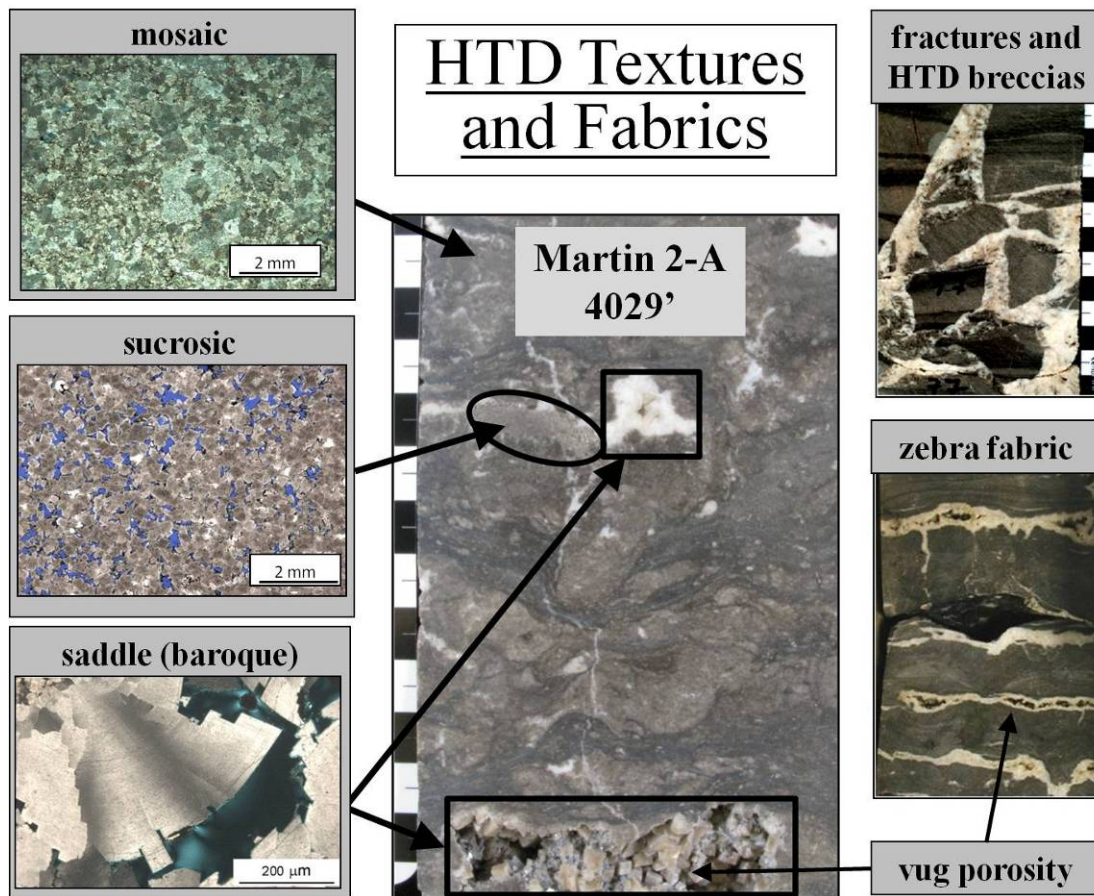
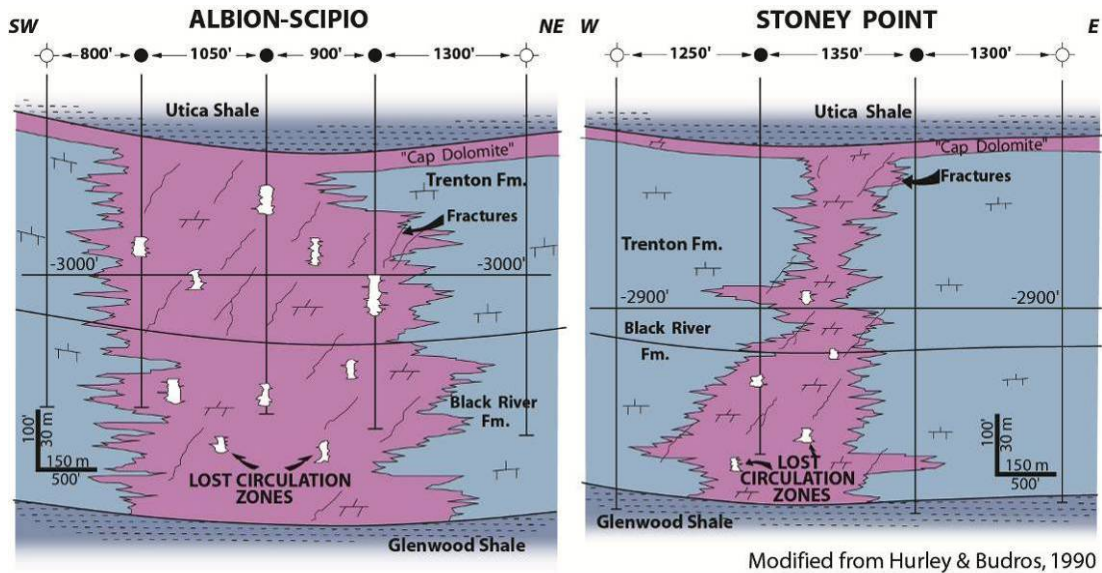


Figure 9. Core slab photographs and thin-section photomicrographs showing characteristic TBR HTD textures. White coarse-crystalline saddle dolomite outlines/fills vugs and fractures. Sucrosic dolomite coinciding with burrow texture is located adjacent to saddle dolomite in the Martin 2-A sample. Matrix consists of low-, to no permeability mosaic dolomite. Breccia/fault sample (upper right) shows angular lithoclasts “floating” in white saddle dolomite, indicating hydraulic fracturing and rapid dolomite crystal formation associated with faults. Zebra fabric (lower right, core in image approximately 4 inches wide) consists of bedding parallel saddle dolomite-lined vugs, indicating burial timing is sufficiently early to allow separation at bedding planes by HTD-fluid (Davies and Smith, 2006; Langhorne (Taury) Smith, 2009, personal communication). Note the heterogeneity of textures in Martin 2-A core slab. Scale bars are in centimeters.

## Dolomite and Dolomitization

The reservoir facies of the TBR are dominated on a regional scale by dolomite associated with fracturing and faulting related to wrench tectonics. This association is observed in New York, Ohio, and Indiana, as well as the Michigan Basin. Study of fault-associated dolomite reservoirs has resulted in development of models of dolomitizing-fluid migration along structural features. However, the source and conditions of fluids at the time of migration remain somewhat debatable.

Taylor and Sibley (1986) recognize three dolomite types related to TBR in the Michigan Basin: regional dolomite, cap dolomite, and fracture-related dolomite (Figures 8 and 10). The regional dolomite occurs throughout the entire TBR interval, or as dolomite inter-bedded within limestone (Taylor and Sibley, 1986). The regional dolomite is limited to western portions of the Michigan Basin, outside of Albion-Scipio localities. The cap dolomite extends across the southern Michigan Basin, ranges 3-30 ft (1-9 m) in thickness at the top of the Trenton, and is characterized by high iron content ( $\text{FeCO}_3$  2-15 mol%) and an anhedral interlocking crystal mosaic (Taylor and Sibley, 1986). The prevailing hypothesis of the origin of the cap dolomite cites dewatering of the overlying Utica Shale (Taylor and Sibley, 1986; Hurley and Budros, 1990). Fracture related dolomite is chemically and texturally distinct from the cap. Fracture dolomite is primarily non-ferroan, consisting of coarse sub- to euhedral crystals, with relatively depleted  $\delta^{18}\text{O}$  values (Taylor and Sibley, 1986). A brown, vuggy, and sucrosic fracture-related dolomite is also recognized (Prouty, 1989). Fracture dolomite, as implied, lines and fills fractures and related vugs. The sucrosic dolomite, along with a mosaic crystalline dolomite, occurs as the matrix in which the fracture and vug lining dolomite is found. Zoned, white, saddle (baroque) dolomite crystal morphologies are likely indicative of hydrothermal origin (Machel



Modified from Hurley & Budros, 1990

Figure 10. Schematic cross-sections of Albion-Scipio and Stoney Point reservoirs. Dolomite is depicted in purple, limestone in blue, and lost circulation of drilling fluid in white. Fractures have been interpreted with little well control. Note lateral extensions of dolomite away from vertical columns with no indication of formational control. (Figure modified after Hurley and Budros, 1990)

and Lonnee, 2002; Davies and Smith, 2006), and line pore space, fill vugs, and replace calcite matrix in TBR dolomites (Figure 9).

Landes (1946) first attributed dolomitization of the Lima-Indiana trend to vertical fluid migration of magnesium-bearing brines along fractures. This concept is given support by a number of studies in which laterally discontinuous dolomite is recognized to occur in relationship to faults in the Michigan Basin (Ells, 1962; Beghini and Conroy, 1966; Rooney, 1966; Prouty, 1989; Hurley and Budros, 1990; and Davies and Smith, 2006). Karsting of the TBR in the Albion-Scipio trend has been invoked in reservoir development modeling by Rooney (1966) and DeHaas and Jones (1989), on the basis of a hypothesized sub-aerial unconformity at the top of the Trenton. However, evidence questioning the validity of this interpretation include

submarine hardground characteristics of phosphate and pyrite mineralization (Keith, 1989), and the lack of vadose or phreatic zone cave features, younger sediment deposits, and other karst features on the scale observed in reservoirs at the Trenton-Utica contact (Hurley and Budros, 1990). Landes (1946) also recognizes the relationship between Lima-Indiana trend reservoir dolomite and hydrothermal alteration indicative of Mississippi Valley-Type (MVT) Pb-Zn mineralization. An increase in saddle dolomite associated MVT mineralization with depth at the Albion-Scipio trend supports upward vertical migration of dolomitizing fluid (Wilson *et al.*, 2001).

Geochemical and geothermal data further support the HTD development model. Depleted  $\delta^{18}\text{O}$  values relative to surrounding limestone reflect high dolomite homogenization temperatures calculated from dolomite crystal fluid inclusions (Allen and Wiggins, 1993; Grammer *et al.*, 2007). The homogenization temperatures are elevated 70°C (Allen and Wiggins, 1993; Grammer *et al.*, 2007) relative to ambient formation temperatures calculated through basin modeling (Cercione, 1984). Furthermore, dolomite homogenization temperatures exceed maximum burial temperatures, with the assumption that an additional 1 kilometer of Late Paleozoic and Mesozoic sediment has been eroded from the Basin maximum burial thickness (Smith, 2006).

Global observation of high-temperature fault-related dolomite has led to development of a structurally-controlled HTD model, including Albion-Scipio and Stoney Point reservoir development (Davies and Smith, 2006) (Figure 11). In this model magnesium-rich brines advect into host limestone from basement or deep sedimentary aquifers via active fault conduits. High pressure-temperature brines extend away from main fault conduits where high pressure gradients, combined with



permeability in host rock or vertical buoyant forces, result in fluid intrusion. Porosity is developed through dissolution enhancement and mineralogical conversion of calcite into dolomite, both of which may be enhanced by hydraulic fracturing. Rapid fluid-pressure reduction due to existing or newly-created dissolution porosity also decreases brine solubility and results in mineral (dolomite) precipitation. Repeated hydrothermal mineralization events likely reduce porosity associated with the most frequently traveled conduits, resulting in relatively poor reservoir quality at major structural features. Included in this model are vertical barriers to upward migration of HTD fluids such as internal shale and overlying cap-rocks. At the barriers, pooling of HTD is generally associated with enhanced porosity development.

Machel and Lonnee (2002) call attention to the ambiguity in the term “hydrothermal dolomite” as it is applied with numerous definitions. In this study HTD is defined as the dolomite mineralization which occurred at temperatures elevated relative to the ambient formation conditions.

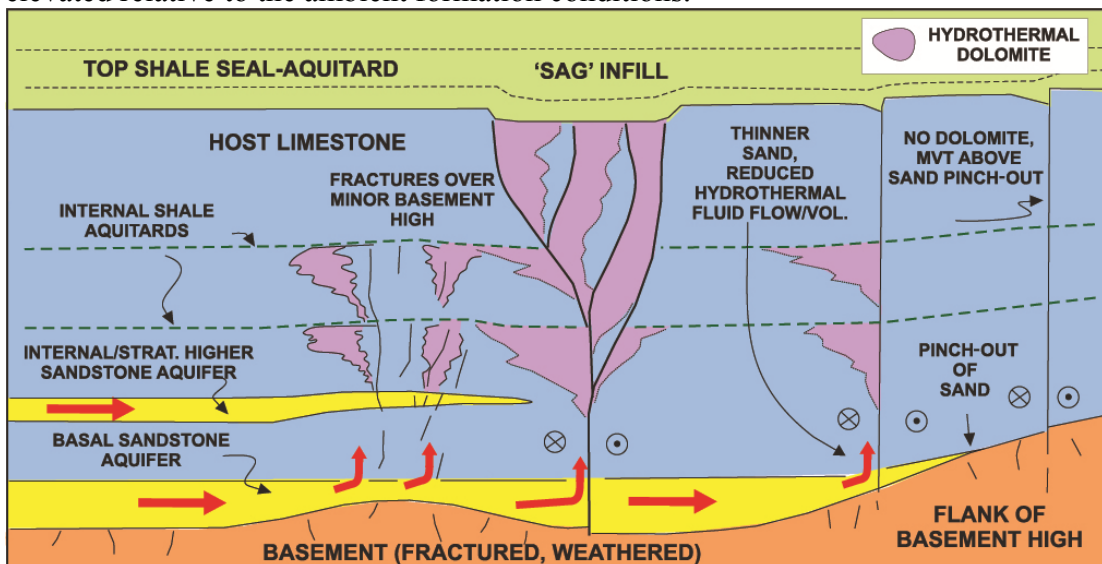


Figure 11. Schematic diagram showing the structurally-controlled hydrothermal dolomite model. Control on reservoir distributions limited to structure and internal aquitards, where host formation rock-fabric related to

deposition is not addressed. See text for further explanation. (Figure from Davies and Smith, 2006)

### Controls on the Lateral Distribution of HTD

Only vaguely addressed, however, in these structural HTD models are controls on the lateral extensions of HTD development and dispersal. Hydraulic-fracturing, pooling of dolomitizing fluid at vertical barriers, and higher local permeabilities are each cited as a possible control on extension of reservoir HTD. Lateral extension of reservoir facies extending 100s of meters away from vertically distributed fault-zone HTD are documented at Albion-Scipio and Stoney Point (Hurley and Budros, 1990). The question then is what controls the reservoir development away from the main fault planes?

Wilson *et al.* (2001) attribute lateral variability in HTD geometries to mechanical rock behavior, where lithology controls fracturing. However, the notable lack of fractures in high porosity and permeability burrows of the Black River Group (Schulz, 2011) does not support rock mechanics and fracturing as an exclusive developmental control. Primary rock fabric does, however, control the mechanical behavior of rock by way of texture (mud content), grain type, and nature of grain contact, cementation, and mineralogy at the time of fracture. If rock mechanical behavior controls lateral variability in high-porosity HTD, then that relationship inherently imposes depositional facies and early diagenetic control on reservoir development, each of which are related to sequence stratigraphic positioning (e.g. surfaces more or less susceptible to meteoric diagenesis, changes in lithology, constituent components, facies geometries, and relative location related to symmetric or asymmetric sea level fluctuations).

The primary reservoir exploration strategies currently being utilized in the search for HTD reservoirs relies mainly on the identification of the structural-sag features observed in 3D seismic data. Given that the seismically identifiable structural features are likely also primary vertical fluid conduits, they then represent lower reservoir quality because of porosity reduction at fluid conduits that have experienced multiple HTD-fluid migrations (Davies and Smith, 2006; Murray Matson, 2010, personal communication). Identifying controls on HTD development laterally away from primary structural surfaces would greatly augment seismic exploration and subsequent drilling, by working to avoid non-productive step-out wells from the major structural surfaces.

Previous study of TBR deposition has focused primarily on the Black River interval, with attention paid to the Trenton Group only to broad regional or localized areas outside of this study's focus. Additionally, reservoir studies at Albion-Scipio and Stoney Point have neglected or dismissed depositional reconstruction as a critical tool in describing reservoir formation processes (Beghini and Conroy, 1966; Rooney, 1966; Taylor and Sibley 1986; Prouty, 1989; Keith 1985, 1986, 1989; DeHaas and Jones, 1989; Hurley and Budros, 1990), with the exception of few recent studies (Schulz, 2011; and Thornton, 2011). Therefore, a detailed depositional study of the Trenton Group and incorporation of Albion-Scipio and Stoney Point reservoir data offers opportunity to better define the local depositional system and its evolution, and also to test the hypothesized depositional controls on reservoir formation processes in the interval as outlined in recent work.

## METHODOLOGY

### Core Data

#### Core Description

Development of a depositional model for TBR carbonates requires core-based description of depositional facies and their vertical stacking patterns. Lithofacies established through core description allows for interpretations of depositional environment and sequence-/cyclostratigraphically significant surfaces and intervals, while also constraining probable depositional geometries, and establishing vertical stacking patterns of facies.

Fourteen conventional cores taken from the TBR interval were chosen for depositional modeling in this study (Table 1). These cores, stored at the Michigan Geological Repository for Research and Education (MGRRE), are all located in the Albion-Scipio trend, Stoney Point field, or the four counties surrounding those structural features (Branch, Calhoun, Hillsdale, and Jackson) (Figure 12). The cores chosen in the vicinity of the Albion-Scipio trend were based on the criteria that they contain either the Trenton Group stratigraphic interval, or contain the Black River Shale.

Core was described on a centimeter-scale, using Swanson's (1981) Sample Examination Manual as a guide. The described interval was stratigraphically constrained to the top of the Trenton Group at highest and 40 feet (12 meters) below the Black River Shale at lowest. This lower boundary is designed to capture Black River Shale within a complete depositional cycle, which range from 20 to 30 feet (6 – 9 meters) thick in the Black River Group (Schulz, 2011). Capturing the Black River

Permit #	Well	Abbreviation	County	Field	Trenton Group	Black River Shale	Core Analysis	Feet described
37385	Arco Conklin 1-31	AC 1-31	Hillsdale	SP	Y	N	Y	197
37239	Arco Dunn 1-14	AD 1-14	Calhoun	n/a	N	Y	Y	35
37838	Arco Gardner 1-16	AG 1-16	Hillsdale	SP	N	Y	Y	19
21064	Buehrer 1	B 1	Hillsdale	A-S	Y	Y	Y	339
36587	Casler 5-30	C 5-30	Jackson	SP	N	Y	Y	103
33673	Faist 2-12	F 2-12	Jackson	n/a	Y	Y	Y	382
22196	Hergert 2	H 2	Hillsdale	A-S	N	Y	N	28
22381	Mann 6	M 6	Hillsdale	A-S	N	Y	limited	73
22083	Martin 2-A	M 2-A	Calhoun	A-S	Y	N	Y	99
22460	McMahon 4	MCM 4	Calhoun	A-S	Y	N	Y	78
21381	Rowe A-2	R A-2	Hillsdale	A-S	Y	Y	Y	346
31253	Rzepke 1-27	RZ 1-27	Branch	n/a	N	Y	Y	26
21833	Skinner 1	S 1	Hillsdale	A-S	N	Y	Y	62
31407	Stetler 1-33	ST 1-33	Branch	n/a	N	Y	Y	34

Table 1. Information for cores used in this study. “Field” column denotes Albion-Scipio trend (A-S), Stoney Point field (SP), or other (n/a) well locations. “Feet Described” measures linear feet described in each core. See Figure 12 for core and county locations. Core name abbreviations are used in figures and text henceforth.

Shale within a depositional cycle is significant in that it enables facies mapping at a defined isochronous surface. Facies distributions are thereby temporally constrained in a depositional sequence context. Mapping at this surface also supplies critical facies distribution data to be incorporated into a continuous stratigraphic record through the entirety of the overlying Trenton Group.

Core descriptions include lithology, grain types, textural classification (Dunham, 1962; and Embry and Klovan 1971), dominant pore types (Choquette and Pray, 1970), sedimentary structures, diagenetic features, color (Rock Color Chart, Geological Society of America, 1991), and depositional cyclicity. Additions to Swan’s Sample Examination Manual developed specifically to address observations in this study include development of a bioturbation index, “grain-bed” thickness and frequency measurements, and supplements addressing burrow diameter and filling

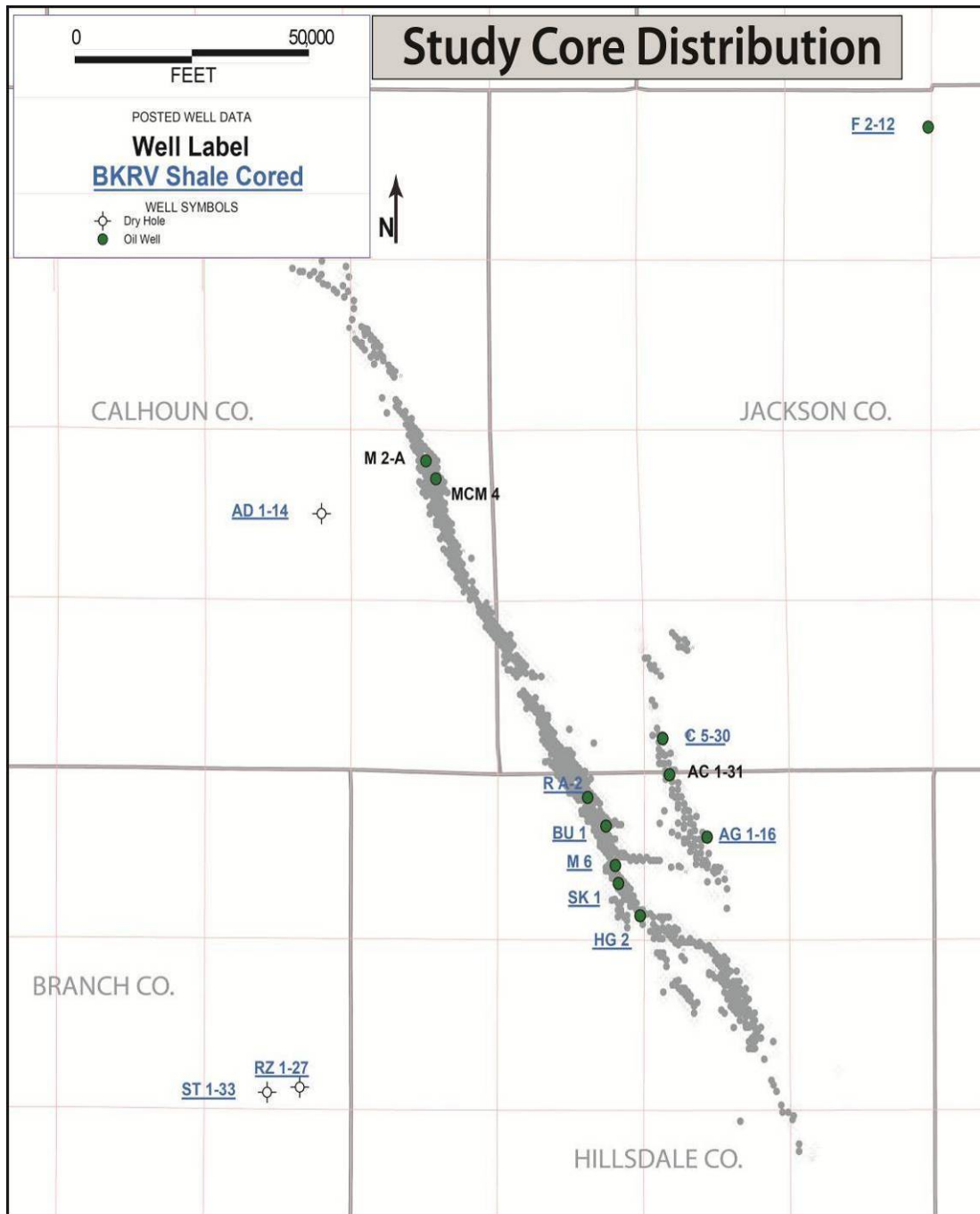


Figure 12. Distribution of core used in this study in relationship to the Albion-Scipio trend and Stoney Point field. Core taken from wells that produced oil are shown as green circles, producing wells shown as gray circles, and dry wells shown as crossed-hollow circles. Cores that capture the Black River Shale are labeled in blue and underlined, and cores only

containing the Trenton Group are labeled in black. Note concentration of cores along the two producing fields (Albion-Scipio located at West, Stoney Point at East). Refer to Table 1 for core abbreviations and selection information.

grains (Appendix A and B). These additional observations will be discussed in subsequent sections. Thin sections were obtained throughout the entire described core. Thin section descriptions with associated photomicrographs (Appendix D) further constrain the hand sample-scale core observations. Thin section samples were impregnated with blue epoxy to highlight the distribution of porosity. Lithofacies were classified from core and thin section observations, which were then used to interpret depositional facies (see Depositional Reconstruction chapter). Descriptions, facies interpretations and identification of stacking patterns, thin section sampling depths, well engineering data (i.e. initial production tested and perforated intervals), and petrophysical and wire-line log data were then plotted in a graphical core description chart modified from Swanson (1981) (Figure, 13) (Appendix C).

Pervasive dolomitization in some cored intervals obscures or obliterates primary fabrics at the core or thin section scale. This diagenetic overprint can impede the ability to identification of sedimentary criteria necessary for facies determination (e.g. structures and gains). However, the comparison between core and thin section sampling-scales, and augmentation of thin section observations with the white card-reflected light petrographic technique (Zenger, 1979; and Folk, 1987) combine to reveal grain type and sedimentary structure data for interpretation of the depositional environment.

### Bioturbation Index

The activity of burrowing organisms is a well-documented characteristic of

subtidal carbonate platform deposits (Enos, 1983; Ekdale *et al.*, 1984; Flugel, 2004),

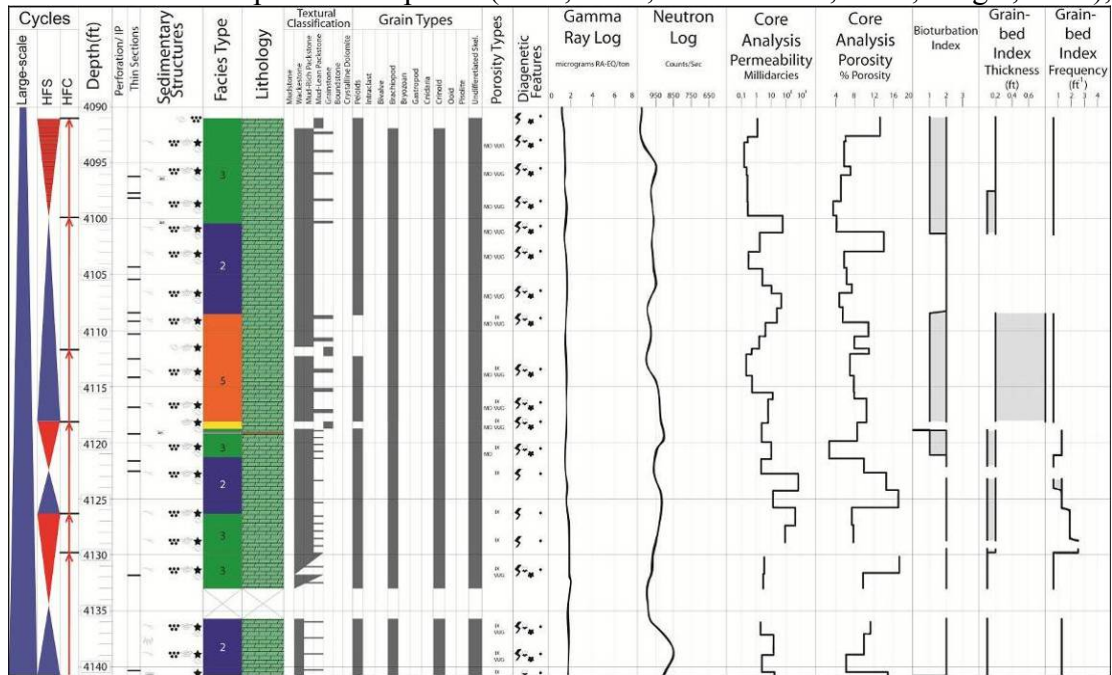


Figure 13. Example of graphic core description log. The combination of these parameters into a single display aids in analysis and interpretation of subsurface cores. See text for description of core log information.

where biologic alteration of primary depositional features and grain reworking may determine the distribution of porosity and permeability pathways (Flugel, 2004; Thornton, 2011). Bioturbation is extensive throughout the TBR section (Hurley and Budros, 1991; and Wilson *et al.*, 2001; Schulz, 2011), owing to shallow (<150 m) subtidal sedimentation in semi-restricted basin (i.e. reduced wave energy and tidal currents) environmental conditions, which allowed burrowing communities to thrive.

As bioturbation constitutes a key depositional characteristic of the TBR carbonates, a numerical bioturbation index was developed for this study, in order to capture the visual estimation of bioturbation in core based on bedding preservation and burrow abundance, boundaries, and burrow overlap (Table 2, after Taylor and Goldring, 1993). Plotting the bioturbation index as a graphic log alongside core



descriptions and physical property measurements (whole core analysis, wire line logs) provides a supplementary tool in interpretation and analysis of described sections.

<b>Bioturbation Index #</b>	<b>Percent Bioturbated</b>	<b>Classification</b>	<b>Description</b>
0	0	No bioturbation	- bedding completely intact with no burrow traces
1	1-30	Sparse bioturbation	bedding is distinct, burrows do not overlap
2	31-60	Moderate bioturbation	- bedding is identifiable, but becoming less distinct - burrow boundaries are distinct with overlap observable but not dominant
3	61-99	Intense bioturbation	- bedding is completely disturbed, but discernible - burrow boundaries overlap with later burrows discrete
4	100	Total bioturbation	-complete bioturbation -bedding is not identifiable due to repeated reworking

Table 2. Bioturbation Index used to visually describe and classify the percentage of sediment, primary bedding, reworking of sedimentary structures, and burrow preservation, density and overlap. (Modified after Taylor and Goldring, 1993)

Dominant burrow diameters and the nature of burrow fill (e.g. Dunham's (1962) textural classification and grain types) were also documented in addition to the bioturbation index and biogenic environmental/sedimentological indicators (e.g. borings in consolidated or semi-consolidated substrate).

### Grain-bed Indexes

Grain-beds, or packstone-to-grainstone beds and seams (<0.5 ft thick) composed of grain concentrations are distributed throughout the TBR interval. These grain beds are insufficient alone to base a set of criteria for unique lithofacies or depositional environment interpretation, however, observations regarding the thickness, frequency, and character of the beds prove to be useful attributes in the facies analyses conducted in this study.

Broadly categorized as grain concentrations, these beds contain a variety of grain-types and sedimentary structures with Dunham textural classifications ranging from grainstone, to high grain concentration wackestone (i.e. high percentage of total volume composed of grains and approaching a grain supported texture). The grain-beds are commonly interpreted as representing storm winnowing/deposition, but also spillover of sediments from sand bodies (e.g. shoals) (Aigner, 1985). The thickness and frequency of grain-bed deposits are purely numerical measurements that are graphically represented on core descriptions, and intended to be combined with the sedimentological observations discussed in this study (Figure 14). The thickness and frequency along with the texture and sedimentary structures of the grain-beds, and also the facies in which they occur (i.e. above and below), are considered together in context to represent a water depth proxy, and as such they are employed as a facies analysis tool in this study.

### Whole Core Analysis

Petrophysical data were available from full diameter core analysis in the MGRRE database. These data include percent porosity, maximum horizontal permeability, horizontal permeability 90° from maximum values, vertical

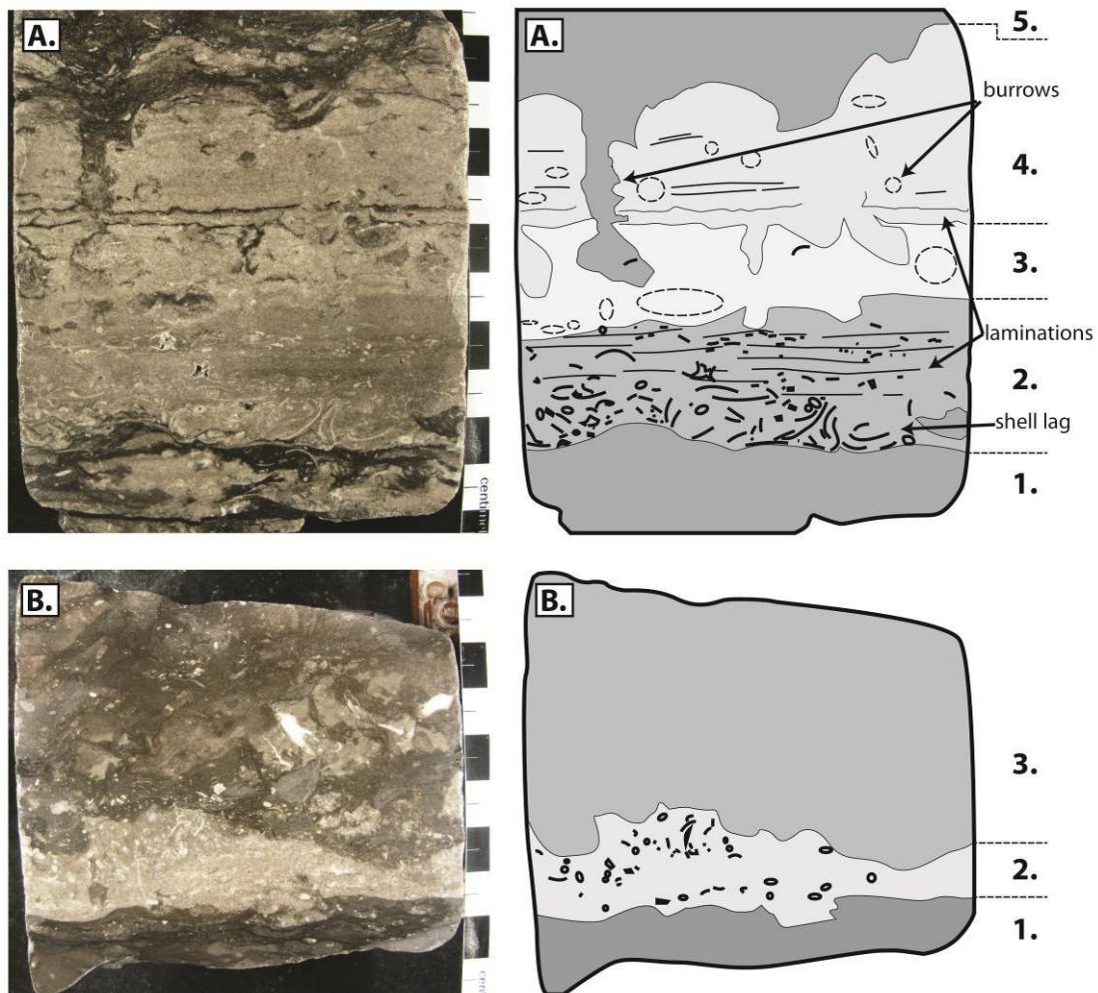


Figure 14. Core photos and interpretive outlines illustrating a variety of grain-bed characteristics. **Sample (A)** is interpreted to represent the deposition of two tempestite (storm) deposits. The first begins with scour of bed A1, followed by deposition of a bioclastic lag (shell lag, bottom of A2) that fines-up into a laminated sand. Horizon A3 contains burrows and reworked sediment likely from the A2 horizon or subsequent deposits. The second tempestite initiates at the planed A3-A4 contact where a lag deposit is lacking, likely due to reworking of the upper portions of the previous tempestite deposit (A2 and A3). The storm deposit at A4 is capped by a characteristic irregular, burrowed surface (Aigner, 1985). **Sample (B)** is interpreted to represent a high energy event sand deposit, possibly through winnowing fine grains at the sediment-water interface, or mobilization of grains from an adjacent bathymetric high during a storm.

The thickness and frequency parameters of these grain beds offer insight

into relative water depth (or increased storm activity) when plotted with core description in log format. However, the range in grain bed characteristics shown here demonstrates that depositional structures, character, and surrounding deposits are a necessary context for environmental interpretations of the beds. Samples from M 2-A core, scales are in cm.

permeability, fluid saturation, grain density, and bulk density measurements. Core analyses indicate the capability of the rock sample to house and/or transmit fluids effectively. Grain density indicates mineralogy, where values distinguish between limestone and dolomite. When grain density data were not available or proved inconclusive, dilute (5-10% concentration) hydrochloric acid testing and alizarin-red etch-staining techniques were applied directly to rock and thin section samples (Scholle and Ulmer-Scholle, 2003). High frequency sampling (generally 1 ft, 0.33 m intervals) and direct measurements of rock properties are advantages of whole core analyses over wire-line log data for formation reservoir attributes. Whole core analysis data are the fundamental measures of reservoir quality in this study and provide the basis for comparison of reservoir-facies and reservoir-stratigraphic relationships (Appendix E).

### Wire-line Logs

Wire-line logs record physical attributes as well as proxies of a rock formation's character (e.g. neutron logs are used to porosity from measured hydrogen atom concentrations). Tool measurements and relevance to rock character are explained well by Asquith and Gibbons, (1982) and Doveton (1994), and are summarized below.

Gamma-ray logs (GR) measure natural radioactivity, giving an indication of elemental makeup of the constituent rock material (e.g. low values in clean carbonate

material and high values detecting K-bentonites). Neutron logs indicate porosity by measuring hydrogen ion concentration, assumed to represent pore fluid. The gamma-ray log is useful in locating and correlating radiogenic K-bentonite beds in the TBR. Geophysical log curves were provided by the MGRRE facility, where they have been scanned and imported into database software, calibrated, and digitally traced, allowing for identification of K-bentonites and stratigraphic correlation over the study area.

### Data Limitations

Spatial distribution of core data is limited in both stratigraphic coverage and spatial distribution. Development of a core-based depositional model is inherently limited in the three-dimensional aspect: core is essentially a 1-D data set, where interpretational errors are introduced upon inter-well correlation (i.e. 2-D and 3-D). However, core provides the only well-constrained rock sample in the study area. The issue of vertical core coverage is amplified by incomplete vertical overlap of cored formation intervals (e.g. stratigraphic intervals that are time equivalent). Incomplete overlap of cores is attributable to the variable depths desired by the driller of the core, but also introduced to a degree by sampling of the multiple target strata in this investigation (i.e. core containing the Black River Shale and the Trenton Group). The aerial distribution of cores is also limited, with most cores being near the linear Albion-Scipio and Stoney Point fields, and few cores (4 utilized in this study) from wells outside the two trends. Despite the issues described above, core coverage is sufficient for development of a depositional model, K-bentonite constrained paleogeographic reconstructions, and a larger scale (3<sup>rd</sup> order) sequence stratigraphic framework, however, complete core overlap is required to fully evaluate a high

resolution sequence stratigraphic framework (e.g. 4<sup>th</sup> and 5<sup>th</sup> order, Kerans and Tinker, 1997).

Determining controls on reservoir distribution away from structural planes requires the inclusion of major faults and fracture location data in the analysis of reservoir quality. Two-dimensional and 3-D seismic data sets (Davies and Smith, 2006) were not accessible for incorporation into this project, and therefore the project is limited to the use of a limited number of published fault distribution maps (e.g. Ells, 1962; and Hurley and Budros, 1990). The whole core analysis data are limited in only two cores (Table 1), where they were completely absent or limited by staggered sampling.

## DEPOSITIONAL SYSTEM RECONSTRUCTION

Analyzing the development of ancient sedimentary systems requires the understanding of depositional facies as they relate to one another at the surface of deposition, and also the evolution of those relationships through time. Although general facies relationships can be described through establishing a depositional setting and idealized facies models, defining facies relationships and spatial distributions in dynamic ancient sedimentary systems requires the identification of synchronous, genetically-related strata. The following TBR depositional system reconstruction addresses these spatial-temporal facies and stratigraphic relationships through sequential development of: a generalized depositional model from core observations; multiple K-bentonite constrained paleogeographic reconstructions; a K-bentonite constrained chronostratigraphic framework; and a sequence stratigraphic framework, which integrates depositional cyclicity/facies stacking patterns, paleogeography, and the chronostratigraphic framework.

In describing the TBR interval, a depositional model is developed in order to address facies-characteristic rock fabrics and their genetic relationships. Additional chronostratigraphic and sequence stratigraphic approaches were used to define the evolution of the sedimentary system. Integrating these datasets provides a well-constrained reconstruction of the TBR interval. Additional analysis of depositional patterns shown in the system reconstruction may offer insights into causal mechanisms of those changes during system evolution, providing a predictive tool for Basin-scale depositional models, as well as insight into the control of depositional fabric on reservoir development. That is, this effort provides a reservoir prediction tool related to depositional patterns.

## Facies Associations

Seven lithofacies were identified in the fourteen cores (total coverage of 1820 linear ft, 555 m) (Table 3) and defined on the basis of texture, grain types, sedimentary structures, and environmental indicators (e.g. degree of storm influence as a paleodepth proxy, sedimentary reducing-oxidizing environments, intraclastic grains). Based on characteristics consistent with an epeiric ramp-platform setting with differing fair weather and storm hydrodynamic influences (Burchette and Wright, 1992), the facies group into three ramp sub-environments: 1) low-energy outer ramp

<b><u>Diagnostic Attributes</u></b>	<b><u>F6</u></b>	<b><u>F5</u></b>	<b><u>F4</u></b>	<b><u>F3</u></b>	<b><u>F2</u></b>	<b><u>F1</u></b>
<b>Dominant facies texture</b>	packstone - grainstone	packstone- wackestone	grainstone	packstone - grainstone	wackestone	mudstone- wackestone
<b>Gross thickness (ft)</b>	16.8	100.6	54.1	575.2	584.0	28.4
<b>Average thickness (ft)</b>	8.4	4.6	1.3	6.9	6.9	1.7
<b>Number of intervals</b>	2	22	43	84	84	17
<b>Grain bed mean thickness (ft)</b>	0.7	0.2	n-a	0.2	0.15	<0.1
<b>Grain bed mean frequency (ft<sup>-1</sup>)</b>	1.3	0.9	n-a	0.4	0.8	1.1
<b>Dominant grain bed texture</b>	packstone	packstone	n-a	packstone - grainstone	packstone	wackestone
<b>Burrow fill sediment (dominant)</b>	grain-mud mix	grain	grain	grain	mud-grain mix	mud-grain mix

Table 3. Diagnostic attributes of depositional facies. “Dominant” and attribute mean values are calculated from the numerical coding of attributes recorded during core description. See Appendix A for detailed outline. “n-a” denotes not-available/not-applicable.

mud-rich deposits, basinward of shoal complexes, 2) moderate and episodically high-energy foreshoal mid-ramp, and 3) inner ramp shoal complex of high-energy shoals and low-energy intershoal depressions (Figure 15).



## Deeper Platform Environment

### Facies 1: Mudstone to Wackestones

*Observations:* Facies 1 is a moderate to totally bioturbated carbonate mudstone to wackestone. The few grains associated with this facies (less than 10%) are peloids, with minor brachiopod, crinoid, gastropod and bryozoan shells and fragments. Concentration of organic material is common, giving this facies a characteristic dark gray-black color in core sample (Figure 16 and 17). Pyrite crystals are common in thin section and core. *Thalassinoides* and *Chondrities* burrow traces (*Cruziana* ichnofacies, Ekdale et al., 1984) are common. Pressure solution of carbonate results in the presence of abundant wispy stylolitization and stylolaminations (Flügel, 2004) in this facies. Facies 1 is commonly thinly bedded with gradational bedding contacts and represents a minor volume of the total described core (Table 3).

*Interpretation:* This facies represents outer ramp deposition (Figure 15) or deposition in a restricted environment where circulation and/or carbonate production is limited. Limited skeletal grains and preserved laminations with the accumulation of micrite indicates a low energy environment of deposition (Flügel, 2004), at or below storm-wave base.

Variable conditions of water circulation and oxygenation are indicated in the sediments of Facies 1. The dysaerobic/anaerobic conditions commonly required for the preservation of organic matter and development of authigenic pyrite (Flügel, 2004) indicate restricted circulation, while intermittent oxygen enrichment is indicated by *Thalassinoides* trace fossils (Ekdale et al., 1984). This combination suggests that Facies 1 experienced time intervals of both restricted, and poor to

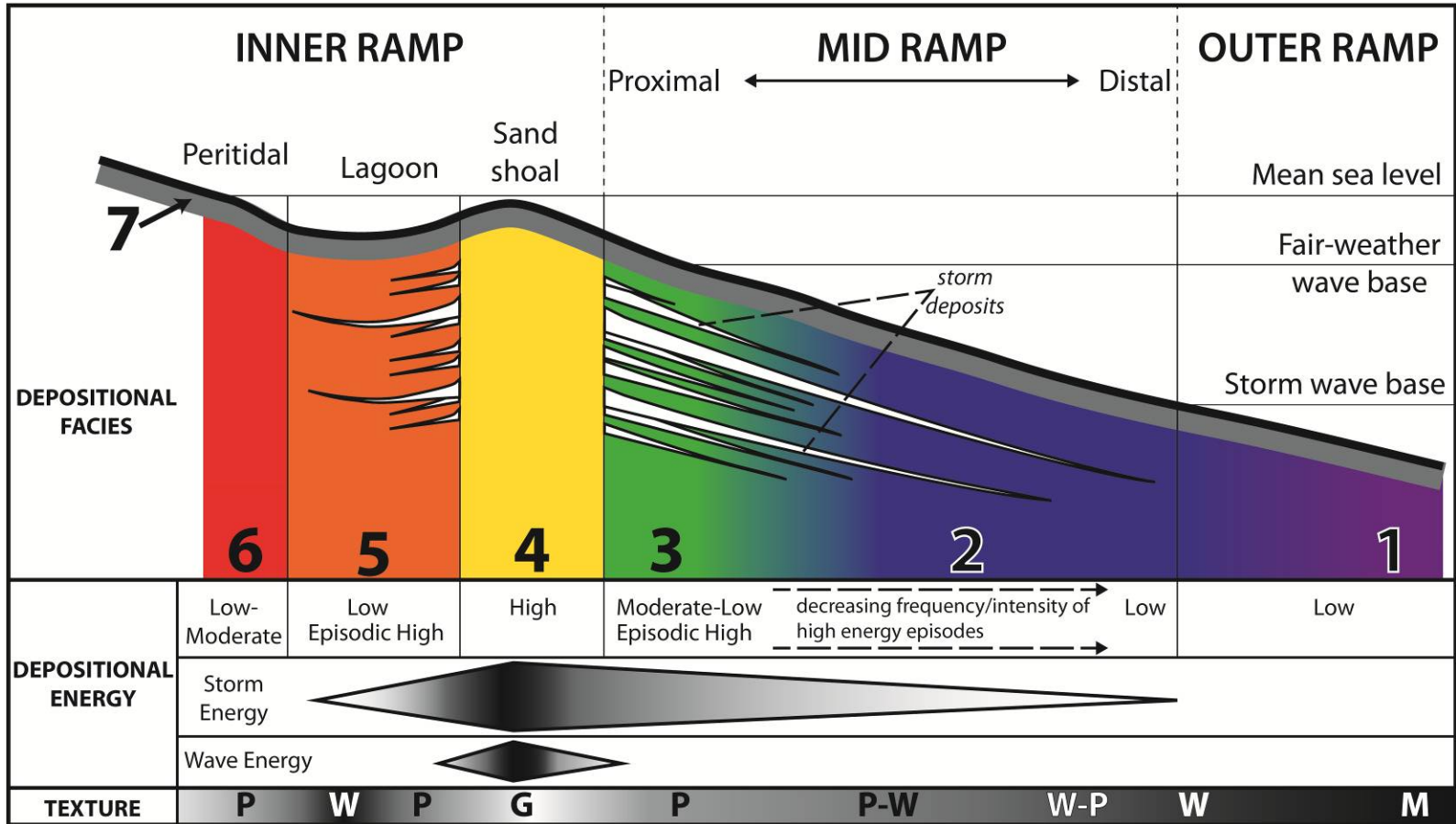


Figure 15. Schematic overview of the TBR depositional profile. The depositional energy gradient on the ramp platform is characterized by a gradual energy increase from a deeper outer ramp position, to shallower wave and micro-tide influenced inner ramp locations. Rock textures reflect the ramp-energy conditions (M = mudstone, W = wackestone, P = packstone, G = grainstone). Storm deposits vary in thickness, frequency, and amalgamation, in addition to lateral extension into deeper ramp environments. Storm deposition is controlled by magnitude and frequency of events and ramp position (see text for discussion). Note: facies color scheme is intended to show lateral relationships at the depositional surface, not vertical continuity of facies. Storm deposits show the episodic deposition and variable lateral extension over time.

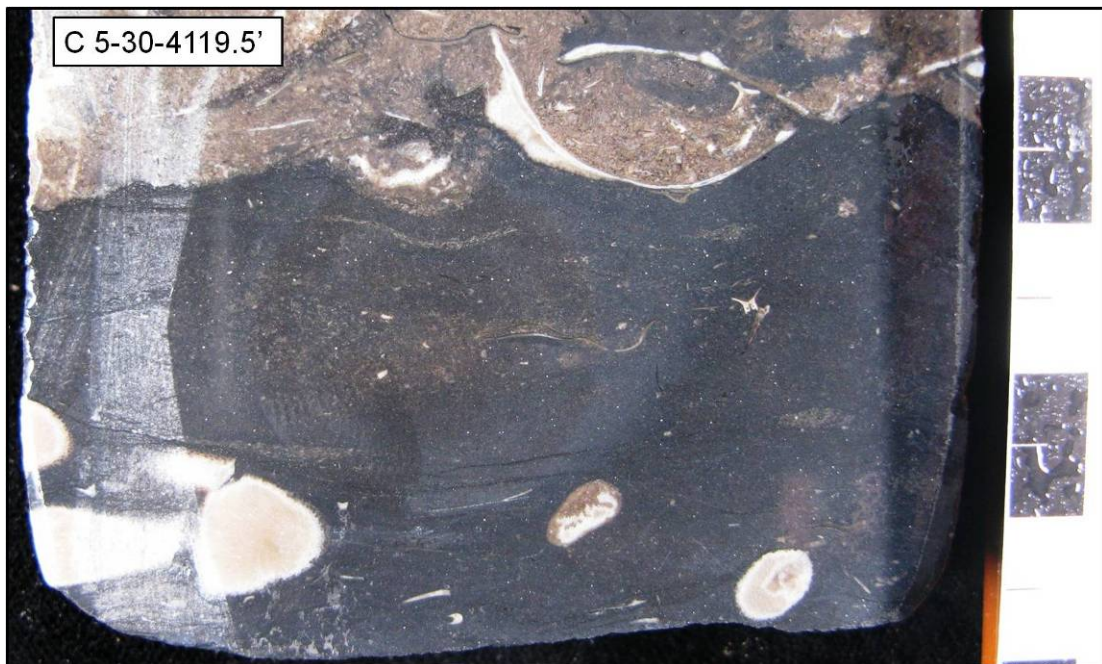


Figure 16. Facies 1- Core photograph showing very dark gray-black mudstone to sparse skeletal wackestone. Scale is in centimeters.

moderate circulation.

#### Facies 2: Biotubated Peloidal-bioclastic Wackestone

*Observations:* Moderately, to totally bioturbated brachiopod, peloidal

wackestones containing abundant skeletal debris and ranging from feet to tens's of feet thick are distributed throughout the TBR (Figure 18). Brachiopod, crinoid, and ostracode bioclasts and peloids are the dominant grain types (approximately 70%) in this facies. Additional grains include pelecypod and gastropod bioclasts, with few bryozoan and trilobite fragments.

Grain micritization is prevalent in wackestone textures, and variable in grain-beds. The presences of packstone grain-beds, composed of winnowed bioclasts and very fine to medium sand sized (64 – 500  $\mu\text{m}$ ) fragmented and abraded skeletal fragments, are also characteristic (Table 3). Associated with the grain beds in this facies are irregular laminations (micro-hummocks?), irregular non-planar basal contacts, and normal grading upsection to wackestone texture. Pervasive bioturbation commonly obscures sedimentary structures, however, burrow fill is noteworthy in that the texture is characterized by both grain dominant and grain-mud mixed textures, with few (less than 15%) mud-filled burrows (Figure 19, Table 3). Grains that fill burrows are dominantly medium silt to fine sand sized (16 – 250  $\mu\text{m}$ ) bioclast fragments and peloids. Wispy stylolites and burrow-bounding stylonodular fabrics (Flügel, 2004) are distributed throughout this facies.

*Interpretation:* Distal mid-ramp to outer ramp deposition (Figure 15) is indicated by storm generated packstone grain-beds and associated sedimentary structures deposited in wackestones (Burchette and Wright, 1992; Aigner, 1985). Normal marine salinity and circulation conditions are indicated by a diverse fauna and abundant bioturbation.

Storm events lower the effective wave base from fair weather conditions, thereby increasing hydrodynamic energy at depositional surfaces that are low-energy in ambient conditions. Mid- to outer ramp storm influence is shown here as ambient

wackestone sedimentation punctuated by storm wave and current sediment reworking. The storm events are manifested in Facies 2 as grain-beds with characteristic partial to complete winnowing of mud, mechanical abrasion of bioclasts, and import of silt to sand sized grains. The grain-beds show scoured and erosive bases, graded laminar and undulate-laminar bedding, and gradational upper bed transitions with increased bioturbation, indicating storm deposition in a distal position relative to shore or shoals. Normal grading and transitional upper bedding contacts result from waning storm influences. Storm influences are also indicated where primary bedding has been obliterated by bioturbation or grain-beds are not evident, but where event deposits are preserved as abraded grain concentrations (packstone-wackestone) deposited in burrow voids during storms (i.e. the tubular tempestite of Tedesco and Wanless, 1988, see Figure 7). The thin, discrete storm generated packstone grain-beds with either distinct sedimentary structures and/or the character of burrow filling sediment in bioturbated wackestones point to a depositional environment below fair-weather wave base, but above storm-wave base.



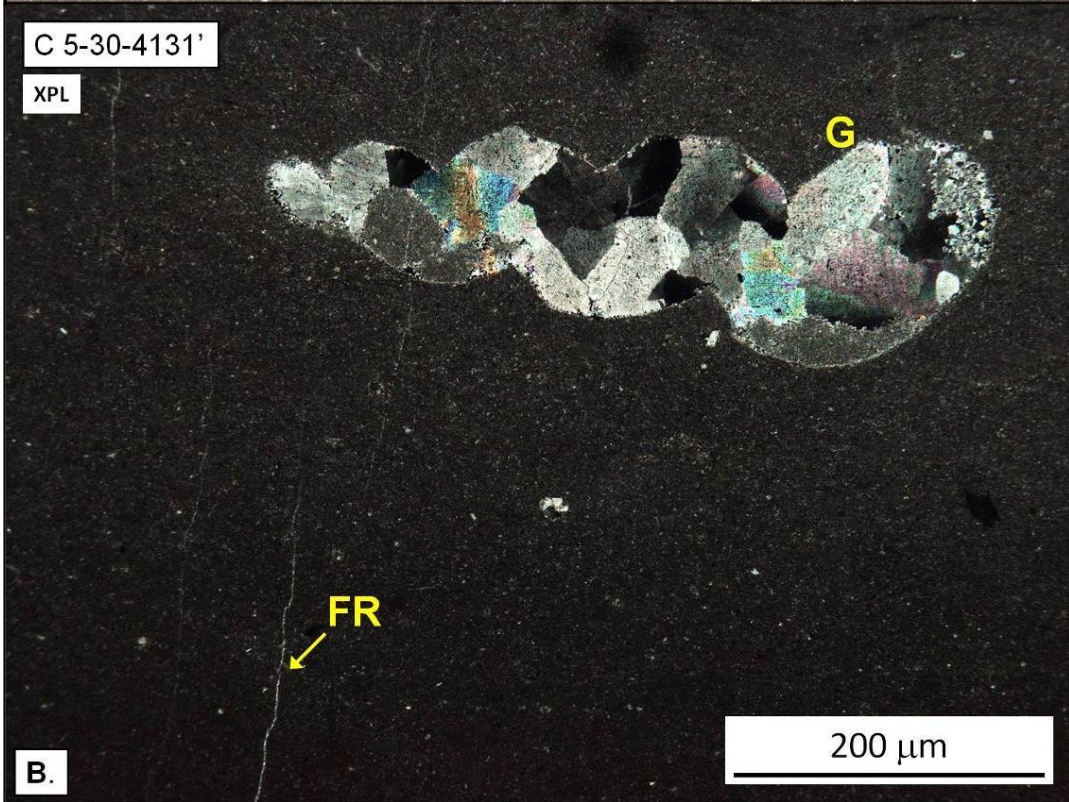
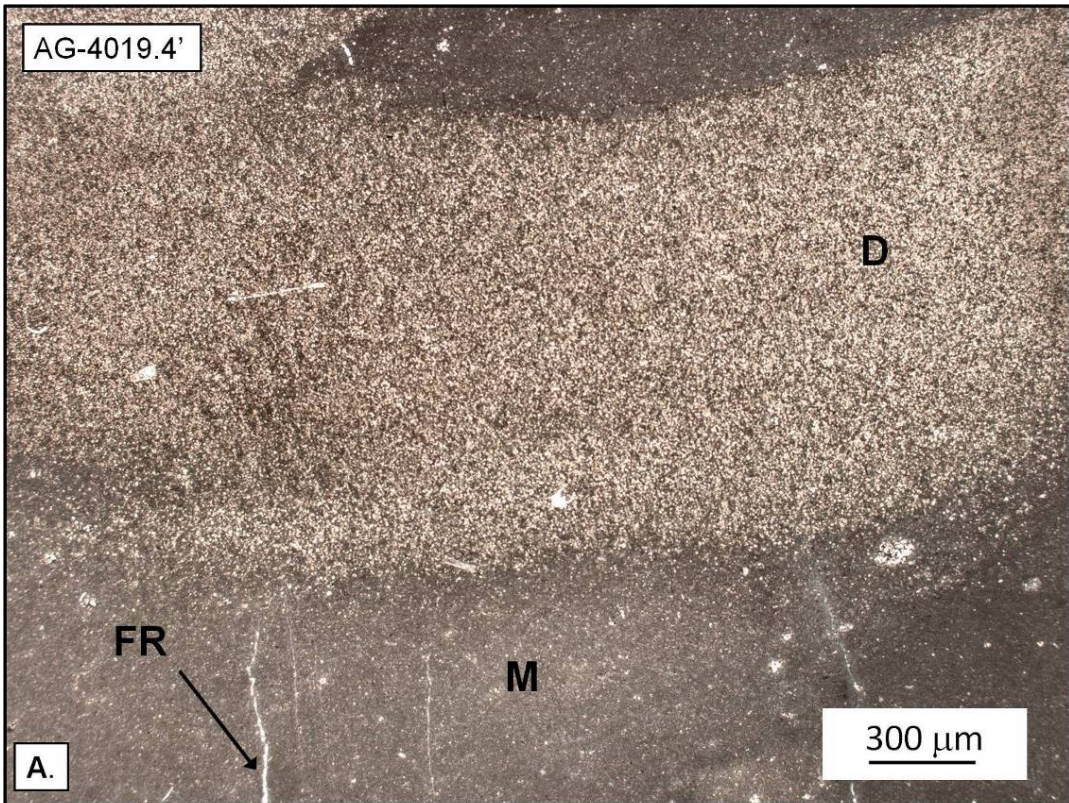




Figure 17. Facies 1- (Thin section photomicrographs) A.) Mudstone (M) with sparse (<5%) bioclasts, abundant euhedral dolomite (D) rhombs (<15  $\mu\text{m}$ ), and calcite filled micro-fractures (FR). Sample shown in plane-polarized light (PPL). B.) Mudstone with calcite filled micro-fractures (FR) and mold of a single gastropod shell (G) filled with anhedral-mosaic calcite. Sample shown in crossed-polarized light (XPL).

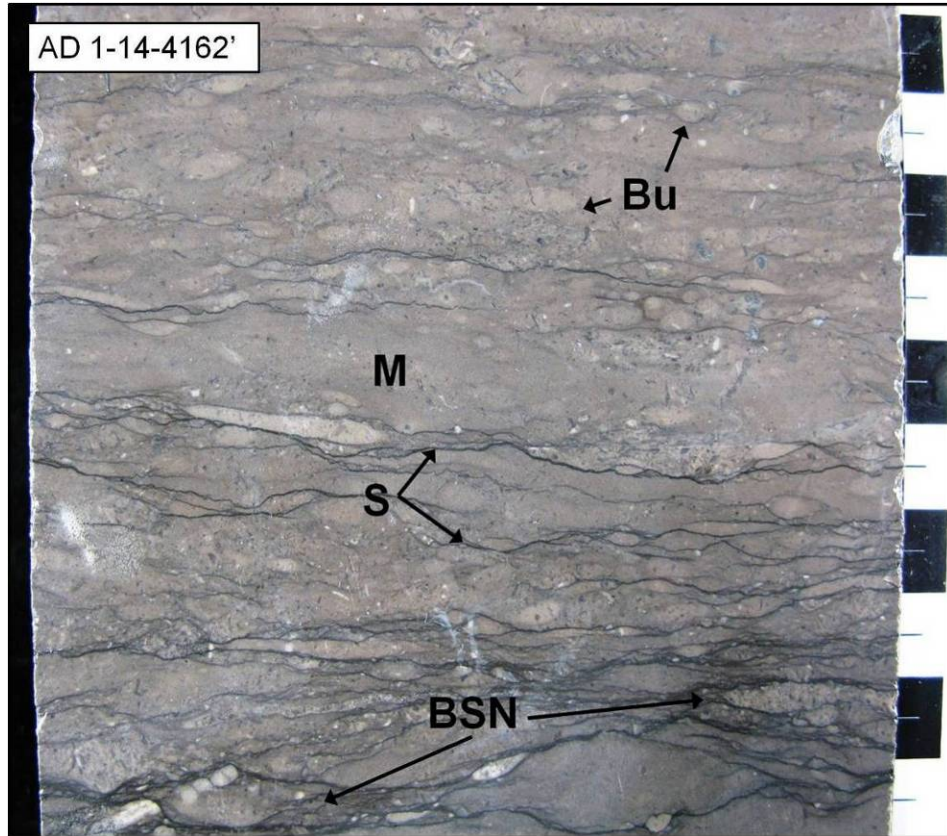


Figure 18. Facies 2- Core photograph showing moderately bioturbated wackestone to mudstone textures. Stylolites (S) and burrow-bounding stylonodular fabrics (BSN) are distributed throughout Facies 2. Bu = burrow; M = mud; scale is in centimeters.

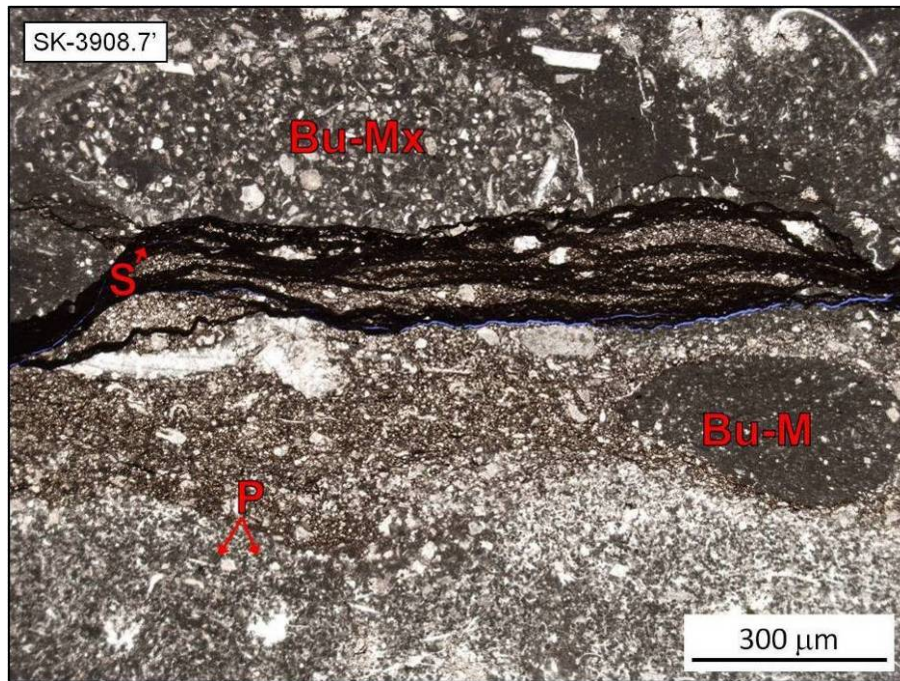


Figure 19. Facies 2- Thin section photomicrograph impregnated with blue epoxy to highlight porosity. Peloid (P) and bioclastic packstone (below prominent stylolite (S)) and wackestone (above S) textures are shown in this sample, where textural inversions occur in grain-mud mixed burrow fill (Bu-Mx, wackestone to peloid-bioclastic packstone here), and mud-dominated burrow fill (Bu-M, mudstone here). Sample is shown in PPL.

### Shallower Platform Environment

#### Facies 3: Bioturbated Bioclastic Packstone-grainstone

*Observations:* Facies 3 consists of moderately to intensely bioturbated packstone to grainstone textures composed primarily (approximately 68%) of brachiopod, crinoid, and peloid grains (Figures 20 and 21). Accessory grains include bryozoan, pelecypod, gastropod, trilobite, and ostracode bioclasts, with a few fragments of tabulate coral (1 – 8 cm) that occur in out-of-growth position. A minor occurrence (15% of total) of branching bryozoan packstones and rudstones are also



included in this facies.

Grains show variable stages of micritization whereby unaltered grains, grains enveloped by superficial micrite, and completely micritized grains commonly occur in the same deposit. Wispy stylolites and burrow-bounding stylonodular fabrics (*Cruziana*-type burrows) are distributed throughout. Burrow fill is grain dominant (80%), with minor occurrences of mud dominant (2%), and grain-mud mixed fill.

Grain-beds in Facies 3 consist of mud-lean packstones and grainstones that show an increased frequency of occurrence, maximum thickness, and range of thickness relative to Facies 2 (Table 3). In addition to thicker individual grain-bed deposits, amalgamation of the beds contributes to apparent thickening of the deposits (e.g. Figure 14a). The character of the grain-beds is variable, from moderate to well sorted, bioturbation-homogenized sand sized crinoid (64 – 400  $\mu\text{m}$ ) and brachiopod fragment (up to centimeter scale in length) deposits, to well sorted laminated/cross-laminated, fine to medium skeletal-peloidal sands (125 – 500  $\mu\text{m}$ ). Tabular intraclasts (0.25 – 2.0 cm) are also deposited in some grain-beds (Figure 20b). The beds have sharp bases, characterized by planar, sub-planar, and undulate-irregular contacts, often displaying fluid and burrow escape structures (Figure 22).

*Interpretation:* Facies 3 is interpreted as mid-ramp deposits, proximal to shoals (Figure 15). Well-circulated, normal marine conditions during deposition are indicated by abundant stenohaline, filter feeding crinoids (Kammer and Ausich, 2004). The increased abundance of filter feeding organisms (crinoid and bryozoan), higher faunal diversity, and abundant *Cruziana*-type burrows further support shallower, well circulated waters in this facies (Dodd and Stanton, 1981) relative to Facies 1 and 2.

Variable grain micritization illustrates that grains in the same deposit have

experienced different durations of exposure at the sea bed, where they were subjected to algal, fungal, or microbial borings (Bathurst, 1966, 1971). Differences in residence times were affected by a combination of normal low to moderate-energy conditions, with low sedimentation rates, and intermittent high-energy storm events that reworked, exhumed, imported, and rapidly deposited grains. The multiple exhumations of grains and repeated storm-generated mixing resulted in grains with variable degrees of micritization.

Planar laminated, well abraded, and well sorted grain-bed sands are likely produced during storms and/or derived from a high-energy shoal environment. Sharp, horizontal basal contacts, and fluid and burrow escape structures indicate erosion and rapid deposition, respectively (Figure 22). Shoal spillover (Ball, 1967), and high-energy storm events in shoal-proximal environments, are typically characterized by grain-beds (Aigner, 1985). A range of storm energies resulted in winnowing/deposition events that affected Facies 3, as shown by the increase in grain-bed maximum thickness, range of thickness, and frequency of bed occurrence (Table 3), combined with the observed grain-bed amalgamation. This wider spectrum of storm energies suggests that storms of variable magnitude affected this facies more frequently than in the distal deep-ramp settings of Facies 1 and 2 (e.g. weaker, more frequent storms with shallower wave base vs. stronger, rarer events with deeper wave base) (Kreisa, 1981; Aigner, 1985). This wider range of storm energies, including the addition of what were likely smaller magnitude storms and shoal spillover deposits, indicate a relatively shallower environment of deposition, often adjacent to active shoals.

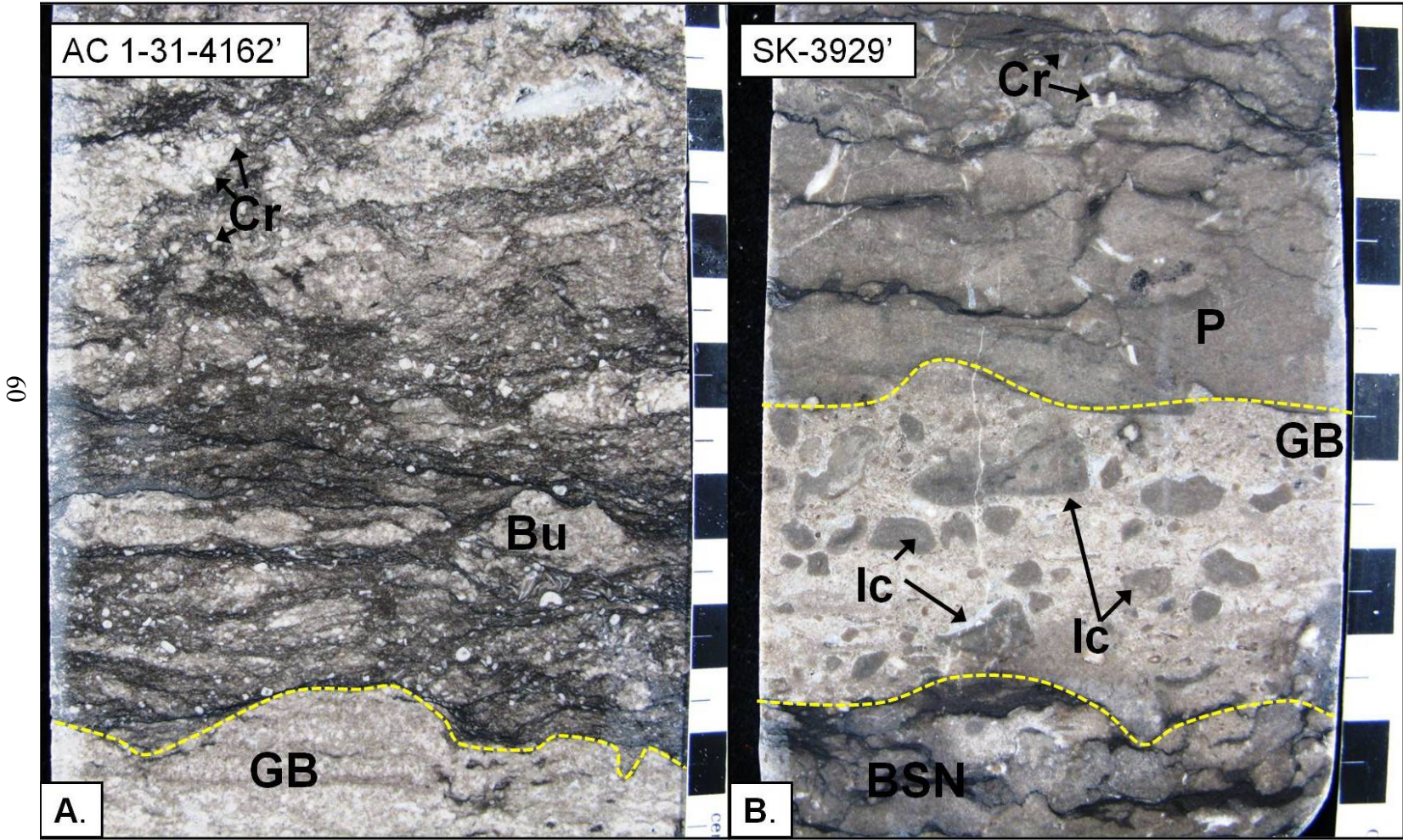


Figure 20. Facies 3- Core photographs. A.) Peloid-crinoid (Cr) packstone to grainstone, with moderate bioturbation (Bu= burrow) and lamination preserved in grainstone to packstone grain-beds (GB, below dashed yellow line). B.) Intensely bioturbated peloid packstone with burrow bounding stylonodular fabric (BSN) and a grain bed (GB, outlined with dashed yellow lines) composed of intraclast (Ic) grainstone. Burrow fill in each sample is grain dominant. Scales are in centimeters.

#### Facies 4: Grainstone Shoal

*Observations:* Cross-stratified, well abraded and sorted skeletal grainstones occur in intervals one to five feet thick in the TBR cores (Figure 23). Undifferentiated bioclastic, crinoid, and brachiopod sands (grain size of 125  $\mu\text{m}$  – 2 mm) compose the majority of allochems in these grainstones (approximately 75%). Additional constituents include peloids, and well rounded composite-grain intraclasts (Figure 24). Composite-grain intraclasts are composed of a variety of skeletal material and micrite (e.g. brachiopod, crinoid wackestone-packstone textures). Bioturbation is absent to moderate. Where evident, bioturbation disrupts strata and burrows are commonly filled with sediment consistent with overlying textures.

*Interpretation:* Wave or current agitated shoal deposition in an inner ramp setting, above fair weather wave base, is indicated by the cross-stratification, highly abraded grains with textural maturity, and lack of bioturbation of Facies 4 (Figure 15). Prolonged exposure to high energy conditions is indicated by the high degree of grain abrasion and rounding. Composite grains are derived from semi-lithified or lithified substrates and were continually reworked and rounded in an active shoal environment. Compound grains are comprised of platy allochems (i.e. brachiopod fragments) within a micrite matrix, indicating that these clasts were assimilated from previously existing surrounding deposits, or alternatively, that they were imported



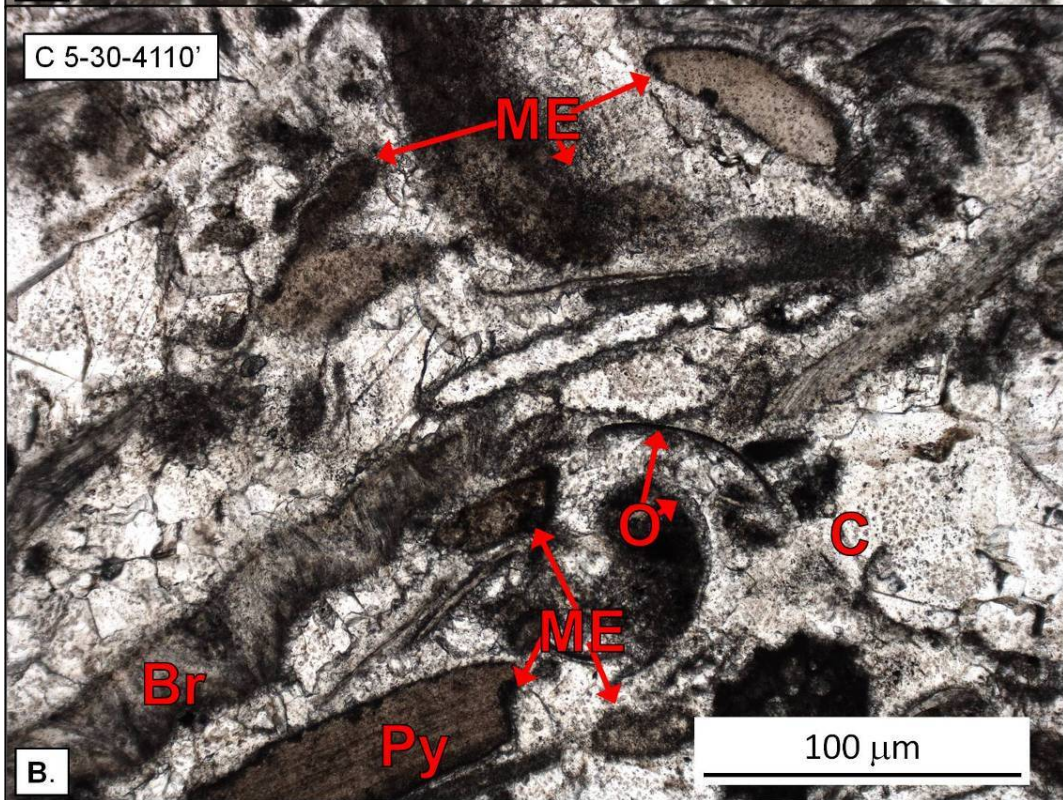
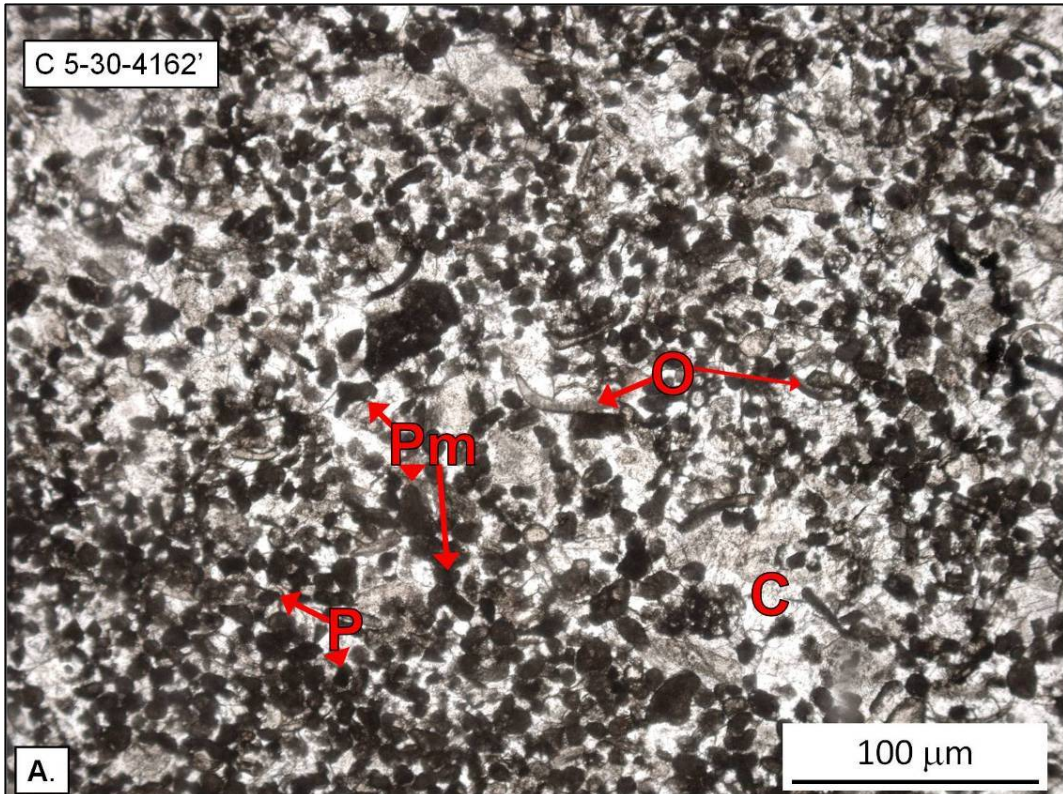




Figure 21. Facies 3- Thin section photomicrographs. A.) Peloid (P) ostracode (O) grainstone, where primary (depositional) porosity is filled with blocky-crystalline calcite (C). Peloids show geometries consistent with fecal pellet (semi-spherical and cylindrical, P) and micritized bioclast (kinked-angular, platy, Pm) origins. B.) Bioclastic grainstone with development of micritic envelopes (ME) at grain surfaces and micritized grains. Br = brachiopod, Py = pelecypod, and the same abbreviations as in A. Samples are shown in PPL.

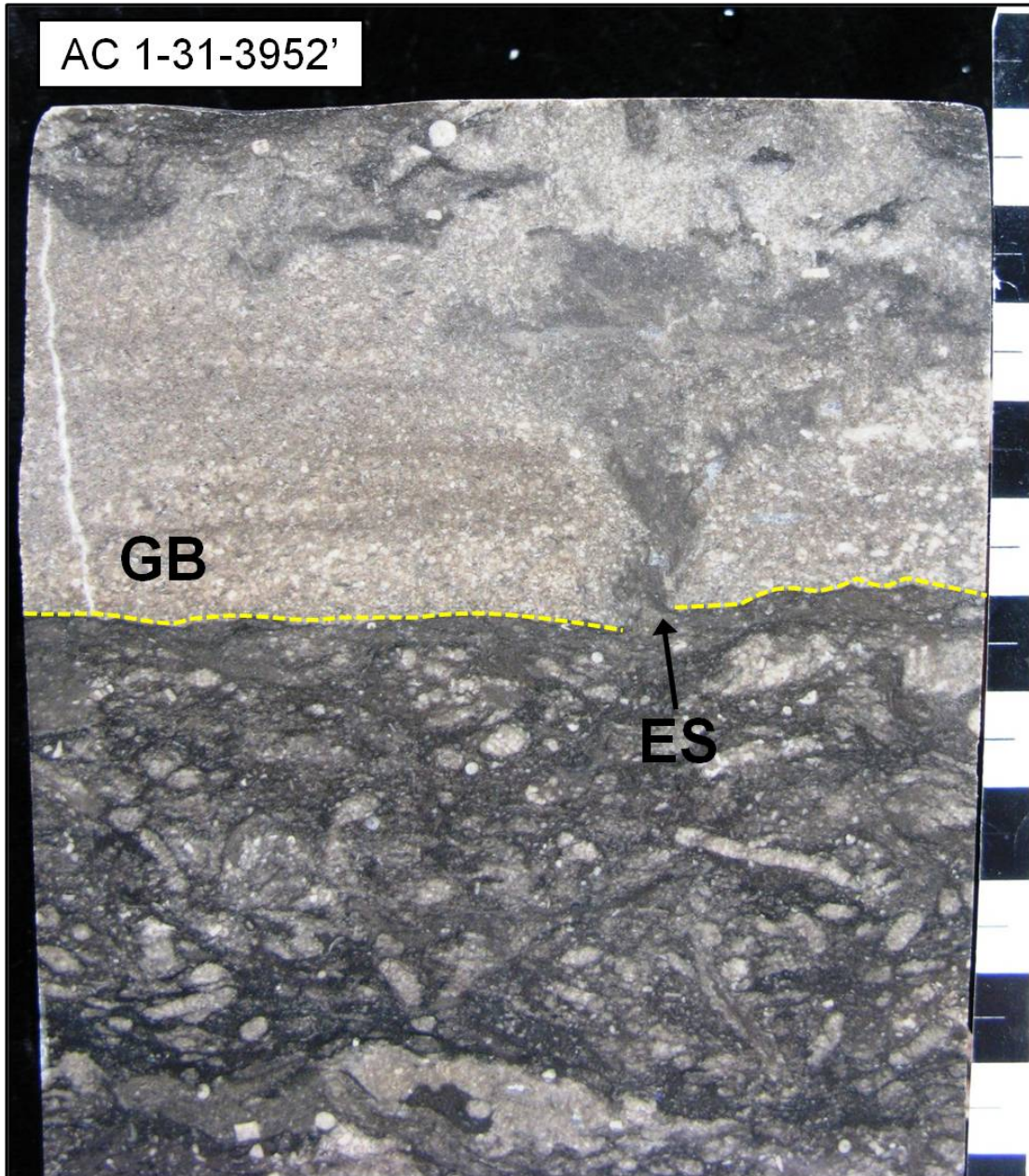




Figure 22. Core photograph showing a grain-bed with characteristics found in Facies 3. An erosive, sharp basal contact (dashed yellow line) is overlain by a laminated and normally graded skeletal grainstone grain-bed (GB) with an irregular upper contact. Rapid deposition typical of grain-beds is shown here by the fluid (or burrow?) escape structure (ES) cutting the basal contact, and incorporating sediment from below. Scale is in centimeters.

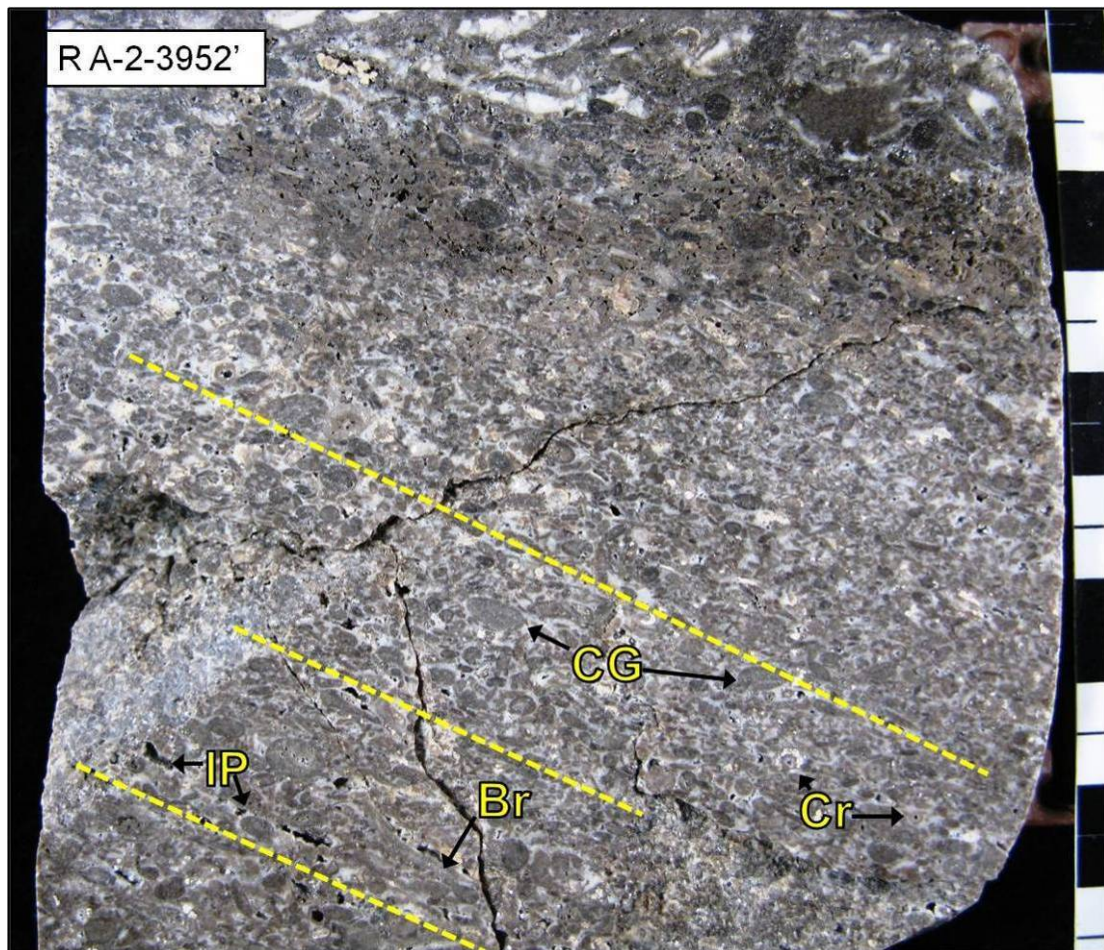


Figure 23. Facies 4- Core photograph showing high-angle cross-bedded grainstone. Grains include crinoid (Cr) and brachiopod (Br) fragments, and composite-grain intraclasts (CG). Composite-grains are sub-spherical, well rounded, and consist of bioclastic wackestones to packstones, showing a textural maturity consistent with a wave or current agitated shoal environment. Primary interparticle pore (IP) spaces are filled by white dolomite, however few interparticle voids remain. High angle

bedding is outlined by dashed yellow lines. Open fractures are an artifact of coring. Scale is in centimeters.

into a lower energy depositional environment from nearby active shoals. Bioturbation was likely absent during shoal activity, however, reduction in local energy levels likely resulted in shoal inactivity and the resultant sediment stabilization allowed organisms to burrow in shoal sands.

#### Facies 5: Mottled Packstone-wackestone

*Observations:* Burrow-mottled packstone-wackestone with dark mudstone pockets and grain-rich beds are deposited in intervals that average five feet thick (Table 3), but that may be up to 18 feet thick in some TBR cores. Characteristic grains in Facies 5 are peloids and unabraded brachiopod fragments, within a dominant wackestone-packstone texture (Figure 25). Abundant ostracode grains are also visible in thin section samples (Figure 26). Additional minor gastropod, pelecypod, and undifferentiated skeletal fragments are observed in this facies. Intense to moderate bioturbation of sediments containing peloids, large platy grains (e.g. brachiopod and pelecypod grains commonly 0.5 – 3.0 cm long), and mud results in chaotic grain orientations. The platy grains commonly shelter peloidal and dark, mud-rich deposits. Color contrasts between dark peloid-mud rich rock and light gray-yellow peloidal sands contribute to a mottled appearance. Packstone to grainstone grain-beds consist of individual brachiopod shell beds, peloid-dominated beds, and beds containing undifferentiated skeletal fragments, crinoids, bryozoans, and intraclasts. Grains show variable stages of micritization. Texturally immature skeletal fragments, grains enveloped by superficial micrite, and completely micritized grains all commonly occur. Deposits with the characteristics of this facies are found in



association with Facies 3 and 4.

*Interpretation:* Facies 5 is interpreted as being deposited in inner ramp semi-restricted lagoons, likely protected by nearby shoals based upon: abundant peloids, ostracode grains, and large brachiopod and bivalve fragments; color and textural mottling; grain-bed composition and structures; textural complexity; and stratigraphic position and facies relationships (Figure 15). Modern deposits in restricted pools, or lagoons shoreward of, and adjacent to, energy absorbing shoals of the Persian-Arabian Gulf document similar peloid wackestones and unabraded brachiopod wackestones with dark colored, reduced micrite (“blackened mud” of Kendall and Skipwith, 1969b; Purser and Evans, 1973). This depositional association is also documented in epeiric carbonate ramps in the geologic record (Jehn and Young, 1976, Lee et al., 2001). Abundant ostracode fragments found in Facies 5 thin sections further support a restricted or protected environment (Standard Microfacies 9 and 19, Wilson, 1975).

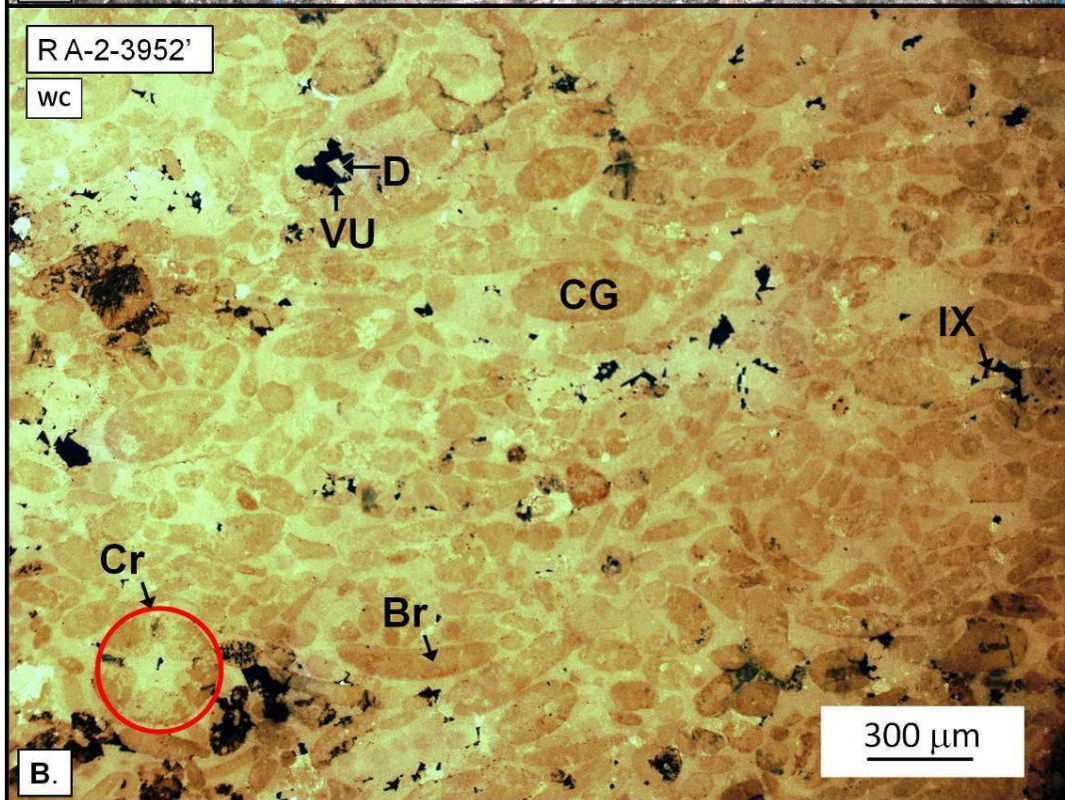
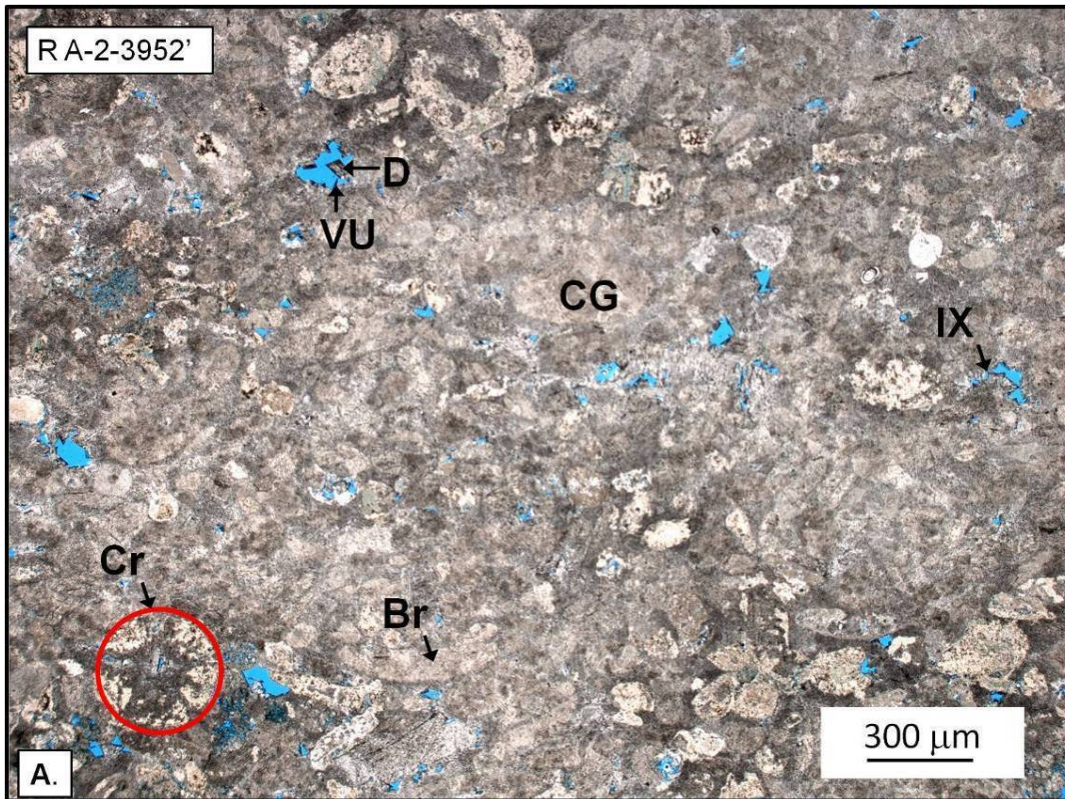


Figure 24. Facies 4- Thin section photomicrographs and example of white card observation technique. (Blue epoxy impregnated thin section photomicrographs) A.) Crinoid (Cr), composite-grain (CG), brachiopod (Br) grainstone with vugular (VU) and intercrystalline porosity (IX) development. Dolomite (D) fills original interparticle porosity (replaces calcite cement?). Dolomitization obscures grain and rock textures, impeding interpretation of depositional fabric. Sample shown in PPL. B.) The same thin section and sample orientation shown in A., but viewed with reflected light white-card technique (Zenger, 1979; and Folk, 1987) in which an intense light source is reflected from an oblique position, revealing grain outlines and Dunham textures. Note cross-section of crinoid ossicle (circled in red) and pores. Thin section sample taken from core shown in Figure 22.



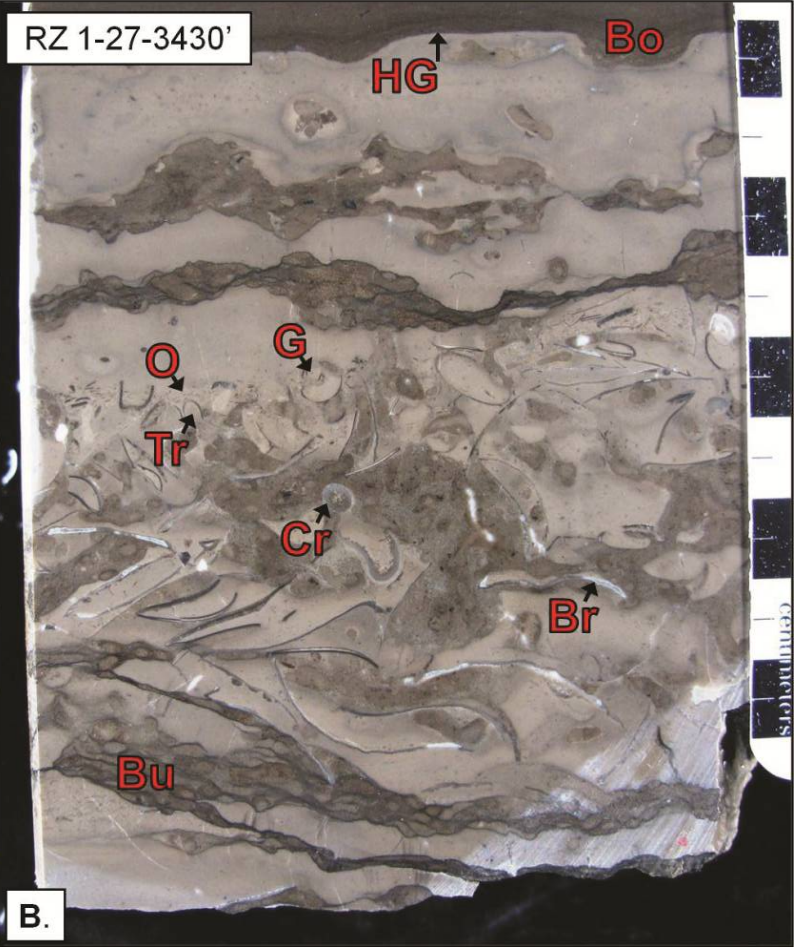
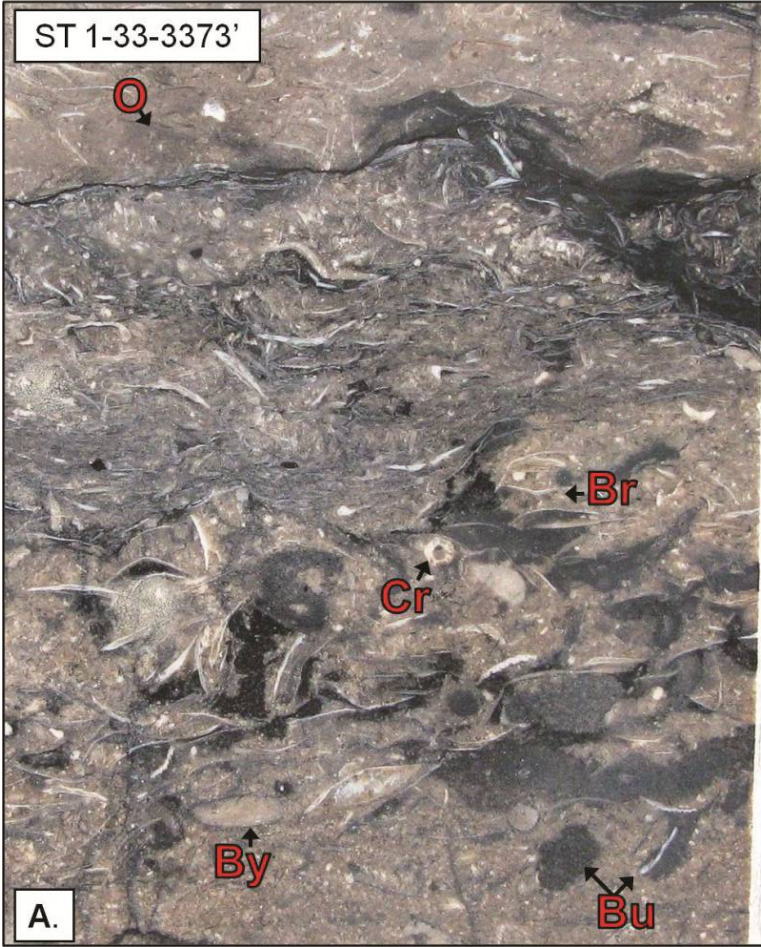


Figure 25. Facies 5- Core photographs. A.) Brachiopod (Br)-peloid packstone showing oxidized (tan) and reduced (dark gray) sediments mixed through bioturbation (Bu = burrow). Brachiopod fragments dominate texture, and show variable degrees of abrasion/fragmentation. Additional grains include crinoid (Cr) and bryozoan (By) fragments and ostracode (O) grains. B.) Peloid-brachiopod wackestone to packstone showing mixed oxidized and reduced sediment textures similar to that shown in A. Grain composition is similar to A., with the addition of trilobite (Tr) and gastropod (G) fragments. A well-defined hardground surface (HG) showing borings (Bo) is present at the top of the core sample, representing non-deposition and possibly exposure. Scales are in centimeters.

Variability in the degree of restriction within the lagoons is suggested by distinctive color and textural mottling. Kendall and Skipwith (1969b) document reducing environments resulting in “blackened” mud within a foot of the sediment-water interface in modern Persian-Arabian Gulf lagoon deposits. Wilson (1975) discusses restricted lagoon floor deposits that are episodically oxidized due to increased circulation by storm or wave activity events. A mottled combination of these two redox environments is observed in Facies 5, owing to mixing of sediments by bioturbation. The stratigraphic/facies association of Facies 5 with shoal and proximal foreshoal facies (Facies 3 and 4), indicates lagoon development in a leeward position relative to energy absorbing bathymetric highs on the TBR platform.

Variable grain-bed composition and sedimentary structures indicate that internal attributes of the deposits depend upon both kinetic strength of the event and position within the lagoon. Relatively low-energy events (e.g. lower magnitude, frequent storms) are deposited in shoal-proximal positions as wackestones locally



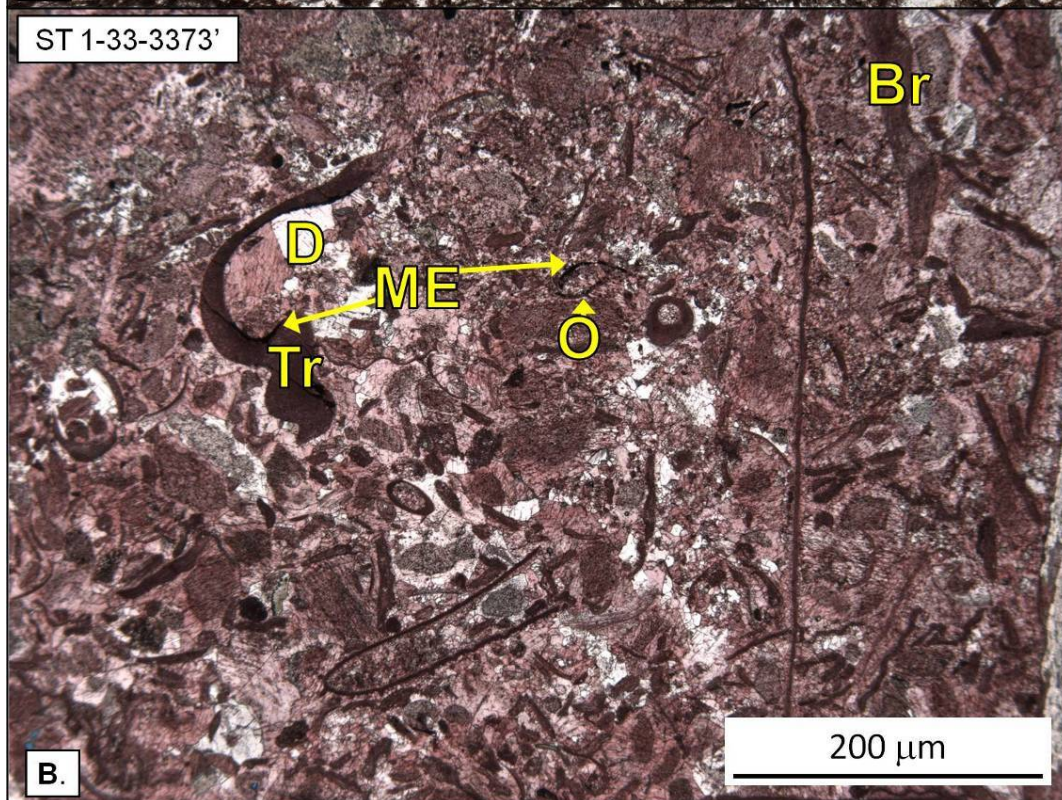
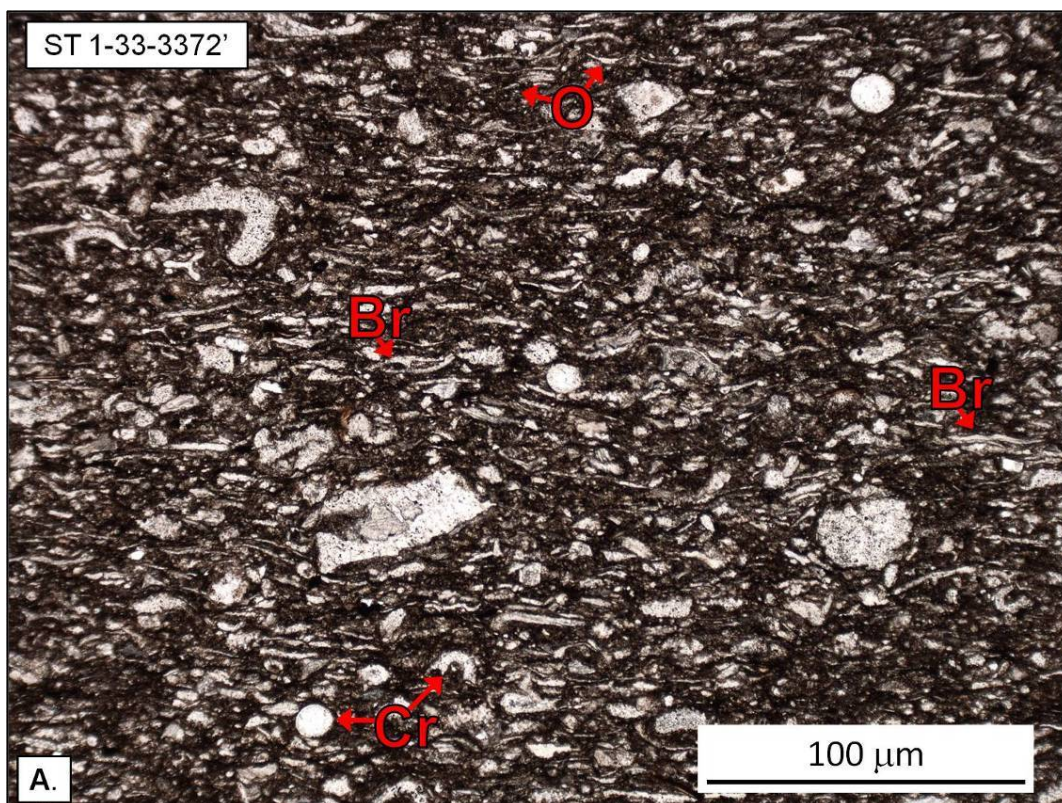


Figure 26. Facies 5 Thin section photomicrographs. A.) Ostracode (O)-crinoid (Cr) wackestone to packstone, with few brachiopod fragments (Br). B.) Ostracode-brachiopod packstone to grainstone treated with Alizarin-red, highlighting calcite and leaving dolomite (D) unaltered. Dunham texture and grain-types are similar to the sample shown in B, with the addition of trilobite fragments (Tr) and micrite envelopes (ME) developed at grain surfaces.

winnowed to brachiopod packstones, laminated peloid packstones, and shoal spillover grainstone deposits. Events with higher kinetic energy (e.g. large storms, and/or tsunamis generated by Taconic tectonics) mobilize and deposit variable grains over the entire effected inner and mid-platform. High energy events are shown in lagoon deposits by the import of grains with high faunal diversity (crinoid, bryozoan) and mixed textural maturity (undifferentiated abraded skeletal and intraclastic grains) grain-beds. Variable grain micritization is indicative of sediment reworking, as discussed for Facies 3.

#### Facies 6: Oxidized Fenestral Packstones

*Observations:* Light gray-buff colored peloidal packstones with solution enhanced “birdseye” (augen or eye shaped) fenestral pores are interbedded with moderately to intensely bioturbated peloid-brachiopod wackestones. These units (bedding approximately 1.5 ft thick) occur in five to eight foot intervals in the upper Black River Group, (Figure 27). Buff colored packstones show distinct horizontally oriented fenestrae and vertical cylindrical vugs (commonly 20 mm long and 2 mm wide), with few brachiopod shell molds. Relict peloids comprise the majority (80%) of the identifiable grains (Figure 28). Oxidation halos surround pores and minor fractures. Bioturbated peloid/brachiopod/gastropod wackestones are characterized by stylonodular fabric that outlines individual *Cruziana*-type burrows. The degree of



bioturbation in the fenestral packstone is difficult to determine because of

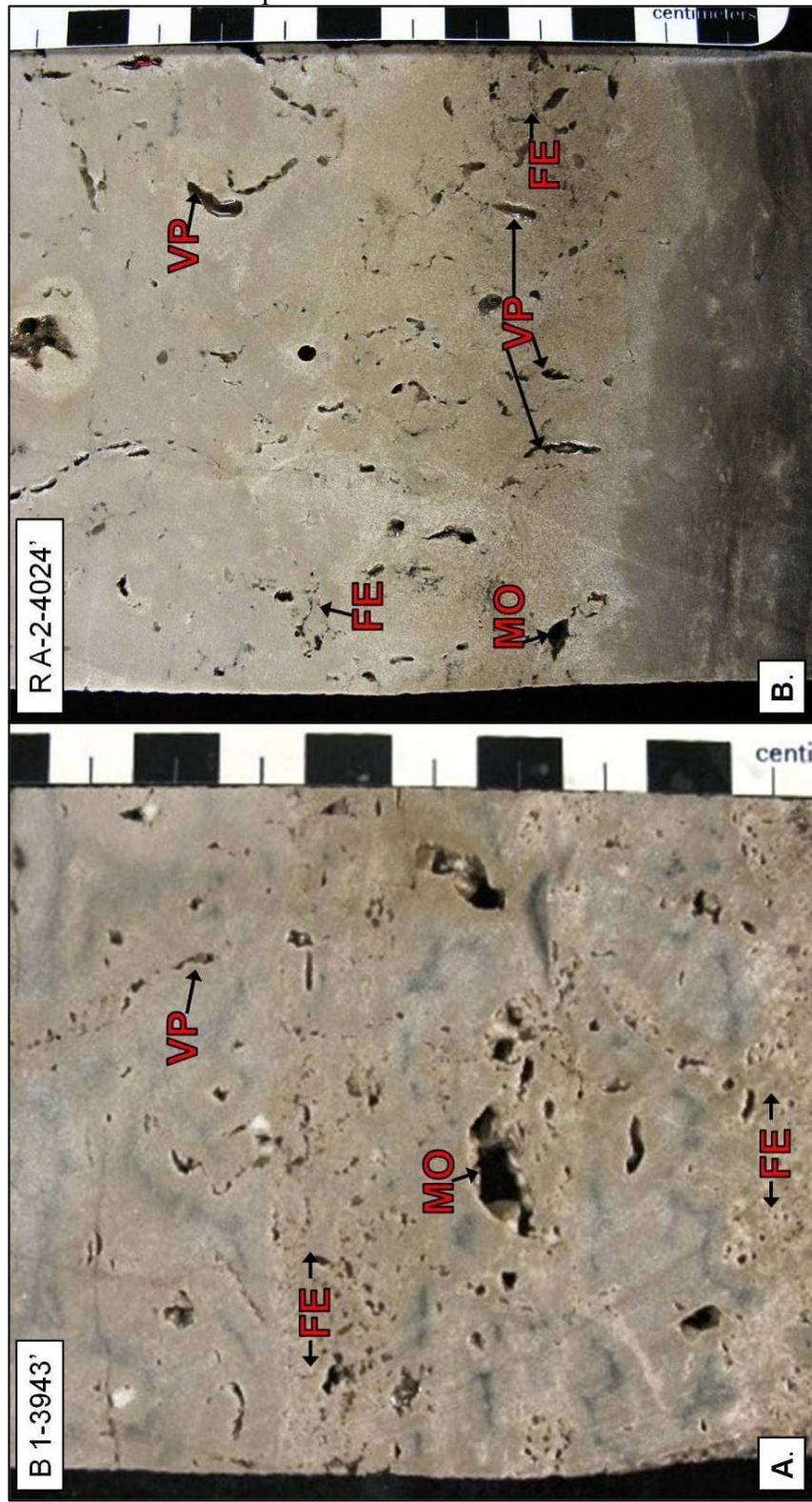




Figure 27. Facies 6- Core photographs. A.) Oxidized peloidal packstone with horizontally elongate fenestral pores (FE), vertically oriented cylindrical pores (VP), and moldic pores (MO, brachiopod). B.) Oxidized peloidal packstone with fenestral porosity, vertically oriented cylindrical pores, and (brachiopod) moldic porosity overlying a reduced moderately bioturbated peloidal packstone to wackestone. Features observed in A. and B. are consistent with a lower intertidal, to upper-most subtidal environment of deposition. Scales are in centimeters.

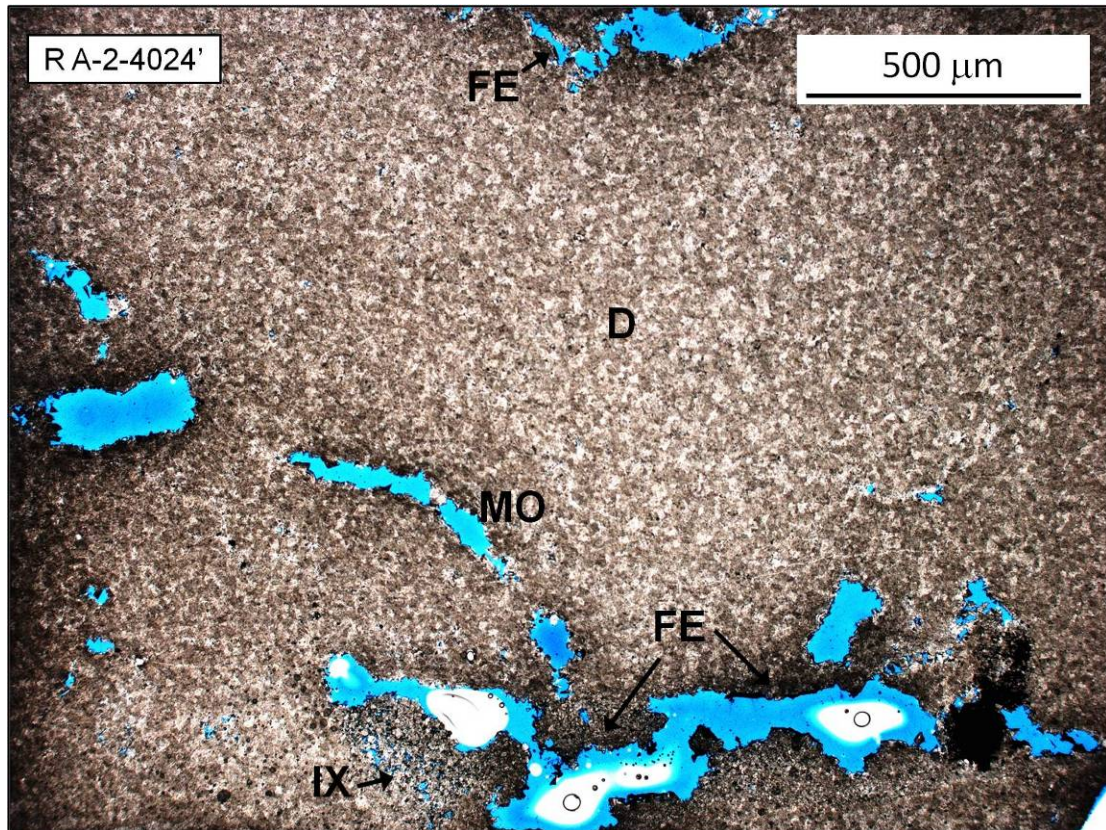


Figure 28. Facies 6- Thin section photomicrograph. Section is impregnated with blue epoxy, highlighting solution enhanced fenestral (FE), moldic (MO, platy skeletal fragment), and intercrystalline (IX) porosity in a peloidal packstone-grainstone. Peloids are replaced by dolomite (D), however grain outline relicts show packstone-grainstone texture. Hydrocarbons (black) partially occlude fenestral pores in lower right of image. White color at center of blue epoxy filled pores represents removal of incomplete impregnation by epoxy.

dolomitization. Distinct internal bedding and lamination is absent, however, well-developed localized fenestral clusters are assumed to represent a bedding proxy (Figure 27).

*Interpretation:* Peritidal deposition in an inner ramp location, consistent with shallow subtidal and lower intertidal positions, is indicated by the oxidized peloidal-fenestral packstones interbedded with bioturbated wackestones (Figure 15). The formation of fenestral pores is attributed to gas production associated with the decay of organic material, lateral migration of water and/or gas, and/or desiccation, all occurring within peritidal environments (Grover and Read, 1978; Shinn, 1983a). While Shinn (1983a) indicates that caution must be used when utilizing the presence of fenestral pores as an exclusive indicator of tidal-flat deposition, the cyclic assemblage of oxidized beds with birdseye fenestral and vertically oriented tubular-vug porosity, interbedded with reduced bioturbated wackestones are consistent with documented examples of modern (Shinn 1983b) and Ordovician (Cressman and Noger, 1976; Grover and Read, 1978) peritidal deposits. The origin of vertically oriented tubular or cylindrical vugs associated with birdseye fenestrae are attributed to burrowing worms in TBR-correlative Ordovician peritidal carbonate deposits (Cressman and Noger, 1976; Grover and Read, 1978), and worm burrows, gas escape structures, and terrestrial plant roots in modern peritidal carbonate environments (Shinn et al., 1969; Shinn, 1983b). The vertical tubular vugs are likely preserved worm burrows (*Skolithos* ichnofacies) or gas-escape structures, as Ordovician deposits predate the evolution of terrestrial plants (Copper, 2002).

An assemblage of key sedimentary structures and features are commonly used in designating intertidal deposits (Cressman and Noger 1976; Grover and Read, 1978; Shinn, 1983; Riding 2000). However, mud laminae, laminated cyanobacteria,

desiccation cracks, and soil clasts are notably lacking in the Black River peritidal facies. The absence of these features in the Black River peritidal deposits suggest that the deposits were likely not formed in a supratidal to uppermost intertidal environment that was regularly exposed. A dominantly subaqueous, lower intertidal to sub-tidal zone of deposition, in a reduced-stress environment of normal marine salinities that supported grazing and burrowing organisms (e.g. gastropod and burrowing crustaceans, respectively) is further indicated by the absence of cyanobacterial mats or laminated structures from Black River tidal deposits (Riding, 2000). The interpretation of lower intertidal and shallow sub-tidal deposition of Facies 5 is therefore supported by the cyclic interbedding of oxidized fenestral packstone, and reduced bioturbated wackestones.

#### Ramp-Platform Independent Deposits

##### Facies 7: Volcanic Tephra

Facies 7 is composed of K-bentonites, representing the deposition of volcanic tephra, or ash beds. The K-bentonites are light grayish green and/or dark gray in core samples, show fissile partings, and contain few bioclasts (Figure 29). Individual K-bentonite bed thicknesses vary from less than a centimeter to approximately 15 centimeters; however volcanic sediments are also incorporated into carbonate beds (1 – 2 feet thick). Deposition of this facies is ubiquitous over the TBR platform and not limited by depth or environmental constraints. That is, the geologically instantaneous, regional deposition of an ash bed blankets all depositional facies and is independent of spatial-depositional relationships (i.e. Walther's Law of the Correlation of Facies). Preservation of ash beds is variable however, because upon introduction into the system, the volcanoclastic sediments are subject to the active processes taking place at





Figure 29. Facies 7- Core photographs (Black River Shale). Volcanic ash deposited throughout the TBR interval are altered to K-bentonites. The thicknesses of the K-bentonite beds vary from a less than one to 15 centimeters. Observed thickness in core is dependent on the volume deposited, preservation potential, and core maintenance and preservation (see difference between A and B). The two core samples of the Black River Shale K-bentonite show here exemplify the dark gray to light gray color, fissile partings, and low bioclastic content characteristic of TBR ash deposits. Scales are in centimeters.

the surface of deposition (e.g. winnowing of fine grains in high-energy environments, homogenization with sediment through bioturbation, ponding of ash in low energy depressions). Fortunately, the Black River Shale and E-Shale K-bentonites are identifiable in all cores used in this study.

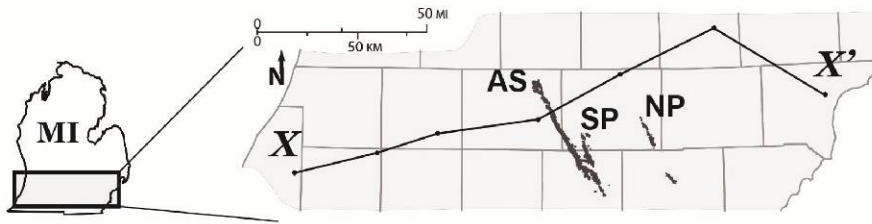
#### K-Bentonite Chronostratigraphy

The spatial relationships of the depositional facies, are constrained through the development of a chronostratigraphic framework, defined by the presence of K-bentonite beds. Isochronous bentonite beds record characteristics of the two-dimensional depositional surface within a sedimentary system at an instant in geologic time (Wheeler, 1958), and therefore constitute the building blocks of the chronostratigraphic framework and the distribution of individual facies at a single point in time. The Black River Shale and E-Shale volcanic tephra beds are assumed to have been deposited over a geologically instantaneous time period of days to weeks (Schmincke and van den Bogaard, 1991; Leslie and Bergstrom, 1997), and are used in this study as isochronous surfaces. These markers are readily identifiable by the physical characteristics in core (Figures 29 and 30) and correlation of core to wire-line log responses (Figure 31).



Figure 30. Facies 7- Core photographs (E-Shale).

Paleogeographic reconstructions are mapped at the intersection of two-dimensional K-bentonite surfaces with one-dimensional core-well bores and the associated depositional facies described in core. These reconstructions provide a vital insight not only facies to distributions at a two defined times and stratigraphic positions, but also a reference for evaluating the genetic stratigraphic and facies relationships during the evolution of the TBR depositional system where such surfaces are not available. This K-bentonite chronology is particularly valuable where there are problems with the vertical continuity or, stratigraphic overlap of cores.



# Michigan Basin K-bentonites

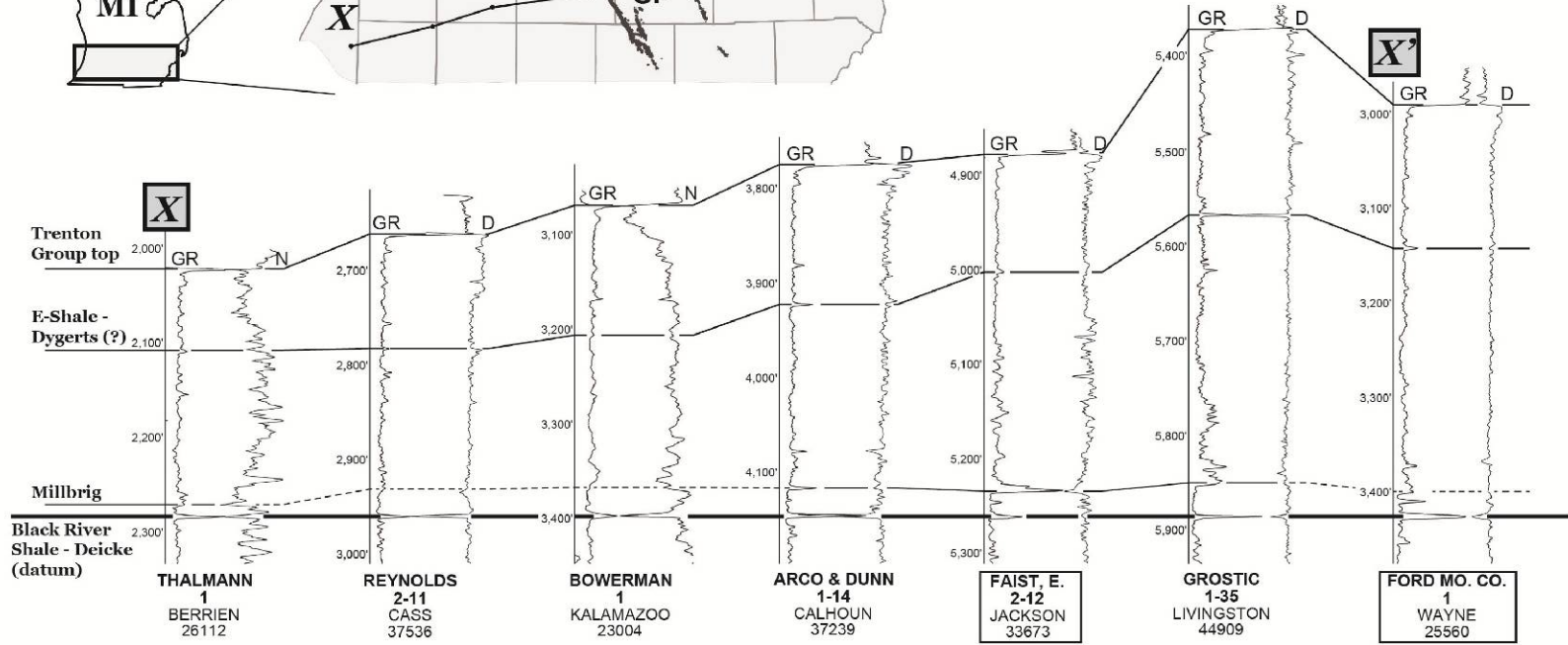




Figure 31. Wire-line log cross-section showing regional continuity of K-bentonites in the Michigan Basin TBR interval. Bentonites identified by Kolata et al. (1996) in the Ford Mo. Co. 1 and Faist, E. 2-12 (well information in boxes) wire-line logs, show continuity of the Black River Shale throughout the southern Michigan Basin. Also documented here is this study's correlation between Kolata et al.'s (1996) Dygerts K-bentonite and the Michigan Basin E-Shale, based on stratigraphic position, wire-line log signature, and mineralogical composition. The Millbrig K-bentonite has been omitted as a chronostratigraphic surface in this study because of inconsistent log signatures (dashed) in Michigan Basin locations. Well name, number, county, and drilling permit number are shown at the base of logs. The wire-line logs used show relative changes in formation gamma-ray (GR), and neutron (N) or density (D) measurements. Locator map shows wells utilized cross-section for Albion-Scipio (AS), Stoney Point (SP), and Napoleon (NP) fields, and Michigan county outlines are included. Note that the Arco & Dunn 1-14 wire-line data shown in the X-X' cross-section also serves as the TBR type-log in this study (see Figure 3).

### Black River Shale

The Black River Shale is a recognized stratigraphic marker bed in the Michigan Basin, located approximately 20 to 30 ft (6-9 m) below the top of the Black River Group (Hurley and Budros, 1990). On the basis of chemical analyses and stratigraphic position, Kolata et al. (1996) connects the Black River Shale to the extensive (230,000 mi<sup>2</sup>, 600,000 km<sup>2</sup>; Huff and Kolata, 1990) Deicke K-bentonite bed (Figure 5b). Variable dating methods of the Deicke has yielded a number of age estimates (e.g, 457.1 ± 1.0 Ma, apatite Nd and Sr isotopes TN, USA, Samson, et al., 1989; 454.5 ± 0.5 Ma, zircon <sup>238</sup>U/<sup>206</sup>Pb, NL, CA, Tucker and McKerrow, 1995; 449.8 ± 2.3 Ma, biotite <sup>40</sup>Ar/<sup>39</sup>Ar from, KY, USA, Min, et al. 2001), with 454 to 455 Ma the commonly accepted range. The Black River Shale has proven to be a useful isochronous stratigraphic surface in previous regional oceanographic, paleogeographic (Leslie and Bergstrom, 1997; Holmden et al., 1998; Kolata et al.,



1998), and high-resolution depositional reconstructions during the Mohawkian (Emerson, 2002, Brett et al. 2004). To date, however, no study has incorporated this marker as a chronostratigraphic surface in the depositional reconstruction of the TBR in the Michigan Basin.

#### Facies Reconstruction: Black River Shale

A complex facies mosaic, superimposed on the low declivity ramp dipping into the basin center is shown by the facies distributions at the time of Black River Shale deposition in Figures 32 and 33a. The cross-section displays of facies distributions constrained by the Black River Shale indicate a complex facies mosaic in the inner, mid, and outer ramp settings. Facies cross-sections additionally illustrate probable facies geometries consistent with strike and dip orientations (e.g. shoal facies (yellow) are oriented elongate to strike, see Modern Analogs section for further discussion). Paleogeography at the time of Black River Shale emplacement shows a well-developed NW/SE depositional strike and NE dip orientation and suggests basin centered subsidence. Distinctive facies mosaics consistent with mid- and inner ramp environments, are outlined by the Black River Shale depositional system. The mid-ramp facies association is composed of widespread deposition of Facies 2 with isolated bathymetric highs (Facies 3). Up depositional slope, and away from the basin center, the inner ramp association shows the development of shoals and lagoons. Facies 3 is interpreted as deposited adjacent to shoal activity, and therefore suggesting that this shoal-lagoon complex developed surrounded by this facies. The complex facies mosaic below and above the Black

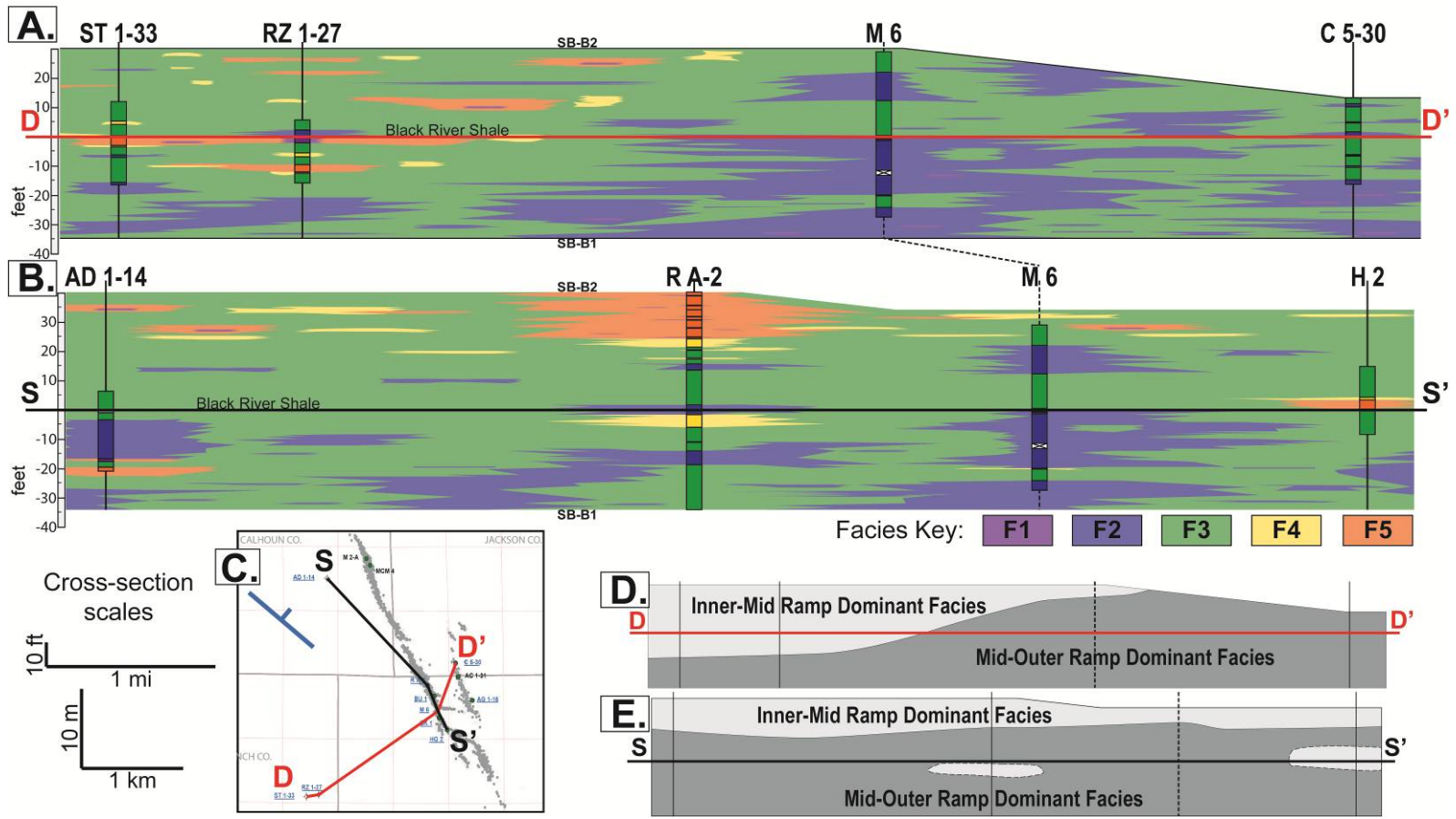


Figure 32. Facies cross-sections showing strike and dip orientations in the in the Albion-Scipio and Stoney Point study area. Cross-section interval is constructed with the Black River Shale as the datum, and includes facies observed in core (core data indicated in bold box) through one depositional sequence based on facies stacking patterns (TR-B2, bound by surfaces SB-B1 and SB-B2, see Figures 35 and 36 and the following text discussion). Lateral and vertical facies shown between wells are based on facies controlled probabilistic models with K-bentonite and modern analog constraints (see text discussion). Cross-sections suggest a heterogeneous distribution of facies mosaics at depositional surfaces, albeit in distinct inner, mid, and outer ramp assemblages. Dip (A., D-D') and strike (B. S-S') orientations (C., note blue strike-dip, symbol) show the partitioning of facies assemblages into inner-mid and mid-outer ramp dominant environments (indicated by shading in D. and E., respectively) in both a lateral and vertical sense. Dip section D-D' shows a shift in inner-mid ramp facies to the northeast. Strike section S-S' also shows an up-section shift from mid-outer ramp facies to inner-mid ramp facies. These lateral and vertical facies distributions support a northwest-southeast trending strike and northeast dip in the TBR depositional system. Facies distributions further imply trends in facies distribution and vertical stacking pattern indicate changes in accommodation over time. Note: core M 6 is common to both sections (dashed lines).

River Shale surface reveals a high degree of depositional heterogeneity, which strongly deviates from previous accounts of “layer cake” deposition in the Michigan Basin TBR carbonates (Taylor and Sibley 1986; Keith, 1989; Hurley and Budros, 1990).

### E-Shale

The E-Shale marker bed, located approximately 150 feet below the Trenton-Utica contact, is also a common subsurface correlation tool used in the southern Michigan Basin (Hurley and Budros, 1990). The E-shale's ash-fall origin is indicated by x-ray diffraction showing pyrogenic sanidine concentrations, (33 weight %, Feutz, 2012), mapped regional continuity, and stratigraphic positioning (Figure 31).

Furthermore, this study shows that the marker equivalently correlates to the stratigraphic position of the Dygerts K-bentonite (Willman and Kolata, 1978), established in the Michigan Basin by Kolata *et al.* (1996) (Figure 31). Chemical fingerprinting has not, however, unequivocally identified a volcanic origin this bed. The available evidence supports the interpretation of the E- Shale as being volcanic in origin. As such, it is therefore employed here as an isochronous surface throughout the study area.

#### Facies Reconstruction: E-Shale

In this study, the E-Shale depositional surface intersects fewer cores over a relatively smaller region than the Black River Shale; however, the core coverage is sufficient to show a similar facies mosaic distribution (Figure 33b). This younger bentonite captures a deeper/lower energy depositional system relative to the Black River Shale, with widespread Facies 2 deposition and Facies 3 occurring on isolated bathymetric highs.

#### Facies and Sequence Stacking Patterns

#### Approach

Cyclic deposition on epeiric carbonate platforms is well documented throughout the sedimentary record (Wilson, 1975), and is particularly pronounced during the marine inundation of the North American craton during the Middle Ordovician (Holland and Patzkowski 1996; Witzke and Bunker, 1996; Pope and Read, 1997; Emmerson 2002; and Brett *et al.*, 2004). Like time equivalent cyclic deposits, the TBR interval cores show depositional cycles related to change in

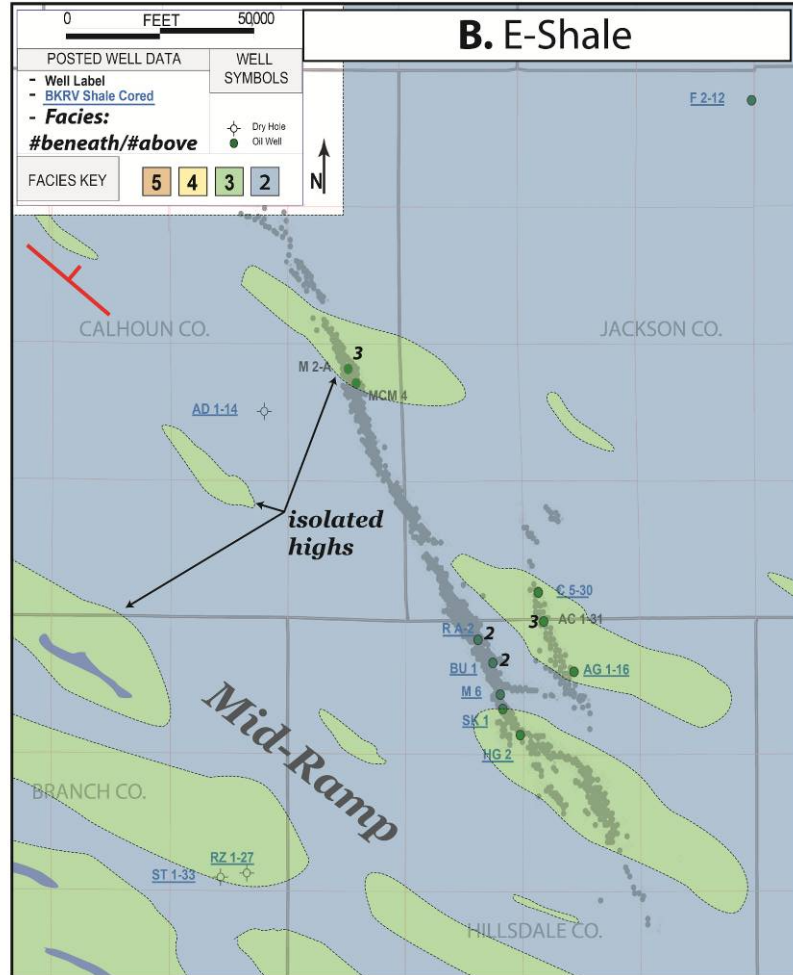
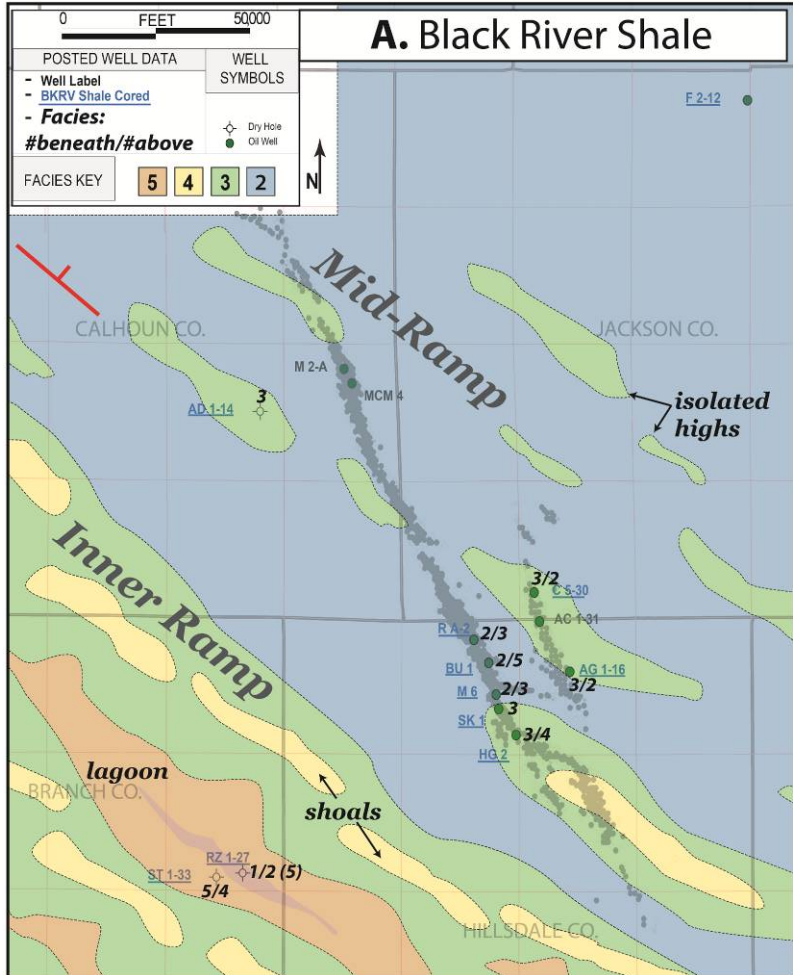


Figure 33. K-bentonite constrained facies distributions. Paleogeographic distributions of facies show probable distributions, relationships, and geometries at isochronous bentonite surfaces. Well labels underlined blue and black indicate where core intersects the Black River (A.) and E-Shale (B.) surface, respectively. Facies below and above the bentonite surface are denoted in black italics and separated by a slash (i.e. *below/above*). Facies distributions show distinct assemblages consistent with mid and inner ramp settings. Bathymetric relief is indicated where relatively shallower water depth facies are juxtaposed (laterally and vertically) against relatively deeper facies. This suggests a distribution of isolated highs, shoals, and intershoal depressions, or lagoons on the platform. Lateral migration of facies is indicated where deposits differ above and below the bentonite surface, and gives further indication of depositional environment through defining the likely laterally adjacent (or incipient) facies type. Paleogeographic facies distributions are consistent with strike and dip interpretations from cross section display (Figure 32). Strike and dip symbol is show in red. Note that no palinspastic correction is accounted for in these maps.

relative depositional energy at multiple scales, which are likely caused by fluctuation in relative sea level. Definition and evaluation of facies stacking patterns in the TBR gives a better understanding of, not only the facies distributions as they occur in core, but also the factors influencing those distributions at different scales (e.g. change in relative sea level, autogenic facies cyclicity).

#### Sequence and Cyclostratigraphy

The ideal sequence and cyclostratigraphic method for system reconstruction groups genetically-related depositional units through integration of rock based core, outcrop, and diagenetic data with acquired seismic and wire-line log data (Sarg, 1988; Kerans and Tinker, 1997; and Grammer *et al.*, 2000). Vertical stacking and lateral relationships of facies, within and between units, are controlled by changes in relative sea level. Changes in relative sea level (the sum of autogenic and allogenic processes affecting local and regional water depths) control the available space for sediment

accumulation, which is generally referred to as accommodation. Accommodation is reflected in the sedimentary record by hydrodynamic and biologic environmental indicators, each of which also serves as the basis for identifying depositional facies. Therefore, the patterns of change in depositional facies reflect change in accommodation (specifically relative sea level fluctuation) within these units, which yields a predictive tool for depositional system reconstruction away from data points (Sarg, 1988; Grammer *et al.*, 2000).

Best practices in high-resolution stratigraphy dictate that an inductive approach should be followed for system reconstruction, because relative sea level changes are documented to occur at multiple spatial and temporal scales (Kerans and Tinker, 1997). In this approach, the smallest scale genetic rock-unit, the high-frequency cycle (HFC, Kearns and Tinker, 1997) is identified as the primary building block of a stratigraphic hierarchy, from which successively larger-scale sequences are constructed and integrated with larger-scale geophysically acquired data (e.g. wire-line logs and seismic). This “bottom-up” approach constrains three-dimensional depositional models (and related hydrocarbon reservoir models) with the smallest scale rock-based HFC unit, and in doing so attempts to maintain the predictive integrity at that highest resolution scale. The integrity of models at this scale is important for reservoir characterization, as it is the scale commonly controlling fluid-flow (Grammer *et al.*, 2004; Stoudt and Raines, 2004).

#### The TBR Approach

The sequence stratigraphic approach used in this study deviates from the above outlined ideal approach, as the data available are incomplete in the study area. The rock-data is limited to core, without the aid of outcrop to provide a lateral

constraints. As discussed, vertical overlap of core is also incomplete, compromising confidence in the correlation of HFCs. Additionally, the majority of depositional facies in the TBR are limited to a subtidal environment, and show no consistent shoaling to exposure, which is a common measure of changes in accommodation space in ideal stratigraphic analyses (e.g. Goldhammer, *et al.*, 1990). The TBR interval does, however, exhibit a hierarchy in depositional cyclicity, consisting of three spatial magnitudes, defined as: large-scale sequences, high frequency sequences (HFSs), and highest-frequency cycles (HFCs) (likely correlating with 3<sup>rd</sup> order, 4<sup>th</sup> order, and HFC-scales outlined in Kearns and Tinker (1997) respectively, on the basis of package thicknesses and frequencies from extrapolated dates in the TBR and comparison with time-equivalent regional deposits (Figure 3)). Because of these data limitations, the sequences in this study are based on the idealized facies successions related to change in accommodation at a larger magnitude (large-scale sequences) relative to HFCs.

The idealized facies stacking pattern used in this study (Figure 34) was determined by the vertical succession of depositional facies according to Walther's Law of the Correlation of Facies (i.e. conformable vertical successions of facies reflect laterally adjacent facies successions at a given depositional surface (Middleton, 1973; Kerans and Tinker, 1997)). However, the chronostratigraphic framework developed through mapping of K-bentonite and the resulting facies reconstructions show complex facies heterogeneity at depositional surfaces, providing considerable insight into the overall TBR depositional system in this region. Additionally, the facies relationships and distribution in the bentonite reconstructions give further insight into the vertical stacking of facies within a composite stratigraphic framework.



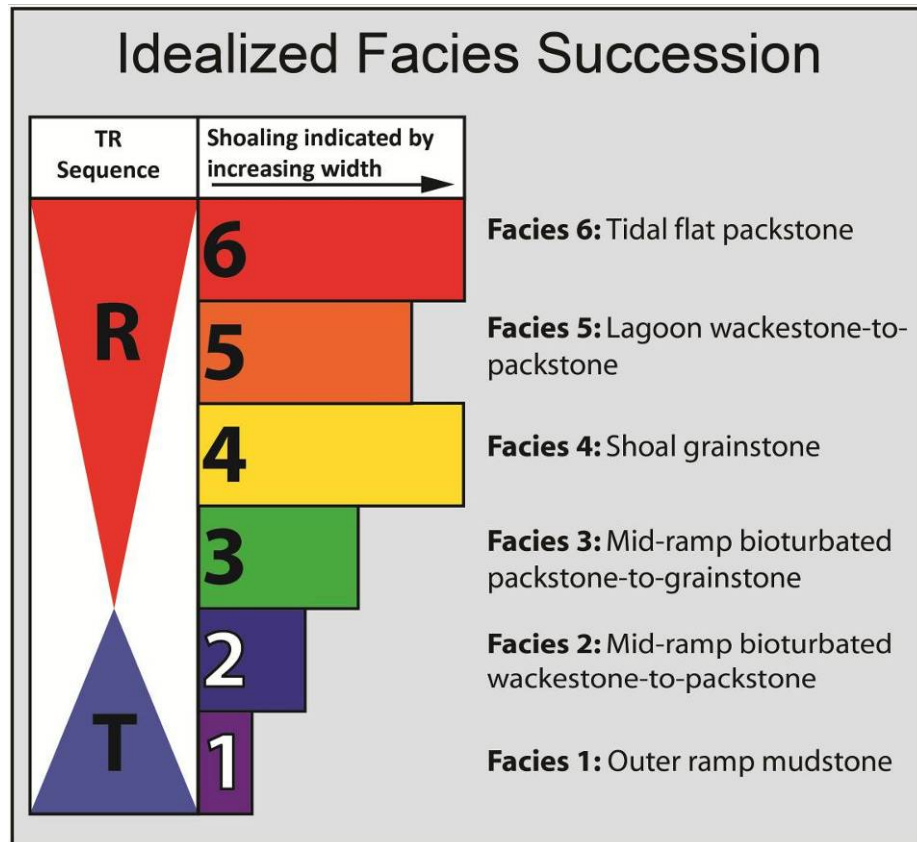


Figure 34. Idealized vertical succession of TBR depositional facies over a transgressive-regressive cycle of relative sea level change. The transgressive hemi-cycle (blue triangle) initiates by increase in water depth as platform flooding initiates (F1, F2). The depositional system shifts from transgression to regression (red triangle) at a turnaround point (point where triangles meet) at the F2/F3 contact. During the regressive hemi-cycle a shoaling upward trend progresses to peritidal facies (F6), with relative increases in water depths where lagoons form in intershoal and backshoal bathymetric depressions.

The heterogeneity observed in the distribution of synchronous facies exhibited by paleogeographic reconstructions of TBR deposition show complex, but systematic depositional trends within a multi-scale sequence hierarchy (Figures 35, 36). These “cycles” are characterized by four large-scale transgressive-regressive (T-R)

sequences, within an overall longer-term transgressive trend. The large-scale depositional sequences are each composed of HFS T-R “cycles”, commonly shoaling to inner ramp facies at HFS terminations. The upper boundaries of the large-scale and HFS are marked by facies shifts to relatively deeper water facies.

All scales of the sequence hierarchy were determined through analysis of vertical stacking patterns of facies in core (HFC also reflect textural changes in a single facies interval, see HFSs and HFCs section) using the idealized facies succession (Figure 34). Facies stacking pattern analysis followed a workflow from a single well (1-D), cross-section (2-D), and composite cross-section (e.g. fence diagram, 3-D) correlations. At the large-scale, however, the facies heterogeneities mosaic distributions (Figures 32 and 33) required that the vertical facies analysis consider facies assemblages reflecting ramp-sub-environments (i.e. outer, mid, and inner ramp associations, as discussed in Facies Associations section) commonly in place of a vertically continuous facies interval. Thus, the sequence boundaries at the large-scale mark rapid deepening of facies assemblages across the platform.

### Stacking Pattern Hierarchy

#### Large-scale Sequences

The large-scale sequences range in thickness from 100 to 150 feet (30 to 46 meters). Analysis of the entire TBR sequence indicates that the system follows an overall transgressive trend. This trend correlates to a deepening of the dominant facies types and environmental associations of platform sub-environments. Depositional facies from core show this transgressive trend as inner and mid-ramp facies dominating the two basal large-scale sequences (TR-B2 and TR-T1), a shift to mid-ramp facies in TR-T2 sequence, and the distal mid- and outer ramp facies

dominating the capping TR-T3 sequence (Figure 36).

Intertidal peloidal packstones and grainstones of the upper Black River Group mark the base of the complete large-scale T-R sequences (SB-B1). The SB-B1 surface is overlain by peloid and crinoid rich wackestones and packstones, which progressively shoal-up to inner ramp skeletal shoal-lagoon complexes in the regressive leg of TR-B2. Of the complete large-scale sequences, TR-B2 shows the highest energy/shallowest hydraulic conditions, however a slight asymmetry showing a thicker transgressive portion of this cycle indicates the system's deepening trend through the sequences.

The overlying TR-T1 sequence shows a facies stacking pattern similar to TR-B2, however a mid-ramp dominated packstone-wackestone facies association caps this sequence rather than a shoal-lagoon complex. This difference indicates relatively deeper environments and lower energy at maximum regression. The proximal mid ramp Facies 3 dominates this sequence, with additional occurrences of the relatively lower and higher energy environments of Facies 2 and 4, respectively.

The transgressive trend of large-scale sequences continues in TR-T2 and TR-T3, where mid-ramp and muddy distal mid-ramp/outer ramp facies associations dominate, respectively. Considering available rock data within the TR-T2 sequence, an equal proportion of proximal and distal mid-ramp facies constitute the majority of the depositional environments recorded, with a regressive cap of Facies 3. Sequence TR-T3 shows a clear dominance of the deep/low energy Facies 2. These upper two sequences show a strong asymmetry favoring transgressive facies stacking patterns consistent with an overall lower order transgressive trend.

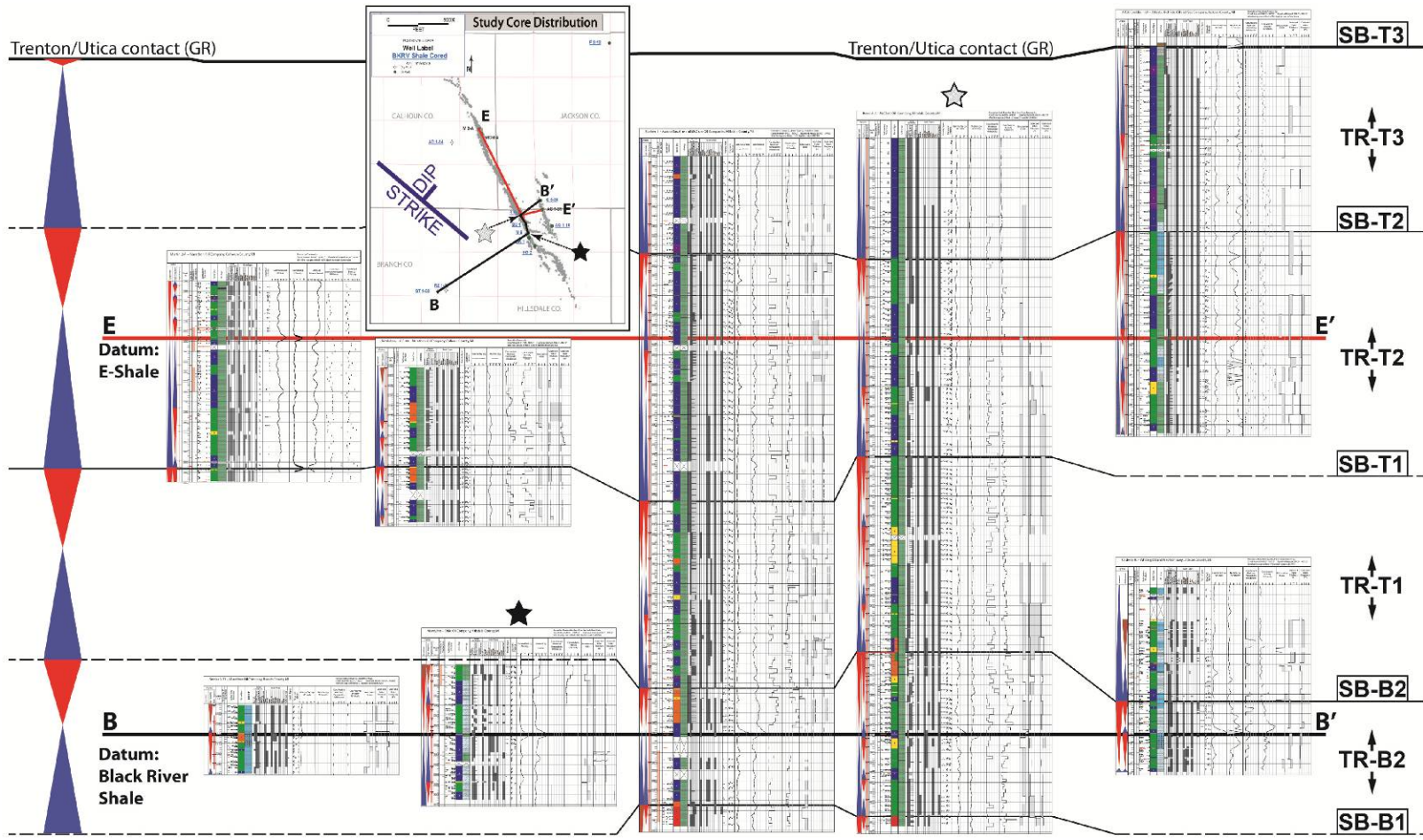


Figure 35. Stratigraphic framework synthesis: detailed core-log view. Stratigraphic framework of the TBR interval constructed from sedimentary logs, isochronous K-bentonite surfaces, and TR depositional sequences. The Black River Shale (B-B') and E-Shale (E-E') each provide an isochronous datum, allowing for the integration of vertically limited core with continuous and overlapping sections into a single composite stratigraphic section. Facies stacking patterns described from core and recorded on sedimentary logs define the T-R sequences. Sequences and their bounding surfaces (TR and SB respectively) are alphanumerically coded by stratigraphic group (e.g. Trenton = T) and chronological order. T-R sequence triangles at left represent a composite of facies stacking pattern data over the study area at the large-scale. Sequence boundaries inferred without core control shown with dashed lines. Stars above logs and on locator map denote changes in cross-section orientation relative to depositional strike and dip.

### HFSs and HFCs

Two to three HFSs compose the large-scale sequences, where complete large-sequences are observed in single cores. Asymmetries in T versus R dominance of a HFS commonly reflect the large-scale T-R-trend in which they occur: that is, HFSs reflect a dominant transgressive or regressive trend, depending on the large-scale T-R stacking trend. The general agreement between the dominance of a T/R hemicycle in HFS's and large-scale trends show systematic links in the development of depositional cyclicity at differing magnitude and time scales. This relationship illustrates the interplay, or superimposition of higher order relative sea level cyclicity on the lower order trends (e.g. "fourth" order superimposed on "third").

The utility of HFC's is limited in the evaluation of facies stacking patterns. These cycles define shoaling and/or deepening-up depositional trends at a foot-scale in core, commonly showing multiple cycles within an individual facies interval (e.g. multiple shoaling-up cycles within a single defined facies interval). Additionally, shallower facies (inner ramp) are generally more sensitive to water depth (relative sea

S6

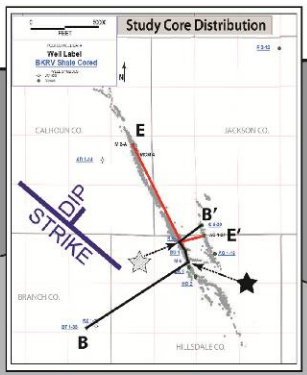
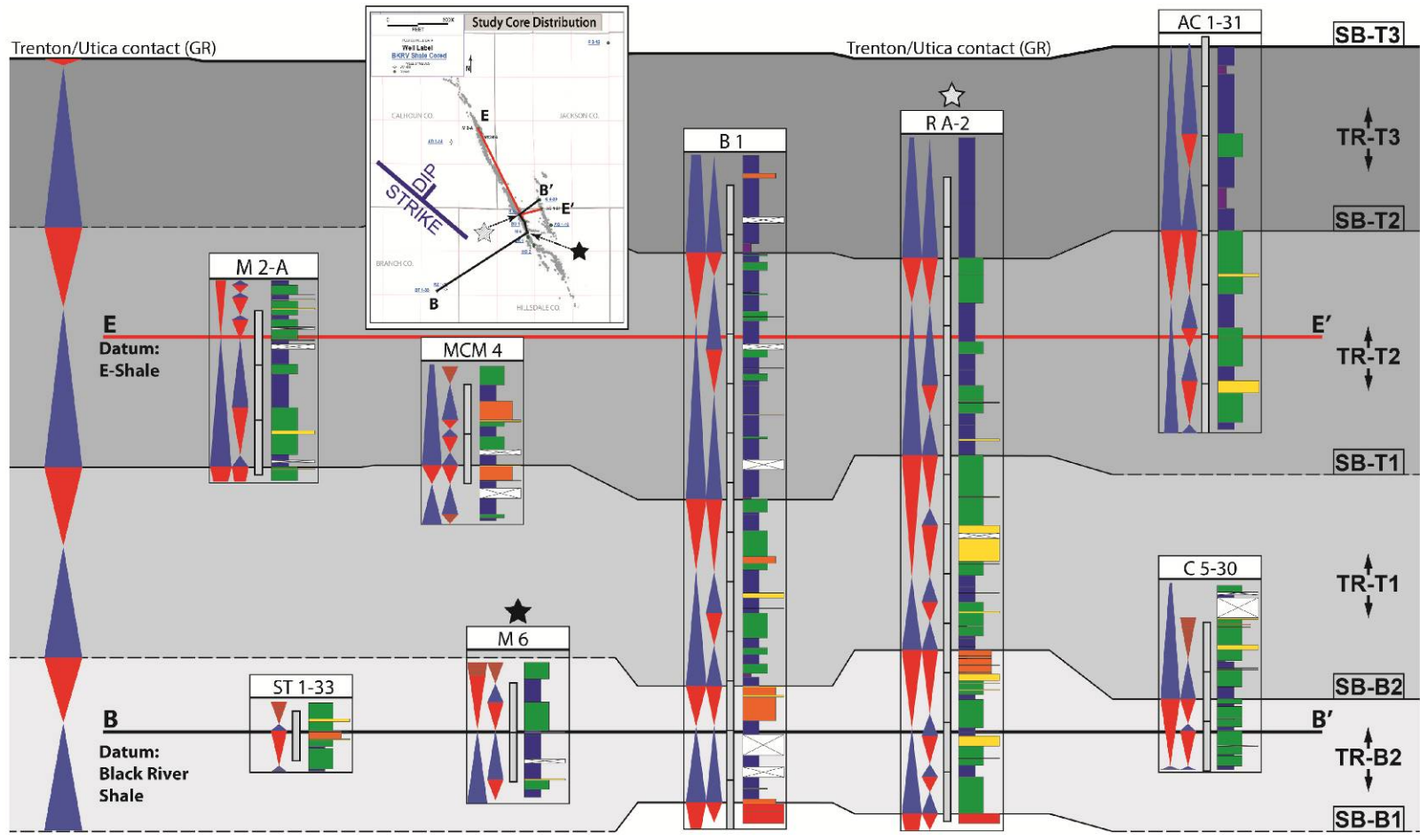


Figure 36. Stratigraphic framework synthesis: detailed facies view. Detailed view of TR facies stacking patterns at multiple-scales in the TBR stratigraphic framework. Facies stacking patterns show four complete large-scale TR sequences composed of multiple small-scale sequences, with the trend of the overall system becoming increasingly transgressive-dominant through time. High frequency-scale (HFS) TR sequences show asymmetry, with transgressive or regressive hemicycles dominating as a reflection of large-scale sequence framework position (e.g. regressive hemicycles dominate HFS TR sequences when located in a large-scale regressive position). T-R sequence triangles at left represent a composite of facies stacking pattern data over the study area at the large-scale. Highest-frequency cycles (HFCs) are not shown on this section. White crossed-out boxes indicate missing core.

level) changes relative to deeper facies (mid and outer ramp), and therefore shallower facies record more sea level cyclicity relative to deeper facies, even though the magnitude of change is the same over the platform (e.g. Goldhammer *et al.*, 1990). The HFC's do, however, correlate to stacking patterns, in that cycles commonly show a higher- and lower-frequency of occurrence in regressive and transgressive trends, respectively, of both the HFS and large scale-sequences. Thus, because the character of the HFCs can vary over short intervals (e.g both coarsening-up and fining-up trends over a 5-10 ft interval) they are used here simply as an aid in evaluating the vertical facies patterns that compose the HFS and large-scale sequences. Therefore the HFC is limited in use to a qualitative constraint on the TBR facies stacking pattern stratigraphic framework.

The heterogeneity in the distribution of depositional facies shown at chronostratigraphic surfaces (Figure 33) illustrates the complexity of the subtidal facies mosaics in the TBR. Cross-section display of core-facies data, vertically constrained at the Black River Shale (Figure 32) indicate, however, that facies are partitioned in inner, mid, and outer ramp mosaic-assemblages. This complex mosaic of facies, combined with the depositional disruption caused by reworking of the



sediment by frequent storms and pervasive bioturbation, results in very weak to no correlation within HFSs and HFCs over the study area. Furthermore, HFSs and HFCs show limited regional consistency in a sequence context and sense of relative sea level change at an instant in time (K-bentonites), suggesting that the use of the highest frequency signals as a basis for cyclostratigraphic frameworks where data are limited to subtidal-dominated shallow carbonate platform deposits similar to the TBR may be problematic. Although the correlation of the HFSs and HFCs is problematic, analysis of patterns in the internal makeup of the HFSs and the vertical succession of both the HFSs and HFCs generally show agreement within the large-scale sequence framework (Figure 36).

#### Implications of Stacking Patterns

Vertical stacking patterns of facies define the large-scale sequences by documenting changes in accommodation, or relative sea level over the TBR platform. A purely autogenic mechanism of sequence development (over 100 vertical feet) throughout the study region (c.a. 525 mi<sup>2</sup>) is improbable. Facies analysis and stratigraphic reconstruction show no evidence of autocyclicality at these scales. However, the stacking patterns do show marked shifts in facies at correlative stratigraphic positions at the large-scale in regionally distributed core. Therefore, it is reasonable to conclude that the T-R sequence hierarchy is developed, in part, as response to allocyclic changes in relative sea level.

Assuming that the sequence framework of the TBR deposits primarily reflects system responses to allocyclic controls, then similar changes would be recorded in time-equivalent marine rocks. Comparison of TBR accommodation trends with time-equivalent deposits on the Laurentian craton show similarities in temporal scale and

direction (increase vs. decrease) in the change of relative sea level (Figure 37). The agreement of the temporal scale and direction of change in accommodation in deposits distributed across the craton supports allogenic controls on large-scale TBR T-R “cyclicality”. Additionally, given that regional relative sea level changes are correlative, it is reasonable to consider a eustatic signal as the probable influence on the craton-scale changes in relative sea level.

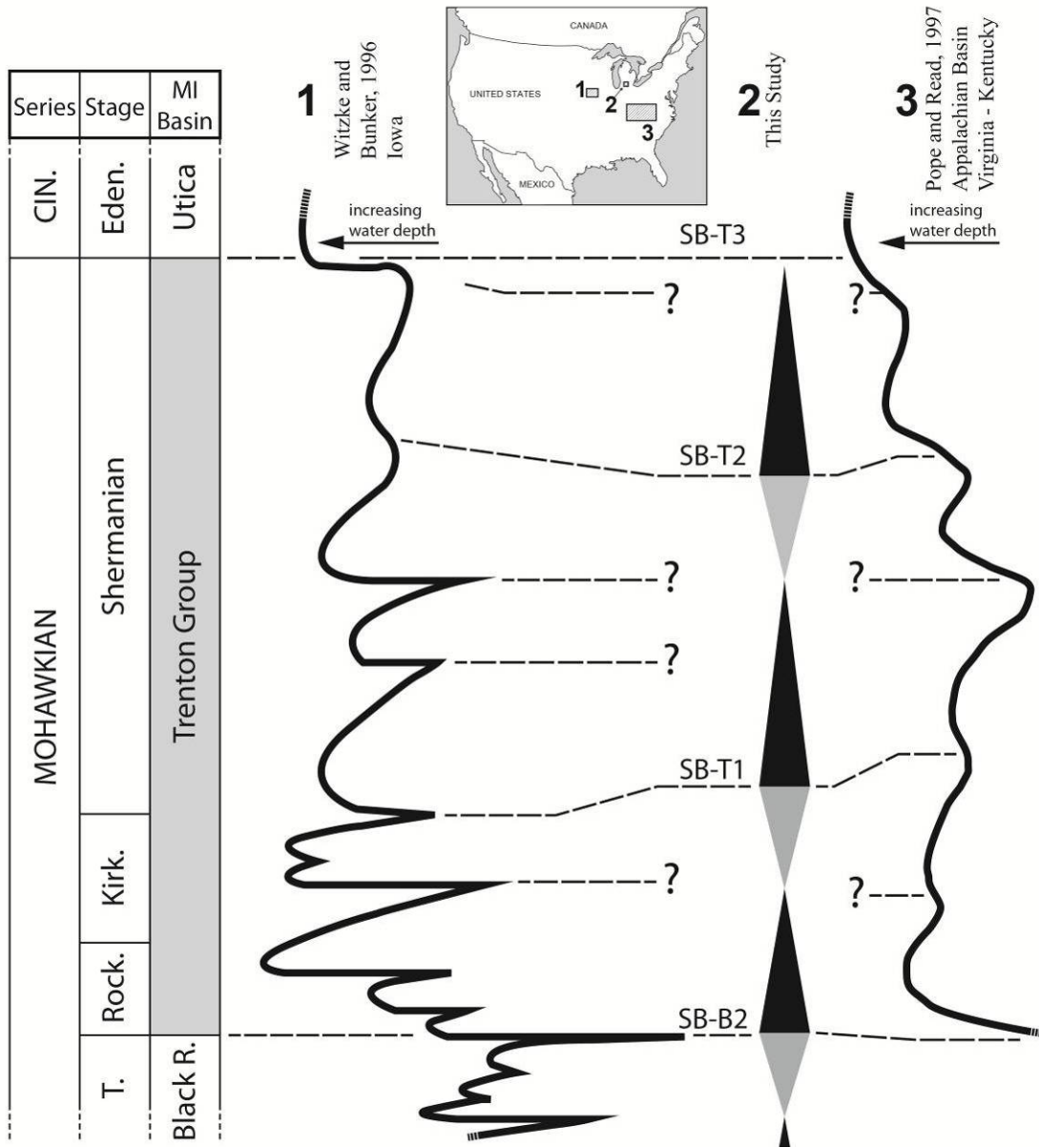


Figure 37. Comparison of Mohawkian changes in relative sea level on the Laurentian craton. Curve numbers correspond to the study areas identified on the map. The composite T-R trend recorded in Michigan Basin TBR cores (No. 2, T = black triangles, R = gray triangles, see Figures 34 and 35 for composite stratigraphic column) shows limited correlation with outcrop-based Iowa and Virginia-Kentucky (outcrop) curves. The TBR sequence boundaries are interpreted as correlating with inflection points succeeding sea level minimums on curves. Because of problems in correlating small-scale TBR T-R sequences in this study, no attempt is made here to compare them with the outcrop-derived curves. However, the higher frequency cyclicity shown in outcrop curves (interpreted and labeled “?”) correlates loosely with the number of small-scale TBR cycles within large-scale sequences (2 to 3). This suggests that craton-wide changes in relative sea level occur at similar scales, frequencies, and direction (increase vs. decrease). Relative sea level curves are scaled to North American Stage boundaries (time-rock units). T. = Turinian, Rock. = Rocklandian, Kirk. = Kirkfieldian, Eden. = Edenian, Cin. = Cincinnati. Modified after Witzke and Bunker, 1996; Pope and Read, 1997; and Catacosinos *et al.*, 2000.

### Issues with Stacking Pattern Causal Mechanisms

Although the above discussion implies allocyclic influences on TBR facies stacking patterns at the large-scale, distinguishing allogenic from autogenic drivers of accommodation is problematic. Moreover, assigning the relative contributions of these mechanisms to the development of sequences at the HFS and HFC-scale is even more questionable. The following section outlines the factors pertinent to cycle/sequence development in the TBR.

#### Autogenic Facies Controls

Autogenic controls on depositional cyclicity are well documented in the study of both ancient (Pratt and James, 1986; Cowan and James, 1996) and modern deposits (Rankey, 2002; Eberli *et al.*, 2005; Harris, 2010; Rankey and Reeder, 2011). The

generation of autocyclic shallow water carbonate strata has also been shown in forward models (Drummond and Wilkinson, 1993a, 1993b). Addressing the autogenic controls on change in accommodation is necessary when evaluating the mechanisms contributing to depositional evolution and sequence development. The following discussion addresses the effects of sedimentation rates, sediment compaction, and storm influences on these factors and the overall TBR depositional system.

### Sedimentation Rates

Sedimentation rates reflect the autogenic mechanisms of carbonate sediment production and preservation potential for the deposit, and additionally provide insight into the hydrodynamic regimes of depositional environments. Definition of this parameter is therefore crucial to understanding the development of sediment bodies, of sedimentary facies, and of stacking patterns, whether they are of autogenic or allogenic derivation. Constrained sedimentation rates are required to understand if changes in relative sea level are caused through local controls on vertical sedimentary accretion, or by a broader scale change in sea level (e.g. eustacy). However, the quantitative evaluation of depositional rates is currently not possible over the platform at the facies-scale, as only one high-confidence dated surface has been identified (Black River Shale).

The calculation of sedimentation rates in the TBR would be problematic even if the temporal components of sedimentation rate were to be well-constrained. Substantial error is introduced into averaging sedimentation through time, as the nature of bedding and stratification inherently incorporates periods of sedimentation and intervals of non-deposition (Sadler, 1981). This issue is exacerbated in the TBR, where sedimentation is strongly influenced by episodic storm activity.

Post-depositional alterations to preserved carbonate deposits may also substantially alter preserved sedimentation rates. Burial dissolution and stylolitization remove rock material (commonly 20-35%), but these processes also redistribute that carbonate material and contribute to the development of burial cements in nearby pore spaces (Scholle and Halley, 1985). Furthermore, the reservoir formation processes of normal faulting and structural deformation with HTD-diagenetic alterations (dissolution and dolomitization) additionally reduce the accuracy of any calculated sedimentation rates, as the majority of current rock data are limited in availability to reservoir rocks subjected to these processes. Therefore, calculated sedimentation rates in the TBR would, at best, represent “sediment preservation rates” in diagenetically and structurally altered reservoir rock.

#### Sediment Compaction

Near surface compaction of sediments constitutes a component of subsidence in carbonate sedimentary systems. The compaction of sedimentary bodies is dependent on sediment type (Goldhammer, 1997), which varies by facies and depositional environment. Thus, differential compaction may occur between sedimentary facies and platform environments, resulting in apparent dips in strata, from the facies-scale up to platform-scale, that are different from original, depositional gradients. Furthermore, bathymetric relief due to differential compaction may impact facies development (Hunt *et al.*, 1996).

Goldhammer (1997) reviews previous work regarding carbonate sediment compaction, and establishes that mechanical compaction rates are primarily controlled by sediment type. This relationship is also influenced by near surface sediment diagenetic controls on sediment competency, such as early carbonate cementation in sand sized grains (e.g. Enos and Sawatsky, 1981; and Grammer *et al.*,

1993, 1999) and chemical compaction. The development of local bathymetric relief through sedimentary compaction/subsidence (e.g. between sedimentary facies bodies), therefore, is fundamentally influenced by autogenic depositional controls on the distribution of sediment types and sedimentary character (i.e. Dunham texture).

The local variability in sediment compaction is likely to have contributed to the variable bathymetric relief observed in the TBR paleogeographic reconstructions. Differential compaction of laterally adjacent sediments—where sediment type and character defines depositional facies—suggests that changes in accommodation were, in part, autocyclic. However, further investigation of the autogenic control on lateral changes in accommodation at a facies-scale, the resulting effects on the vertical stacking patterns of facies observed in core, and the relative contribution of this autocyclicality to the multi-scale stratigraphic framework of the TBR, is not currently possible due to the absence of laterally continuous data in the study area (i.e. as may be seen in outcrop).

#### Storm Activity

As demonstrated in the discussion of the TBR depositional model, storm activity strongly influenced deposition on the platform. Storm activity is controlled by global (allogenic) climatic circulation patterns (Barron, 1994). However, storm influence can also be categorized as an autogenic process within the TBR system, as it affected sedimentation rates, and possibly the organization of the depositional system through controls on facies distributions and relationships.

Storms influenced the TBR facies mosaic through the reworking of sediment at the depositional surface by waves and currents. Storm events impacted sedimentation rates in this section through rapid sedimentation, the winnowing of existing deposits, and general redistribution sediments on the platform (Aigner, 1985;

Drummond and Sheets, 2001). The influence of storms on quantitative sedimentation rates, however, is currently poorly understood, which adds to the uncertainty in TBR sedimentation rates outlined above.

The influence of storm activity on depositional organization in the TBR was a relative increase in wave energies and induction of storm-generated bottom currents (Duke, 1990). Storm-related episodic changes in the overall energy influencing the hydrodynamic conditions on the TBR platform likely influenced the stability of facies/bathymetric relationships (i.e. bathymetric relief influenced through storm-current channelization and the resulting facies mosaic). However, these processes are poorly understood in epeiric seas (Duke, 1990). The role of storms in the depositional organization of TBR facies will be further discussed in the Depositional Analog section.

### Tectonics

A complex tectonic history of the Michigan Basin raises questions regarding the use of facies stacking patterns as a measure of regional or global sea level fluctuation. Problems with using Michigan Basin relative sea level approximations determined from facies focuses on the notion of linear subsidence and the use of the Laurentian craton as a static reference point for sea level reconstruction.

Howell and van der Pluijm (1990, 1999) show Michigan Basin subsidence was episodic at the second order-scale (10-100 MY), and that the style of subsidence was variable over Basin development (e.g. narrow vs. broad subsidence, basin tilting). They conclude that little Basin-centered subsidence occurred during deposition of the TBR interval. However, their proposed mechanisms for episodic Basin subsidence at this scale relies on in-plane lithospheric stresses induced through activity associated with the Taconic orogeny. Assuming that these lithospheric



stresses were episodic, it is reasonable to question whether those or other tectonic factors (e.g. far-field basement fault reactivation (Ettensohn, 2002), and see Future Considerations section) combined with the far-field stresses could also have affected a more subtle, episodic and/or local subsidence in the Michigan Basin and influenced facies stacking patterns.

Furthermore, Coakley and Gurnis (1995) document dynamic tilting of the Laurentian craton, including the Michigan Basin, toward the East. This tilting likely resulted in an accompanying response of relative sea level over the affected area (c.a. 1,000 km craton-ward from the Laurentian margin, Howell and van der Pluijm, 1999), and suggests that the craton is not a stable reference point from which to compare possible regional or eustatic sea level changes.

#### Depositional Analogs

The necessity of comparing observable geologic processes with the rock record has been recognized since Hutton proposed uniformitarianism in the modern foundations of geological sciences in the 18<sup>th</sup> century. Walther focused and clarified this concept to aid in the understanding of depositional components and processes through time with his Law of the Correlation of Facies (Middleton, 1973). Moreover, the study of modern analogs and associated depositional facies, stacking patterns, and diagenetic alteration is fundamental to understanding and modeling the distribution and heterogeneity of subsurface reservoir facies (Grammer *et al.*, 2004, Harris, 2010).

The study of carbonate reservoirs provides insight into subsurface porosity development, pore types and distributions, and the relationships between porosity and permeability (Choquette and Pray, 1970; Moore, 2001). The comparison of subsurface observations with modern depositional environments and diagenetic

studies aids in deciphering the development of petrophysical rock properties. Modern analogs also enhance understanding of the sedimentary processes that formed deposits presently in the subsurface, including the spatial distribution of facies and the dependence of petrophysical properties on facies types. Modern depositional environments and processes analogous to TBR carbonates are then key to understanding facies, facies relationships, their lateral and vertical distribution in the subsurface, as well as any relationship between facies and reservoir quality. This is particularly the case as regards preferential dolomitization of depositional facies and HTD processes in the Albion-Scipio reservoirs.

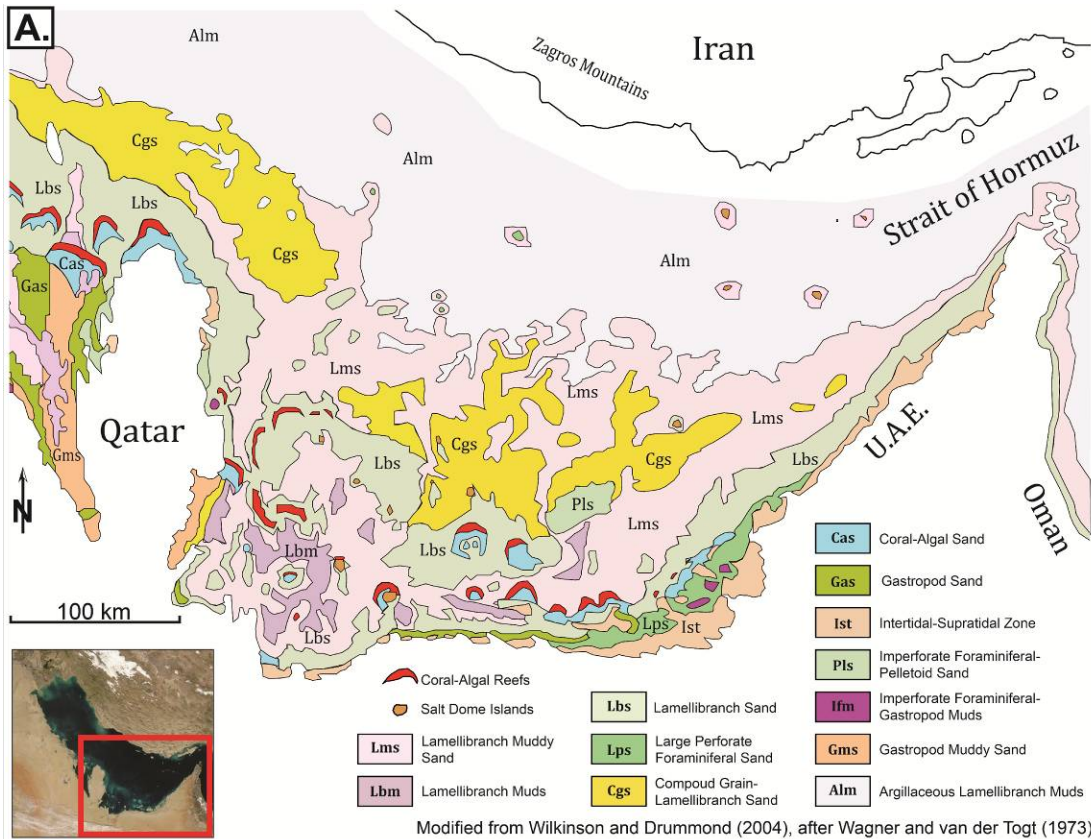
The integration of observations from modern processes in analog systems constrains interpretive depositional models that are derived from fragmentary subsurface data. In conjunction with a stratigraphic framework, the analog constraints on an interpretive model yields geologically reasonable and justifiable geometric attributes of a depositional system. The process of model development and the model itself both offer insight into depositional and reservoir facies development, the spatial distribution of facies, and relationships between deposition and reservoir. The products of the modeling process are constrained depositional and reservoir models that provide valuable guides for efficient hydrocarbon exploration and reservoir management.

No actualistic depositional analog to the Michigan Basin TBR deposits exists on the modern Earth surface. This is due to the deep interior cratonic position of the Michigan Basin during deposition. However, the Holocene Persian Gulf and the Great Pearl Bank Barrier (GPB), and the Great Bahama Bank (GBB) depositional systems each include characteristics that can be used to better understand TBR depositional and stratigraphic evolution. Additionally, contrasting characteristics and

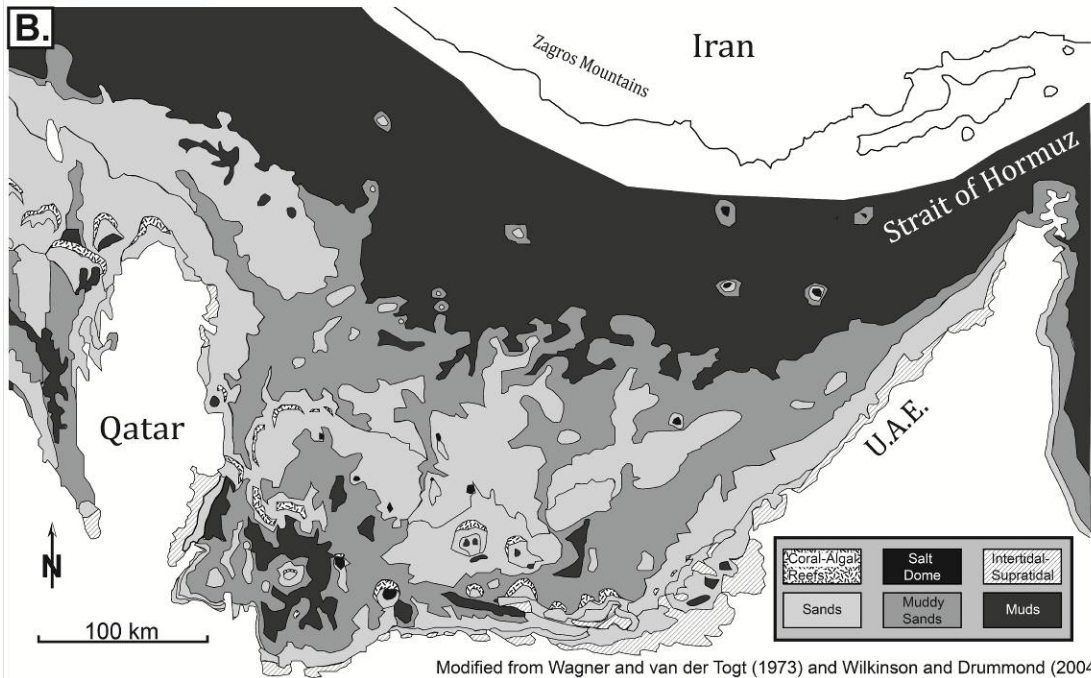
attributes of modern depositional environments with one another in the context of TBR observations provides insight into this epeiric carbonate environment. By combining an Ordovician outcrop-derived shallow-epeiric depositional model *and* modern observations with TBR interpretations, considerable insight into the development of the TBR depositional system is provided.

#### The Persian (Arabian) Gulf and the Great Pearl Bank Barrier (GPB)

The southern Persian Gulf is a shallow (maximum 330 ft, 100 m), arid-subtropical (24°-30°N), carbonate platform located entirely on the continental shelf (Purser, 1973a; Purser and Seibold, 1973) (Figure 38 and 39). The GPB is a prominent shoal complex in the southern Persian Gulf. The GPB depositional system is characterized by facies mosaics of foreshoal, shoal, and backshoal-lagoon deposits (Kendall and Skipwith, 1969b; Purser and Seibold, 1973; Wagner and van der Togt, 1973; Wilkinson and Drummond, 2004) with local hardground formation and variable degrees of bioturbation (Alsharhan and Kendall, 2003). Although the classification of this system as a carbonate ramp is contested by some because of the tectonic, eustatic, and depositional disequilibrium in the region (Riegl *et al.*, 2010), the gentle slopes toward the basin axis (35 cm/km; Hughes, 1997) in the location of the GPB sufficiently meet criteria for a ramp classification for comparison with the Michigan Basin TBR interval.



Modified from Wilkinson and Drummond (2004), after Wagner and van der Togt (1973)



Modified from Wagner and van der Togt (1973) and Wilkinson and Drummond (2004)

Figure 38. Maps showing facies type and generalized texture in the southern Persian Gulf. Facies map (A.) shows variability in facies type and heterogeneous distribution over the Persian Gulf ramp-shoal environments. Generalized textural map (B.) shows facies data simplified to reflect dominating constituent sedimentary material, also reflecting heterogeneity in distribution as in A. Variability in facies and textural distributions at the depositional (isochronous) surface display similarities to TBR paleogeographic reconstructions at the bentonite constrained isochronous surfaces, showing that the observed heterogeneity in facies distributions in reconstructions are consistent with distributions in this modern analog. Satellite image inset outlines map location in red box. Figures are modified from Wagner and van der Togh (1973) and Wilkinson and Drummond (2004); inset provided courtesy of NASA.

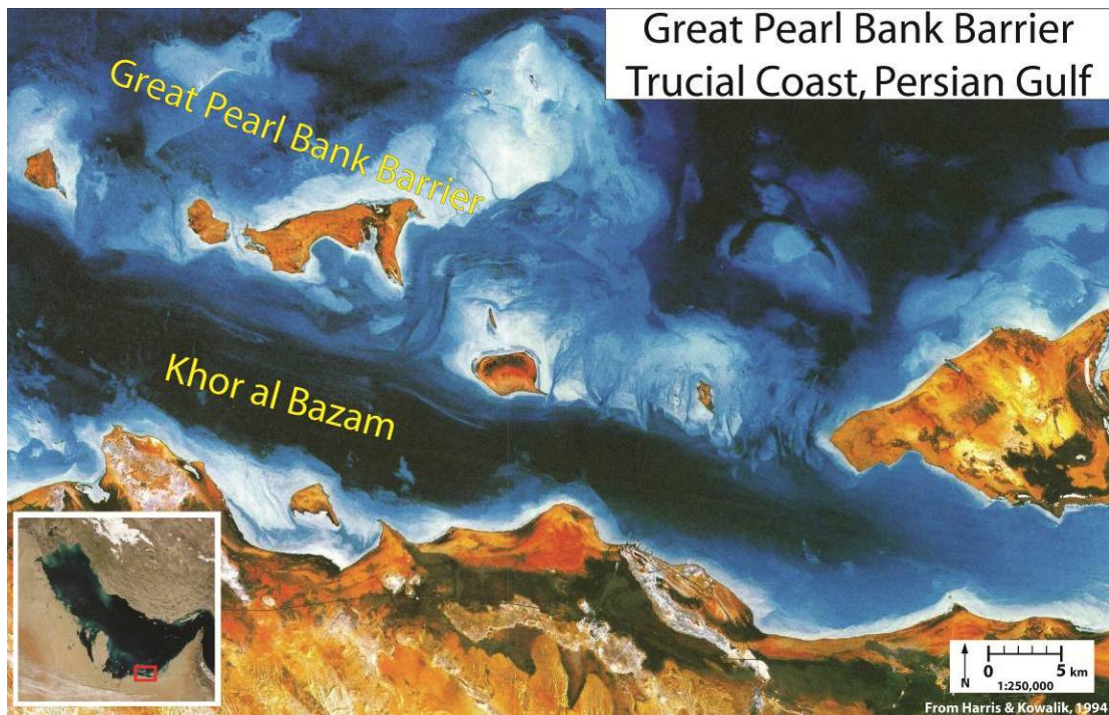


Figure 39. Satellite image showing the Great Pearl Bank Barrier and Khor al Bazam at the Persian Gulf Trucial Coast (U.A.E.). (GPB = Great Pearl Bank Barrier) Red box in inset indicates the location of the high-resolution image. Shallow water is generally indicated by lighter blue colors. Dark blue colors generally indicate relatively deeper water, sediment stabilization by sea grasses, or reduced sediments. Orange colors indicate subaerial exposure. Note the juxtaposition of active shoal sands (white sediments on GPB) on the GPB and deeper/stabilized

environments in a facies mosaic distribution. Images modified from Harris and Kowalik, 1994; insets provided courtesy of NASA.

Basinward, or in the foreshoal environments of the GPB, the sedimentary bodies generally consist of carbonate sands on bathymetric highs that grade into muddy sands in adjoining lows (Purser, 1973b). The sedimentary relationships associated with individual bathymetric highs are variable and depend on the fair-weather wavebase (and water depth) as well as the mechanism responsible for creation of bathymetric relief. The genesis of positive bathymetric relief in the foreshoal facies mosaics is varied, and commonly attributed to coral reef build-ups, salt diapirism, sedimentary shoals, and antecedent topography/structural deformation of bedrock. The geometries of the positive features are likewise varied, and reflect the mechanism of formation, wave agitation regime (i.e. depth relative to storm and fair-weather wavebase and sea level), and orientation relative to dominant wind direction (i.e. the formation of “crests” and fringing reefs on windward and “sediment tails” or dip-parallel spit features on leeward flanks of features).

The GPB shoal and associated lagoons dominate the sedimentary features offshore of the U.A.E. The GPB is developed on a shore-oblique Pleistocene structural hinge-line related to the Zagros fold-thrust belt (Lomando, 1999). At a maximum of 50 km wide (31 mi, dip direction) and 200 km (124 mi) in strike-parallel length, this shoal-complex is subdivided into three sub-environments by Hughes (1997): the subtidal/subaerial sand barrier, the enclosed backshoal lagoon, and the dip-parallel channels that dissect the Barrier. Grains in the GPB shoal are dominantly composed of cross-stratified rounded and angular mollusc and gastropod bioclasts (Bathurst, 1971; Hughes, 1997). Shallow-shoal grainstone deposits (6.6 ft, 2 m, at shallowest, average 16-33 ft, 5-10 m) transition in dip directions into deeper-water

foreshoal and lagoon packstones and wackestones with constituent grains similar to the shoal environment (Hughes, 1997). The dip-parallel channels (commonly 33 ft, 10 m deep; Hughes, 1997) offer limited connection of shoal and lagoon waters to the open Gulf, predominantly through tidal fluctuations. The tidal channels commonly terminate at flood and ebb tidal deltas where ooid formation and deposition is associated with channel-focused tidal agitation (Kendall and Skipwith, 1969a; Loreau and Purser, 1973). Additional ooid generation and deposition at coast and tide-parallel sand bars also shows strong tidal influences (Loreau and Purser, 1973).

Shoreward of the GPB, the Khor al Bazam and smaller restricted lagoons are characterized by protection from open Gulf waters by the GPB. Additional sedimentological characteristics of the lagoon include abundant bioclastic (molluscan and gastropod) and mud-peloidal sediments, and bioturbation by crabs, thalassinid shrimps, and worms (Kendall and Skipwith, 1969b; Evans *et al.*, 1973; Purser and Evans, 1973; and Hughes, 1997). Kendall and Skipwith (1969b) note the correlation of increased carbonate mud content in deposits positioned closer to the central lagoon axis, or away from shoal and coastal complexes. They also document “blackening of grains” in the lagoon axis, and correlate this phenomenon to an increase in reducing conditions with greater water depths in the lagoons.

The Khor al Bazam lagoon bathymetric profile shallows from maximum water depths of 82 feet (25 m) where it abuts open Gulf waters in the west, to where the GPB merges with the U.A.E. coastline c.a. 80 miles (130 km) to the east (Kendall and Skipwith, 1969a). Adjacent to the GPB complex, the northern lagoon margin is characterized by steep slopes, shoal spill-over, accretion of skeletal sand-wedges, and decimeter/meter-scale intercalation of low (mud) and high (sand) energy deposits (Purser and Evans, 1973) in the north, which contrasts with the gentle dips from the



lagoon axis toward the coastline in the south (Purser and Evans, 1973). The southern lagoon margin gently slopes from mud-rich reducing environments at the lagoon-axis up to intertidal and arid-supratidal environments (sabkha) at the Persian Gulf coastline.

#### Problems with the Persian Gulf as a TBR Analog

Differences in the depositional and geological settings of the Persian Gulf and TBR are, however, noteworthy when drawing comparisons between these systems. Chief among these issues are the contrasts in the climatic conditions and structural settings. The Persian Gulf is located in an arid climate, and therefore evaporite prone, whereas no evidence for evaporite deposition is shown in TBR core. The development and differentiation of depositional facies is strongly controlled by underlying structure in the Persian Gulf (Purser, 1973b; Lomando, 1999) where structure, antecedent topography, and salt diapirism contribute to the development of foreshoal bathymetric highs and the GPB complex. Michigan Basin structure is poorly understood during the time of TBR deposition, but it does not correspond to the tectonic drivers in the Persian Gulf.

A difference in general depositional morphology also makes direct comparison of these systems problematic. The Persian Gulf lagoons terminate up-dip at coastal deposits, which together with the GPB restricts lagoon waters, and results in limited circulation in the lagoons. Although the TBR shows development of restricted lagoons, rock data show no indication of regionally exposed coastline that contributed to this restriction.

### Comparable TBR Deposits in the Persian Gulf

Despite the issues with an actualistic comparison of the TBR with the modern Persian Gulf, components of these depositional systems show significant similarities. Outlined below are features common to these systems that offer insight into facies development and relationships in the TBR interval.

*Shoal:* The cross-stratification and mixing of rounded and angular grains, indicate high-energy deposition in both TBR and GPB shoal environments. Additional characteristics common to the GPB and TBR shoal facies include local hardground formation and the intercalation of shoal-sourced grainstones with lower energy packstones and wackestones. Although the recognition of hardground formation in the TBR core is limited, the prevalence of compound grains in shoal deposits indicates that early (or shallow-burial) cementation consolidated sediments sufficiently to maintain competent compound grains that were subsequently incorporated into active shoals. This implies that a relationship similar to the active shoals and local hardground formation at the GPB also occurred in the TBR. The intercalation of shoal sands with wackestone and packstone textures illustrates the close juxtaposition of these deposits and their respective high and low energy environments at the GPB. This interbedded relationship in TBR core suggests a similar juxtaposition of shoal grainstones (Facies 4), foreshoal packstones and wackestones (Facies 3), and backshoal lagoon (Facies 5) environments in the TBR depositional model (Figure 15) (e.g. French and Kerans, 2004).

*Semi-restricted lagoon:* The attributes of the GPB-backshoal Khor al Bazam lagoon gives insight into the shoal-protected semi-restricted lagoons in the TBR. Key features common to the TBR and Persian Gulf deposits are the restricted environments indicated by the reduced lagoon deposits, and the aforementioned

intercalation of the shoal and lagoon deposits. The documentation that reducing environments are more prevalent with greater water depths (Kendall and Skipwith, 1969b) suggests that the restriction of circulation in the Khor al Bazam may result in water column stratification, and therefore oxygen deficiencies at depth. Although no water depth relationship with reducing conditions can currently be established in the TBR lagoons, the association of shoal and reduced lagoon deposits in TBR facies stacking patterns suggests restricted energy conditions and circulation in TBR lagoons similar to those in the Persian Gulf.

*Shoal-lagoon complex:* Although the GPB dimensions are influenced by underlying structure, the close juxtaposition of the GPB shoal with lagoon environments is maintained over 200 km. It is reasonable, therefore, to assume that the TBR shoals (and associated lagoons) developed with comparable scales—that is, in discontinuous belts kilometers wide and 10's of kilometers parallel to strike directions. The dip-parallel channels that contribute to the discontinuous nature of the shoal are also associated with flood and ebb delta features at channel terminations. Although the tidal influence developing the flood and ebb tidal deltas in the modern GPB was likely less pronounced in the TBR, similar storm-surge, shoal spill-over (e.g. Figure 22), or possibly smaller tidal deltas are developed in locations adjoining TBR shoal deposits.

Because there is evidence supporting lagoon restriction, it is reasonable to conclude that the TBR lagoons formed surrounded by bathymetric relief that restricted the depression, such as within a wide bank (e.g. a depression within Facies 3), surrounded by shoals, between a shoal and an emergent tidal island, or a similar combination of positive features surrounding a depression. The bentonite-defined paleogeographic mapping indicates that a belt of shoals and intershoal lagoons

formed a complex facies belt in a strike elongate orientation (Figure 33).

#### Great Bahama Bank (GBB)

The GBB is a shallow (generally 23-33 ft, 7-10 m in depth) aerially extensive (37,000 mi<sup>2</sup>, 96,000 km<sup>2</sup>) humid-subtropical (22°-26°N Lat.) isolated carbonate platform (Tucker and Wright, 1990) (Figures 40 and 41). The present platform geometry developed through aggradation, progradation, and lateral accretion of smaller platforms that originally developed through tectonic activity (Eberli and Ginsburg, 1987).

The GBB is positioned such that dominant southeasterly trade winds traverse the platform (average 20-23 ft/s, 6-7 m/s), resulting in relatively high energy island, reef, and skeletal/oolitic sand shoal features developed at the eastern platform margin (Enos and Perkins, 1976; Bergman *et al.*, 2010). The GBB is tidally dominated (2.3 ft, 0.7 m average tidal amplitude, average velocities 1 ft/s, 0.32 m/s, but up to 6.5 ft/s, 2 m/s (Bergman *et al.*, 2010)), resulting in development of local tidal shoals, channels, and associated ebb and flood deltas at eastern platform margins. The focusing of these energies at the eastern margin of the GBB is a dominating control not only on the local development of high energy facies, but also on the development of the protected, lower energy platform interior leeward of the marginal positive features (Bergman *et al.*, 2010). The tidal flat complex developed on the low energy western (leeward) side of Andros Island also exemplifies this energy-orientation relationship with facies development.

Constituting the aerial majority of GBB, the platform interior has previously been characterized by heavily bioturbated, muddy peloidal “blanket” sands with a dominant packstone texture deposited below fair-weather wave-base and above storm

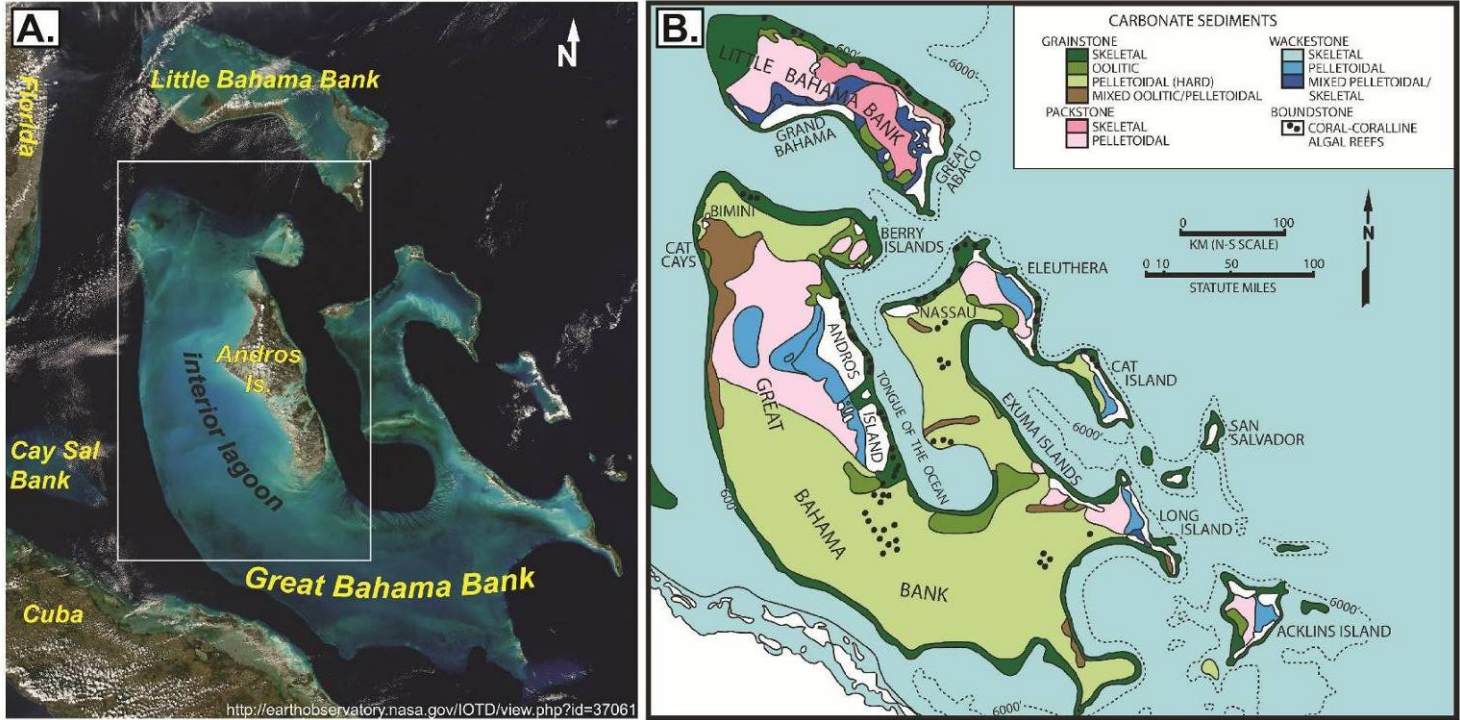


Figure 40. Satellite image showing the Great Bahama Bank and general facies map of the Great Bahama Bank. (GBB = Great Bahama Bank). Water depth in A. is generally indicated by color, where light blue represents shallow (c.a. less than 25 m) and dark blue corresponds to deeper water. Packstone, wackestone, and light green grainstone textures in B. are bioturbated peloidal and skeletal deposits similar to those deposited on the TBR platform (note the widespread shallow water environments in the platform interior—labeled here as “interior lagoon”). White box in A. is the location of Figure 41 maps. A. Image provided courtesy of NASA; B. Modified from Enos, 1974.

wave-base (Figure 40) (Ball, 1967; Enos, 1983; Tedesco and Wanless, 1990; Bergman *et al.*, 2010). However, recent study of the interior platform facies shows heterogeneity in the “blanket sands” (Reijmer *et al.*, 2009) (Figure 41). The low-relief platform interior deposits are marked on the surface by few GBB-interior wind-generated shoals that form isolated bathymetric highs (Bergman *et al.*, 2010) on the interior platform and at the western platform margin (Ball, 1967). Although facies variability on the GBB interior platform is recognized, published literature points toward no consensus regarding the controls on this variability: Bergman *et al.*, (2010) suggest wind generated currents as the principle controlling mechanism; Ball (1967) attributes the development of high-energy facies or shoals in the GBB interior lagoon to storm-action.

Sediments in the GBB-interior are predominantly homogenized through pervasive bioturbation (Ball, 1967). The burrowing organisms in this environment—specifically the decapod shrimp *Callinassa*—produce fecal grains and extensive burrow networks (Shinn, 1968; Bathurst, 1975; Elkdale *et al.*, 1984; Tedesco and Wanless, 1990). Coarse-grained, high-energy storm-lags, and local hardground horizons show preserved bedding planes, and constitute the majority of recognizable sedimentary structures remaining after burrowing-homogenization of sediments (Ball, 1967). Tropical cyclones (ranging in recurrence from 16 in 100 years, Ball, 1967; to

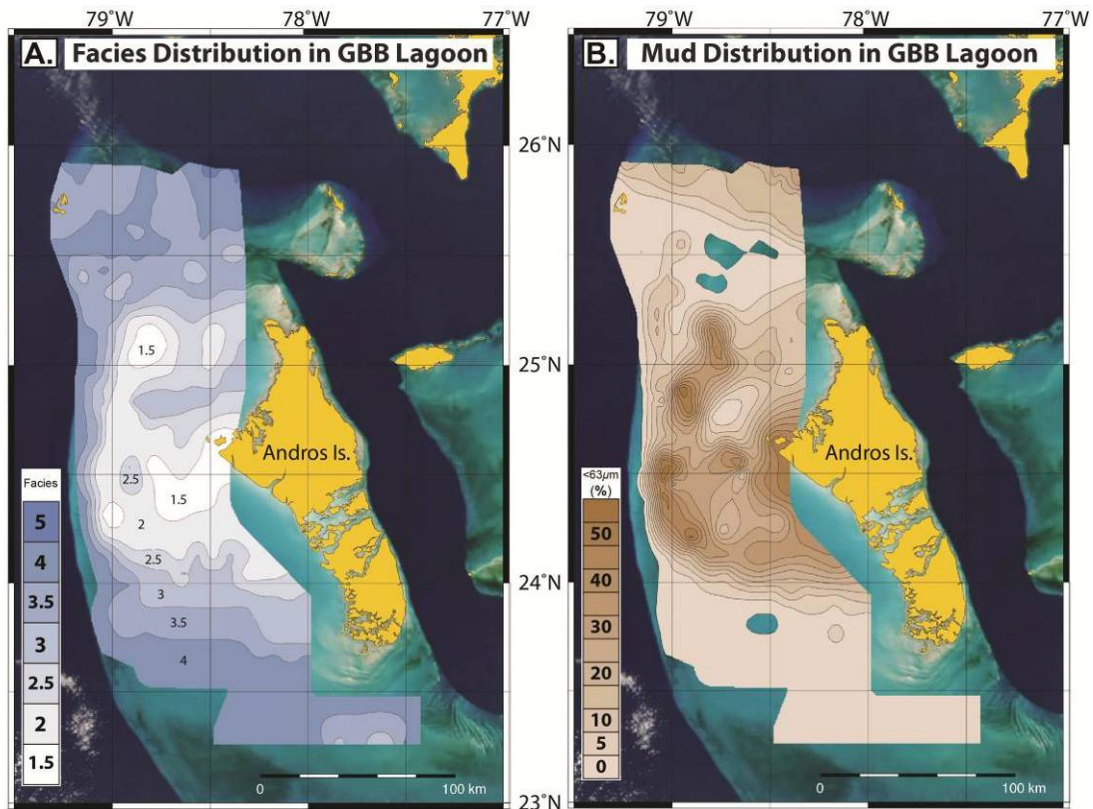


Figure 41. Maps showing detailed facies (A.) and carbonate mud distribution (B.) in the GBB interior lagoon. A. facies: Mud-rich wackestone = 1.5; Wackestone = 2; Mud-rich packstone = 2.5; Packstone = 3; Mud-lean packstone = 3.5; Grainstone = 4; Rudstone = 5. Facies distribution shows somewhat concentric relationships in which textures transition in a complex mosaic. Mud fraction distribution (B.) also shows complex, concentric-gradational distributions over the interior lagoon. The facies and mud-abundance mosaic distribution in the interior GBB platform share a striking similarity to the facies distributions in TBR paleogeographic reconstructions. (Figures modified from Reijmer *et al.*, 2009).

4-5 storms in 10 years, Meyer *et al.*, 2003) and seasonal winter storms frequently traverse the GBB, episodically elevating platform interior hydrodynamic conditions. Although the affect of high energy storm conditions in the platform interior is evident in lag-deposits and coarse-grain burrow fills, the degree that storms impact



sedimentation patterns and facies morphology/geometry on the platform top is disagreed upon by some researchers (Ball, 1967; Hine, 1977; Rankey *et al.*, 2004; Rankey, 2009; and Reeder and Rankey, 2009).

#### Problems with the GBB as a TBR Analog

The fundamental difference between Michigan Basin TBR deposits and the GBB is that this modern environment exists on an isolated carbonate platform surrounded by open deep water (>200 m, 656 ft) ocean, whereas the TBR-study area was deposited surrounded by epeiric seas in an interior cratonic position. The platform margin and slope environments adjoining the GBB illustrate the differences between isolated platforms and ramp geometries. The steep margin-slope geometries of the GBB strongly controls the tidal circulation on the platform, where tidal exchange with open ocean waters at the platform margin is sufficient to develop high energy shoals and associated ooid production. This contrasts with the Michigan Basin TBR where tidal energies were likely relatively lower because of dampening by surrounding shallow seas and regional arches.

#### Comparable TBR Deposits on the GBB

Like the Persian Gulf, a direct comparison between all aspects of the TBR and GBB is limited by differences in geological setting. However, also as with the Persian Gulf, components of the GBB depositional system offer key insights into facies development and relationships in the TBR.

*Mid and outer ramp facies:* Facies mapping on the GBB platform interior show concentrically deposited sediment bodies that transition laterally into adjacent facies in a mosaic distribution (Reijmer *et al.*, 2009). This study's depositional

system reconstructions from core indicate a comparable facies mosaic in mid and outer ramp environments of the TBR. Like the mid and outer ramp TBR, the GBB interior platform shows a range of textures from wackestone to grainstone, where muddy textures show variable mud fractions (Figure 41) (Reijmer *et al.*, 2009). Although no study conducted to date specifically details the controls on the facies variability on the GBB interior platform (Figure 41), fair-weather wind (Bergman *et al.*, 2010) and storm (Ball, 1967) generated currents are proposed as likely hydrodynamic formation mechanisms for the facies mosaic. Observations in core indicate that a similar facies mosaic developed in TBR in response to, or because of variable bathymetry. The controls and formation mechanisms for the TBR mid and outer ramp variable bathymetry and associated facies mosaic will be further discussed in the Analog Synthesis section.

*Bioturbation:* The GBB example is instructive in better understanding the pervasive bioturbation shown in mid-ramp facies in TBR core (Figure 40b). Shinn (1968) shows that the majority of the GBB platform interior west of Andros Island is subjected to extensive bioturbation by the decapod shrimp *Callinasa*, which generates modern burrow networks analogous to the TBR *Thalassinoides*-type burrows. Shinn's work, with support from later work by Tedesco and Wanless (1988), additionally shows that the majority of burrows are preserved in the rock record through the filling of burrow voids by sediments that contrast with the burrowed substrate (commonly coarser grained sediments filling the burrows). Burrow filling sediments also preserve the evidence of bioturbation in the TBR, where burrow overlap commonly results in the development of coarse grained networks (Schulz, 2011) (see Figure 7). These observations in the modern GBB interior platform settings, combined with facies interpretations, support that the TBR

was deposited on a relatively shallow platform environment where burrowing organisms thrived.

### Analog Synthesis

The ultimate goal of incorporating modern analogs into depositional modeling of ancient systems is to depict the interpreted system with realistic sedimentary attributes. At the very least, modern depositional environments provide insight into facies attributes at a 2-D depositional surface with limited data regarding topographic relief, or depth dimension (3-D) of the analogous ancient system. These modern datasets provide crucial sedimentological information, especially when reconstructing a stratigraphic framework at identified 2-D isochronous surfaces (i.e. chrono- and/or sequence stratigraphy), such as done here in the TBR.

The TBR facies show strong similarities to the GPB shoal-lagoon complex, and the GBB interior platform deposits. In each of these modern settings lower-energy, pervasively bioturbated packstones and wackestones coexist with higher-energy sand shoals and/or mud winnowed sediment bodies distributed in a complex facies mosaic. A similar facies mosaic is shown in the facies distributions and the relationship between low and higher-energy deposits at the bentonite-defined surfaces in the TBR.

### Development of the Facies Mosaic

Unresolved through this discussion of modern depositional analogs, however, are the processes by which facies are developed in the mosaic distribution on the TBR platform. Comparing and contrasting the modern analogs, along with ancient depositional analogs may offer insight into these processes.

*Variable bathymetry—facies and controls:* Although some of the Persian Gulf's texturally mature foreshoal deposits are documented as structurally generated (Purser, 1973b), facies mapping shows that the development of isolated bathymetric highs and associated texturally mature sediment bodies is not limited to structural features (Wagner and van der Togt, 1973; Wilkinson and Drummond, 2004), indicating hydrodynamic controls. Facies mapping on the GBB interior platform (Reijmer *et al.*, 2009) also indicates that the control on texture and facies distribution is not limited to the platform dominating eastern margin energy-barriers. The question pertinent to facies development in the TBR is then, what factors other than structure (GPB) and barriers (Andros Island, GBB) cause the development of these modern mosaic facies distributions?

The facies variability on the GBB platform interior and the mid and outer ramp environments of the TBR are likely the result of the interplay between tidal, wind, and storm generated currents. Fringing reefs on windward margins in the Persian Gulf likely influence sedimentation on mid ramp bathymetrically positive features by providing sediment and an energy barrier resulting in sediment stabilization (Purser, 1973b). What this biologic influence on Persian Gulf "shoal" development outlines is the lack of biologic controls on the development of similar facies patterns (geometries) in the GBB platform interior as they are shown in facies maps (Reijmer *et al.*, 2009; Figure 41), and paleogeographic reconstructions in the TBR (Figure 33). This implies that, unlike the structural and biologic controls on the mid-ramp analogous Persian Gulf deposits, the GBB interior platform and TBR mid and outer ramp deposits are fundamentally controlled through the distribution of hydrographic energy.

Published research indicates that the facies distribution on the GBB platform

interior is likely developed through wind and storm generated currents. As tidal influence is diminished but not eliminated in the interior platform, it is likely that the combined effects of tidal action, wind driven currents, and episodic high-energy storms sculpt the observed depositional morphology and associated textures/facies. The TBR mid-ramp facies likely also developed in response to the focusing of variable sources of hydraulic energies, in addition to the previously outlined autogenic facies controls (e.g. sediment compaction).

A similar combination of tidal and storm influence developing a facies mosaic of tidal-island complexes is hypothesized by Pratt and James (1986). In this model they propose that rather than an expansive channelized tidal flat occupying the entirety of the shelf, Ordovician carbonates at the eastern margin of Laurentia (Newfoundland) are characterized by numerous low-relief supratidal islands surrounded by sub- and intertidal banks. This facies mosaic relationship was explained through a constructive relationship between tidal and storm activity. The model proposes that tidal exchange developed relatively broad tidal flow-pathways, which were further developed through the superimposition of episodic higher-energy storm-induced currents. The result of the constructive relationship between tidal and storm currents is the development of numerous isolated bathymetric highs. The model further proposes that the sediment “islands” migrate with tidal and storm current generated erosion and deposition. This model has been used to explain the development of bathymetric differentiation and the resulting facies mosaic in a Trenton Group paleoenvironmental reconstruction in a Michigan Basin flank (Ontario) outcrop study (Brookfield and Brett, 1988).

Neglected, however, in the Pratt and James tidal-island model, and in any previous Michigan Basin TBR model, is the influence of wind-driven currents on the

development of facies mosaics. The large aerial extent of inundation in the TBR Michigan Basin presented significant fetch beneath the southeasterly tradewinds. The Michigan Basin water surface area at TBR-time was larger than the GBB interior platform environment. Therefore it is reasonable to conclude that wind-driven currents similar to those influencing facies on the GBB were also generated in the Michigan Basin during TBR deposition.

It is proposed here that the TBR mid-ramp facies mosaic distributions (and implications of variable bathymetry therein) in the study area developed through a similar mechanism, considering the facies/textural distributions shown in the TBR paleogeographic reconstructions, analogous facies distributions of the GBB interior lagoon, the Pratt and James model for variable bathymetric topography development, and wind-driven currents in the Michigan Basin. The constructive hydrologic actions of diminished tidal flow and low-energy wind-driven currents likely provided a broad channel in which storm surge/currents further sculpted the seafloor morphology.

*Peritidal facies:* The TBR inner ramp facies geometries also likely developed through the combined tide, storm, and wind-driven hydraulic action, as outlined above. In both the GBB and Persian Gulf examples the intertidal components are predominantly connected to a subaerially exposed land mass. This contrasts with the TBR peritidal system because of the apparent lack of exposed land in the region, at least based upon available core. The development of TBR intertidal deposits can, however, be explained through applying the Pratt and James tidal-island model in the context in which it was developed: intertidal deposits. This would constitute all of the factors outlined in the above discussion of the application of the Pratt and James model to TBR mid ramp facies, with the exception of a relatively shallower depositional setting where the positive relief (shallower) features represent tidal

deposits. It is noteworthy to acknowledge that upper intertidal or supratidal deposits likely exist in the TBR interval and simply are not captured and/or preserved in the available core.

### Summary of Depositional Reconstruction

The depositional system of the TBR interval is considerably more complex than previously published accounts favoring layer cake sedimentation and stratigraphy. Facies analysis from core shows that the TBR depositional environments are consistent with a storm-dominated low-declivity epeiric ramp, characterized by inner, mid, and outer ramp sub-environments. Mapping of cross-sections and paleogeographic depositional surfaces with K-bentonite constraints indicates that the facies were deposited in heterogeneous mosaics within these sub-environments with well-defined depositional strike-dip orientations. The integration of modern analogs and ancient depositional models into depositional environment reconstruction of the TBR provides substantial support to interpretations made from core and mapping. Furthermore, the facies heterogeneities and striking similarities between the TBR deposits and modern analogs show the insufficiencies in designating this, or likely most any neritic carbonate interval, as characterized by blanket sedimentation and layer cake stratigraphy without a detailed facies analysis.



## RESERVOIR ASPECTS

The reservoir aspect of this study was limited to core data acquired within the structurally defined Albion-Scipio trend and Stoney Point field (Table 1) because HTD reservoir-quality development is fundamentally dependent on structural controls (i.e. Figures 6 and 11). It is noteworthy that at reservoir scale (km-scale) HTD processes are fundamentally controlled by structure, and therefore the position of cores relative to primary structural features (i.e. faults) also controls the development of reservoir attributes. Although fault/fracture distribution data is limited, core used in this study is considered representative of the reservoirs as a whole because of the spread in core distribution (Figure 12) and variation in reservoir aspects in the cores over all of the depositional facies.

Although HTD processes generate reservoir quality with variable lateral extent, well control in the study area shows that HTD processes are spatially limited to approximately one kilometer away from the primary fault zones. Therefore, non-reservoir limestone core data attained tens of kilometers outside of these zones is omitted from this discussion of reservoir aspects. Additionally, reservoir analysis does not include Facies 7—K-bentonites—because of resolution limitations of whole core analysis data.

### Reservoir Type

In order to test the hypothesis that depositional facies control HTD reservoir quality development away from primary faults, reservoir type must be defined (Table 4). The goal of differentiating reservoir type is to identify petrophysically similar rocks-types from core and whole core analysis so that these and additional reservoir

attributes (Table 5) can be evaluated in the context of depositional facies.

Considering the available quantitative reservoir data, measured permeability ( $K$ ) best represents the reservoir type because these values reflect pore connectivity and the overall pore network, and to a degree pore types. The division of petrophysical data into reservoir type is designed to account for the skewing of calculated averages in fractured (FR, permeability values  $\geq 1000$  mD), non-fractured (NF, permeability values  $< 1000$  mD), producible (PD, permeability values  $> 0.1$  mD), non-productible (NP, permeability values  $\leq 0.1$  mD), and high-quality (HQ, permeability values between 0.1 and 1000 mD) reservoir intervals of the formation. Although the TBR HTD reservoirs undoubtedly contain fractures and faults, in order to best represent meaningful statistical metrics of petrophysical data the NF reservoir-type is used as the primary definition of reservoir in this discussion (Figure 42). The HQ reservoir-type is used for the comparison of reservoir quality where average values are not affected by FR or NP data, allowing for the examination of these values where all rock is reservoir.

<b>Reservoir Types</b>	<b>Abbreviation</b>	<b>Lower <math>K</math> cut-off (mD)</b>	<b>Upper <math>K</math> cut-off (mD)</b>
<b>Gross</b>	<b>GR</b>	n-a	n-a
<b>Fractured</b>	<b>FR</b>	$\geq 1,000$	n-a
<b>Non-Fractured</b>	<b>NF</b>	n-a	$< 1,000$
<b>Non-Productible</b>	<b>NP</b>	n-a	$\leq 0.1$
<b>Producible</b>	<b>PD</b>	$> 0.1$	n-a
<b>High-Quality</b>	<b>HQ</b>	$> 0.1$	$< 1,000$

Table 4. Individual reservoir types defined with minimum and maximum permeability values. GR includes all whole core analysis ( $K$ ,  $\Phi$ ) data. FR denotes core samples with permeability measurements that exceed a permeability cut-off assumed here to represent fracture conduits, where NF includes all data with the FR removed. NP constitutes rock with extremely low permeability, where PD represents GR data with NP removed. HQ reservoir contains permeabilities between NP and FR

maximum and minimum constraints, respectively. NF reservoir is the reservoir-type used in the discussion of reservoir aspects of the TBR unless otherwise noted. Permeability ( $K$ ) is measured in milli-Darcies

Reservoir Attributes		F1	F2	F3	F4	F5	F6		
Lith.	limestone%	15	7	20	15	16	0		
	dolomitic limestone%	0	18	13	6	18	0		
	dolomite%	85	84	67	79	66	100		
Petrophysical Attributes	Dominant pore types		VU, IX	IX, VU	IX, MO, VU	IX	IX, MO, VU	VU, FE, MO	
	Feet fractured (% total)		0	113 (19)	63 (11)	7 (13)	11 (11)	3 (18)	
	Feet with ZVU (% total)		6 (21)	217 (37)	115 (20)	3 (6)	0	0	
	Average $\Phi$ (%) and $K$ (mD)	Gross: All Whole Core Data	$\Phi$	3.0	3.4	3.4	3.6	3.7	4.1
			$K$	2.5	187.4	86.9	84.3	28.3	5.5
			$n$	26	407	449	51	81	13
		Fractured (F) ( $K \geq 1,000$ mD)	$\Phi$	n-a	6.9	5.8	2.4	n-a	n-a
			$K$	n-a	6,065.0	4,165.3	3,000.0	n-a	n-a
			$n$	0	12	8	1	0	0
		Non-Fractured (NF) ( $K < 1,000$ mD)	$\Phi$	3.0	3.3	3.3	3.6	3.7	4.1
			$K$	2.5	8.8	12.9	25.9	28.3	5.5
			$n$	26	395	441	50	81	13
		Producible Reservoir ( $K > 0.1$ mD)	$\Phi$	3.8	5.1	4.5	4.6	5.9	4.7
			$K$	4.8	453.8	175.7	138.5	54.4	10.1
			$n$	13	168	222	31	42	7
HQ Reservoir ( $K > 0.1$ , <1,000mD)		$\Phi$	3.8	5.0	4.4	4.7	5.9	4.7	
		$K$	4.8	22.2	26.5	43.2	54.4	10.1	
		$n$	13	156	214	30	42	7	

Table 5. Summary of reservoir attributes and reservoir-types compared with depositional facies. Lithology (Lith.) gives indication to the amount (%) of ft) of examined core that was partially or completely dolomitized by HTD processes. Dominant pore types show indicate the pores that contribute a minimum of 20% to the total occurrence of facies porosity, where the dominant type is listed first (VU = vugular, FE = fenestral, MO = moldic, IX = intercrystalline, ZVU = zebra-fabric vug). “Feet fractured” and “Feet with ZVU” show the measurement of feet and the percentage of facies gross footage (in parentheses after ft value) containing fractures and ZVU textures, respectively. Average porosity ( $\Phi$  in %) and permeability ( $K$  in mD) calculations show values for individual depositional facies within defined reservoir-types. The average values show the benefit of removing NR (values not shown, but contained in GR) and FR ( $n$ =number of measurements), in that average

permeability varies over orders of magnitude while porosity values remain relatively constant when the extremes are removed. Focusing on the NF (and HQ) reservoir-types thereby gives representative depositional facies permeability values for majority of reservoir rock without substantially altering porosity values or removing numerous data points.

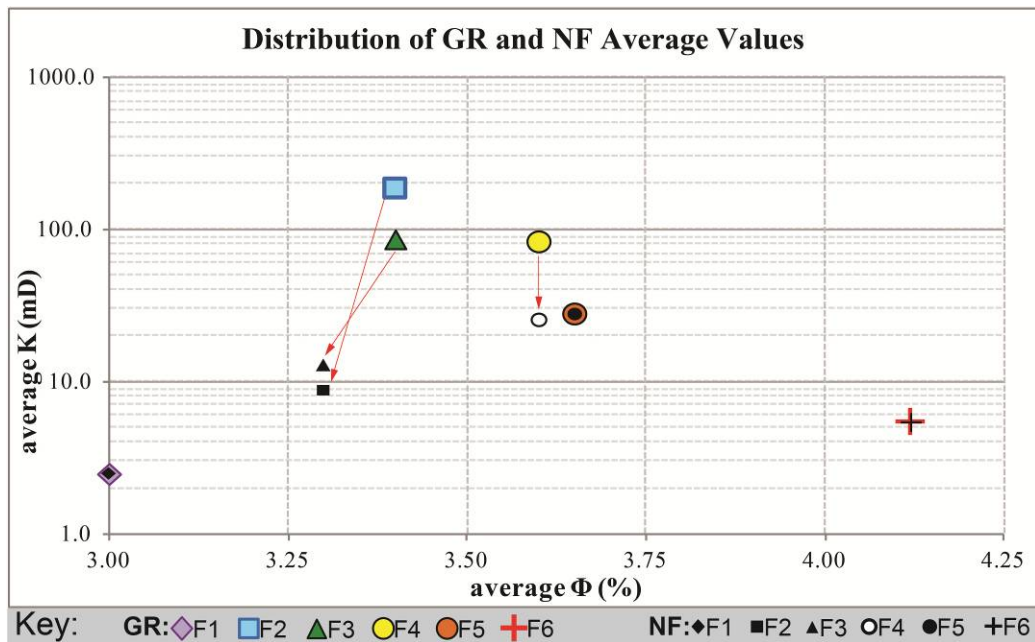


Figure 42. Plot showing the porosity-permeability relationships for GR and NF reservoir-types. Red arrows indicate the shift in values from GR to NF when FR reservoir-types are removed. This shows that the FR reservoir data skew average permeabilities over an order of magnitude, and also that removing the FR data changes average porosities by a fraction of a percent. Because the limited FR data alters average permeability values significantly, removing these values gives a more representative mean values for facies throughout the reservoirs. Note Facies 1, 5, and 6 contain no FR reservoir type, and therefore NF and GR values are equal.

### Comparison of Reservoir and Depositional Aspects

The evaluation of reservoir potential and attributes within depositional and stratigraphic subdivisions and trends contributes to the understanding of how

reservoir distribution and quality is related to those aspects in the TBR. Depositional reconstructions show that depositional and stratigraphic controls are genetically linked in the TBR. Therefore, if relationships between depositional and reservoir aspects are established, then the ties between depositional fabric (i.e. facies), facies geometries, facies associations, and the stratigraphic organization in facies stacking patterns provide a better understanding of the distribution of reservoir quality in the subsurface. Moreover, with a positive correlation of reservoir parameters with depositional aspects it may be possible to develop a tool utilizing depositional reconstruction constraints for reservoir quality prediction away from observations.

#### Depositional Facies vs. Reservoir Attributes and Type

The variability in reservoir type observed during core description and evident in whole core porosity and permeability data, suggests that additional semi-quantitative reservoir attribute data regarding lithology (mineralogy), fracture, and pore type (Table 5) are necessary to supplement whole core measurements (Figure 43). The reservoir attributes illustrate the highly heterogeneous nature of reservoir in this interval, while outlining subtle trends within depositional facies divisions.

The core lithologies indicate that each depositional facies is highly dolomitized (60-100% of core described). However, each depositional facies, with the exception of Facies 6, contain intervals within the Albion-Scipio trend and Stoney Point field that remain limestone. Reservoir heterogeneity is also outlined by the variability in dominant pore type and the distribution of fracture and zebra vug intervals in the facies. Reservoir attributes show identifiable relationships with depositional facies, where some attributes show good correlation within depositional divisions. Relationships between reservoir attributes and depositional facies are

outlined below.

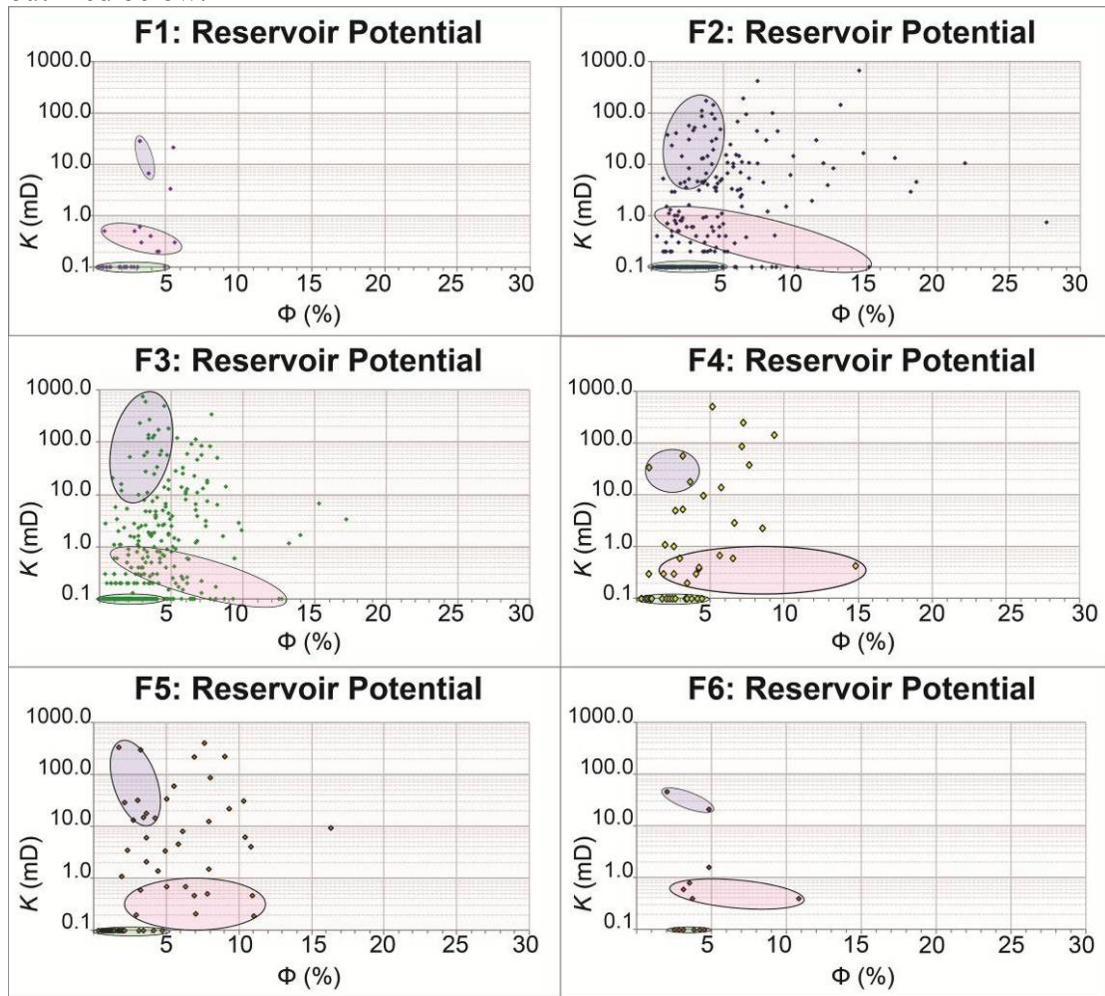


Figure 43. Porosity vs. permeability cross-plots showing NF reservoir data for individual depositional facies. Blue circles outline moderate to high-permeability ( $K$ ), low porosity ( $\Phi$ ) data field. These data are attributed to fractures or touching vugs (including those found in association with zebra-fabric) and low matrix porosities and permeabilities. Red circles outline moderate to high-porosity, low permeability data. NP reservoir-type (green circles) plot along the x-axis, indicating that any existing pores are completely isolated. Plotting porosity-permeability relationships gives insight into the occurrence of reservoir quality in the individual depositional facies (F).

Dominant pore type shows a positive correlation with HQ reservoir-type permeabilities, where depositional facies with a dominant intercrystalline pore type

(F2, 3, 4, and 5) record average permeabilities increased by greater than 10 mD relative to the other facies. Average porosity measurements for the HQ reservoir show consistent values around 5%. These porosity and permeability values for the HQ reservoir-type support Thornton's (2011) conclusion that intercrystalline pore type contributes significantly to the overall rock permeability.

Fracture and vug development in TBR rocks is variable in the context of depositional facies. Fractures are developed in all depositional facies except Facies 1. Facies 2 contains the highest fractured-feet percentage. Zebra fabric and the characteristic bedding parallel vugs (see Figure 9) are developed dominantly in the mid and outer ramp facies (Facies 1, 2, and 3). The dominance of mid ramp Facies 2 and 3 in the TBR interval core (90% of all core) may generally explain the prevalence of zebra fabric associated with these rock types, as they volumetrically constitute the majority of the interval subjected to HTD-alteration.

#### Primary and Secondary Reservoir

Reservoir attributes and porosity-permeability cross plots show that depositional Facies 3 constitutes the primary NF reservoir in the TBR. Facies 2 is considered secondary in terms of reservoir quality, based on relatively lower average permeability measurements for NF reservoir and a prevalence of isolated pores.

*Facies 3:* Averages of NF reservoir-type whole core measurements show well developed permeabilities (12 mD) in Facies 3, with porosity comparable to all facies (c.a. 3%). Intercrystalline is the dominant pore-type in this facies, and is primarily associated with high-permeability zones in burrow networks (Thornton, 2011) (Figure 44). Because burrows overlap in three-dimensions, deposits with intercrystalline porosity development associated with burrow-filling sediments create



porous-permeable networks of reservoir quality. Intercrystalline porosity in burrow networks and grain-beds significantly contribute to reservoir quality in the Facies 3 primary TBR reservoir. Moldic/vuggy pores are the secondary pore type in Facies 3.

*Facies 2:* Non-fractured average permeabilities are lower in Facies 2 relative to Facies 3. Intercrystalline porosity is the dominant pore-type in Facies 2, however, the development of isolated vugs and zebra fabric vugs is also prevalent in this facies, and therefore reservoir quality is considered secondary to the primary Facies 3 reservoir.

#### Reservoir Roles of Other Depositional Facies

The following section summarizes the quantitative porosity-permeability relationships in the NF reservoir-type for each depositional facies (Figure 43). Porosity-permeability data distributions (Figure 43) are divisible into petrophysically similar fields based on inferred pore types and associated permeabilities.

*Facies 1:* This facies likely acts as a baffle or barrier to vertical fluid flow in the TBR HTD reservoirs. Porosity-permeability relationships show three subsets of Facies 1: an impermeable and low porosity baffle, a low reservoir storage potential and well developed permeability field, and reservoir quality field. The well developed permeability field is likely related to portions (20%) of Facies 1 with zebra fabric development or partially filled fractures. The very low vertical permeability of the zebra-fabrics and overall low porosity and permeability of Facies 1 designate it as a reservoir baffle or barrier.

*Facies 4:* This facies shows NF average porosity and permeability values slightly higher than Facies 2 and 3. However, because this facies constitutes a minor amount of described core (< 5% total feet, average thickness 1.25 ft) it is

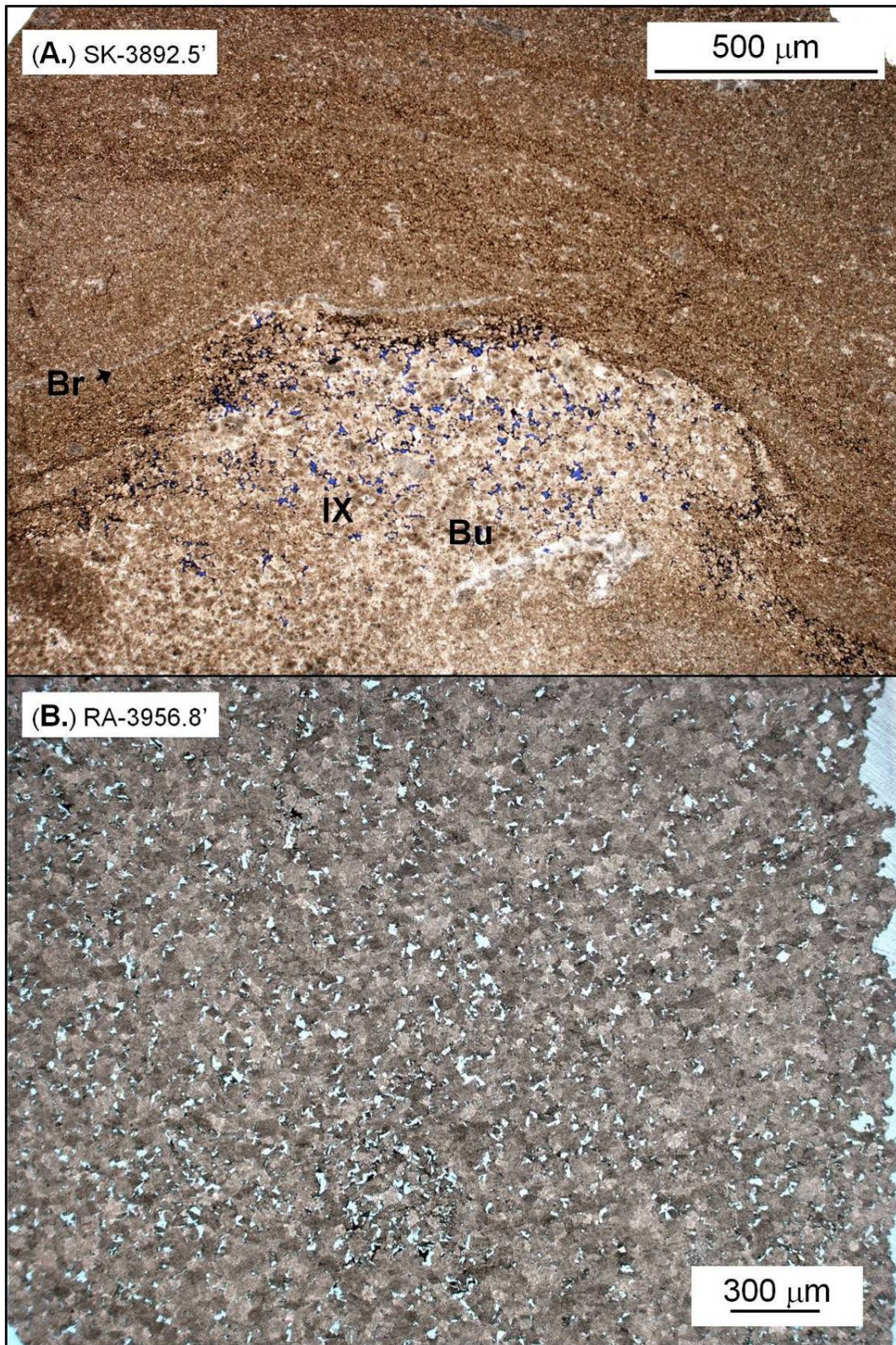




Figure 44. Thin-section photomicrographs showing intercrystalline porosity occurring in association with burrows in Facies 3. (A.) An individual burrow with intercrystalline porosity enclosed in non-porous matrix. (B.) Cross-section view of intercrystalline porosity distribution within a single burrow. B=brachiopod; IX=intercrystalline porosity; Bu=burrows.

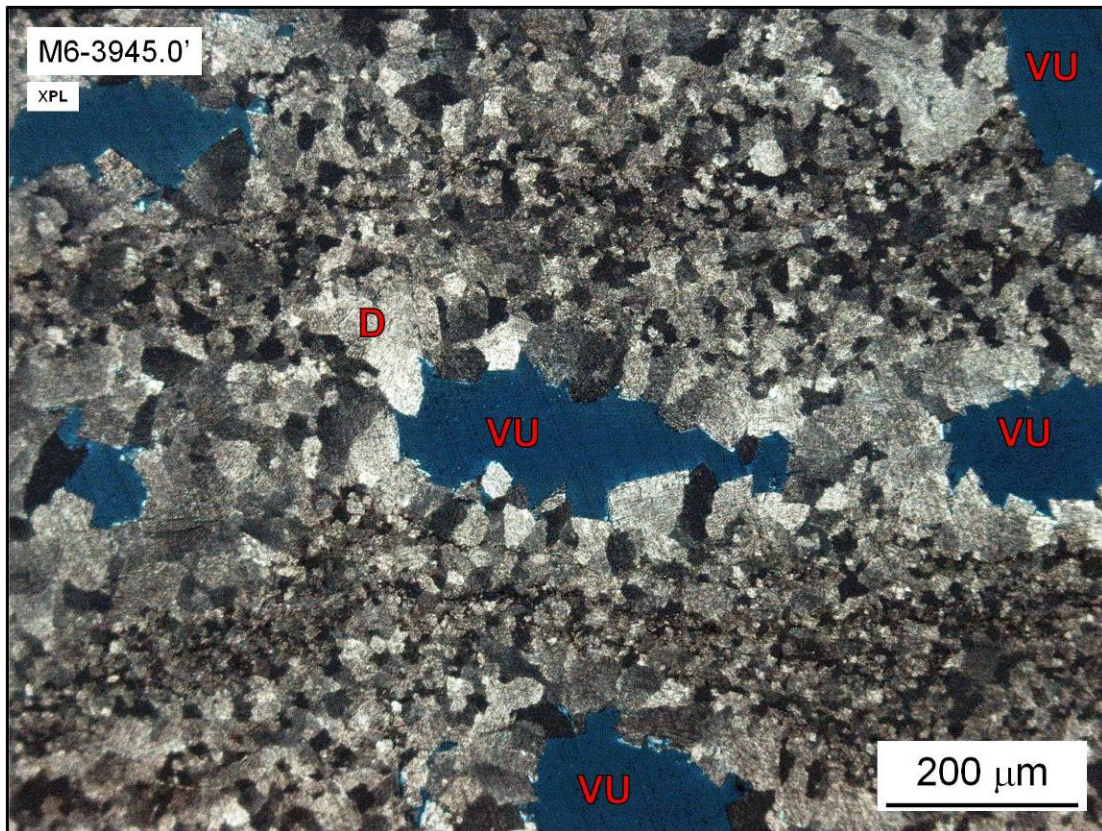


Figure 45. Thin-section photomicrograph showing isolated vug porosity occurring in dolomitized Facies 2. Although porosity values are high, permeability is low, owing to the isolation of pores in impermeable matrix. D=dolomite; VU=vug.

#### Reservoir Roles of Other Depositional Facies

The following section summarizes the quantitative porosity-permeability

relationships in the NF reservoir-type for each depositional facies (Figure 43). Porosity-permeability data distributions (Figure 43) are divisible into petrophysically similar fields based on inferred pore types and associated permeabilities.

*Facies 1:* This facies likely acts as a baffle or barrier to vertical fluid flow in the TBR HTD reservoirs. Porosity-permeability relationships show three subsets of Facies 1: an impermeable and low porosity baffle, a low reservoir storage potential and well developed permeability field, and reservoir quality field. The well developed permeability field is likely related to portions (20%) of Facies 1 with zebra fabric development or partially filled fractures. The very low vertical permeability of the zebra-fabrics and overall low porosity and permeability of Facies 1 designate it as a reservoir baffle or barrier.

*Facies 4:* This facies shows NF average porosity and permeability values slightly higher than Facies 2 and 3. However, because this facies constitutes a minor amount of described core (< 5% total feet, average thickness 1.25 ft) it is considerably less volumetrically significant than the primary reservoir, and considered as a tertiary level reservoir.

*Facies 5:* No clear correlation between porosity and permeability is shown in this facies. Reservoir quality in Facies 5 reflects the mottled texture characteristic of the depositional fabric and variety of pore types. A lack of significant fracture and zebra-fabric intervals (10% and 0%, respectively) show no dominant mechanical relationships to reservoir formation in Facies 5. Therefore, no clear relationships between depositional fabrics and HTD reservoir development exist in Facies 5.

*Facies 6:* The limited development and/or preservation of isolated fenestral birdseye and vertically oriented cylindrical pores in Facies 6 result in poor reservoir quality. A weak negative correlation exists between porosity and permeability in this

facies. The negative correlation is likely attributed to few (n=2) minor fractures recording moderate permeabilities (10 to 45 mD) with poorly developed porosity, and isolated fenestral and cylindrical pores with low permeabilities and moderate porosities. Facies 6 may act a baffle or barrier to fluid flow. This is supported by the assumption that the peritidal environment was likely subjected to early diagenesis/cementation which preserved the characteristic fenestral and cylindrical pores through burial (e.g. Shinn *et al.*, 1980; Shinn, 1983a).

#### NF Reservoir-type vs. T-R Trends in Facies Stacking Patterns

Primary reservoir (Facies 3) porosity and permeability trends show an apparent correlation of reservoir quality development with T-R trends in the facies stacking pattern framework (Figures 46 and 47). Patterns in reservoir quality development are also evident in the comparison of different scales of stacking patterns (i.e. large-scale vs. HFS sequences). The analysis of patterns in these data groupings (T or R, large or HFS) places reservoir quality development in depositional and stratigraphic contexts, thereby enhancing predictability of reservoir distribution. This analysis indicates the degree that changes in relative sea level controlled HTD reservoir formation processes, through its control on depositional fabrics.

In order to evaluate reservoir quality distribution in the facies stacking pattern framework, porosity and permeability data are reduced to average and median values. Utilizing both of these statistical metrics allows for their comparison, which further constrains reservoir relationships within the stratigraphic framework (Figures 46 and 47). The median values aid in this analysis through accounting for the skewing of mean values by outliers in data populations.

*Porosity trends:* Analysis of NF reservoir data within the facies stacking

pattern framework shows that primary and secondary reservoir (Facies 3 and 2) porosities are preferentially developed in transgressive (T) trends. Primary and secondary reservoir porosities show higher porosities for T relative to regressive (R) trends at the large-scale (Figure 46, plots C.—D.). Comparisons additionally indicate that primary and secondary reservoir porosities are relatively higher at HFSs (vs. large) when considering only R trends (Figure 46, plots E.—F.). The accessory reservoirs in Facies 4 and 5, however, show opposing trends: higher porosities developed in large-scale R relative to large-scale T (Figure 46, plots C.—D.); higher porosity in HFS R relative to large-scale R (Figure 46, plots E.—F.). Primary reservoir porosity is also slightly higher at the large-scale relative to the HFS in exclusively T trends (Figure 46, plots G.—H.).

*Permeability trends:* Plotting NF reservoir data with facies stacking pattern constraints indicates that primary reservoir permeabilities are also relatively higher in T relative to R trends at the large-scale (Figure 44, plots C.—D.). The primary reservoir permeability trends also reflect the above porosity trends with relatively higher values for HFSs (vs. large) when considering only R trends (Figure 47, plots E.—F.) and large-scale relative to the HFS in exclusively T trends (Figure 47, plots G.—H.).

The analysis of patterns of permeability data distribution with depositional and stratigraphic parameters gives an established sedimentological framework to evaluate reservoir quality distribution. Moreover, the general agreement in porosity and permeability trends for the primary reservoir division show a link between porosity, permeability, depositional facies, and stratigraphic hierarchy.

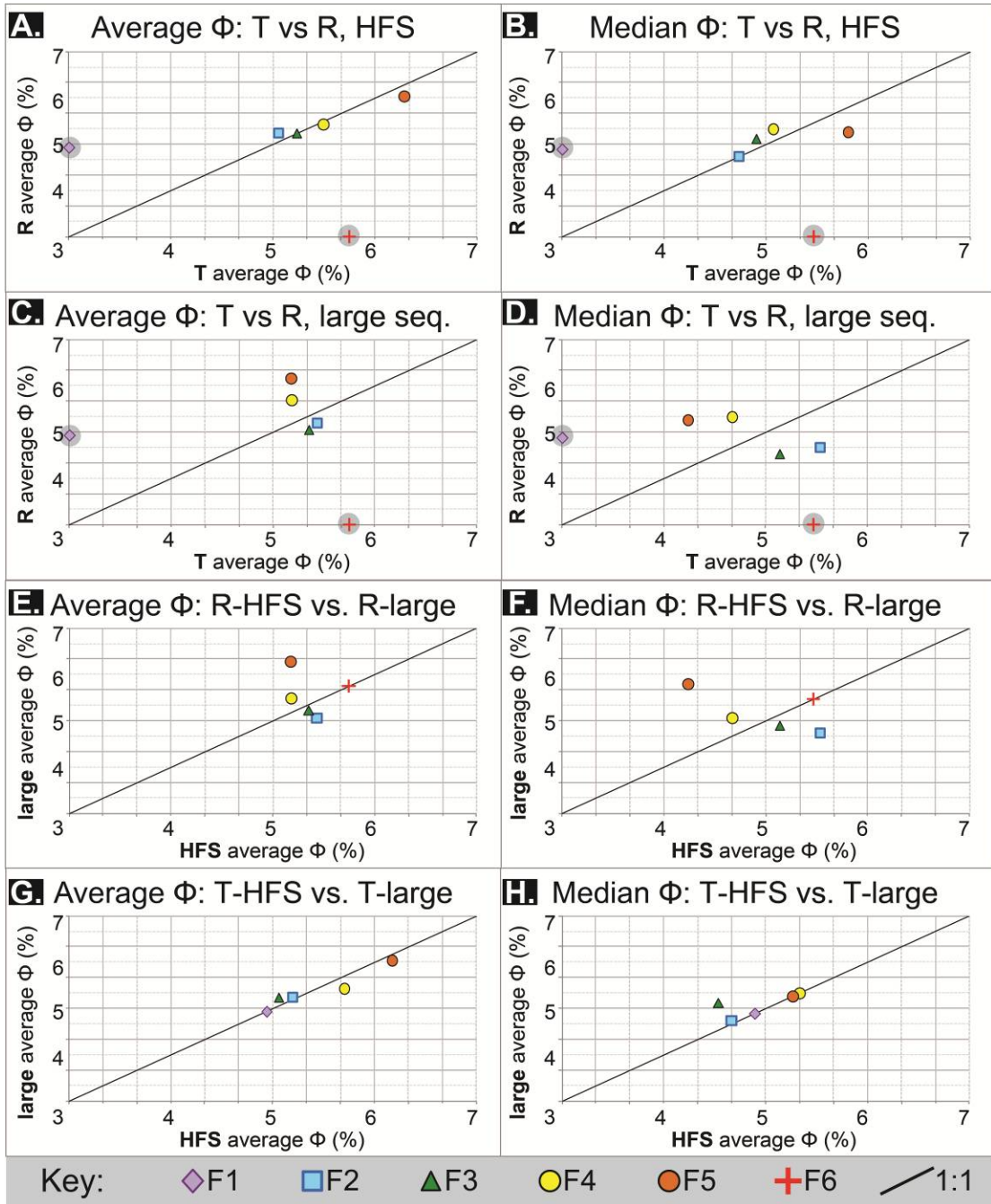


Figure 46. Plots showing facies relations of average and median NF porosity variability with position in T and R trends in large and HFS sequence hierarchy. For reference the 1:1 line is also plotted. Displacement off the 1:1 line indicates higher average values for the data population plotted on the axis toward which the point is displaced. This displacement



suggests that porosity ( $\Phi$ ) is preferentially developed in a given trend (e.g. higher primary reservoir porosity in T trends, plots C. and D.) or facies stacking hierarchical position (e.g. higher primary reservoir porosity at the HFS for R trends, plots E. and F.). Data points outlined in gray circle indicate null values for the opposing axis. Plots exclusively showing R (E. and F.) and T (G. and H.) do not contain F1 or F6, respectively, because these facies are not present in those stacking intervals.

### Facies and Stacking Pattern Controls on Reservoir Quality Distribution

The relationship of the NF reservoir-type with porosity and permeability indicate that facies stacking pattern trends (and inferred relative sea level trends) are useful as an aid in defining reservoir quality distribution in core, and provides a possible predictive tool for reservoir distribution in the TBR interval. The reservoir quality relationship with stratigraphic trend is likely a function of changes in accommodation controlling depositional fabric in the facies, rather than regional syndepositional/early burial diagenetic events, as no indication of such widespread event is shown in core (e.g. exposure and dissolution). The trends in primary and secondary reservoir porosity, permeability, and HTD distribution/character are likely related to the depositional fabric of Facies 2 and 3. The following section contains interpretations and hypothetical explanations of these relationships.

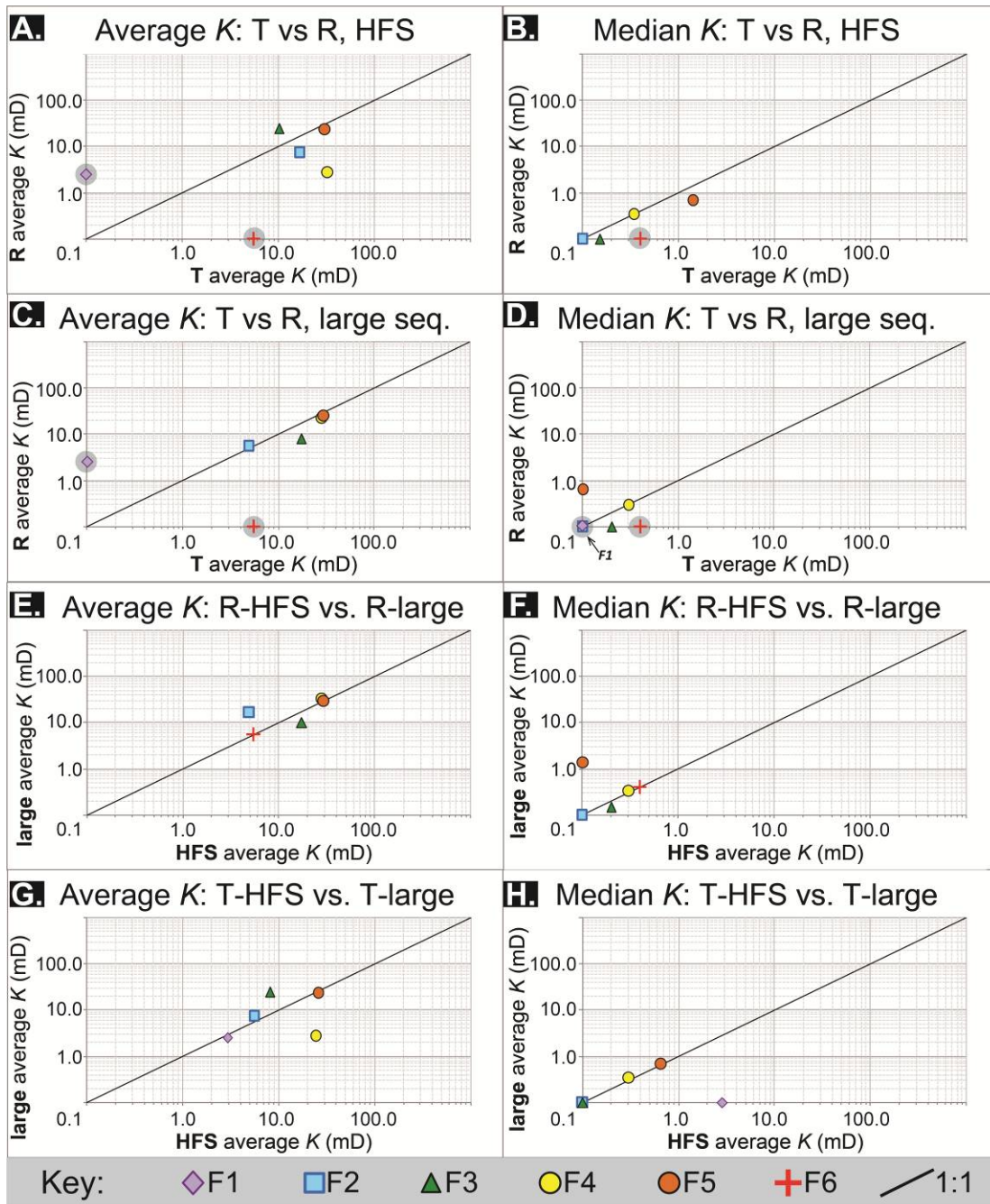


Figure 47. Plots showing average and median NF permeability variability with position in T and R trends and large and HFS sequence hierarchy. Permeability values are plotted with reference to a 1:1 line. Displacements from the 1:1 line indicate permeability ( $K$ ) trends similar to those shown in porosity plots (Figure 46) (e.g. higher primary reservoir permeability in T trends, plots C. and D.; higher primary

reservoir permeability at the HFS for R trends, plots E. and F.). Data points outlined in gray circle indicate null values for the opposing axis. Plots exclusively showing R (E. and F.) and T (G. and H.) do not contain F1 or F6, respectively, because these facies are not present in those stacking intervals.

### Controls on Reservoir Quality Distribution

The prevalence of zebra fabric and fracture development in Facies 2 relative to other volumetrically significant facies (i.e. Facies 3) suggests that these attributes are partially controlled by depositional fabric. A two-fold increase in percentage of core with fractures and zebra-fabrics in Facies 2 relative to 3 indicates that the secondary reservoir (Facies 2) was more susceptible to mechanical alteration during structural deformation and HTD diagenesis. This implies that HTD-fluid interaction with the primary depositional fabrics of Facies 3 may have had a stronger control on reservoir quality development, because the primary reservoir was less altered by structural/HTD mechanics (relative to Facies 2), while porosity and permeability remains relatively equal between the two facies.

#### Facies 2

The secondary reservoir (Facies 2) is primarily composed of bioturbated brachiopod-peloidal wackestones and shows the most extensive development of fractures and zebra-fabric related vugs of all depositional facies. Grain-beds in these deposits are thin, with dominant packstone textures. The preferential channelization of HTD fluids through burrow galleries, as earlier proposed, is likely limited in these deposits because of the mix of mud and grain-rich sediments in the burrow fill. The dominant control on HTD reservoir formation in this facies is therefore likely

mechanical and related to depositional texture and sedimentary composition.

Mechanical properties of carbonate rocks are controlled by numerous factors: the sedimentary facies as it is characterized by constituent material, pore types, and grain size, arrangement, and contacts; diagenetic alteration; and existing mechanical anisotropy (e.g. fractures) (Dürrast and Siegesmund, 1999; Westphal et al., 2004; Barbier et al. 2012). The sedimentological controls on mechanical behavior in Facies 2 likely dominates these factors, as early diagenesis appears limited primarily to cementation and no evidence points toward existing fractures prior to structural and HTD alteration. The mud-dominant textures with thin packstone grain-bed (storm deposit) units behaved mechanically as a structurally-competent, brittle unit, with a dominant horizontal anisotropy (grain-beds) (e.g. Wennberg *et al.*, 2006). These mechanical properties, controlled by sedimentary texture in this facies, are conducive to fracture development (e.g. Wennberg *et al.*, 2006) and likely the development of zebra-fabrics associated with grain-beds. Development of intercrystalline porosities likely developed in association with coarse grain burrow fill and as a general HTD overprint throughout the facies.

### Facies 3

Reservoir quality in Facies 3 is likely generated primarily through a depositional fabric control on HTD fluid-pathways with subordinate mechanical controls. The highly heterogeneous depositional fabric in the primary reservoir of Facies 3 limits the categorization of mechanical behaviors as outlined with Facies 2. This relative heterogeneity compared to Facies 2 results from increased skeletal grain diversity, dominantly grain-rich burrow fill sediments (mud-lean packstone and grainstone textures), variable mud content, and variable grain-bed texture and

thicknesses in the primary reservoir.

The porous and permeable zones in the primary fabric of this facies (e.g. coarse grain burrow fill, grainstone grain-beds), however, likely acted as preferential HTD fluid-pathways. Primary porosity in grainstone textures was likely preserved in burrow filling sediment, grain-beds, and general deposition though early burial, and therefore was present at the time of structural and HTD deformation and invasion of dolomitizing fluids.

### Summary of Reservoir Aspects

Facies 3 shows the characteristics necessary for the development of lateral extension of HTD reservoir quality away from primary vertical faults, in that laterally continuous, permeable, coarse-grain filled burrow galleries provide preferential HTD-fluid pathways. Additional implications outlined in the above discussion are also noteworthy: controls on the HTD process are likely related to depositional fabric through the distribution of primary porosity and permeability *and* mechanical-sedimentological character.

Inevitably, however, these interpretations must be considered in light of the underlying issue of primary structural control on HTD reservoir distribution and the lack of data defining the location of major faults in these reservoirs. Because of limited structural data, these analyses address the lateral development of HTD reservoir quality away from faults semi-quantitatively. The fracture distribution in core is estimated by assuming that it is directly related to proximity to major fault-zones. Despite the fact that no well-constrained structural data is currently available for a quantitative spatial analysis of reservoir quality-structural relationships, the detailed analyses and interpretations included in this study from core are assumed to

be representative of reservoir formation processes at the Albion-Scipio trend and Stoney Point field.

A noteworthy aspect of reservoir development not included in this study involves the degree that impermeable deposits (e.g. K-bentonites) impede HTD fluid-migration along vertically oriented faults. This component of HTD development/reservoir quality formation has previously been documented (Davies and Smith, 2006; and Sharp *et al.*, 2010) as well as proposed for Albion-Scipio and Stoney Point reservoirs (Hurley and Budros, 1990). More recent work by Feutz (2012), evaluating the role of baffles and barriers to vertical migration of HTD fluids indicates that they exhibit substantial control on reservoir quality formation in these TBR reservoirs.

## SUMMARY AND CONCLUSIONS

This study increases understanding of epeiric carbonate sedimentation through detailed facies analysis, paleogeographic reconstruction at isochronous surfaces, and facies stacking pattern analysis in the southern Michigan Basin TBR interval. Additional insight was gained into HTD-processes, distribution, and reservoir characterization through the analysis of reservoir data in the context of a detailed depositional model and facies stacking pattern hierarchy. The following are key conclusions from this study:

1. The TBR was deposited on a storm-dominated low-declivity epeiric ramp. Depositional facies associations are consistent with outer ramp, mid-ramp, and inner ramp sub-environments. Variability in depositional facies type and character show a marked contrast with previous layer-cake or blanket depositional models for this interval in the Michigan Basin.

2. Analysis of grain-bed distribution (thickness, frequency) and character (sedimentary structures, grain size and type) is a useful aid in the facies analysis of these dominantly sub-tidal ramp deposits.
3. Facies mapping at isochronous K-bentonite surfaces indicates considerable heterogeneity in the TBR facies-mosaic within ramp sub-environments (Figure 48). Cross-sectional and paleogeographic mapping at these isochronous surfaces provides additional insight into facies distributions by illustrating well-constrained facies distributions at time equivalent depositional surfaces. K-bentonite mapping also indicates that the ramp dipped toward the northeast, or basin center.
4. The comparison of the TBR depositional system with modern depositional analogs gives critical insight and understanding to facies development, relationships, and geometries on this epeiric carbonate ramp. The striking similarities in facies type and relationship that the TBR shares with Holocene analogs further discount previous simplistic layer cake depositional models for the TBR. Additionally, evaluating the mechanisms for the genesis of depositional morphology and facies characteristics in modern and ancient deposits aids in understanding of sedimentological and stratigraphic development within the TBR.
5. Analysis of facies stacking patterns identifies stratigraphic organization within a three tiered hierarchy: large-scale sequences, high-frequency scale (HFS) sequences, and high-frequency cycles (HFC). This stratigraphic organization likely represents combined allocyclic and autocyclic signals at the HFC and HFS scales. However, large-scale “cyclicality” in facies stacking patterns shows temporal scales and



accommodation trends that correspond to regional time-equivalent deposits, indicating allogenic influences at this hierarchical level.

6. The evaluation of reservoir aspects of the TBR interval at Albion-Scipio and Stoney Point shows that depositional fabric controls reservoir quality development *and* the characteristics of pore types and pore connectivity (permeability). Facies 3 constitutes the primary TBR reservoir, and is characterized by intercrystalline and vuggy pore types related to coarse grained burrow fill and grain-bed deposition. Facies 2 is considered secondary reservoir, characterized by the development of fractured and zebra fabric reservoir related to the impermeable and mechanically-rigid nature of the facies.
7. Primary reservoir porosity and permeability correlates to position within the stratigraphic framework, where higher values correlate to large-scale transgressive trends identified through facies stacking patterns. This relationship between facies/stratigraphic position and reservoir characteristics develops a hydrocarbon exploration and/or reservoir characterization/management tool that can be used to identify best practices in future HTD hydrocarbon reservoir development, in the Michigan Basin TBR and globally.

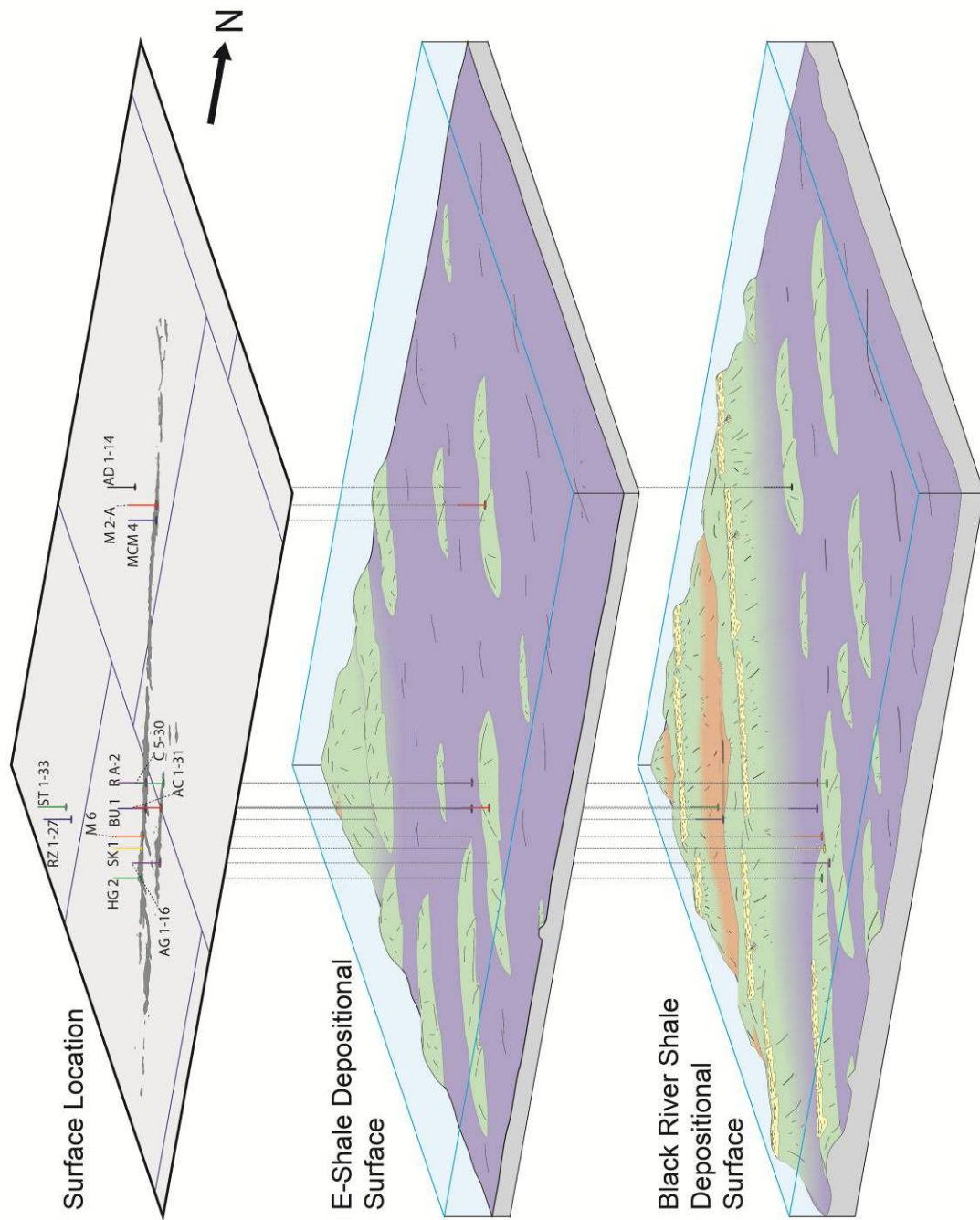


Figure 48. Depositional platform morphologies reconstructed to represent time-slices at the isochronous K-bentonite surfaces—compatible with facies, cross-section, and modern analog analysis. Well bores are represented as vertical lines. Surface well locations are color coded and correspond to

where facies data from core intervals intersect bentonites. Surface Location shows the Albion-Scipio and Stoney Point wells (dark gray) and Michigan county lines for reference. Relief at depositional surfaces has no scale; however it is exaggerated to represent relative water depths. Note: the dimensions of the surface and bentonite surfaces are identical to those in Figure 12.

### Considerations for Future Work

This study substantially increases the information regarding the deposition and stratigraphy in the southern Michigan Basin TBR deposits. However, numerous aspects of this interval warrant further investigation in order to better understand the deposition, stratigraphy, and HTD-emplacement in the TBR, as well as HTD processes in general.

A specific issue requiring future work is apparent mass-transport deposition (mass-transport deposits or MTDs) in a TBR core northeast of the Albion-Scipio trend primary study area (in F 2-12 core). Below are descriptions and preliminary interpretations regarding these MTDs that follow the layout of facies discussions employed in the Depositional Reconstruction section of this study. The purpose of this full description is intended to provide preliminary documentation of these deposits for future use.

#### MTDs

*Observation:* A single core used in this study (F 2-12) contains deposits of polymictic breccias and conglomerates (Dunham textural equivalent to lithoclastic rudstones and floatstones). The deposits are composed of sub-rounded to very angular (Powers, 1953) sand to small cobble sized clasts (63  $\mu\text{m}$  – 128 mm, largest identifiable in core) in an undifferentiated skeletal fragment-crinoid wackestone to

mudstone matrix (Figure 49). Matrix grains include bryozoan, ostracode, gastropod, and pelecypod fragments.

Individual lithoclast composition is variable. Approximately 70% of the lithoclasts consist of peloid, brachiopod, and crinoid wackestone to packstone, with a minor occurrence of skeletal grainstone and mudstone textured clasts. Larger clasts show overturned primary bedding structures (Figure 49). Lithoclasts commonly contact and show suturing by pressure solution. Individual breccia deposits range from less than a foot to over 25 feet thick. Breccia bedding contacts show basal scour, while upper boundaries transition to peloid crinoid wackestones and mudstones. Basal contacts deviate up to 25 degrees from horizontal. Internal bedding structures show normal graded bedding in deposits less than four feet thick (thin), and show reverse graded bedding, chaotic grain orientation, and random size distribution throughout deposits greater than four feet thick.

*Interpretation:* Breccias in the F 2-12 core are interpreted to be mass-transport deposits (MTDs). Multiple beds containing lithoclasts composed of texturally very immature mud to cobble sized breccias indicate mass-transport depositional mechanisms. The F 2-12 core shows evidence of individual and combined turbidity-flow, grain-flow, and debris-flow transport modes (as defined by Nardin et al., 1979; and Cook and Mullins, 1983).

Reverse graded bedding is indicative of grain-flow deposits, where grain-to-grain contact supports the flow above the substrate, dispersive pressure concentrates larger grains toward the top of the flow at the zone of minimum internal shear, and smaller sediments settle through space between larger contacting clasts and deposit at

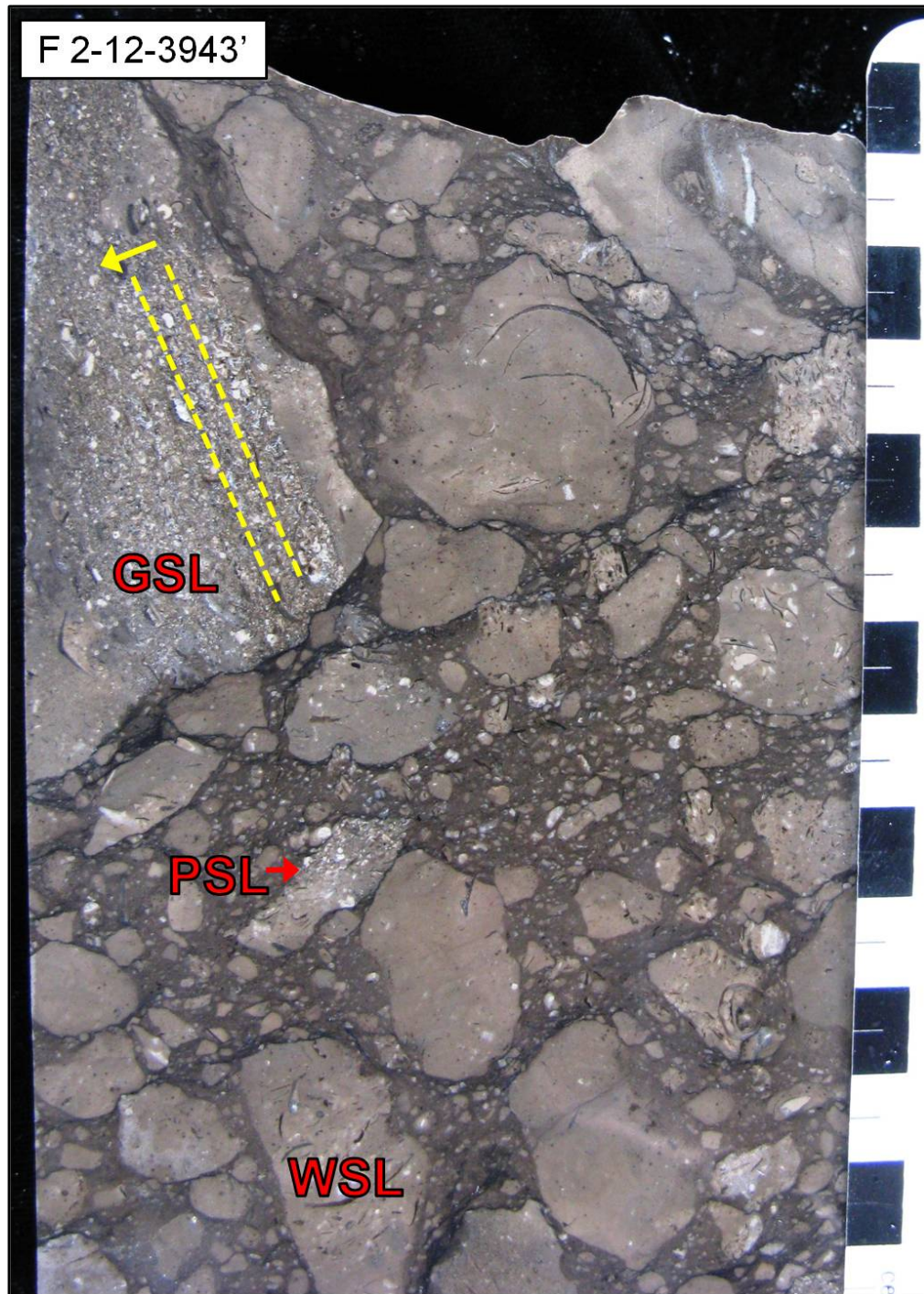


Figure 49. MTD- Core photograph showing debris flow breccia. Sample shows sand to cobble sized ( $63 \mu\text{m} - 75 \text{mm}$ ) grainstone (GSL), packstone (PSL), and wackestone (WSL) lithoclasts within a wackestone matrix. Bedding

in the labeled grainstone clast is overturned (dashed yellow line, arrow points toward younger depositional laminae within the clast). Scale is in centimeters.

the flow base (Lowe, 1976; Cook and Mullins, 1983). The angle of slope required for development of grain-flow ranges from 9 to over 30 degrees (Cook and Mullins, 1983). Debris-flow deposits are characterized by poor sorting with chaotic grain orientations and are transported on slopes less than 0.1 degree under the support of fine grained matrix strength (Hampton, 1979). Turbidity-flow deposits transport sediment through support by fluid turbidity, and are readily recognized as containing Bouma Sequence characteristics of basal scour, normal graded bedding, and bedforms associated with a decreasing-up energy regime (Hsu, 1989).

These MTDs are interpreted as deposited on a localized margin-slope and unrelated to the deposition at the Alboin-Scipio trend and Stoney Point field. The F 12 core contains MTDs with variable character over 300 feet (90 meters) of core, suggesting that depositional relief is persistent though TBR deposition proximal to this core location. Observations indicating bathymetric relief include depositional surfaces inclined from horizontal, grain-flow deposits requiring a minimum 9-degree slope, and episodic deposition over the 300 vertical feet (90 meters) of core. The deposition of peloidal-skeletal wackestones to packstones between mass-transport deposits in the F 2-12 core is consistent with textures elsewhere on the platform during TBR deposition. Additionally, textures of lithoclasts in mass-transport deposits show environments of deposition consistent with Facies 2 and 3 (i.e. lithoclasts show no distinct shoal, tidal flat, or reef deposition). Continuity of regional K-bentonite accumulation in the F 2-12 core (notably the Black River Shale and E-Shale) suggest that breccia emplacements were syndepositional with the Albion-Scipio and Stoney Point TBR deposits. Core taken in the vicinity (surface distance of

2,000 ft, 600 m) of the F 2-12 core show similar MTDs (Feutz, 2012), however no well data outside of that range indicate MTDs or a continuity in the bathymetric relief necessary for the generation of these deposits.

Similar ambient depositional textures to the TBR mid and outer ramp facies, combined with evidence for localized bathymetric relief and/or lack of regional structural continuity of relief indicate that the MTDs are local phenomena and have no genetic relationship to Albion-Scipio and Stoney Point reservoir rock deposition (i.e. shoal-ramp depositional models). Although implications held in MTDs are noteworthy to Michigan Basin deposition during the TBR interval (e.g. the distribution of bathymetric relief and possible tectonic or cosmogenic-impact structure (Milstein, 1994) mechanisms for local relief development), they are beyond scope of the present goal of modeling the deposition of the Albion-Scipio and Stoney Point reservoir rocks. Further or specific interpretation of the F 2-12 MTDs without detailed study amounts to speculation. These MTDs are therefore only addressed here for future consideration.

#### Additional Future Considerations

The following list includes additional important subjects and questions for future research regarding the issues addressed in this study:

1. Investigate MTDs. What is/are the mechanism(s) of debris and/or grain flow emplacement? Do these deposits indicate significant relief at a regional or local margin and where is the bathymetric relief located? How was the depositional relief generated? How do these deposits fit into the low-declivity ramp model?
2. Test the depositional model put forth in this study through the



incorporation of new (unavailable to this investigation) core extracted from the TBR at Napoleon field. Are depositional facies consistent with the facies associations and depositional orientations outlined here? Does ramp geometry follow the present Michigan Basin structure (i.e. depositional strike coincident with structural contours on Trenton Group top), is it consistent with orientations at Albion-Scipio, or does it have a completely different orientation?

3. Chemically fingerprint E-shale and other K-bentonites in the TBR to further constrain depositional and stratigraphic models with additional isochronous surfaces, allowing for further quantitative intra/inter-basin correlation of these event deposits.
4. Date E-shale and other bentonite surfaces in the interval. Do absolute age constraints and provide quantification necessary for calculation of sedimentation (preservation) rates? Does this quantification give insight into the cyclicity order of the facies stacking pattern hierarchy (e.g. 3<sup>rd</sup>, 4<sup>th</sup>, HFC)? Do dates provide constraints for comparison/correlation of the TBR T-R trends with regional relative sea level curves?
5. Construct a biostratigraphic framework (e.g. brachiopoda, Emmerson, 2002) for comparison with, and integration into sequence and chronostratigraphy, further temporally constraining this interval.
6. Investigate mechanical controls of facies and associated textures and rock-fabrics on HTD-processes proposed here. Is it possible to construct a mechanical stratigraphic framework? How does a mechanical stratigraphic framework compare to facies distributions and/or porosity permeability relationships in core?

7. Is it possible to calibrate facies in core to modern log suites (i.e. FMI logs in Rice Creek unit of Albion Scipio trend, Napoleon Field, or additional recent TBR drilling activity) based on mechanical facies attributes proposed here?
8. Continue analysis of TBR depositional modeling through the remainder of the Black River Group (deeper) with the workflow outlined here.
9. How does the depositional/stratigraphic model compare with 3-D seismic data acquired during recent TBR hydrocarbon exploration activity? Are these sequences and the facies/stacking pattern associated petrophysical characteristics resolvable? Do reservoir trends show geometries consistent with the depositional geometries outlined here?
10. If incorporated into a 3-D geobody simulation (e.g. PETREL model), how does this model (statistically) correlate to wire-line log or 3-D seismic data? Does this give additional insight into fault distribution and/or reservoir-depositional facies relationships?

## BIBLIOGRAPHY

- Ahr, W.M., 1973. The carbonate ramp – an alternative to the shelf model, Gulf Coast Association of Geological Societies Transactions, v. 23, p. 221-225.
- Aigner, T., 1985. *Storm Depositional Systems: Dynamic stratigraphy in modern and ancient shallow-marine sequences*. Springer, Berlin, 174 p.
- Allen, J. R. and Wiggins, W. D., 1993. *Dolomite Reservoirs – Geochemical Techniques for Evaluating Origin and Distribution*. - AAPG Continuing Education Course Note Series No. 36, 129 p.
- Alsharhan, A. S., Kendall, C. G. St. C., 2002. Holocene costal carbonates and evaporites of the southern Arabian Gulf and their ancient analogues, Earth-Science Reviews, v. 61, p. 191 -243.
- Anselmetti, F.S. and Eberli, G.P., 1999, The velocity-deviation log: A tool to predict pore type and permeability trends in carbonate drill holes from sonic and porosity or density logs: AAPG Bulletin, v. 83, n. 3, p. 450-466.
- Asquith, G.B. and Gibson, C., 1982. *Basic Well Log Analysis for Geologists, AAPG Methods in Explorations Series*, 216 p.
- Barbier, M., Hamon, Y., Callot, J-P., Floquet, M., Daniel, J-M., 2012. Sedimentary and diagenetic controls on the multiscale fracturing pattern of a carbonate reservoir: The Madison Formation (Sheep Mountain, Wyoming, USA), Marine and Petroleum Geology, v. 29, p. 50-67.
- Barron, E.J., and Moore, G.T., 1994. *Climate Model Application in Palaeoenvironmental Analysis*, SEPM Short Course No. 33, 344 p.
- Ball, M.M., 1967. Carbonate sand bodies of Florida and the Bahamas, Journal of Sedimentary Petrology, v. 37, p. 556-591.
- Bathurst, R.G.C., 1971. *Carbonate Sediments and Their Diagenesis*, Elsevier, Oxford, Developments in Sedimentology, no. 12, 658 p.
- Bathurst, R.G.C., 1966. Boring algae, micrite envelopes and lithification of molluscan biosparites, Journal of Geology, v. 5, p. 15-32.
- Beghini, V.G., and Conroy, T.R., 1966. A history of the Trenton Albion-Scipio trend of Michigan, 5<sup>th</sup> Annual Ontario Petroleum Institute Conference Proceedings, London, Ontario, p. 1-21.

- Bellinger, S., 2009. West Bay Exploration, group of industry partners continue successful Trenton-Black River exploration, development work in Calhoun, Jackson counties, *Oil and Gas News*, v. 115, n. 44, 3 p.
- Bergman, K.L., Westphal, H., Janson, X., Poiriez, A., and Eberli, G.P., 2010. Controlling parameters on facies geometries of the Bahamas, an isolated carbonate platform environment, *In: Westphal, H., Riegl, B., and Eberli G.P. (eds.), Carbonate Depositional Systems: assessing dimensions and controlling parameters*, Springer Science, New York, p. 5-80.
- Beyer, S.R., Simo, J.A., and Byers, C.W., 2008. Lithofacies, K-bentonite geochemistry, and sequence stratigraphy of the Ordovician (Mohawkian-Cincinnatian) Galena Group, northeastern Iowa, *Geoscience Wisconsin*, v. 19, pt. 2, p. 23-48.
- Blakey, R. <http://www4.nau.edu/blakey.html>, accessed 6-2010.
- Brett, C.E. and Brookfield, M.E., 1984. Morphology, faunas and genesis of Ordovician hardgrounds from southern Ontario, Canada, *Palaeogeography, Palaeoclimatology, Palaeoecology*, v. 46, n. 4, p. 233-290.
- Brett, C.E., McLaughlin, P.I., Cornell, S.R., and Baird, G.C., 2004. Comparative sequence stratigraphy of two classic Upper Ordovician successions, Trenton Shelf (New York–Ontario) and Lexington Platform (Kentucky–Ohio): Implications for eustasy and local tectonism in eastern Laurentia, *Palaeogeography, Palaeoclimatology, Palaeoecology*, v. 210, p. 295-329.
- Brookfield, M.E., 1982. Glacio-Eustatic sedimentary cycles in Trenton Limestone (Middle Ordovician) of southern Ontario (Abstract), *AAPG Bulletin*, v. 66, p. 1165.
- Brookfield, M.E., and Brett, C.E. 1988. Paleoenvironments of the Mid-Ordovician (Upper Caradocian) Trenton limestones of southern Ontario, Canada: Storm sedimentation on a shoal-basin shelf model, *Sedimentary Geology*, v.57, p.75-105.
- Budai, J.M., and Wilson, J.L., 1991. Diagenetic history of the Trenton and Black River Formation, *In: Catacosinos, P.A., and Daniels, Jr., P.A. (eds.) Early Sedimentary Evolution of the Michigan Basin*, Geological Society of America Special Paper 256, p. 73–88.
- Buehner, J.H., and Davis, S.H., 1968. Albion-Pulaski-Scipio-trend field: Symposium on Michigan oil and gas fields, *Michigan Basin Geological Society*, p. 37-47.
- Burchette, T.P., and Wright, V.P., 1992. Carbonate ramp depositional systems, *Sedimentary Geology*, v. 79, p. 3-57.

- Catacosinos, P.A., Harrison, W.B., Reynolds, R.F., Westjohn, D.B., and Wollensak, M.S., 2000. Stratigraphic nomenclature for Michigan, Michigan Dept. of Environmental Quality, Geological Survey Division and Michigan Basin Geological Society.
- Catacosinos, P.A., Daniels, P.A., Harrison, W.B., 1990. Structure, stratigraphy and petroleum geology of the Michigan Basin. *In*: Leighton, M.W., Kolata, D.R., Oltz, D.F., and Eidel J.J. (eds) *Interior Cratonic Basins*, AAPG, Tulsa, Oklahoma, AAPG Memoir 51, p. 561-601.
- Cercone, K.R., 1984. Thermal history of the Michigan Basin, AAPG Bulletin, v. 68, no. 2, p. 130–136.
- Chen, D., Qing, H., Yang, C., 2004. Multistage hydrothermal dolomites in the Middle Devonian (Givetian) carbonates from the Guilin area, South China, *Sedimentology*, v. 51, p. 1029-1051.
- Choquette, P.W., Pray, L.C., 1970. Geologic nomenclature and classification of porosity in sedimentary carbonates, AAPG Bulletin, v. 54, p. 207-244.
- Coakley, B., and Gurnis, M., 1995. Far-field tilting of Laurentia during the Ordovician and constraints on the evolution of a slab under an ancient continent, *Journal of Geophysical Research*, v. 100, p. 6313–6327.
- Cook, H.E., and Mullins, H.T., 1983. Basin margin environment, *In*: Scholle, P.A., Bebout, D.G., Moore, C.H., (eds.), *Carbonate Depositional Environments*, AAPG Memoir 33, p. 540-617.
- Copper, P., 2002. Silurian and Devonian reefs: 80 million years of global greenhouse between two ice ages. *In*: Kiessling W., Flugel, E., and Golonka, J. (eds.) *Phanerozoic Reef Patterns*, SEPM Special Publication 72, p. 181-238.
- Cohee, G.V., 1948. Cambrian and Ordovician rocks in Michigan Basin and adjoining areas: AAPG Bulletin, v. 32, p. 1417-1448.
- Cowan C.A., and James, N.P., 1996. Autogenic dynamics in carbonate sedimentation: meter-scale shallowing-upward cycles, Upper Cambrian, Western Newfoundland, Canada, *American Journal of Science*, v. 296, p. 1175-1207.
- Cressman, E.R., and Noger, M.C., 1976. Tidal-flat environments in the High Bridge Group (Middle Ordovician) of central Kentucky, University of Kentucky-Lexington, Kentucky Geological Survey, Series X, Report of Investigation 18, 15 p.
- Davies, G.R., and Smith, L.B., 2006. Structurally controlled hydrothermal dolomite facies: An overview. AAPG Bulletin, v. 90, no. 11, p. 1641-1690.

- DeHaas, R.J., and Jones, M.W., 1989. Cave-levels of the Trenton-Black River Formations in central southern Michigan, *In: Keith, B.D., (ed.) The Trenton Group (Upper Ordovician Series) of Eastern North America*, AAPG Studies in Geology 29, p. 237-266.
- Dodd, J.R., and Stanton, Jr., R.J., 1981. *Paleoecology, Concepts and Applications*, Wiley-Interscience Publication, New York, 559 p.
- Doveton, J. H., 1994. *Geological Log Interpretation: reading the rocks from wireline logs*: SEPM Short Course 29, 169 p.
- Drummond, C.N., and Wilkinson, B.H., 1993a. Aperiodic accumulation of cyclic peritidal carbonate, *Geology*, v. 21, p. 1023-1026.
- Drummond, C.N., and Wilkinson, B.H., 1993b. Carbonate cycle stacking patterns and hierarchies of orbitally-forced eustatic sealevel change, *Journal of Sedimentary Petrology*, v. 63, p. 369-377.
- Drummond, C.N., and Sheets, H., 2001. Taphonomic reworking and stratal organization of tempestite deposition: Ordovician Kope Formation, Northern Kentucky, U.S.A., *Journal of Sedimentary Research*, v. 71, n. 4, p. 621-627.
- Duke, W.L., 1990. Geostrophic circulation or shallow marine turbidity currents? The dilemma of paleoflow patterns in storm-influenced prograding shoreline systems, *Journal of Sedimentary Petrology*, v. 60, n. 6, p. 870-883.
- Dunham, R.J., 1962. Classification of carbonate rocks according to depositional texture, *In: Ham, W. E., (ed.), Classification of Carbonate Rocks – A Symposium*, AAPG Memoir 1, p. 108-121.
- Dürrast, H. and Siegesmund, S., 1999. Correlation between rock fabrics and physical properties of carbonate rocks, *International Journal of Earth Sciences*, v. 88, p. 392-408.
- Eberli G.P., Ginsburg R.N., 1987. Segmentation and coalescence of Cenozoic carbonate platforms, Tertiary northwestern Great Bahama Bank, *Geology*, v. 15, p. 75-79.
- Eberli, G.P., Harris, P.M., Grammer, G.M., and Cruz, F.E.G., 2005. *Field Guide to the CSL-AAPG Seminar on Sequence Stratigraphy and Reservoir Distribution in a Modern Carbonate Platform, Bahamas*, University of Miami Comparative Sedimentology Laboratory Sedimenta CD Series No. 3.
- Ekdale, A.A., Bromley, R.G., and Pemberton, S.G., 1984. Ichnology – *Trace Fossils in Sedimentology and Stratigraphy*, SEPM Short Course No. 15, 317 p.

- Ells, G.D., 1962. Structures associated with the Albion-Scipio oil field trend, Michigan Geological Survey, East Lansing, Michigan, p. 86.
- Ells, G.D., 1966. Albion-Scipio trend: Michigan's syncline oil fields (abstract), AAPG Bulletin, v. 50, p. 612.
- Embry, A.F. and Klován, J.E., 1971. A late Devonian reef tract on northeastern Banks Island Northwest Territories, Bulletin Canadian Petroleum Geologists, v. 19, p. 730-781.
- Emerson, N.R., 2002. Sedimentology, sequence stratigraphy, and brachiopod biostratigraphy of the Ordovician (Mohawkian) Decorah Formation, Midcontinent, USA, Ph.D. thesis, University of Wisconsin, Madison, Wisconsin, 490 p.
- Enos, P., 1974. Surface sediment facies of the Florida-Bahamas Plateau map series MC-5, no. 4, Geological Society of America, Boulder, Colorado, USA.
- Enos, P., and Sawatsky, L.H., 1981. Pore networks in Holocene carbonate sediments, Journal of Sedimentary Petrology, v. 51, p. 961-985.
- Enos, P., 1983. Shelf Environment, *In*: Scholle, P.A., Bebout, D.G., Moore, C.H., (eds.), *Carbonate Depositional Environments*, AAPG Memoir 33, p. 268-296.
- Ettensohn, F.R., Hohman, J.C., Kulp, M.A., and Rast, N., 2002. Evidence and Implications of Possible for Field Responses to Taconian Orogeny: Middle-Late Ordovician Lexington Platform and Sebree Trough East-central United States, Southeastern Geology, v. 41, no. 1, p. 1-36.
- Evans, G., Murray, J.W., Biggs, H.E., Bate, R., and Bush, P.R., 1973. The oceanography, ecology, sedimentology and geomorphology of parts of the Trucial Coast Barrier Island Complex, Persian Gulf, *In*: Purser, B.H., (ed.) *The Persian Gulf: Holocene Carbonate Sedimentation and Diagenesis in a Shallow Epicontinental Sea*, Springer, New York, p. 233-278.
- Fara, D.R., and Keith, B.D., 1989. Depositional facies and diagenetic history of the Trenton Limestone in northern Indiana. *In*: Keith, B.D. (ed.) *The Trenton Group (Upper Ordovician Series) of Eastern North America*, AAPG, Tulsa, Oklahoma, AAPG Studies in Geology, no. 29, p. 277-298.
- Fara, D.R., and Keith, B.D., 1984. Depositional facies and diagenetic history of Trenton limestone in northern Indiana (Abstract), AAPG Bulletin, v. 68, p. 1919.
- Feutz, P.J., 2012. Evaluating the effects of thin shales on the lateral distribution of hydrothermal dolomite reservoirs, Albion-Scipio and Stoney Point fields,



- Michigan Basin, unpublished M.S. Thesis, Western Michigan University, Kalamazoo, Michigan, 281 p.
- Fisher, J.H., Barratt, H.W., Droste, J.B., and Shaver, R.H., 1988. Michigan Basin. *In*: Sloss, L.L. (ed.) *Sedimentary Cover – North American Craton*, Geological Society of America, Boulder Colorado, The Geology of North America, v. D-2, p. 361-382.
- Flügel, E., 2004. *Microfacies of Carbonate Rocks*, Springer, New York, p. 976.
- Folk, R.L., 1987. Detection of organic matter in thin-sections of carbonate rocks using a white card, *Sedimentary Geology*, v. 54, p. 193-200.
- Fowler, J.H. and Kuenzi, W.D., 1978. Keweenawan turbidites in Michigan (deep borehole red beds): a founded basin sequence developed during evolution of a proto-oceanic rift system, *Journal of Geophysical Research*, v. 83, p. 5833–5843.
- French, V.L., and Kerans, C., 2004. Accommodation-controlled systems-tract-specific facies partitioning and resulting geometric development of reservoir grainstone ramp-crest shoal bodies. *In*: Grammer, G.M., Harris, P.M., and Eberli, G.P. (eds.) *Integration of Outcrop and Modern Analogs in Reservoir Modeling*, AAPG, Tulsa, Oklahoma, AAPG Memoir 80, p. 171-190.
- Goldhammer, R.K., Dunn, P.A., and Hardie, L.A., 1990. Depositional cycles, composite sea-level changes, cycle stacking patterns, and the hierarchy of stratigraphic forcing: Examples from Alpine Triassic platform carbonates, *Geological Society of America Bulletin*, v. 102, n. 5, p. 535-562.
- Goldhammer, R.K., 1997. Compaction and decompaction algorithms for sedimentary carbonates, *Journal of Sedimentary Research*, v. 67, n. 1, p. 26-35.
- Grammer, G.M., Ginsburg, R.N., Swart, P.K., McNeill, D.F., Jull, A.J.T., and Prezbindowski, D.R., 1993. Rapid growth rate of syndepositional marine aragonite cements in steep marginal slope deposits, Bahamas and Belize, *Journal of Sedimentary Petrology*, v.63, p. 983-989.
- Grammer, G.M., Crescini, C.M., McNeill, D.F., and Taylor, L.H., 1999. Quantifying rates of syndepositional marine cementation in deeper platform environments—New insight into a fundamental process, *Journal of Sedimentary Research*, v. 69, p. 202-207.
- Grammer, G.M., Eberli, G.P., Van Buchem, F.S.P., Stevenson, G.M., Homewood, P.W., 2000. Application of high resolution sequence stratigraphy in developing an exploration and production strategy for a mixed carbonate/siliciclastic system (Carboniferous) Paradox Basin, Utah, USA, *In*: Homewood, P.W., and

- Eberli, G. P. (eds.), *Genetic Stratigraphy on the Exploration and Production Scales: Case Studies from the Pennsylvanian of the Paradox Basin and the Upper Devonian of Alberta*, *Elf Aquitaine Memoir* 24, p. 29-69.
- Grammer, G.M., Harris, P.M., and Eberli, G.P., 2004a. *Integration of Outcrop and Modern Analogs in Reservoir Modeling*, AAPG Memoir 80, Tulsa, Oklahoma, 394 p.
- Grammer, G.M., Harris, P.M., and Eberli, G.P., 2004b. Integration of outcrop and modern analogs in reservoir modeling: Overview with examples from the Bahamas, *In: Grammer, G. M., Harris, P. M., and Eberli, G. P. (eds.), Integration of Outcrop and Modern Analogs in Reservoir Modeling*, AAPG Memoir 80, p. 1-22.
- Grammer, G.M., Harrison III, W.B., Gillespie, R., 2007. Establishing the relationship between fracture-related dolomite and primary rock fabric on the distribution of reservoirs in the Michigan Basin, DOE Final Report, DOE Award DE-FC26-04NT15513, 308p, DOI: [10.2172/948838](https://doi.org/10.2172/948838).
- Grover, G. and Read, J.F., 1978. Fenestral and associated vadose diagenetic fabrics of tidal flat carbonates, Middle Ordovician New Market Limestone, Southwestern Virginia, *Journal of Sedimentary Petrology*, v. 48, n. 2, p. 453-473.
- Hampton, M.A., 1979. Buoyancy in debris flows: *Journal of Sedimentary Petrology*, v. 49, n. 3, p. 753-758.
- Harris, P.M. and Kowalik, W.S. (eds.), 1994. *Satellite Images of Carbonate Depositional Settings: Examples of Reservoir- and Exploration-Scale Geologic Facies Variation*, AAPG Methods in Exploration Series No. 11, 147 p.
- Harris, P.M., 2010. Delineating and quantifying depositional facies patterns in carbonate reservoirs: Insight from modern analogs, *AAPG Bulletin*, v. 94, no. 1, p. 61-86.
- Haq, B.U. and S.R. Shutter, 2008. A chronology of Paleozoic sea-level changes, *Science*, v. 322, October 2008, p. 64-68.
- Harding, T.P., 1974. Petroleum traps associated with wrench faults, *AAPG Bulletin*, v. 58, no. 7, p. 1290-1304.
- Hine, A.C., 1977. Lily Bank, Bahamas: history of an active oolite sand shoal, *Journal of Sedimentary Petrology*, v. 47, n. 4, p. 1554-1581.
- Holland, S.M., and Patzkowsky, M.E., 1996. Sequence stratigraphy and long-term paleoceanographic change in the Middle and Upper Ordovician of the eastern United States, *In: Witzke B.A., Day, J., and Ludvigson, G.A. (eds.) Paleozoic*

*sequence stratigraphy: Views from the North American craton*, Geological Society of America Special Paper 306, p. 117-129.

- Holmden, R.A., Creaser, K., Muehlenbachs, S.A., Leslie, S.A., and Bergstrom, S.M., 1998. Isotopic evidence for geochemical decoupling between ancient epeiric seas and bordering oceans: Implications for secular curves, *Geology*, v.26, p. 567-570.
- Howell, P.D. and van der Pluijm, B.A., 1990. Early history of the Michigan Basin: subsidence and Appalachian tectonics, *Geology*, v. 18, p. 1195-1198.
- Howell, P.D., and van der Pluijm, B.A., 1999. Structural sequences and styles of subsidence in the Michigan basin, *GSA Bulletin*, v. 111, no. 7, p. 974-991.
- Hsu, K.J., 1989. *Physical Principles of Sedimentology*, Springer-Verlag, Berlin, 233 p.
- Huff, W.D. and Kolata, D.R., 1990. Correlation of the Ordovician Deicke and Millbrig K-bentonites between the Mississippi Valley and the Southern Appalachians, *AAPG Bulletin*, v. 74, p. 1736-1747.
- Huff, W.D., Bergström, S. M., and Kolata, D. R., 1992. Gigantic Ordovician volcanic ash fall in North America and Europe: Biological, tectonomagmatic, and event-stratigraphic significance, *Geology*, v. 20, p. 875-878.
- Huff, W.D., Kolata, D.R., Bergstrom, S.M., and Zhang, Y-S, 1996. Large-magnitude Middle Ordovician volcanic ash falls in North America and Europe: dimensions, emplacement and post-emplacement characteristics, *Journal of Volcanology and Geothermal Research*, v. 73, p. 285-301.
- Hughes, G.W., 1997. The Great Pearl Bank Barrier of the Arabian Gulf as a possible Shu'aiba analogue, *GeoArabia*, v. 2, n. 3, p. 279-304.
- Hunt, D., Allsop, T., Swarbrick, R.B., 1996. Compaction as a primary control on the architecture and development of depositional sequences: concept framework, applications, and implications, *In: Howell, J.A., and Aitken, J.F. (eds.) High Resolution Sequence Stratigraphy: Innovations and Applications*, Geological Society of London Special Publication No. 104, p.321-345.
- Hurley, N.F., and R. Budros, 1990. Albion-Scipio and Stoney Point fields-U.S.A., Michigan Basin, *In: Beaumont, E.A., and Foster N.H. (eds.) Treatise of Petroleum Geology Atlas of Oil & Gas Fields, Stratigraphic Traps I*. AAPG, p. 1-32.
- Irwin, M.L., 1965. General theory of epeiric clear water sedimentation, *AAPG Bulletin*, v. 49, n. 4, p. 445-460.

- Ives, R.E., 1960. Trenton-Black River Formation development in Michigan, The Interstate Oil Compact Commission Committee Bulletin, v. 2, no. 1, p. 37-48.
- Jehn, P.J., and Young, L.M., 1976. Depositional environments of the Pitkin Formation, Northern Arkansas, Journal of Sedimentary Petrology, v. 46, n. 2, p. 377-386.
- Jennette, D.C., and Pryor, W.A., 1993. Cyclic alternation of proximal and distal storm facies: Kope and Fairview Formations (Upper Ordovician), Ohio and Kentucky, Journal of Sedimentary Petrology, v. 63, n. 2, p. 183-203.
- Kammer, T.W., and Ausich, W.I., 2006. The "Age of Crinoids": A Mississippian biodiversity spike coincident with widespread carbonate ramps, Palaios, v. 21, p. 238-248.
- Keith, B.D., 1985. Facies, diagenesis and the upper contact of the Trenton limestone of northern Indiana, In: Cercone, K.R., and Budai, J.M. (eds.) *Ordovician and Silurian Rocks of the Michigan Basin*, Michigan Basin Geological Society Special Paper 4, p. 15-32.
- Keith, B.D., 1986. Reservoirs resulting from facies-independent dolomitization: Case histories from the Trenton and Black River carbonate rocks of the Great Lakes area, Carbonates and Evaporites, v. 1, no. 1, p. 74-82.
- Keith, B.D., 1989. Regional Facies of Upper Ordovician Series of Eastern North America. In: Keith, B.D. (ed.) *The Trenton Group (Upper Ordovician Series) of Eastern North America*, Tulsa, Oklahoma, AAPG Studies in Geology, no. 29, p. 1-16.
- Kendall, G.St.C., and Skipwith P.A.D'E., 1969a. Geomorphology of a recent shallow-water carbonate province: Khor al Bazam, Trucial Coast, southwest Persian Gulf, Geological Society of America Bulletin, v. 80, p. 865-892.
- Kendall, G.St.C., and Skipwith P.A.D'E., 1969b. Holocene shallow-water carbonate and evaporite sediments of Kohr al Bazam, Abu Dhabi, southwest Persian Gulf, AAPG Bulletin, v. 53, n. 4, p. 841-869.
- Kennett, J.P., 1982. *Marine Geology*. Prentice Hall, Englewood Cliffs, N.J., USA. 752 p.
- Kerans, C., and Tinker, S.W., 1997. *Sequence Stratigraphy and Characterization of Carbonate Reservoirs*, SEPM Short Course Notes No.40, Society for Sedimentary Geology, Tulsa, Oklahoma, 121 p.

- Keulegan, G.H., and Krumbein, W.C., 1949. Stable configuration of bottom slope in a shallow sea and its bearing on geological processes, *Transactions, American Geophysical Union*, v. 30, n. 6, p. 855-861.
- Kolata, D.R., Huff, W.D., and Bergström, S.M., 1996. Ordovician K-bentonites of eastern North America, *Geological Society of America Special Paper 313*, 84 p.
- Kolata, D.R., Huff, W.D., and Bergström, S.M., 1998. Nature and regional significance of unconformities associated with the Middle Ordovician Hagan K-bentonite complex in the North American midcontinent, *Geological Society of America Bulletin*, v.110, n. 6, p. 723-739.
- Kreisa, R.D., 1981. Storm-generated sedimentary structures in subtidal marine facies with examples from the Middle and Upper Ordovician of southwestern Virginia, *Journal of Sedimentary Petrology*, v. 51, n. 3, p. 823-848.
- Landes, K. L., 1946. Porosity through dolomitization, *AAPG Bulletin*, v. 30, p. 305-318.
- Lee, Y.I., Hyeong, K.S., Yoo, C.M., 2001. Cyclic sedimentation across a Middle Ordovician carbonate ramp (Duwibong Formation), Korea, *Facies*, v. 44, p. 61-74.
- Leighton, M.W., 1990. Introduction to Interior Cratonic Basins, *In: Leighton, M.W., Kolata, D.R., Oltz, D.F., and Eidel J.J. (eds) Interior Cratonic Basins*, AAPG, Tulsa, Oklahoma, AAPG Memoir 51, p. 1-29.
- Leslie, S.A., and Bergstrom, S.M., 1997. *Use of K-bentonite bed as time-planes for high-resolution lithofacies analysis and assessment of net rock accumulation rate: An example from the upper Middle Ordovician of eastern North America*, *Geological Society of America Special Paper 321*, p. 11-21.
- Lindsay, R.F., Cantrell, D.L., Hughes, G.W., Keith, T.H., Mueller III, H.W., and Russell, S.D., 2006. Ghawar Arab-D reservoir: Widespread porosity in shoaling-upward carbonate cycles, Saudi Arabia, *In: Harris, P.M., and Weber, L.J. (eds) Giant hydrocarbon reservoirs of the world: From rocks to reservoir characterization and modeling: AAPG Memoir 88/ SEPM Special Publication*, p. 97-137.
- Lomando, A.J., 1999. Structural influences on facies trends of carbonate inner ramp systems, examples from the Kuwait-Saudi Arabian coast of the Arabian Gulf and northern Yucatan, Mexico, *GeoArabia*, v. 4, p. 339-360.
- Loreau, J.-P. and Purser, B.H., 1973. Distribution and ultrastructure of Holocene ooids in the Persian Gulf, *In: Purser, B.H., (ed.) The Persian Gulf: Holocene*

- Carbonate Sedimentation and Diagenesis in a Shallow Epicontinental Sea*, Springer, New York, p. 279-328.
- Lowe, D.R., 1976. Grain flow and grain flow deposits: *Journal of Sedimentary Petrology*, v. 46, n. 1, p. 188-199.
- Machel, H.G. and Lonnee, J., 2002. Hydrothermal dolomite – a product of poor definition and imagination, *Sedimentary Geology* v., 152, p. 163–171.
- Melzer, S.E., Budd, D.A., 2008. Retention of high permeability during shallow burial (300 to 500 m) of carbonate grainstones, *Journal of Sedimentary Research*, v. 78, p. 548 -561.
- Meyer, D.L., Bries, J.L., Greenstein, B.J, and Debrot, A.O., 2003. Preservation of *in situ* reef framework in regions of low hurricane frequency: Pleistocene of Curacao and Bonaire, southern Caribbean, *Lethaia*, v. 36, p. 273-285.
- McKerrow, W.S., Dewey, J.F., and Scotese, C.R., 1991. The Ordovician and Silurian development of the Iapetus Ocean, *In*: Bassett, M.G. (ed.), *The Murchison Symposium special paper in Palaeontology*, p. 165–178.
- Michigan Department of Natural Resources and Environment  
[www.michigan.gov/dnre](http://www.michigan.gov/dnre), accessed 10-18-2010.
- Middleton, G.V., 1973. Johannes Walther's law of facies, *Geological Society of America Bulletin*, v. 84, p. 979-988.
- Milstein, R.L., 1994. The Calvin Impact Crater, Cass County, Michigan: Identification and analysis of a subsurface ordovician astrobleme. Ph.D. Dissertation, Oregon State University, Corvallis, Oregon, 114 p.
- Min, K., Renne, P.R., and Huff, W.D., 2001.  $^{40}\text{Ar}/^{39}\text{Ar}$  dating of Ordovician K-bentonites in Laurentia and Baltoscandia, *Earth and Planetary Science Letters*, v. 185, p. 121-134.
- Moore, C. H., 2001. *Carbonate Reservoirs: Porosity evolution and diagenesis in a sequence stratigraphic framework*: Amsterdam, Elsevier, 444 p.
- Morrow, D.W., 1978. Dolomitization of Lower Paleozoic burrow-fillings, *Journal of Sedimentary Petrology*, v. 48, no. 1, p. 295-306.
- Nader, F.H., Swennen, R., Ellam, R.M., 2007. Field geometry, petrography and geochemistry of a dolomitization front (Late Jurassic, central Lebanon), *Sedimentology*, v. 54, p. 1093-1119.

- Nadon, G.C., Simo, J.A., Dott, R.H., Jr., and Byers, C.W., 2000. High-resolution sequence stratigraphic analysis of the St. Peter Sandstone and Glenwood Formation (Middle Ordovician), Michigan Basin, U.S.A., AAPG Bulletin, v. 84, p. 975-996.
- Nardin, T.R., Hein, F.J., Gorsline, D.S., and Edwards, B.D., 1979. A review of mass movement processes, sediment and acoustic characteristics, and contrasts in slope and base-of-slope systems versus canyon-fan-basin floor systems, *In*: Doyle, L.J. and Pikley, O.H. (eds.), *Geology of Continental Slopes*, SEPM Special Publication no. 27, Tulsa, Oklahoma, p. 49-60.
- NASA <http://earthobservatory.nasa.gov/IOTD/view.php?id=37061>, accessed 1-16-2012.
- Plint, A.G., N. Eyles, C.H. Eyles and R.G. Walker 1992. Controls of sea-level changes. *In*: Walker, R.J. and James, N.P. (eds.), *Facies Models: Response to Sea-Level Change*. Geological Association of Canada, St. John's, Newfoundland, p. 15-25.
- Pope, M.C., and Read, J.F., 1997. High-resolution surface and subsurface sequence stratigraphy of Late Middle to Late Ordovician (Late Mohawkian-Cincinnatian) foreland basin rocks, Kentucky and Virginia, AAPG Bulletin, v. 81, no. 11, p. 1866-1893.
- Pope, M.C., and Read, J.F., 1998. Ordovician metre-scale cycles: Implications for climate and eustatic fluctuations in the central Appalachians during a global greenhouse, non glacial to glacial transition, *Palaeogeography, Palaeoclimatology, Palaeoecology*, v. 138, p. 27-42.
- Powers, M.C., 1953. A new roundness scale for sedimentary particles, *Journal of Sedimentary Petrology*, v. 23, p. 117-119.
- Pratt, B.R., and James, N.P., 1986. The St. George Group (Lower Ordovician) of western Newfoundland: tidal flat island model for carbonate sedimentation in shallow epeiric seas, *Sedimentology*, v. 33, p. 313-343.
- Pratt, B.R., and Holmden, C. (eds.), 2008. *Dynamics of Epeiric Seas*, St. John's, Newfoundland & Labrador, Canada, Geological Society of Canada Special Paper No. 48, 406 p.
- Pratt, B.R., and Holmden, C., 2008. Introduction. *In*: Pratt, B.R., and Holmden, C. (eds.) *Dynamics of Epeiric Seas*, St. John's, Newfoundland & Labrador, Canada, Geological Society of Canada Special Paper No. 48, p. 1-7.
- Prouty, C.E., 1989. Trenton exploration and wrenching tectonics – Michigan Basin and environs. *In*: Keith, B.D. (ed.) *The Trenton Group (Upper Ordovician*



- Series) of Eastern North America*, Tulsa, Oklahoma, AAPG Studies in Geology, no. 29, p. 207-236.
- Purser, B.H. (Ed.), 1973a. *The Persian Gulf: Holocene Carbonate Sedimentation and Diagenesis in a Shallow Epicontinental Sea*. Springer, New York, 471p.
- Purser, B.H., 1973b. Sedimentation around bathymetric highs, *In: Purser, B.H., (ed.) The Persian Gulf: Holocene Carbonate Sedimentation and Diagenesis in a Shallow Epicontinental Sea*, Springer, New York, p. 157-178.
- Purser, B.H. and Evans, G., 1973. Regional sedimentation along the Trucial Coast, SE Persian Gulf. *In: Purser, B.H., (ed.) The Persian Gulf: Holocene Carbonate Sedimentation and Diagenesis in a Shallow Epicontinental Sea*, Springer, New York, p. 211–231.
- Purser, B.H. and Seibold, E., 1973. The principal environmental factors influencing Holocene sedimentation and diagenesis in the Persian Gulf. *In: Purser, B.H., (ed.) The Persian Gulf: Holocene Carbonate Sedimentation and Diagenesis in a Shallow Epicontinental Sea*, Springer, New York, p. 1–9.
- Rankey, E.C., 2002. Spatial patterns of sediment accumulation on a Holocene carbonate tidal flat, northwest Andros Island, Bahamas, *Journal of Sedimentary Research*, v. 72, p. 591-601.
- Rankey, E.C., Enos, P., Steffen, K., and Druke, D., 2004. Lack of impact of Hurricane Michelle on tidal flats, Andros Island, Bahamas: integrated remote sensing and field observations, *Journal of Sedimentary Research*, v. 74, n. 5, p. 654-661.
- Rankey, E.C., Reeder, S.L., 2011. Holocene oolitic marine sand complexes of the Bahamas, *Journal of Sedimentary Research*, v. 81, p. 97–117.
- Read, J.F., 1998. Phanerozoic carbonate ramps from greenhouse, transitional and ice-house worlds: clues from field and modeling studies. *In: Wright, V.P., and Burchette, T.P. (eds) Carbonate Ramps*. Geological Society, London, Special Publications, 149, p. 107-135.
- Read, J.F., 1995. Overview of carbonate platform sequences, cycle stratigraphy and reservoirs in greenhouse and icehouse worlds. *In: Read, J.F., Kearns, C., Weber, L.J., Sarg J.F, and Wright, F.M., (eds.), Milankovitch Sea Level Changes, Cycles and Reservoirs on Carbonate Platforms in Greenhouse and Ice-house Worlds: SEPM Short Course 35*, p. 1-102.
- Read, J.F., 1985. Carbonate platform models. *AAPG Bulletin*, v. 69, p. 1-21.

- Reeder, S.L. and Rankey, E.C., 2009. A tale of two storms: an integrated field, remote sensing and modeling study examining the impact of hurricanes Frances and Jeanne on carbonate systems, Bahamas, *In: Swart, P.K., Eberli, G.P., and McKenzie, J.A. (eds.), Perspectives in Carbonate Geology: a Tribute to the Career of Robert Nathan Ginsburg*, International Association of Sedimentologists Special Publication No. 41, p. 75-90.
- Reijmer, J.J.G., Swart, P.K., Bauch, T., Otto, R., Reuning, L., Roth, S., and Zechel, S., 2009. A re-evaluation of facies on Great Bahama Bank I: new facies maps of western Great Bahama Bank, *In: Westphal, H., Riegl, B., and Eberli G.P. (eds.), Carbonate depositional systems: assessing dimensions and controlling parameters*, Springer Science, New York, p. 29-46.
- Riegl, B., Poiriez, A., Janson, X., and Bergman, K.L., 2010. The Gulf: facies belts, physical, chemical, and biological parameters of sedimentation on a carbonate ramp, *In: Westphal, H., Riegl, B., and Eberli G.P. (eds.), Carbonate depositional systems: assessing dimensions and controlling parameters*, Springer Science, New York, p. 145-213.
- Riding, R., 2000. Microbial carbonates: the geological record of calcified bacterial-algal mats and biofilms: *Sedimentology*, v. 47, p. 179-214.
- Rock-Color Chart Committee, 1991. *Rock-Color Chart*, 7<sup>th</sup> Ed., Geological Society of America, unpaginated.
- Rooney, L.F., 1966. Evidence of unconformity at top of Trenton Limestone in Indiana and adjacent states, *AAPG Bulletin*, v. 50, p. 533-546.
- Ross, J.R.P., and Ross, C.A., 1992. Ordovician sea-level fluctuations. *In: Global Perspectives on Ordovician Geology*, Proceedings of the sixth International Symposium on the Ordovician System, University of Sydney, Australia, p. 327-335.
- Sadler, P.M., 1981. Sediment accumulation rates and the completeness of stratigraphic sections, *Journal of Geology*, v. 89, p. 569-584.
- Samson, S.D., Patchett, P.J., Roddick, J.C., and Parish, R.R., 1989. Origin and tectonic setting of Ordovician bentonites in North America: Isotopic and age constraints, *Geological Society of America Bulletin*, v. 101, p. 1175-1181.
- Sarg, J.F., 1988. Carbonate sequence stratigraphy, *In: Wilgus, C.K., Posamentier, H., Ross, C.A., and Kendall, C.G.St.C., (eds.), Sea Level Changes: an Integrated Approach*, SEPM Special Publication No. 42. p. 155-181.

- Schmincke, H.-U., and van den Bogaard, P., 1991. Tephra layers and tephra events, *In: Einsele, G., Ricken, W., and Seilacher, A., (eds.), Cycles and Events in Stratigraphy*, Springer-Verlag, New York, p. 392-429.
- Scholle, P.A. and Ulmer-Scholle, D.A., 2003. *A Color Guide to the Petrography of Carbonate Rocks: Grains, Textures, Porosity, Diagenesis*, AAPG Memoir 77, Tulsa, Oklahoma, 474 p.
- Scholle, P.A. and Halley, R.B., 1985. Burial diagenesis: Out of sight, out of mind!, *In: Schneidermann, N. and Harris, P.M., (eds.) Carbonate Cements*, SEPM Special Publication No. 36, p. 309-334.
- Schutter, S.R., 1992. Ordovician hydrocarbon distribution in North America and its relationship to eustatic cycles, *In: Webby, B.D. and Laurie, J.R., (eds.), Global Perspectives on Ordovician Geology*, Balkema, Rotterdam, p. 421-432.
- Sharp, I., Gillespie, P., Morsahad, D., Tabner, C., Karpuz, R., Verges, J., Horbury, A., Pickard, N., Garland, J., Hunt, D., 2010. Stratigraphic architecture and fracture-controlled dolomitization of the Cretaceous Khami and Bangestan groups: an outcrop case study, Zagros Mountains, Iran, *In: van Buchem, F.S.P., Gedes, K.D., and Esteban, M. (eds.) Mesozoic and Cenozoic Carbonate Systems of the Mediterranean and the Middle East: Stratigraphic and Diagenetic Reference Models*, Geological Society of London, Special Publication, v.329, p. 343-396.
- Shinn, E.A., 1968. Burrowing in recent lime sediments of Florida and the Bahamas, *Journal of Paleontology*, v. 42, n. 4, p. 879-894.
- Shinn, E.A., Lloyd, R.M., and Ginsburg, R.N., 1969. Anatomy of a modern carbonate tidal-flat, Andros Island, Bahamas, *Journal of Sedimentary Petrology*, v. 39, n. 3, p. 1202-1228.
- Shinn, E.A., Robbin, D.M., and Steinen, R.P., 1980. Experimental compaction of lime sediment, Program with Abstracts, AAPG Annual Meeting, Denver, CO, USA, p. 120.
- Shinn, E.A., 1983a. Birdseyes, fenestrae, shrinkage pores, and loferites: A reevaluation, *Journal of Sedimentary Petrology*, v. 53, n. 2, p. 619-628.
- Shinn, E.A., 1983b. Tidal flat environment, *In: Scholle, P.A., Bebout, D.G., Moore, C.H., (eds.), Carbonate Depositional Environments*, AAPG Memoir 33, p. 172-210.
- Schulz, J.E., 2011. Facies control on reservoir quality in hydrothermal dolomite, Albion-Scipio trend, Michigan Basin. unpublished M.S. Thesis, Western Michigan University, Kalamazoo, MI, 279 p.

- Smith, Jr. L.B., 2006. Origin and reservoir characteristics of Upper Ordovician Trenton-Black River hydrothermal dolomite reservoirs in New York, AAPG Bulletin, v. 90, no. 11, p. 1691-1718.
- Stoudt, E.L., and Raines, M.A., 2004. Reservoir characterization in the San Andres Formation of Vacuum Field, Lea County, New Mexico: Another use of the San Andres Algerita Outcrop Model for improved reservoir description, *In*: Grammer, G. M., Harris, P. M., and Eberli, G. P. (eds.), *Integration of Outcrop and Modern Analogs in Reservoir Modeling*, AAPG Memoir 80, p. 191-214.
- Swanson, R.G., 1981. *Sample Examination Manual*, AAPG Methods in Exploration Series, 118 p.
- Taylor, T.R., and Sibley, D.F., 1986. Petrographic and geochemical characteristics of dolomite types and the origin of ferroan dolomite in the Trenton Formation, Ordovician, Michigan Basin, U.S.A., *Sedimentology*, v. 33, p. 61-86.
- Taylor, A.M. and Goldring, R., 1993. Description and analysis of bioturbation and ichnofabrics, *Journal of the Geological Society of London*, v. 150, p. 141-148.
- Tedesco, L.P., and Wanless, H.R., 1991. Generation of sedimentary fabrics and facies by repetitive excavation and storm infilling of burrow networks, Holocene of south Florida and Caicos Platform, *BWI: Palaios*, v. 6, p. 326-343.
- Thornton, J.E., 2011. Prediction of petrophysical properties of Trenton-Black River (Ordovician) Reservoirs by comparing pore architecture and permeability to sonic velocity, Michigan Basin, USA, unpublished M.S. Thesis, Western Michigan University, Kalamazoo, Michigan, 431 p.
- Trevail, R.A., 1988. Distribution of Middle Ordovician altered volcanic ash beds (K-bentonites), southwestern Ontario, Geological Association of Canada/Canadian Association of Petroleum Geologists, Program with Abstracts, v. 13, p. A126.
- Tucker M.E., and Wright, V.P., 1990. *Carbonate Sedimentology*, Blackwell Science Ltd., Oxford, 482 p.
- Tucker, R.D. and McKerrow, W.S., 1995. Early Paleozoic chronology: A review in light of new U-Pb zircon ages from Newfoundland and Britain, *Canadian Journal of Earth Science*, v. 32, p. 368-379.
- Wagner, C.W., and van der Togt, C., 1973. Holocene sediment and their distribution in the southern Persian Gulf, *In*: Purser, B.H., (ed.) *The Persian Gulf: Holocene Carbonate Sedimentation and Diagenesis in a Shallow Epicontinental Sea*, Springer, New York, p. 123-155.

- Wanless, H.R., Tedesco, L.P., Tyrrell, K.M., 1988. Production of subtidal tubular and surficial tempestites by Hurricane Kate, Caicos Platform, British West Indies, *Journal of Sedimentary Petrology*, v. 58, no. 4, p. 739-750.
- Westphal, H., Eberli, G.P., Smith, L.B., Grammer, G.M., and Kislak, J., 2004. Reservoir characterization of the Mississippian Madison Formation, Wind River basin, Wyoming, *AAPG Bulletin*, v. 88, n. 4, p. 405-432.
- Wennberg, O.P., Svana, T., Azizzadeh, M., Aqrawi, M.M., Brockbank, P., Lyslo, K.B., and Ogilvie, S., 2006. Fracture intensity vs. mechanical stratigraphy in platform top carbonates: the Aquitanian of the Asmari Formation, Khaviz Anticline, Zagros, SW Iran, *Petroleum Geoscience*, v. 12, p. 235-245.
- Wheeler, H.E., 1958. Time-stratigraphy, *AAPG Bulletin*, v. 42, p. 1047-1063.
- Wilkinson, B.H., and Drummond, C.N., 2004. Facies mosaics across the Persian Gulf and around Antigua—stochastic and deterministic products of shallow-water sediment accumulation, *Journal of Sedimentary Research*, v. 74, n. 4, p. 513-526.
- Willman, H.B., and Kolata, D.R., 1978. The Platteville and Galena Groups in northern Illinois, *Illinois State Geological Survey Bulletin* 502, 75 p.
- Wilson, E.N., Hardie, L.A., and Phillips, O.M., 1990. Dolomitization front geometry, fluid flow patterns, and the origin of massive dolomite: the Triassic Latemar Buildup, northern Italy, *American Journal of Science*, v. 290, p. 741-796.
- Wilson, J.L., 1975. *Carbonate Facies in Geologic History*, Springer-Verlag, New York, 471 p.
- Wilson, J.L., Budai, J.M., Sengupta, A., 2001. Trenton-Black River Formations of Michigan Basin. *AAPG Search and Discovery Article #10020*
- Witzke, B.J., and Bunker, B.J., 1996. Relative sea-level changes during Middle Ordovician through Mississippian deposition in the Iowa area, North American craton, *In: Witzke B.A., Day, J., and Ludvigson, G.A. (eds.) Paleozoic sequence stratigraphy: Views from the North American craton*, Geological Society of America Special Paper 306, p. 307-330.
- Yao, Q., Demicco, R.V., 1997. Dolomitization of the Cambrian Carbonate Platform, southern Canadian Rocky Mountains: dolomite front geometry, fluid inclusion geochemistry, isotopic signature, and hydrogeologic modeling studies, *American Journal of Science*, v. 297, p. 892-938.

Zenger, D.H., 1979. Primary textures in dolostones and recrystallized limestones: a technique for their microscopic study, *Journal of Sedimentary Petrology*, v. 49, p. 677-687.

APPENDIX A – Core Descriptions



## Abbreviations and Definitions

<b><u>Core Color Key (Rock Color-Chart Committee GSA, 1991)</u></b>			
<b>Color</b>	<b>Value</b>	<b>Color (cont.)</b>	<b>Value (cont.)</b>
Pale greenish yellow	10Y 8/2	Brownish gray	5YR 4/1
Dark yellowish brown	10YR 4/2	Pale brown	5YR 5/2
Pale yellowish brown	10YR 4/2	Light brownish gray	5YR 6/1
Moderate yellowish brown	10YR 5/4	Pinkish gray	5YR 8/1
Very pale orange	10YR 8/2	Black	N 1
Greenish black	5GY 2/1	Grayish black	N 2
Light grayish green	5GY 8/1	Dark gray	N 3
Olive gray	5Y 4/1	Medium dark gray	N 4
Light olive gray	5Y 6/1	Medium gray	N 5
Dusky yellow	5Y 6/4	Medium light gray	N 6
Yellowish gray	5Y 7/2	Light gray	N 7
Brownish black	5YR 2/1	Very light gray	N 8
Dusky brown	5YR 2/2		

<b><u>Pore Type Key</u></b>			
<b>Code</b>	<b>Pore types</b>	<b>Code</b>	<b>Pore (cont.)</b>
IX	Intercrystalline	FR	Fracture
IP	Interparticle	VUG	Vug
MO	Moldic	WX	Intracrystalline
FE	Fenestral	WP	Intraparticle

Pressure Solution definitions (from Flugel, 2004)

- Stylobedding: Pseudo-bedding caused by parallel pressure solution
- Stylo laminated: Laminated appearance due to swarms of parallel stylolites
- Stylo nodular: Nodules and lenses of densely packed grains separated by stylolites
- Stylo mottled: Patchy enrichment of insoluble stylocumulate
- Stylo breccoid: Originates from selective pressure solution
- Stylo cumulate: Insoluble residue accumulated along a pressure-solution surface

Colors described from core (capitalized in text) relate to the above

standardized color chart key. Pore-type abbreviations in descriptions also follow the above keys. Locations of thin-section samples are indicated by TS. Cycle tops reflect no specific sequence hierarchy; however commonly coincide with the HFC-scale. Key features and deviations from general descriptions are shown indented below general description.

**ARCO Conklin 1-31 – Atlantic Richfield Oil and Gas Company**

**Permit #37385, Jackson County, MI**

**Cored Interval: 3899.5' – 3685.0'      Examined Interval: 3899.5' – 3703.0'**

**Core footages are (-5') relative to wire-line logs**

**Top Trenton: 3705.0' (From core)**

**Formations: Trenton Gp. and Utica Shale**

**3899.5 – 3894.4' = Facies #2. Dolomite. Wackestone interbedded with skeletal packstone.** Medium dark gray, Brownish gray, Pale brown, moderately bioturbated, peloid (40%), crinoid (40%), undifferentiated skeletal fragment, brachiopod, wackestone-to-packstone, with interbedded crinoid (70%), undifferentiated skeletal fragment, brachiopod, packstone/grainstone (0.2' thick, one per-foot). Wispy stylolites occur throughout. Burrows are commonly filled with coarse skeletal material and range in diameter 1.0 – 1.5 cm. White crystalline dolomite replaces skeletal fragments, lines vugs, and fills veins (0.1 x 8.0 cm, n=2). Porosity is IX (IP) in burrow fill and some packstone beds, and minor MO (crinoid) and zebra fabric VU (5-8%).

3897.0 TS

3896.6 TS

3896.4 TS

**3894.4 – 3889.7' = Facies #3. Dolomite. Burrow mottled packstone with interbedded grainstone.** Brownish gray, Medium dark gray, Pale brown, moderate/intensely bioturbated, crinoid (40%), peloid (20%), brachiopod (20%), undifferentiated skeletal fragment packstone-to-wackestone with interbedded crinoid (40%), peloid (30%), brachiopod (20%), undifferentiated skeletal fragment, grainstone/packstone (0.1 thick, deposited one or two per foot). Basal contacts of thin grainstone/packstone are sub-planar with fluid-escape structures, upper contacts are dominantly gradational. Burrow diameter ranges 1.0 – 2.0 cm, with dominantly grain-rich fill. Wispy stylolites occur throughout, with minor development of burrow-bounding stylonodular fabric. White crystalline dolomite replaces skeletal fragments, lines vugs, and fills sub-vertical veins/HTD breccias. Porosity is minor IX in grain-rich zones and bed parallel zebra fabric VU (5%).

Laminated peloid grainstone: 3894.4 – 3894.2', 3892.0 – 3891.9'

HTD breccia: 3890.3 – 3890.1'

3891.0 TS

**3889.7 – 3879.7' = Facies #3. Dolomite. Burrow-mottled packstone-to-wackestone interbedded with skeletal packstone.** Pale yellowish brown, Brownish gray, Dark gray, moderate/intensely bioturbated packstone-to-wackestone, with interbedded crinoid (70%), undifferentiated skeletal fragment, brachiopod, peloid (?) packstone (0.3 – 0.4' thick, occurring one per two-to three feet). Burrow diameter ranges 1.0 – 2.0 cm, with dominantly grain-rich fill. Wispy, burrow-bounding, and low-amplitude suture stylolites are distributed throughout. White crystalline dolomite replaces skeletal fragments, lines molds and vugs, and occludes grainstone porosity/replaces cement. Porosity is minor WP and MO (crinoid), minor IX in grainstone horizons and burrow fill, and both isolated and zebra fabric VU throughout (5-8%).

Cycle top: 3892.9', 3882.6'

3889.05 TS

3880.7 TS

**3879.7 – 3873.4' = Facies #4. Dolomite. Grainstone interbedded with packstone.** Very pale orange, Pale yellowish brown, moderate/sparsely bioturbated, crinoid (80%), undifferentiated skeletal fragment, grainstone with interbedded crinoid (70%), undifferentiated skeletal fragment, packstone (0.4 – 0.5' thick, occurring one per two feet). Burrow diameter is 1.0 cm, and fill is commonly grainstone. Grainstones contain few sedimentary structures, however one is cross-bedded. Wispy stylolites and white crystalline dolomite occur throughout. Minor IX in grainstones adjacent to packstone and FR, however IX and VU (<1.5 cm) is well developed in packstone texture (8-10%).

Cycle top: 3873.4'

3877.8 TS

3877.0 TS

3876.9 TS

3876.1 TS

3874.2 TS

**3873.4 – 3866.2 = Facies #2. Dolomitic limestone. Burrow-mottled wackestone interbedded with packstone.** Pale brown, Brownish gray, Medium dark gray, moderate/intensely bioturbated crinoid (70%), undifferentiated skeletal fragment (15%), brachiopod, peloid (?) wackestone-to-packstone interbedded with undifferentiated skeletal fragment (70%), crinoid (20%), brachiopod, peloid packstone-to-grainstone (.01 – 0.3' thick, occurring one per one/two feet) with sub-planar and irregular contacts. Burrow diameter ranges 1.0 – 2.0 cm, and burrow fill is same texture as pack-grainstone interbeds. Stylolitic throughout. White crystalline dolomite replaces skeletal fragments and lines pores throughout. Porosity is IX, MO (crinoid), VU (pinpoint, and large up to 8.0 cm), throughout, with minor local FR (8-10%).

3868.1 TS

3867.8 TS

3867.5 TS

**3866.2 – 3861.0' = Facies #3. Limestone. Packstone interbedded with skeletal grainstone.** Pale brown, Medium gray, Brownish gray, moderately bioturbated, peloid (60%), undifferentiated skeletal fragment (20%), crinoid (15%), brachiopod packstone-to-wackestone interbedded with crinoid (70%), brachiopod, bivalve, undifferentiated skeletal fragment, grainstone (0.2 – 0.6' thick, at one per foot). Wispy stylolites distributed throughout. Burrow diameter ranges 1.0 – 2.0 cm, and fill consists of coarse skeletal material. Grainstone beds are commonly bound by undulate-irregular basal contacts with fluid/burrow escape structures, and gradational upper contacts. Porosity is limited to minor FR (<5%).

Cycle top: 3866.0'

Fissile shale: 3864.6'

Exposure surface (?): 3862.0'

3861.8 TS

3861.0 TS

**3861.0 – 3851.4' = Facies #3. Dolomitic limestone. Packstone interbedded with skeletal grainstone.** Pale brown, Medium gray, Brownish gray, moderately bioturbated, peloid (60%), undifferentiated skeletal fragment (20%), crinoid (15%), brachiopod packstone-to-wackestone interbedded with crinoid (70%), brachiopod, bivalve, undifferentiated skeletal fragment, grainstone (0.1 – 0.2' thick, at one per one/two feet). Wispy stylolites distributed throughout. Burrow diameter ranges 1.0 – 2.0 cm, and fill consists of coarse skeletal material. Grainstone beds are commonly bound by undulate-irregular basal contacts with fluid/biogenic escape structures, and gradational upper contacts. White dolomite replaces skeletal fragments and outlines zebra fabric in all textures. Porosity is minor development of IX in burrow fill and grainstone, zebra and pin-point VU (5%).

Cycle top: 3853.1'

3861.9 TS

3860.3 TS

**3851.4 – 3851.3' = Facies #8. Shale.** Dark gray, laminated fissile shale. [Core-Log correlation]

**3851.3 – 3846.9' = Facies #3. Dolomite. Packstone interbedded with skeletal grainstone.** Pale yellowish brown, Brownish gray, Dark gray, sparse/moderately bioturbated, peloid (40%), crinoid (30%), undifferentiated skeletal fragment, brachiopod packstone interbedded with grainstone (0.1 – 0.2' thick, at one per foot). Burrow diameter ranges 1.0 – 2.0 cm, and fill consists of coarse skeletal material. Grainstone beds are bound by undulate-irregular basal contacts. White dolomite occurs in veins (0.1 x 3.0 cm) and outlines zebra fabric. Porosity is minor IX in burrow fill and zebra fabric VU throughout (<5%).

Cycle top: 3846.9'

**3846.9 – 3839.7' = Facies #2. Dolomite. Wackestone interbedded with packstone.** Pale yellowish brown, Brownish gray, Dark gray, sparse/moderately bioturbated, peloid (40%), crinoid (30%), undifferentiated skeletal fragment, brachiopod wackestone-to-packstone interbedded with packstone-to-grainstone (0.1 – 0.2' thick, at one per foot). Burrow diameter ranges 1.0 – 2.0 cm, and burrow fill texture is commonly that of overlying bed (i.e. wackestone fill in packstone bed). Packstone beds are bound by undulate-irregular basal contacts. White dolomite occurs in veins (0.1 x 3.0 cm, n=5) and outlines zebra fabric. Anhydrite also occludes VU porosity. Porosity is minor IX in burrow fill and well developed VU zebra fabric (8%).

Cycle tops: 3839.7'

3842.9 TS

**3839.7 – 3829.6' = Facies #2. Dolomite. Wackestone coarsening-up to packstone.** Pale yellowish brown, Brownish gray, Dark gray, moderately bioturbated, crinoid (60%), brachiopod (20%), peloid wackestone-to-packstone with interbedded packstone (0.1

– 0.3' thick, at one/two per foot). General texture coarsens-up from wacke-mudstone to packstone with discrete packstone beds. {CU-tops 3836.8', 35.8', 33.5', 29.6'}. Burrow diameter ranges 1.0 – 2.0 cm, and burrow fill texture is commonly that of overlying bed (i.e. wackestone fill in packstone bed). Interval is capped by laminated undifferentiated skeletal fragment (50%), peloid (30%), crinoid, brachiopod grainstone. Porosity is dominated by zebra VU, with minor IX in packstone zones (8%).

Cycle tops: 3833.5', 3829.6'

3831.6 TS

**3829.6 – 3819.4 = Facies #3/5. Dolomitic limestone. Wackestone coarsening-up to grainstone.** Pale yellowish brown, Brownish gray, Dark gray, moderately bioturbated, crinoid (60%), brachiopod (20%), peloid wackestone-to-packstone with interbedded laminated/bedded grainstone (0.4' thick, at one per two feet). Texture generally coarsens-up from wacke-mudstone to packstone with discrete packstone beds. Grainstone beds become planar based toward top of the interval. Burrow diameter ranges 0.5 – 1.5 cm, with both grain-rich and mud-rich fill. Porosity is zebra VU, with minor IX (IP) in grainstones and burrow fill (8%).

CU cycle tops: 3826.6', 3823.3', 3821.0'

3826.6 TS

3824.0 TS

3823.6 TS

3821.0 TS

**3819.4 – 3814.1' = Facies #3/5. Limestone. Packstone interbedded with grainstone.** Pale yellowish brown, Medium gray, Light olive gray, moderately bioturbated, peloid (50%), crinoid (30%), brachiopod, undifferentiated skeletal fragment, packstone-to-wackestone, with interbedded grainstone-to-packstone (0.1 – 0.3' thick, at one per one-two feet). Wispy stylolites and burrow-bounding stylonodular fabric distributed throughout, and few (n=6) low-amplitude suture stylolites. Burrow diameter ranges 0.5 – 1.5 cm, with grain-rich fill. Grainstone beds are planar-based in lower half of the interval, and become irregular/undulate in upper half. No visible porosity.

Cycle top: 3818.4'

3819.0 TS

**3814.1 – 3797.9' = Facies #3. Limestone. Packstone interbedded with grainstone.** Pale yellowish brown, Medium gray, Light olive gray, moderately bioturbated, peloid (50%), crinoid (30%), brachiopod, undifferentiated skeletal fragment, packstone-to-wackestone, with interbedded grainstone-to-packstone (0.1 – 0.4' thick, at one per foot, and decreasing in frequency toward top). Wispy stylolites and burrow-bounding stylonodular fabric distributed throughout. Burrow diameter ranges 0.5 – 1.5 cm, with grain-rich fill. Grainstone beds based by irregular/undulate contacts. Porosity is minor IX in grainstone.

Chert nodule: 3807.8'

Cycle top: 3812.2'

3809.7 TS  
3807.5 TS  
3806.1 TS  
3799.0 TS

**3797.9 – 3786.8' = Facies #2. Dolomitic limestone. Burrow-mottled wackestone.**

Brownish gray, Olive gray, Pale yellowish brown, moderate/intensely bioturbated, peloid (80%), crinoid, brachiopod, undifferentiated skeletal fragment, wackestone with wispy stylolites, burrow-bounding stylonodular fabric, and few low-amplitude suture stylolites (n=5) distributed throughout. Burrow diameter is <1.0 cm, with both grain-rich and mud-rich fill textures. White dolomite is sparsely distributed throughout as randomly oriented veins (0.2 x 2.0 cm, one per foot) and zebra fabric veins (n=3). Porosity is minor IX and small VU in few burrows (<5%). Note: no grain-rich interbeds (tempestites?).

Cycle top: 3793.6'

3788.0 TS

**3786.8 – 3776.1' = Facies #1. Dolomite. Burrow-mottled wackestone-to-mudstone.**

Brownish gray, Olive gray, Pale yellowish brown, moderate/intensely bioturbated, peloid (50%), crinoid (30%), undifferentiated skeletal fragment, brachiopod wackestone-mudstone with wispy stylolites, burrow-bounding stylonodular fabric, and low-amplitude suture stylolites distributed throughout. Burrow diameter is <1.0 cm, with mud-rich fill. White dolomite is sparsely distributed throughout as crinoid fragment replacement, randomly oriented veins (0.2 x 2.0 cm, one per two feet), and zebra fabric veins (n=3). Included is thin fissile shale, likely volcanic ash. Porosity is minor zebra VU (<5%). Note: no grain-rich interbeds (tempestites?).

Shale: 3783.9'

Cycle tops: 3776.1'

3782.1 TS

**3776.1 – 3766.8' = Facies #2. Dolomite. Wackestone interbedded with peloid packstone.**

Brownish gray, Olive gray, Pale yellowish brown, moderately bioturbated, peloid (50%), crinoid (30%), undifferentiated skeletal fragment, brachiopod wackestone-to-packstone with peloid (70%), undifferentiated skeletal fragment, crinoid packstone beds (0.2' thick, at one per three feet). Packstone contacts with wackestone are undulate. Wispy stylolites are distributed throughout, with few (n=3) low-amplitude suture stylolites. Burrow diameter ranges 0.5 – 2.5 cm, and burrows are commonly filled with peloid and undifferentiated skeletal fragment grains. White dolomite fills vertically oriented hairline fractures (>10.0 cm long) and replaces skeletal fragments. Porosity is IX in burrow fill and packstone textures, with minor development of pinpoint VU (<5%).

Cycle top: 3766.8'

3769.1 TS

**3766.8 – 3760.6' = Facies #2. Dolomite. Wackestone interbedded with peloid packstone.**

Brownish gray, Olive gray, Pale yellowish brown, moderately bioturbated, peloid



(40%), crinoid (40%), undifferentiated skeletal fragment, brachiopod wackestone-to-packstone with one peloid (70%), undifferentiated skeletal fragment, crinoid packstone bed (0.4' thick, at one per six feet). Packstone-wackestone contacts are undulate. Wispy stylolites are distributed throughout. Burrow diameter ranges 0.5 – 2.5 cm, and burrows are commonly filled with peloid and undifferentiated skeletal fragment grains. White dolomite fills vertically oriented hairline fractures, lines zebra fabric vugs and replaces skeletal fragments. Porosity is IX in burrow fill, with minor development of pinpoint and zebra (n=1) VU (<5%).

Cycle top: 3760.6'

3765.0 TS

**3760.6 – 3748.4' = Facies #3. Dolomite. Burrow-mottled packstone-to-wackestone.**

Brownish gray, Olive gray, Pale yellowish brown, intensely bioturbated, peloid (40%), crinoid (40%), undifferentiated skeletal fragment, brachiopod packstone-to-wackestone. Burrows commonly overlap, and are filled with peloid and undifferentiated skeletal fragment grains. Wispy stylolites are distributed throughout, with few low-amplitude suture stylolites (n=5). Interval contains a fracture zone (0.5 x >40.0 cm) of fluid migration, lined with white dolomite and pyrite. White dolomite also fills vertically oriented hairline fractures, lines zebra fabric vugs and replaces skeletal fragments. Porosity is minor zebra VU and FR, however core is broken, and FR porosity is difficult to assess.

Cycle top: 3748.4'

Missing core: 3756.8 – 3756.2', 3754.7 – 3754.0'

**3748.4 – 3734.7' = Facies #2. Dolomite. Wackestone coarsening-up to packstone.** Dark gray, Brownish gray, Pale yellowish brown, moderately bioturbated, crinoid (40%), undifferentiated skeletal fragment (30%), brachiopod (20%), peloid wackestone coarsening-up to packstone with few discrete packstone beds (0.1 – 0.3' thick, at one per five feet). Discrete packstone beds have undulate contacts. Burrow diameter ranges 1.0 – 3.0 cm, with both grain-rich and mud-rich fill. White dolomite lines and fills fractures, veins, and zebra fabrics. Minor IX and VU porosity is developed in grain rich textures, and minor zebra VU and FR porosity also occurs (5-7%).

Cycle tops: 3744.0', 3738.7', 3734.7'

3747.9 TS

**3734.7 – 3720.9' = Facies #1/2. Dolomite. Wackestone.** Dark gray, Brownish gray, Pale yellowish brown, moderately bioturbated, crinoid (40%), undifferentiated skeletal fragment (30%), brachiopod (20%), peloid wackestone-to-packstone with thin few (n=2) laminated peloid undifferentiated skeletal fragment packstone horizons (0.1' thick, at two per seven feet). Burrow diameter ranges 1.0 – 3.0 cm, with both grain-rich and mud-rich fill. Minor development of IX porosity in association with grain rich texture (<5%).

Cycle tops: 3724.0'

3732.0 TS

**3720.9 – 3718.7' = Facies #2/3. Dolomite. Burrow-mottled peloid packstone.** Pale yellowish brown, Medium gray, Brownish gray, moderately bioturbated and stylomottled, peloid (80%), crinoid, brachiopod, packstone-to-wackestone. Burrow diameter ranges 1.0 – 3.0 cm, with grain-rich fill. Internal structure lacks in this bed. No visible porosity.

3718.8 TS

**3718.7 – 3714.5' = Facies #1. Dolomite. Dark mudstone-to-wackestone.** Grayish black, Black, Brownish black mudstone-to-wackestone with few crinoid, brachiopod, and trilobite fragments, stylolite swarms, and laterally discontinuous mud-rich packstone 'pockets' (n=3). Burrow diameter ranges 1.0 – 3.0 cm, with both grain-rich and mud-rich fill. White dolomite occurs in hair-line veins. No visible porosity. [Note: upon polishing, what seemed to be hydrocarbons were released from these rocks]

**3714.5 – 3705.0' = Facies #2. Dolomite. Coarsening-up mudstone-to-packstone.** Medium gray, Brownish gray, moderate/intensely bioturbated mud-to-wackestone and packstone with few crinoid, brachiopod, and trilobite fragments, stylolite swarms, and laterally discontinuous mud-rich packstone 'pockets'. Burrow diameter ranges 1.0 – 3.0 cm, with both grain-rich and mud-rich fill. Deposits coarsen-up from mudstone to packstone in short intervals. No visible porosity.

Cycle tops: 3713.7', 3712.3', 3711.1', 3710.3', 3708.0', 3706.7'

Trenton Top: 3705.0'

3706.0 TS

**3705.0 – 3703.0' = Shale.** Medium gray, Light olive gray, laminated shale. Utica Shale.

**ARCO Dunn 1-14 – Atlantic Richfield Oil and Gas Company**

**Permit #37239, Calhoun County, MI**

**Cored Interval: 4141.0' – 4199.0'      Examined Interval: 4176.0' – 4141.0'**

**Core is (-5') relative to wire-line logs**

**Black River Shale: 4150.9' (from core)**

**Formation: Black River Gp.**

**4176.0' – 4174.4' – Facies #5/1. Limestone. Burrowed mudstone.** Yellowish gray, Medium light gray, moderately bioturbated mudstone with sparse crinoid fragments and infrequent stylolitization. No visible porosity.

**4174.4' – 4172.0' – Facies #3. Limestone. Peloidal packstone intercalated with skeletal grainstones.** Yellowish gray, Medium light gray, moderately/intensely bioturbated peloidal packstone intercalated with an undifferentiated skeletal fragment (90%), intraclast (5%), oncolite grainstone-to-packstone (0.1' thick, occurring two in three feet). The interval is sparsely stylolaminated. Included in the interval is a likely hardground as represented by vertical borings surrounded by alteration halos. No visible porosity.

Hardground: 4172.8'

**4172.0' – 4165.8' – Facies #1/2. Limestone. Bioturbated wackestone-to-mudstone.**

Medium light gray, Light olive gray, Grayish pink, moderately bioturbated wackestone-to-mudstone. Stylonodular fabric dominates pressure solution features, however stylomottling and wispy/stylolamination is present. Burrows are often bound by stylonodular texture and filled with grains, such as crinoids and undifferentiated skeletal fragments. Sparse white crystalline calcite filled veins/fractures (0.1cm x 3.0 cm). Also contained in the interval is a possible hardground given evidence by borings. Grains include brachiopods (50%), undifferentiated skeletal fragments (20%), crinoids, bryozoans, and a single stromatoporoid(?) fragment. No visible porosity.

Hardground(?): 4166.6'

**4165.8' – 4161.9' – Facies #2. Limestone. Peloid wackestone-to-packstone.** Medium light gray, Light olive gray, Grayish pink, moderately burrowed, peloid, crinoid, brachiopod wackestone-to-packstone with moderate stylomottling and stylolamination development. The basal section of the interval contains randomly oriented calcite filled veins. Included is a brachiopod, crinoid, undifferentiated skeletal fragment grainstone horizon (4163.0'). Porosity is a single brachiopod mold, partially filled with crystalline calcite.

Grainstone: 4163.1 – 4163.0'

Cycle top: 4161.9'

4159 TS

**4161.9' – 4154.9' – Facies #2. Limestone. Peloid wackestone-to-packstone.** Medium light gray, Pale green yellow, Greenish black, sparse/moderately bioturbated peloidal packstone with sparsely distributed stylolaminated intervals (0.2' thick). Skeletal grains occur as an apparent stylocumulate wackestone, where constituent grains include brachiopods, crinoids, bryozoans. Burrow filling material is identical to surrounding grains. Chert nodules occur and increase in frequency upward in the

interval. Interval is capped by a gastropod (40%), brachiopod (25%), crinoid (10%) packstone (upper 0.1'). Porosity is IP (peloids).

Chert nodules: 4159.8', 4158.7', 4158.3', 4156.8'

Cycle top: 4154.9'

**4154.9' – 4152.0' – Facies #3. Limestone. Peloidal packstone intercalated with skeletal packstones.** Medium light gray, Pale green yellow, Greenish black, sparsely bioturbated, peloidal packstone with skeletal packstone intercalations (0.1'-0.2' thick, occurring once in 0.5'). Packstone consists of undifferentiated skeletal fragments, brachiopod, and gastropod grains, in addition to one interval described as a bryozoan (1 cm diameter) grainstone-to-packstone. Interval contains very sparse wispy stylolites and white calcite filled veins. Porosity is minor IP (bryozoan, n=2).  
Chert nodules: 4154.5', 4153.0'

4153 TS

4152 TS

**4152.0' – 4150.9' – Calcareous Shale.** Light gray, fissile shale. Black River Shale.

**4150.9' – 4143.0' – Facies #3. Limestone. Peloidal packstone intercalated with skeletal grainstones.** Medium light gray, Light olive gray, Grayish pink, moderately bioturbated peloid (80%), brachiopod (10%), crinoid, gastropod packstone. Grainstone intercalations fine upward in each horizon, and consist of undifferentiated skeletal fragments, brachiopod, intraclast, gastropod, and crinoid grains (0.1'-0.2' thick, occurring once in 0.5'). Packstones contain very sparse nodular and low amplitude suture stylolites, where the grainstone horizons do not contain readily visible pressure solution. No visible porosity.

Cycle top: 4149.5'

**ARCO Gardner 1-16 – Atlantic Richfield Oil and Gas Company**

**Permit #37838, Hillsdale County, MI**

**Cored Interval: 4027.0' – 3971.0'      Examined Interval: 4027.0' – 4008.6'**

**Core footages are (-2') relative to wire-line logs**

**Black River Shale: 4117.0' (from core)**

**Formation: Black River Gp.**

**4027.0' – Bottom of Core**

**4027.0' – 4026.6' – Facies #4. Limestone. Skeletal grainstone.** Medium light gray, Medium gray, undifferentiated skeletal fragment (70%), crinoid (10%), brachiopod (10%), gastropod skeletal grainstone, bound at the base by an undulatory contact and fluid escape structures incorporating sediment from below. Elongate grains are dominantly horizontally oriented; however the interval is not laminated. No visible porosity.

Cycle Top: 4026.6'

**4026.6' – 4021.0' – Facies #2. Limestone. Wackestone-to-peloidal packstone.** Medium light gray, Medium gray, Light brownish gray, Brownish gray, moderately bioturbated, wispy, to burrow-bounding stylonodular fabric. Burrow diameters range from 0.2 cm – 2.0 cm, with grain-rich fill. Grains include peloids (60%), brachiopods (20%), gastropods (10%), crinoids (10%) No visible porosity.

Cycle Top: 4021.0'

**4021.0' – 4017.2' – Facies #3. Limestone. Packstone-to-wackestone.** Medium light gray, Light brownish gray, Brownish gray, wispy stylonitic, bioturbation increasing from sparse at the base to moderate at the top of the interval. Grains include peloids (50%), gastropods (20%), large (~2 cm) bryozoans (20%), brachiopods, and crinoids. Burrow diameters range from 0.2 cm – 2.0 cm, with grain-rich fill. Included in the interval are two, 0.1' thick skeletal packstones at 2' spacing, consisting of undifferentiated skeletal fragment (60%), bryozoan (20%), gastropod (10%), crinoid, and brachiopod grains. No visible porosity.

4019.0' TS

**4017.2' – 4017.0' – Shale (calcareous).** Dark gray, fissile. Black River Shale.

**4017.0' – 4011.6' – Facies #2 and 3. Dolomitic Limestone. Burrow mottled wackestone-to-packstone.** Light brownish gray, Medium light gray, Brownish gray, stylonodular, moderately/intensely bioturbated peloidal wackestone-to-packstone, transitioning upward into skeletal dominated packstones. Skeletal grains include crinoids (50%), brachiopods (20%), bivalves, gastropods, and undifferentiated skeletal fragments. Burrow diameters range from 1.0 cm – 3.0 cm, with grain-rich fill. This coarsening upward cycle repeats up in three occurrences, with bases at 4017.0', 4015.3', and 4013.4'. Included in this interval is a coarse, white crystalline anhydrite filled vug at 4014.4'. No visible porosity.

Cycle Top: 4011.6'

4017.0' TS

4012.0' TS

**4011.6' – 4008.6' – Facies #2. Limestone. Wackestone.** Light brownish gray, Medium dark gray, sparsely/moderately bioturbated (burrow diameters 0.5 cm – 1.0 cm, with grain-rich and mud-rich fill), stylomottled/stylonodular wackestone. Grains include brachiopods (60%), crinoids (20%), undifferentiated skeletal fragments, and peloids. No visible porosity.

**Buehrer 1 – Aurora Gasoline Company and McClure Oil Company**

**Permit #21064, Hillsdale County, MI**

**Cored Interval: 3964.0' – 3910.0'      Examined Interval: 3948.8' – 3610.0'**

**Core footages are (-4') relative to wire-line logs**

**Top Black River: 3900.0' (from core)**

**Black River Shale: 3980.0' (from core)**

**Formations: Trenton Gp. and Black River Gp.**

**3948.8 – 3942.0' = Facies #6 (A). Dolomite. Burrowed wackestones interbedded with fenestral packstones.** Brownish gray, Brownish black, moderate/intensely bioturbated, brachiopod (50%), peloid (50%) wackestone interbedded with oxidized, Very pale orange, Pale yellowish brown, peloid (90%), brachiopod packstone (likely tidal flat). Wackestones shallow-up to oxidized packstones in cycles. Wackestone is sometimes stylolaminated. White crystalline dolomite partially occludes porosity throughout. Porosity is MO, with additional development of VU and FE porosity in packstone beds (8%).

Cycle tops: 3946.6'; 3942.0'

Missing Core: 3945.0 – 3944.5'; 3943.0 – 3942.0'

**3942.0 – 3938.0' = Facies #6. Dolomite. Bedded grainstone.** Pale brown, Dusky yellowish brown, sparsely bioturbated peloid (60%), brachiopod (20%), crinoid, undifferentiated skeletal fragment, grainstone-to-packstone with wispy stylolites throughout and few low-amplitude suture stylolites (n=2). Bedding is 0.75 – 0.1' thick and oriented 5 – 10° from horizontal, with horizontally oriented grains. White dolomite replaces skeletal fragments and cement occludes IP porosity throughout. Porosity is dominantly MO and VU, with minor development of keystone VU (<10%).

Cycle Top: 3939.6'; 3938.0'

**3938.0 – 3935.5' = Facies #5. Dolomite. Bioturbated packstone-to-wackestone.** Light brownish gray, Brownish gray, moderate/intensely bioturbated, peloid (60%), crinoid packstone-to-wackestone, with wispy, burrow-bounding stylonodular, and few low-amplitude suture stylolites (n=2) throughout. Burrows are >2.0 cm, and commonly amalgamate. Included in the interval is a laminated peloidal packstone. Porosity is IX in dolomitized burrows (5-8%).

Laminated packstone: 3936.6 – 3936.5'

Cycle top: 3935.5'

**3935.5 – 3914.6' = Facies #2. Dolomite. Bioturbated wackestone with bryozoan packstone bed.** Brownish gray, Dusky yellowish brown, Light brownish gray, intense/moderate bioturbated, peloid (60%), bryozoan, brachiopod, crinoid, wackestone with wispy stylolites and stylomottled fabric. Included in this interval is a bryozoan (70%) crinoid packstone-to-wackestone, with bryozoan skeletal fragments 1.0 – 10.0 cm in length. Burrows are filled with crystalline dolomite, and diameter ranges 1.0 – 2.0 cm, commonly amalgamate. White dolomite fills hair-line veins, which are dominantly vertically oriented (0.1 x <10.0 cm). Porosity is dominantly IX in burrow fill, with additional minor VU (pinpoint, <0.5 cm) (5%).

Bryozoan packstone: 3931.9 – 3931.0'

Chert nodules: 3929.8', 3927.4', 3917.8'



Cycle tops: 3931.1', 3927.3', 3918.1', 3914.6'

Missing core: 3931.0 – 3928.8', 3924.3 – 3919.4', 3917.1 – 3914.6'

**3914.6 – 3912.3' = Facies #2. Dolomite. Bryozoan wackestone.** Grayish brown, Dusky yellowish brown, Light brownish gray, moderate/intensely bioturbated, bryozoan (80%), peloid, undifferentiated skeletal fragment wackestone with wispy stylolites throughout. Burrow diameter ranges 1.0 – 4.0 cm and commonly overlap. Bryozoan skeletal fragments range 1.0 – 10.0 cm in length. White dolomite hairline veins occur vertically and sub-vertically oriented throughout. Porosity is IX in burrow fill dolomite (4%).

Missing core: 3913.8 – 3912.9'

**3912.3 – 3902.0' = Missing Core.**

**3902.0 – 3898.1' = Facies #2. Dolomite. Wackestone with grain concentrated horizons. Black River Shale (absent).** Brownish gray, Brownish black, Dusky yellowish brown, moderately bioturbated, peloidal (50%), crinoid wackestone with interbedded brachiopod (70%), crinoid wackestone-to-packstone (0.1' thick, occurring at one per two feet). Wispy stylolites and burrows 1.0 – 3.0 cm in diameter occur throughout. White dolomite commonly replaces skeletal fragment grains. Porosity is dominated by IX in mud matrix, with minor development of WP (crinoid) (<5%).

**Facies #8. Black River Shale:** 3900.0 (driller report)

Chert nodule: 3901.7'

Missing core: 3901.0 – 3899.7'

**3898.1 – 3897.8' = Missing Core.**

**3897.8 – 3897.0' = Facies #3. Dolomite. Skeletal packstone.** Brownish gray, Light brownish gray, Dusky yellowish brown, non-/sparsely bioturbated, brachiopod (40%), crinoid (30%), undifferentiated skeletal fragment, mud-rich packstone. Few white dolomite hair-line veins (n=4). Porosity is well developed IP with additional shelter porosity, WP, MO, and minor IX (10%).

**3997.0 – 3996.2' = Missing Core.**

**3996.2 – 3995.0' = Facies #2. Dolomite. Bioturbated brachiopod wackestone-to-packstone.** Brownish gray, Light brownish gray, Dusky yellowish brown, moderate/intensely bioturbated, brachiopod (60%), crinoid (30%), gastropod, peloid wackestone-to-packstone with one thin (0.1' thick) brachiopod packstone bed. Wispy stylolites are distributed throughout. Burrows (1.0 – 4.0 cm diameter) are filled with crystalline dolomite. White dolomite occurs as hair-line veins and partially occludes porosity. Porosity is IX in burrow fills, poorly developed as VU (<0.3 cm, n=10), and well developed IP specific to the brachiopod packstone bed.

**3895.0 – 3894.5' = Missing Core**

**3894.5 – 3883.0' = Facies #5. Dolomite. Mudstone/wackestone interbedded with laminated grainstone.** Brownish gray, Light brownish gray, Dusky yellowish brown, moderately bioturbated mudstone-to-brachiopod (60%) crinoid, bryozoan

wackestone with interbedded peloid (80%), crinoid, brachiopod, undifferentiated skeletal fragment, bryozoan, often laminated, packstone-to-grainstone (0.1 – 0.3' thick, occurring at one/two per foot) with wispy stylolites throughout. Burrows are commonly 2.0 – 4.0 cm in diameter and filled with coarser skeletal material. White dolomite replaces some skeletal fragments and fills hair-line veins (<5.0 cm in length). Porosity is well developed sucrosic IX in grainstones, with additional minor development of MO, WP, FR, and VU (8 – 10%).

Intraclasts: 3888.3'

Chert nodules: 3894.5', 3885.7', 3889.5'

Cycle tops: 3888.3', 3885.4'

Missing core: 3893.4 – 3893.0', 3890.2 – 3889.6', 3887.1 – 3886.4

**3883.0 – 3882.0' = Facies #4. Dolomite. Laminated skeletal grainstone.** Brownish gray, Pale brown, laminated undifferentiated skeletal fragment (60%), crinoid, compound grains (undifferentiated skeletal fragment, brachiopod, crinoid with maximum dimension of 1.5 cm), brachiopod, mollusk grainstone. White dolomite fills a single vein (13.0 cm long). Porosity is dominantly MO (brachiopod), with additional IX (5%).

Stylolite swarm/shale: 3882.3

**3882.0 – 3878.0 = Facies #5. Dolomite. Mudstone-to-wackestone with interbedded laminated packstones.** Dark yellowish brown, Dusky yellowish brown, sparsely bioturbated mudstone-to-brachiopod wackestone interbedded with laminated brachiopod (40%), peloid (40%), undifferentiated skeletal fragment packstone (0.2' thick, occurring one per two feet). Wispy stylolites throughout. White dolomite fills veins (1.0 x 0.3 cm). Porosity is dominantly IX, with additional MO and VU developed in association with abundance of skeletal grains.

Cycle top: 3879.7'

Missing core: 3880.5 – 3880.0'

**3878.0 – 3877.8' = Missing Core.**

**3877.8 – 3877.0' = Facies #4. Dolomite. Cross-bedded skeletal grainstone.** Pale brown, Brownish gray, Very light gray, cross-bedded, crinoid (40%), undifferentiated skeletal fragment (20%), micritized-rounded grains (20%), brachiopod grainstone-to-packstone. Micritized grains likely were originally compound grains and crinoid fragments. Bedding is 0.2 – 0.3' thick. Included in skeletal grain component is a tabulate coral fragment. Porosity is dominantly MO (brachiopod) and WP (coral), with additional minor development of VU and IX (5%).

Cycle top: 3877.0'

**3877.0 – 3876.7' = Missing Core.**

**3876.7 – 3873.0' = Facies #2. Dolomite. Bioturbated wackestone-to-mudstone.** Brownish gray, Dusky yellowish brown, Grayish brown, moderate/intensely bioturbated, peloid (30%), brachiopod, crinoid wackestone-to-mudstone with wispy stylolites throughout. Burrow diameter ranges of 2.0 – 4.0 cm, commonly overlapping, and burrow fill is commonly peloid packstone-to-grainstone. Grain-rich horizons (tempestites?) conspicuously lack in this interval. White dolomite fills veins up to 6.0

cm long with dominantly vertical orientation, replaces skeletal fragments, and fills/occludes VU porosity. Porosity is small (0.75 cm maximum diameter) VU and burrow fill IX (6%).

Chert nodule: 3875.0'

Cycle tops: 3873.0'

**3873.0 – 3871.0' = Facies #1. Dolomite. Mudstone-to-wackestone interbedded with laminated grainstone.** Light brownish gray, Brownish gray, Dusky yellowish brown, moderately bioturbated mudstone-to-peloid, crinoid, undifferentiated skeletal fragment wackestone interbedded with commonly laminated peloid/undifferentiated skeletal fragment grainstone (0.1' thick, occurring two/three per foot). Burrow diameter ranges 2.0 – 4.0 cm. Wispy stylolites are distributed throughout. White dolomite fills veins up to 6.0 cm long with dominantly vertical orientation, replaces skeletal fragments, and fills/occludes VU porosity. Porosity is sucrosic IX and minor development of small (<0.5 cm) VU in grainstone beds.

Missing core: 3872.3 – 3871.9'

**3871.0 – 3866.4' = Facies #3. Dolomite. Skeletal packstone interbedded with wackestone.** Light brownish gray, Brownish gray, Dusky yellowish brown, crinoid (60%), undifferentiated skeletal fragment, brachiopod packstone-to-grainstone interbedded with moderately bioturbated mudstone-to-peloid, crinoid, undifferentiated skeletal fragment wackestone (0.1 – 0.2' thick, occurring at one per foot). Bedding contacts are sub-planar to slightly undulate. Burrow diameter ranges 1.0 – 4.0 cm and burrow fill is commonly the same texture as the overlying bed. Porosity is IX in grain/packstones (5%).

Cycle tops: 3870.4', 3868.0', 3867.5', 3866.4'

**3866.4 – 3866.0' = Missing Core.**

**3866.0 – 3861.7' = Facies #2. Dolomite. Bioturbated wackestone with packstone pockets.** Brownish gray, Dark yellowish brown, Dusky yellowish brown, moderate/intensely bioturbated, brachiopod (50%), crinoid (30%), peloid, bryozoan wackestone with laterally discontinuous packstone deposits (<0.1' thick, occurring one/two per foot) and wispy stylolites throughout. Burrow diameter ranges 1.0 – 4.0 cm Porosity is IX in burrow fill, with additional minor WP, MO, and VU development.

Chert nodule: 3865.7'

Missing core: 3863.2 – 3862.3'

**3861.7 – 3858.0' = Facies #3. Dolomite. Skeletal packstone-to-grainstone interbedded with bryozoan wackestone.** Brownish gray, Dark yellowish brown, Dusky yellowish brown, Very light gray, moderate/intensely bioturbated, crinoid (30%), brachiopod (30%), undifferentiated skeletal fragment, bryozoan, mollusk packstone-to-grainstone interbedded with sparse/moderately bioturbated brachiopod (60%), crinoid, undifferentiated skeletal fragment wackestone and wispy stylolites throughout. Bed thickness for each texture ranges 0.2 – 0.4' thick. The mud fractions of packstone beds are dark in color (Dusky yellowish brown) and commonly sheltered by brachiopod fragments. Porosity is MO/VU associated with saddle dolomite and few zebra fabric vugs (n=2).

Chert nodule: 3860.5'

Cycle top: 3860.8'

**3858.0 – 3853.4' = Facies #2. Dolomite. Brecciated and bioturbated wackestone with packstone beds.** Light brownish gray, Light olive gray, moderate/intense bioturbated, brachiopod (30%), crinoid (30%), bryozoan, gastropod, peloid wackestone interbedded with brachiopod (30%), crinoid (30%), bryozoan, gastropod, peloid packstone-to-grainstone (0.1 – 0.3' thick, occurring one per two feet) and wispy stylolites throughout. Burrow diameter ranges 1.0 – 4.0 cm and burrow fill is commonly packstone and grainstone textures. White dolomite replaces skeletal fragments and is prevalent in veins and HTD breccia. Porosity is IX in burrow fill, MO and VU in grainstones, and VU in HTD breccia (8-9%).

HTD breccia: 3857.7 – 3857.5'

Cycle tops: 3856.5', 3854.5'

**3853.4 – 3850.8' = Facies #3/5. Dolomite. Skeletal wackestone interbedded with thinning-up grainstone.** Light brownish gray, Brownish gray, Medium gray, moderately bioturbated, undifferentiated skeletal fragment (60%), brachiopod (15%), crinoid (15%), bryozoan wackestone interbedded with undifferentiated skeletal fragment (60%), brachiopod (15%), crinoid (15%), intraclast, bryozoan grainstone (0.7 – 0.2' thick with decreasing thickness higher in the interval, occurring one per foot in basal section and three per foot in upper half of interval). Wispy stylolites occur throughout mud-rich textures. Burrow diameter ranges 1.0 – 4.0 cm and burrow fill is coarsely crystalline dolomite. Porosity is IX in burrow fill and grainstone textures, and sparse (n=1) VU (6%).

Hardground: 3853.3'

Intraclasts (1.0 mm – 3.0 cm): 3852.6'

Chert nodule: 3852.0'

**3850.8 – 3850.2' = Missing Core.**

**3850.2 – 3843.6 = Facies #3. Dolomite. Laminated packstone interbedded with bryozoan wackestone.** Light brownish gray, Brownish gray, Light olive gray, sparse bioturbation, laminated undifferentiated skeletal fragment (40%), crinoid (30%), brachiopod, bryozoan packstone-to-grainstone interbedded with wackestone-to-packstone (each bed thickness 0.1 – 0.3') with wispy stylolites associated with mud-rich texture. Bedding contacts are sub-planar to undulate. Few (n=2) wackestone grains are exclusively large bryozoan grains (1.0 x 3.0 cm). Burrow diameter ranges 2.0 – 4.0 cm, and burrow fill texture is the same as that of the overlying bed. Porosity is MO (crinoid) and VU and IX in grain-rich burrow fill (5-7%).

Cycle top: 3843.6'

Missing core: 3848.0 – 3846.5'

**3843.6 – 3840.7' = Facies #3. Dolomite. Skeletal packstone interbedded with bryozoan wackestone.** Light brownish gray, Brownish gray, Light olive gray, sparse bioturbation, undifferentiated skeletal fragment (40%), crinoid (30%), brachiopod, bryozoan packstone interbedded with wackestone-to-packstone (each bed thickness 0.1 – 0.3') with wispy stylolites associated with mud-rich texture. Bedding contacts are sub-planar to undulate. Few (n=2) wackestone intervals are characterized by large bryozoan grains (1.0 x 3.0 cm) exclusively. Burrow diameter ranges 2.0 – 4.0 cm,

and burrow fill texture is the same as that of the overlying bed. Porosity is MO (crinoid) and VU and IX in grain-rich burrow fill (5-7%).

Cycle top: 3840.7'

**3840.7 – 3839.9' = Missing Core.**

**3839.9 – 3833.0 = Facies #2. Dolomite. Brecciated wackestone with packstone intercalations at high-frequency.** Brownish gray, Pale brown, Medium dark gray, moderately bioturbated, crinoid (40%), brachiopod (20%), undifferentiated skeletal fragment, bryozoan wackestone interbedded with undifferentiated skeletal fragment, peloid packstone (0.1' thick, occurring one/two per foot) and wispy stylolites throughout. Packstone beds are bound by undulate basal contacts, irregular upper contacts, and appear to be laminated, however apparent laminations may be attributable to pressure solution/stylolitization. Burrow diameter ranges 1.0 – 4.0 cm and burrow fill is both grain-rich and mud-rich, reflecting the overlying bed texture. Included in the interval is a Medium dark gray, Grayish black shale. White dolomite commonly replaces skeletal fragments, fills sub-vertical veins, and is abundant in zebra fabric and (incipient) HTD breccia. Porosity is dominantly zebra fabric VU (n=6, at one/two per foot), with additional very minor FR (8%).

Shale: 3838.6 – 3838.4'

HTD breccia: 3836.0 – 3835.6'

Cycle tops: 3838.6', 3833.6'

**3833.0 – 3832.3' = Missing Core.**

**3832.3 – 3830.9' = Facies #4. Dolomite. Skeletal grainstone.** Brownish gray, Pale brown, Medium dark gray, non-/sparsely bioturbated, undifferentiated skeletal fragment, crinoid, brachiopod grainstone. White dolomite replaces grains and cement/occludes primary porosity, obscuring depositional fabric. Porosity is IX and zebra VU (n=1) (7%).

**3830.9 – 3819.0' = Facies #2. Dolomite. Bioturbated wackestone with laminated packstone intercalations at high-frequency.** Brownish gray, Medium dark gray, Grayish black, moderate/intensely bioturbated, crinoid (40%), brachiopod (30%), undifferentiated skeletal fragment, gastropod wackestone interbedded with undifferentiated skeletal fragment (60%), brachiopod, crinoid packstone-to-grainstone (0.1 – 0.3' thick, occurring two/three per foot) with wispy stylolites throughout. Packstone-to-grainstone beds are often laminated and bound by planar and sub-planar surfaces. Burrow diameter ranges 1.0 – 2.0 cm and burrow fill is dominantly filled with coarse grains. White dolomite fills veins/fractures and occludes porosity. Porosity is limited to grain rich textures, where sucrosic IX, FR (n=1), VU and zebra VU constitute pore types (6%).

Cycle tops: 3828.0', 3824.4', 3820.2'

Missing core: 3827.3 – 3826.7', 3820.1 – 3819.6'

**3819.0 – 3816.5' = Facies #3. Dolomite. Bioturbated wackestone with laminated packstone intercalations at high-frequency.** Brownish gray, Medium dark gray, Grayish black, moderate/intensely bioturbated, crinoid (40%), brachiopod (30%), undifferentiated skeletal fragment, gastropod wackestone interbedded with

undifferentiated skeletal fragment (60%), brachiopod, crinoid packstone-to-grainstone (0.1 – 0.3' thick, occurring two/three per foot) with wispy stylolites throughout. Packstone-to-grainstone beds are often laminated and bound by planar and sub-planar surfaces. Burrow diameter ranges 1.0 – 2.0 cm and burrow fill is dominantly filled with coarse grains. White dolomite fills veins/fractures and occludes porosity. Porosity is limited to grain rich textures, where sucrosic IX, VU and zebra VU constitute pore types (6%).

**3816.5' – 3815.6' = Missing Core.**

**3815.6' – 3812.3' = Facies #5. Dolomite. Bioturbated skeletal wackestone with thick packstone beds.** Brownish gray, Medium dark gray, Grayish black, moderate/intensely bioturbated, crinoid (40%), brachiopod (30%), undifferentiated skeletal fragment, gastropod wackestone interbedded with undifferentiated skeletal fragment (60%), brachiopod, crinoid packstone-to-grainstone (0.4' thick, occurring one per foot) with wispy stylolites throughout. Packstone-to-grainstone beds are often laminated and bound by planar and sub-planar surfaces. Burrow diameter ranges 1.0 – 2.0 cm and burrow fill is dominantly filled with coarse grains. White dolomite fills veins/fractures and occludes porosity. Porosity is limited to grain rich textures, where sucrosic IX (dominates) with minor VU constitute pore types (6%).  
Cycle Top: 3812.3'

**3812.3 – 3807.3' = Facies #3. Dolomite. Wackestone-to-packstone interbedded with skeletal grainstone.** Brownish gray, Olive black, Medium light gray, Light brownish gray, moderate/sparsely bioturbated, bryozoan (40%), brachiopod (30%), crinoid (20%), undifferentiated skeletal fragment, wackestone-to-packstone interbedded with undifferentiated skeletal fragment, peloid packstone-to-grainstone (0.1 – 0.2' thick, occurring two per foot) with wispy stylolites throughout and few (n=6) low-amplitude suture-stylolites. Laminations are identifiable in each texture in select beds. Bedding contacts are dominated by sharp, planar and sub-planar surfaces, however some contacts are characterized as low amplitude undulate (compactional?) surfaces. Burrow diameter ranges 1.0 – 2.0 cm and burrow fill is coarse grained. Bryozoan fragments are 0.4 cm in maximum dimension. White dolomite replaces skeletal fragments. Porosity is dominated by IX in grain-rich texture and burrow fill, with additional development of minor MO/VU in all textures (6%).  
Cycle Top: 3807.3'  
Missing core: 3810.4 – 3809.6', 3808.8 – 3808.5'

**3807.3 – 3805.2' = Missing Core.**

**3805.2 – 3799.2' = Facies #3. Dolomite. Bryozoan wackestone-to-packstone with thick grainstone beds.** Brownish gray, Olive black, Medium light gray, Light brownish gray, moderately bioturbated, bryozoan (40%), brachiopod (30%), crinoid (20%), undifferentiated skeletal fragment, wackestone-to-packstone interbedded with undifferentiated skeletal fragment, peloid grainstone (0.1 – 0.5' thick, occurring two per foot) with wispy stylolites and low-amplitude suture-stylolites (one/two per foot) throughout. Grainstones are bound by planar and sub-planar basal contacts and gradational and undulate upper contacts, and beds fine-upward in upper half of interval. Burrow diameter ranges 1.0 – 2.0 cm and burrow fill is grain-rich. Porosity

is IX/IP in select (more commonly the thicker) grainstones and burrow fill, saddle dolomite occluded WP/MO/zebra VU (n=1), and small (<0.5 cm) VU throughout (8%).

Cycle top: 3799.2'

Missing core: 3801.1 – 3800.7', 3800.2 – 3800.0'

**3799.2 – 3798.6' = Missing Core.**

**3798.6 – 3791.5' = Facies #2. Dolomite. Heavily dolomitized wackestone.** Brownish gray, Dark gray, Light brownish gray, sparsely bioturbated, crinoid (40%), brachiopod (40%), bryozoan, undifferentiated skeletal fragment, wackestone-to-mudstone interbedded with wackestone-to-packstone (0.1' or less thick, occurring one per two feet). Interval is capped by a 0.2' thick, laminated, undifferentiated skeletal fragment, crinoid, brachiopod packstone-to-grainstone with fluid-escape structures at the base. Bedding contacts throughout are irregular/undulate. Dolomitization obscures depositional fabric (incipient HTD breccia, broken and rotated bedding). White dolomite fills vertical veins, replaces skeletal fragments, and occludes some zebra fabric vugs. Porosity is dominated by zebra fabric VU (n= >8) with additional minor development of MO/VU throughout (10%).

Cycle top: 3791.5'

Missing Core: 3798.0 – 3796.9', 3796.4 – 3795.3', 3793.4 – 3792.6'

**3791.5 – 3790.9' = Missing Core.**

**3790.9 – 3784.7' = Facies #2 and 3. Dolomite. Wackestone-mudstone interbedded with packstone-to-grainstone.** Brownish gray, Medium dark gray, Pale brown, sparse/moderately bioturbated, crinoid (40%), undifferentiated skeletal fragment (40%), brachiopod, bryozoan, wackestone-to-mudstone interbedded with packstone-to-grainstone (0.1 – 0.2' thick, occurring one per foot) with wispy stylolites and sharp, sub-planar bedding contacts throughout. Burrow diameter ranges 1.0 – 2.0 cm and burrow fill is coarse grain skeletal sand. White dolomite commonly occludes moldic and vug pores, replaces cement/fills primary porosity. Porosity is IX in grain-rich textures and MO/VU (<0.5 cm diameter (5-8%).

Cycle tops: 3788.4', 3784.7'

Missing core: 3789.3 – 3788.6', 3786.3 – 3786.0'

**3784.7 – 3784.2' = Missing Core.**

**3784.2 – 3767.4 = Facies #1 and 2. Dolomite. Heavily dolomitized and brecciated wackestone-mudstone interbedded with packstone-to-grainstone.** Brownish gray, Medium dark gray, Pale brown, sparse/moderately bioturbated, crinoid (40%), undifferentiated skeletal fragment (40%), brachiopod, bryozoan, wackestone-to-mudstone interbedded with packstone-to-grainstone (0.1 – 0.2' thick, occurring one per two/three feet) with wispy stylolites and sharp, sub-planar bedding contacts throughout. Burrow diameter ranges 1.0 – 2.0 cm and burrow fill is coarse grain skeletal sand. Primary depositional fabric is commonly partially or completely obscured by dolomitization. White dolomite commonly occludes moldic and vug pores, replaces cement/fills primary porosity. Porosity is dominantly zebra VU

(greater than two per foot) and VU associated with HTD breccia, with additional minor IX in grain-rich textures and small MO/VU (<0.5 cm diameter (6%).

Missing core: 3782.6 – 3781.7', 3781.0 – 3780.6', 3779.5 – 3779.0',  
3777.7 – 3776.4', 3775.3 – 3774.4', 3772.7 – 3770.0', 3769.6 – 3768.7'

**3767.4 – 3763.9' = Missing Core.**

**3763.9 – 3752.1' = Facies #2 and 3. Dolomite. Bioturbated wackestone interbedded with skeletal packstone, capped by laminated packstone.** Dark gray, Brownish gray, Light brownish gray, moderate/intensely bioturbated, crinoid (60%), brachiopod (15%), undifferentiated skeletal fragment wackestone-to-mudstone interbedded with crinoid (40%), brachiopod (40%), undifferentiated skeletal fragment packstone-to-grainstone (0.1 – 0.2' thick, occurring one per two/three feet) with wispy stylolites, irregular, gradational basal (grain-rich) bedding contacts, and gradational upper contacts throughout. Burrow diameter ranges 0.2 -2.0 cm. Interval is capped by a laminated undifferentiated skeletal fragment, peloid packstone with a horizontal/planar upper contact. Porosity is dominated by zebra fabric VU, with development of minor IX.

Cycle top: 3752.1'

**3752.1 – 3740.4' = Facies #2 and 4. Dolomite. Bioturbated wackestone interbedded with skeletal packstone, capped by cross-bedded grainstone.** Dark gray, Brownish gray, Light brownish gray, moderate/intensely bioturbated, crinoid (60%), brachiopod (15%), undifferentiated skeletal fragment wackestone-to-mudstone interbedded with crinoid (40%), brachiopod (40%), undifferentiated skeletal fragment packstone-to-grainstone (0.1' thick, occurring one per four feet) with wispy stylolites, irregular, gradational basal (grain-rich) bedding contacts, and gradational upper contacts throughout. Burrow diameter ranges 0.2 -2.0 cm. Interval is capped by a 0.3' thick, bedded/ cross-bedded, crinoid grainstone. Porosity is dominated by IX with minor development of zebra fabric VU (n=3).

Cycle top: 3740.4'

Missing core: 3750.7 – 3749.9', 3748.3 – 3745.8'

**3740.4 – 3732.6' = Facies #2. Dolomite. Bioturbated wackestone interbedded with skeletal packstone.** Brownish gray, Brownish black, Light brownish gray, moderate/intensely bioturbated, crinoid (70%), brachiopod, undifferentiated skeletal fragment, wackestone interbedded with packstone (0.1' thick, occurring one per two feet) with wispy stylolites throughout. Burrow fill is dominantly mud-rich, however some grain rich burrow fill occurs in the interval. Packstone beds are bound at the base by equal proportions of discrete and gradational contacts, infrequently showing fluid escape structures in each. Upper contacts of packstone beds are commonly irregular/undulate and transitional. White dolomite dominates zebra fabric, often occluding zebra vugs, but also replaces skeletal fragments. Porosity is zebra VU, saddle dolomite lined VU, and minor development of IX in grain-rich deposits.

Cycle top: 3732.6'

**3732.6 – 3723.3' = Facies #2. Dolomite. Bioturbated wackestone interbedded with skeletal packstone.** Brownish gray, Brownish black, Light brownish gray, moderate/intensely bioturbated, crinoid (70%), brachiopod, undifferentiated skeletal



fragment, wackestone interbedded with packstone (0.1' thick, occurring one/two per foot) with wispy stylolites throughout. Burrow fill is dominantly mud-rich, however some grain rich burrow fill occurs in the interval. Packstone beds are bound at the base and top by undulate contacts. White dolomite dominates zebra fabric, often occluding zebra vugs, but also replaces skeletal fragments. Porosity is dominantly IX in grain-rich deposits, with additional minor zebra VU, sub-spherical VU (commonly <0.75 cm, but also 2.0 – 5.0 cm diameter) (5-8%).

Cycle top: 3728.5', 3723.3'

**3723.3 – 3720.0' = Facies #3 (4?). Dolomite. Packstone coarsening-up to grainstone cycles.** Pale yellowish brown, Pinkish gray, Brownish gray, moderately bioturbated, crinoid (60%), brachiopod (20%), undifferentiated skeletal fragment packstone-to-wackestone that coarsens/cleans-upward (CU) to structure-less grainstone (beds up to 0.7' thick). Wispy stylolites occur throughout. Porosity is MO/VU with additional minor development of IX/IP in grainstone beds (<5%).

CU cycle tops: 3722.4', 3720.8', 3720.0'

**3720.0 – 3711.4' = Facies #2. Dolomite. Wackestone interbedded with skeletal packstone-to-grainstone.** Brownish gray, Light brownish gray, Light olive gray, moderately bioturbated, crinoid (70%), brachiopod (25%), undifferentiated skeletal fragment, wackestone-to-packstone interbedded with packstone-to-grainstone (0.1' thick, occurring one per foot) with wispy stylolites throughout. Packstone-to-grainstone bed bounding surfaces are characterized as gradational basal contacts and well-defined, undulate upper contacts. Burrow diameter ranges 1.0 – 2.0 cm and burrow fill is both grain-supported and mud-supported. Included in the interval is a Dark gray, thin (0.05' thick), laminated shale. Porosity is IX, with additional pinpoint VU, with few MO and larger VU (5%).

Shale: 3717.1'

Cycle tops: 3718.1', 3714.5'

**3711.4 – 3702.1' = Facies #3. Dolomite. Packstone interbedded with skeletal grainstone.** Brownish gray, Light brownish gray, Light olive gray, moderately bioturbated, crinoid (70%), brachiopod (25%), undifferentiated skeletal fragment, packstone-to-wackestone interbedded with packstone-to-grainstone (0.1 – 0.6' thick, occurring one/two per foot) with wispy stylolites throughout. Packstone-to-grainstone bed bounding surfaces are characterized as gradational basal contacts and well-defined, undulate upper contacts. Burrow diameter ranges 1.0 – 2.0 cm and burrow fill is both grain-supported and mud-supported. Porosity is IX, with additional pinpoint VU, with few MO (5%).

Missing core: 3707.8 – 3705.0'

**3702.1 – 3692.5' = Facies #2 and 3. Dolomite. Wackestone interbedded with skeletal packstone-to-grainstone.** Brownish gray, Light brownish gray, Light olive gray, moderately bioturbated, crinoid (70%), brachiopod (25%), undifferentiated skeletal fragment, wackestone-to-packstone interbedded with packstone-to-grainstone (0.1 – 0.5' thick, occurring two per foot) with wispy stylolites throughout. Packstone-to-grainstone bed bounding surfaces are characterized as gradational basal contacts and well-defined, undulate upper contacts. Burrow diameter ranges 1.0 – 2.0 cm and burrow fill is both grain-supported and mud-supported. Packstone-to-grainstone beds

increase in thickness and become increasingly laminated upward. Porosity is IX in grain-rich textures with minor zebra VU, few MO and larger VU (5-8%).

Missing core: 3697.5 – 3697.0', 3696.4 – 3695.9', 3695.4 – 3694.8'

**3692.5 – 3692.0' = Missing core.**

**3692.0 – 3688.2' = Facies #3. Dolomite. Packstone interbedded with skeletal grainstone**

Dusky yellowish brown, Pale yellowish brown, Brownish black, moderately bioturbated, crinoid (50%), undifferentiated skeletal fragment (30%), peloid, brachiopod, packstone-to-wackestone interbedded with packstone-to-grainstone (0.2' thick, occurring one/two per foot) and wispy stylolites throughout. Burrow diameter ranges 1.0 – 2.0 cm and burrow fill is both grain-supported and mud-supported. Bedding contacts are an inconsistent mixture of sub-planar and undulate. Included in the interval is a thin (<0.1'), fissile shale, which appears to be out of place considering surrounding depositional texture and character. White dolomite fills veins and zebra fabric (n=2). Porosity is limited to IX in a single grainstone bed (3689.0').

Shale: 3691.5'

Cycle top: 3688.2'

**3688.2 – 3680.9' = Facies #2 and 3. Dolomite. Wackestone interbedded with skeletal packstone, capped by thick packstone.**

Dusky yellowish brown, Pale yellowish brown, Brownish black, moderately bioturbated, crinoid (50%), undifferentiated skeletal fragment (30%), peloid, brachiopod, wackestone-to-packstone interbedded with packstone-to-grainstone (0.1' thick, occurring one per one/two feet) and wispy stylolites throughout. Burrow diameter ranges 1.0 – 2.0 cm and burrow fill is both grain-supported and mud-supported. Bedding contacts are an inconsistent mixture of sub-planar and undulate. Packstone texture dominates the grain-rich bed in the upper 1.25' of the interval. White dolomite fills veins and lines zebra fabric (n=3). Porosity is minor development of IX in grain-rich beds, minor FR, and few (n=3) zebra VU (5%).

Cycle top: 3680.9'

Missing core: 3686.5 – 3685.7'

**3680.9 – 3678.8' = Missing Core.**

**3678.8 – 3667.9' = Facies #2. Dolomite. Brecciated and bioturbated wackestone**

**interbedded with skeletal packstone.** Dark yellowish brown, Medium dark gray, Brownish gray, moderate/intensely bioturbated, crinoid (70%), brachiopod (15%), undifferentiated skeletal fragment wackestone-to-packstone interbedded with peloid, undifferentiated skeletal fragment, crinoid, brachiopod packstone (0.1 – 0.2' thick, occurring one per three feet) with wispy stylolites, high density in sections, throughout. Burrow diameter is dominantly 1.0 cm with grain-rich burrow fill. Bedding contacts are dominantly planar and sub-planar with infrequent undulate boundaries. White dolomite occurs as HTD breccia zebra fabric. Porosity is IX in grain-rich beds and burrow fill, VU associated with HTD breccia and zebra fabric, and minor MO (crinoid) (<8%).

Mudstone (?): 3677.7' – 3677.5'

HTD breccia: 3674.4'

Cycle tops: 3677.7', 3667.9'  
Missing core: 3674.5 – 3673.5', 3673.1 – 3672.4'

**3667.9 – 3663.6' = Facies #2 and 3. Dolomite. Wackestone-to-packstone with high frequency packstone-to-grainstone interbeds.** Moderate yellowish brown, Light brownish gray, Brownish gray, Dark gray, moderate/intensely bioturbated, crinoid (60%), brachiopod (30%), undifferentiated skeletal fragment, wackestone-to-packstone interbedded with packstone-to-grainstone (0.1 – 0.4' thick, occurring two/four per foot) with wispy stylolites throughout mud-rich beds. Burrow diameter is 1.0 – 4.0 cm with burrow fill commonly reflecting the overlying bed fabric. Bedding contacts are a mix of planar and undulate. White dolomite is distributed throughout as veins and zebra fabric. Porosity is dominated by zebra VU (n=4) and IX in grain-rich deposits, with minor development of MO/VU (5-8%).

Cycle top: 3663.6'

**3663.6 – 3658.8' = Facies #2. Dolomite. Bioturbated wackestone interbedded with skeletal packstone and shale/stylolite swarms.** Brownish gray, Medium dark gray, Pale brown, moderate/intensely bioturbated, crinoid (50%), brachiopod (30%), undifferentiated skeletal fragment, gastropod, bryozoan wackestone-to-packstone with interbedded packstone-to-grainstone (0.1' thick, occurring one/two per foot) with wispy stylolites and irregular bedding contacts throughout. Burrow diameter is 1.0 – 4.0 cm with burrow fill commonly reflecting the overlying bed fabric. Included in the interval are two Dark gray shales (or dense stylolitic swarms) and bedded (0.1' thick) crinoid, brachiopod packstone. White dolomite occurrence is dominated by zebra fabric with few veins. Porosity is minor development of IX in packstone-grainstone beds, MO/VU, and zebra VU (n=2) (<5%).

Shale: 3660.8 – 3660.7'

Bedded skeletal packstone: 3660.2 – 3660.1'

Cycle top (major?): 3660.7'

**3658.8 – 3649.8' = Facies #1 and 2. Dolomite. Wackestone-to-mudstone with packstone horizons and beds.** Dusky brown, Brownish gray, Medium dark gray, moderately bioturbated, crinoid (40%), brachiopod (40%), undifferentiated skeletal fragment, gastropod, peloid wackestone-to-mudstone with packstone laminations and beds (<0.05 – 0.2' thick) with wispy/burrow-bounding stylolites throughout, and few (n=2) low-amplitude suture-stylolites. Burrow diameter ranges 0.5 – 3.0 cm and burrow fill is grain-supported throughout. Packstone increase in thickness, from the basal 2/3 where horizons/laminations show horizontal grain orientation and sharply contact wacke-mudstone, up-to sparsely bioturbated, often laminated beds (0.1 – 0.2' thick, occurring one per foot) in the uppermost 1/3. Porosity is dominantly zebra VU (n=5), with minor IX development where packstone beds occur (5%).

Cycle top: 3654.8'

**3649.8 – 3648.0' = Missing Core.**

**3648.0 – 3644.2' = Facies #2. Dolomite. Bioturbated wackestone with high frequency (laminated) packstone beds.** Dusky brown, Brownish gray, Light brownish gray, intense/moderately bioturbated, crinoid (50%), undifferentiated skeletal fragment/peloid (30%), brachiopod, mollusk wackestone-to-packstone with

interbedded packstone (0.1' thick, occurring two/three per foot). Burrow fill texture commonly is the same as the overlying bed. Included in the interval is a fining-up laminated packstone with an irregular base and undulate upper contact. Porosity is IX in grain-rich zones (packstone, burrow fill), with minor development of saddle dolomite occluded VU (<1.0 cm, n=2) (<5%).

Fining-up packstone: 3644.0 – 3644.3'

Cycle top: 3644.2'

**3644.2 – 3639.1' = Facies #2. Dolomite. Wackestone and mud-rich/sheltered packstone beds.** Brownish gray, Medium dark gray, Light brownish gray, moderately bioturbated, brachiopod (40%), crinoid (20%), mollusc, gastropod, undifferentiated skeletal fragment, wackestone with mud-rich packstone-to-wackestone beds (0.2' thick, occurring at the base and top) with wispy stylolites throughout. Packstone beds contain 40% Dark gray mud and unabraded skeletal fragments, primarily brachiopods. White dolomite fills few (n=4) vugs and vertically oriented veins (n=2, <5.0 cm). Porosity is minor IX and WP/MO (<5%).

Cycle top: 3639.1'

Missing core: 3643.8 – 3641.1'

**3639.1 – 3634.1' = Facies #2. Dolomite. Wackestone interbedded with skeletal packstone.** Medium dark gray, Brownish gray, Pale brown, moderately bioturbated, crinoid (40%), peloid (20%), brachiopod, gastropod, wackestone-to-packstone with interbedded packstone (0.1' thick, occurring one per two feet) with undulate bedding contacts and wispy stylolites throughout. Burrow diameter ranges 1.0 – 2.0 cm and burrow fill is skeletal fragments (<2.0 cm). Porosity is minor IX in burrow fill and packstone beds (<5%).

Cycle top: 3634.1'

**3634.1 – 3621.4' = Facies #1. Dolomite. Wackestone with packstone horizons and beds.** Medium dark gray, Brownish gray, Pale brown, moderately bioturbated, crinoid (40%), peloid (20%), brachiopod, gastropod, wackestone with intercalated medium sand sized skeletal packstone horizons (0.1 and <0.1' thick, occurring one per foot) with sharp planar bedding and wispy stylolites throughout. Burrow diameter ranges 1.0 – 2.0 cm and burrow fill is dominantly identical to wackestone matrix, however some are filled with skeletal fragments. White dolomite occurs as vertical and sub-vertical hair-line veins (five per foot) and replaces select skeletal fragments. Porosity is minor IX in burrow fill and random zones, minor zebra VU (n=2) and FR (n=1) (<5%).

**3621.4 – 3620.7' = Missing Core.**

**3620.7 – 3619.2' = Facies #5/3. Dolomite. Laminated grainstone with interbedded wackestone.** Light brownish gray, Brownish gray, Medium dark gray, non-/sparsely bioturbated, often laminated, crinoid (60%), undifferentiated skeletal fragment (10%), brachiopod (10%), bryozoan grainstone-to-packstone (0.1 – 0.3' thick) interbedded with brachiopod, crinoid, bryozoan wackestone (0.1 – 0.2' thick) with wispy stylolites throughout. White dolomite replaces skeletal fragments and occludes shelter and vugular porosity. Porosity is IX in packstone and minor development of IX/WP/MO throughout.

Cycle top: 3619.2'

**3619.2 – 3610.0' = Facies #2. Dolomite. Bioturbated wackestone-to-packstone.** Brownish gray, Dusky yellowish brown, Light brownish gray, moderate/intensely bioturbated, crinoid (35%), peloid/undifferentiated skeletal fragment (35%), brachiopod, gastropod, wackestone-to-packstone with skeletal packstone burrow fill (0.1 – 3.0 cm diameter). White dolomite fills/partially occludes porosity, lines fractures (>10.0 cm), and replaces skeletal fragments. Porosity is dominated by IX in burrow fill, with additional development of small VU (<0.5 cm) (5-7%).

Cycle top: 3613.0'

**End of core.**

**Casler 5-30 – Whiting Oil and Gas Company**

**Permit #36587, Jackson County, MI**

**Cored Interval: 4081.0' – 4191.0'      Examined Interval: 4174.2' – 4081.0'**

**Top Black River Shale: 4154.5' (from core)**

**Top Black River: 4127.0' (?)**

**Formations: Black River Gp., Black River Shale, Trenton Gp.**

**4174.2' – 4172.3' = Facies #2. Dolomitic Limestone. Burrow-mottled packstone-to-grainstone.** Light brownish gray, Brownish gray, intensely bioturbated and stylomottled, with chert nodules. Burrows, with diameter range of 0.5 – 2.5 cm are the only observable sedimentary structure. Burrow fill is dominantly a mix of grain-rich and mud-rich sediments. Grains include peloids (90%), crinoids, and brachiopod. No visible porosity.

Chert nodules: 4173.1', 4172.8'

Cycle top: 4172.3'

4172.5 TS

**4172.3' – 4167.8' = Facies #3. Dolomitic Limestone. Burrow mottled packstone-to-grainstone.** Light brownish gray, Brownish gray, intensely bioturbated and stylomottled, homogenized grainstone (basal 0.3') transitioning up-to moderately bioturbated and stylolaminated mud-lean packstone. Burrow diameter ranges 0.2 – 3.0 cm, with grain rich burrow fill. Interval capped by hardground, represented by borings filled with dark organic rich sediment. Minor occurrence of calcite veins (<3mm) occur in the interval. Grains include peloids (70%), brachiopod (5%), crinoids, and gastropods. No visible porosity.

Hardground: 4167.8'

4170.5 TS

**4167.8' – 4167.4' = Facies #2/1. Dolomitic Limestone. Burrow-mottled wackestone .** Medium dark gray, Brownish gray, moderately bioturbated, peloidal wackestone to mud-rich packstone. Burrow fill consists of Light brownish gray peloidal (60%), crinoid (20%), undifferentiated skeletal fragment packstone-to-grainstone. Burrow diameter ranges 0.5 – 1.0 cm. No visible porosity.

4172.5 TS

**4167.4' – 4161.0' = Facies #3. Dolomitic Limestone. Peloidal packstone-to-grainstone.** Light brownish gray, Brownish gray, moderately bioturbated, mud-rich packstone interbedded with skeletal grainstone (0.1 – 0.2' thick, occurring one per three feet). Burrows are two dominant sizes, with diameter ranges 0.3 – 1.0 cm, and 1.0 – 3.0 cm. The smaller diameter burrows are filled with a mix of mud-rich and grain-rich sediment, where the larger variety is dominated by grain-rich fill. Anastomosing stylolites and stylolaminations occur throughout. Grains include peloids (80%), crinoids, brachiopod, gastropods, and bryozoans. No visible porosity.

Missing Core: 4162.9' – 4162.4'

Cycle top: 4161.0'

4164.5 TS

**4161.0' – 4154.8' = Facies #3. Limestone. Packstone with skeletal grainstone beds.** Light brownish gray, Olive gray, brown moderately bioturbated peloid (80%), crinoid, brachiopod packstone with increasing grainstone intercalations and chert nodules upward in the interval. Stylolaminations and burrow-bounding stylonodular fabric is distributed throughout. Burrows (0.5 – 3.0 cm diameter) are filled with coarse, mud-lean sediments. Undifferentiated skeletal fragment (30%), brachiopod (20%), crinoid (20%), bryozoan grainstone beds (0.1 – 0.3' thick, occurring one-to-two per foot) fine upward in grain-size from scour surfaces/ball-and-flow structures. Crystalline calcite replacement of brachiopod fragments occurs in grainstone horizons (n=2). No visible porosity.

Grainstone horizons: 4157.3 – 4157.2', 4156.5 – 4156.4', 4155.5 – 4155.2'

Chert nodules: 4160.0', 4159.0', 4158.0', 4155.6', 4155.2'

Cycle top: 4155.5'

4156 TS

**4154.8' – 4154.5' = Facies #8. Shale. Argillaceous mudstone/calcareous shale.** Light gray, Pale green yellow, Brownish black, Black, fissile. **Black River Shale.**

**4154.5' – 4152.1' = Facies #2. Dolomitic Limestone. Burrow-mottled packstone.** Medium gray, Light brownish gray, moderately bioturbated, peloid (90%), crinoid, brachiopod, mud-rich packstone. Burrow diameter ranges 1.0 – 2.0 cm, with a combination of mud-rich and grain-rich fill, and associated burrow-bounding stylonodular fabric. Very sparse calcite veins (1cm x 1mm) occur in upper 1' of interval. Intervals of Brownish black stylolaminations (<0.1') occur in the interval at a frequency of two per foot, possibly representing episodic volcanic eruptions subsequent to Black River Shale deposition. Porosity includes IP in prominent stylolaminations, and minor IP/IX in surrounding limestone.

Stylolaminations: 4154.2', 4153.9', 4153.6'

**4152.1' – 4149.1' = Facies #3 and 4. Dolomitic Limestone. Packstone interbedded with skeletal grainstone.** Light brownish gray, Brownish gray, moderately bioturbated peloid (70%), brachiopod (5%), crinoid packstone with thin undifferentiated skeletal fragment (70%), brachiopod grainstone beds (0.1 – 0.2' thick, occurring one-to-two per foot). Included in the interval is a laminated/horizontal grain orientation grainstone. Interval capped by vertical borings, representative of a likely hardground, filled with relatively darker (dark grey/brown) sediments consistent with the overlying interval. Very minor FR porosity (<4%).

Hardground: 4150.7', 4149.1'

**Facies #4.** Laminated grainstone: 4150.2 – 4150.1'

Chert nodules: 4149.5', 4150.3'

Cycle top: 4149.1'

4152 TS

4149.5 TS

**4149.1' – 4138.0' = Facies #3. Dolomitic Limestone. Packstone-to-grainstone.** Light brownish gray, Grayish pink, Brownish gray, moderately bioturbated, with burrow-bounding stylonodular fabric and very sparse low-amplitude suture-stylolites. Burrow diameter ranges 1.0 – 3.0 cm, with Light brownish gray, coarse grained fill. Skeletal and intraclast grain content increases, and peloid/mud component decreases-up in the interval. Interval is capped by vertical borings, likely representing a hardground. Grains include peloids (60%), crinoids (10%), brachiopod, undifferentiated skeletal fragments, and intraclasts. Porosity includes VU and partially calcite filled FR in chert and minor IX/IP surrounding chert.

Chert nodules: 4143.4', 4142.9', 4142.3', 4139.2'

Hardground: 4138.0'

Missing Core: 4141.1' – 4140.3'

4148.5 TS

4144.5 TS

4139 TS

**4138.0' – 4137.8' = Facies #4. Limestone. Skeletal grainstone.** Light brownish gray, Grayish pink, laminated, to cross-laminated undifferentiated skeletal grainstone. Included in this interval is a non-laminated (structure-less, bioturbated?) undifferentiated skeletal fragment (50%), brachiopod (20%), intraclast (10%), crinoid grainstone. No visible porosity.

Hardground: 4137.8'

Cycle top: 4137.8

**4137.8' – 4135.0' = Facies #5. Limestone. Burrow-mottled packstone-to-wackestone interbedded with skeletal packstone.** Light brownish gray, Light gray, Brownish black, intensely/totally bioturbated, peloidal packstone interbedded with thin, undifferentiated skeletal fragment (60%), brachiopod (20%), crinoid (10%) mud-lean packstone (0.1' thick, occurring one-to-two per foot). Burrow diameter ranges 1.0 – 2.0 cm, with both mud-rich and grain-rich fill. Wispy and low-amplitude suture stylolites are distributed throughout. No visible porosity.

**4135.0' – 4132.6' = Facies #5. Dolomitic Limestone. Peloidal packstone-to-wackestone.**

Light brownish gray, Brownish gray, moderately bioturbated, peloid, crinoid (<5%) packstone-to-wackestone with burrow-bounding stylonodular fabric. Burrow diameter ranges 0.5 – 3.0 cm, where fill is relatively lighter in color (Light brownish gray) and coarser grained than burrowed sediments. No visible porosity.

Chert nodule: 4134.8'

4133.5 TS

**4132.6' – 4123.5' = Facies #3. Dolomitic Limestone. Burrow-mottled packstone interbedded with skeletal grainstones.** Light brownish gray, Brownish gray, Olive gray, totally bioturbated, peloidal packstone with wispy/stylolamination intervals interbedded with thin undifferentiated skeletal fragment (80%), crinoid, brachiopod grainstones (0.1' thick, occurring one per foot). Burrow diameter, where identifiable, ranges 0.2 – 2.0 cm, with grain-rich packstone and grainstone fill. No visible porosity.



**Facies #8. Shale (<0.1')**: 4124.0'  
Hard/firmground: 4127.3'  
Cycle top: 4127.3'

4131 TS  
4130.5 TS  
4126 TS  
4124.3 TS

**4123.5' – 4121.0' = Facies #3. Limestone. Burrowed packstone-to-grainstone.** Light brownish gray, Brownish gray, Medium gray, moderate/ intensely bioturbated, peloidal (50%), crinoid (20%), brachiopod packstone with two undifferentiated skeletal fragment grainstone horizons (0.25' thick). Burrow diameter ranges 0.5 – 3.0 cm, with grain-rich fill. No visible porosity.

Skeletal grainstones: 4121.25', 4121.5'  
4121 TS

**4121.0' – 4119.9' = Facies #2. Limestone. Peloidal wackestone-to-packstone.** Dark gray-to-Brownish gray, sparse/moderately bioturbated, laminated (or stylolaminated) undifferentiated skeletal fragment (40%), peloidal (40%), crinoid wackestone-to-packstone. Burrow diameter ranges 0.7 – 1.5 cm, with mud-rich fill. Pyrite and few white dolomite veins distributed throughout interval. No visible porosity.

4120.5 TS

**4119.9' – 4119.5' = Facies #1 and 2. Limestone. Mudstone-to-wackestone.** Black, Brownish gray, mudstone-to-Black, Brownish black, Brownish gray, brachiopod (50%), crinoid (20%), bryozoan (10%), undifferentiated skeletal fragment wackestone. Mudstone dominates in basal 0.2'. Bioturbation is none-to-sparse, with a diameter of 1.0 cm and mud fill. No visible porosity.

**4119.5' – 4114.0' = Facies #3. Dolomitic Limestone. Packstone interbedded with skeletal grainstone.** Brownish gray, Grayish pink, moderately bioturbated peloid (80%), crinoid, brachiopod packstone with relatively lighter color (Brownish gray) and coarse grained burrow filling sediments and moderately distributed burrow-bounding stylonodular fabric. Packstone is interbedded with undifferentiated skeletal fragment (70%), crinoid, brachiopod grainstone-to-mud-lean packstone, which increase in skeletal grain completeness, frequency of occurrence, and decrease in grain abrasion, upward in the interval. Very minor development of FR porosity, the majority of which is occluded by white dolomite.

Skeletal grainstone: 4118.0' – 4117.5', 4116.8' – 4116.6', 4114.7' – 4114.5'

Fracture/vein filled with white crystalline calcite: 4116.0'; 4115.0'

4118 TS  
4115 TS

**4114.0' – 4112.0' = Facies #4. Dolomitic Limestone. Laminated skeletal grainstone.** Light brownish gray, Light olive gray, laminated-to-cross laminated undifferentiated

skeletal fragment (70%), brachiopod (15%), crinoid grainstone. In upper 0.5' of the interval large brachiopod fragments dominate grains, laminations cease, and a mud fraction (mud-lean packstone) is included in constituent sediments. No visible porosity.

Cycle top: 4112.0'

4112.5 TS

**4112.0' – 4108.0' = Facies #2. Limestone. Peloidal packstone.** Light gray, Light brownish gray, Brownish black, moderately bioturbated, peloid (70%), undifferentiated skeletal fragment (10%), brachiopod (10%), crinoid packstone-to-grainstone with stylonodular-to-wispy/stylolaminated fabric. Burrow diameter ranges 0.5– 2.0 cm, with dominantly grain-rich burrow fill. No visible porosity.

4110 TS

**4108.0' – 4097.8' = Facies #5/3. Dolomitic Limestone. Burrow-mottled peloidal packstone-to-grainstone.** Light gray, Light brownish gray, Brownish black, intensely bioturbated, peloidal (70%), crinoid (10%), brachiopod (10%), bryozoan packstone-to-grainstone with peloidal packstone horizons (devoid of skeletal grains), with intervals of mud-rich packstone-to-wackestone . Interval displays stylolaminated-to-stylonodular fabric. Burrow diameter ranges 0.5 – 0.3 cm, with coarse grained filling sediments. Interval includes chert and thin shale/mudstone horizon. No visible porosity.

Chert nodule: 4108.0'

Shale: 4102.1' – 4102.0'

4105 TS

4102 TS

**4097.8' – 4097.0' = Facies #4/3. Dolomitic Limestone. Undifferentiated skeletal grainstone.** Light brownish gray, grain distribution/sedimentary structure is homogeneous, includes very sparse (2 count) brachiopod fragments. No visible porosity.

4172.5 TS

**4097.0' – 4088.0' = Missing Core.**

4172.5 TS

**4088.0' – 4086.9' = Facies #2. Limestone. Burrow-mottled peloidal packstone-to-wackestone.** Light gray, Light brownish gray, intensely bioturbated peloidal packstone-to-wackestone. No visible porosity.  
Vertical fracture partially filled with white, coarsely crystalline calcite: 4084.6'

4087 TS

**4086.9' – 4086.3' = Missing Core.**

**4086.3' – 4081.0' = Facies #3. Limestone. Peloidal packstone.** Light gray, Light brownish gray, moderately bioturbated, stylolaminated peloidal (70%), crinoid, brachiopod, bryozoan packstone. No visible porosity.

4082 TS

**Faist, E. 2-12 – TOTAL Petroleum Inc.**

**Permit #33673, Jackson County, MI**

**Cored Interval: 5255.0' – 4873.0'      Examined Interval: 5254.8' – 4873.0'**

**Perforations: 5156.0 – 5180.0'**

**Top Trenton: 4879.5' (From core)**

**Top Black River: 5197.0' (From core)**

**Black River Shale: 5230.7' (From core)**

**Formations: Utica, Trenton, and Black River**

**5254.8 – 5252.8' = Limestone. Burrowed mudstone.** Very light gray, Pale yellowish brown, sparse/moderately bioturbated mudstone with few crinoid grains (<3%). Wispy stylolites and stylomottling distributed throughout. Burrow diameter is commonly 1.0 cm. Minor FR porosity occurs in chert nodules.

Chert nodules:                    5254.8', 5253.4'

5253.0 TS

**5252.8 – 5236.0' = Burrow mottled wackestone with thin mass transport deposit.** Pale yellowish brown, Medium light gray, Brownish gray, moderately bioturbated, brachiopod (40%), crinoid (20%), peloid (?), gastropod wackestone-to-packstone with wispy and low-amplitude suture stylolites. Burrow diameter range 0.4 – 1.0 cm. Bedding planes orient 10-20° from horizontal. Included is clast-supported mass transport breccia with sub- angular to sub-rounded lithoclasts, and thin fissile shale. No visible porosity.

Shale (fissile):    5243.5 – 5243.3'

Debris flow breccia:    5240.7 – 5240.1'

5250.2 TS

5249.4 TS

5245.3 TS

5244.1 TS

5243.3 TS

5242.9 TS

**5236.0 – 5231.2' = Burrow mottled fining-up packstone.** Pale yellowish brown, Light brownish gray, Medium gray, moderate/intensely bioturbated, brachiopod (60%), crinoid (20%), undifferentiated skeletal fragment (15%), bryozoan, gastropod packstone-to-grainstone and wackestone. Texture transitions as grain size fines-up from complete skeletal fragment grainstone/packstone, to laminated undifferentiated skeletal fragment, crinoid, brachiopod packstone, then to wackestone. Skeletal grainstone/packstone grains orient parallel to antecedent bedding at 10-20° from horizontal, however the sparsely bioturbated packstone laminations are horizontal. Interval is capped by wackestone with undulate basal contact. No visible porosity.

Chert nodule:                    5231.6'

5232 TS

**5231.2 – 5230.7' = Shale.** Very light gray, Yellowish gray fissile shale. **Black River Shale.**

**5230.7 – 5221.8' = Limestone. Graded skeletal packstone-mudstone beds.** Pale yellowish brown, Light brownish gray, Medium light gray, undifferentiated skeletal fragment (60%), crinoid (15%), brachiopod (15%), gastropod packstone that fines-up to laminated mudstone. All bedding is sub-horizontal (10-20° from horizontal) and wispy stylolites are distributed throughout. Each fining-up deposit (0.4 – 0.8') begins at a sub-planar scour surface overlain by skeletal packstones. No visible porosity. Chert nodule: 5220.1'

**5221.8 – 5209.8' = Limestone. Bryozoan-skeletal packstone interbedded with wackestone.** Brownish gray, Medium gray, Light olive gray, sparse/moderately bioturbated, brachiopod (40%), crinoid (20%), undifferentiated skeletal fragment, bryozoan, gastropod, oncoid(?) packstone (0.3 – 0.5' thick) interbedded with sometimes laminated wackestone-to-mudstone (0.2' thick), with wispy stylolites distributed throughout. Bryozoan fragment diameters measure up to 1.5 cm in discrete horizons. Bedding (15-20° from horizontal) is irregular and non-planar in packstone beds, and bedding contacts are commonly undulate and chaotic. Porosity is limited to a single, partially calcite cement occluded MO (brachiopod).  
Bryozoan (large) packstone-wackestone: 5221.1', 5220.7'

**5209.8 – 5204.0' = Limestone. Skeletal packstone interbedded with wackestone.** Brownish gray, Medium gray, Light olive gray, sparse/moderately bioturbated, brachiopod (40%), crinoid (20%), undifferentiated skeletal fragment, gastropod, bryozoan packstone (0.3 – 0.5' thick) interbedded with sometimes laminated wackestone-to-mudstone (0.2' thick), with wispy stylolites distributed throughout. Bedding (15-20° from horizontal) is irregular and non-planar in packstone beds, and bedding contacts are commonly undulate and chaotic. Brachiopod fragments infrequently shelter dark mud. No visible porosity.  
Brachiopod sheltered mud: 5205.1 – 5205.3'

**5204.0 – 5198.0' = Limestone. Skeletal wackestone-to-packstone.** Light brownish gray, Light gray, Dark gray, moderately bioturbated, undifferentiated skeletal fragment (60%), crinoid (15%), brachiopod (15%), bryozoan wackestone-to-packstone with wispy/stylolaminated fabric. Grains in this interval are un-oriented. Bedding is sub-horizontal (15-20° from horizontal). Burrow diameter ranges 0.5 – 1.5 cm. No visible porosity.

5198.0 TS

**5198.0 – 5186.2' = Limestone. Mass transport breccia.** Medium light gray, Light brownish gray, Olive gray, sub-angular, to sub-rounded clast and matrix supported mass transport deposit (Dunham equivalent: lithoclastic rudstone/floatstone). Lithoclasts are composed of peloid (60%), crinoid (30%), brachiopod wackestone and packstone. Clast-supported breccia (clasts 2.0 – 6.0 cm diameter) at base transition-up to mudstone and minor skeletal debris matrix-supported, bimodal breccia (clasts coarse sand sized; 2.0 – 3.0 cm diameter). Breccia texture transition repeats. Minor wispy stylolites are distributed throughout. Upper 2' contain vertical stylolites.  
Clast supported breccia: 5198.0', 5189.5', 5186.2'

5193.0 TS

**5186.2 – 5164.2' = Dolomitic limestone and dolomite. Massive skeletal grainstone.** Light brownish gray, Pale yellowish brown, undifferentiated skeletal fragment (60%), crinoid (20%), brachiopod grainstone-to-packstone with horizontal and sub-vertical (30° from vertical) wispy and low-amplitude suture stylolites. Significant sedimentary structure lacks. Porosity consists of local zones of well developed IX (IP) (15% within) and minor VU, each containing residual hydrocarbon. Vugs are sometimes oriented parallel to sub-vertical stylolites, but no dominant orientation occurs.

5172.0 TS

**5164.2 – 5142.4' = Dolomite. Skeletal wackestone-to-packstone.** Pale yellowish brown, Light brownish gray, Medium gray, peloid (?), crinoid (50%), undifferentiated skeletal fragment (30%), brachiopod wackestone-to-packstone with horizontal and sub-vertical (30° from vertical) oriented wispy/low-amplitude stylonodular and stylomottled fabric. Porosity is IX and VU throughout, and well developed VU (measuring >3.0 x 2 cm) in zones.

*[Possibly mass transport deposit, difficult to tell in <1/4 of core].*

**5142.4 – 5150.5' = Dolomite. Massive skeletal grainstone.** Light brownish gray, Pale yellowish brown, undifferentiated skeletal fragment (60%), crinoid (20%), brachiopod grainstone-to-packstone with sparsely distributed horizontal and sub-vertical (30° from vertical) wispy and low-amplitude suture stylolites. Significant sedimentary structure lacks. Porosity consists of local zones of poorly developed IX (IP) (5% within) and minor VU.

**5150.5 – 5133.0' = Limestone. Mass transport breccia.** Light brownish gray, Brownish gray, Olive gray, Medium light gray, sub-angular, to sub-rounded clast and matrix supported mass transport deposit (Dunham equivalent: lithoclastic rudstone/floatstone). Lithoclasts are composed of peloid (60%), crinoid (30%), brachiopod wackestone and packstone. Matrix is mudstone at base, with increasing crinoid and brachiopod fragment wackestone near top. No visible porosity.

5144.0 TS

**5133.0 – 5130.2' = Dolomite. Skeletal grainstone.** Light brownish gray, Pale yellowish brown, undifferentiated skeletal fragment (60%), crinoid (30%), brachiopod grainstone with horizontal and vertical and sub-vertical dissolution seams. Porosity is minor IX (IP) and VU (<5%).

5131.0 TS

**5130.2 – 5107.0' = Dolomite. Homogenized skeletal packstone.** Light brownish gray, Pale yellowish brown, Medium gray, crinoid, brachiopod, peloid (?) packstone-to-grainstone, with well developed sub-vertical (20 – 30° from vertical) stylolites and horizontal suture stylolites. Sub-vertical stylolites often result stylocumulate pseudo-beds. Sedimentary structures are notably absent, possibly owing to soft-sediment

deformations. Porosity is IX and VU in isolated zones (commonly (2.0 – 5.0 cm dimensions), and minor FR (<5%).

5122.0 TS

5110.0 TS

**5107.0 – 5089.0' = Dolomitic limestone. Skeletal packstone interbedded with grainstone.**

Light brownish gray, Pale yellowish brown, Medium gray, crinoid, brachiopod, peloid (?) packstone-wackestone interbedded with undifferentiated skeletal fragment (60%), crinoid (30%), brachiopod grainstone, each with well developed sub-vertical (20 – 30° from vertical) stylolites and horizontal suture stylolites. Texture contrasts are evident; however additional sedimentary structures are notably absent. Porosity is minor IX and VU (<5%).

Skeletal grainstone: 5105.2 – 5104.1', 5096.0 – 5094.5'

5104.0 TS

5096.2 TS

5093.4 TS

**5089.0 – 5078.0' = Limestone. Homogenized packstone with grainstone interbeds.**

Pale yellowish brown, Yellowish gray, Very light gray, crinoid (80%), brachiopod, undifferentiated skeletal fragment grainstone-to-packstone interbedded with Brownish gray, Medium gray, crinoid (60%), brachiopod (30%), undifferentiated skeletal fragment packstone-to-wackestone. Grainstone beds (0.5' thick, at one per one/two feet) share non-planar, undulate contacts with packstones. Packstones contain sub-vertical (20 – 30° from vertical) stylolite swarms. Depositional fabric internal to bedding appears homogenized, but evidence of burrowing lacks.

5085.5 TS

**5078.0 – 5069.8' = Limestone. Homogenized packstone-to-wackestone with packstone interbeds.** Brownish gray, Medium light gray, Dark yellowish brown, crinoid (60%), undifferentiated skeletal fragment, brachiopod, packstone-to-wackestone with interbedded packstone (0.5' thick, one per one/two feet). Bedding contacts are irregular, non-planar, and often undulate. Sedimentary structure internal to bedding is mottled and nodular. Sub-vertical stylolites are prevalent throughout. Minor IP and FR (weathered stylolite?) porosity (5%).

5072.0 TS

**5069.8' – 5052.8' = Dolomite. Mottled wackestone.** Medium light gray, Brownish gray, Dark yellowish brown, crinoid (70%), undifferentiated skeletal fragment, brachiopod, bryozoan wackestone-to-mudstone with mottled and nodular fabric owing to vertical and horizontal pressure dissolution. Minor FR, MO/WP (crinoid), and IX porosity.

5058.0 TS

**5052.8' – 5036.5' = Limestone. Mass transport deposit.** Brownish gray, Light brownish gray, Medium light gray, mass transport deposit composed of sub-rounded, to sub-

angular undifferentiated skeletal fragment (40%), crinoid (30%), brachiopod packstone and wackestone; laminated peloid (60%), crinoid, gastropod, brachiopod, packstone; and few crinoid, brachiopod, undifferentiated skeletal fragment grainstone lithoclasts and mudstone-to-wackestone matrix (Dunham equivalent: lithoclastic rudstone/floatstone). Interval consists of matrix support of clasts at base and top, and clast support in center third. Clast size and density is highest in the middle third of the interval, where large clasts (>8.0 cm) are commonly fractured with muddy matrix infill. No visible porosity.

5048.8 TS

**5036.5 – 5035.7' = Limestone. Mottled wackestone.** Crinoid, undifferentiated skeletal fragment, wackestone with mottled and nodular fabric owing to vertical and horizontal pressure dissolution. No visible porosity.

**5035.7 – 5018.2' = Limestone. Mass transport deposit.** Light brownish gray, Brownish gray, Medium light gray, mass transport deposit composed of sub-rounded, to sub-angular mudstone; peloid, crinoid, brachiopod wackestone; few (<10%) laminated skeletal packstone lithoclasts, and mudstone-to-wackestone matrix with crinoid fragments (Dunham equivalent: lithoclastic rudstone/floatstone). Texture is variable between clast- and-matrix support displaying no apparent organization. Interval is capped by mottled and nodular mudstone. No visible porosity.

Mottled mudstone: 5018.3 – 5018.2'

**5018.2 – 5012.8' = Limestone. Mass transport deposit.** Light brownish gray, Brownish gray, Medium light gray, mass transport deposit composed of sub-rounded, to sub-angular: mudstone; peloid, crinoid, brachiopod wackestone; and few (<10%) laminated skeletal packstone lithoclasts, and mudstone-to-wackestone matrix with crinoid fragments (Dunham equivalent: lithoclastic rudstone/floatstone). Large clasts (>5.0 cm) are commonly fractured with matrix infill. Texture is variable between clast- and matrix-support displaying no apparent organization. Interval is capped by a thin mottled and nodular mudstone. No visible porosity.

Mottled mudstone: 5012.85 – 5012.8'

**5012.8 – 5005.1' = Limestone. Mass transport deposit.** Light brownish gray, Brownish gray, Medium light gray, mass transport deposit composed of sub-rounded, to sub-angular: mudstone; peloid, crinoid, brachiopod wackestone; few (<10%) laminated skeletal packstone lithoclasts, and mudstone-to-wackestone matrix with crinoid fragments (Dunham equivalent: lithoclastic rudstone/floatstone). Large clasts (>5.0 cm) are commonly fractured with matrix infill. Texture is variable between clast- and matrix-support displaying no apparent organization. No visible porosity.

5011.9 TS

**5005.1 – 4990.1' = Limestone. Mottled wackestone-mudstone with floating lithoclasts.** Brownish gray, Dark yellowish brown, Dark gray, crinoid (70%), undifferentiated skeletal fragment, brachiopod, gastropod, wackestone-to-mudstone with equant-to-tabular “floating” mud-supported lithoclasts ranging 1.0 – 5.0 cm with variable dimensions. Wackestone texture is mottled in appearance, lacking significant



depositional structures aside from fining-up to stylolaminated mudstones. Lithoclasts are composed of peloid (60%), brachiopod, crinoid packstone-to-wackestone, constituting <10% of total rock. Larger lithoclasts commonly are fractured with matrix infill. Elongate lithoclasts commonly parallel bedding and horizontal stylolites in orientation. Wispy stylolites are distributed throughout. No visible porosity.

Mudstone (cycle top?): 5000.8', 4997.3'

5002.0 TS

**4990.1 – 4981.4' = Limestone. Mass transport deposit.** Dark yellowish brown, Brown black, Pale brown, mass transport deposit composed of sub-rounded to angular, dominantly (80%) peloid (60%), brachiopod, crinoid packstone-to-wackestone, but also brachiopod (70%), crinoid (15%), undifferentiated skeletal fragment grainstone lithoclasts (Dunham equivalent: lithoclastic rudstone/floatstone). Dominant (80%) lithoclast size ranges 1.0 – 1.5 cm, however clasts >6.0 cm sparsely occur. Texture is variable between clast- and matrix-support, however the basal half is dominantly matrix-supported, and the upper half clast-supported. No visible porosity.

4987.2 TS

**4981.4 – 4969.5' = Limestone. Mottled wackestone-mudstone with floating lithoclasts and mass transport deposit.** Brownish gray, Dark yellowish brown, Dark gray, crinoid (70%), undifferentiated skeletal fragment, brachiopod, gastropod, wackestone-to-mudstone with equant-to-tabular “floating” mud-supported lithoclasts ranging 1.0 – 10.0 cm with variable dimensions, however large clasts are commonly elongate. Wackestone texture is mottled in appearance, lacking significant depositional structures aside from fining-up to stylolaminated mudstones. Lithoclasts are composed of peloid (60%), brachiopod, crinoid packstone-to-wackestone. Included are large (>15.0 and 10.0 cm) laminated skeletal grainstone clasts with fractures filled by wackestone-mudstone matrix, and a matrix-supported mass transport deposit. Wispy stylolites are distributed throughout. No visible porosity.

Mudstone (cycle top?): 4975.6'

Mass transport deposit: 4975.3 – 4974.2'

4977.0 TS

**4969.5 – 4969.3' = Limestone. Skeletal packstone-to-wackestone.** Light gray, laminated, undifferentiated skeletal fragment (60%), crinoid (20%), brachiopod packstone-mudstone. Packstone is bound by a discrete, sub-planar, and scoured base, which is overlain by a thin Dark gray crinoid wackestone (0.1.'). No visible porosity.

**4969.3 – 4965.0' = Limestone. Mottled wackestone-mudstone with floating lithoclasts and mass transport deposit.** Medium dark gray, Brownish gray, Dark yellowish brown, sparsely bioturbated, crinoid (70%), brachiopod, peloid (?), wackestone-to-mudstone with equant-to-tabular “floating” mud-supported lithoclasts ranging 1.0 – 5.0 cm with variable dimensions (<15% of total rock). Lithoclasts are composed of peloid (60%), brachiopod, crinoid packstone-to-wackestone. Burrow diameter ranges 0.3 – 1.0 cm. Random orientation wispy stylolites are distributed throughout.

Included in is a matrix supported mass transport deposit with bed contacts oriented 20 – 30° from horizontal. Interval is capped by a thin (0.1' thick) crinoid wackestone. No visible porosity.

Mass transport deposit: 4965.5 – 4965.4'

**4965.0 – 4949.3' = Limestone. Mottled wackestone-mudstone with floating lithoclasts and thin mass transport deposits.** Brownish gray, Dark yellowish brown, Medium dark gray, sparse/moderately bioturbated, crinoid (60%), brachiopod, wackestone-to-mudstone containing <15% equant-to-tabular “floating” mud-supported lithoclasts ranging 1.0 – 5.0 cm with variable dimensions. Wackestone texture is mottled in appearance, lacking significant depositional structures aside from fining-up to stylolaminated mudstones. Lithoclasts are composed of peloid (60%), brachiopod, crinoid packstone-to-wackestone. Few large lithoclasts are fractured with matrix infill. Included are matrix- and clast-supported mass transport deposits. Wispy stylolites are distributed throughout. No visible porosity.

Mass transport deposits (clast): 4965.0 – 4963.6', 4959.4 – 4957.6'

Mass transport deposits (matrix): 4961.1 – 4960.8', 4956.8 – 4956.4

Cycle tops: 4960.8', 4953.8'

**4949.3 – 4936.8' = Limestone. Mottled wackestone-mudstone with thin mass transport deposits.** Brownish gray, Dark yellowish brown, Medium dark gray, moderately bioturbated, crinoid (60%), brachiopod, wackestone-to-packstone. Wackestone texture is burrow mottled in appearance. Interval has been incompletely diagenetically altered, resulting in a “blotchy” or fringed appearance at diagenetic front. Included are minor mass transport deposits. Wispy stylolites are distributed throughout. No visible porosity.

Mass transport deposit: 4938.3 – 4938.2'

4944.0 TS

**4936.8 – 4927.5' = Limestone. Burrow mottled wackestone.** Brownish gray, Dark yellowish brown, moderately bioturbated, crinoid (60%), brachiopod (25%), undifferentiated skeletal fragment, bryozoan wackestone-to-packstone with a thin skeletal packstone bed. Wispy stylolites are distributed throughout. No visible porosity.

Skeletal packstone: 4932.6 – 4932.5'

Cycle top: 4927.5'

**4927.5 – 4927.0' = Limestone. Mottled wackestone-mudstone.** Brownish gray, Dark yellowish brown, Medium dark gray, moderately bioturbated, crinoid (60%), brachiopod, wackestone-to-packstone. Wackestone texture is burrow mottled in appearance. Interval has been incompletely diagenetically altered, resulting in a “blotchy” or fringed appearance at diagenetic front. Wispy stylolites are distributed throughout. No visible porosity.

**4927.0 – 4923.0' = Missing Core**

**4923.0 – 4913.5' = Limestone. Mottled wackestone-mudstone.** Brownish gray, Dark yellowish brown, Medium dark gray, moderately bioturbated, crinoid (60%),

brachiopod, wackestone-to-packstone. Wackestone texture is burrow mottled in appearance. Interval has been incompletely diagenetically altered, resulting in a “blotchy” or fringed appearance at diagenetic front. Wispy stylolites are distributed throughout. No visible porosity.

4922.0 TS

- 4913.5 – 4911.2’ = Limestone. Skeletal wackestone.** Grayish black, crinoid (60%), brachiopod (25%), undifferentiated skeletal fragment, wackestone with wispy stylolites distributed throughout. No visible porosity.
- 4911.2 – 4902.8’ = Limestone. Mottled wackestone-mudstone.** Brownish gray, Dark yellowish brown, Medium dark gray, moderately bioturbated, crinoid (60%), brachiopod, wackestone-to-packstone. Wackestone texture is burrow mottled in appearance. Interval has been incompletely diagenetically altered, resulting in a “blotchy” or fringed appearance at diagenetic front. Wispy stylolites are distributed throughout, with few stylolite swarms. Minor FR porosity.
- 4902.8 – 4901.5’ = Limestone. Mass transport deposit.** Pale yellowish brown, Dusky brown matrix-supported mass transport deposit composed of sub-rounded to angular peloid, crinoid, brachiopod wackestone-to-packstone clasts and mud matrix (Dunham equivalent: lithoclastic rudstone/floatstone). Deposit is truncated by a planar contact at top. No visible porosity.
- 4901.5 – 4900.3’ = Limestone. Graded and laminated skeletal grainstone.** Light brownish gray, Pale brown, sparsely bioturbated, laminated, undifferentiated skeletal fragment (60%), crinoid (30%), brachiopod, grainstone. Grains fine-up from planar based coarse sand-sized skeletal fragments, to fine sand-sized fragments at an irregular/undulate upper bounding surface. No visible porosity.
- 4900.3 – 4892.2’ = Limestone. Mottled mudstone-to-wackestone.** Brownish gray, Dark yellowish brown, Medium dark gray, sparsely bioturbated mudstone-to-crinoid (60%), brachiopod wackestone. Texture is burrow mottled in appearance. Interval has been incompletely diagenetically altered, resulting in a “blotchy” or fringed appearance at diagenetic front. Included are minor mass transport deposits. Wispy stylolites are distributed throughout. No visible porosity.  
Cycle tops: 4897.5’, 4892.2
- 4892.2 – 4891.3’ = Dolomitic limestone. Mudstone.** Dark yellowish brown, Grayish black mudstone.
- 4891.3 – 4889.5’ = Limestone. Mottled wackestone-mudstone with floating lithoclasts.** Dark gray, Brownish black mudstone-to-crinoid wackestone with Light brownish gray “floating” mud-supported lithoclasts ranging 1.0 – 3.0 cm. Mudstone-wackestone texture is mottled in appearance. Lithoclasts are sometimes fractured with matrix infill. Wispy stylolites are distributed throughout. No visible porosity.
- 4889.5 – 4875.9’ = Limestone/dolomite. Burrow mottled wackestone with rip-up intraclasts.** Brownish gray, Medium gray, moderately bioturbated, crinoid (40%),

undifferentiated skeletal fragment (30%), brachiopod, wackestone with wispy stylolites throughout. Included at the top of the interval are tabular rip-up intraclasts.

Cap dolomite (bottom): 4884.5'

Trenton Top: 4875.9'

4880.2 TS

4877.5 TS

4877.0 TS

**4875.9 – 4873.0' = Shale.** Medium dark gray, Dark gray, laminated shale with few (<3%) crinoid and brachiopod fragments. **Utica Shale.**

**Hergert 2 – McClure Oil Company**

**Permit #22196, Hillsdale County, MI**

**Cored Interval: 3892.0' – 4063.5'      Examined Interval: 3933.8' – 3905.8'**

**Core footages are (+6') relative to wire-line logs**

**Top Black River Shale: 3923.8' (from core)**

**Formations: Black River Gp.**

**3933.8' – 3926.5' = Facies #3. Limestone. Intercalated packstone-to-grainstone.** Light olive gray, Brownish black, Light gray, Medium dark gray, moderately bioturbated peloid packstone intercalated with brachiopod, peloid grainstone (<0.1' – 0.1' thick, at one per one/two feet). Interval contains wispy stylolites, small burrows with grain-rich fill (0.5 cm diameter), chert nodules containing white crystalline calcite fractures, and grains including peloids, brachiopod, and very sparse bryozoans. No visual porosity.

Chert nodules: 3931.0', 3930.3', 3927.5'

Cycle top: 3926.5'

3927.45 TS

3927.1 TS

**3926.5' – 3924.0' = Facies #3. Limestone. Intercalated grainstone-to-packstone.** Light olive gray, Brownish black, Light gray, Medium dark gray, moderately bioturbated grainstone lacking grain orientation intercalated with peloidal packstone-to-grainstone (0.1' thick, at one per one/two feet). Burrow diameter ranges 0.5 – 2.0 cm, and skeletal grains fill dominates. Grainstones contain wispy stylolites, and grains including bryozoans, intraclasts, crinoids, brachiopods. No visual porosity.

3924 TS

**3924.0' – 3923.8' = Facies #8. Shale. Calcareous shale/argillaceous mudstone.** Brownish black, Medium dark gray, and fissile. Black River Shale/Deicke metabentonite.

**3923.8' – 3923.6' = Facies #4. Limestone. Peloidal packstone-to-grainstone.** Light brownish gray, laminated and cross-laminated, with very sparse burrows. Fining upward from basal crinoids to exclusively peloids. No visual porosity.

Cycle top: 3923.6'

**3923.6' – 3919.5' = Facies #5. Limestone. Peloid packstone-to-wackestone.** Light brownish gray, Brownish gray, moderately bioturbated, with stylonodular texture commonly bounding burrows (1.0 cm diameter, mud-rich and grain-rich fill) and very sparsely distributed, low amplitude suture-stylolites. Grains include peloids, crinoids, brachiopod, undifferentiated skeletal fragments, gastropods. Apparent sheltering of dark-organic rich sediments by brachiopod fragments. No visual porosity.

3922 TS

**3919.5' – 3918.5' = Facies #4. Limestone. Undifferentiated skeletal and intraclastic grainstone.** Light brownish gray, Brownish gray, fining upward from basal

unbraided skeletal fragments to undifferentiated skeletal fragments and peloids. Identifiable grains include crinoids, brachiopod, peloids, and intraclasts. No visual porosity.

Cycle top: 3918.5'

**3918.5' – 3912.7' = Facies #3. Limestone. Burrow mottled packstone-to-grainstone.**

Brownish black, Light gray, Medium dark gray, intensely bioturbated, peloid, crinoid, brachiopod packstone intercalated with undifferentiated skeletal fragment crinoid grainstone (0.2' thick, at one per two feet). Burrow diameter ranges 2.0 – 4.0 cm, and skeletal grains fill dominates. Burrow-bounding stylonodular and stylomottled fabrics dominate packstone. Grainstones devoid of sedimentary structure/grain orientation. No visual porosity.

Cycle top: 3912.7'

**3912.7' – 3908.0' = Facies #3. Limestone. Peloid skeletal packstone-to-grainstone.** Light brownish gray, Brownish gray, laminated and cross-laminated peloidal packstone-to-grainstone intercalated with homogeneous (devoid of sedimentary structure/grain orientation) crinoid, brachiopod, peloid, undifferentiated skeletal fragments grainstone (0.2' thick, at one per two feet). Burrow diameter ranges 2.0 – 4.0 cm, and skeletal grains fill dominates. Homogeneous grainstone intervals are moderately burrowed. Laminated grainstone stones are sparsely burrowed, and capped by vertical burrows filled with skeletal material from above. Very sparse, low amplitude suture-stylolites. No visual porosity.

Cycle top: 3908.0'

3911.95 TS

**3908.0' – 3905.8' = Facies #3. Limestone. Burrowed packstone-to-grainstone.** Light brownish gray, Brownish gray, moderately burrowed, with well developed burrow-bounding stylonodular and anastomosing stylolite fabrics. Burrow diameter ranges 2.0 – 4.0 cm, and skeletal grains fill dominates. Grains include peloids, crinoids, and brachiopods. No visual porosity.

Cycle top: 3905.8'

3907 TS

**Mann, H 6 – Ohio Oil Company**

**Permit #22381, Hillsdale County, MI**

**Cored Interval: 3935.0' – 4084.0'      Examined Interval: 4007.6' – 3935.0'**

**Core footages are (+3') relative to wire-line logs**

**Top Black River Shale: 3974.2' (from drillers report, core)**

**Formations Black River Shale, Black River Gp., Trenton Gp.**

**4007.6' – 4003.2' = Facies #2. Dolomitic Limestone. Bioturbated wackestone-to-packstone.** Light brownish gray, Dark yellowish brown, Brownish gray, moderately/intensely bioturbated, wispy stylolites and stylomottled around coarser grained burrow fill wackestone-to-packstone. Burrow diameter ranges 0.5 cm to 1.5 cm, with larger burrows filled with coarser, relatively lighter colored sediment. Peloid (40%), undifferentiated skeletal fragment (30%), brachiopod, crinoid, ostracode grainstones (0.075' – 0.15' thick, at inconsistent 0-4 occurrences per foot) interbedded with peloid (20%), undifferentiated skeletal fragment (20%), crinoid (20%), brachiopod wackestone-to-packstone. Very sparse calcite filled veins/fractures (0.1 cm x 5.0 cm) with dominant bedding horizontal and vertical orientations occur in the interval (n=6). Interval is capped by a possible bored surface, indicating firm/hardground. No visible porosity.  
Firm/hardground:      4003.2'

**4003.2' – 3998.8' = Facies #3. Dolomitic Limestone. Peloidal packstone intercalated with skeletal grainstones.** Light brownish gray, Brownish gray, Medium dark gray, Pale brown, moderately bioturbated, wispy stylolites and stylomottled around coarser grained burrow fill, with few (n=6) low-amplitude suture stylolites peloid (70%), brachiopod, crinoid wackestone-to-packstone. Burrow diameter ranges 1.0 – 2.0 cm. Included in the interval is a laminated peloidal (70%), undifferentiated skeletal fragment, gastropod, brachiopod packstone that fines-up to stylolamiated wackestone. Limited IP porosity development in packstones (<5%).  
Laminated packstone:    4002.8' – 4002.7'  
Chert nodule:      3999.1'  
Cycle tops:      4002.8'; 4000.7'

**3998.8' – 3998.6' = Facies #4. Dolomitic Limestone. Laminated skeletal intraclastic grainstone.** Light brownish gray, laminated/cross-laminated, crinoid (50%), undifferentiated skeletal fragment (20%), intraclast (20%), brachiopod grainstone. Intraclasts are tabular-to-equant with sub-rounded surfaces, ranging 0.2 cm to 2.0 cm in dimensions. No visible porosity.

**3998.6' – 3990.3' = Facies #2. Dolomitic Limestone. Peloid packstone-to-wackestone.** Brownish gray, Medium dark gray, Pinkish gray, moderately/intensely bioturbated, wispy stylolitic and burrow-bounding stylonodular peloid packstone-to-wackestone. Burrow diameter ranges 0.5 cm to 1.5 cm, with grain rich fill. Brachiopod dominated (70%) skeletal packstones 0.1' thick intercalate once in two feet. Grains include peloids (60%), brachiopod (20%), crinoids, gastropods, tabular coral (inverted orientation form growth position, approximate height ~0.5'). Porosity is limited to WP in tabular coral fragment (<5%).  
Cycle tops:      3996.5', 3990.3'

3995.8' TS

3990.5' TS

**3990.3' – 3988.3' = Missing core.**

**3988.3' – 3986.8' = Facies #2. Dolomite. Wackestone-to-peloidal packstone.** Light brownish gray, Brownish gray, Medium light gray, Pale yellowish brown, sparsely/moderately bioturbated coarsening-up wackestone-to-mud-rich packstone, where basal texture is peloid (60%), crinoid (40%) wackestone that transitions to a peloid (50%), brachiopod (30%), crinoid mud-rich packstone. Burrow diameter ranges 0.5 cm to 1.0 cm, and fill reflects the texture of overlying bed. No visible porosity.

Cycle Top: 3986.8'

3987.5' TS

**3986.8' – 3986.4' = Missing core.**

**3986.4' – 3983.6' = Facies #2. Dolomite. Wackestone-to-packstone.** Pale yellowish brown, Dark yellowish brown, Medium dark gray, moderately bioturbated, wispy stylolitic, peloid (250%), undifferentiated skeletal fragment (30%) wackestone coarsening-up to brachiopod dominated packstone. Burrows up to 2.0 cm in diameter are filled with coarse crystalline dolomite. Interval contains vertical to sub-vertical white dolomite filled fractures (0.5 cm x 4 cm) and associated vertical stylolites. Porosity containing residual hydrocarbons is developed as IX in dolomitized burrow fill (5%).

Cycle Top: 3983.6'

3985.4' TS

3983.6' TS

**3983.6' – 3976.0' = Facies #2. Dolomitic Limestone. Wackestone-to-packstone.** Grayish brown, Light brownish gray, Brownish gray, Very light gray, moderately bioturbated, peloid (50%), gastropod (15%), brachiopod (15%), crinoid (10%), bryozoan wackestone-to-packstone, with wispy/low amplitude suture stylolites and burrow-bounding stylonodular fabrics. Packstone horizons (0.1' thick) with horizontally oriented grains occur at zero/two per foot. Interval also contains a bryozoan (95%), crinoid packstone horizon. Minor development (n=6) of white dolomite veins (0.2 cm x 3 cm). Minor porosity is developed in peloidal packstones as IX/MO, where molds are not bound by euhedral dolomite crystal faces, but are dominantly sub-spherical (4 - 6%).

Bryozoan packstone horizon: 3977.0' – 3977.1'

Chert nodules: 3981.9', 3980.9', 3979.5', 3978.3', 3977.5'

Cycle top: 3976.0'

**3976.0' – 3975.6' = Facies #2. Dolomite. Bryozoan brachiopod packstone.** Grayish brown, Light brownish gray, Brownish gray, Very light gray, moderately bioturbated, brachiopod (50%), bryozoan (30%), gastropod (10%), crinoid mud-rich packstone. Interval transitions upward from a dominant grain-type of bryozoan (1 cm – 2 cm diameter) to brachiopod. No visible porosity.



Cycle top: 3975.6'

**3975.6' – 3973.9' = Facies #2. Dolomite. Peloidal packstone.** Grayish brown, Brownish gray, Light brownish gray, sparsely bioturbated, peloid packstone with wispy stylolites. Includes sub-horizontal white (saddle) dolomite filled fractures (0.5 cm x 5.0 cm) and randomly orientated hair-line fractures (0.1 cm x 3.0 cm). No visible porosity.

Missing core: Drillers report - drilled **Black River Shale: 3975.0' – 3974.2'**

**Facies #8.** Dark gray, fissile shale: 3974.1' – 3974.0'

Cycle top: 3973.9'

**3973.9' – 3959.4' = Facies #3. Dolomite/dolomitic limestone. Laminated peloidal packstone-wackestone-skeletal packstone cycles.** Pale yellowish brown, Light brownish gray, Brownish gray, moderately bioturbated, coarsens-upward from laminated peloid (85%) intraclast packstone, to peloid wackestone, to brachiopod (50%), crinoid, undifferentiated skeletal fragment, bryozoan packstone. Peloidal packstones contain laminations, cross-laminations, hummocky cross-laminations, and muddy sediments in burrow fills (0.7 cm diameter) consistent wackestone component of the interval. Interval also contains skeletal grainstone intercalations 0.1' thick composed of similar grains and grain proportions of skeletal packstones and are bound at the base and top by irregular surfaces. Wispy stylolites and stylomottled fabric dominates mud supported texture, however low amplitude suture stylolites are present (n=6). No visible porosity.

Cycle tops: 3971.1', 3968.6', 3965.2', 3963.5', 3962.2', 3959.4'

Missing core: 3961.5' – 3960.5'

3974.3' TS

3967.5' TS

**3959.4' – 3959.2' = Missing core.**

**3959.2' – 3947.7' = Facies #2. Dolomite/dolomitic limestone. Burrowed peloidal wackestone-to-packstone.** Light brownish gray, Pale brown, Dark yellowish brown, Brownish gray, moderately/intensely bioturbated, stylomottled and burrow-bounding stylonodular, peloid (60%), brachiopod (20%), crinoid wackestone intercalated with peloid (60%), brachiopod (20%), crinoid packstones (0.1' thick, occurring one per one/two feet). Grain supported intercalations are sometimes laminated. Burrow diameter ranges 0.2 cm to 2.0 cm (1.0 cm – 2.0 cm size dominate) and coarse burrow fill is commonly replaced by coarse crystalline dolomite mosaic, but also are filled with mud. White coarsely crystalline dolomite also lines dominant sub-vertical fractures (0.1–0.5 cm x 1.0–8.0 cm), subordinate random orientated fractures/veins, and replaces shell fragments. No visible porosity.

Cycle tops: 3952.5', 3947.7'

3956.4' TS

**3947.7' – 3944.5' = Facies #3. Dolomite. Peloidal packstone intercalated with skeletal grainstones.** Very pale orange, Light brownish gray, Dark gray, sparsely bioturbated, peloid (80%), crinoid, brachiopod packstone-to-wackestone intercalated with crinoid

(60%), brachiopod (20%), bryozoan, intraclast, trilobite grainstone-to-packstones (0.1' thick, one per one/two feet). Saddle dolomite often lines crinoid fragments molds. Pervasive dolomitization in upper half of the interval obscures non-skeletal grains and matrix, replaces skeletal fragments throughout, and developed MO, VU, WP, and IX (pinpoint vugs) porosity (5-8%).

Cycle top: 3944.5'

3947.0' TS

3945.0' TS

**3944.5' – 3941.5' = Facies #3. Dolomite. Peloidal packstone.** Light brownish gray, Brownish gray, Dark gray, moderately bioturbated, peloid (70%), crinoid, undifferentiated skeletal fragment, packstone, with wispy stylolitic and burrow-bounding stylonodular textures. Burrow diameter ranges 1.0 – 2.0 cm, where apparent coarse grain fill dominates. Pervasive dolomitization obscures grain and depositional texture identification. Matrix replacement (mosaic) and white saddle dolomite occurs throughout, with development of saddle dolomite lined bedding parallel-elongated vugs (zebra fabric, 3.0 cm x 1.0 cm) and equant vugs (0.5 cm). Additional porosity is developed in IX pinpoint vugs located in matrix replacing dolomite. Vugs commonly contain residual hydrocarbon. Porosity is IX, VU, MO (15%).

**3941.5' – 3940.0' = Facies #3. Dolomite. Peloidal packstone intercalated with skeletal grainstones.** Dark gray, Light olive gray, depositional texture is obscured by dolomitization. Primary fabric is likely moderately bioturbated, peloidal packstone-to-wackestone, with burrow-bounding stylonodular fabric. Matrix replacing dolomite crystal mosaic dominates, but also contains saddle dolomite filled vugs. Porosity includes IP and IX (<5%).

Cycle top: 3940.0'

**3940.0' – 3939.5' = Facies #3. Dolomite. Peloidal packstone.** Light brownish gray, Brownish gray, Dark gray, moderately bioturbated, peloid (70%), crinoid, undifferentiated skeletal fragment, packstone, with wispy stylolitic and burrow-bounding stylonodular textures. Pervasive dolomitization obscures grain and depositional texture identification. Matrix replacement (mosaic) and white saddle dolomite occurs throughout, with development of saddle dolomite lined bedding parallel-elongated vugs (zebra fabric, 3.0 cm x 1.0 cm), equant vugs (0.5 cm), and bedding parallel/sub-horizontal fractures. Additional porosity is developed in IX pinpoint vugs in matrix replacing dolomite. Vugs commonly contain residual hydrocarbon. Porosity is IX, VU, MO (10%).

Chert nodules: 3939.8', 3938.4'

3938.6' TS

**Martin et al. 2-A – Marathon Oil Company**

**Permit #22083, Calhoun County**

**Cored Interval: 4085.2 – 4184.6'      Examined Interval: 4184.6' – 4085.2'**

**Core footages are (0') relative to wire-line logs**

**Top of E-Shale: 4113.0'**

**Perforated Interval: 4108 - 4120', 4128 – 4140'**

**Formations: Trenton**

**4184.6 – 4179.0' = Facies #3. Dolomite. Burrow-mottled packstone to wackestone with coarse-grained burrow fills and thin (<0.2') skeletal grainstone horizons.** Grains are predominantly crinoids with brachiopods and trilobites. Coarse-grained burrow fills commonly exhibit intercrystalline porosity. Minor amounts of stylolites. Grainstone horizons = 4182.0', 4183.3'

**4179.0 – 4178.7' = Facies #4. Dolomite. Finely laminated skeletal grainstone topped with borings.** Minor dissolution porosity.

**4178.7 – 4177.5' = Facies #3. Dolomite. Burrow-mottled packstone to wackestone with coarse-grained burrow fills.** Grains include bryozoans and undifferentiated skeletal debris. Minor intercrystalline porosity is found in burrows. Stylolites are common. Cycle tops = 4178.7'

**4177.5 – 4175.5' = Facies #2. Dolomite. Sucrosic texture, likely burrow-mottled wackestone with coarse-grained burrow fills.** Grains include crinoids and undifferentiated skeletal debris. Porosity types include intercrystalline and vuggy. Stylolites are common.

**4175.5 – 4174.4' = Missing core.**

**4174.4 – 4171.7' = Facies #2. Dolomite. Burrow-mottled wackestone with ~0.3' thick grainstone horizon at 4173.7'.** Coarse-grained burrow fills are common. Stylolites frequently bound nodules. Grains include crinoids and undifferentiated skeletal debris. Cycle tops = 4174.3'

**4171.7 – 4163.6' = Facies #3. Dolomite. Burrow-mottled packstone to wackestone with coarse-grained burrow fills and skeletal grainstone horizons (<0.3' thick).** Grains include brachiopods, crinoids, peloids and undifferentiated skeletal debris. Very minor intercrystalline porosity in coarse-grained burrow fills near top of section. Small (~1 mm) vugs associated with saddle dolomite. Stylolites are common.

**4163.6 – 4161.4' = Facies #3. Burrow-mottled packstone to wackestone with coarse-grained burrow fills.** Grains include bryozoans, crinoids, peloids and minor brachiopods. Minor stylolites.

**4161.4 – 4159.7' = Facies #4/5. Sparsely-burrowed skeletal/tidal flat (?) grainstone.** Grains include peloids and undifferentiated skeletal debris. Porosity types include minor fenestral and intercrystalline. Minor stylolites. Shaley/carbonaceous partings at

4160.3’.

Cycle tops = 4159.7’

**4159.7 – 4150.4’ = Facies #3. Dolomite. Burrow-mottled packstone to wackestone with coarse-grained burrow fills and skeletal grainstone horizons** (4158.0’, 4156.1’, 4153.4’, 4152.7’, 4152.3’ and 4150.5’) Grains include peloids, intraclasts, crinoids and undifferentiated skeletal debris. Minor void-lining saddle dolomite and fracture breccias. Porosity types include intercrystalline in burrow fills/grainstone horizons and non-selective vugs. Stylolites are common.

Cycle tops = 4156.6’

**4150.4 – 4148.0’ = Facies #3. Dolomite. Burrow-mottled packstone to grainstone with coarse-grained burrow fills and thin (<0.2’) grainstone horizons** (4149.3’). Grains include intraclasts, bryozoans, crinoids and gastropods. Stylolites are common.

Cycle tops = 4148.0’

**4148.0 – 4145.0’ = Facies #2. Dolomite. Burrow-mottled wackestone with coarse-grained burrow fills.** Shale horizon (~ 1cm) at 4146.6’. Grains include intraclasts, peloids and undifferentiated skeletal debris. Stylolites are common.

**4145.0 – 4137.6’ = Facies #2. Dolomite. Burrow-mottled wackestone to packstone with coarse-grained burrow fills.** Grains include peloids, crinoids and intraclasts. Saddle dolomite very commonly lines voids and replaces matrix. Vertical fracture (~ 5mm thick, from 4138.8 – 4137.6’) occluded with saddle dolomite and truncated by stylolites. Porosity is vuggy. Stylolites are common.

**4137.6 – 4131.5’ = Facies #2. Dolomite. Burrow-mottled wackestone with coarse-grained burrow fills.** Grains include crinoids, peloids and intraclasts. Skeletal lag surface at 4136.5’. Minor vuggy porosity and zones with abundant intercrystalline porosity. Stylolites are common.

Cycle tops = 4136.5’

**4131.5 – 4131.0’ = Facies #3. Dolomite. Burrow-mottled packstone.** Grains include crinoids and peloids. Intercrystalline porosity. Stylolites are common.

**4131.0 – 4126.7’ = Facies #3. Dolomite. Burrow-mottled packstone with coarse-grained burrow fills and grainstone horizons** (~ 0.2 – 0.5’ thick). Grains include crinoids, peloids, brachiopods and undifferentiated skeletal debris. Porosity types include vuggy and intercrystalline (primarily within grainstone horizons and coarse-grained burrow fills). Vugs are lined with saddle dolomite. Stylolites are common.

Cycle tops = 4126.7’

**4126.7 – 4119.3’ = Facies #2. Dolomite. Burrow-mottled wackestone with coarse-grained burrow fills and grainstone horizons.** Grains include crinoids, peloids and undifferentiated skeletal debris. Porosity types include vuggy and intercrystalline. Fracture breccias at 4129.9’. Saddle dolomite commonly lines vugs and replaces matrix. Stylolites are common.

**4119.3 – 4116.7’ = Missing core.**

- 4116.7 = 4115.0' = Facies #2. Dolomite. Burrow-mottled wackestone.** Grains include peloids and undifferentiated skeletal debris. Vuggy porosity is common. Saddle dolomite often lines vugs and replaces matrix. Stylolites are common.
- 4115.0 – 4114.7' = Missing core.**
- 4114.7 – 4114.2' = Facies #2. Dolomite. Burrow-mottled wackestone.** Grains include peloids and undifferentiated skeletal debris. Vuggy porosity is common. Saddle dolomite often lines vugs and replaces matrix. Stylolites are common.
- 4114.2 – 4109.3' = Facies #3 and 1. Dolomite and shale. Burrow-mottled packstone to wackestone with coarse-grained burrow fills and grainstone horizons (4113.0').** Grains include crinoids, intraclasts, peloids and undifferentiated skeletal debris. Shale horizon at 4112.9'. Dolomite occluded fractures from 4110.0 – 4109.5'. Intercrystalline porosity is found in burrow fills. Stylolites are common. Cycle tops = 4112.9'
- 4109.3 – 4108.8' = Missing core.**
- 4108.8 – 4180.6' = Facies #2. Dolomite. Burrow-mottled mudstone to wackestone with coarse-grained burrow fills.** Grains include undifferentiated skeletal debris. Stylolites are common.
- 4108.6' – 4108.3' = Facies #4. Dolomite. Sparsely-burrowed, laminated grainstone.** Grains include undifferentiated skeletal debris, which are abraded and well-sorted. Stylolites are common. Saddle dolomite replaces matrix and occludes fractures. Porosity is intercrystalline.
- 4108.3 – 4108.0' = Missing core.**
- 4108.0 – 4107.3' = Facies #4. Dolomite. Sparsely-burrowed, laminated grainstone.** Grains include undifferentiated skeletal debris, which are abraded and well-sorted. Stylolites are common. Saddle dolomite replaces matrix and occludes fractures. Porosity is intercrystalline.
- 4107.3 – 4104.5' = Burrow-mottled packstone to wackestone with coarse-grained burrow fills and grainstone horizons (4107.1').** Grains include crinoids, peloids and trilobites. Minor replacement of matrix by saddle dolomite. Stylolites are common. Intercrystalline porosity is found in burrow fills and grainstone horizons. Hardground at 4104.5'. Cycle tops = 4104.5'
- 4104.5 – 4104.3' = Facies #2. Dolomite. Sparsely-burrowed mudstone.** No distinctive textures.
- 4104.3 – 4102.3' = Facies #2. Dolomite. Burrow-mottled wackestone with coarse-grained burrow fills and grainstone horizons (4102.5').** Grains include peloids and undifferentiated skeletal debris. Microfractures are occluded by saddle dolomite.

Stylolites are common. Intercrystalline porosity is found in burrow fills and grainstone horizons.

**4102.3 – 4099.4' = Facies #3. Dolomite. Burrow-mottled packstone with coarse-grained burrow fills and grainstone horizons (4101.4').** Grains include peloids, crinoids and undifferentiated skeletal debris. Microfractures are both open and occluded by saddle dolomite. Stylolites and organics are common. Intercrystalline porosity is found in burrow fills and grainstone horizons.

**4099.4 – 4099.1' = Facies #4. Dolomite. Sparsely-burrowed, laminated skeletal grainstone.** Grains include undifferentiated skeletal debris that is abraded and well-sorted. Microfractures are occluded with saddle dolomite.

**4099.1 – 4095.2' = Facies #3. Dolomite. Burrow-mottled packstone with coarse-grained burrow fills and grainstone horizons (4098.0', 4096.4', 4095.2').** Grains include peloids, crinoids and brachiopods. Stylolites throughout. Intercrystalline porosity is found within grainstone horizons and burrow fills. Minor replacement of matrix by saddle dolomite.

**4095.2 – 4094.8' = Facies #2. Dolomite. Burrow-mottled mudstone to wackestone.** Grains include crinoids, peloids and intraclasts. Minor amounts of matrix-replacive saddle dolomite and stylolites. Sparse intercrystalline porosity.

**4094.8 – 4094.4' = Facies #4. Dolomite. Sparsely-burrowed, laminated skeletal grainstone.** Grains include undifferentiated skeletal debris that is well-sorted and abraded. Microfractures are occluded with saddle dolomite. Intercrystalline porosity.

**4094.4 – 4092.3' = Facies #2. Dolomite. Burrow-mottled wackestone to packstone with coarse-grained burrow fills.** Grains include peloids and crinoids. Saddle dolomite commonly replaces matrix and occludes fractures. Intercrystalline porosity. Stylolites are common.

**4092.3 – 4092.0' = Facies #4. Dolomite. Sparsely-burrowed, laminated skeletal grainstone.** Grains include undifferentiated skeletal debris that is well-sorted and abraded. Microfractures are occluded with saddle dolomite. Intercrystalline porosity.

**4092.0 – 4087.3' = Facies #3. Dolomite. Burrow-mottled packstone to wackestone with coarse-grained burrow fills and grainstone horizons (4091.6').** Grains include peloids, crinoids and undifferentiated skeletal debris. Shale horizons at 4089.1' and 4088.6'. Replacement of matrix by saddle dolomite is common. Porosity types include intercrystalline (within burrow fills) and vugs (often lined/occlude by saddle dolomite).

**4087.3 - 4085.2' = Facies #2. Dolomite. Burrow-mottled wackestone to mudstone with coarse-grained burrow fills and grainstone horizons (4085.9').** Grains include peloids, crinoids, gastropods and brachiopods. Intercrystalline porosity is common in burrow fills. Stylolites are common.

**McMahon, J. & B. #4 – Marathon Oil Company**

**Permit #22460, Calhoun County, MI**

**Cored Interval: 4170.0 – 4091.0'**

**Examined Interval: 4168.7 – 4091.0'**

**Formation: Trenton**

**4168.7 – 4167.5' = Facies #2. Dolomite. Burrow-mottled wackestone.** Medium gray, Brownish gray, Light brownish gray, moderately bioturbated, crinoid (40%), undifferentiated skeletal fragment (30%), brachiopod (20%), peloid wackestone-to-packstone with packstone burrow-fill (1.0 – 2.0 cm), grain concentrated accumulations, and wispy stylolites distributed throughout. White dolomite replaces skeletal fragments and fills fractures and lines pores. Porosity is well developed IX (IP) in grain-rich zones, WP/MO (crinoid), and minor VU (5-10%).

**4167.5' – 4165.8' = Dolomite. Wackestone interbedded with skeletal grainstone.** Medium gray, Brownish gray, Light brownish gray, moderately bioturbated, crinoid (40%), undifferentiated skeletal fragment (30%), brachiopod (20%), peloid wackestone-to-packstone interbedded with Pale yellowish brown, undifferentiated skeletal fragment (60%), crinoid, brachiopod, (cross-bedded?) grainstone (0.2 – 0.4' thick, at one per foot). Burrow diameter ranges 1.0 – 2.0 cm, with grain-rich burrow fill. Wispy stylolites are distributed throughout. Porosity is well developed IX and VU (5-10%).

Cycle top: 4165.8'

4167.2 TS

**4165.8 – 4162.1' = Facies #3. Dolomite. Wackestone with interbedded packstone.** Medium gray, Brownish gray, Pale yellowish brown, moderate/sparsely bioturbated, crinoid (40%), brachiopod (40%), undifferentiated skeletal fragment, wackestone-to-packstone interbedded with crinoid, brachiopod, undifferentiated skeletal fragment packstone-to-grainstone (0.2' thick, at one per foot) and mud-rich brachiopod packstone horizons. Burrow diameter ranges 1.0 – 2.0 cm, with grain-rich burrow fill. Wispy stylolites are distributed throughout. Grain-rich horizons are bound at by sub-planar basal and transitional upper contacts. White dolomite replaces skeletal fragments, lines pores and filled hair-line veins. Porosity is well developed IX and zebra VU, and minor WP/MO (brachiopod and crinoid) (10%).

Cycle top: 4162.1'

4164.6 TS

**4162.1 – 4148.8' = Facies #2. Dolomite. Wackestone with grain-rich horizons.** Medium gray, Brownish gray, Pale yellowish brown, moderate/sparsely bioturbated, crinoid (40%), brachiopod (40%), undifferentiated skeletal fragment, wackestone interbedded with crinoid, brachiopod, undifferentiated skeletal fragment packstone (0.2' thick, at one per foot) and mud-rich brachiopod packstone-wackestone horizons. Each bed shows little internal structure. Burrow diameter ranges 1.0 – 2.0 cm, with both mud-rich and grain-rich burrow fill. Wispy stylolites are distributed throughout. Grain-rich horizons are bound irregular and undulate contacts. White dolomite replaces skeletal fragments, lines pores and filled hair-line veins. Porosity is well developed IX and minor zebra VU and WP/MO (brachiopod and crinoid) (10%).

Missing core: 4161.2 – 4160.3', 4157.7' – 4152.1', 4151.2 – 4150.4'

4159.0 TS  
4158.9 TS  
4158.8 TS  
4153.5 TS

**4148.8 – 4148.3' = Facies #4. Dolomite. Laminated skeletal grainstone.** Pale yellowish brown, laminated, sparse/moderately bioturbated, crinoid (60%), brachiopod (30%), undifferentiated skeletal fragment grainstone with sharp, scoured, and sub-planar base. Porosity is occluded by white dolomite, with minor zebra VU remaining (<5%).  
Cycle top: 4148.3'

**4148.3 – 4141.3' = Facies #5/3. Dolomite. Wackestone with interbedded skeletal packstone.** Medium gray, Light brownish gray, sparse/moderately bioturbated, crinoid (60%), brachiopod (30%), undifferentiated skeletal fragment wackestone-to-packstone interbedded with packstone (0.1 – 0.3' thick, at one per two feet) and thin packstone stringers (<0.05). Burrow diameter ranges 1.0 – 2.0 cm, with both mud-rich and grain-rich burrow fill. Wispy stylolites are distributed throughout. White dolomite lines pores and occludes zebra VU. Porosity is well developed IX in grain rich textures, and poorly developed MO/WP and VU (5-10%).

4148.1 TS  
4147.5 TS  
4142.6 TS

**4141.3 – 4140.8' = Facies #4. Dolomite. Laminated skeletal grainstone.** Pale yellowish brown, planar based, laminated undifferentiated skeletal fragment, crinoid grainstone. Grain-size coarsens upward. Primary porosity is completely occluded by white dolomite, however secondary porosity is developed as IX and VU (8%).  
Cycle top: 4140.8'

**4140.8 – 4135.7' = Facies #2. Dolomite. Wackestone interbedded with skeletal packstone.** Medium gray, Brownish gray, Light brownish gray, moderately bioturbated, brachiopod (40%), crinoid (40%), undifferentiated skeletal fragment wackestone interbedded with peloid, undifferentiated skeletal fragment packstone (0.1' thick, at one per foot). Beds are bound by irregular and undulate contacts. Burrow diameter is commonly 1.5 cm and filled with dominantly skeletal grains. Wispy stylolites occur throughout, with few (n=2) low-amplitude suture stylolites. Porosity is very well developed sucrosic IX in burrow fill and packstone beds, and minor VU.  
Cycle top: 4135.7'

4140.5 TS

**4135.7 – 4133.0' = Missing Core.**

**4133.0 – 4129.8' = Facies #3. Dolomite. Wackestone coarsening-up to packstone cycles.** Brownish gray, Olive gray, Pale yellowish brown, moderately bioturbated, crinoid (40%), brachiopod (20%), peloid, undifferentiated skeletal fragment wackestone



repeatedly coarsening-up to packstone with interbedded discrete packstone-grainstone beds (0.1' thick). Burrow diameter ranges 1.0 – 2.0 cm, with dominantly grain-rich burrow fill. Porosity is IX and minor isolated VU (5-8%).

Cycle tops: 4131.9', 4129.8'

4131.9 TS

4131.8 TS

**4129.8 – 4121.1' = Facies #3 and 2. Dolomite. Packstone-to-wackestone with interbedded skeletal packstone.** Brownish gray, Olive gray, Pale yellowish brown, moderately bioturbated, crinoid (40%), brachiopod (20%), peloid, undifferentiated skeletal fragment packstone-to-wackestone with skeletal packstone beds (0.1 – 0.2' thick, at two per foot, decreasing in frequency-up). Burrow diameter ranges 1.0 – 2.0 cm, with grain-rich burrow fill. Packstone interbeds are mixture of sharp/planar-basal and undulate-basal contacts. Porosity is well developed sucrosic IX porosity in zones of grain concentrations and minor MO (crinoid) (8%).

Cycle tops: 4125.3', 4123.7', 4121.1'

Missing core: 4129.5 – 4128.7', 4123.2 – 4122.1'

4122.5 TS

4121.7 TS

**4121.1 – 4118.9' = Facies #3. Dolomite. Packstone-to-wackestone with interbedded skeletal packstone.** Brownish gray, Olive gray, Pale yellowish brown, sparse/moderately bioturbated, crinoid (50%), brachiopod, undifferentiated skeletal fragment, peloid packstone-to-wackestone with skeletal packstone beds (0.1 – 0.2' thick, at one per foot). Burrow diameter ranges 1.0 – 2.0 cm, with both mud-rich and grain-rich burrow fill. Packstone interbeds are mixture of sharp/planar-basal and undulate-basal contacts. Porosity is well developed sucrosic IX porosity in burrow fill and minor MO (crinoid) (8%).

Fissile shale: 4119.2 – 4119.1'

4119.2 TS

**4118.9 – 4118.1' = Facies #4. Dolomite. Skeletal grainstone.** Pale yellowish brown, brachiopod (60%), crinoid (30%), undifferentiated skeletal fragment grainstone with undulate contacts and no internal structure. The lack of sedimentary structure suggests total bioturbation subsequent to deposition. White dolomite occludes primary porosity, however MO, VU, and IX porosity is moderately developed (5-8%).

**4118.1 – 4108.5' = Facies #5. Dolomite. Packstone-to-wackestone with thick grainstone interbeds.** Brownish gray, Olive gray, Pale yellowish brown, sparse/moderately bioturbated, crinoid (50%), brachiopod, undifferentiated skeletal fragment, peloid packstone-to-wackestone interbedded with skeletal grainstone beds (0.2 – 0.8' thick, at one per two feet). Burrow diameter ranges 1.0 – 2.0 cm, with dominantly grain-rich burrow fill. Porosity is dominantly IX, with additional MO and VU (5-8%).

Cycle tops: 4117.1', 4112.7', 4111.5', 4108.5'

Massive grainstone: 4112.3 – 4111.5'

4116.7 TS  
4114.1 TS  
4113.6 TS  
4110.3 TS  
4109.2 TS  
4109.1 TS

**4108.5 – 4101.4' = Facies #2. Dolomite. Crinoid brachiopod wackestone.** Brownish gray, Olive gray, Pale yellowish brown, moderately bioturbated, crinoid (40%), brachiopod (20%), peloid, undifferentiated skeletal fragment wackestone-to-packstone. Burrow diameter ranges 1.0 – 2.0 cm, with both mud-rich and mud-rich burrow fill. Porosity is well developed sucrosic IX and VU (8%).

4108.5 TS  
4105.3 TS  
4104.3 TS

**4101.4 – 4097.6' = Facies #3. Dolomite. Packstone-to-wackestone interbedded with grainstone.** Brownish gray, Olive gray, Pale yellowish brown, sparse/moderately bioturbated, crinoid (50%), brachiopod, undifferentiated skeletal fragment, peloid packstone-to-wackestone interbedded with skeletal grainstone beds (0.1 – 0.2' thick, at one per two feet). Burrow diameter ranges 1.0 – 2.0 cm, with both mud-rich and grain-rich burrow fill. Grainstone interbeds are mixture of sharp/planar-basal and undulate-basal contacts, and sometimes laminated. Grainstone skeletal grains become less abraded and fragmented in the upper section of the interval. Porosity is dominantly zebra VU, with additional MO and VU (5-8%).

Cycle top: 4099.0'

4098.2 TS  
4097.8 TS  
4097.7 TS

**4097.6 – 4091.0' = Facies #3. Dolomite. Packstone-to-wackestone interbedded with packstone.** Brownish gray, Olive gray, Pale yellowish brown, sparse/moderately bioturbated, crinoid (50%), brachiopod, undifferentiated skeletal fragment, peloid packstone-to-wackestone interbedded with skeletal mud-rich packstone beds (0.2' thick, at one per two feet). Burrow diameter ranges 1.0 – 2.0 cm, with both mud-rich and grain-rich burrow fill. Packstone interbeds are mixture of sharp/planar-basal and undulate-basal contacts. Porosity is dominantly zebra VU, with additional MO and VU (5%). Interval is capped by a laminated undifferentiated skeletal fragment, peloid packstone.

Cycle top: 4091.0'

4096.2 TS

**Rowe A-2 – McClure Oil Company**

**Permit #37239, Hillsdale County, MI**

**Cored Interval: 4030.0' – 3680.0'      Examined Interval: 4026.1' – 3680.0'**

**Core footage is (+5) relative to wire-line logs**

**Top Black River: 3942.7' (From core)**

**Top Black River Shale: 3980.0' (From core)**

**Formations: Black River Gp. and Trenton Gp.**

**4026.1 – 4022.0' = Facies #6. Dolomite. Tidal flat grainstones interbedded with burrowed wackestones.** Dark yellowish brown, Brownish gray, sparse-to-moderately bioturbated, peloid (80%), gastropod, brachiopod, wackestone-to-packstone interbedded with Light olive gray, Very pale orange, Very light gray, oxidized tidal flat peloidal grainstone-to-packstone. Pack-wackestone beds contain burrows commonly 1.0 cm in diameter, with both coarse-grained and muddy burrow fill. Characteristic of mud rich deposits are poorly developed VU and IX porosities, white crystalline dolomite veins (0.2 x 8.0 cm) and wispy stylolites. Tidal flat beds (0.5 – 0.9' thick) contain laminations, few horizontal (n=2) and vertical (n=5) stylolites, FE, MO (brachiopod), and VU porosity (5-8%).

Cycle tops: 4027.0', 4023.4'

Major cycle tops: 4022.4'

4024.0 TS

**4022.0 – 4011.2' = Facies #3. Dolomite. Bioturbated peloidal packstone.** Pale yellowish brown, Light brownish gray, Very light gray, Medium gray, moderately/intensely bioturbated, peloid (80%), crinoid, brachiopod, packstone-to-wackestone with intercalations of undifferentiated skeletal fragment (80%), intraclast grainstones (0.05 – 0.4' thick), with wispy stylolites throughout. Burrowed packstones contain burrows (0.2 – 1.5 cm diameter) commonly filled with Light brownish gray, coarser grained dolomite (sediments) and associated IX porosity development (~5%). Bioturbation increases from moderate to intense upward in the interval. Saddle dolomite lined vertical fractures (2.0 x 20.0 cm) and skeletal fragment replacement occurs throughout. Additional porosity is minor FR where saddle dolomite does not completely occlude, and minor IP (IX) in grainstones.

Intraclastic grainstones: 4016.0 – 4015.8', 4013.8 – 4013.6'

Cycle tops: 4013.6'

4019.0 TS

4015.0 TS

4014.0 TS

**4011.0 – 4003.2' = Facies #3. Dolomite. Bioturbated packstone with coarse-grained burrow fill.** Dark yellowish brown, Light olive gray, Medium gray, intensely/moderately bioturbated peloid, crinoid, brachiopod packstone-to-wackestone, with horizons of laminated peloid packstone (0.1' thick, at one/foot) and wispy stylolites throughout. Burrow diameter ranges 0.25 – 2.0 cm. Burrow fill is Dark yellowish brown in color and consists of coarse skeletal grains, with well developed IX porosity (10-15%).

Cycle tops: 4003.2'

**4003.2 – 4000.2' = Facies #2. Dolomite. Bioturbated wackestone.** Dark yellowish brown, Light olive gray, Brownish gray, Medium gray, intensely/moderately bioturbated peloid, crinoid (<10%), brachiopod (<10%) wackestone with horizons of laminated/cross-laminated peloid packstone (0.1' thick, at one/foot) and burrow-bounding and wispy stylolites. Burrow diameter ranges 0.5 – 1.0 cm in diameter, with both mud-rich and coarse grained fill. Interval contains bored surface with alteration halos and rip-up clasts immediately above, representing a hardground. No visible porosity.

Hardground: 4003.0'

Cycle tops: 4003.0'

**4000.2 – 3997.7' = Facies #2. Dolomite. Burrow-mottled wackestone with coarse-grained burrow fill.** Dusky brown, Brownish gray, Light olive gray moderate/intensely bioturbated peloid, crinoid (<10%), brachiopod (<10%) wackestone with wispy stylolites and stylomottled fabric. Burrow diameter ranges 0.5 – 1.5 cm, with associated IX (IP) porosity (5-8%). Interval contains white crystalline dolomite veins (0.2 x 1.0 cm).

Chert nodule: 3998.0'

3995.8 TS

3995.0 TS

**3997.7' – 3987.0' = Facies #3. Dolomite. Burrow-mottled wackestone-to-packstone.** Brownish gray, Medium dark gray, Pale yellowish brown, moderate/intensely bioturbated, peloid (40%), bryozoan (20%), brachiopod (15%), undifferentiated skeletal fragment wackestone-to-packstone, with coarse grained burrow-fill (1.0 – 2.0 cm diameter) and wispy/stylomottled fabric. Included in the interval is a skeletal, intraclast grainstone. Porosity (5%) is IX (burrow fill), VU, and MO (bryozoan, brachiopod).

Intraclast grainstone: 3995.0' – 3994.8'

Shale: 3984.0' (<.01')

Chert nodule: 3993.0', 3388.5'

Cycle tops: 3995.5', 3994.1', 3986.5'

3990.5 TS

3988.9 TS

3987.5 TS

**3987.0 – 3981.8' = Facies #4. Dolomite. Interbedded packstones and grainstones.** Dark yellowish brown, Brownish gray, Medium gray, Pale yellowish brown packstones interbedded with grainstones, each composed of peloid (60%), bryozoan (20%), brachiopod (10%), crinoid, and undifferentiated skeletal fragment grains. Interval is sparsely bioturbated (burrow diameter ranges 0.5 – 1.5 cm), contains wispy and low-amplitude suture stylolites, and chert. Grainstones (0.05 - .2' thick) occurring at one or two beds per foot are bound by irregular/sub-planar contacts with packstones. Bryozoans in the interval are up to 1.0 cm in diameter. Porosity consists of minor IP (IX) in grainstones, and bryozoan MO and WP (5 – 9%).

Cycle tops: 3981.8

Chert nodule: 3986.0', 3985.5', 3985.3', 3982.0', 3981.9'

3985.4 TS

3983.6 TS

**3981.8 – 3877.9' = Facies #2. Dolomite. Burrow-mottled wackestone.** Dark yellowish brown, Brownish gray, Medium gray, Pale yellowish brown intense/totally bioturbated peloid (?), brachiopod (40%), undifferentiated skeletal fragment (10%), bryozoan wackestone with wispy stylolites. Bioturbation increases-up, with a dominant 0.75 cm burrow diameter and dominantly mud-rich fill. White dolomite veins (0.3 x 2.0 cm) minor development (n=10). Very minor development of IX porosity in a single location (1.0 x 3.0 cm).

**Facies #8. Black River Shale: 3980.0'**

3980.5 TS

**3977.9 – 3970.2' = Facies #3. Dolomite. Burrow-mottled packstone-to-grainstone.** Dark yellowish brown, Moderate yellowish brown, Medium gray, peloid (60%), crinoid (15%), brachiopod (15%) undifferentiated skeletal fragment packstones interbedded with crinoid (50%), brachiopod (30%), undifferentiated skeletal fragment grainstones, commonly occurring one every two/three feet, at 0.1' thick. Burrow diameter ranges 1.0 – 2.0 cm, with grain-rich fill. Wispy/low-amplitude stylolites and white dolomite filled fractures/veins (0.1 x 3.0 cm) are distributed throughout. Minor IX (IP grainstones), and saddle dolomite lined VU and FR porosity (5%).

Cycle tops: 3977.5', 3971.7'

Chert nodule: 3973.3'

3974.3 TS

**3970.2 – 3963.5' = Facies #3. Dolomite. Burrow-mottled packstone with coarse-grained burrow fill.** Brownish gray, Pale yellowish brown, Dark yellowish brown, Medium gray moderate/intensely bioturbated peloid (70%), crinoid (15%), brachiopod, undifferentiated skeletal fragment, gastropod packstone with skeletal rich packstone-to-grainstone beds (0.1' thick, occurring one-to-two in two vertical feet), and wispy/stylomottled fabric throughout. Interval is capped by a skeletal packstone-to-grainstone in upper 1.0'. Burrows are filled with coarse grain dolomite crystals (diameter ranges 1.0 – 2.0 cm). White crystalline dolomite replaces skeletal grains throughout (>10%). Porosity is minor MO throughout, IX and VU in skeletal rich beds, and IX throughout burrow fills (5-8% total).

**Facies #1. Mudstone/shale: 3963.5'**

Cycle tops: 3963.5'

Chert nodules: 3969.8', 3967.0'

3968.35 TS

3968.15 TS

3967.5 TS

3964.5 TS

3964.3 TS

**3963.5 – 3960.2' = Facies #2. Dolomite. Burrow-mottled wackestone with interbedded skeletal grainstone horizon.** Light grayish green, Pale yellowish brown, Brownish gray, Dark gray, moderately bioturbated peloid (60%), brachiopod (15%), crinoid (15%) wackestone-to-packstone with wispy and low-amplitude suture stylolites. Burrow diameter ranges 1.0 – 2.0 cm, with grain-rich fill. Included in the interval is a crinoid (80%), brachiopod grainstone with minor development of IX (IP), MO, and VU porosity (5%). Additional porosity is IX in apparent peloid-rich horizons.

Skeletal grainstone: 3561.8 – 3961.6'

Cycle tops: 3961.6'

Chert nodules: 3962.0', 3961.2'

3961.7 TS

**3960.2 – 3954.0' = Facies #3. Dolomite. Burrow-mottled packstone-to-grainstone with coarse-grained burrow fills and interbedded skeletal grainstone horizons.** Light grayish green, Pale yellowish brown, Brownish gray, Dark gray, intensely bioturbated peloid (70%), crinoid, brachiopod packstone with laminated and cross-laminated undifferentiated skeletal fragment (50%), crinoid (30%), brachiopod grainstone beds. Individual burrow diameter ranges 1.0 – 2.0 cm (commonly overlap), with coarse skeletal fill. Planar based skeletal grainstones transition-up to peloid packstones. Porosity is well developed in grainstones as IX (cement), IP, MO, VU, and IX in burrow fill (15%).

**Facies #4.** Skeletal grainstone: 3958.9 – 3958.8', 3958.6 – 3958.3', 3956.8 – 3955.0

Cycle tops: 3958.4', 3955.0'

3960.1 TS

3959.05 TS

3958.15 TS

3957.9 TS

3957.4 TS

3957.35 TS

3957.05 TS

3956.8 TS

3956.4 TS

3955.95 TS

3955.75 TS

**3954.0 – 3950.8' = Facies #4. Dolomite. Skeletal grainstone with interbedded burrow-mottled packstone-to-wackestone.** Light brownish gray, Brownish gray, Light gray, crinoid (75%), compound skeletal grain, bryozoan, brachiopod, undifferentiated skeletal fragment grainstone interbedded with moderately bioturbated peloid (70%), brachiopod (10%), crinoid (10%), undifferentiated skeletal fragment packstone-to-wackestone. Grainstones with cm-scale cross-bedding are planar based, and where cross-bedding lacks an irregular surface at basal bed-contact. Burrow diameter ranges 1.0 – 2.0 cm, with dominantly coarse grain burrow fill. Porosity is limited to IX in burrow fill (5%).

Cycle tops: 3952.6', 3950.8'

3952.1 TS

**3950.8 – 3942.7' = Facies #5/3. Dolomite. Burrow-mottled wackestone with interbedded grainstone/packstone, mudstone, and shale.** Dark gray, Pale yellowish brown, Very pale orange, Brownish gray, moderately bioturbated, peloid (60%), brachiopod, crinoid wackestone interbedded with brachiopod (50%), crinoid (30%), undifferentiated skeletal fragment, bryozoan grainstone and mud-rich packstone. Grainstones contain well abraded laminated skeletal fragment, and burrowed packstone intervals within, where brachiopod grains shelter mud deposits. Burrow diameter ranges 1.0 – 2.0 cm, with both mud-rich and grain-rich fill. Minor IX porosity throughout (5%).

**Facies #1.** Mudstone/shale: 3949.8 – 3949.7', 3942.8 – 3942.7'

**Facies #8.** Shale, fissile: 3945.8 – 3845.7'

Major cycle boundary: 3942.7'

Cycle tops: 3947.8', 3948.7'

Chert nodule: 3947.1'

**Top Black River Formation: 3942.7'**

3949.5 TS

3947.0 TS

3945.0 TS

**3942.7 – 3938.4' = Facies #5/3. Dolomite. Burrow-mottled packstone-to-wackestone with interbedded grainstone.** Dark gray, Brownish gray, moderately/intensely bioturbated, peloid (50%), brachiopod (15%), crinoid (10%), bryozoan (10%), undifferentiated skeletal fragment packstone-to-wackestone (0.1 – 0.5' thick) with wispy and low-amplitude suture stylolites. Interbedded are Very light gray, Very pale orange laminated undifferentiated skeletal fragment, crinoid, brachiopod grainstones (0.1 – 0.4' thick, at three beds in two feet). Burrow diameter ranges 1.0 – 3.0 (commonly overlapping), with grain-rich burrow fill. Dark in color and likely organic rich. Minor IX and MO porosity.

**Facies #1.** Mudstone: 3941.8 – 3941.7'

**Facies #4.** Skeletal grainstone: 3939.7 – 3938.7'

Cycle tops: 3941.8', 3938.4'

3938.6 TS

**3938.4 – 3931.2' = Facies #2/5. Dolomite. Burrow-mottled wackestone-to-mudstone with interbedded grainstone.** Dark gray, Brownish gray, moderately/intensely bioturbated, peloid (50%), brachiopod (15%), crinoid (10%), bryozoan (10%), undifferentiated skeletal fragment wackestone-to-mudstone with wispy and low-amplitude suture stylolites (0.1 – 0.7' thick). Interbedded are Very light gray, Very pale orange, laminated undifferentiated skeletal fragment, crinoid, brachiopod grainstones (0.1 – 0.7' thick, at three beds in two feet). Interval is dark in color and likely organic rich. Minor IX, MO and VU porosity (5-10%) throughout, and additional well developed IX porosity (20%) in limited areas of grainstones.

**Facies #1.** Mudstone: 3936.7 – 3936.6', 3933.4 – 3933.3'

Cycle tops: 3936.7', 3933.4'

3935.6 TS

**3931.2 – 3914.3' = Facies #3. Dolomite. Burrow-mottled packstone with grainstone intervals.** Dark gray, Brownish gray, moderate/intensely bioturbated, undifferentiated skeletal fragment (50%), crinoid (15%), brachiopod (10%), bryozoan, peloid packstone-to-wackestone, with coarse-grain burrow fill, laminations, and wispy stylolites and stylolaminations. Burrow diameter ranges 1.0 – 2.0 cm. Intercalated undifferentiated skeletal fragment (50%), crinoid (25%), brachiopod (25%) grainstones (0.05 – 0.9' thick, at one per three-to-five feet). White crystalline dolomite replaces skeletal fragments and fills veins throughout. Minor porosity is developed as IX in burrow fill, and IP, MO, VU in grainstones.

**Facies #1/5.** Mudstone: 3926.4 – 3926.3'

**Facies #4.** Skeletal grainstone: 3919.7 – 3918.8'

Cycle tops: 3926.4', 3918.8'

3925.75 TS

3919.3 TS

**3914.3 – 3901.7' = Facies #2. Dolomite. Wackestone with grainstone and bryozoan packstone horizons.** Medium gray, Brownish gray, Dark yellowish brown, Pale yellowish brown, sparse/moderate bioturbated crinoid (40%), brachiopod (40%), bryozoan, peloid (?) wackestone-to-packstone with wispy stylolites and stylomottling. Interbedded are crinoid (70%), undifferentiated skeletal fragment, brachiopod, grainstones (0.1' thick, one-two per foot), laminated peloid packstone beds (0.1' thick, one-two per foot), and bryozoan packstone beds (0.1' thick, n=3 in basal 6'). Bedding contacts are dominantly irregular and non-planar. Burrow diameter ranges 1.0 – 2.0, with mud-rich and grain-rich burrow fill. White crystalline dolomite replaces skeletal fragment, partially/totally fills MO, VU, and hair-line veins. Porosity is IX and pinpoint VU in all textures, and MO in bryozoan packstones (10%).

Bryozoan packstones (grains up to 1.0 cm diameter): 3914.0 – 3908.0'

**Facies #4.** Skeletal grainstone: 3909.9 – 3909.7'

**Facies #1.** Mudstone/shale: 3906.7 – 3906.6'

Cycle tops: 3909.7', 3906.6', 3901.7'

Chert nodule: 3914.3'

**3901.7 – 3893.8' = Facies #3. Dolomite. Burrow-mottled packstone with grainstone horizons.** Medium gray, Brownish gray, Dark yellowish brown, Pale yellowish brown, sparse/moderate bioturbated crinoid (40%), brachiopod (40%), bryozoan, peloid (?) wackestone-to-packstone with wispy stylolites and stylomottling. Interbedded are crinoid (70%), undifferentiated skeletal fragment, brachiopod, grainstones (0.1' thick, one/two per foot), laminated peloid packstone beds (0.1' thick, one/two per foot), and bryozoan packstone beds (0.1' thick). Burrow diameter ranges 1.0 – 2.0 cm, with dominantly grain-rich fill. Bedding contacts are dominantly irregular and non-planar. White crystalline dolomite replaces skeletal fragment, partially/totally fills MO, VU, and hair-line veins. Porosity is IX and pinpoint VU in all textures, and MO in bryozoan packstones (5-10%).

Skeletal grainstone (Facies #4): 3895.2 – 3895.0', 3994.0 – 3893.8'



Cycle tops: 3893.8'

**3893.8 – 3882.2' = Facies #4. Dolomite. Interbedded, laminated skeletal packstones and grainstones.** Pale yellowish brown, Medium gray, Very light gray, Pinkish gray, undifferentiated skeletal fragment (60%), crinoid, brachiopod, bryozoan grainstone fining-up to mud-rich packstones (0.3 – 0.7' cycles) with laminated peloid packstone interbeds. Bedding contacts are dominantly planar. White crystalline dolomite replaces skeletal fragment, partially/totally fills MO, VU, and vertical hairline veins. Porosity is WP and MO (bryozoan, crinoid), and VU in bedding parallel VU (zebra fabric) (10-15%).

Cycle top: 3882.2'

3887.95 TS

3887.75 TS

3887.00 TS

**3882.2 – 3879.5' = Missing core.**

**3879.5 – 3875.6' = Facies #4. Dolomite. Skeletal grainstone interbedded with packstone.** Pale yellowish brown, Medium gray, Very light gray, Pinkish gray, sparsely bioturbated undifferentiated skeletal fragment (60%), crinoid (10%), brachiopod (10%), bryozoan, grainstone (0.1 -0.4' thick, one/two per foot) interbedded with, and fining-up to brachiopod (40%), crinoid (30%), bryozoan mud-rich packstone. Burrow diameter ranges 1.0 – 2.0 cm, with dominantly grain-rich fill. White crystalline dolomite replaces skeletal fragment, partially/totally fills molds, vugs, and vertical hairline veins. Porosity is IX in grainstones, WP and MO (bryozoan, brachiopod) (5-8%).

Cycle tops: 3875.6'

**3875.6 – 3870.0' = Facies #3. Dolomite. Burrow-mottled packstone with coarse-grained burrow fills and interbedded grainstone.** Medium dark gray, Brownish gray, Pale yellowish brown, moderately bioturbated, peloid (60%), crinoid, brachiopod, bryozoan packstone-to-wackestone, interbedded with undifferentiated skeletal fragment (80%), crinoid, brachiopod grainstones (0.1' thick, at one-two per two feet). Burrow diameter ranges 0.75 – 2.0 cm. Porosity is IX in burrows and grainstone, WP and MO (bryozoan), and zebra fabric VU (5-8%).

Cycle tops: 3870.0', 3855.8'

**3870.0 – 3855.8' = Facies #3 and 4. Dolomite. Burrow-mottled wackestone interbedded with grainstone.** Dark gray, Light brownish gray, Brownish gray, moderate/intensely bioturbated undifferentiated skeletal fragment (60%), crinoid (10%), brachiopod (10%), peloid, bryozoan wackestone-to-packstone interbedded with skeletal grainstones (0.1 – 0.2 thick, one-four per two feet). Grainstones contact wackestones at irregular surfaces, and show evidence of fluid escape. Burrow diameter ranges 1.0 – 3.0 cm (commonly overlapping), with dominantly grain-rich fill. Wispy stylolites occur throughout. White crystalline dolomite replaces skeletal fragment, partially/totally fills vugs and molds. Porosity is poorly developed as IX and MO (bryozoan) throughout, however large zebra fabric pores exceed core dimensions (n=3) (10%).

HTD breccia:	3865.1 – 3864.8'
<b>Facies #4.</b> Cross-bedded grainstone:	3862.2 – 3861.7'
Cycle tops:	3868.3', 3861.7'

**3855.8 – 3840.1' = Facies #3. Dolomite. Burrow-mottled packstone-to-wackestone with coarse-grained burrow fill, interbedded with grainstone.** Dark gray, Light brownish gray, Brownish gray, moderate/intensely bioturbated, undifferentiated skeletal fragment (60%), crinoid (10%), brachiopod (10%), peloid, bryozoan wackestone-to-packstone interbedded with skeletal grainstones (0.1 – 0.2 thick, one-four per two feet). Grainstones contact wackestones at irregular surfaces. Burrow diameter ranges 1.0 – 3.0 cm, with dominantly grain-rich fill. Wispy stylolites occur throughout. White crystalline dolomite replaces skeletal fragment, partially/totally fills MO, VU, and occurs as HTD breccias. Porosity is poorly developed as MO (bryozoan) and IX throughout, however large zebra fabric pores exceed core dimensions (n=6) (20%).

Cycle tops: 3851.0', 3847.7', 3840.1'

**3840.1 – 3825.3' = Facies #2. Dolomite. Wackestone interbedded with grainstone.** Dark gray, Light brownish gray, Brownish gray, sparse/moderately bioturbated, peloid, crinoid (40%), brachiopod (30%), undifferentiated skeletal fragment wackestone-to-packstone with wispy stylolites and crinoid (50%), brachiopod (30%), undifferentiated skeletal fragment grainstones (0.1' thick, at zero/two per foot). Irregular basal contact of grainstones dominates, however upper contacts are transitional with wacke-packstones. Burrow diameter ranges 1.0 – 2.0 cm, with both mud-rich and grain-rich fill. Porosity is very minor FR (n=2), minor IX in grainstones and burrow fill, and large zebra-fabric VU (n=7, 1.0 x >5.0 cm) ( $\phi$  ~15%).

Cross-bedded skeletal grainstone (Facies #4): 3833.9 – 3833.2'  
 Cycle tops: 3837.2', 3833.2', 3828.3'

**3825.3 – 3819.4' = Facies #2. Dolomite. Wackestone-to-packstone with interbedded grainstone.** Dark gray, Light brownish gray, Brownish gray, sparse/moderately bioturbated, peloid, crinoid (40%), brachiopod (30%), undifferentiated skeletal fragment wackestone-to-packstone with wispy stylolites and crinoid (50%), brachiopod (30%), undifferentiated skeletal fragment grainstones (0.1' thick, at zero/two per foot). Irregular basal contact of grainstones dominates, however upper contacts are transitional with wacke-packstones. Burrow diameter ranges 1.0 – 2.0, with mud-rich and grain-rich burrow fill. Dolomite filled fractures with dimensions 0.2 cm x 6.0-10.0 cm are distributed throughout (one/three per foot). Porosity is minor FR and IX, and large (1.0 x 4.0 cm) saddle dolomite lined VU, with all pore types in each rock fabric.

Cycle tops: 3821.3'

**3819.4 – 3812.1' = Facies #3. Dolomite. Wackestone with grainstone beds.** Dark gray, Light brownish gray, Brownish gray, peloid, crinoid (40%), brachiopod (30%), undifferentiated skeletal fragment wackestone with crinoid (50%), brachiopod (30%), undifferentiated skeletal fragment grainstones (0.1 – 0.5' thick, at one per foot). Burrow diameter ranges 1.0 – 2.0, with mud-rich and grain-rich burrow fill. Bedding

contacts are irregular and gradation at both the base and top of grainstones. Porosity is minor as IX (IP) in grainstones (<5%).

**Facies #4.** Skeletal grainstone: 3814.0 – 3813.75'  
Cycle tops: 3813.75'

**3812.1 – 3805.0' = Facies #3. Dolomite. Burrow-mottled packstone-to-grainstone with coarse-grained burrow fills interbedded with grainstone tempestites.** Dark gray, Light brownish gray, Brownish gray, moderately bioturbated peloid (60%), crinoid (20%), brachiopod, gastropod, bryozoan packstone with wispy and low-amplitude stylolites. Interbedded are crinoid (40%), brachiopod (40%), undifferentiated skeletal fragment grainstones (0.2 – 0.3' thick, at one per foot). Packstone burrow diameter ranges up to 2.0 cm, and fill is identical to grainstone character. White coarsely crystalline dolomite occurs throughout. Porosity is minor as IX in grainstones (<5%).  
Cycle tops: 3811.1', 3807.8'

**3805.0 – 3797.7' = Facies #2. Dolomite. Wackestone interbedded with grainstone.** Depositional fabric is obscured by dolomitization. Light brownish gray, Medium gray, Very light gray, sparse/moderately bioturbated peloid (60%), crinoid (20%), brachiopod wackestone-to-packstones interbedded with skeletal grainstones (0.1 – 0.3' thick, at one per two feet). Burrow diameter ranges 1.0 – 2.0, with mud-rich and grain-rich burrow fill. Extensive saddle dolomite filled fractures and breccias. Porosity is VU, FR (10%).  
Cycle tops: 3799.9'

**3797.7 – 3789.0' = Facies #2. Dolomite. Wackestone-to-packstones.** Depositional fabric is obscured by dolomitization. Light brownish gray, Medium gray, Very light gray, sparse/moderately bioturbated peloid, skeletal wackestone-to-packstones. Grain concentrated beds distinctly lack. Burrow diameter ranges 1.0 – 2.0, with mud-rich and grain-rich burrow fill, however muddy fill dominates. Zebra fabrics and white coarsely crystalline dolomite replacement occurs throughout. Minor VU porosity.

**3789.0 – 3783.2' = Facies #3. Dolomite. Burrow-mottled packstone.** Depositional fabric is obscured by dolomitization. Light brownish gray, Medium gray, Very light gray, sparse/moderately bioturbated peloid, skeletal packstone with wispy stylolites and skeletal grainstone beds (0.1' thick, n=2). Burrow diameter ranges 1.0 – 2.0, with grain-rich burrow fill. Vertical fractures dominate basal 5', where random orientation dominates. Saddle dolomite occludes small fractures and minor breccias and replacement is common throughout. Porosity is zebra-fabric associated VU (<8%).  
Cycle tops: 3788.5'

**3783.2 – 3763.3' = Facies #2. Dolomite. Brecciated burrow-mottled wackestone-to-packstone with grainstone horizons.** Depositional fabric is obscured by dolomitization. Light brownish gray, Medium gray, Very light gray, sparse/moderately bioturbated peloid, skeletal wackestone-to-packstone. Burrow diameter ranges 1.0 – 2.0, with mud-rich and grain-rich burrow fill. Saddle dolomite commonly occludes small fractures and breccias. Grains include peloids and skeletal debris. HTD breccia (zebra VU) and minor VU and fracture porosity.  
HTD breccias: 3780.0 – 3779.3', 3778.8 – 3778.0'  
Cycle tops: 3777.1', 3772.5', 3763.3'

**3763.3 – 3749.3' = Facies #3. Dolomite. Heavily dolomitized, burrow-mottled packstone-to-grainstone.** Depositional fabric is obscured by dolomitization. Light brownish gray, Medium gray, Very light gray, moderately bioturbated (likely) peloid, skeletal packstone-to-grainstone with wispy and high-amplitude suture stylolites. Extensively brecciated and vertically/sub-vertically fractured with associated parallel stylolites. Burrow diameter ranges 1.0 – 2.0, with grain-rich burrow fill. Coarsely crystalline saddle dolomite is very common throughout, where some zones are completely recrystallized to white dolomite. Vugular and FR porosity.

Cycle tops: 3760.4'

3750.5 TS

**3749.3 – 3740.7' = Facies #3. Dolomite. Heavily dolomitized, burrow-mottled wackestone-to-packstone.** Depositional fabric is obscured by dolomitization. Light brownish gray, Medium gray, Very light gray, moderately bioturbated (likely) peloid, crinoid, skeletal packstone (sometimes laminated). Grain concentrated beds distinctly lack. Saddle dolomite commonly occludes sub-vertical fracture zones (up to 3.0 cm wide) and breccias. Porosity is minor FR and VU (<5%).

Laminated peloid packstone: 3744.1 – 3744.0'

Cycle tops: 3743.6'

**3740.7 – 3713.9' = Facies #3. Dolomite. Heavily dolomitized, burrow-mottled packstone-to-wackestone.** Depositional fabric is obscured by dolomitization. Light brownish gray, Medium gray, Very light gray, moderate/intensely bioturbated (likely) peloid, crinoid, skeletal wackestone. Zebra fabrics are common and minor saddle dolomite occludes fractures and breccias. Minor VU porosity.

Cycle tops: 3735.7', 3713.9'

3736.00 TS

**3713.9 – 3680.0' = Facies #2. Dolomite. Heavily dolomitized, burrow-mottled wackestone-to-packstone.** Light brownish gray, Medium gray, Very light gray, depositional fabric is obscured by dolomitization. Nearly void of discernable structure and very homogenous. No visible porosity.

Cycle tops: 3704.4'

**Rzepke 1-27 – Marathon Oil Company**

**Permit #31253, Branch County, MI**

**Cored Interval: 3445.0' – 3378.0'      Examined Interval: 3436.0' – 3410.0'**

**Core footage is (-5') relative to wire-line logs**

**Top Black River Shale: 3417.0 (from core)**

**Formations: Black River Shale, Black River Gp.**

**3436.0' – 3432.2' – Facies #3. Limestone. Peloidal packstone-to-wackestone.** Medium light gray, Light brownish gray, Pale yellow brown, sparsely bioturbated, wispy/stylolaminated, laminated, peloidal packstone-to-wackestone. Additional grains are brachiopod fragments (<5%), with increasing abundance in upper 1'. Interval includes white crystalline calcite filled veins/fractures (0.1 cm x 2.0 cm) and cement filled shelter porosity (brachiopod). A brachiopod (90%), undifferentiated skeletal fragment (10%) packstone-to-grainstone horizon with random orientation grains and a basal scour surface, grading-up into laminated peloidal packstone, occurs at 3433.4' (0.1' thick). Interval is capped by bored surface, likely a hardground. No visible porosity.

Hardground: 3432.3'

Chert nodules: 3436.0'; 3435.8'; 3434.3'

**3432.3' – 3431.6' – Facies #4. Limestone. Skeletal grainstone.** Light brownish gray, Very light gray, Pale yellow brown, undifferentiated skeletal fragment (60%), crinoid (30%), brachiopod (30%) grainstone. Horizontally oriented, elongate grains at the semi-planar base transition upward to random orientation grains. No visible porosity.

**3431.6' – 3430.3' – Facies #5. Limestone. Packstone-to-wackestone.** Medium light gray, light brownish gray, brownish gray, intensely bioturbated, peloidal (70%), brachiopod wackestone-to-packstone with a horizon of undifferentiated skeletal fragment (50%), crinoid (30%), brachiopod packstone (0.1' thick). Upper 0.5' of interval shows a concentration of brachiopods sheltering dark carbonate mud. Capped by a hard ground, represented by vertical borings (0.075' length), which are rimmed by diagenetic alteration halos. No visible porosity.

Hardground: 3430.3'

**3430.3' – 3425.2' – Facies #5 and 3. Limestone. Peloidal packstone.** Light brownish gray, Medium light gray, Brownish gray, moderately bioturbated, with sparse brachiopod and crinoid fragments and sparse chert nodules. Included in the interval is a planar based peloid (40%), undifferentiated skeletal fragment (30%), brachiopod (30%), grainstone fining-up to peloidal packstone (0.1' thick). Thick stylolamination intervals (0.1' thick) thin-upward and transition into anastomosing and wispy stylolites. White crystalline calcite veins (0.2 cm x 2.0 cm) occur in the interval. No visible porosity.

Chert nodule: 3427.5'

3426.8 TS

**3425.2' – 3423.8' – Facies #4. Limestone. Skeletal grainstone.** Very pale orange, Pale yellowish brown, fining upward undifferentiated skeletal fragment (60%),

brachiopod (25%), crinoid grainstone. Porosity is a single vug, partially filled by crystalline calcite, likely formed through shelter porosity by a brachiopod.

**3423.8' – 3420.0' – Facies #3. Limestone. Burrow mottled packstone.** Light brownish gray, Pale brown, intensely bioturbated, peloidal (80%) mud-rich packstone. Additional grains include crinoid and brachiopod fragments. Interval includes two, 0.1 – 0.2' thick planar laminated peloidal grainstones at a 1.5' spacing. No visible porosity.

**3420.0' – 3419.5' – Facies #3. Limestone. Skeletal packstone-to-grainstone.** Pale yellowish brown, Light brownish gray, Pale brown, peloidal (30%), bryozoan (30%), crinoid (20%), brachiopod (20%), intraclast mud-rich packstone, with a laminated undifferentiated skeletal fragment grainstone horizon (0.2' thick). Interval is capped by a laminated undifferentiated skeletal fragment peloidal grainstone. No visible porosity.

Chert nodule: 3420.0'

**3419.5' – 3417.3' – Facies #1. Limestone. Burrow mottled mudstone-to-wackestone.** Light brownish gray, Brownish gray, Pale brownish yellow, totally bioturbated and sediment reworked. Grains include brachiopods (<10%) and bryozoans (<5%). Boring structures at 3419.2' represent a firmground/hardground. No visible porosity.

**3417.3' – 3417.0' – Shale. Calcareous shale/argillaceous mudstone.** Medium light gray, Medium gray, fissile, calcareous metabentonite. **Black River Shale.**

**3417.0' – 3414.2' – Facies #2. Limestone. Wackestone.** Medium light gray, Medium gray, moderately/intensely, bioturbated, crinoid (80%), brachiopod wackestone, with dense nodular and anastomosing stylolitization. Dense stylolite swarms may be attributable to episodic volcanic deposits (Black River Shale/metabentonite). Stylomottling associated with burrowing dominated fabric is present in the upper 1.0' of interval. Interval is capped by borings, representing hardground formation. No visible porosity.

Hardground: 3416.2'

**3414.2' – 3410.0' – Facies #3. Limestone. Wackestone-to-packstone intercalated with skeletal grainstones.** Medium dark gray, Dark gray, moderately bioturbated, wispy stylolitic/stylonodular, peloid (60%), undifferentiated skeletal fragment (10%), brachiopod (10%), crinoid, bryozoan wackestone-to-packstone. Undifferentiated skeletal fragment (60%), brachiopod (20%), crinoid (10%), bryozoan grainstones (0.1' – 0.3' thick) lack dominant grain orientation, intercalate at two per foot. In upper 0.5' of interval brachiopods shelter dark carbonate mud. No visible porosity.

Chert nodule: 3412.3'

**Skinner 1 – Marathon Oil Company**

**Permit #21833, Hillsdale County, MI**

**Cored Interval: 4000.0' – 3875.0'      Examined Interval: 3937.4' – 3875.0'**

**Core footages are (+1') relative to wire-line logs**

**Top Black River Shale: 3890.6'**

**Formations: Black River Shale, Black River Gp.**

**3937.4' – 3936.5' = Facies #3. Dolomite. Laminated peloidal packstone-to-skeletal wackestone.** Pale brown, Light brownish gray, laminated peloid (95%) brachiopod, crinoid, packstone overlain by Dark gray, Brownish gray, Light brownish gray, sparsely bioturbated, wispy stylolitic, crinoid (40%), brachiopod (40%), peloid (20%) wackestone with Light brownish gray coarse grain burrow fill (0.5 – 3.0 cm diameter). Packstone-wackestone contact is irregular, with skeletal grain abundant portions of wackestone filling depressions, grading up into mud-dominated. White crystalline dolomite fills vertical veins (0.1 cm x 2.0 cm) and replaces brachiopod and crinoid fragments. Porosity occurs as pinpoint VU (0.1 cm – 0.2 cm), which is limited in distribution to close proximity of white crystalline dolomite.  
Cycle top:      3937.0'

**3936.5' – 3932.8' = Facies #3. Dolomite. Peloidal packstone intercalated with skeletal grainstones.** Pale brown, Moderate yellowish brown, Dark yellowish brown, Brownish black, Grayish black, peloid packstone at base, transitioning upward to structure-less crinoid (60%), undifferentiated skeletal fragment (20%), brachiopod (20%) grainstone-to-packstone intercalated with moderately bioturbated, wispy stylolitic and burrow-bounding stylonodular peloid (80%), crinoid, brachiopod, packstone-to-wackestones, which are laminated in locations. Burrow diameter ranges 1.0 – 2.0 cm, with coarse-grained fill. Skeletal grainstones are 0.3' thick, occur once per-foot in basal portion of interval, and decrease in frequency of occurrence upward. White crystalline (saddle) dolomite commonly replaces crinoid and brachiopod fragments, and also fills hair-line veins (0.1 cm x 3 cm). Porosity is developed as isolated pinpoint VU (<0.2 cm diameter) and minor development of MO/WP pores in skeletal fragments throughout (5%).  
Cycle tops:      3935.5'; 3932.8'

**3932.8' – 3928.0' = Facies #5. Dolomite. Skeletal-intraclastic grainstone and wackestone.** Dark yellowish brown, Pale yellowish brown, Light olive gray, Brownish black, Grayish black, undifferentiated skeletal fragment (40%), crinoid (30%), intraclast (20%), brachiopod grainstone interbedded with moderately bioturbated, brachiopod (40%), peloid (30%), crinoid wackestone. Intraclasts in grainstones are composed of sub-rounded, equant (0.3 cm) and tabular (0.3 cm x 2 cm) shaped grains of (apparent) peloid/crinoid wackestones. Wackestone deposits contain burrows with mud-rich and coarse-grain fill 0.5 – 1.0 cm in diameter, wispy stylolites and burrow-bounding stylonodular fabric, and saddle dolomite replacement of skeletal fragments. Included in this interval is a 0.1' thick laminated peloid packstone. Porosity is developed as pinpoint VU in matrix replacing mosaic-dolomite, and less commonly as IP in few locations of skeletal grainstones.  
Laminated peloid packstone:      3929.7'  
Cycle tops:      3931.0'; 3928.0'

**3928.0' – 3918.8' = Facies #5 and 4. Dolomite. Peloid wackestone-to-packstone with intraclast grainstones.** Brownish gray, Olive gray, Dark gray, Pale yellowish brown, moderately bioturbated, peloid (60%), crinoid (15%), brachiopod (15%), undifferentiated skeletal fragment wackestone-to-packstone containing burrows (0.5 cm to 1.0 cm in diameter) replaced by coarse crystalline dolomite, wispy stylolites and burrow-bounding stylonodular fabric, and saddle dolomite replacement of skeletal fragments (depositional fabric is partially obscured by dolomitization). Included in this interval are 0.1' thick crinoid (60%), undifferentiated skeletal fragment (20%), brachiopod, intraclast grainstones at an occurrence of once in four feet. Grainstones including intraclasts contact underlying beds at a planar base, and contain horizontal grain orientations. Grainstones lacking intraclast are structure-less, and bound by irregular contacts. White dolomite veins (0.2 x 1-10 cm) with a dominant vertical orientation occur throughout. Porosity is poorly developed as IP in grainstones and IX in wackestones (5%).

**Facies #4.** X-laminated intraclast packstone: 3926.5' – 3926.4'

**Facies #4.** Intraclast grainstone: 3922.2' – 3922.1'

Cycle tops: 3926.5', 3920.7', 3918.8'

Missing core: 3924.6' – 3924.0'

3923' TS

3921' TS

**3918.8' – 3914.3' = Facies #5/2. Dolomite. Peloid packstone-to-wackestone.** Pale yellowish brown, Dark yellowish brown, Brownish black, hummocky cross-laminated, peloid (95%), crinoid packstone fining-up to sparsely bioturbated (0.2 cm – 1.0 cm burrow diameters, with both mud-rich and grain-rich burrow fill), peloid (70%), crinoid (15%), brachiopod wackestone-to-packstone (depositional fabric partially obscured by dolomitization). Fining up cycle repeats, with bases at 3918.8' and 3816.8'. Included in the uppermost wackestone portion of the interval is a single tabular coral fragment (height >4cm). White dolomite filled veins and fractures (0.2 cm x 4 cm) occur throughout interval. Porosity is developed as IX in areas of (likely) dolomitized peloids, and poorly developed as saddle dolomite lined skeletal MO pores.

Cycle tops: 3916.8', 3914.3'

Chert nodule: 3917.9'

**3914.3' – 3906.5' = Facies #3 and 4. Dolomite/dolomitic limestone. Peloidal packstone with intraclastic grainstones.** Pale yellowish brown, Pale brown, Grayish black, moderately bioturbated (burrows 0.3 cm -1.5 cm diameter, with grain-rich fill) peloid (80%), crinoid (10%), brachiopod, undifferentiated skeletal fragment wackestone-to-packstone with stylomottled and burrow-bounding stylonodular fabrics. Included are crinoid (70%), undifferentiated skeletal fragment (10%), intraclast (10%), brachiopod, peloid grainstone horizons, each planar at base, but lacking further sedimentary structure/grain orientation. Porosity is poorly developed as IX (IP) where skeletal fragments are dolomitized (<5%).

**Facies #4.** Skeletal intraclast grainstone: 3913.6' – 3913.5', 3910.1' – 3910.0'

Cycle tops: 3911.0', 3906.5'

Chert nodule: 3909.7'



Change from dolomite to dolomitic limestone at 3912.0'

3908.7' TS

**3906.5' – 3893.1' = Facies #2. Dolomite. Burrow mottled wackestone-to-packstone.** Dark yellowish brown, Brownish gray, Grayish black, moderate/intensely bioturbated, peloid (60%), crinoid (15%), brachiopod (10%), bryozoan, gastropod wackestone-to-packstone, with wispy/burrow-bounding stylonodular fabrics and few low-amplitude suture stylolites (n=8). Burrow diameter ranges 1.0 – 2.0 cm, with both mud-rich and grain-rich burrow fill. Included are mud-rich packstone horizons with relatively higher content of skeletal grains, at thickness of 0.1' – 0.2' and occurrences of one-per three feet. Porosity is developed as IX in matrix replacing mosaic-dolomite in a single interval (3894.1' – 3893.3'), and very poorly developed as dolomite lined FR.

Chert nodules: 3899.3', 3896.5', 3896.3', 3894.8'  
Cycle tops: 3899.4'; 3895.1'  
Missing core: 3898.0' – 3896.7'

3902' TS

3901' TS

**3893.1' – 3890.8' = Facies #3. Dolomite. Bryozoan packstone-wackestones.** Brownish black, Pale yellowish brown, bryozoan (50%), crinoid (30%), undifferentiated skeletal fragment, packstone-to-wackestone, increasing in mud content and grain size fining-up to crinoid (60%), brachiopod (20%), undifferentiated skeletal fragment grainstone, and further fining-up to sparse-moderately bioturbated peloid (80%), bryozoan wackestone-to-packstone. Fining-up sequence repeats four times. Bryozoan fragments at the base of cycles range in size 1.0 cm-to-2.0 cm in diameter. Burrows (1.0 – 2.0 cm diameter) are filled with coarse crystalline dolomite relative to matrix replacing mosaic. Skeletal fragments are frequently partially, to completely replaced by white crystalline dolomite. Porosity includes WP and MO in bryozoan and crinoid fragments, IP in skeletal grainstones, and IX in matrix mosaic dolomite in wackestone component.

Cycle tops: 3892.3', 3891.8', 3891.3'  
Chert nodules: 3993.0', 3991.4'

3892.5' TS

**3890.8' – 3890.6' = Missing Core: Facies #8.** Driller's Report indicates interval as **Black River Shale**

**3890.6' – 3888.0' = Facies #3. Dolomite. Fining-up peloidal packstone-to-wackestone.**

Light brownish gray, Dark gray, Pale yellowish brown, laminated peloid (90%), crinoid, brachiopod packstone-to-grainstone fining-up to peloid (70%), crinoid (20%), undifferentiated skeletal fragment wackestone-to-packstone. Interval transitions from sparsely bioturbated at base, to moderate/intensely bioturbated at top, also increasing in dominance of wispy stylolitic/burrow-bounding stylonodular fabric. Burrow diameter ranges 1.0 – 2.0 cm, with grain-rich burrow fill. No visible porosity.

Cycle top: 3888.0'

Missing core: 3889.3' – 3889.0'

3888.2' TS

**3888.0' – 3887.2' = Facies #2. Dolomite. Burrow-mottled peloidal(?) wackestone-to-packstone.** Dark yellowish brown, Moderate yellowish brown, Grayish black, intensely bioturbated, peloid (?), crinoid (30%), brachiopod (10%), wackestone-to-packstone, with wispy stylolites. Burrow diameters range 0.75 cm-to-2.0 cm, with both mud-rich and grain-rich fill. Dolomitization has obscured depositional fabric. Porosity poorly developed as IX in matrix replacing mosaic-dolomite.

3887.6' TS

**3887.2' – 3875.0' = Facies #3. Dolomite. Laminated peloidal packstone-wackestone-skeletal packstone cycles.** Dark yellowish brown, Moderate yellowish brown, Grayish black, laminated peloid (70%), brachiopod, crinoid, packstone-to-grainstone fining-up to moderately bioturbated peloid (70%), brachiopod (10%), crinoid, bryozoan wackestone. Burrow diameter ranges 0.75 – 2.0 cm, with coarse grain fill. Dolomitization has obscured depositional fabric. Wispy stylolite and low-amplitude suture stylolites are sparsely distributed throughout. Included in the interval are laminated peloid (70%), brachiopod (25%), crinoid packstones 0.1' thick, distributed at 0-2 per two feet. Vertically oriented white dolomite filled veins/fractures (0.2 cm x 3-10 cm) are common throughout. Porosity consists of IX in matrix replacing mosaic and MO/VU associated with brachiopod and crinoid fragments (5-10%).

Chert nodules: 3887.0'; 3886.1'; 3879.1'

Missing core: 3978.4' – 3977.8'

3886.6' TS

3877.5' TS

**Stetler 1-33 – Marathon Oil Company**

**Permit #31407, Branch County, MI**

**Cored Interval: 3395.0' – 3350.0'      Examined Interval: 3390.0' – 3355.9'**

**Core footages are (+7') relative to wire-line logs**

**Top Black River Shale: 3371.3' (from core)**

**Formations: Black River Shale, Black River Gp.**

**3390.0' – 3386.9' = Facies #2 and 3. Limestone. Wackestone-to-packstone.** Light brownish gray, Grayish pink, Brownish gray, a very sparsely bioturbated basal wackestone that transitions upward into a laminated peloidal packstone. Burrow diameter ranges 1.0 – 3.0 cm, with both mud-rich and grain-rich burrow fill. Wispy stylolites/stylolaminations distributed throughout the mud dominated section. Veins/fractures filled with crystalline calcite occur sparsely in lower half of the interval. Laminations become more identifiable upward in interval, transitioning into (hummocky) cross-laminations top. Grains include peloids (90%) and gastropods. No visible porosity.

Chert nodule: 3387.5'

3388 TS

**3386.9' – 3378.6' = Facies #3/5. Limestone. Peloidal packstone intercalated with skeletal grainstones.** Light brownish gray, Grayish pink, Brownish gray, moderately bioturbated, stylonodular to stylomottled, peloid dominated packstone intercalated with homogeneous skeletal grainstones (0.1' – 0.2' thick, occurring at one per four feet). Burrow fill is dominated by coarse skeletal debris (1.0 – 3.0 cm diameter). Randomly oriented crystalline calcite filled veins occur sparsely through the interval. A hardground or firmground is indicated by vertical borings. Packstone grains include peloids (70%), crinoids (10%), brachiopods (10%), intraclasts, and gastropods. Grainstones are composed of crinoids (50%), undifferentiated skeletal fragments (30%), brachiopods (20%), and intraclast grains. Porosity consist of a single partially calcite filled crinoid MO, otherwise no visible porosity.

Skeletal Grainstone: 3386.3' – 3386.2', 3385.1' – 3384.9'

Hard or firmground: 3381.4'

3380 TS

**3378.6' – 3376.5' = Facies #2. Limestone. Burrow-mottled peloidal packstone-to-wackestone.** Light brownish gray-to-Brownish gray, moderate/intensely bioturbated with thin discrete stylolite seams (1mm thick) and randomly oriented calcite veins (1 mm x 3 mm). Burrow diameter ranges 1.0 – 3.0 cm, with dominantly grain rich burrow fill. Grains include peloid (50%), ostracodes (15%), crinoids (10%), and brachiopods. No visible porosity.

Hardground: 3376.7'

**3378.6' – 3373.9' = Facies #3 and 4. Limestone. Peloidal packstone intercalated with skeletal grainstones.** Dusky yellow, Brownish black, Gray black, moderately bioturbated with burrow-bounding stylonodular to wispy stylolites. Burrow diameter ranges 1.0 – 3.0 cm with grain rich fill. Interval is capped by an undifferentiated skeletal fragment brachiopod crinoid grainstone with preservation of bedding parallel

grain orientation (1' thick). Grains for each texture include peloids, undifferentiated skeletal fragments, crinoids, and brachiopods. Packstones are dominated by peloids, and grainstones by undifferentiated skeletal fragments. No visible porosity.

**Facies #4. Skeletal Grainstone:** 3374.9' – 3373.9'

Chert nodule: 3376.0'

3374 TS

**3373.9' – 3369.8' = Facies #5. Limestone. Skeletal packstone-to-wackestone.** Brownish black, Gray black, Dusky yellow, sparse/moderately bioturbated packstone with sparse calcite veins (1 mm x 3 mm). Burrow diameter ranges 1.0 – 2.0 cm, with grain rich burrow fill. Larger brachiopod grains in lower section of interval appear to shelter dark (organic rich?) mud. Interval contains chert nodules, one containing internal pyrite mineralization, and a dark (organic rich?) bryozoan brachiopod wackestone interval. Grains include brachiopods, undifferentiated skeletal fragments, peloids, crinoids, bryozoans, and gastropods. No visible porosity.

**Facies #8. Dark gray wackestone,**

**Black River Shale:** 3371.5' – 3371.3'

Chert nodule and pyrite: 3372.5'

Chert nodules: 3370.2'; 3369.8'

3373 TS

3372 TS

**3369.8' – 3368.9' = Facies #4. Limestone. Skeletal grainstone.** Dusky yellow, Brownish black, undifferentiated skeletal fragments (90%), brachiopod, laminated grainstone. No visible porosity.

**3368.9' – 3365.1' = Facies #3. Limestone. Peloidal packstone-to-wackestone.** Medium dark gray, Brownish gray, Light brownish gray, sparsely bioturbated packstone-to-wackestone, with wispy stylolites and burrow bounding stylonodular fabrics. Burrow fill is coarser grained skeletal debris relative to surrounding sediments. Grains include peloids (30%), brachiopods (30%), crinoids (15%), and bryozoans. No visible porosity.

**3365.1' – 3363.7' = Facies #4. Limestone. Laminated skeletal grainstone.** Medium dark gray, Brownish gray, Light brownish gray, graded grainstone, fining-up from near complete brachiopods to medium sand sized undifferentiated skeletal fragments. Fining-up cycles occur in two similarly thick intervals. Grains include undifferentiated skeletal fragments (70%), brachiopods (10%), crinoids (10%), and bryozoans. No visible porosity.

3364 TS

**3363.7' – 3355.9' = Facies #3. Limestone. Bioturbated peloidal packstone.** Medium dark gray, Brownish gray, Light brownish gray, intensely bioturbated packstone with burrow-bounding stylonodular fabric. Burrow diameter ranges 1.0 – 3.0 cm, with grain-rich burrow fill. Grains include peloids (30%), crinoids (30%), brachiopods (30%), and bryozoans (20%). No visible porosity.

3359 TS

APPENDIX B – Core Plates

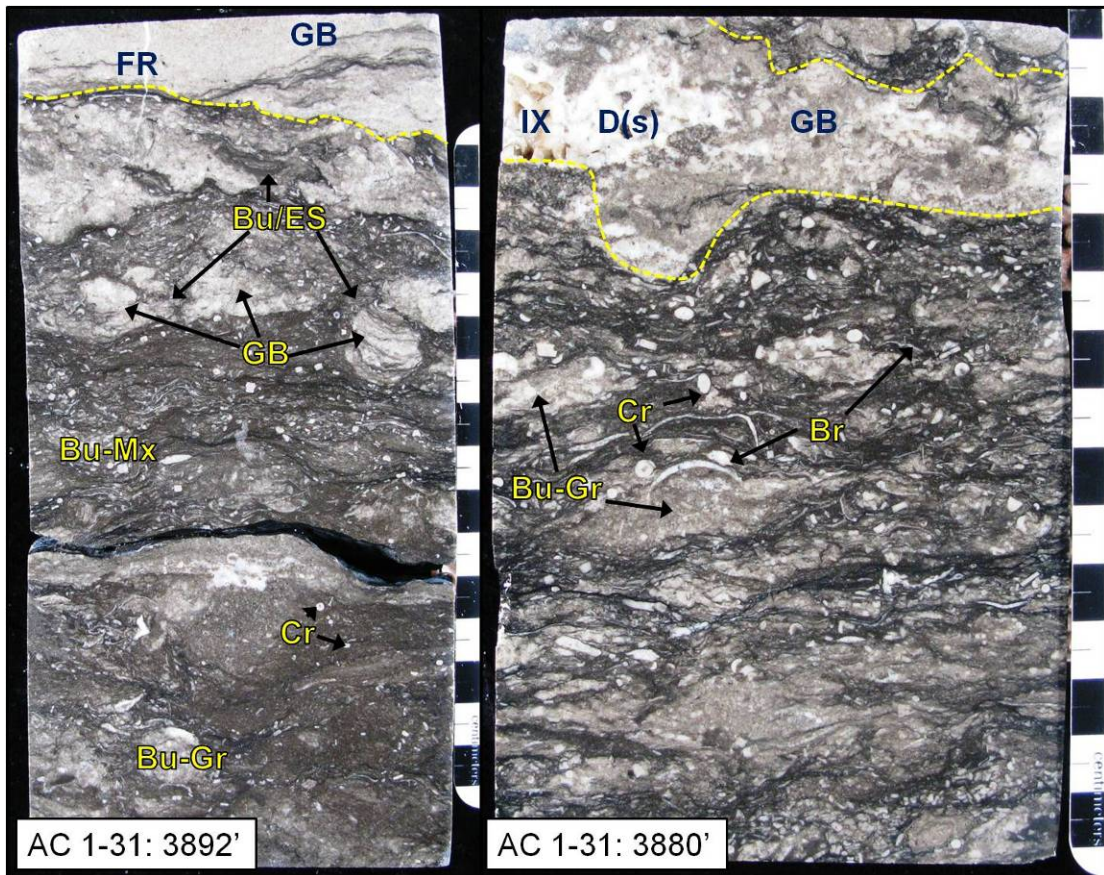
<b>Key to Common Core and Thin Section Image Labels</b>							
<b>Feature Key</b>		<b>Key (cont.)</b>		<b>Key (cont.)</b>		<b>Porosity Key</b>	
<b>Bo</b>	boring	<b>CG</b>	compound grain	<b>Ic</b>	intraclast	<b>IX</b>	intercrystalline
<b>Br</b>	brachiopod	<b>Cr</b>	crinoid	<b>M</b>	mud/mudstone	<b>IP</b>	interparticle
<b>BSN</b>	burrow-bounding stylonodular	<b>C</b>	calcite	<b>ME</b>	micritic envelope	<b>MO</b>	moldic
<b>Bu</b>	burrow	<b>D</b>	dolomite	<b>O</b>	ostracode	<b>FE</b>	fenestral
<b>Bu-Gr</b>	grain dominant burrow fill	<b>FR</b>	fracture	<b>P</b>	peloid	<b>FR</b>	fracture
<b>Bu-M</b>	mud dominant burrow fill	<b>G</b>	gastropod	<b>Py</b>	pelecypod	<b>VU</b>	vug
<b>Bu-Mx</b>	mud-grain mix burrow fill	<b>GB</b>	grain-bed	<b>S</b>	stylolite	<b>WX</b>	intracrystalline
<b>By</b>	bryozoan	<b>HG</b>	hardground	<b>Tr</b>	trilobite	<b>WP</b>	intraparticle
<b>Pg</b>	platy grain	<b>LC</b>	lithoclast	<b>Sk</b>	skeletal fragment	<b>zvu</b>	zebra-fabric vug
<b>Psl</b>	pressure solution	<b>N</b>	normal grading	<b>Cn</b>	coral		
<b>Ct</b>	chert	<b>L</b>	lamination				

- Core plates are labeled with abbreviations shown above unless otherwise noted.
- All scales are in centimeters.
- All images are oriented with shallowest depths at the top of image, except where image is rotated (noted by rotation of text, indicating “top”).
- Few core images show a gray substance in pore spaces. This is grit remnant from polishing that was often not removable.

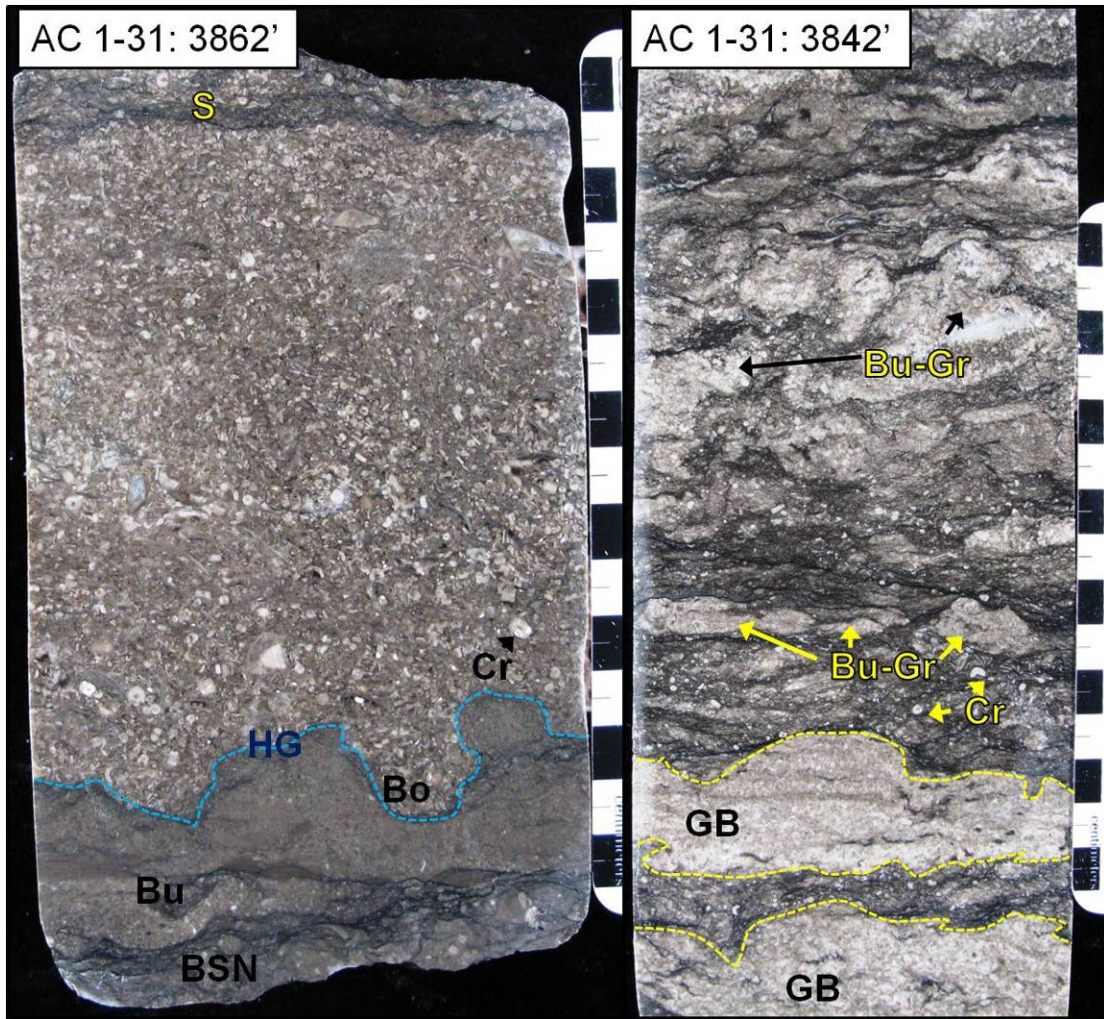
ARCO Conklin 1-31 – Atlantic Richfield Oil and Gas Company

Permit #37385, Jackson County, MI



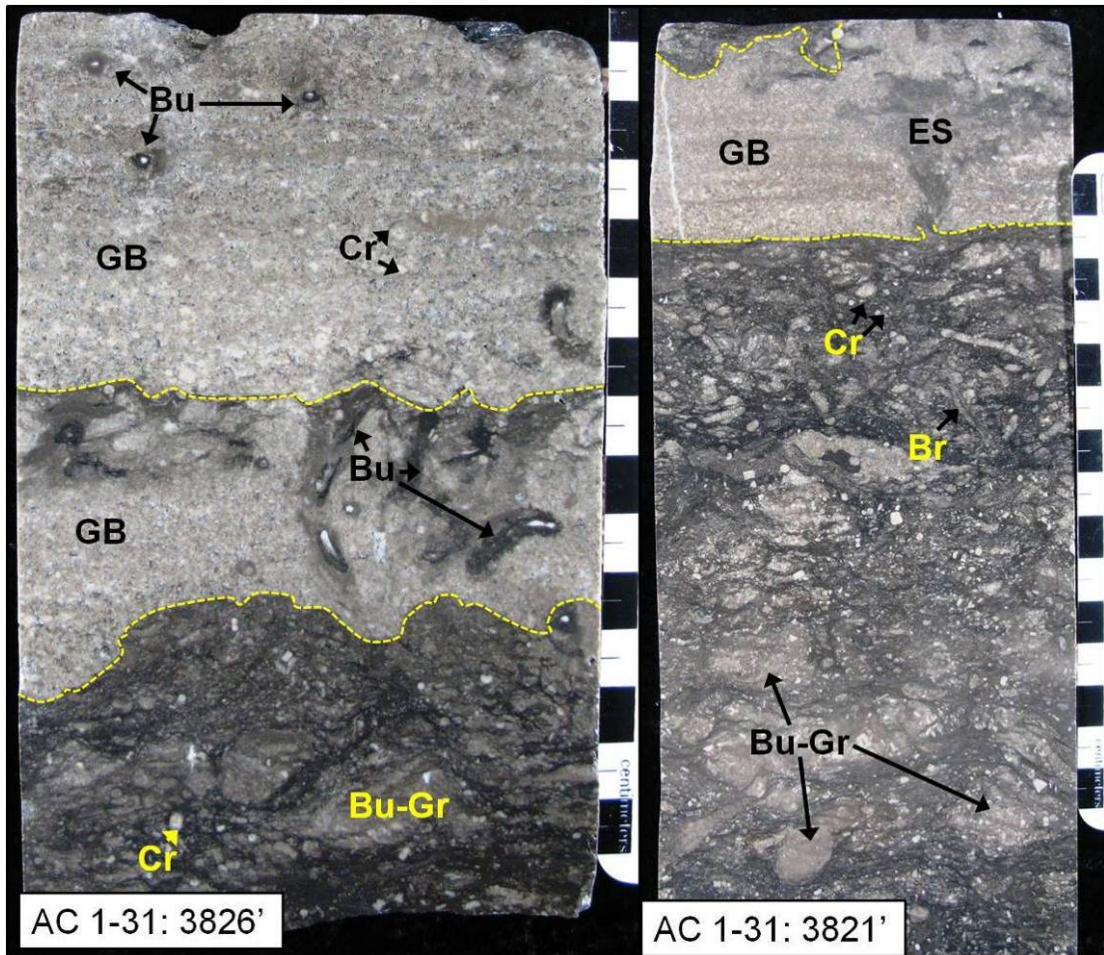


**AC 1-31: 3892'- F3** - Packstone-wackestone with grainstone grain-beds (yellow dashed line) and grain-dominated burrow fill. Grain-beds are dissected by burrows and /or escape structures. **AC 1-31: 3880'- F3** - Packstone with grainstone grain-beds (yellow dashed line). Saddle dolomite lined (D(s)) vugs and intercrystalline porosity is developed through dissolution of grain-bed deposits.

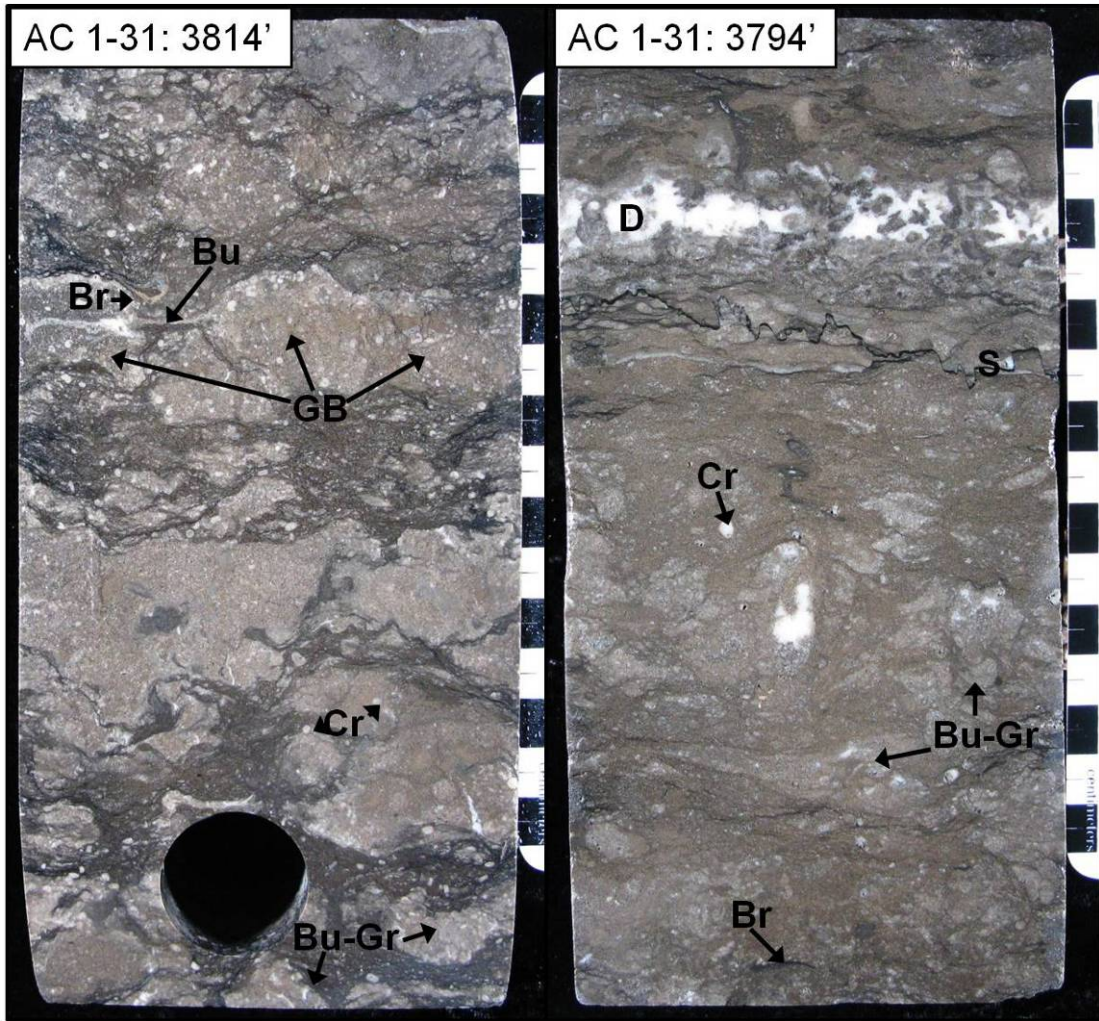


AC 1-31: 3862' – F3 - Peloidal packstone capped by an irregular and bored hardground surface (blue dashed line). Hardground is overlain by a grainstone dominated by crinoidal debris. AC 1-31: 3842'- F2 - Packstone with laminated grain-beds (yellow dashed line) and grain-dominated burrow filling sediments.



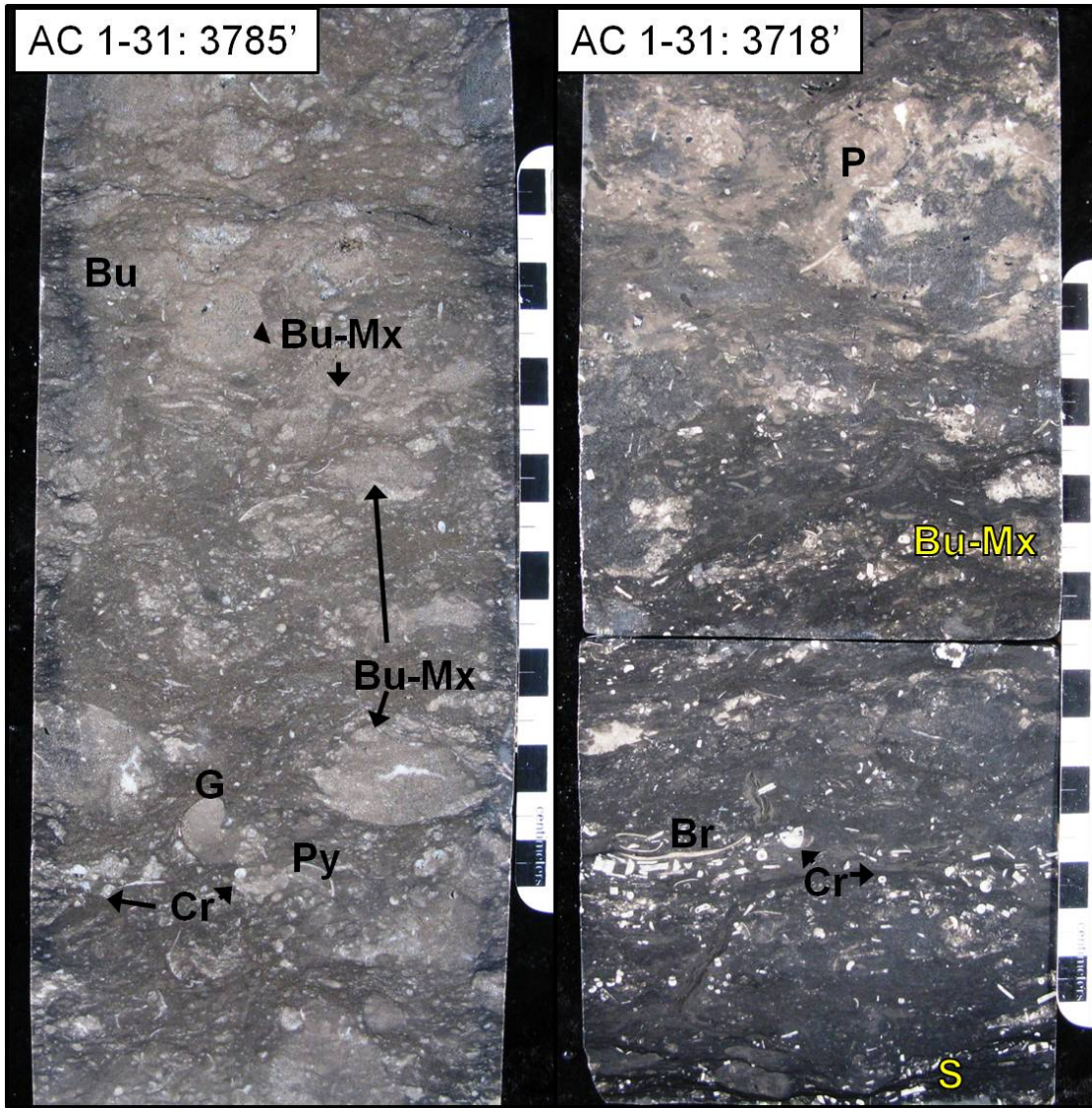


**AC 1-31: 3826'- F3/4** - Packstone-wackestone with amalgamated grainstone grain-beds (yellow dashed lines). Burrow fill is dominantly grain-rich, with mud/grain-mixed sediments in grain-bed burrows. **AC 1-31: 3821'- F3/4** - Packstone with grainstone grain-beds (yellow dashed lines). Burrow fill is dominantly grain-rich. Grain-bed is laminated with a planar-horizontal basal contact interrupted by a fluid/burrow escape structure.



AC 1-31: 3814'- F3 - Packstone-wackestone with burrow dissected grainstone grain-beds and grain-dominated burrow fill. AC 1-31: 3794'- F2 - Peloidal wackestone-packstone with grain-dominated burrow-fill. Horizontally oriented white crystalline dolomite seam may indicate incipient zebra-fabric development.

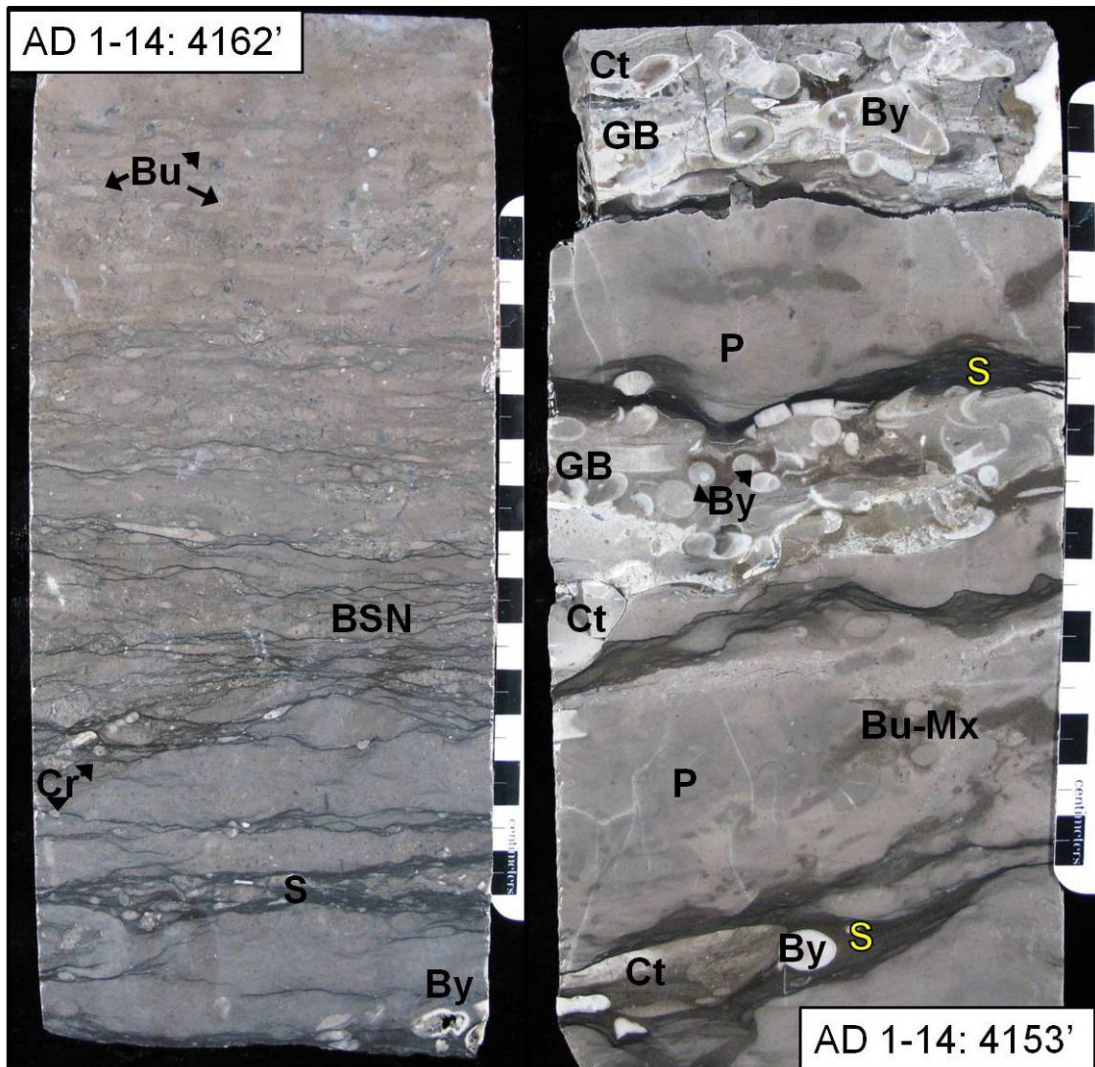




AC 1-31: 3785'- F2 – Wackestone-packstone with grain-mud mixed burrow fill. AC 1-31: 3718'- F1 – Wackestone-mudstone with dark (organic rich reduced?) sediments. Burrow fill is grain-mud mixed with few dominated exclusively by peloids.

ARCO Dunn 1-14 – Atlantic Richfield Oil and Gas Company

Permit #37239, Calhoun County, MI



**AD 1-14: 4162'- F2** – Peloid wackestone-packstone with stylolites and burrow-bounding stylonodular fabric. Burrow Fill is dominantly mud-rich. Minor development of WP in bryozoan fragment in the lower corner of sample. **AD 1-14: 4153'- F3** – Peloidal packstone with large (cm-scale) bryozoan packstone grain-beds. Burrow fill is a grain-mud mix (peloid packstone). Pressure solution seams and stylolites are well developed. Chert nodules are developed throughout this sample.



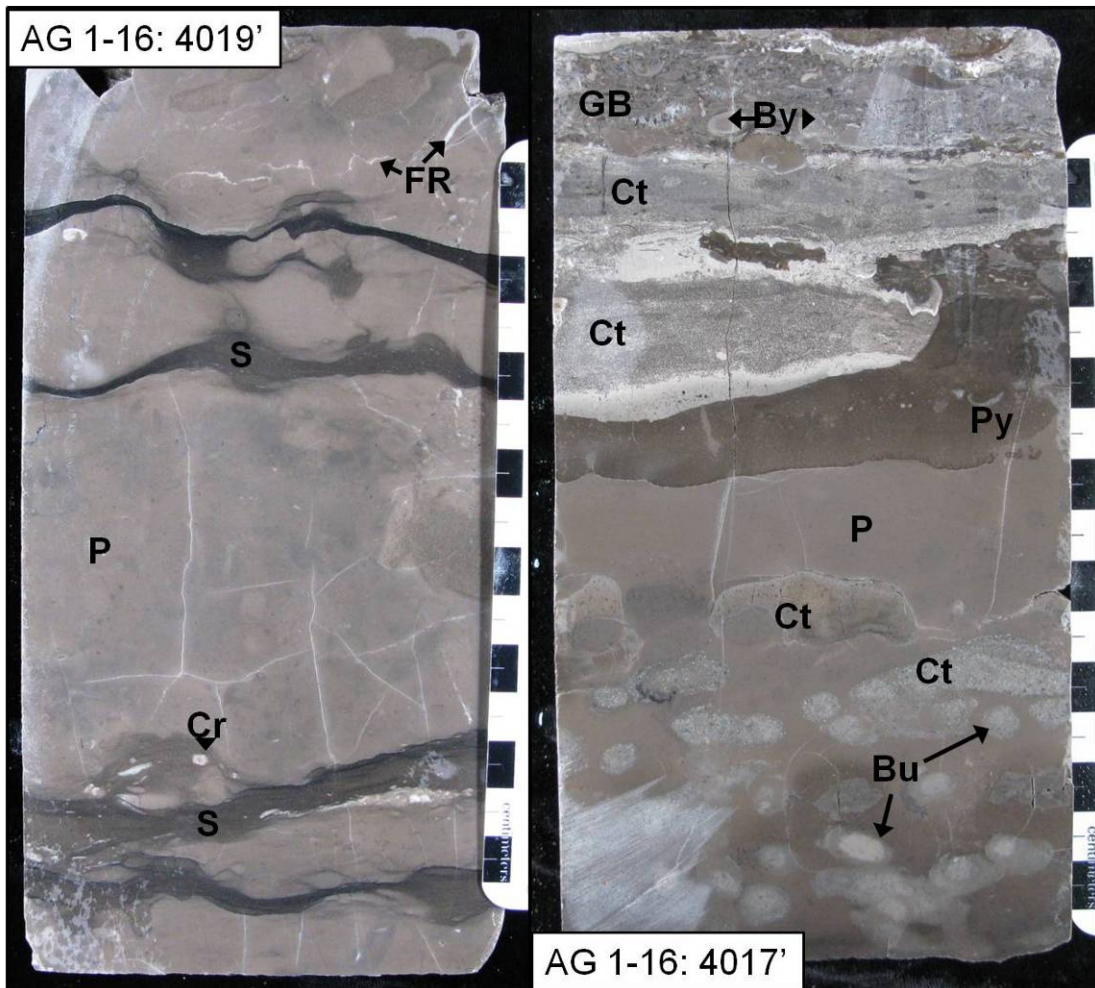


**AD 1-14: 4152'- F3** – Peloid packstone with large (cm-scale) gastropod bioclast. Sample is predominantly composed of peloid grains. **AD 1-14: 4151'- F7** – Calcareous K-bentonite –Black River Shale (in plastic bag).



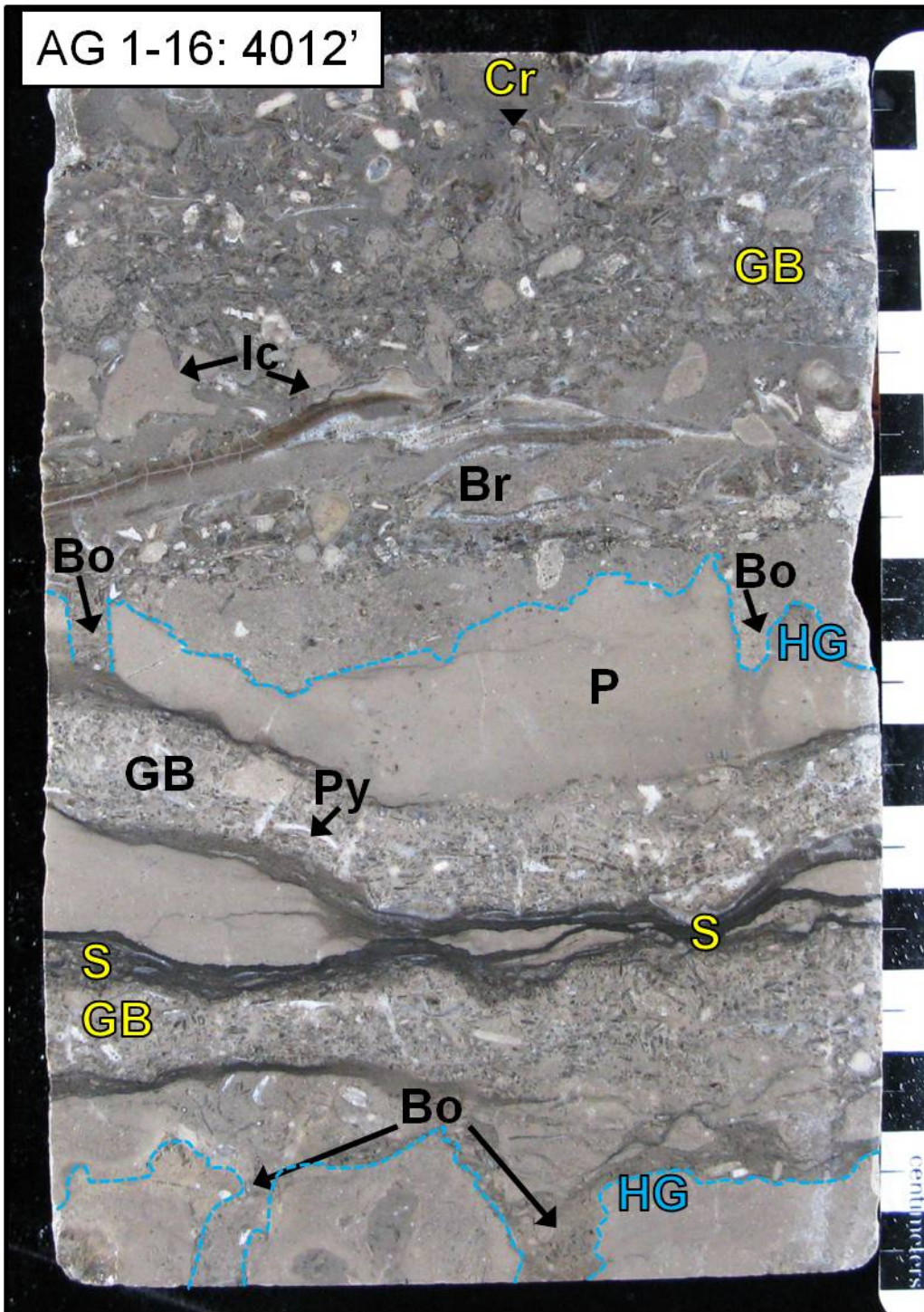
ARCO Gardner 1-16 – Atlantic Richfield Oil and Gas Company

Permit #37838, Hillsdale County, MI



**AG 1-16: 4019'- F3** – Peloid packstone-wackestone with discrete pressure solution and stylolite seams. Fractures and veins are filled with white crystalline dolomite. **AG 1-16: 4017'- F2** - Peloid wackestone-packstone with replacement of burrow filling carbonate grains by chert. Chert is additionally replaces peloids and forms nodules. Sample is capped by packstone grain-bed.

AG 1-16: 4012'

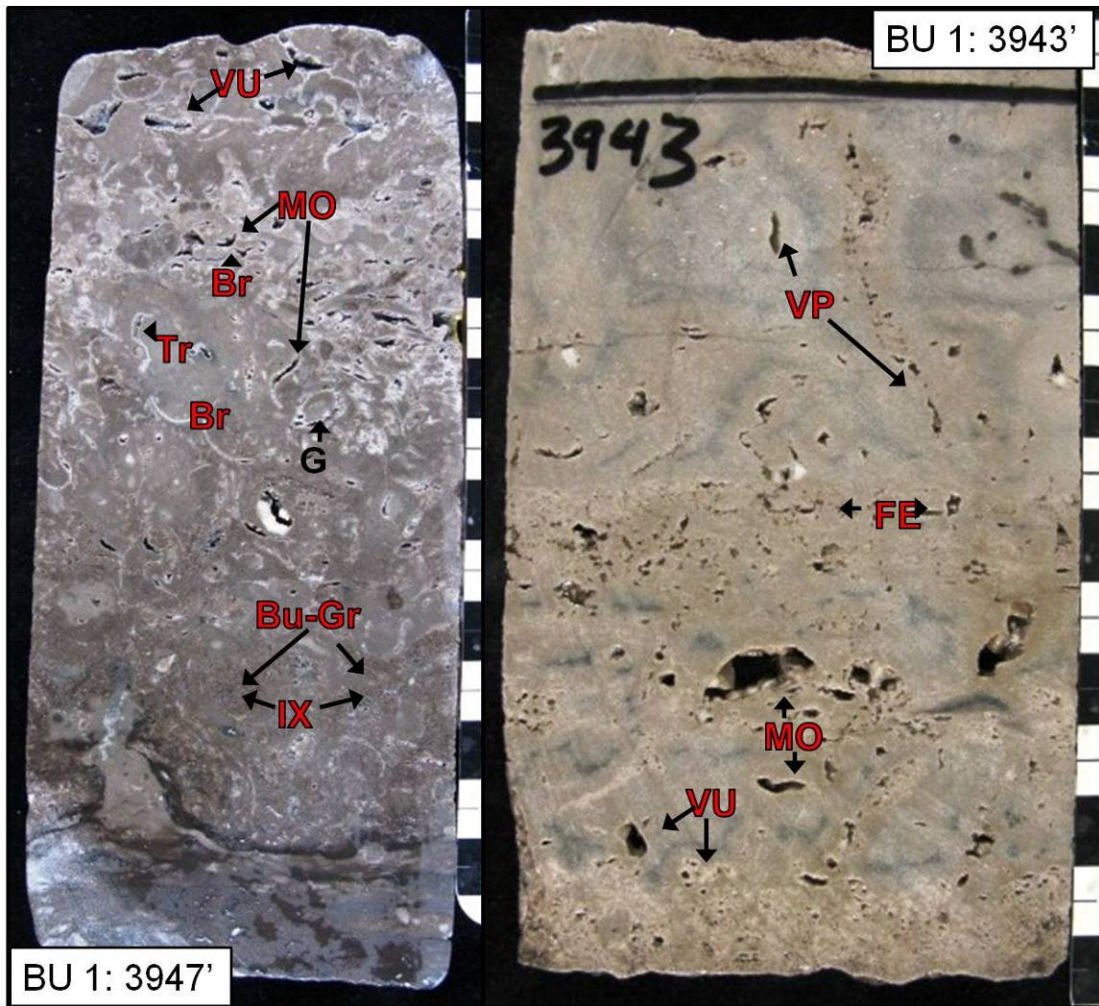


**Ag 1-16: 4012'- F3** – Peloid packstone-wackestone with multiple bored hardgrounds (blue dashed lines) and packstone skeletal grain-beds. Pressure-solution and stylolite seams are well developed at bedding contacts. Intraclast are deposited above hardgrounds and likely derived locally from the indurated substrate.

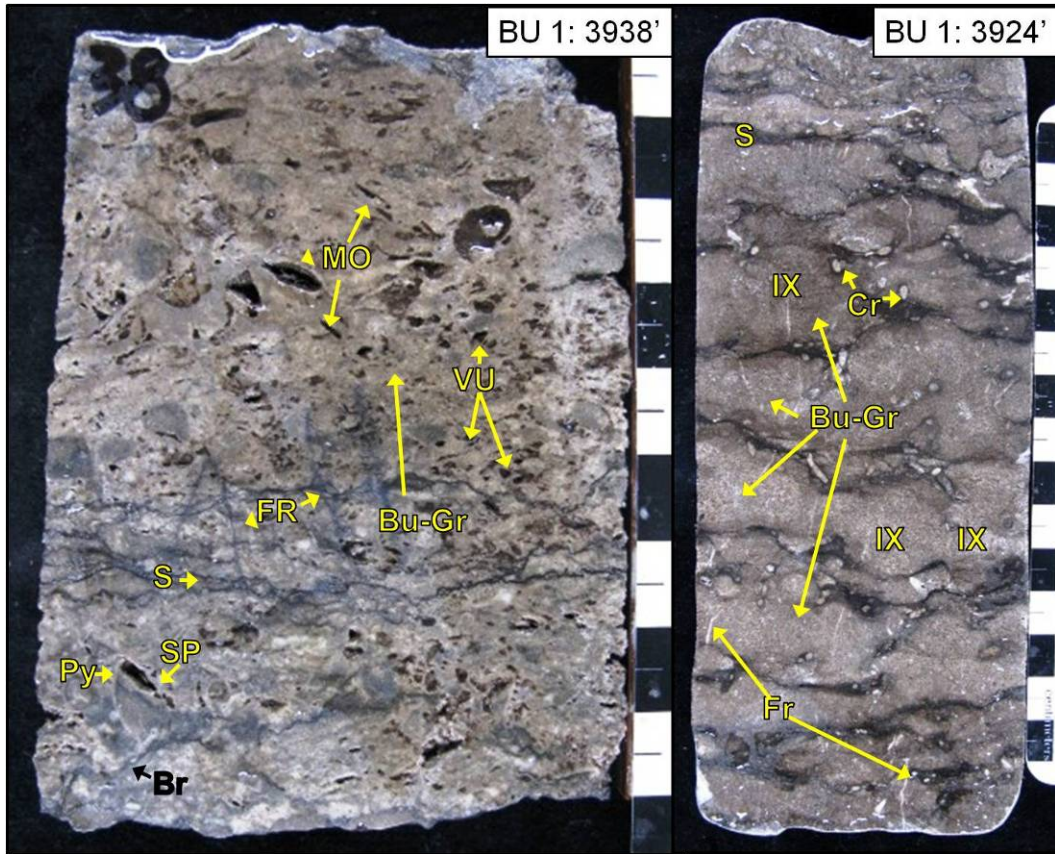
Buehrer 1 – Aurora Gasoline Company and McClure Oil Company

Permit #21064, Hillsdale County, MI



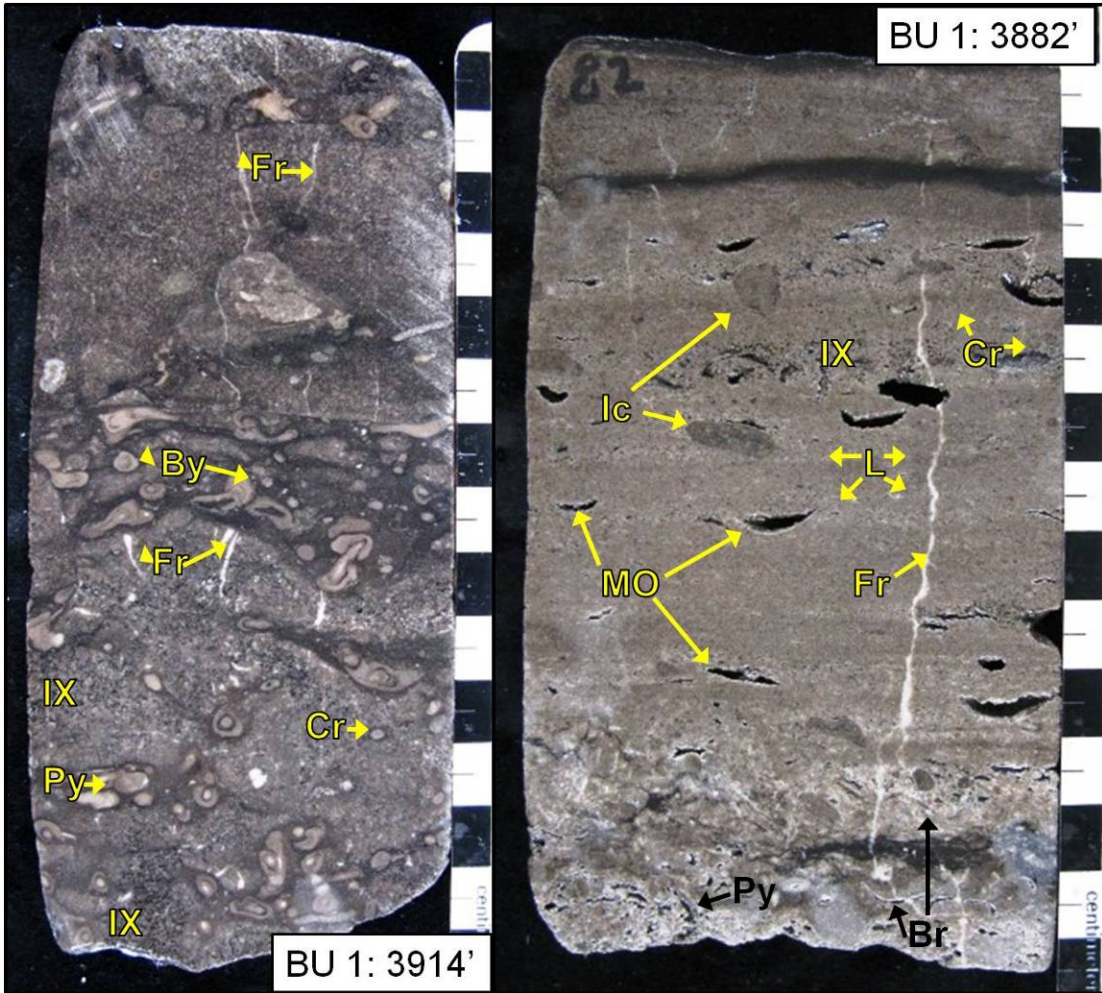


**BU 1: 3947'- F5/3** – Peloid packstone-wackestone with abundant platy (brachiopod/pelecypod) skeletal debris. Moldic and vugular porosity is well developed throughout with minor intercrystalline porosity zones.  
**BU 1: 3943'- F6** – Oxidized fenestral peloidal packstone with vertically oriented vugs. Oxidation halos are common around pores.



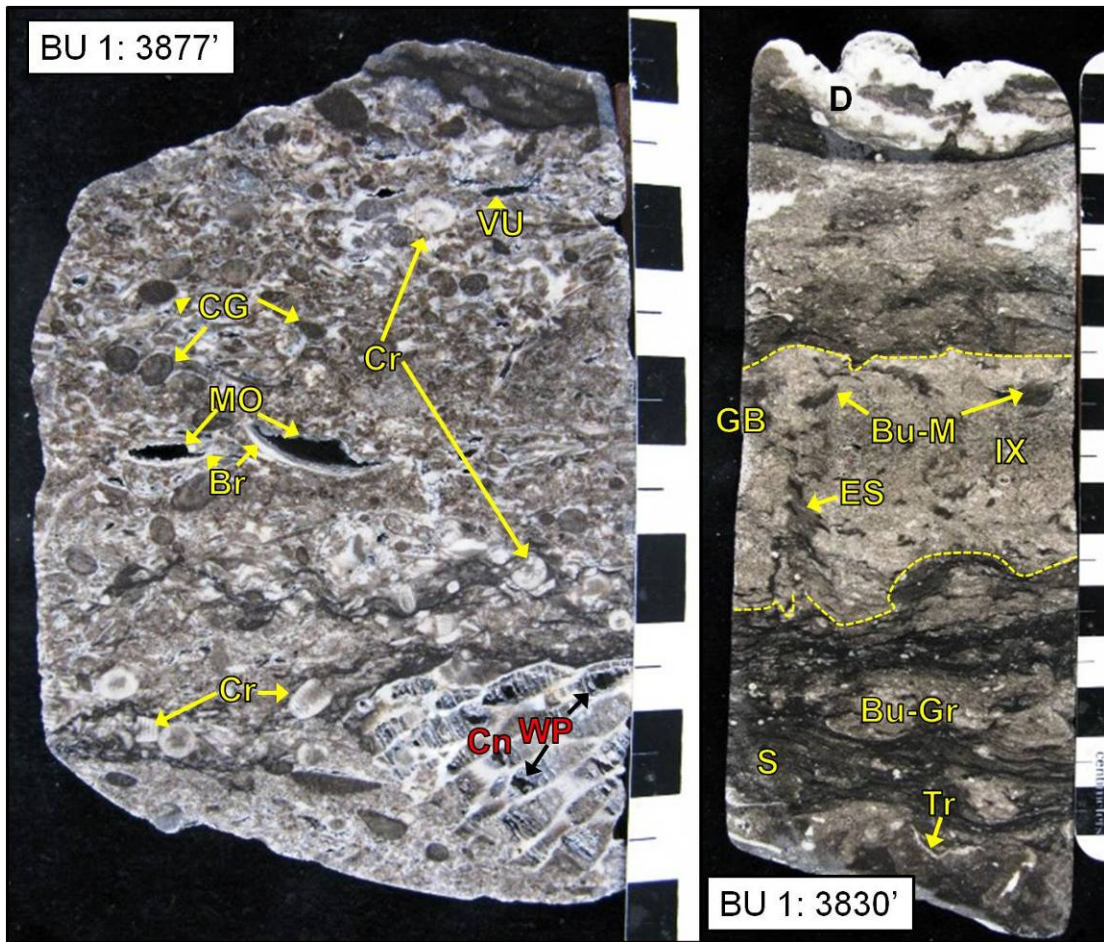
**BU 1: 3938'- F5/3** – Peloid/brachiopod packstone-grainstone with well developed moldic and vugular pores. Shelter porosity (SP) is additionally developed (pelecypod). **BU 1: 3924'- F2** – Wackestone with grain-dominated burrow fill and associated IX porosity. Fractures and veins are filled with white crystalline dolomite.



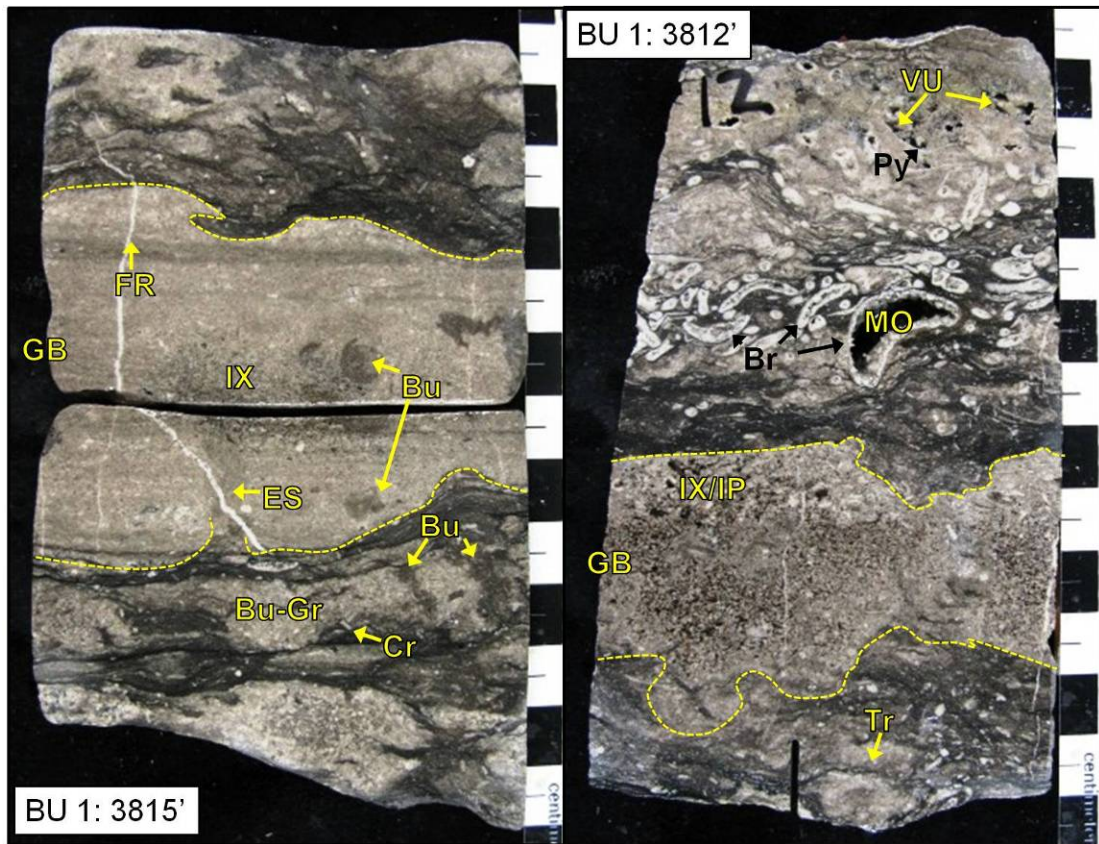


**BU 1: 3914'- F2** – Peloid/crinoid wackestone-packstone with a bryozoan packstone-wackestone grain-bed. Intercrystalline porosity is developed in zones. Fractures/veins are filled with white crystalline dolomite. **BU 1: 3882'- F4** – Laminated (L) grainstone with compound-grain intraclasts. Moldic and intercrystalline porosity is distributed throughout this sample. Fractures are filled with white crystalline dolomite.



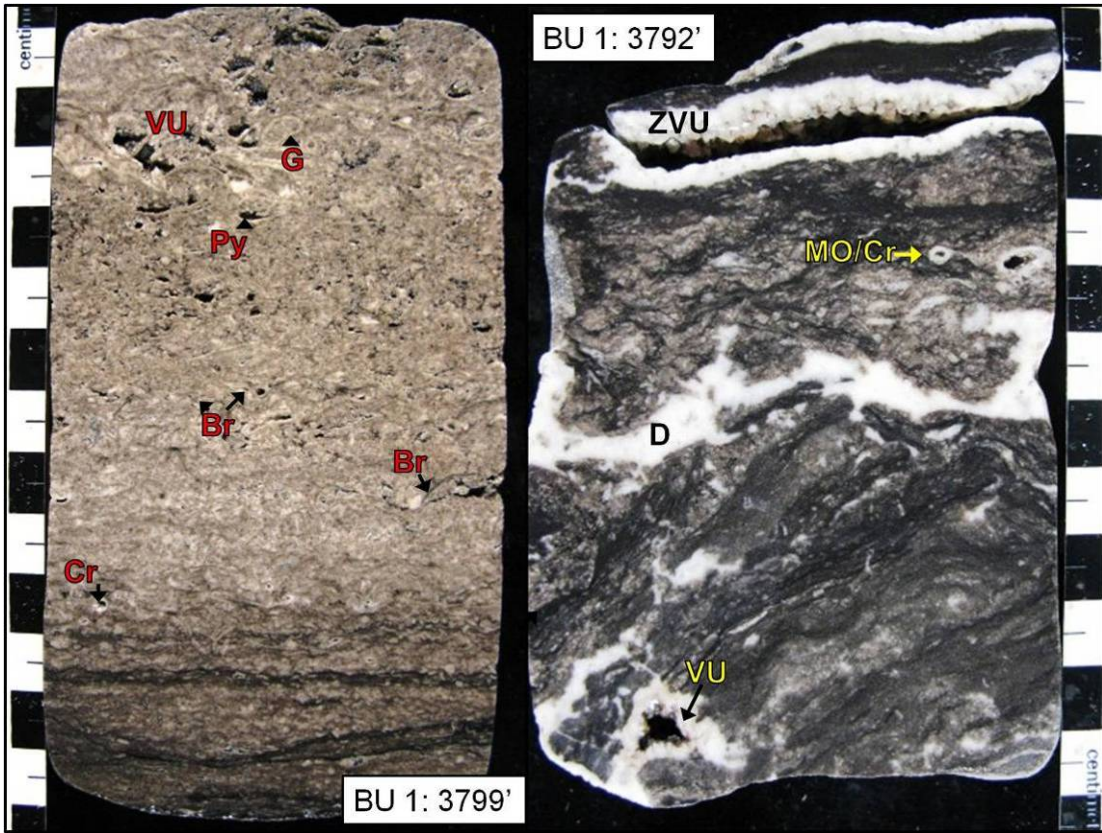


**BU 1: 3877'- F4** – Crinoid/compound-grain grainstone. Moldic (brachiopod) and intraparticle (tabulate coral, Cn) porosity is developed with minor vug porosity. **BU 1: 3830'- F2** – Crinoid wackestone with grainstone grain-beds (yellow dashed lines) showing fluid/burrow escape structures. Burrow fill is dominantly grain-dominated, with mud-dominated fill in grain-bed deposit.

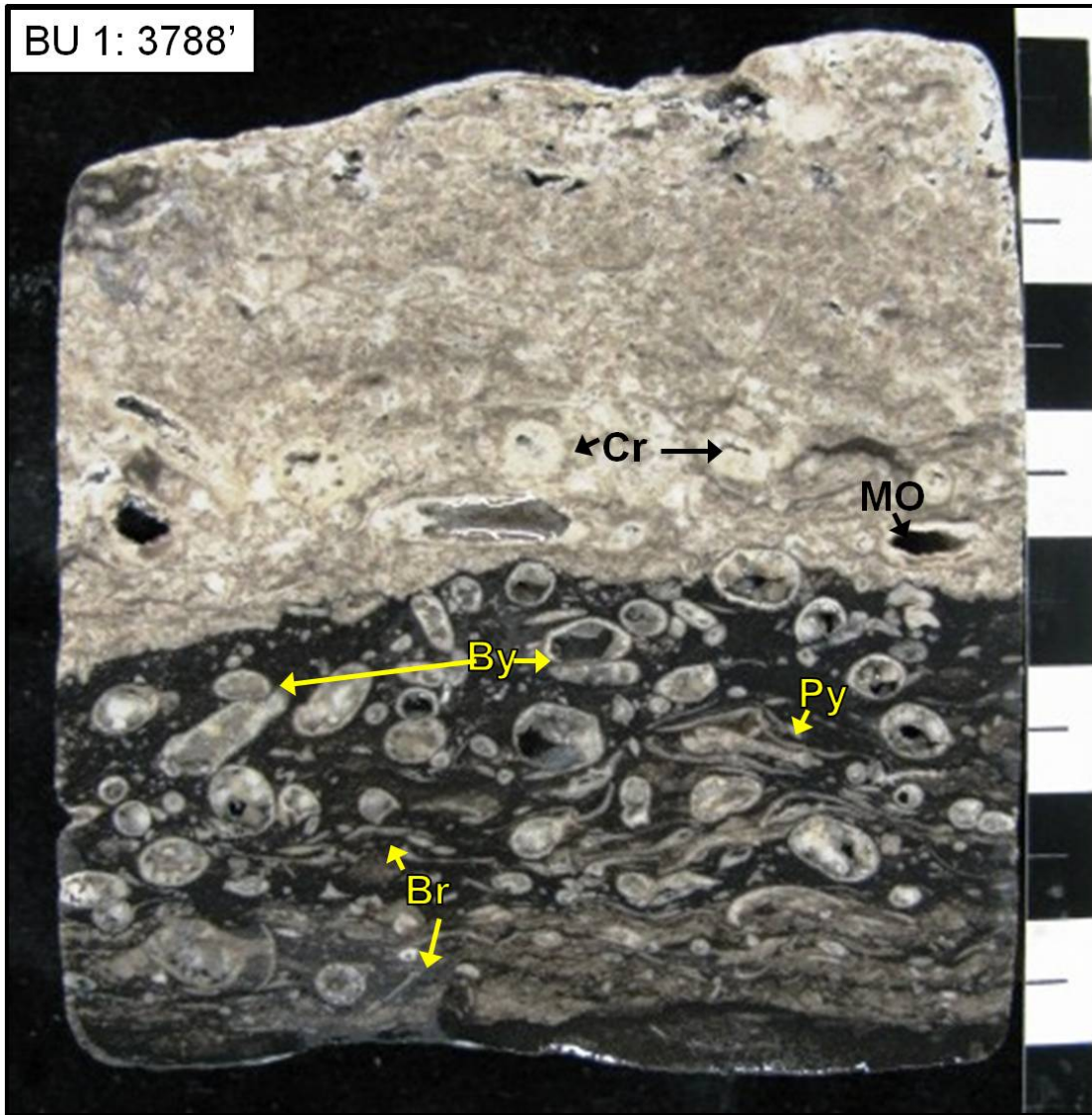


**BU 1: 3815'- F5/3** – Skeletal wackestone with grain-dominated burrow fill and laminated grainstone grain-beds (yellow dashed lines). Grain-bed shows burrow/fluid escape structure and grain-mud mixed burrow fill. Fracture is filled with white crystalline dolomite. **BU 1: 3812'- F3** – Crinoid/brachiopod packstone-wackestone and grainstone grain-bed (yellow dashed lines) with well developed IX porosity. Additional porosity includes MO (brachiopod) and VU.



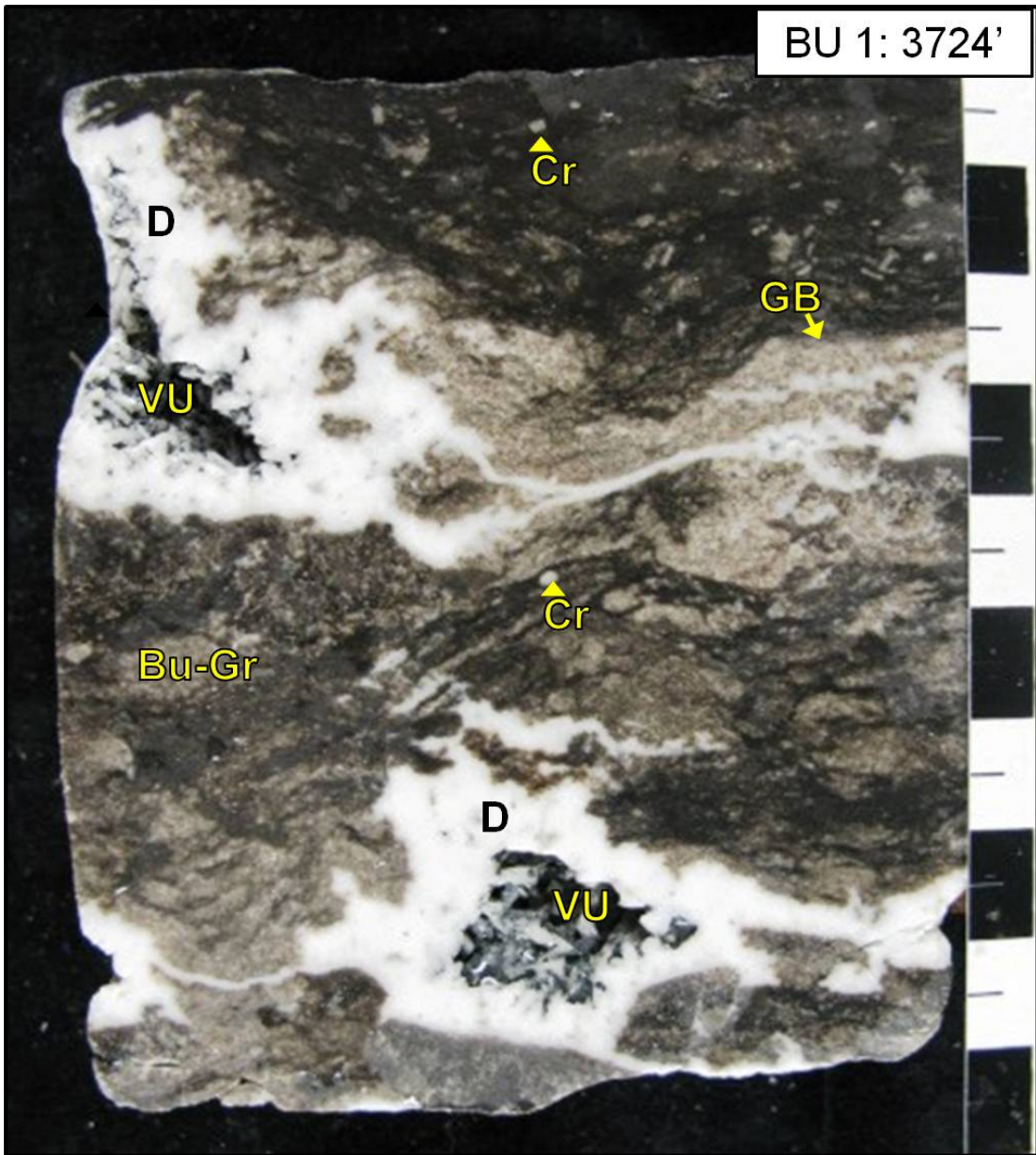


**BU 1: 3799'- F4** – Skeletal grainstone with VU, IX, and IP. **BU 1: 3792'- F2** – Skeletal wackestone with HTD-zebra fabric and zebra vug development.

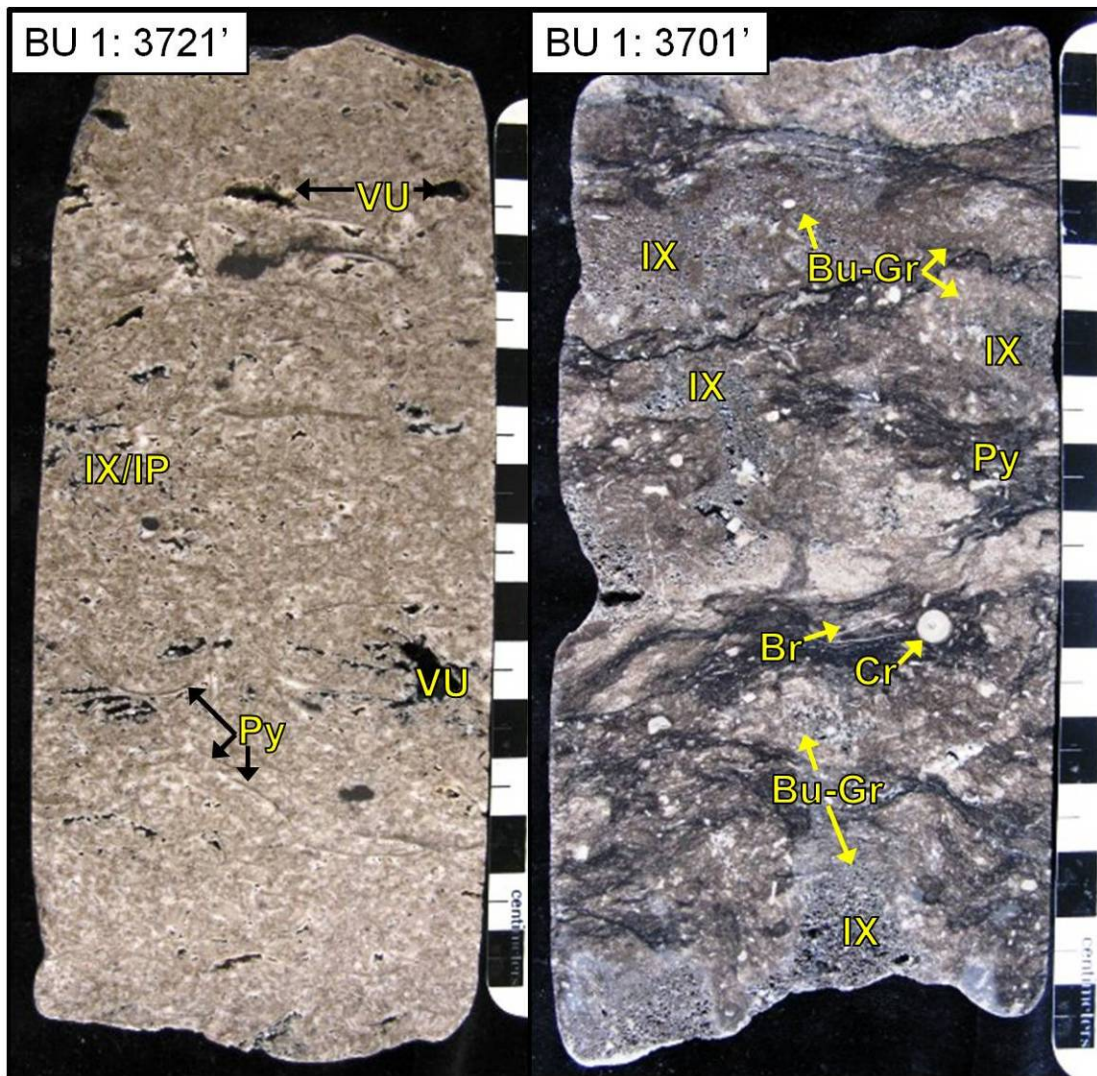


**BU 1: 3788'- F2/3** – Bryozoan mixed-skeletal wackestone-packstone overlain by crinoidal grainstone. Dark gray/black wackestone mud contrasts with light grainstone sediments. Porosity is dominantly moldic with minor intercrystalline development.





**BU 1: 3724'- F2** – Wackestone with packstone grain-bed and grain-dominant burrow fill. Sample shows development of HTD-zebra fabric with white saddle dolomite filled vugs containing residual hydrocarbon. White dolomite veins also extend horizontally in the zebra fabric.

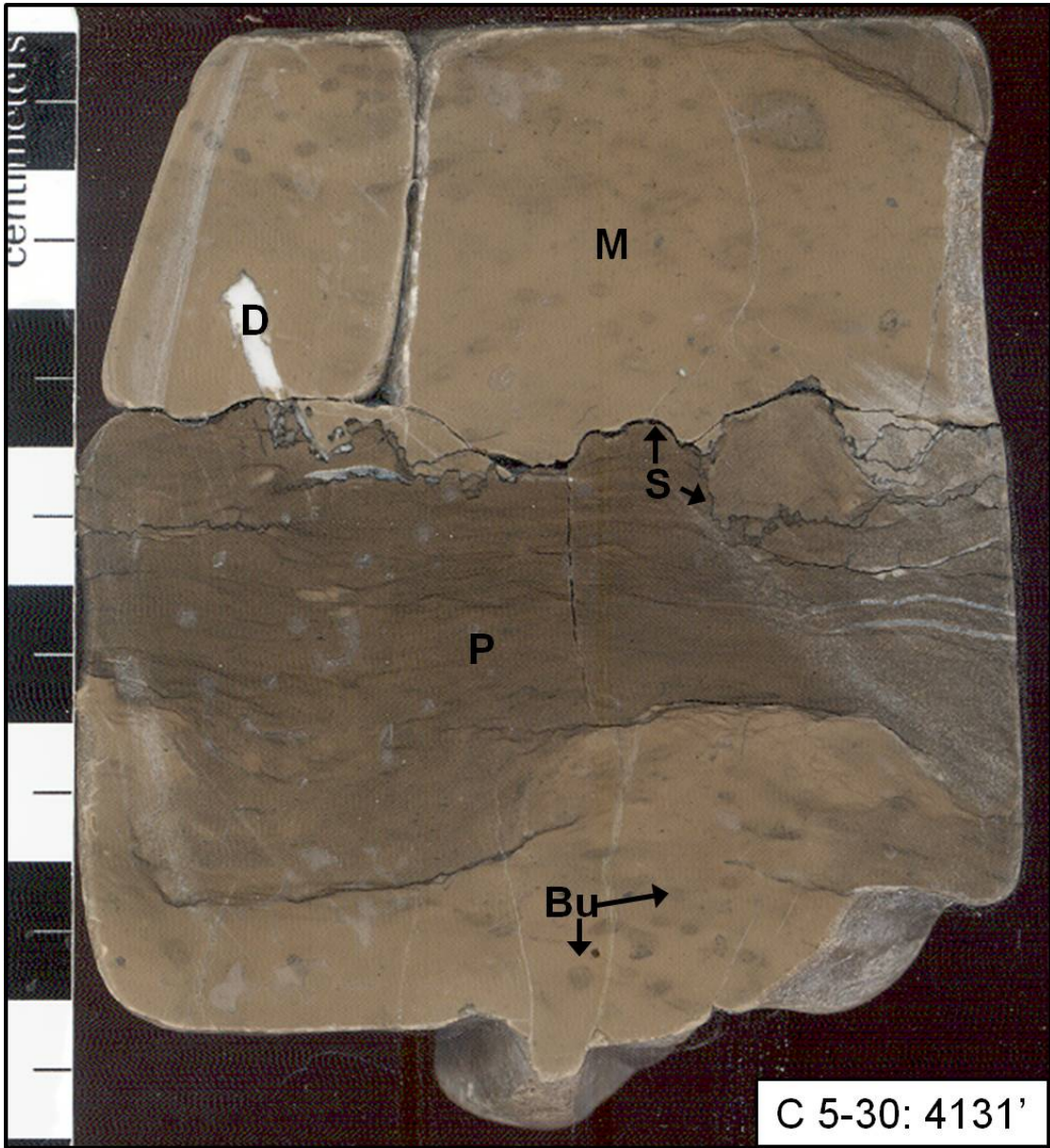


**BU 1: 3721'- F4** – Skeletal grainstone with VU, IX, and IP. Primary pore space/cement is filled/replaced by white crystalline dolomite. **BU 1: 3701'- F3** – Crinoid pelecypod/brachiopod packstone-wackestone with grain-dominant burrow fill. Intercrystalline porosity occurs within grain dominated burrows. Additional VU porosity is developed where pervasive dissolution increases porosity in IX zones.

Casler 5-30 – Whiting Oil and Gas Company

Permit #36587, Jackson County, MI



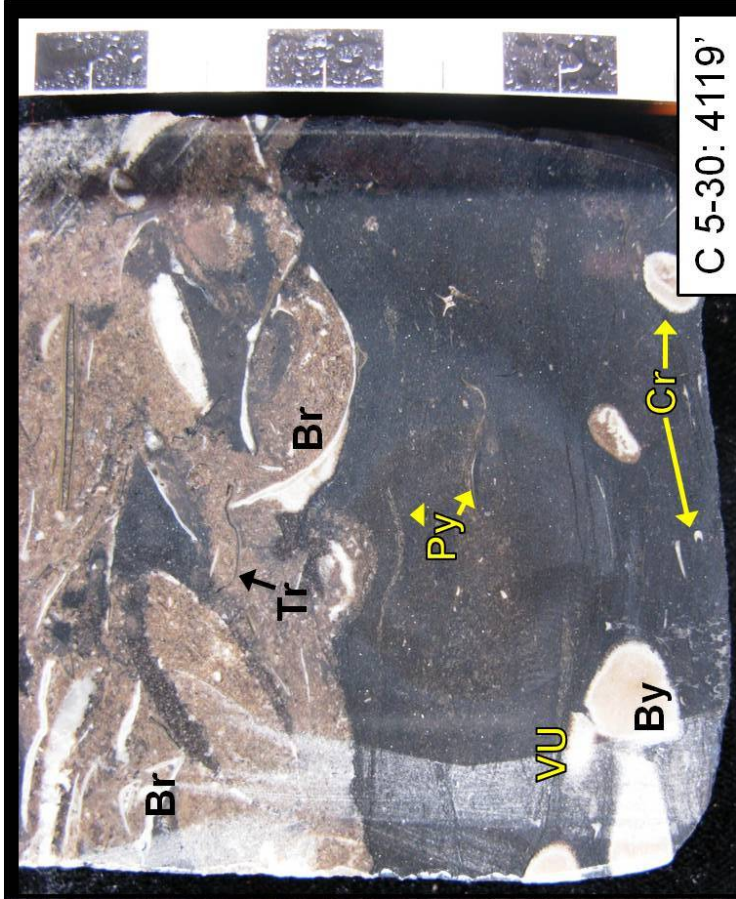


**C 5-30: 4131'- F5** – Peloidal wackestone-mudstone with mud dominant burrow fill. Pressure solution and stylolitization is well developed. Dolomite fills sub-vertical fracture.



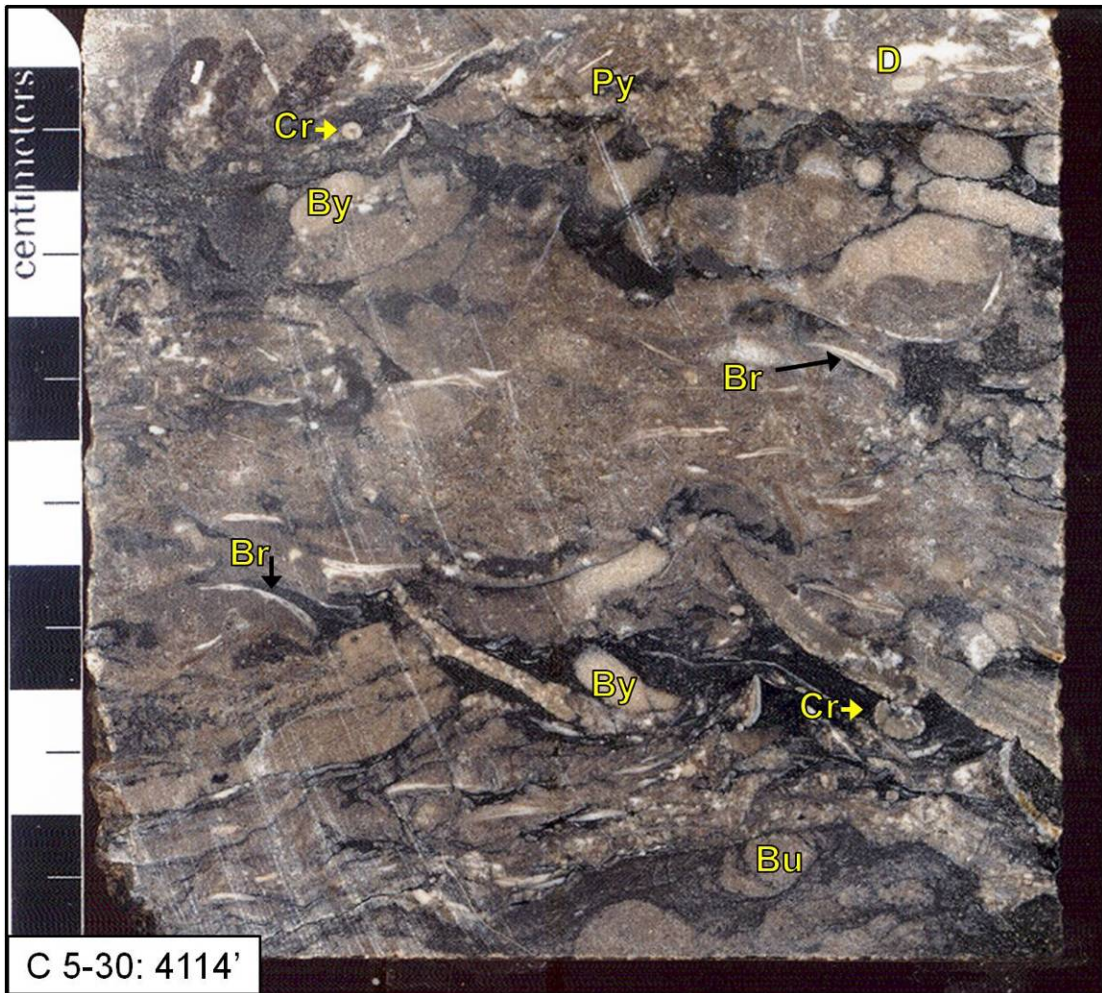


C 5-30: 4122'



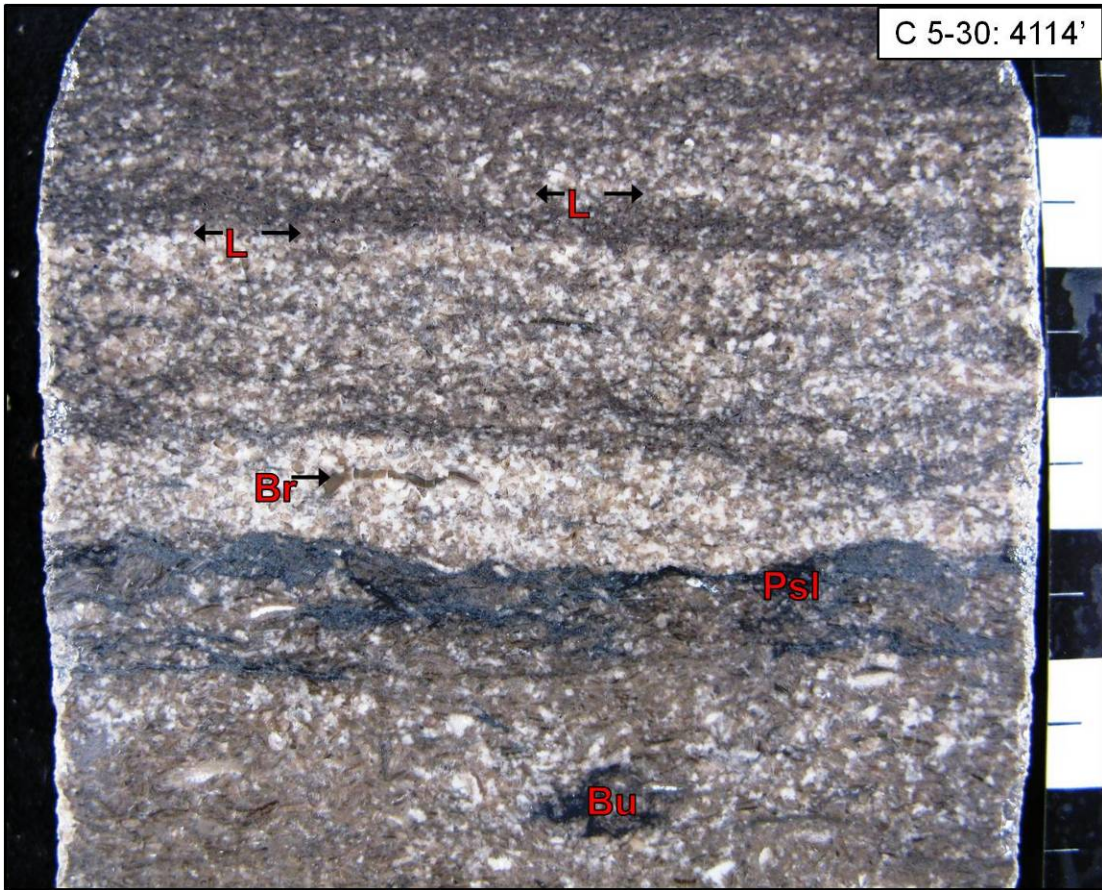
C 5-30: 4119'

C 5-30: 4122'- F3 - Peloidal-skeletal packstone with grainstone bed (GRST) capping this sample. Burrow-bounding stylonodular fabric with grain-rich burrow fill is prominent in the center of this sample. C 5-30: 4119'- F1/5 - Dark gray/black wackestone-mudstone overlain by beige brachiopod skeletal fragment packstone.



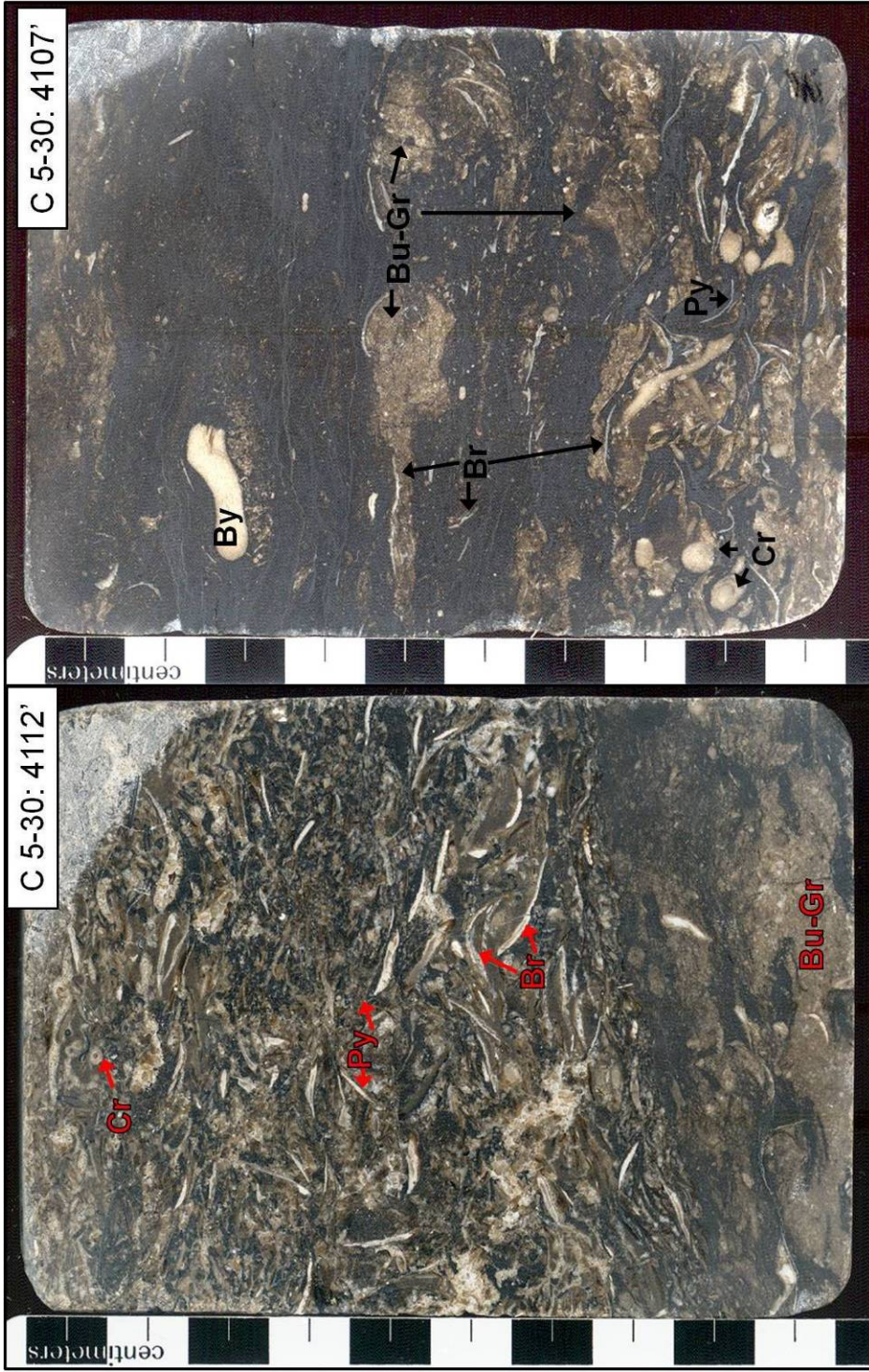
**C 5-30: 4114'- F5** – Skeletal-peloidal packstone with dark grey/black mud-dominated zones showing a mottled texture and color. Burrows are filled with sediments contrasting to the burrowed substrate. Dolomite fills veins or original pore space.





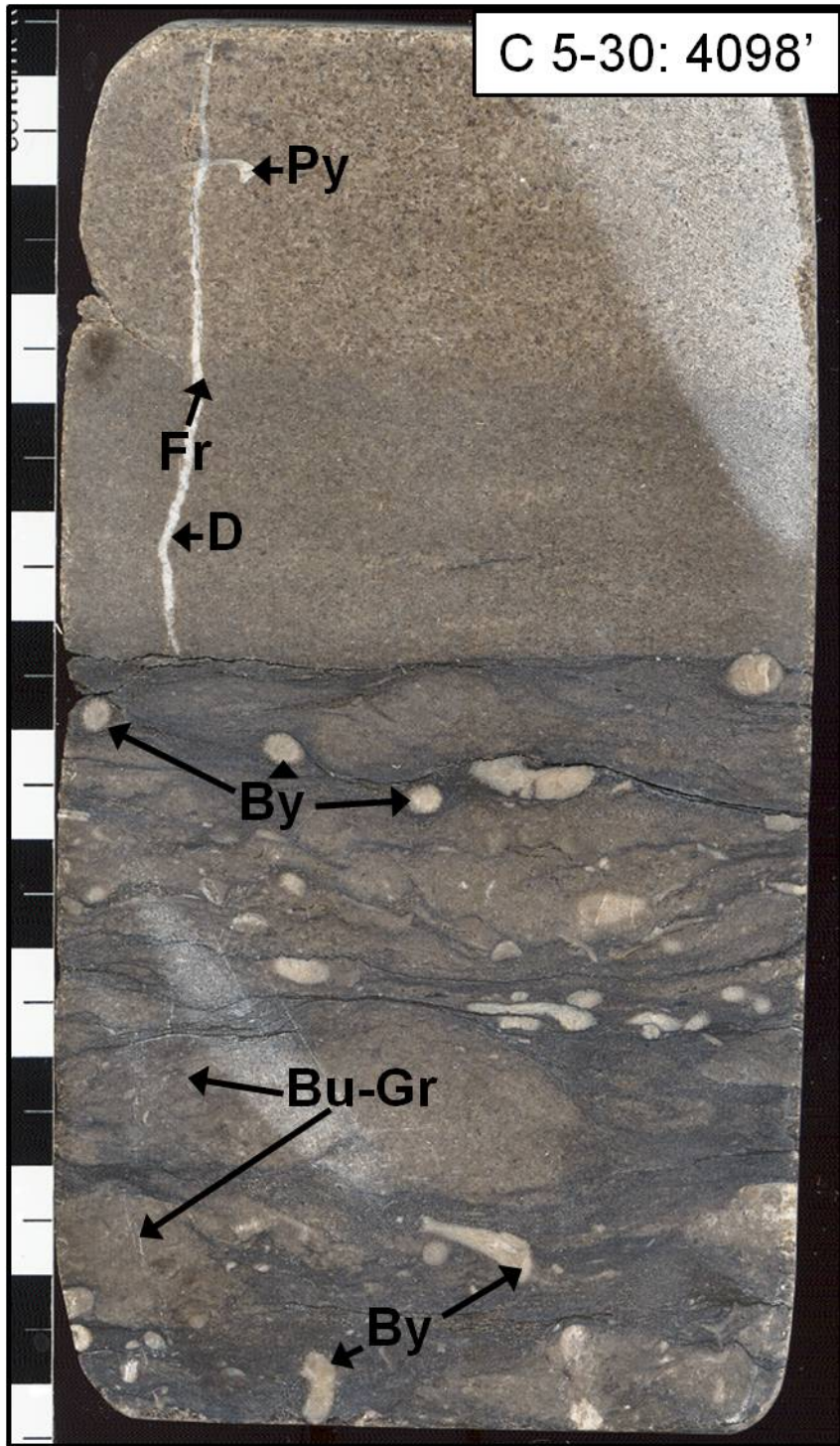
C 5-30: 4114'- F4 – Laminated (L) skeletal fragment grainstone. Pressure solution seam (Psl) follows bedding contact.





C 5-30: -4112'- F5 – Brachiopod-pelecypod packstone showing mottled color and texture characteristic of TBR Facies 5 lagoon deposits. Note mixture of dark (reduced) and relatively lighter sediment (oxidized). C 5-30: -4107'- F5/1 – Skeletal wackestone-packstone overlain by dark gray/black mudstone/skeletal fragment-peloid wackestone. Sample contains grain-dominant burrow filling sediments that are relatively lighter in color (oxidized). Sample exhibits the mixture of dark (reduced) and light (oxidized) sediment characteristic of TBR Facies 5 lagoon (and more restricted/deeper Facies 1) deposits.



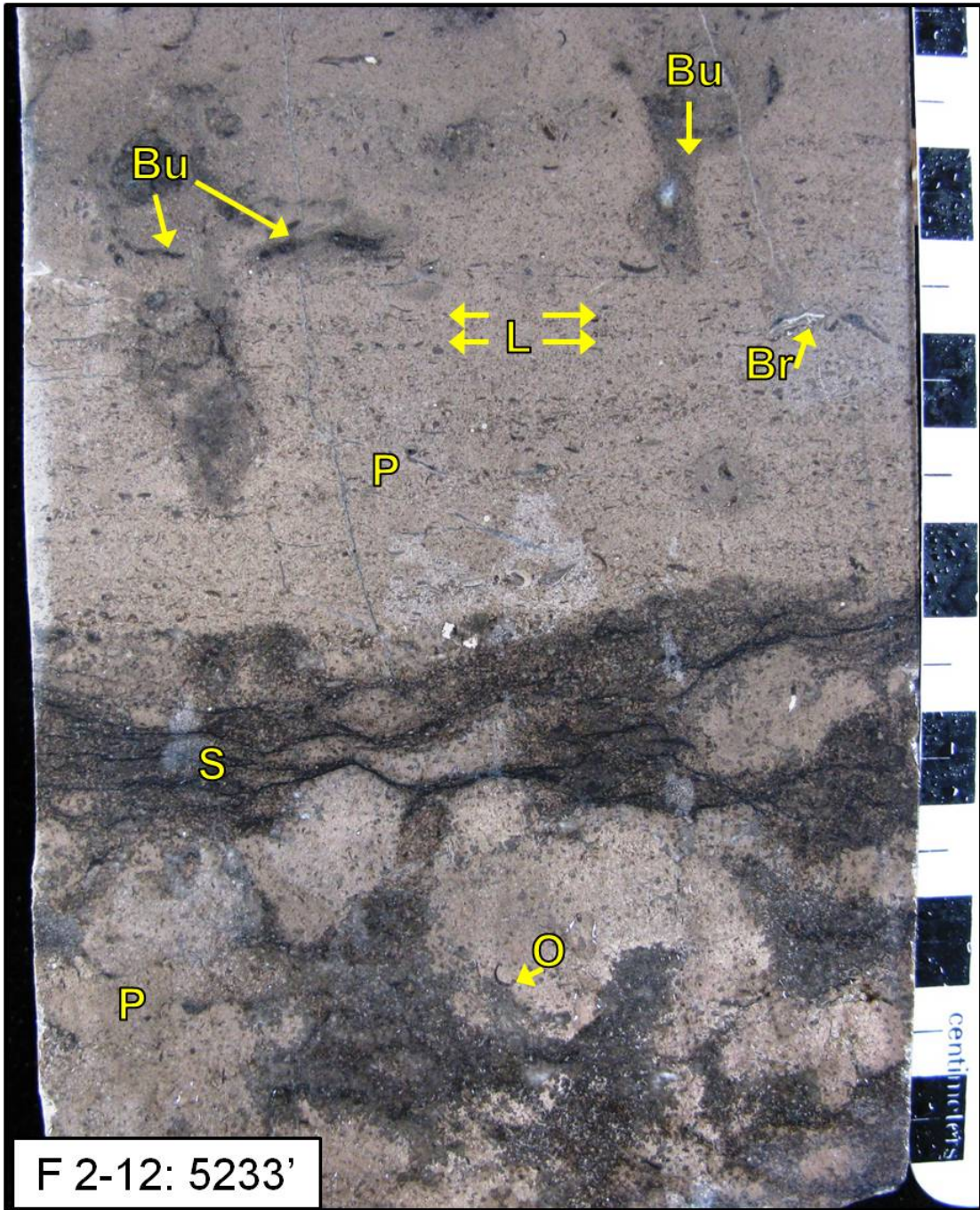


**C 5-30: 4098'- F3** –Peloid-bryozoan packstone-wackestone with grain-dominated burrow fill overlain by a bedded skeletal fragment grainstone. White dolomite fills a prominent vertically-oriented fracture.

Faist, E. 2-12 – TOTAL Petroleum Inc.

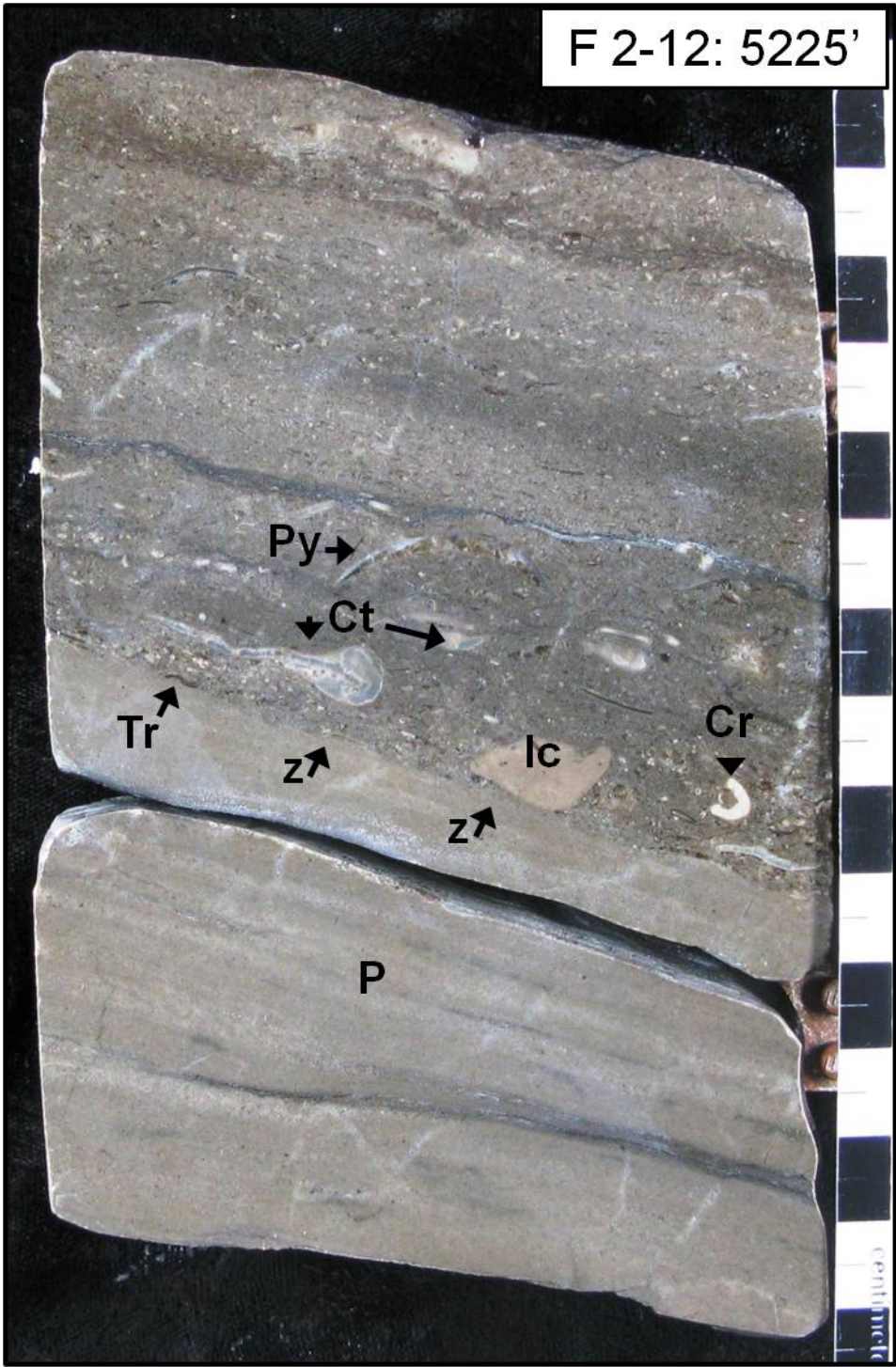
Permit #33673, Jackson County, MI





F 2-12: 5233' – Mottled peloid-ostracode packstone overlain by laminated (L) peloid skeletal fragment grainstone packstone. Laminated packstone contains burrows filled with mud-grain mix.

F 2-12: 5225'

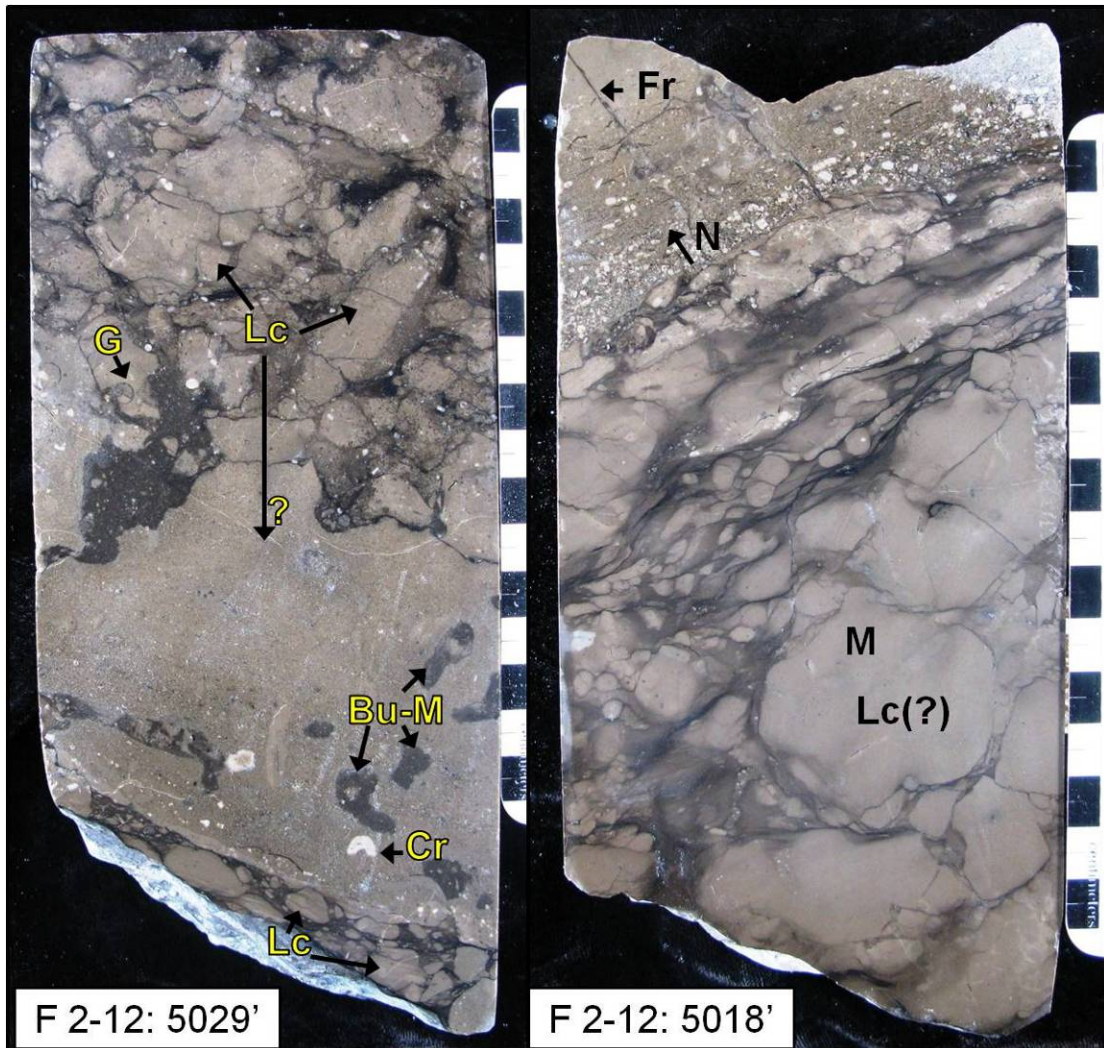




**F 2-12: 5225'** – Laminated peloidal packstone-grainstone overlain by a skeletal intraclastic grainstone. Skeletal grainstone shows normal grading at the bedding contact. Unidirectional flow is additionally indicated at the bedding contact where sediment from the underlying bed is preferentially accumulated on the up-dip side of grains (*Z*) and scoured on the lee of grains. Bedding is apparently inclined approximately 15 degrees from horizontal.

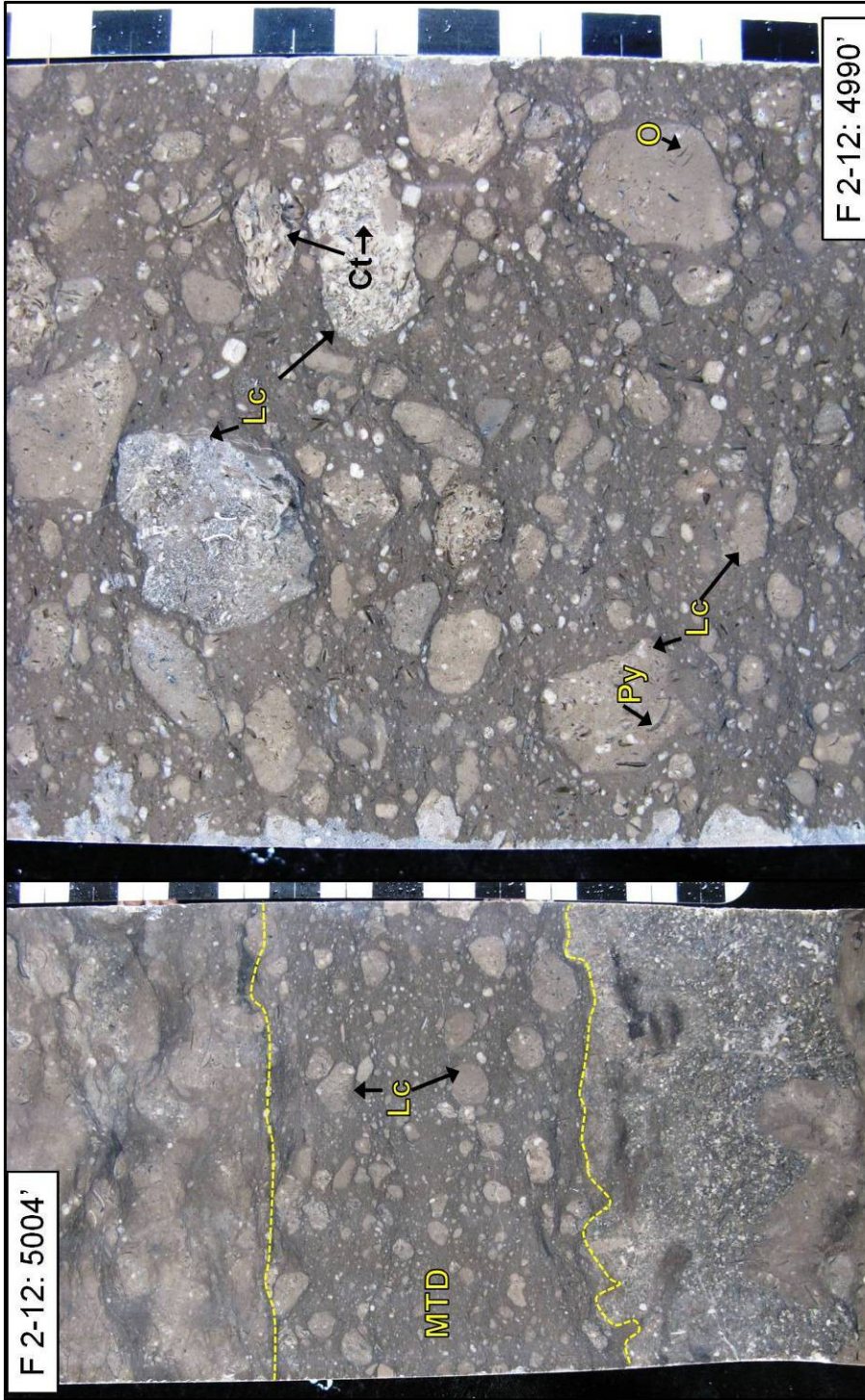


**F 2-12: 5046'** – Skeletal peloidal packstone-wackestone with grainstone burrow fill (?). Pressure solution/stylolite seams (outlined with white lines) are oriented approximately 50 degrees from horizontal, indicating non-vertical stresses applied to the sample, and/or sample rotation from the original pressure solution development orientation.



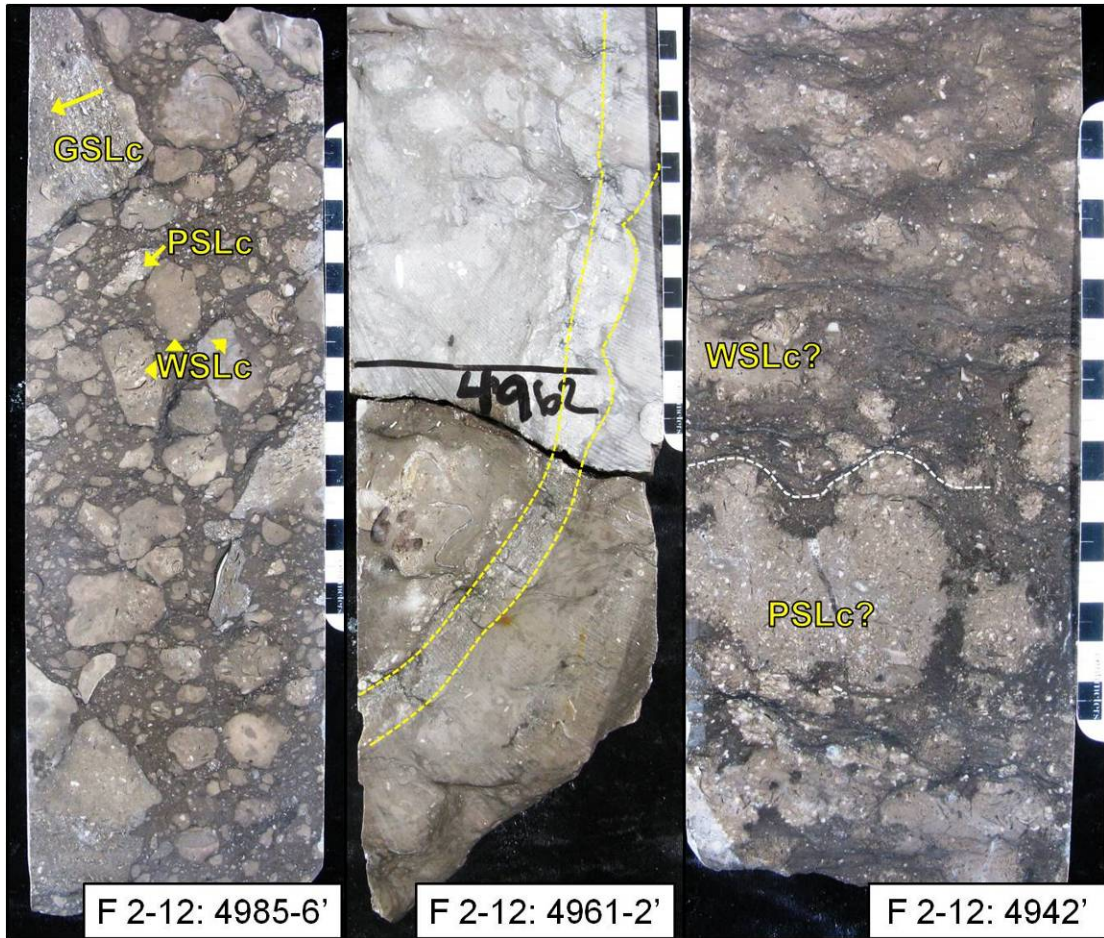
**F 2-12: 5029'** – MTD breccia composed of peloidal-skeletal fragment lithoclasts (Lc). Lithoclasts internally show mud-dominated burrows. Matrix is skeletal wackestone-mudstone. **F 2-12: 5018'** – MTD breccia (?) overlain by normally graded (N, arrow indicating grading direction) skeletal grainstone that transitions up-to packstone-mudstone. Apparent lithoclasts (Lc?) are composed of mud and peloids. Lithoclasts boundaries show less defined outline compared to other F 2-12 MTD, indicating that all of these grains were not completely lithified upon mobilization/deposition. Fracture is filled with calcite.





**F 2-12: 5004'** – Pelloid-skeletal packstone-grainstone containing MTD conglomerate (yellow dashed outline). Lithoclasts (Lc) are composed of skeletal-pelloidal wackestone-packstone, and are sub-angular to sub-rounded. MTD matrix is crinoidal wackestone. **F 2-12: 4990'** – MTD conglomerate. Lithoclasts (Lc) are sub-angular to rounded, and composed of mudstone, wackestone, and packstone textures. Few lithoclasts are replaced by chert (Ct) only within the grain, suggesting that chert replacement occurred prior to mass-transport.





**F 2-12: 4985-6'** – MTD breccia showing highly angular constituent grains composed of a variety of Dunham textures, which include wackestone (WSLc), packstone (PSLc), and grainstone lithoclasts (GSLc). The labeled GSLc show that this block is overturned from original depositional orientation, where the arrow indicates normal grading and points toward depositional-“up”. MTD matrix is skeletal wackestone. **F 2-12: 4961-2'** – Core section showing rotated bedding contacts (yellow outline), likely indicating soft sediment deformation on steep slopes. Note: the color change between core fragments is the difference between polished (lower) and unpolished slabs. **F 2-12: 4942'** – Mottled packstone and wackestone textures showing heterogeneous diagenetic alteration (?) of sediments. Zones of consistent textures are labeled as lithoclasts because pressure solution (white dashed line) follows apparent clast boundaries, indicating suturing. Diagenetic distributions/mechanisms are poorly understood in this and samples like this.

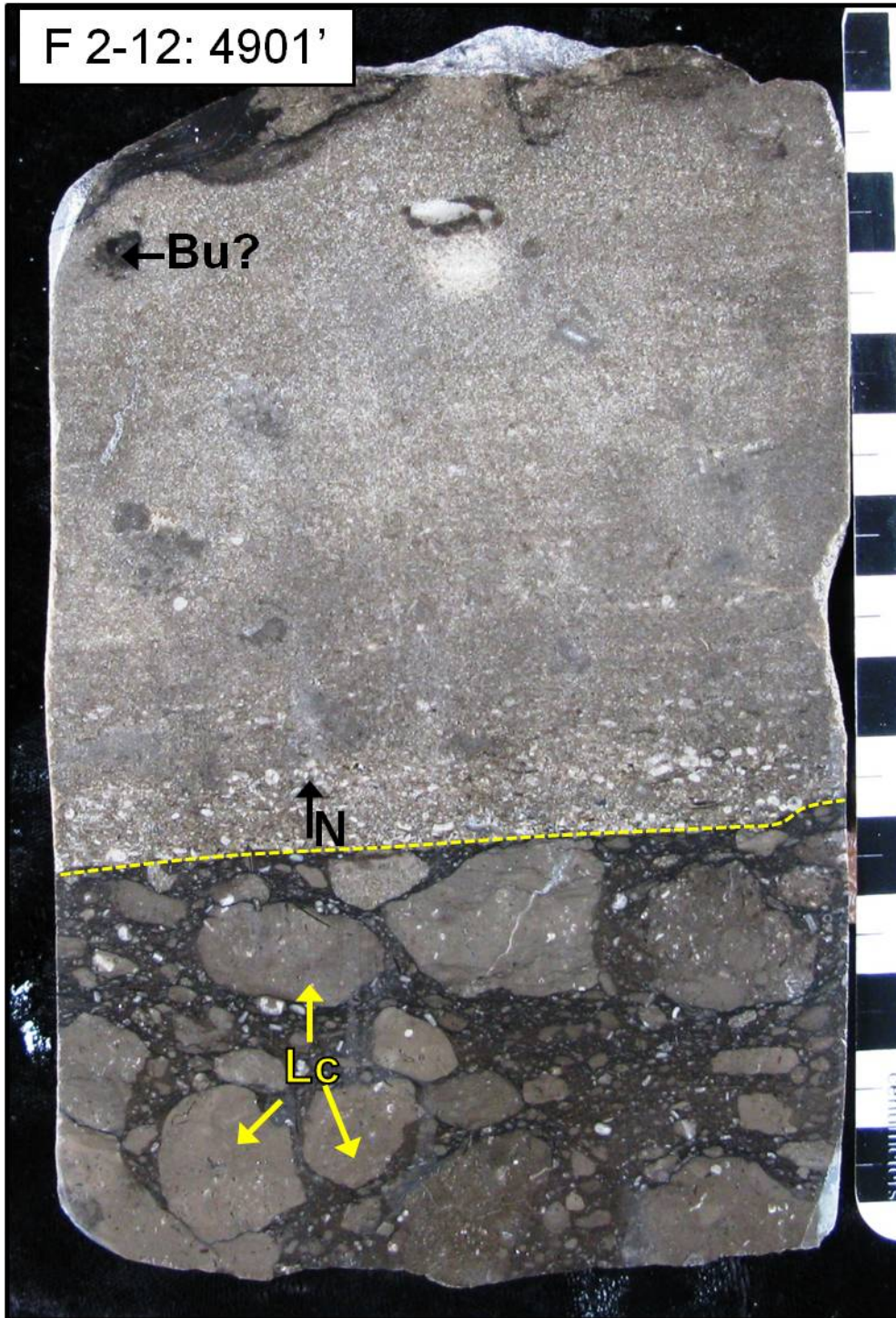


F 2-12: 4901'

←Bu?

↑N

↑  
LC  
↙ ↘



**F 2-12: 4901'** – MTD breccia overlain by a sharp-planar based (yellow dashed line), normally graded (N, arrow indicating grading direction), and laminated skeletal fragment grainstone.

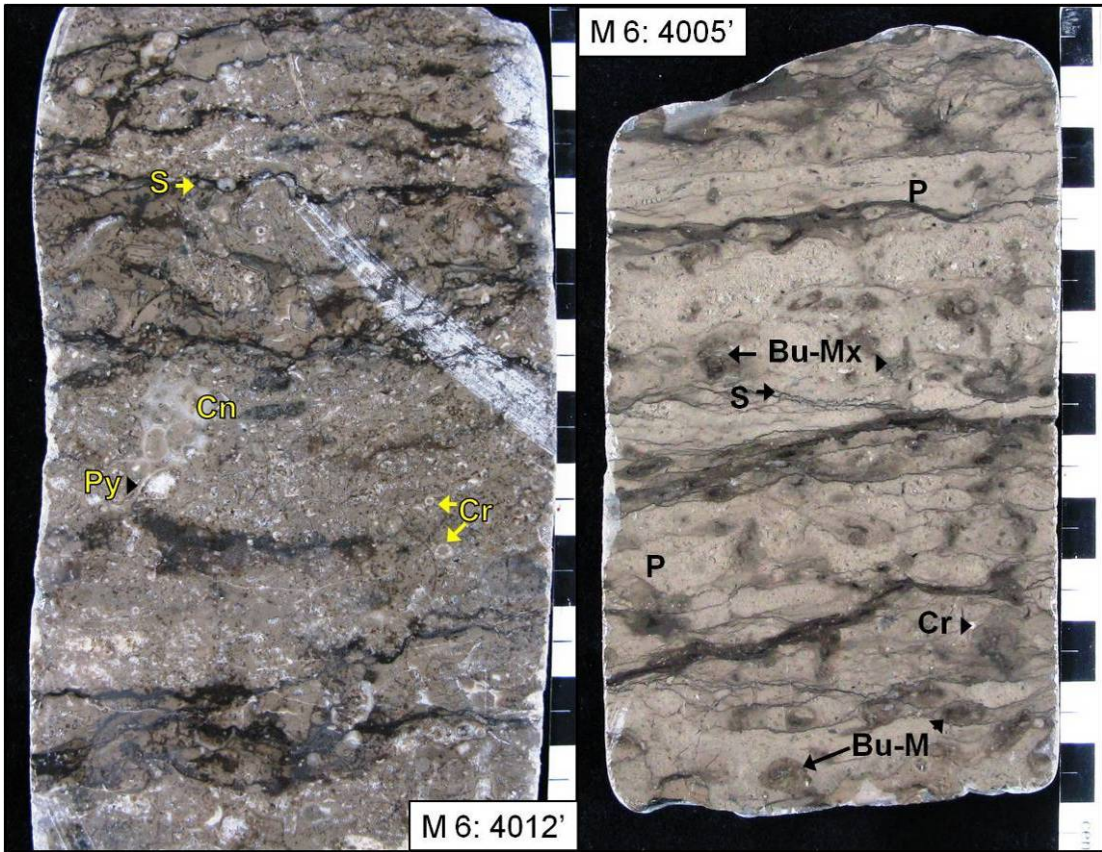
Hergert 2 – McClure Oil Company  
Permit #22196, Hillsdale County, MI



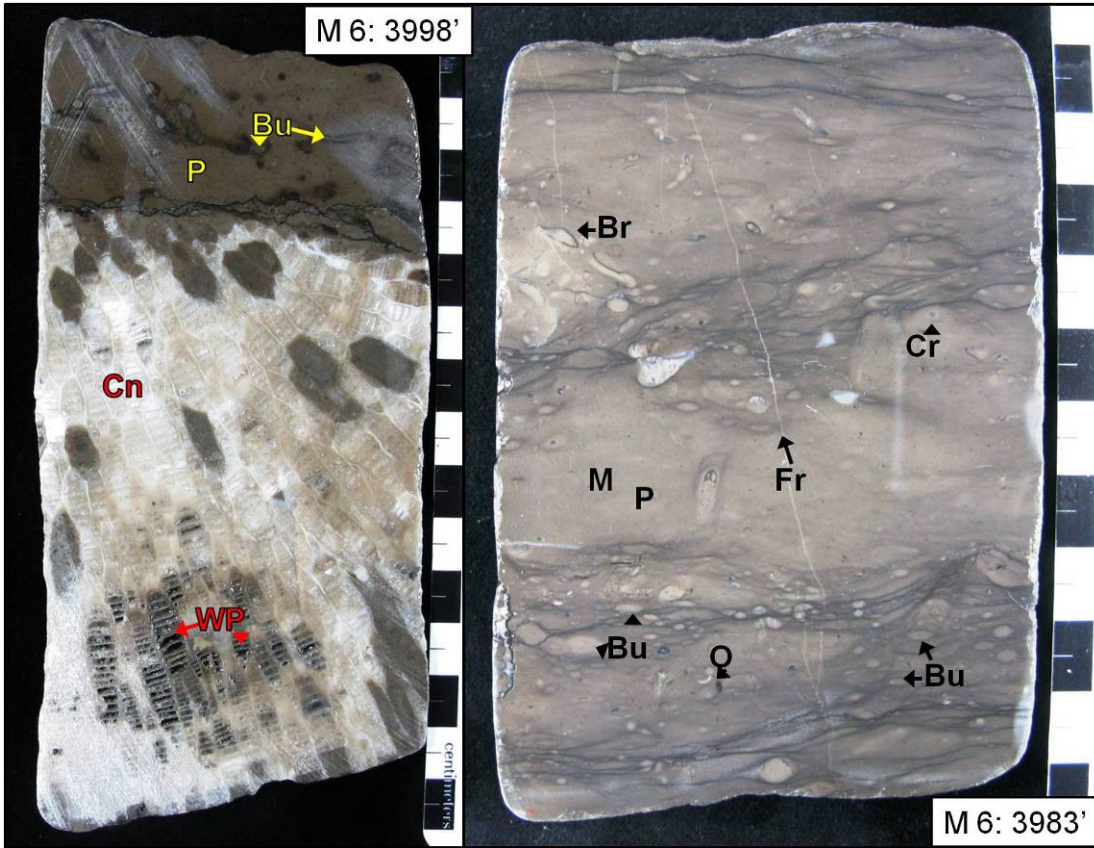
H 2: 3923-4' – F 7 – Black River Shale K-bentonite.

Mann, H 6 – Ohio Oil Company  
Permit #22381, Hillsdale County, MI



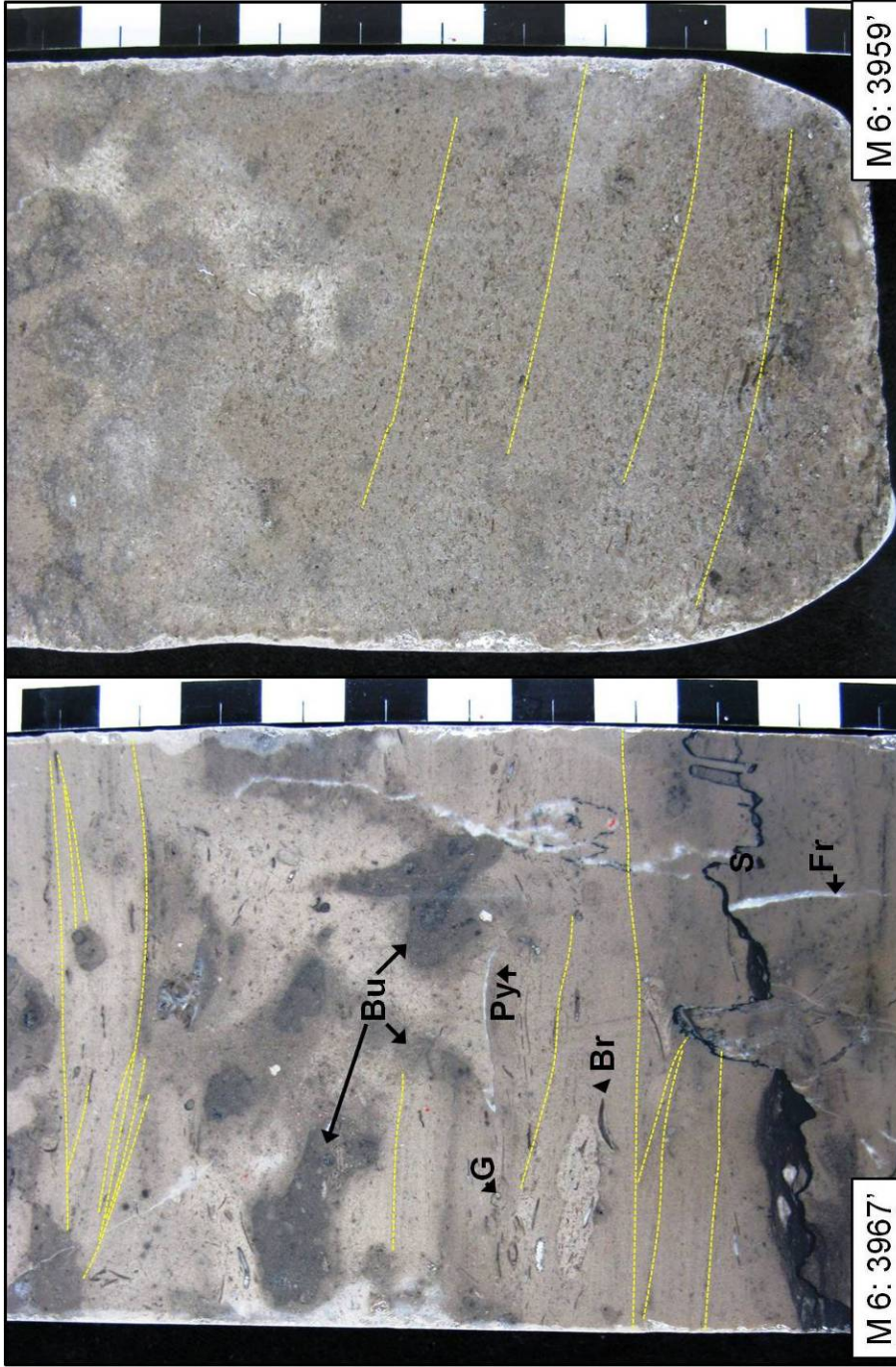


**M 6: 4012'** – F3 – Peloid-skeletal packstone showing general mottled texture of TBR mid-outer ramp facies (Cn = tabulate coral fragment) **M 6: 4005'** – F2 – Peloid-skeletal wackestone-packstone with mud and mud-grain mixed burrow filling sediments and prominent development of pressure solution and stylolites.



**M 6: 3998'** – F2 – Peloid wackestone with large tabulate coral fragment (Cn, framestone) out-of-growth position. Coral contains limited interparticle porosity. **M 6: 3983'** – F2 – Peloid wackestone-mudstone with abundant small burrows (2 - 4 mm diameter).

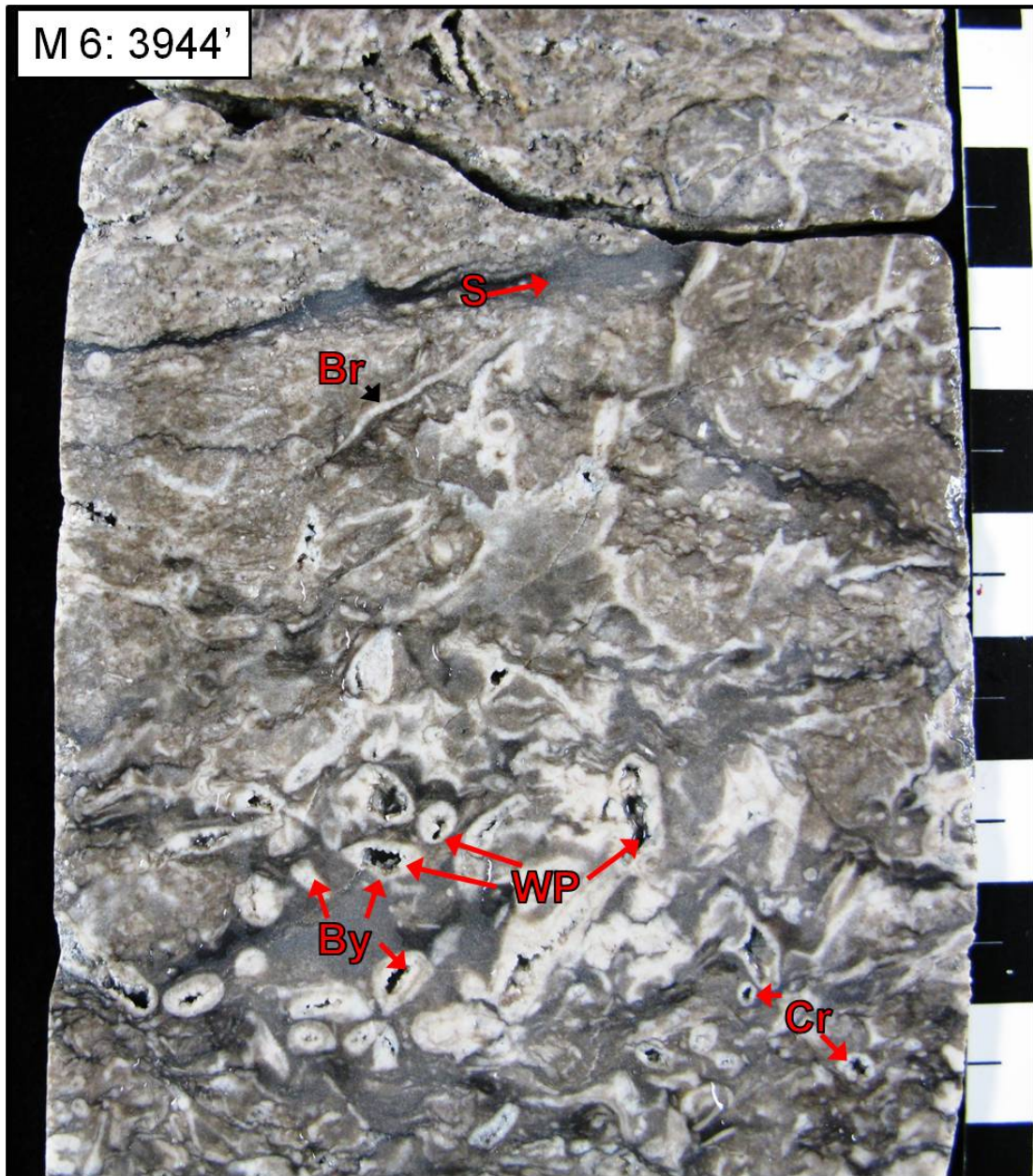




**M 6: 3967'** – Peloid wackestone-packstone overlain by a laminated/hummocky cross-laminated (laminations are outlined with dashed yellow lines) peloid-skeletal fragment packstone-grainstone. Packstone-grainstone contains mud and mud-grain mixed burrow filling sediments. Planar laminations transitioning-up to hummocky cross-laminations are indicative of waning storm energies. Also shown in this sample are white dolomite filled fractures and prominent stylolites.

**M 6: 3959'** – Bedded (cross-bedded?) skeletal fragment-peloid grainstone-packstone transitioning up to a burrow homogenized deposit.



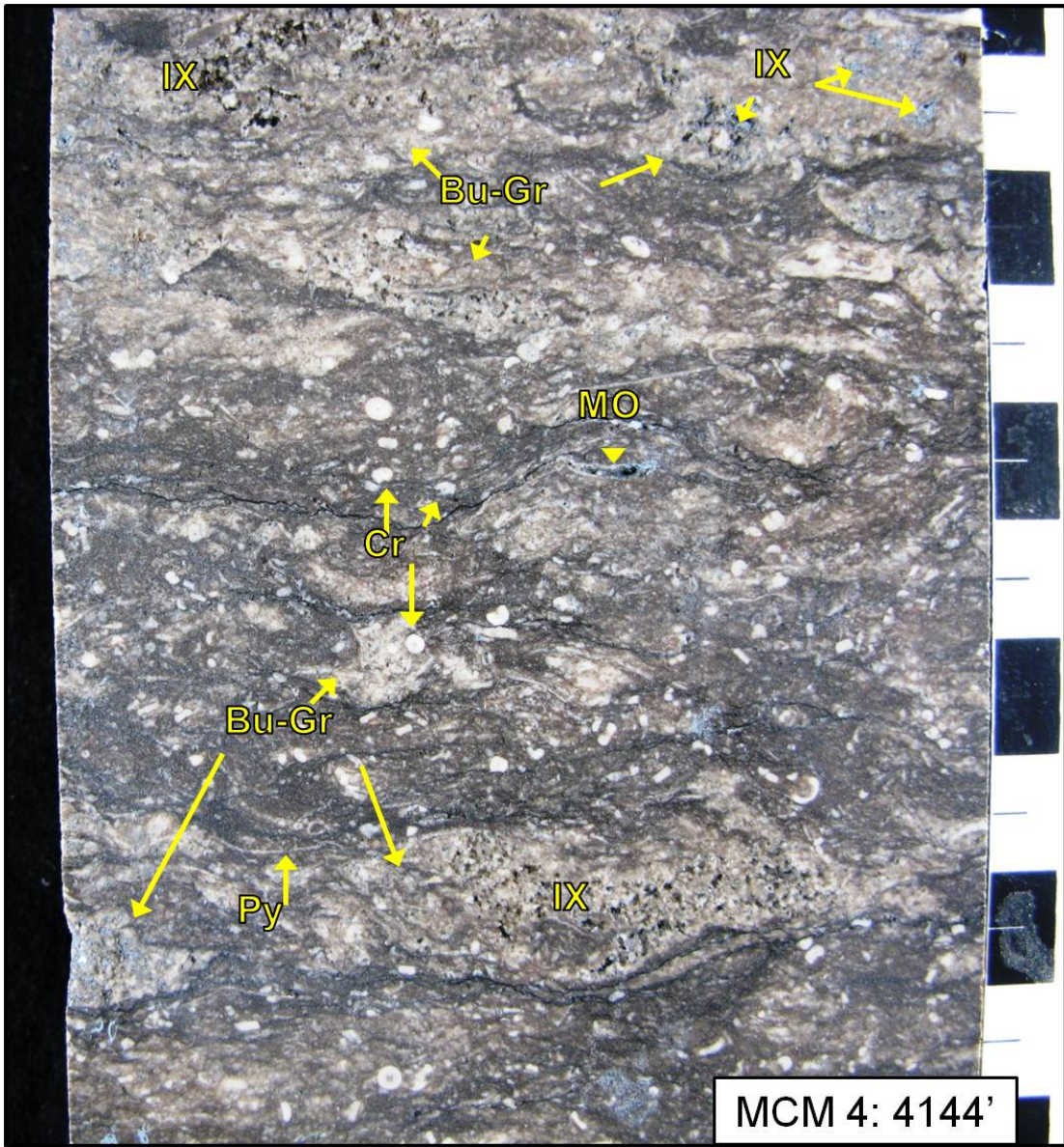


**M 6: 3944' – F3** – Bryozoan packstone and skeletal fragment packstone. Skeletal fragments have been replaced by white dolomite. Interparticle porosity is developed in association with bryozoan and crinoid fragments, with minor IX developed in the upper section of core.

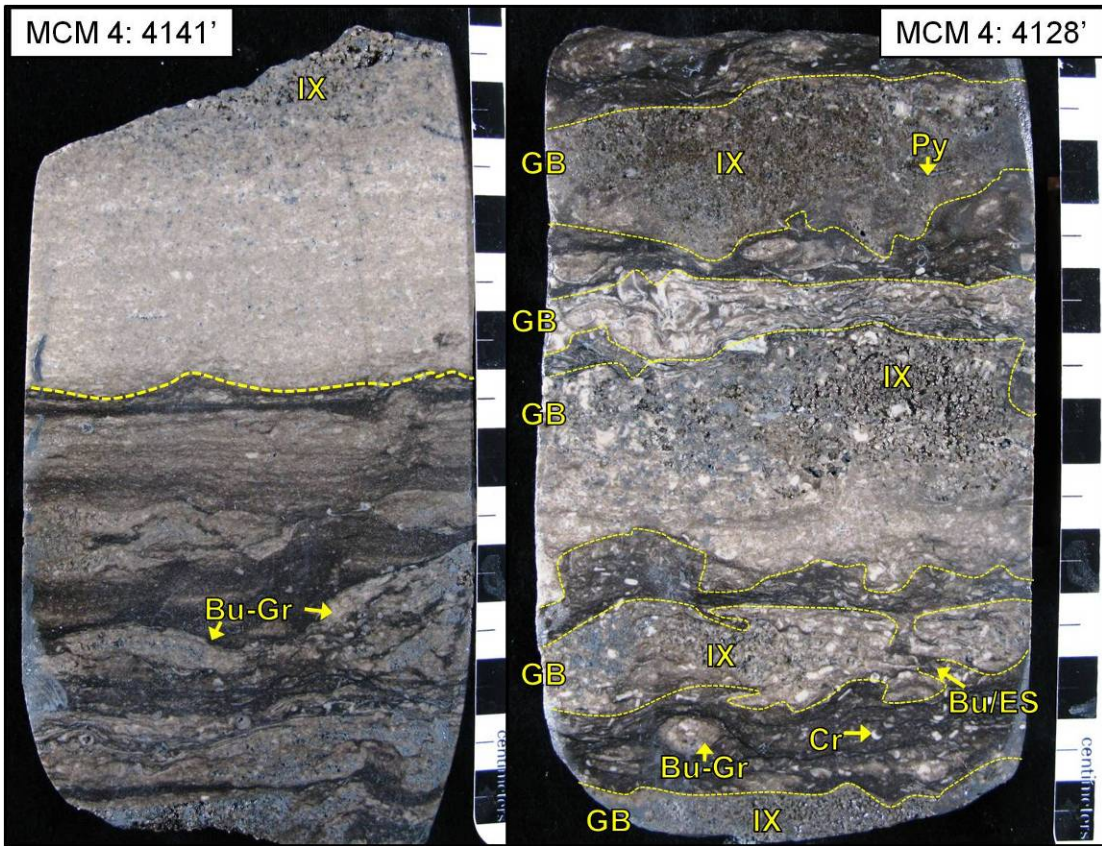
McMahon, J. & B. #4 – Marathon Oil Company

Permit #22460, Calhoun County, MI



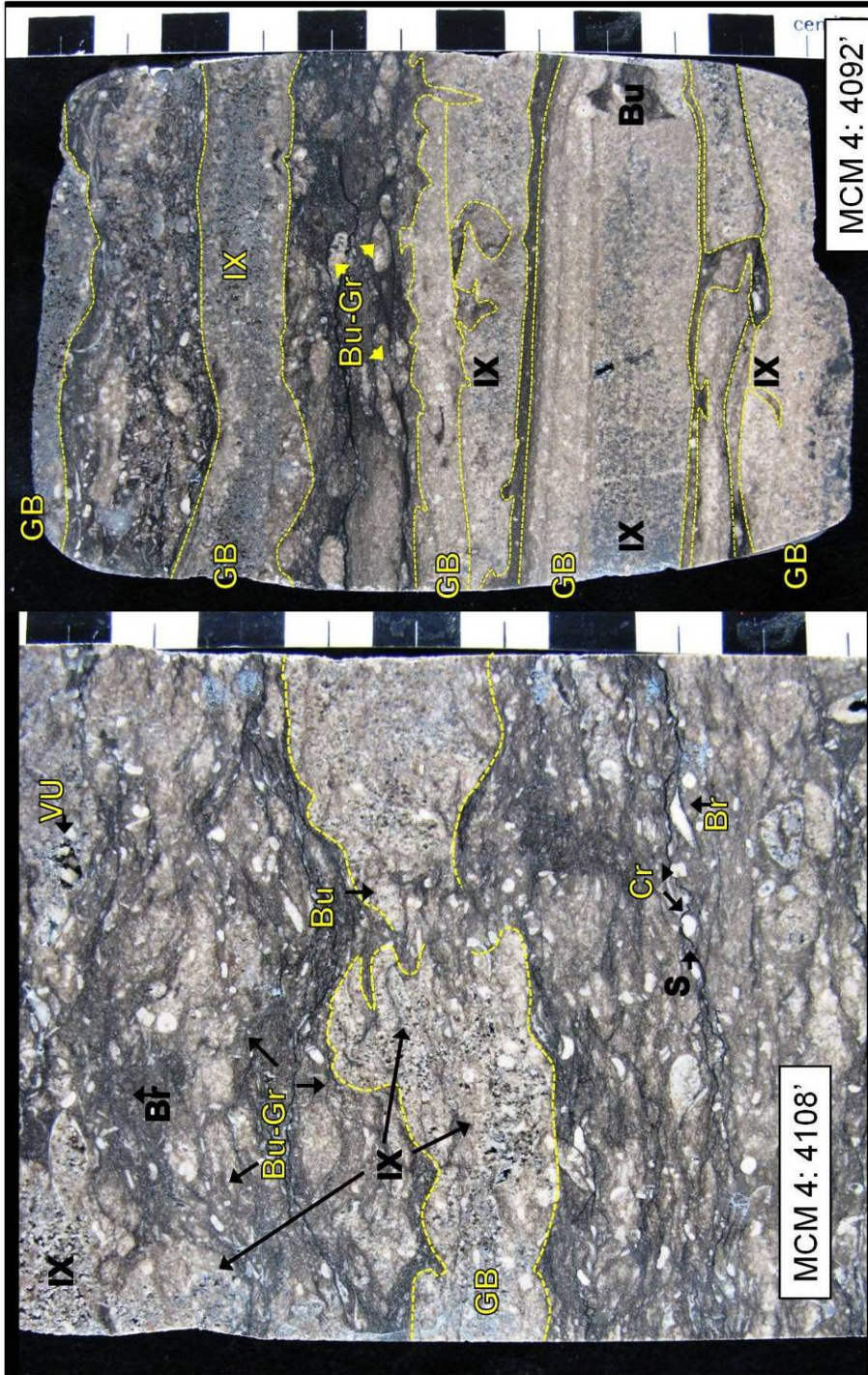


**MCM 4: 4144' – F3/5** – Crinoid wackestone-packstone with grain-dominant burrow filling sediment. Intercrystalline porosity is developed in association with grain-filled burrows.



**MCM 4: 4141' – F3** – Crinoid, brachiopod, peloid packstone-wackestone with packstone-grainstone grain bed (outlined with dashed yellow lines) and grain-dominant burrow fill. Intercrystalline porosity is associated with grain-bed and grain-dominant burrow fill. **MCM 4: 4128' – F3** – Core section dominated by grain-bed deposition (individual grain-beds are outlined with yellow dashed lines). Intercrystalline porosity is associated with grainstone grain-beds.

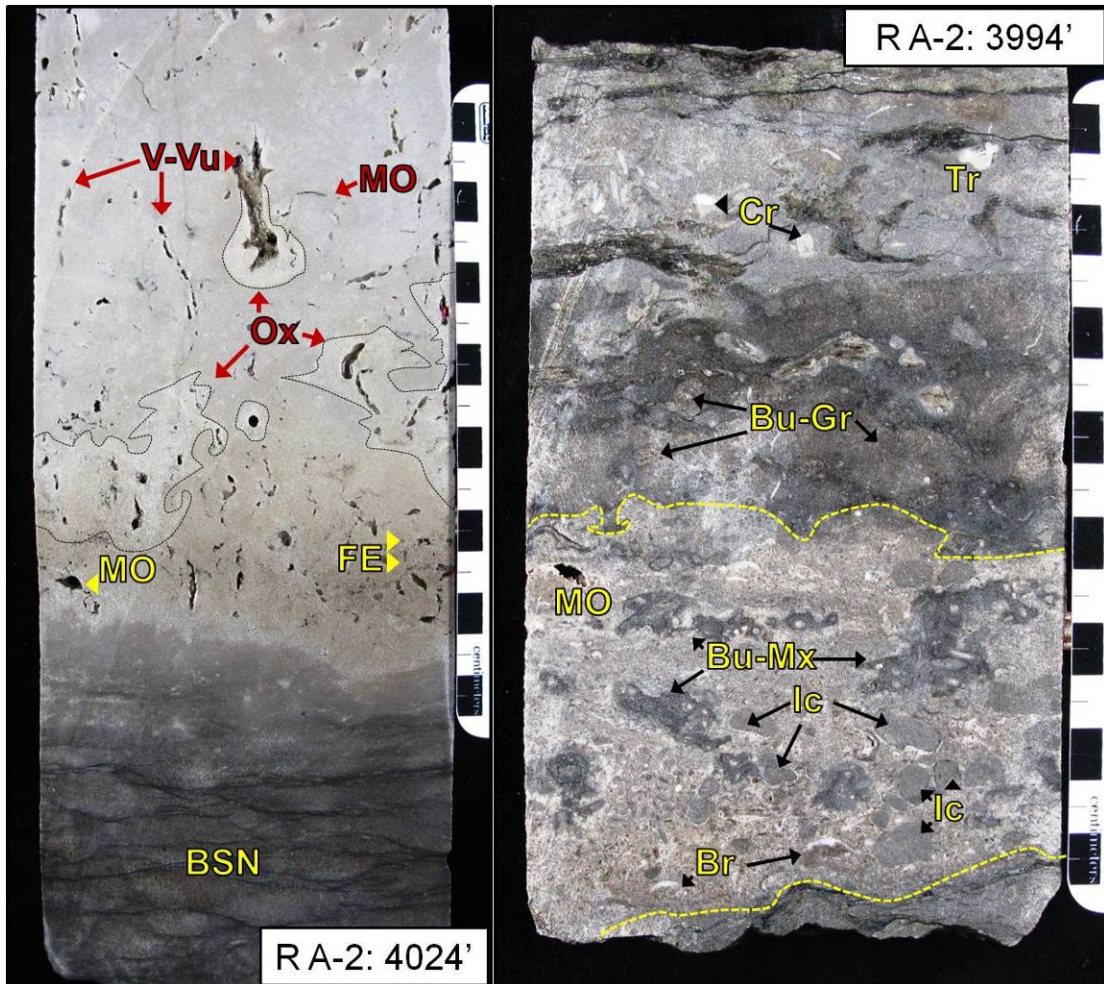




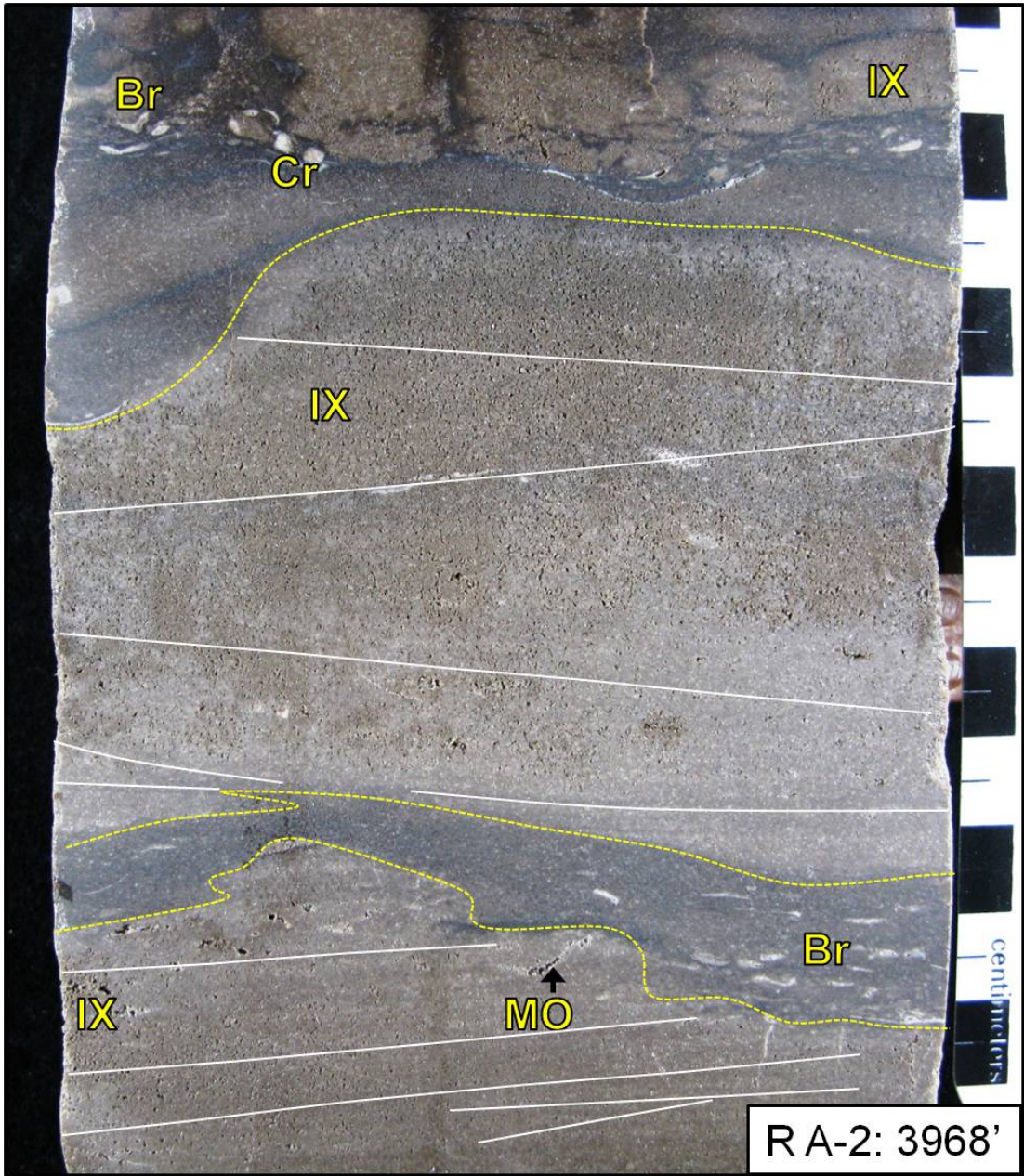
**MCM 4: 4108' – F3** – Crinoid, brachiopod, peloid packstone-wackestone with packstone-grainstone grain bed (outlined with dashed yellow lines) and grain-dominant burrow fill. Intercrystalline and minor vug porosity is associated with grain-bed and grain-dominant burrow fill. **MCM 4: 4092' – F3** – Core section dominated by grain-bed deposition (individual grain-beds are outlined with yellow dashed lines). Sample exhibits grain-bed amalgamation likely owing to higher frequency of storms affecting the depositional surface. Burrowed surfaces and lamination truncation commonly indicates individual grain-bed bounding surfaces. Intercrystalline porosity is associated with grainstone grain-beds.

Rowe A-2 – McClure Oil Company  
Permit #37239, Hillsdale County, MI



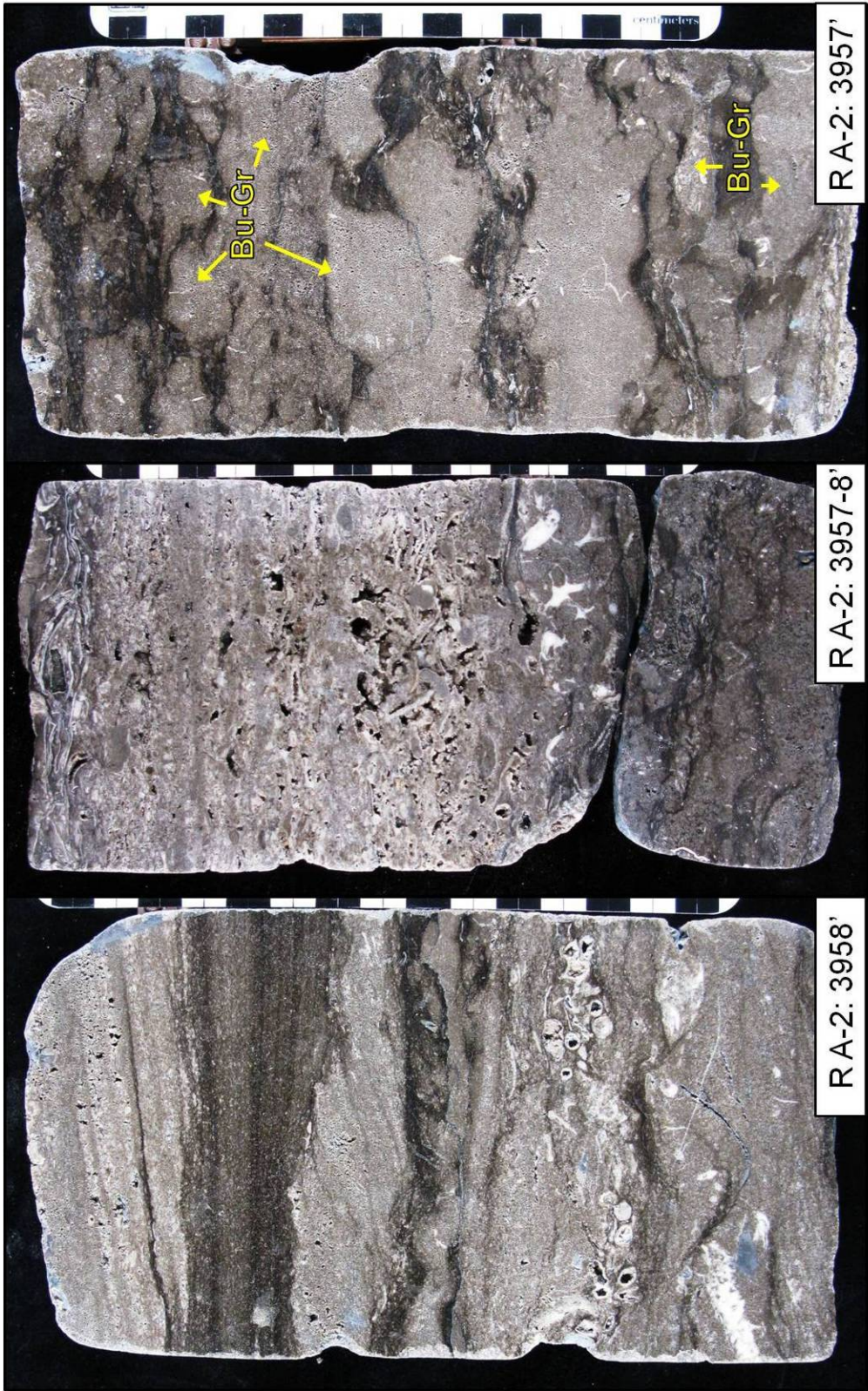


**R A-2: 4024' – F6** – Oxidized fenestral peloid packstone overlying peloid wackestone with burrow-bounding stylonodular fabric. A higher degree of oxidation (Ox) is commonly shown around molds, vugs, and vertically oriented vugs (V-Vu). **R A-2: 3994' – F3** – Peloid packstone-wackestone with intraclastic grainstone grain-bed (outlined with dashed yellow lines). Burrow fill is dominantly grain-dominated.



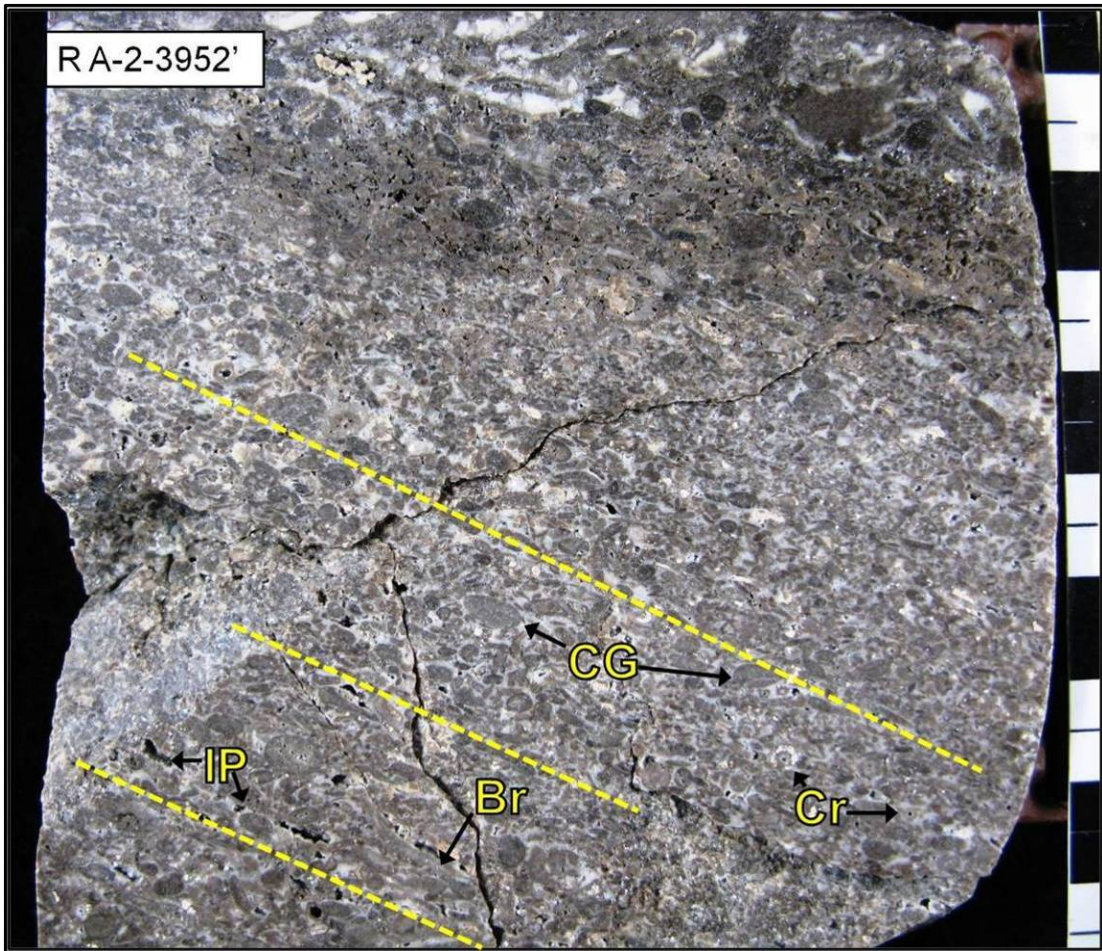
**R A-2: 3968' – F3** – Brachiopod-crinoid wackestone-packstone with grainstone grain-beds (outlined with dashed yellow lines). Grain-beds show cross-lamination (hummocky?) (outlined with white lines). Porosity is limited to IX and MO in grain-bed deposits.



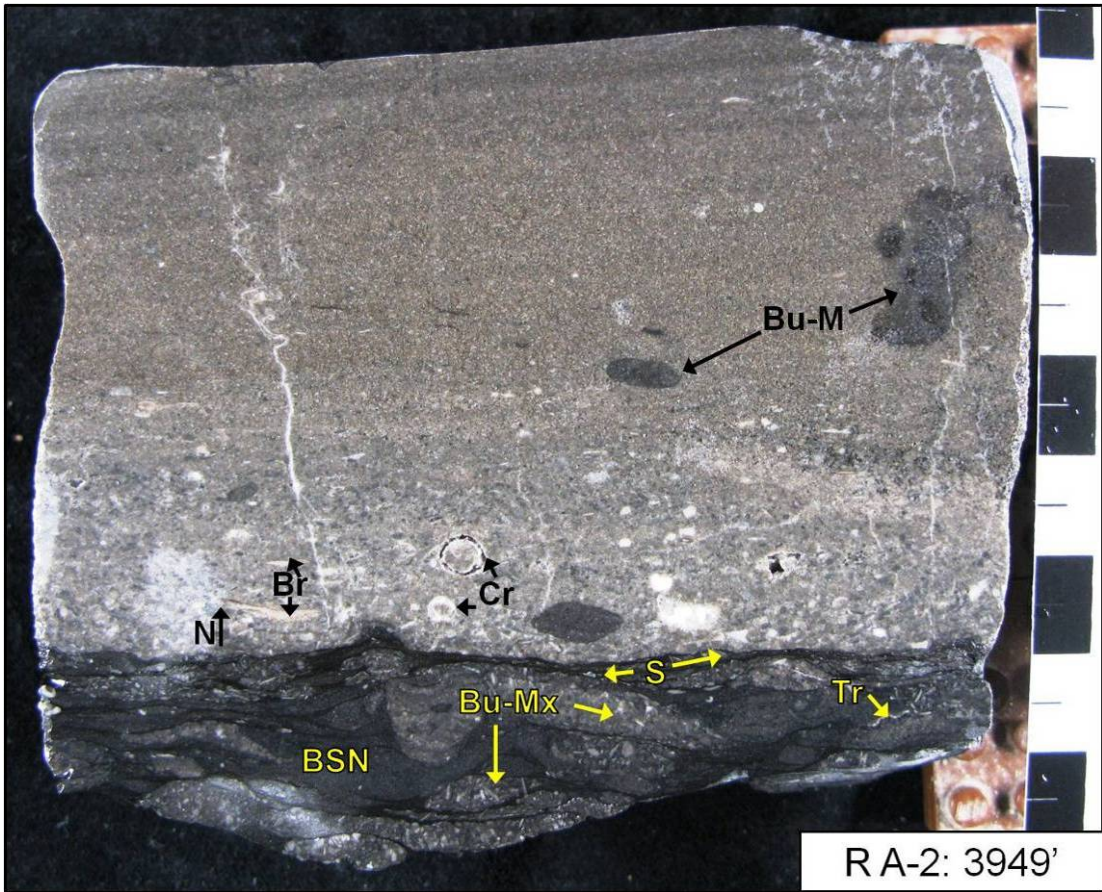


**RA-2: 3957-8' - F3 and 4** - Continuous core from lower left (deepest) to upper right. Interbedding of Facies 3 packstone-grainstone and Facies 4 cross-bedded grainstone. Porosity distribution and character is apparently related to grain-size and sorting, where well sorted-abraded grainstones show IX, and poorly sorted deposits contain VU and IP.



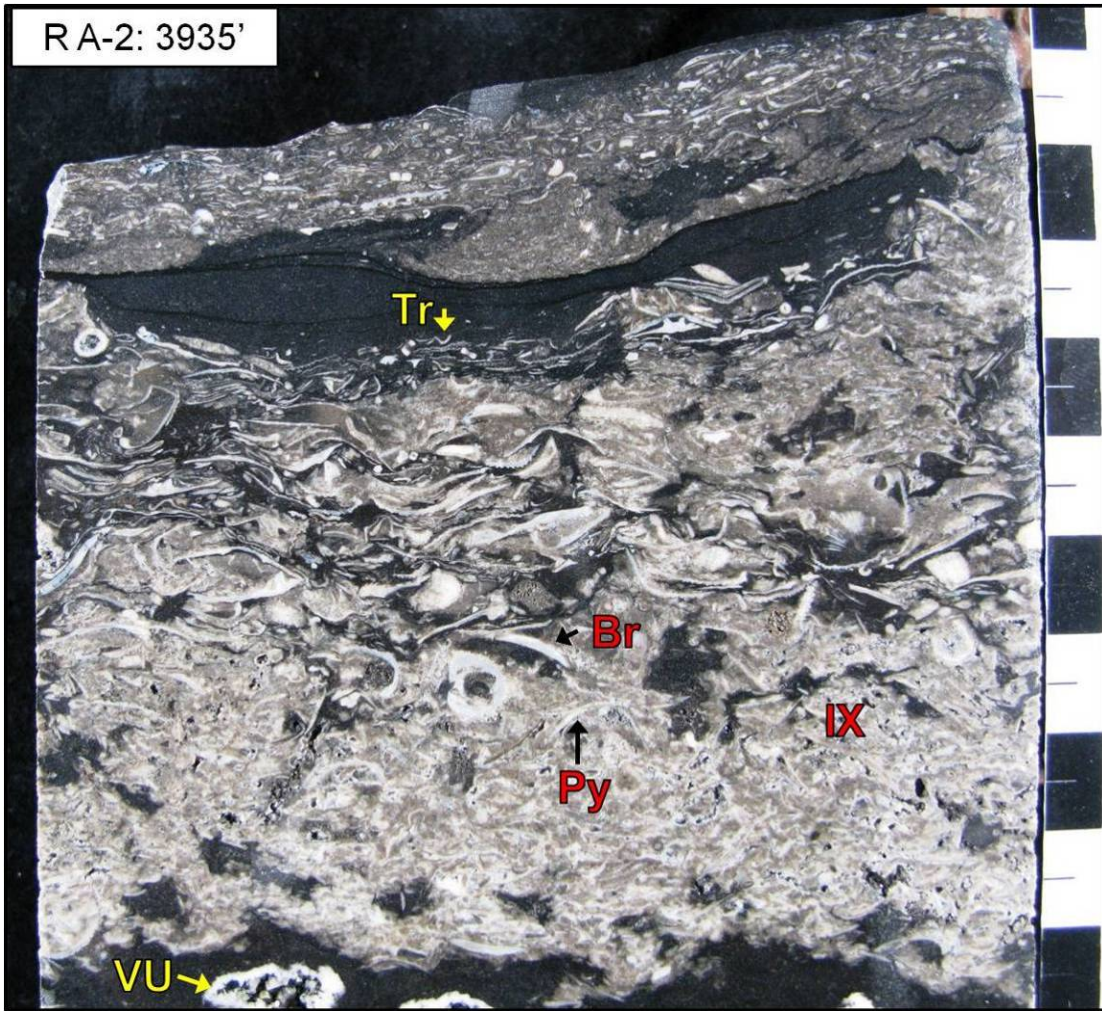


**R A-2: 3952' – F4** – Cross-bedded compound grain –crinoid grainstone. Cross bedding is outlined with yellow dashed lines. Porosity is dominantly IP (IX).



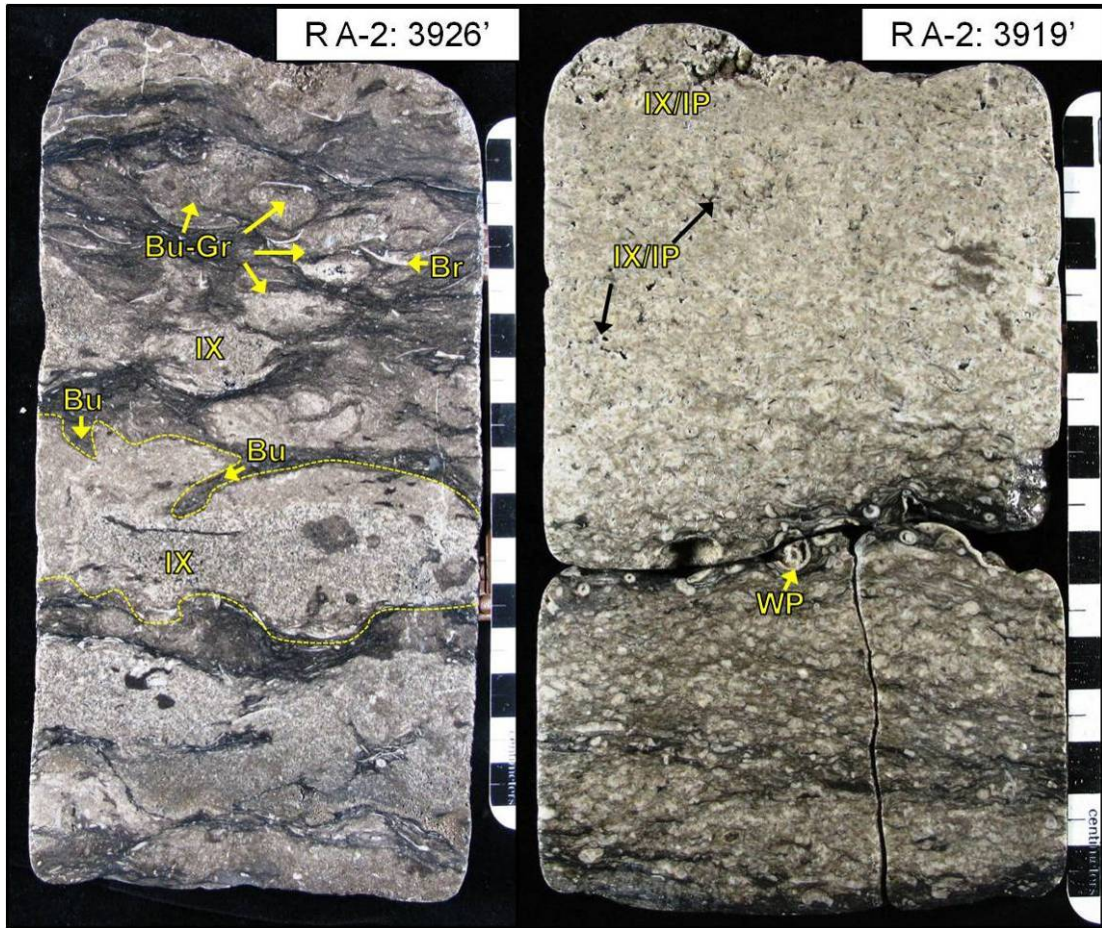
**R A-2: 3949' – F 3 and 5** – Dark gray (reduced?) wackestone-mudstone with burrow-bounding stylonodular fabric and grain-mud mixed burrow fill (F5) overlain by a normally graded (N, arrow pointing in grading direction), laminated, skeletal fragment-peloid packstone-grainstone with mud-dominant burrow fill (F3). White dolomite fills sub-vertical veins. Minor VU and WP (crinoid) porosity is show in this sample.



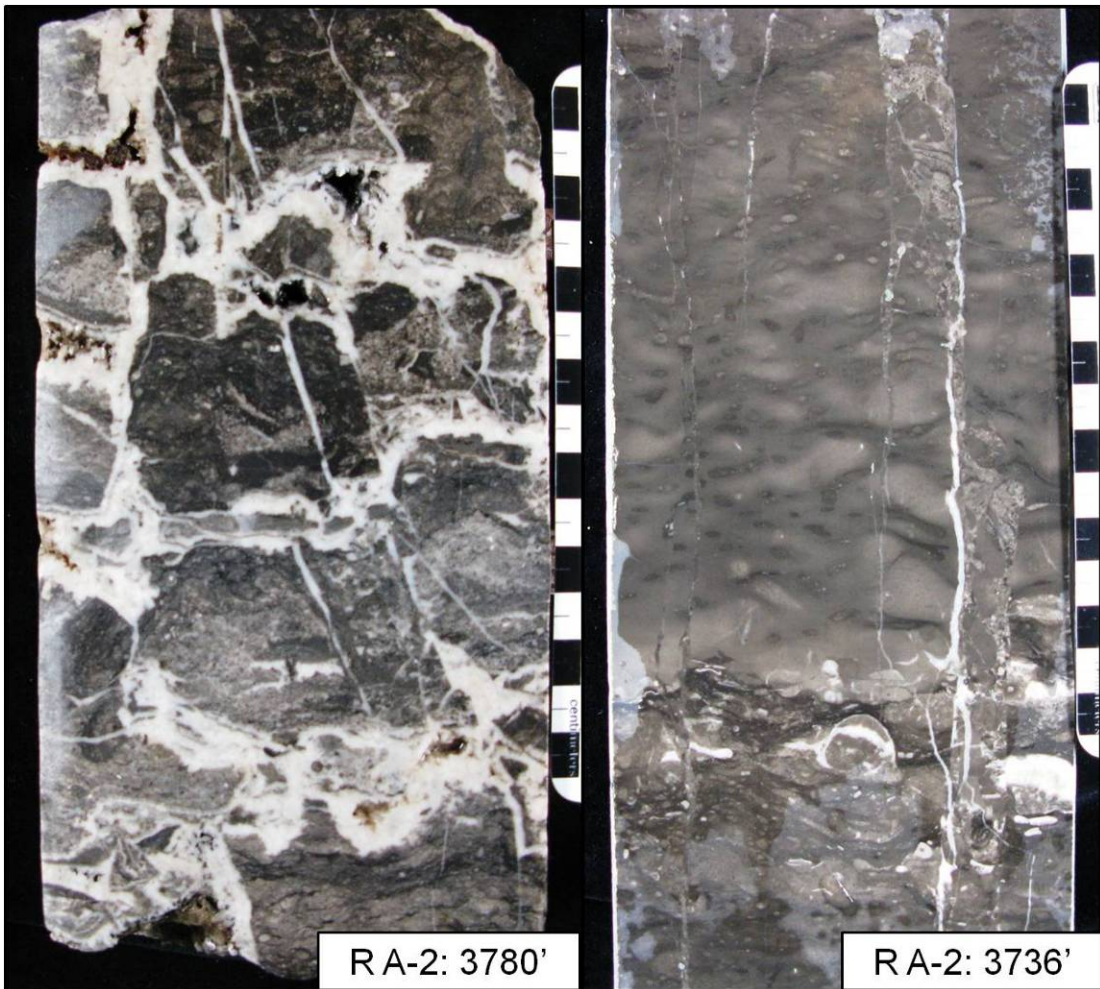


**R A-2: 3935' – F 5** – Dark gray (reduced?) wackestone-mudstone interbedded and intermixed with brachiopod-skeletal fragment packstone. White dolomite replaces bioclasts and fills primary pore space. Porosity is developed as IX where dolomite does not completely occlude IP voids, and dissolution VU occur in reduced wackestone textures.





**R A-2: 3926' – F 3** – Brachiopod-crinoid packstone-wackestone with grainstone grain-beds (outlined with dashed yellow lines) and grain dominant burrow fill. Grain-bed and burrow fill is associated with IX. **R A-2: 3919' – F 4** – Crinoid-skeletal fragment grainstone. Porosity is developed as IX/IP in association with what was likely primary pore space/early marine cement. Minor WP porosity is additionally developed in association with crinoid fragments.

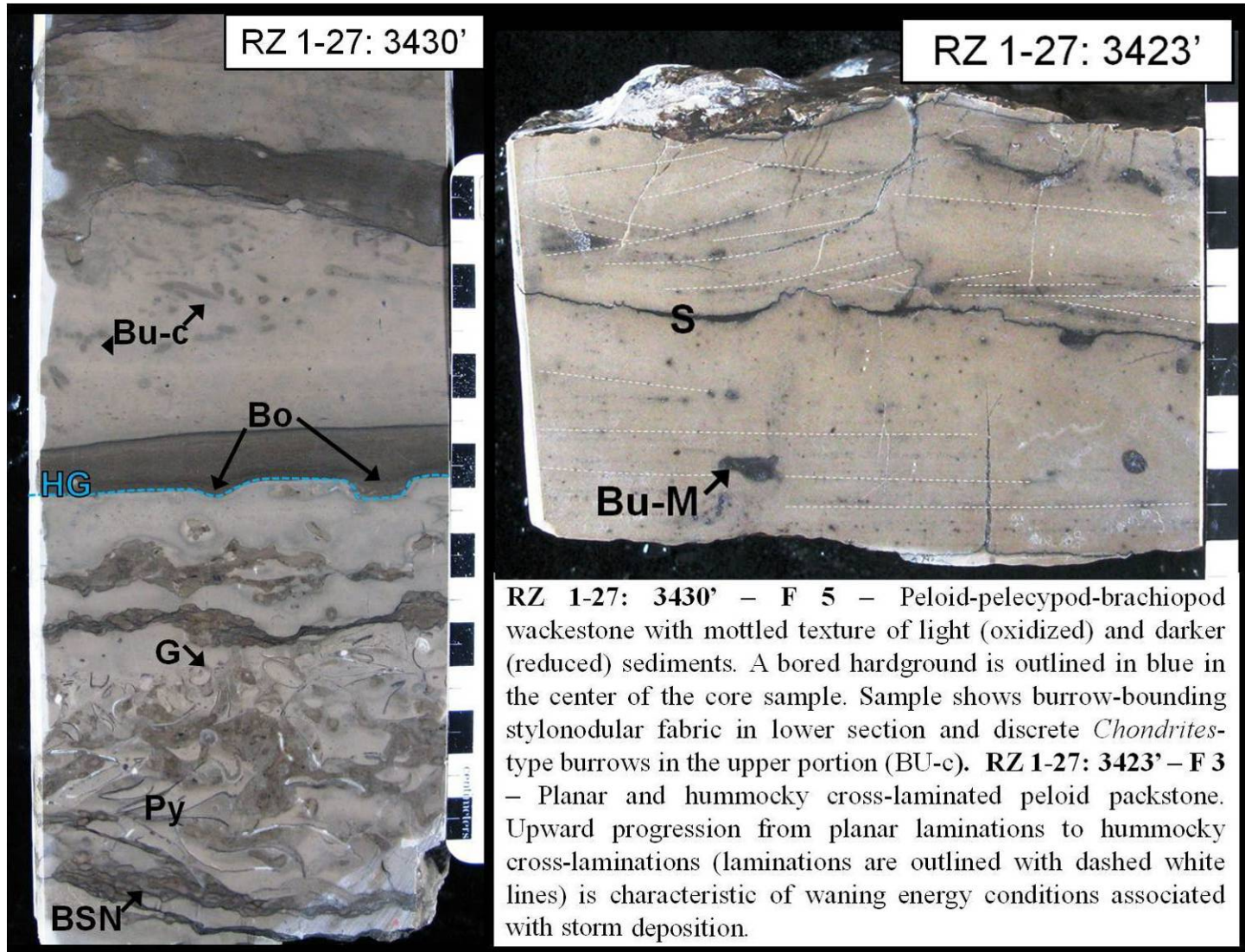


**R A-2: 3780' – F 2** – Wackestone with HTD breccias fabric development and associated saddle dolomite lined vugs. **R A-2: 3736' – F 2** – Pervasively dolomitized wackestone with grain-dominant burrow fill (?). Note the rock-fabric appears “liquefied” due to strong HTD-alteration associated with close proximity to vertically oriented faults and fractures. This rock fabric contrasts with the breccia with well developed vugs in R A-2 3780', which is also in close proximity to faulting.

Rzepke 1-27 – Marathon Oil Company

Permit #31253, Branch County, MI





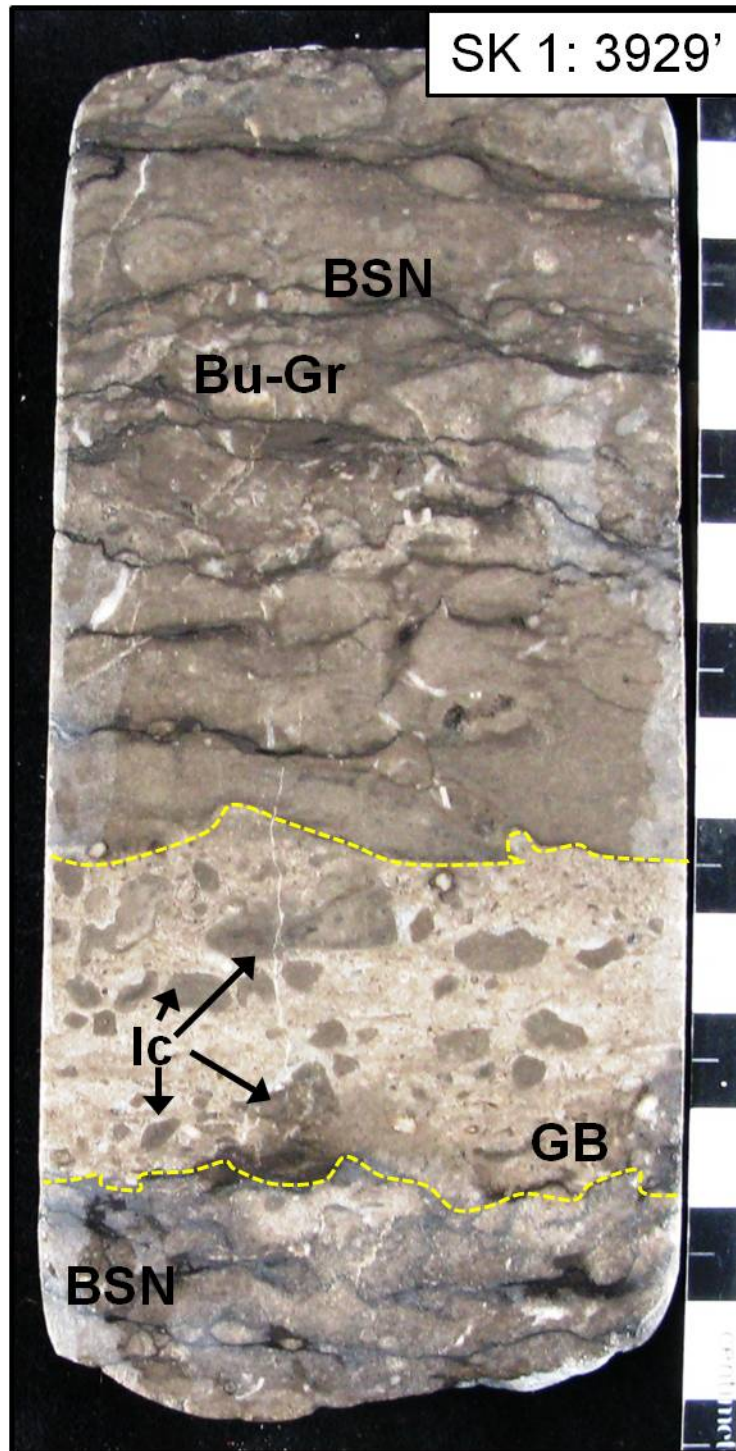




**RZ 1-27: 3117' – F 7** – Black River Shale K-bentonite. No scale, however core width is the same as RZ 1-27: 3430 and 3423 images with scales.

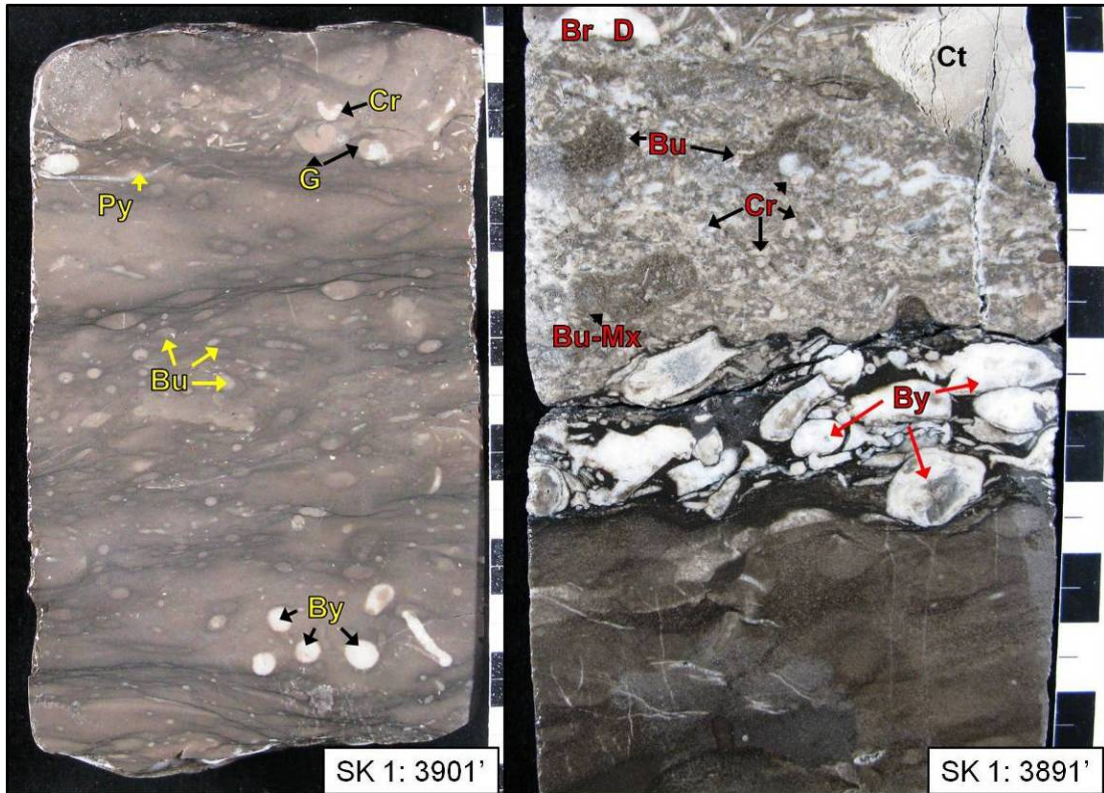
Skinner 1 – Marathon Oil Company  
Permit #21833, Hillsdale County, MI





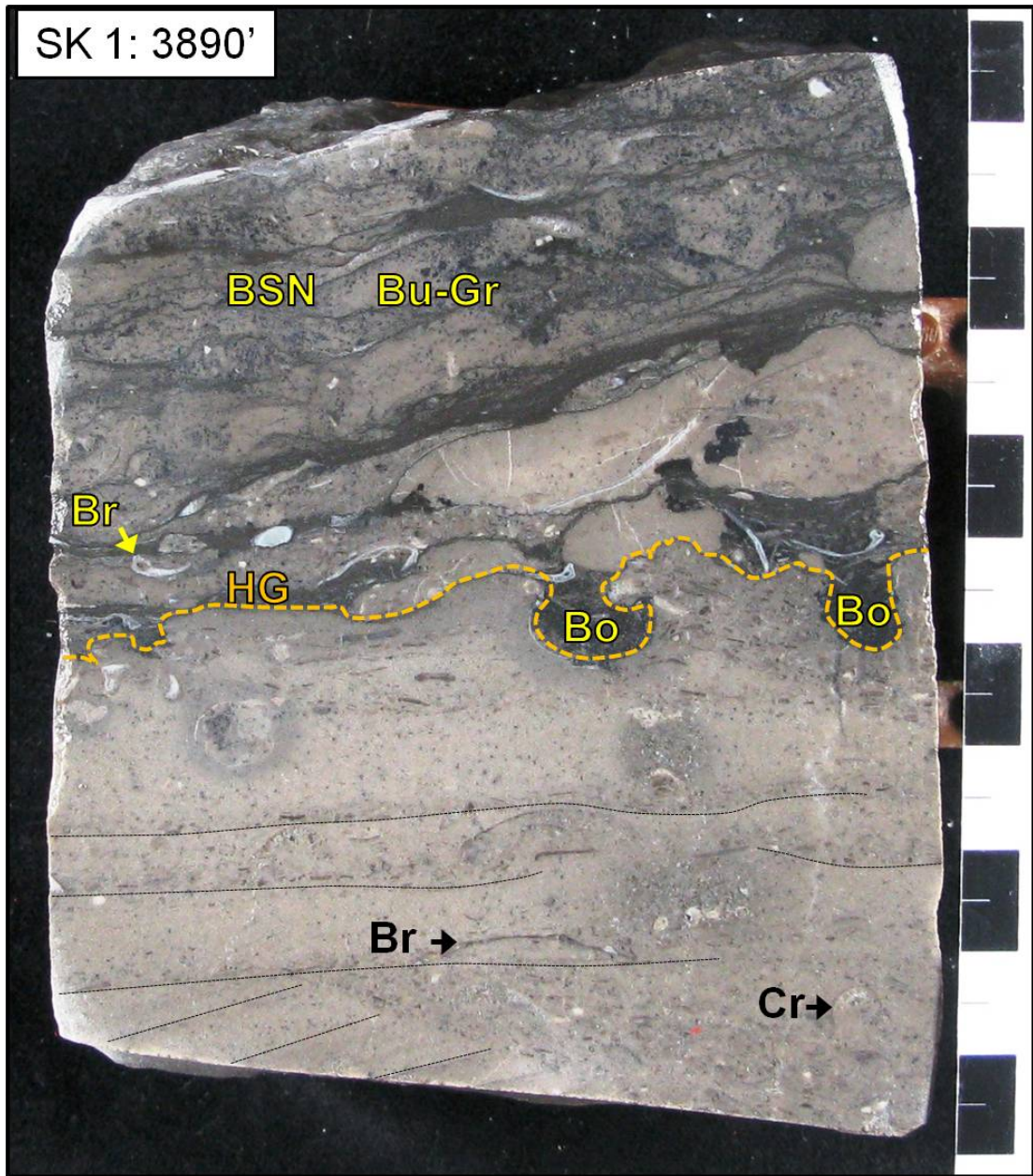
**SK 1: 3929' – F 5/3** – Peloid-crinoid wackestone-packstone with an intraclastic grainstone grain-bed. Burrow fill is dominantly grain-dominated in

burrow-bounding stylonodular fabrics. Intraclastic grainstone may represent storm or near-shoal channel deposition.



**SK 1: 3901'** – F 2 – Peloid wackestone with variable skeletal grains. **SK 1: 3891'** – F 3 – Peloid wackestone-packstone, overlain by large bryozoan fragment (>1 cm) packstone, overlain by a skeletal debris packstone. Skeletal packstone contains burrows with mud-grain mixed fill. Bioclasts are replaced by white dolomite.

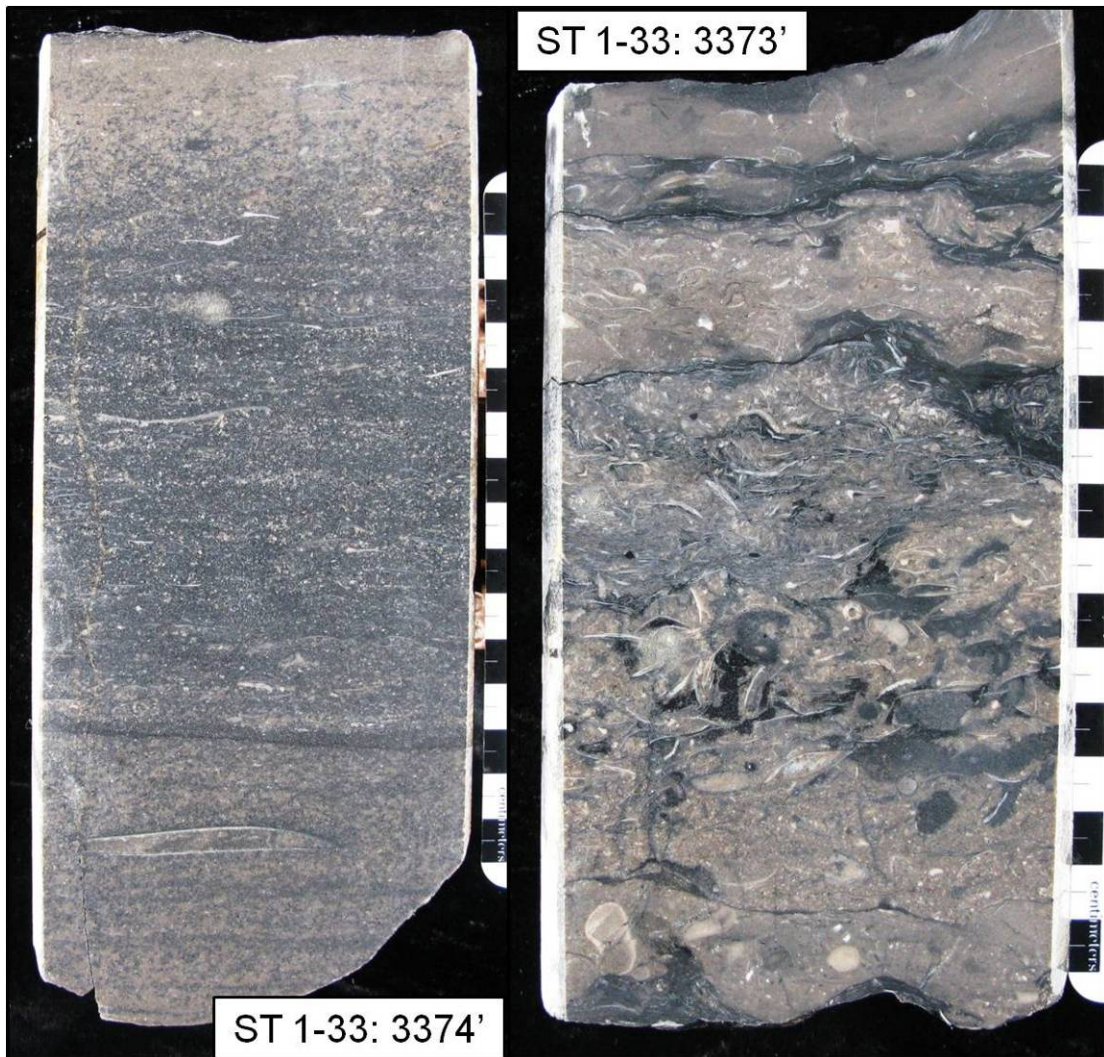




**SK 1: 3890' – F 3** –Laminate and cross-laminated peloid-skeletal fragment packstone-wackestone capped by a bored hardground (outlined with dashed orange line). Laminations lack above hardground, where burrow-bounding stylonodular fabric dominates with grain-dominant burrow fill.

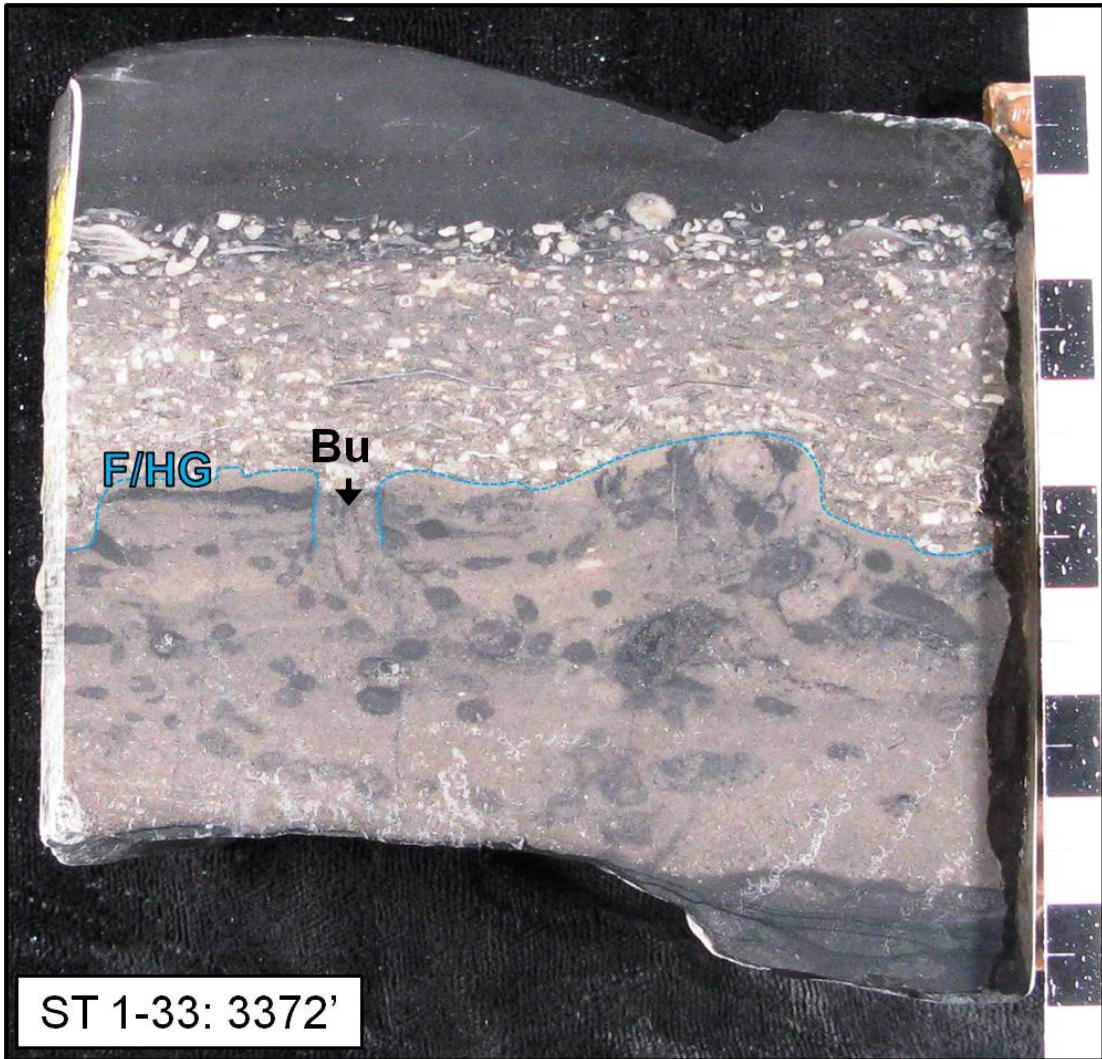
Stetler 1-33 – Marathon Oil Company

Permit #31407, Branch County, MI



**ST 1-33: 3374-3' – F 4 and 5** – Continuous core from lower left (deepest) to upper right. Laminated skeletal fragment grainstone overlain by mottled skeletal packstone-grainstone. Image on right show a mottled mixture of light (oxidized) and dark (reduced) sediments consistent with lagoon settings. This core succession shows a transition from shoal environments (left image) to lagoon settings, indicating a lateral facies shift.





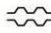




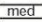




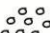













































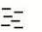









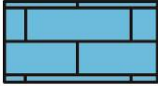






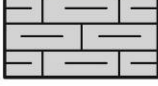
ST 1-33: 3372' – F 5 – Peloid wackestone-packstone capped by a burrowed/bored firm/hardground (outlined with dashed blue line), overlain by a skeletal packstone, overlain by a dark gray/black mudstone.

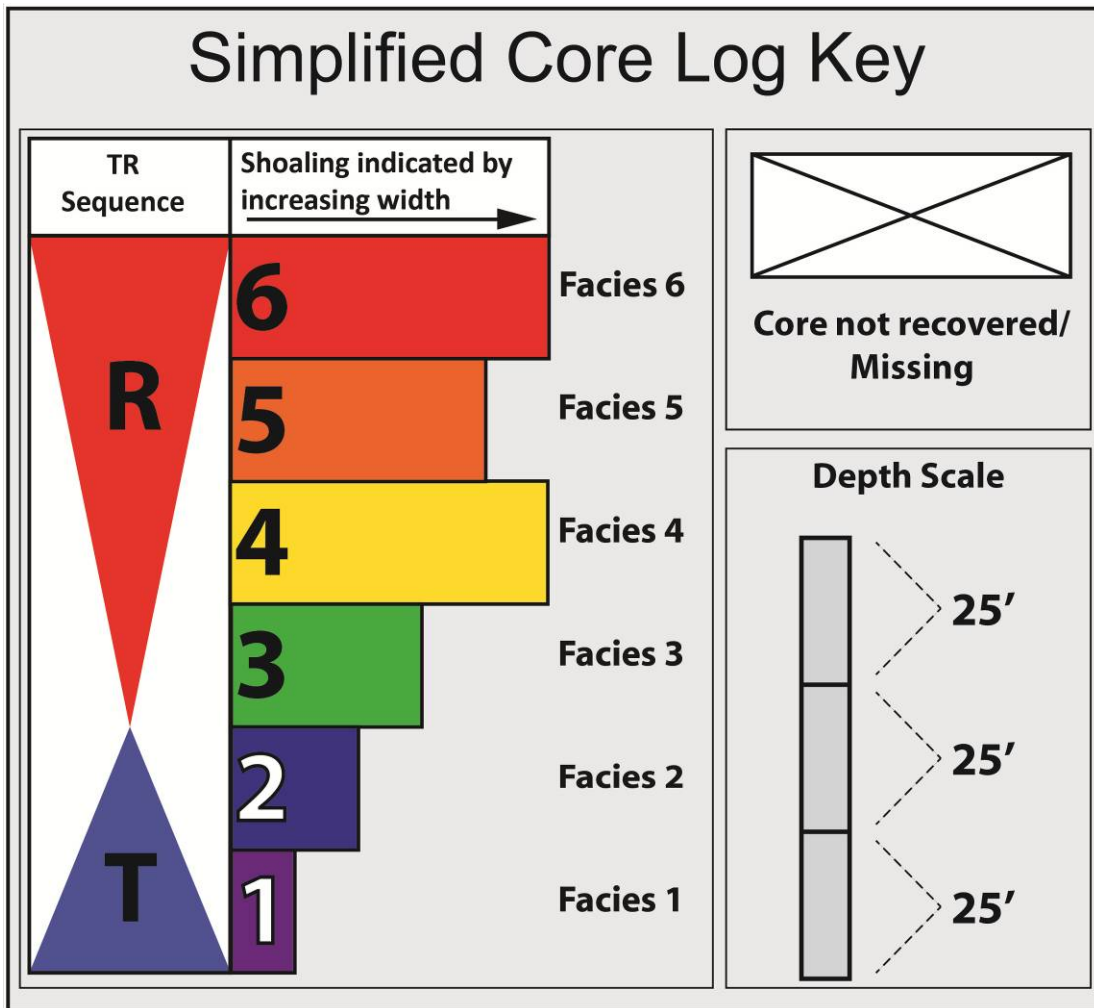


APPENDIX C – Core Log-Graphical Core Description

## Appendix Keys and Introduction

<b>Legend: Grains, Sedimentary Structures, Features and Diagenetic Features</b>					
	Oncolites/Pisolite		Laminated		Fenestral Textures
	Oolites		Thin Bedded		Keystone Vugs
	Coated Grain		Medium Bedded		Brecciated
	Peloids		Wavy Laminated		Layered Internal Sed.
	Pellet		Stromatolitic Algal Laminated		Dolomite Cement
	Intraclast		Cross Bedded		Anhydrite Cement
	Stromatoporoid		Flat Bedded		Cemented
	Trilobite		Inclined Bedded		Partially Filled Vug
	Green Algae		Contorted Bedded		Cemented Vug
	Red Algae		Fining Upward		Open Fracture
	Phylloid Algae		Coarsening Upward		Fracture Swarm
	Brachiopod		Bored Surface		Partially Filled Fracture
	Gastropod		Exposure Surface		Cement Filled Fracture
	Undifferentiated Fossils		Mud Cracked		Anhydrite Filled Fracture
	Coral		Burrowed		Reddish Karst Fill
	Bryozoan		Burrows w/ Alteration Halos		Geopetal Texture
	Echinoderm		Wispy Stylolite		Brecciated Zone
	Molluscs, undifferentiated		Stylolitic		Stylonodular
	Crinoids		Stylolite Swarms		Stylomottled
	Erosional Surface		Argillaceous		Major Boundary (Sequence / Facies)
	Scoured Surface		Anhydritic/Gypsiferous		Minor Boundary (Erosional Surface)
	Hardground		Silicious Nodule		
	Pyritic				

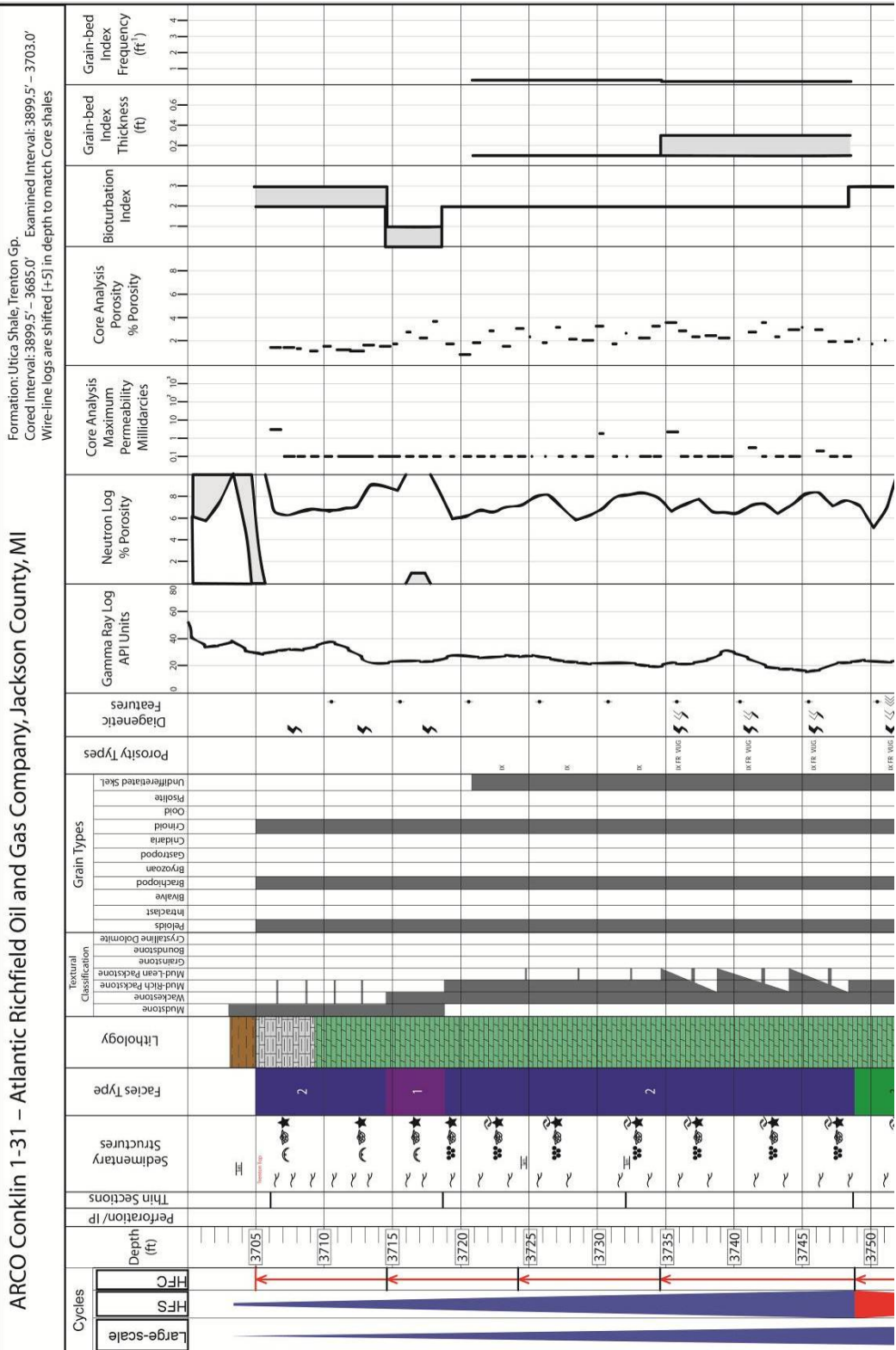
Legend: Pore Types		Legend: Lithology	
IX	Intercrystalline		Limestone
IP	Interparticle		Cherty Limestone
FE	Fenestral		Argillaceous, Dolomitic Limestone
FR	Fracture		Dolomitic Limestone
MO	Moldic		Dolomite
VUG	Vug		Argillaceous Dolomite
WX	Intracrystalline		Shale
WP	Intraparticle		Calcareous Shale



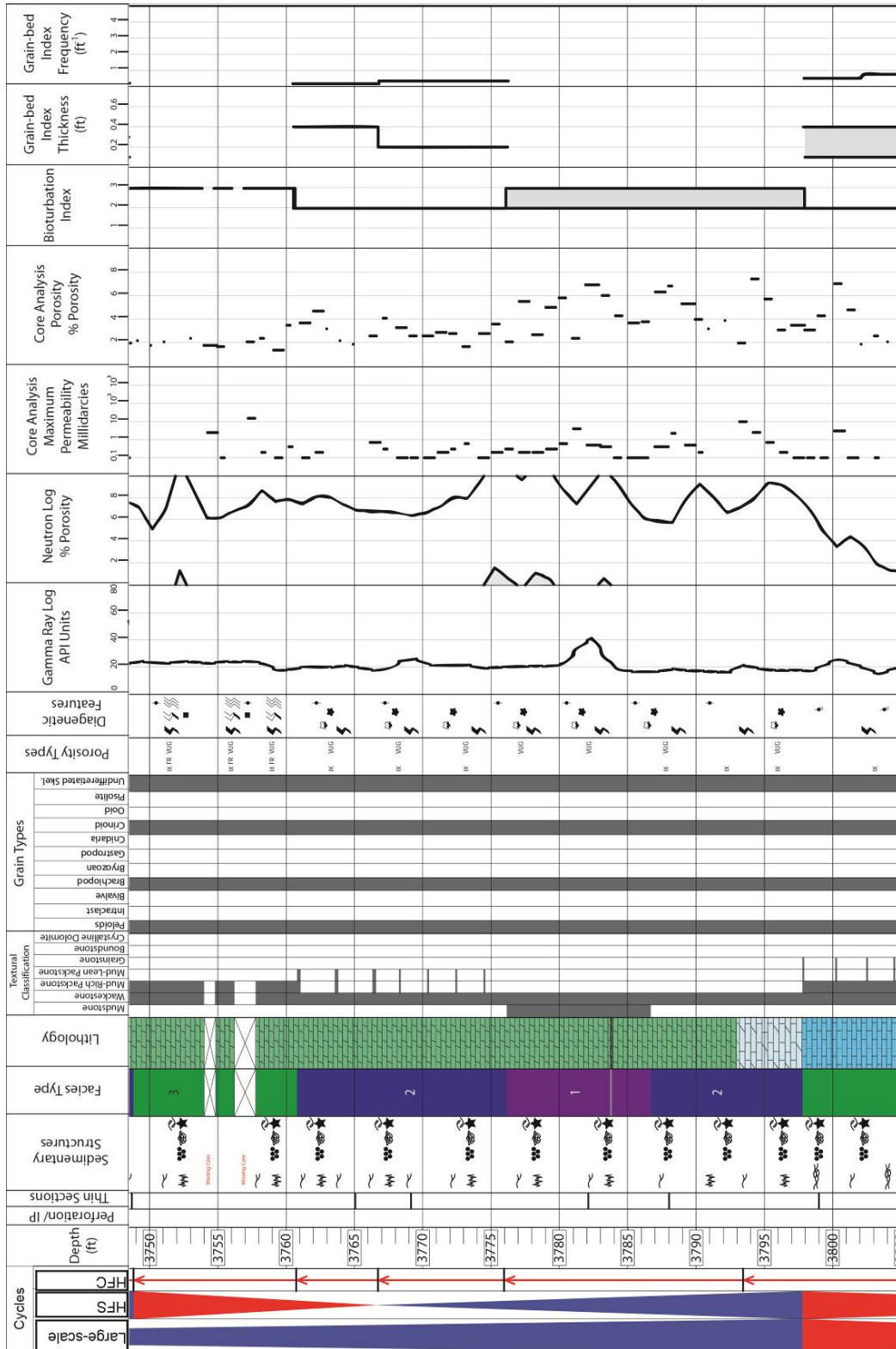
Simplified facies logs are included for each core with the format as shown above. These logs show large-scale (left) and HFS (right) T (blue) and R (red) trends indicated by triangles, as in main text. Facies are coded by color and indicate interpreted relative water depth (shoaling indicated by width) with shallower water shown with larger box.

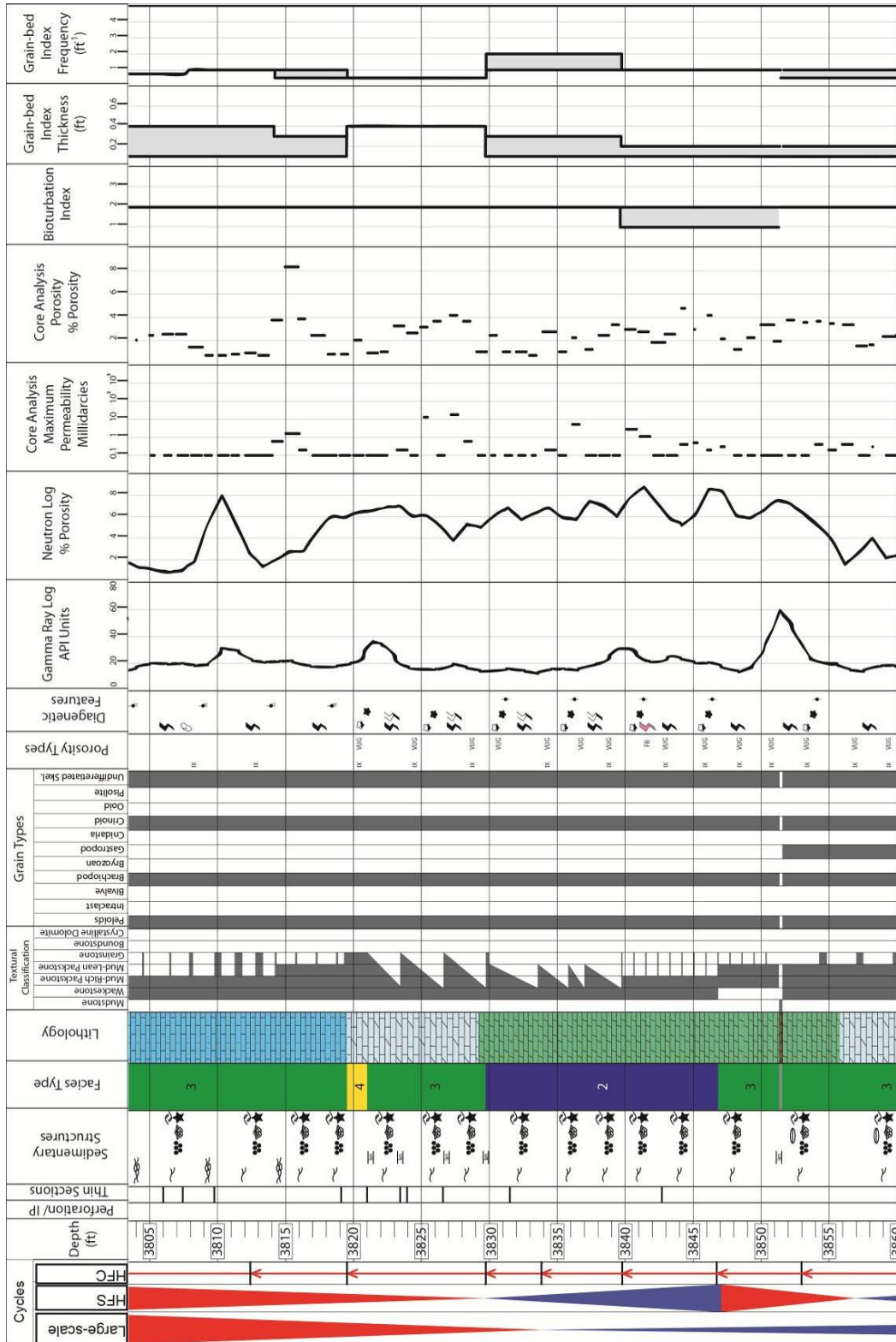
ARCO Conklin 1-31 – Atlantic Richfield Oil and Gas Company

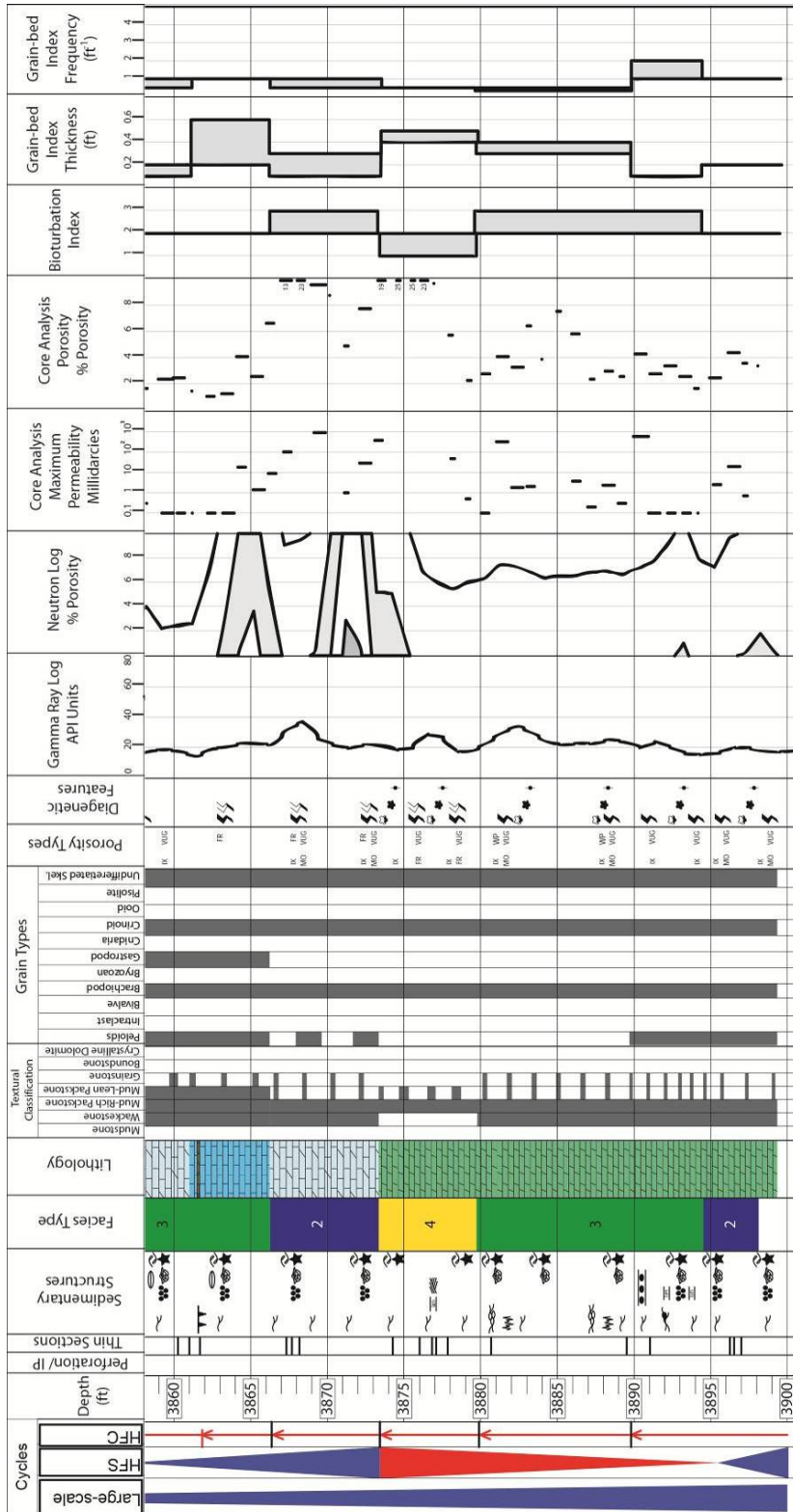
Permit #37385, Jackson County, MI



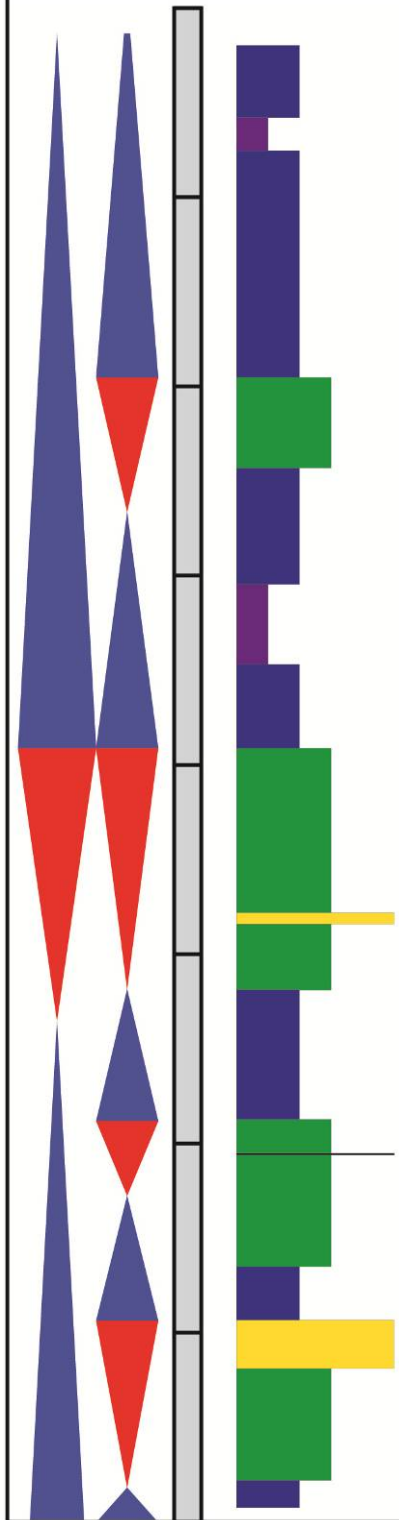






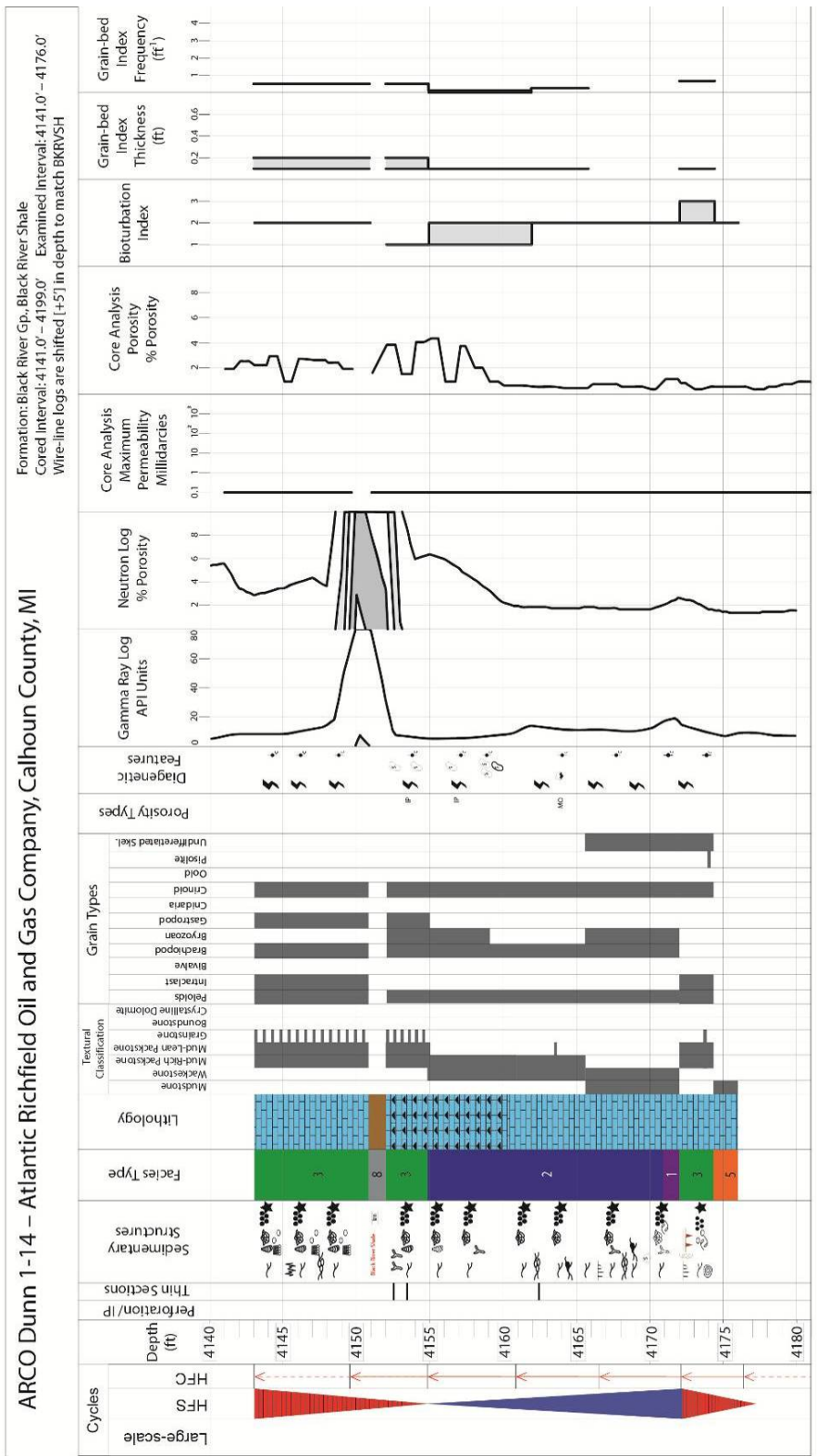


# AC 1-31



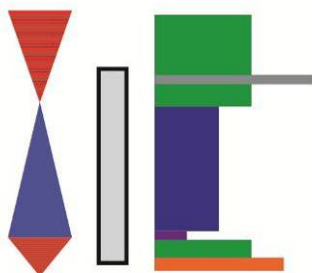
ARCO Dunn 1-14 – Atlantic Richfield Oil and Gas Company

Permit #37239, Calhoun County, MI





AD 1-14

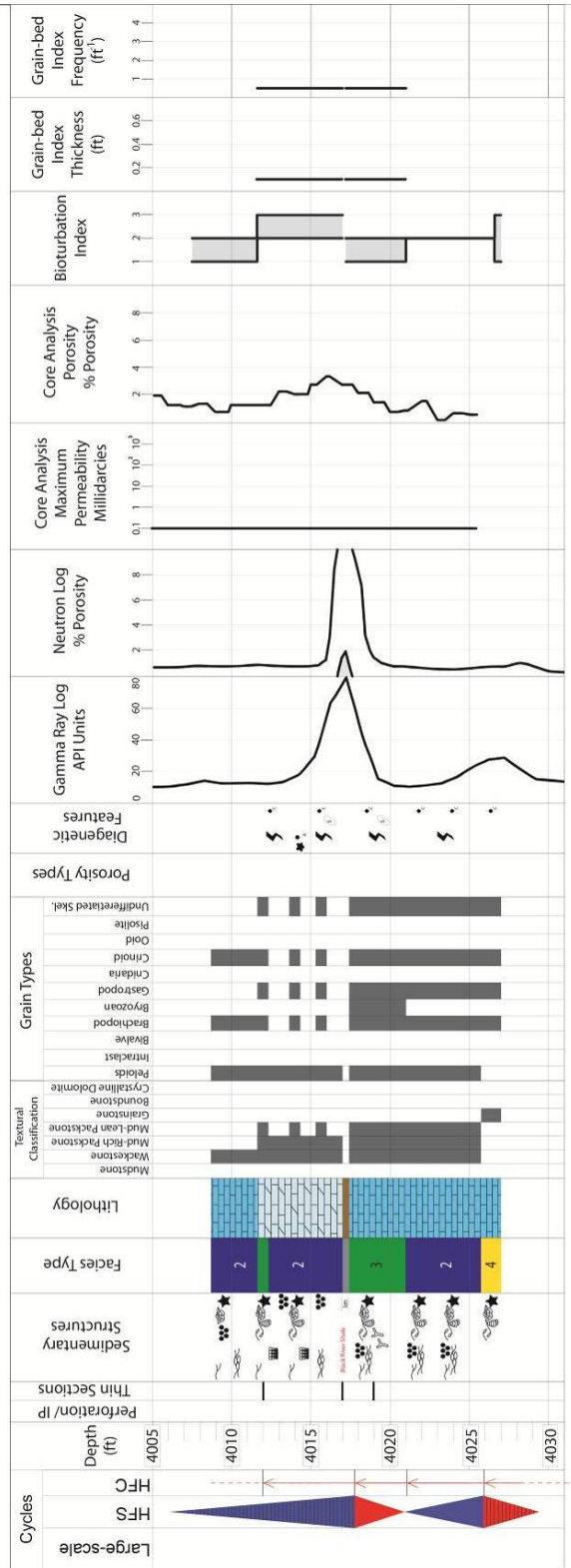


ARCO Gardner 1-16 – Atlantic Richfield Oil and Gas Company

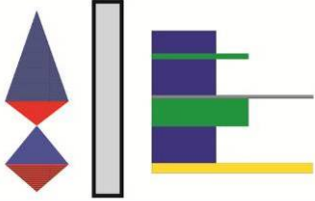
Permit #37838, Hillsdale County, MI

ARCO Gardner 1-16 – Atlantic Richfield Oil and Gas Company, Hillsdale County, MI

Formation: Black River Gp., Black River Shale  
 Cored Interval: 4027.0' – 3971.0' Examined Interval: 4008.6' – 4027.0'  
 Wire-line logs are shifted [+2'] in depth to match BKRVS5H

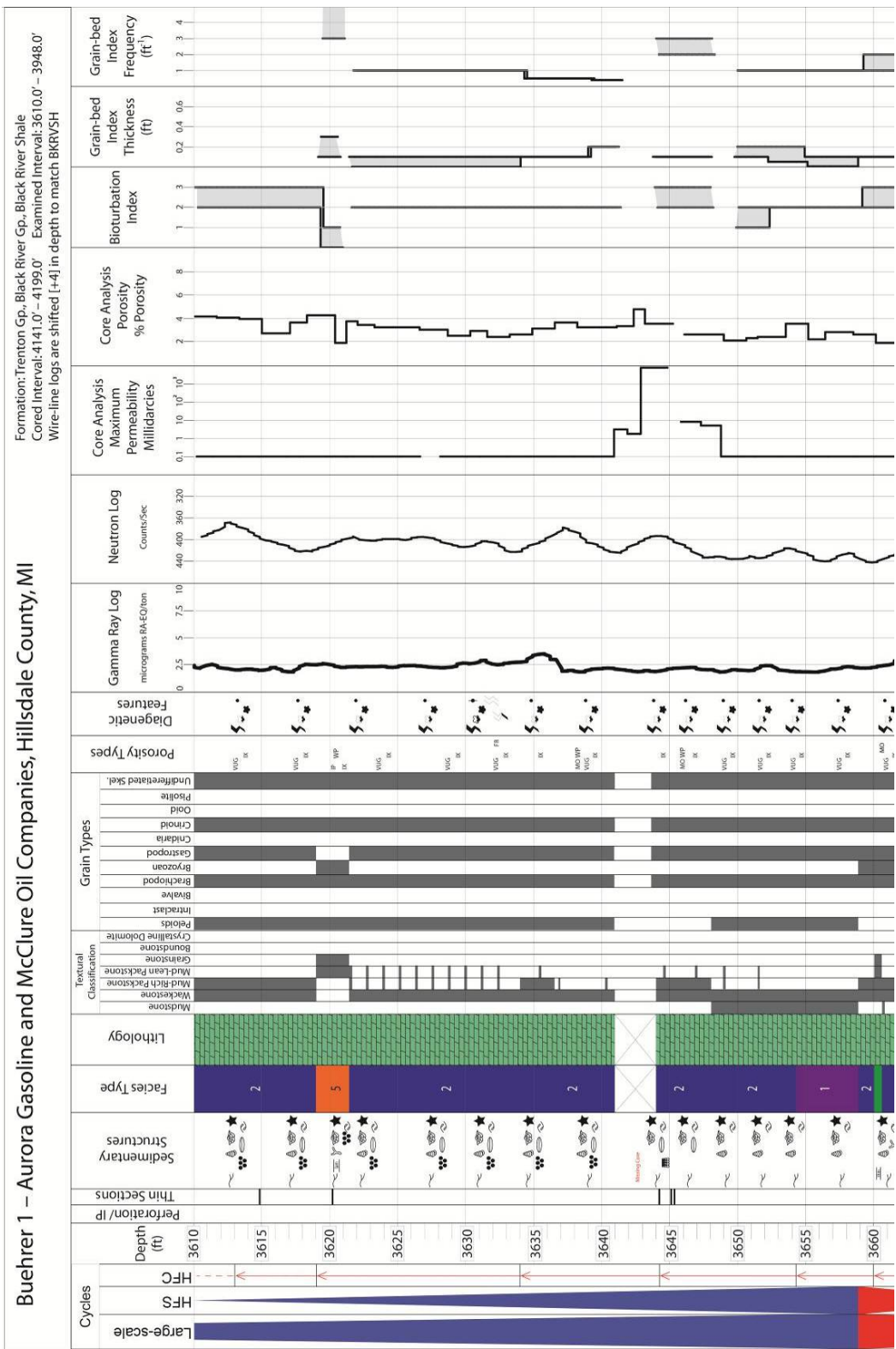


AG 1-16

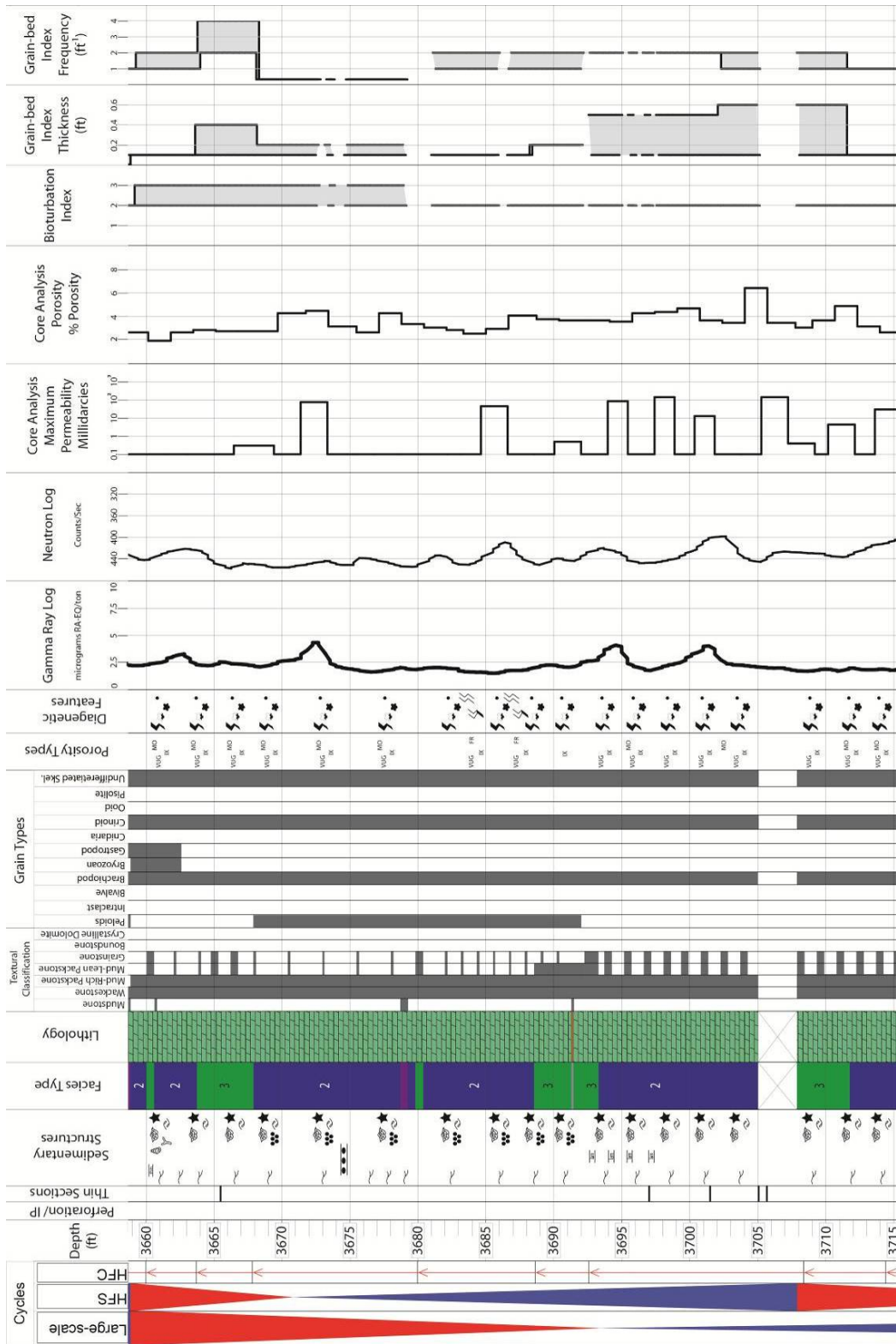


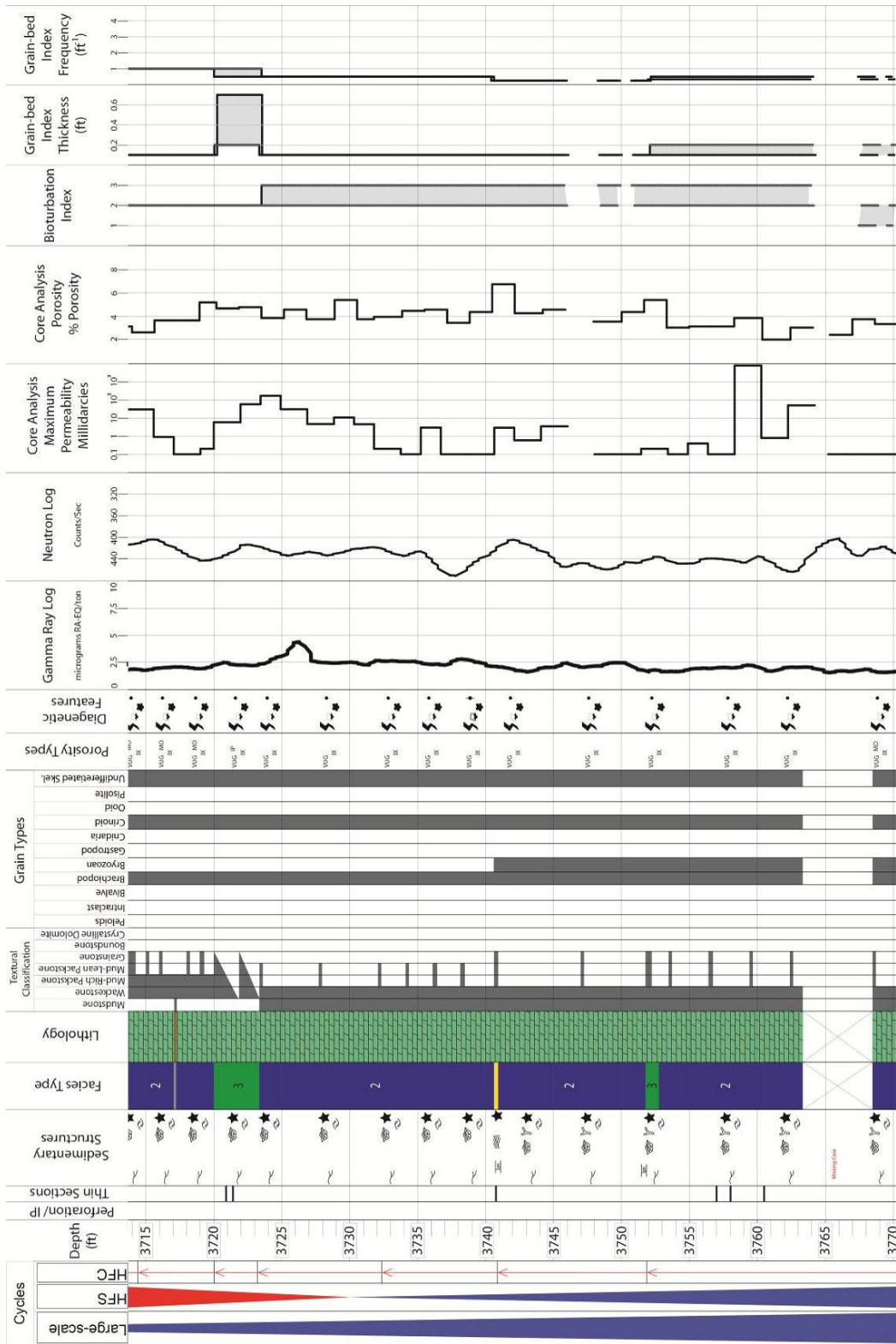
Buehrer 1 – Aurora Gasoline Company and McClure Oil Company

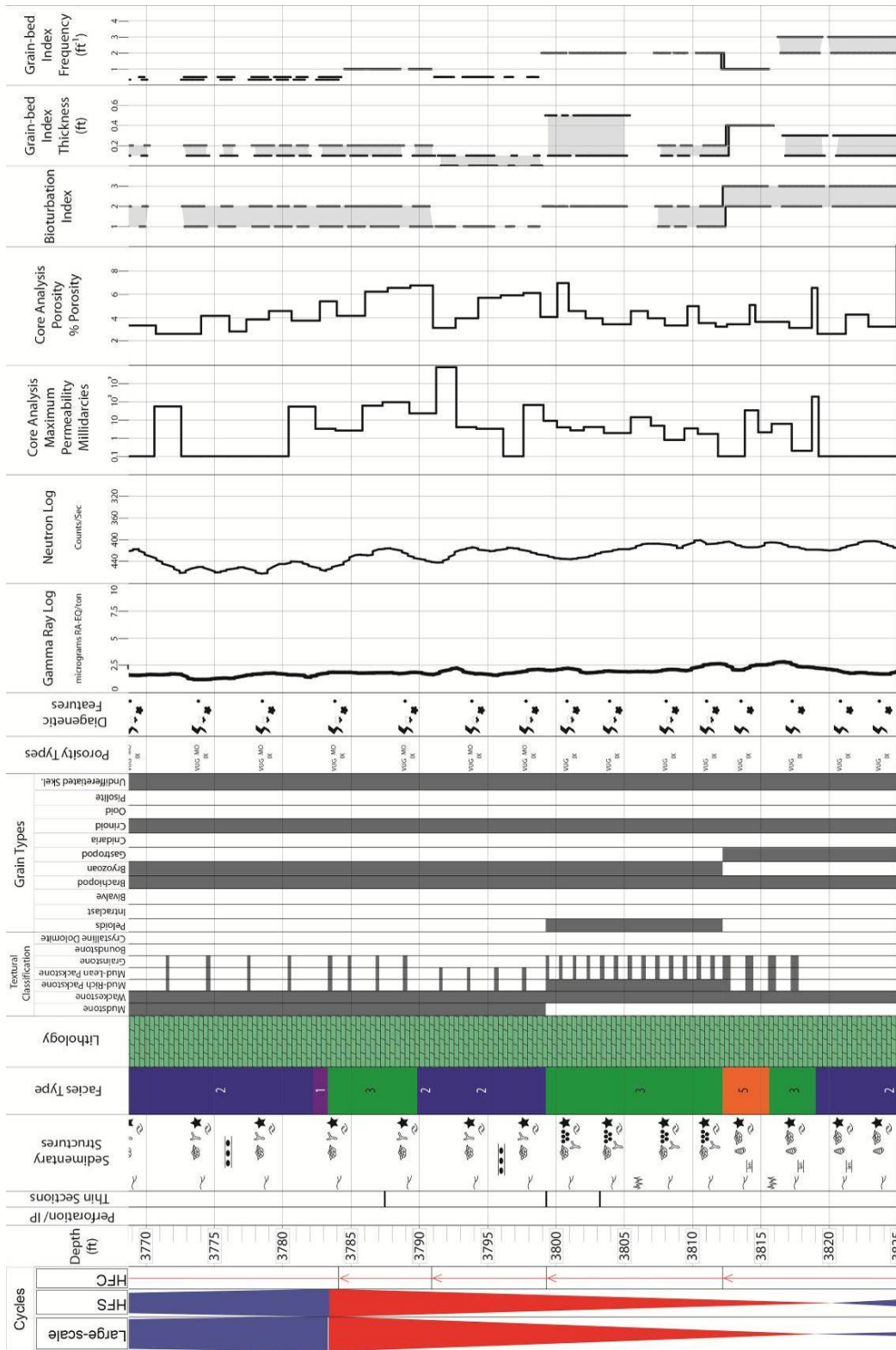
Permit #21064, Hillsdale County, MI

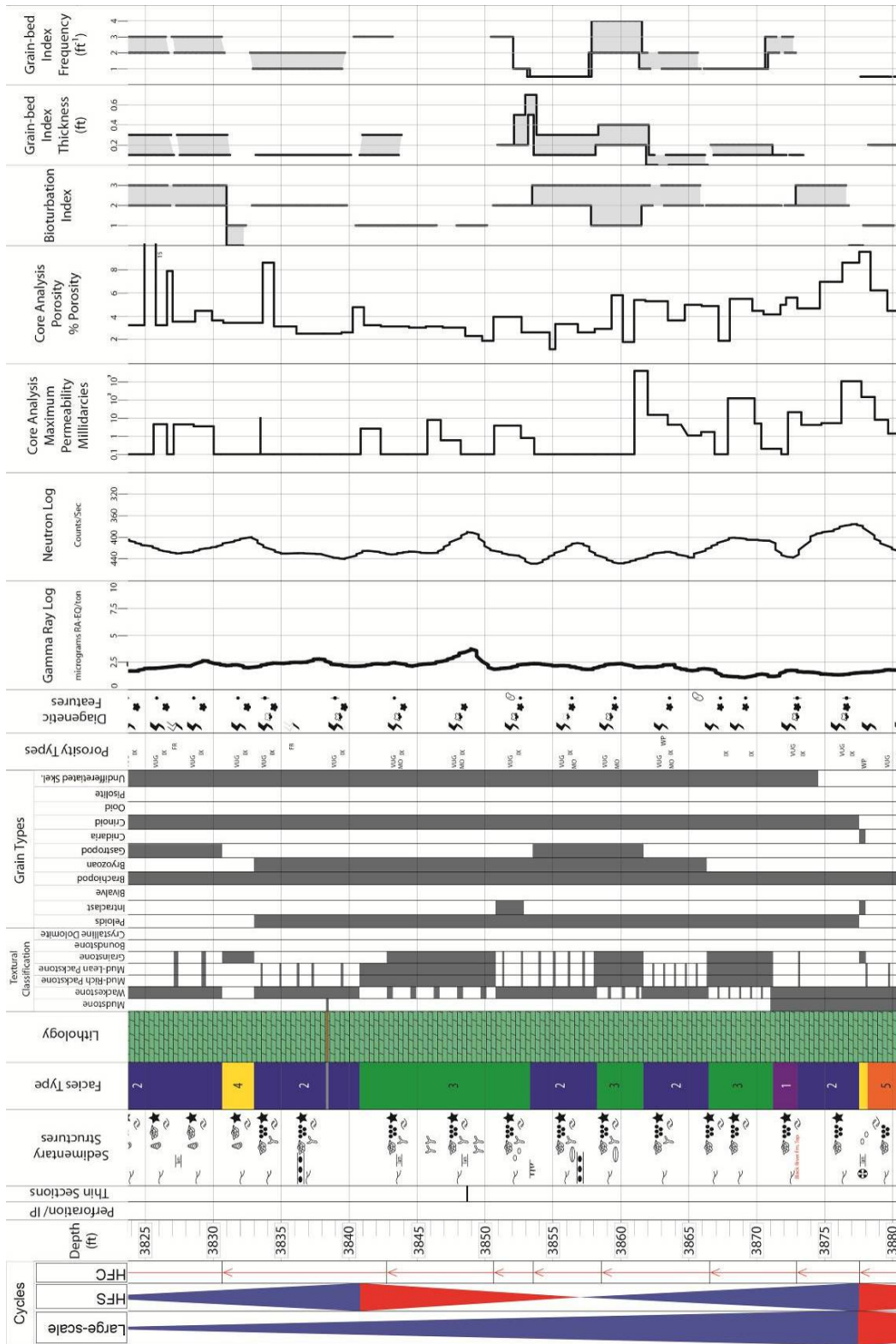


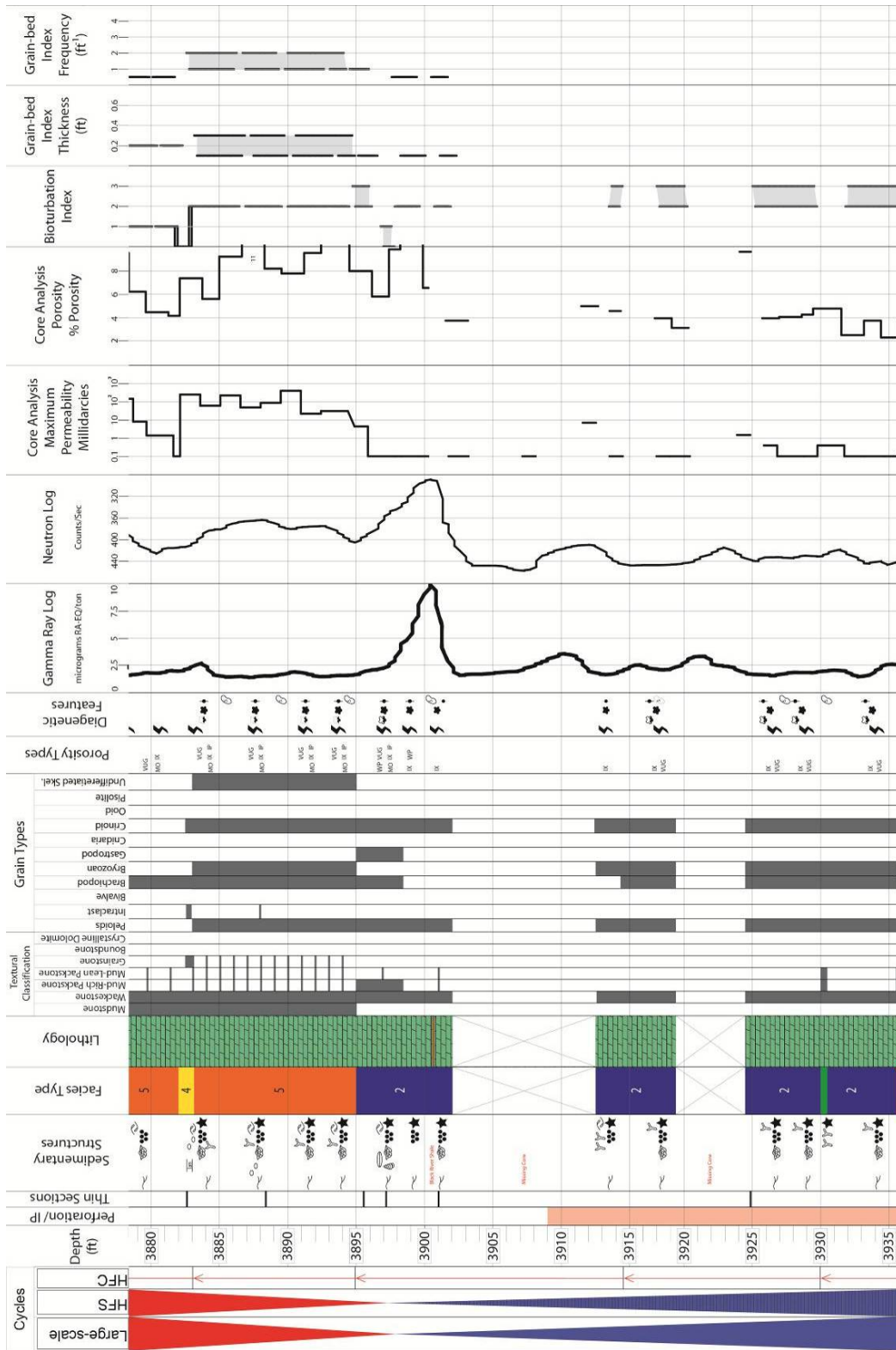




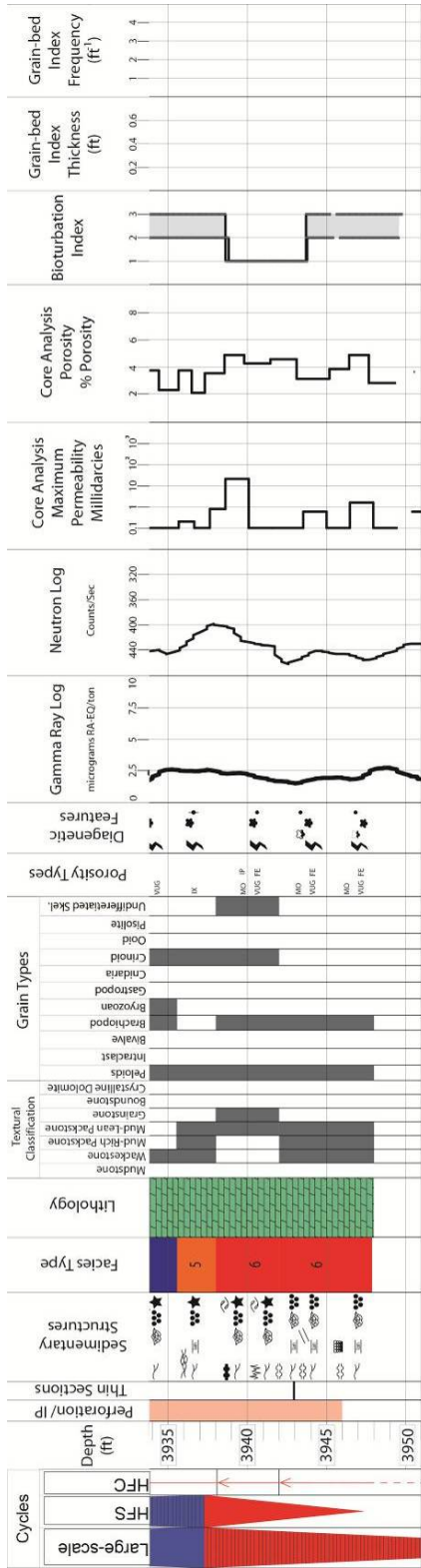




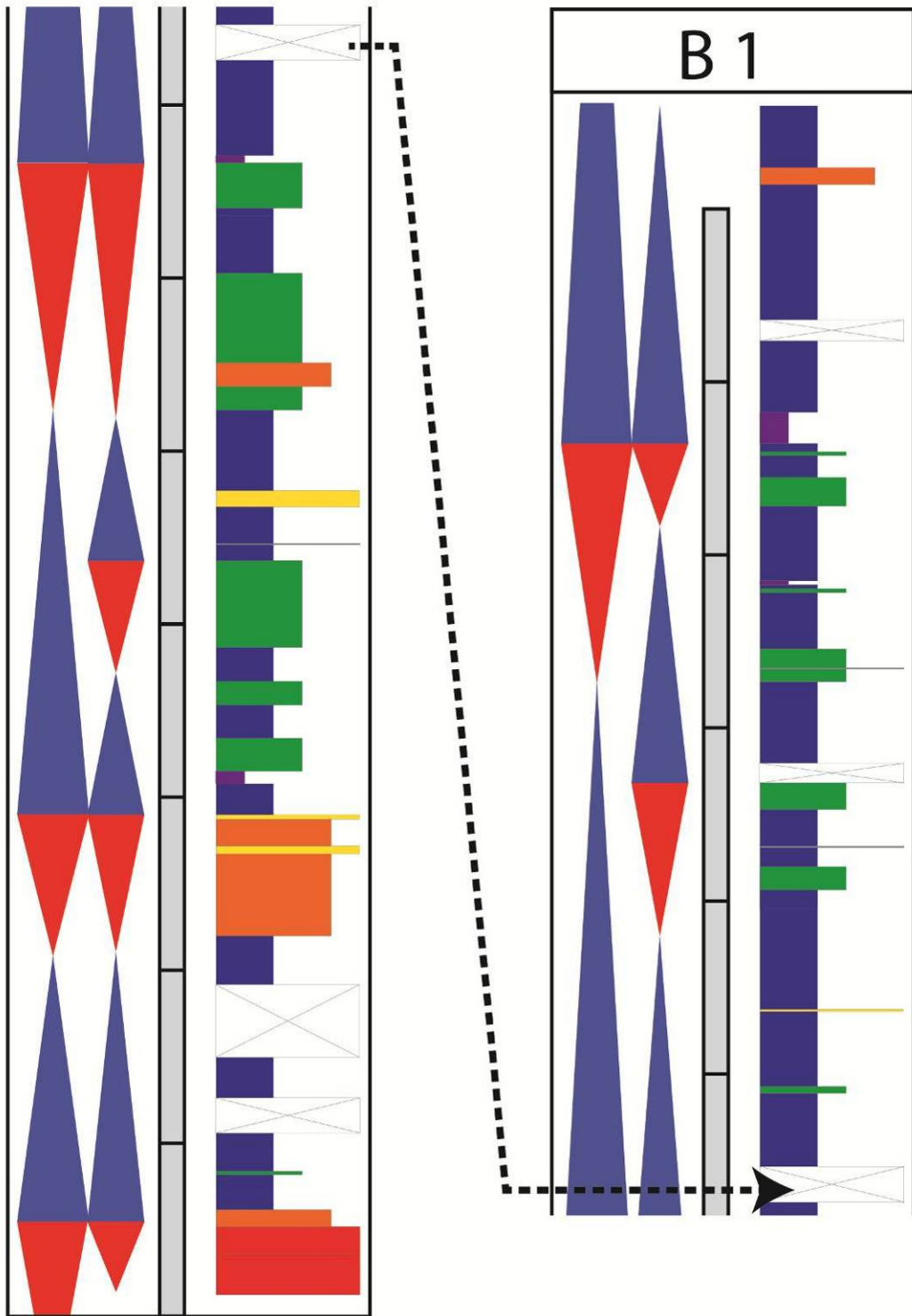










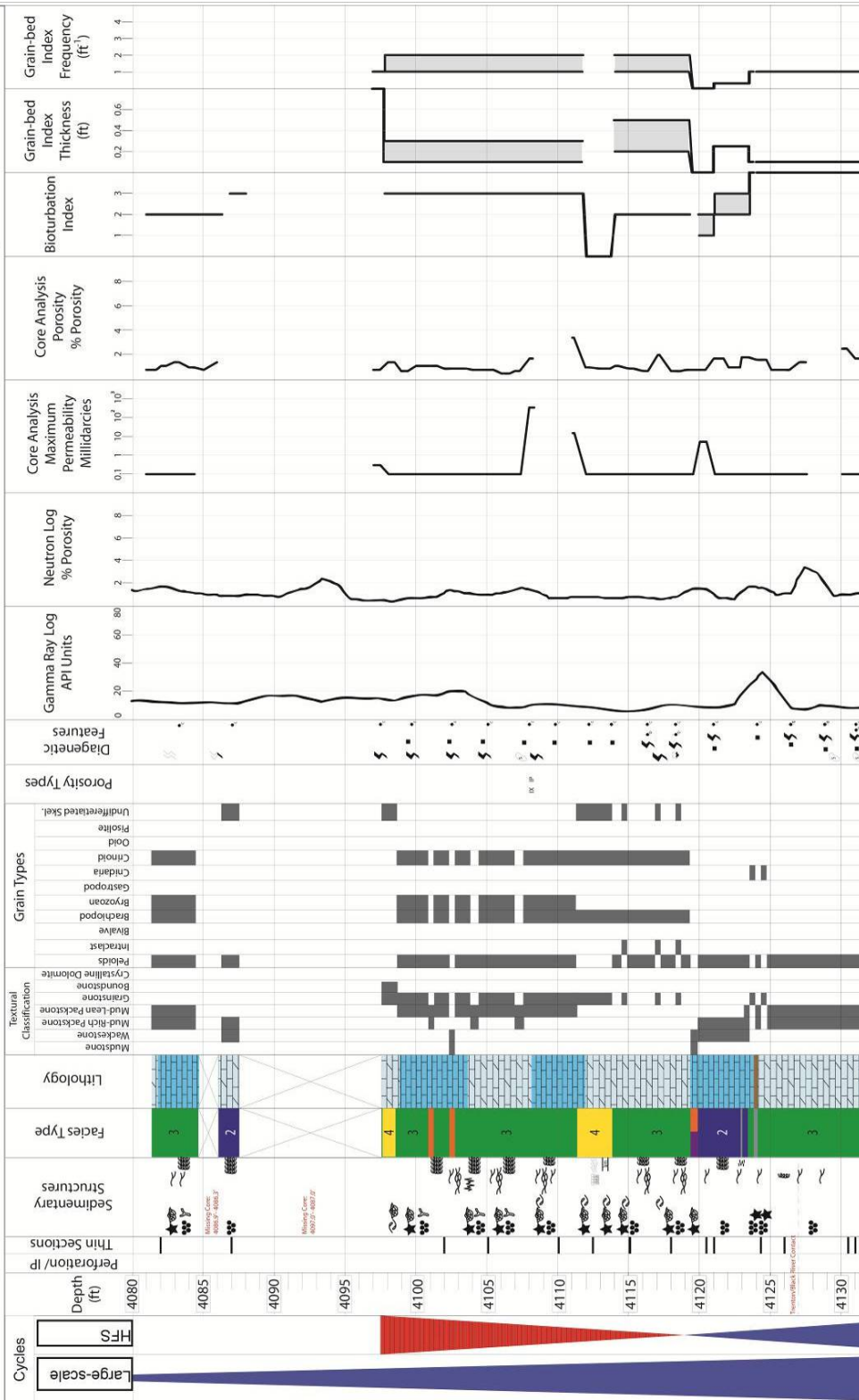


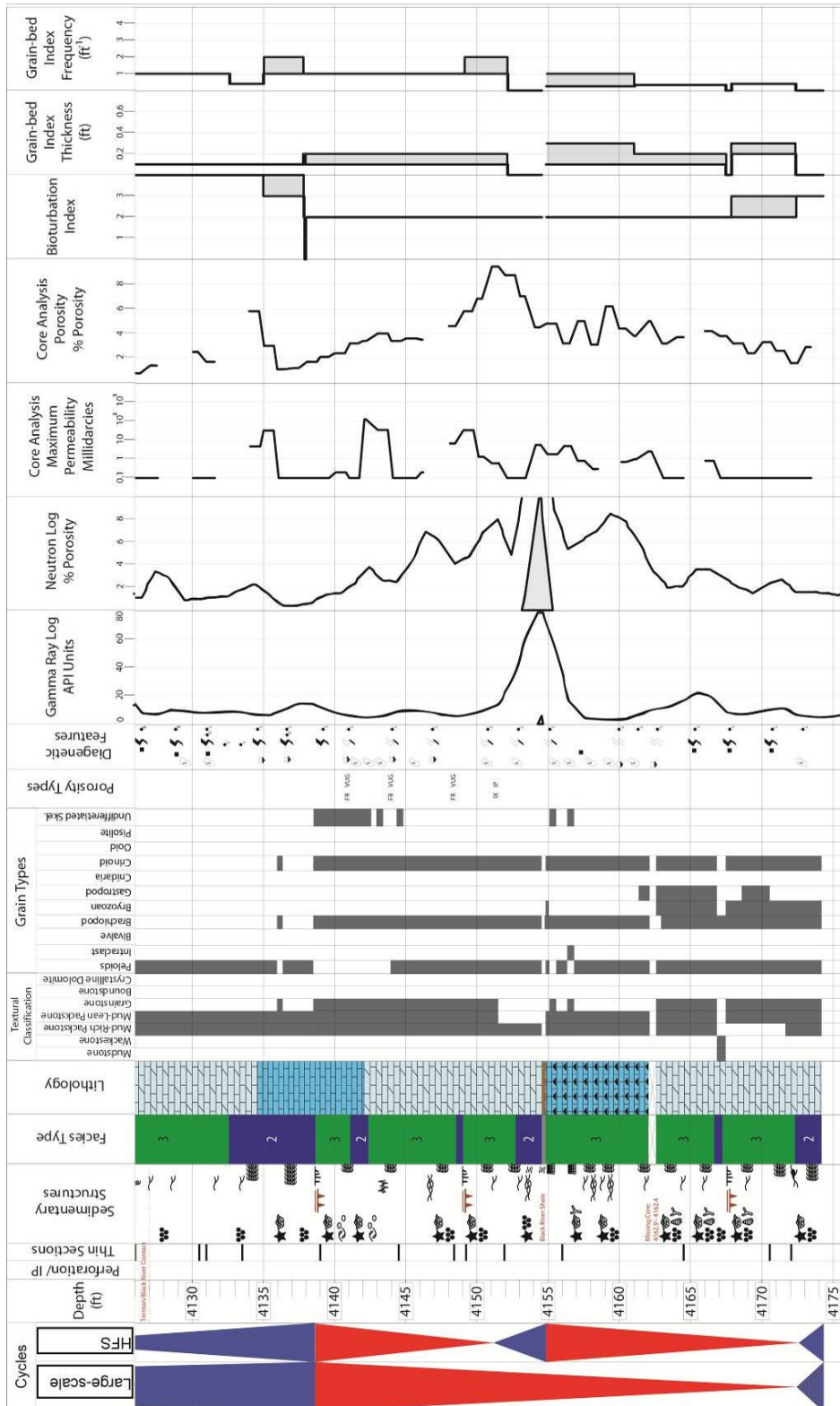
Casler 5-30 – Whiting Oil and Gas Company

Permit #36587, Jackson County, MI

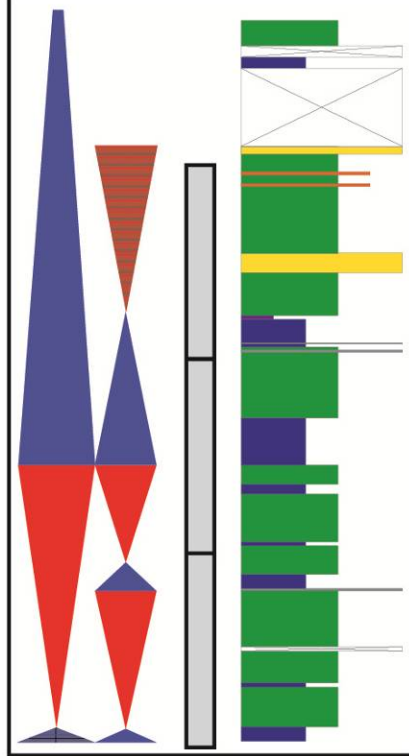
# Casler 5-30 – Whiting Oil and Gas Company, Jackson County, MI

Formation: Black River Gp., Black River Shale, Trenton Gp.  
 Cored Interval: 4081.0' – 4191.0' Examined Interval: 4081.0' – 4174.2'  
 Wire-line logs are shifted [-4'] in depth to match BKRVSJH





# C 5-30



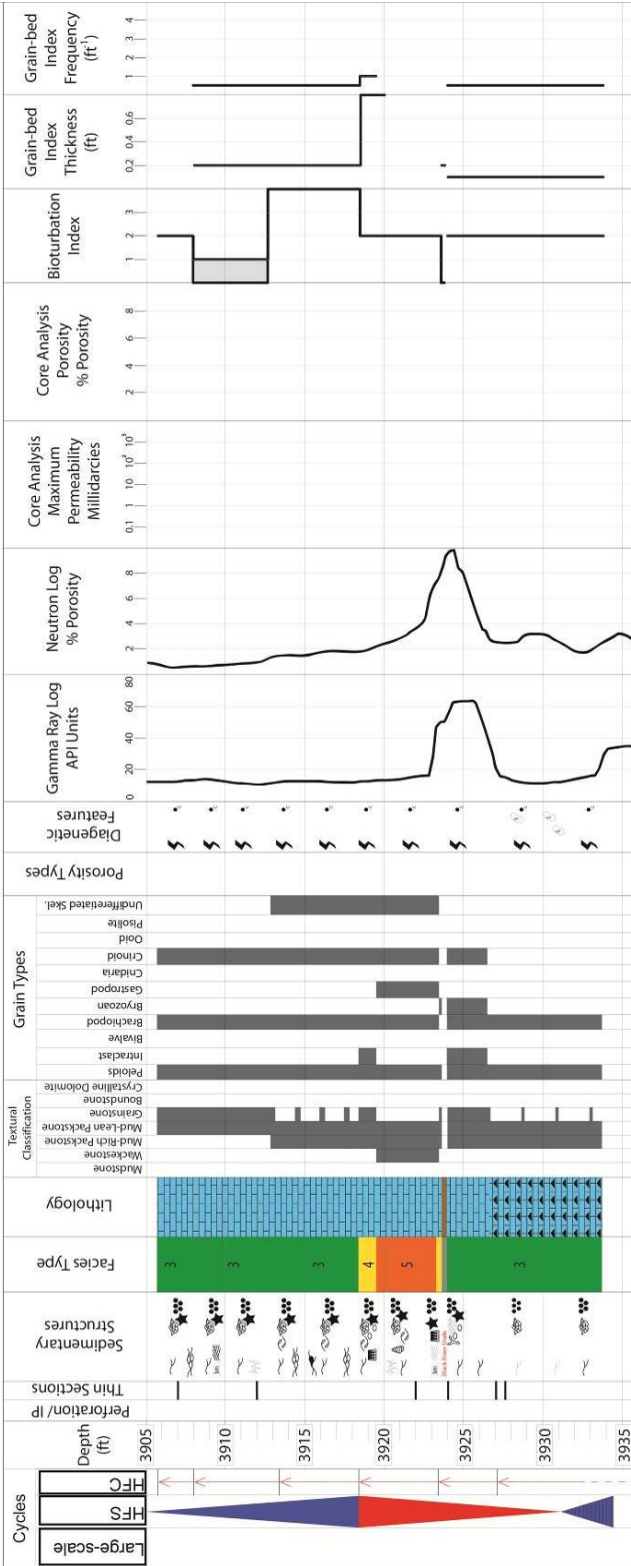
Hergert 2 – McClure Oil Company

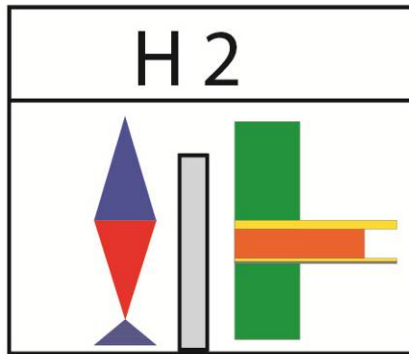
Permit #22196, Hillsdale County, MI



Hergert 2 – McClure Oil Company, Hillsdale County, MI

Formation: Black River Gp., Black River Shale  
 Cored Interval: 3892.0 – 4063.5' Examined Interval: 3933.8' – 3905.8'  
 Wire-line logs are shifted [-6'] in depth to match BKRVSJH

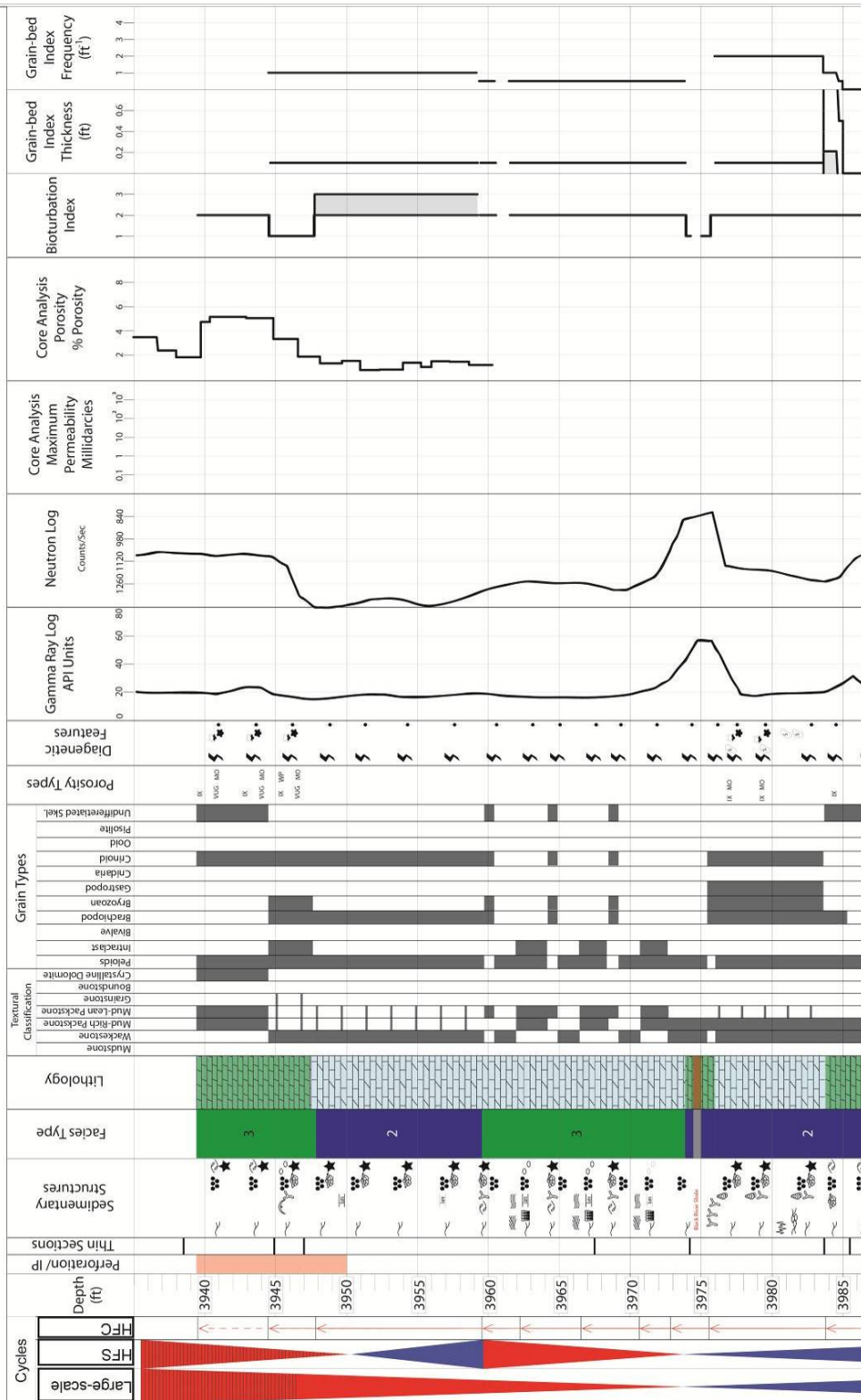


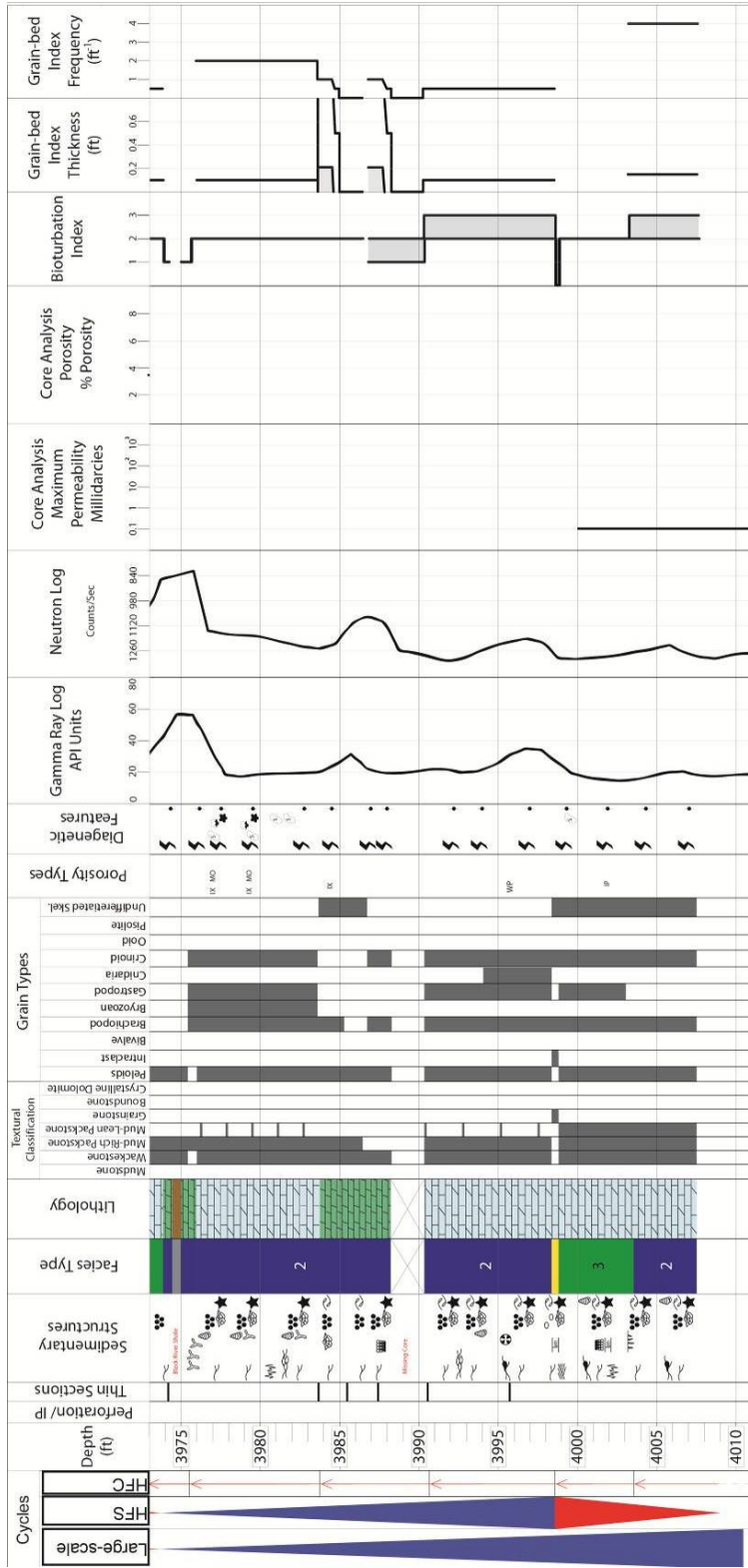


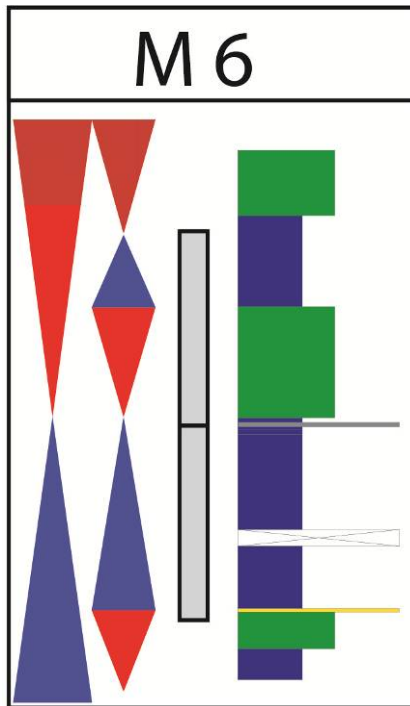
Mann, H 6 – Ohio Oil Company  
Permit #22381, Hillsdale County, MI

Formation: Trenton Gp., Black River Gp., Black River Shale  
 Cored Interval: 3935' - 40847.0' Examined Interval: 3935.0' - 4007.6'  
 Wire-line logs are shifted [-3'] in depth to match BKRVSJH

Mann, H 6 - Ohio Oil Company, Hillsdale County, MI







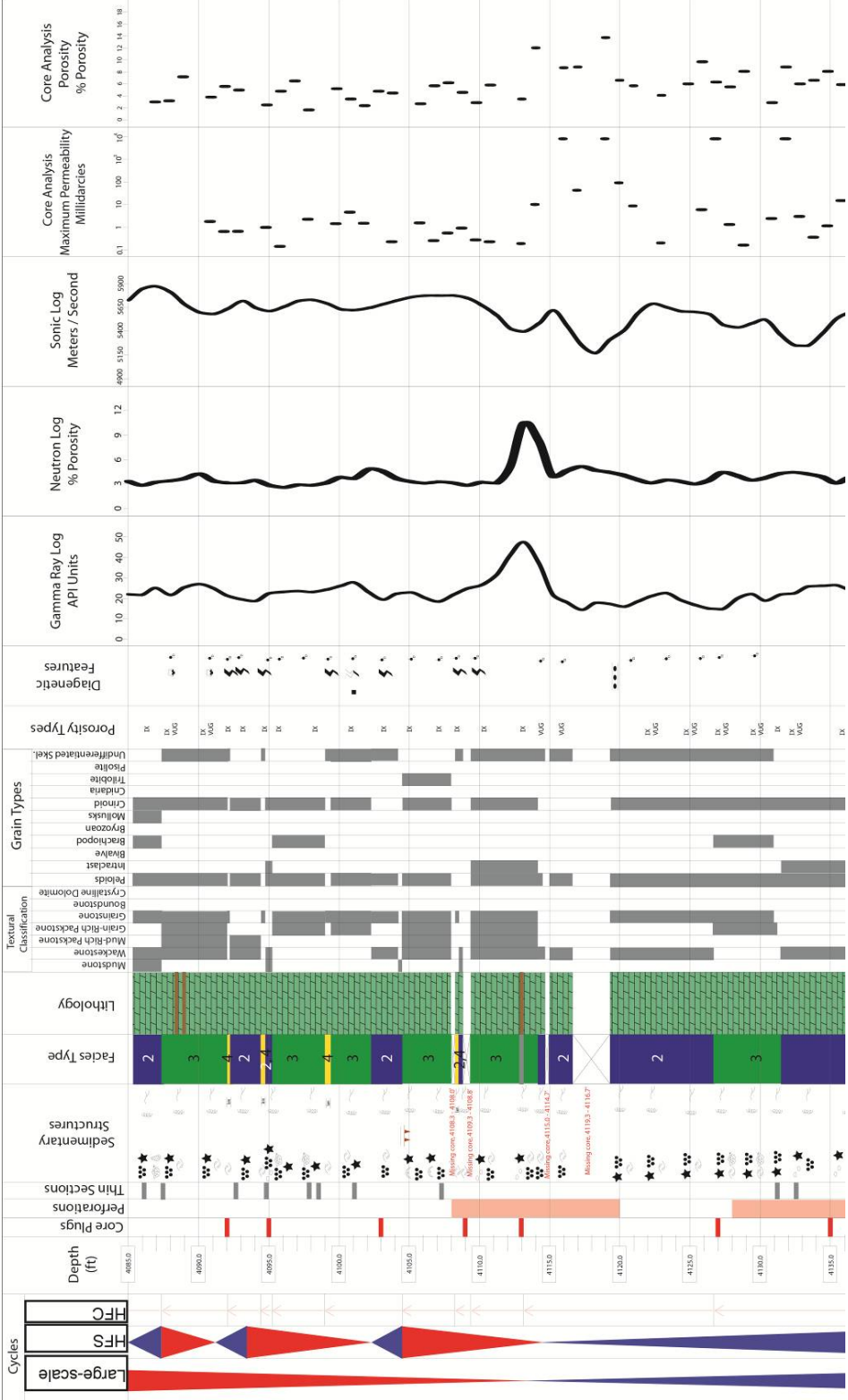


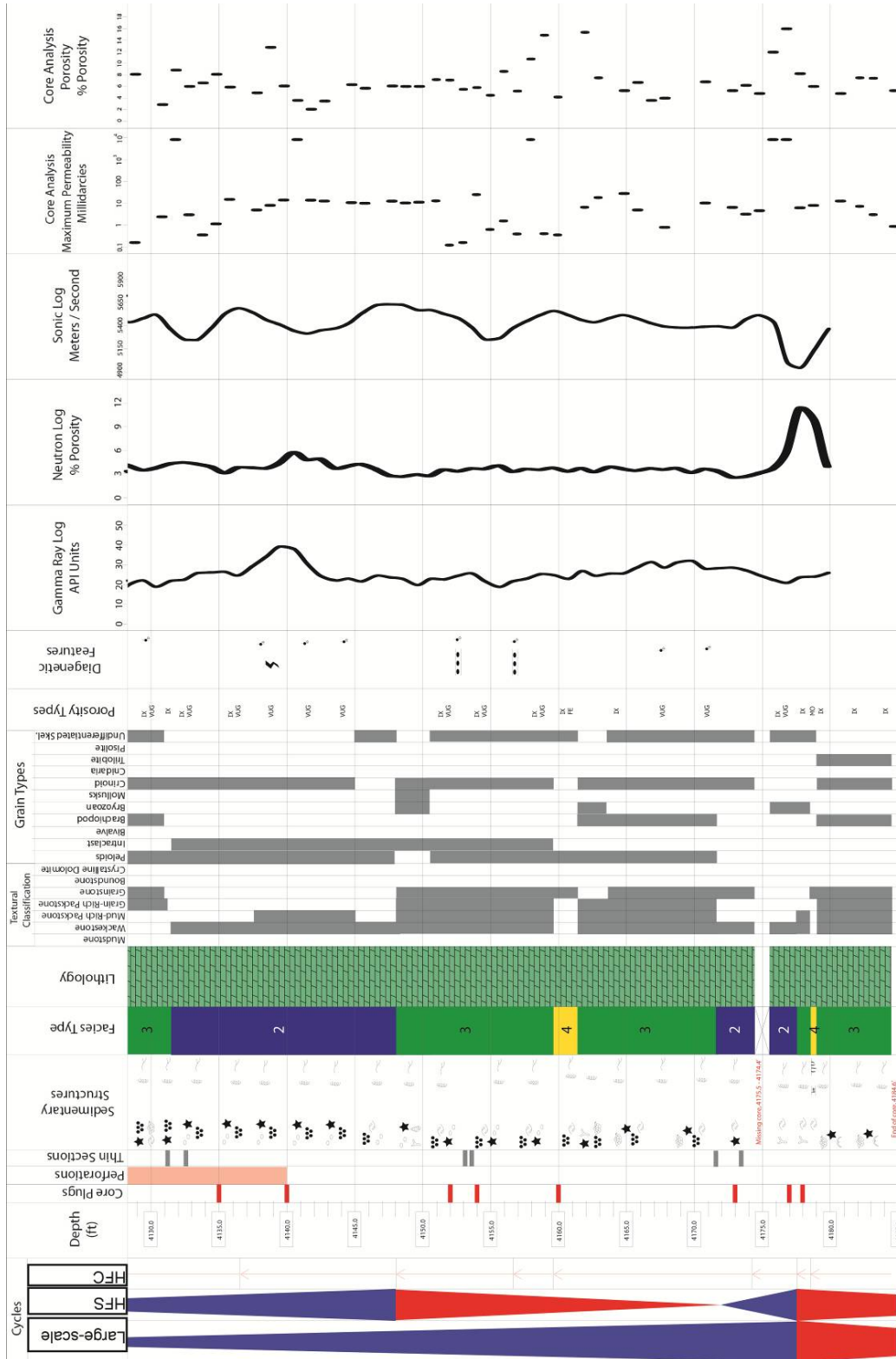
Martin et al. 2-A – Marathon Oil Company

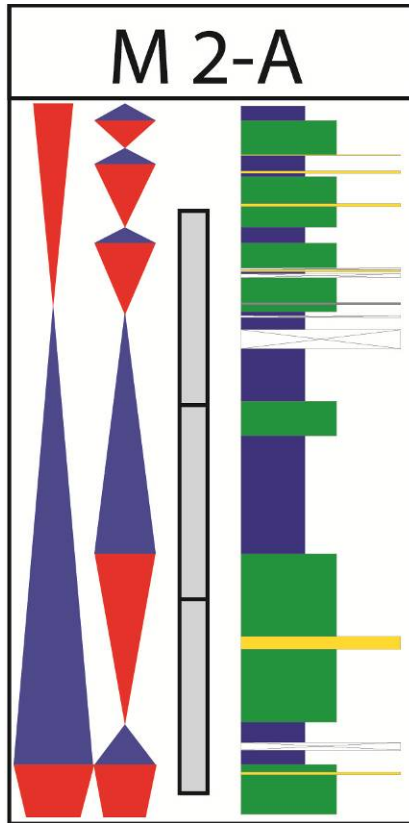
Permit #22083, Calhoun County

# Martin 2-A – Marathon Oil Company, Calhoun County, MI

Formation: Trenton Gp.  
 Cored Interval: 4184.6' – 4085.2'  
 Examined Interval: 4184.6' – 4085.2'  
 Wire-line logs are shifted [+0] in depth to match Core shales

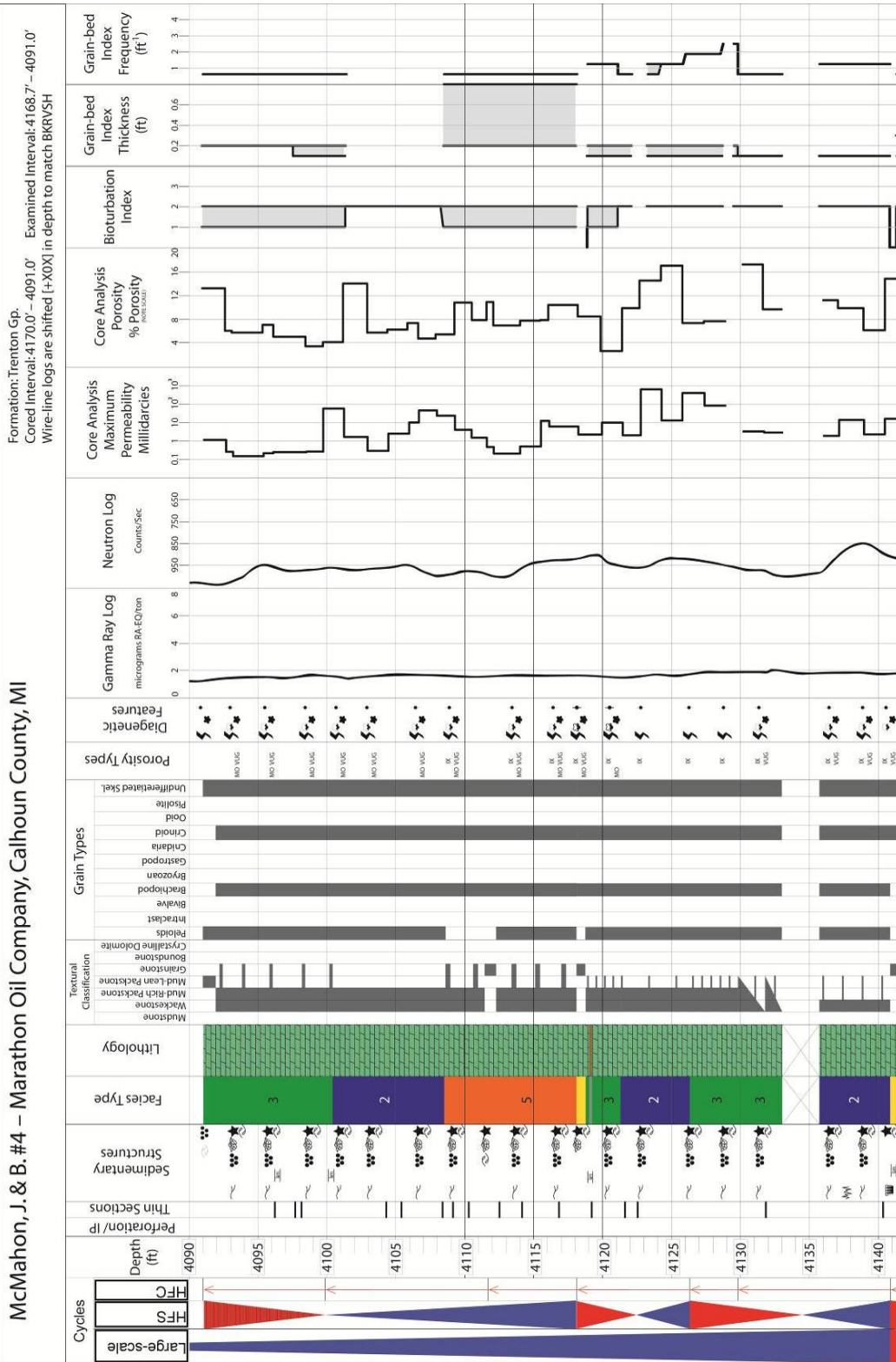




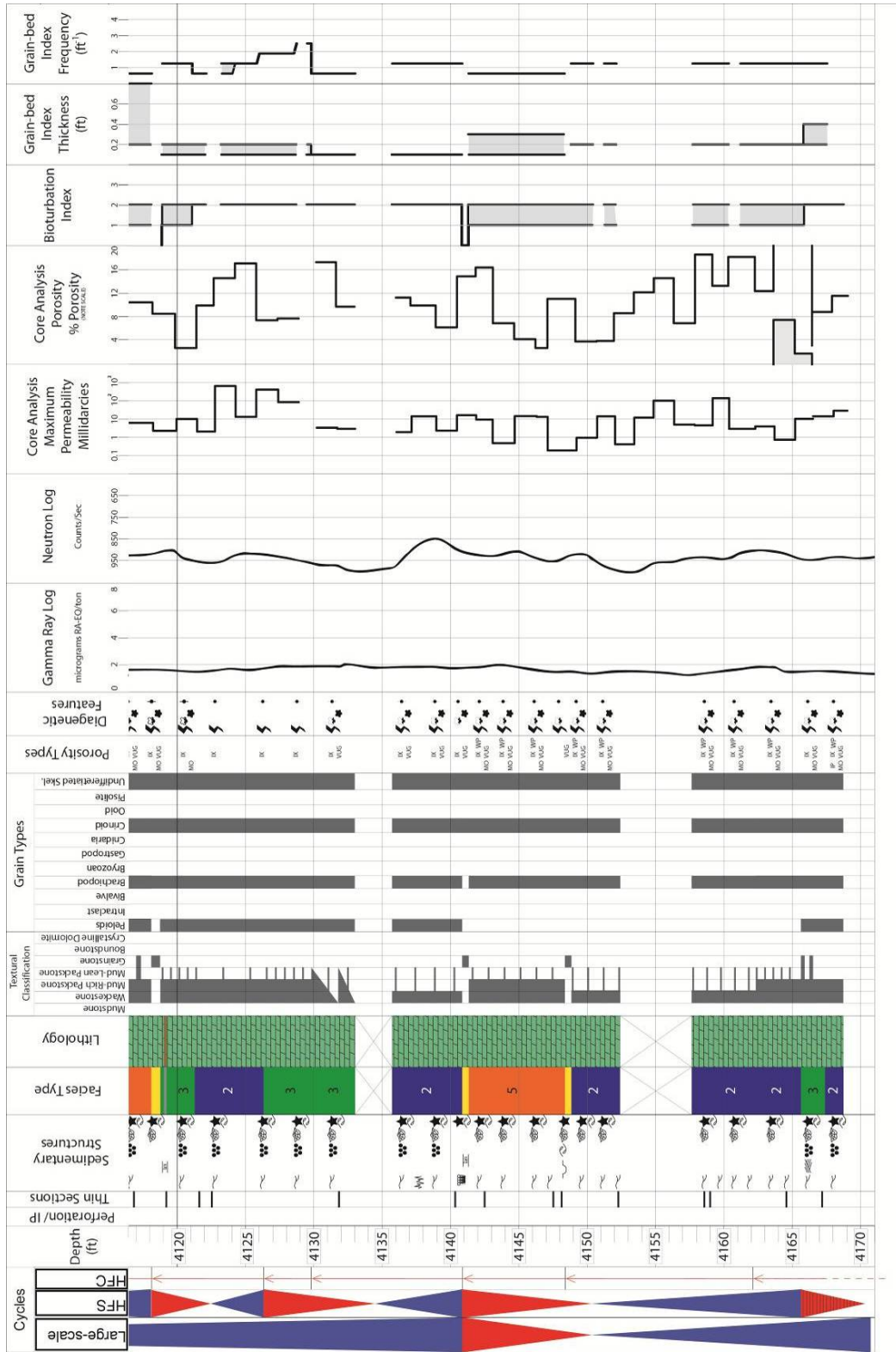


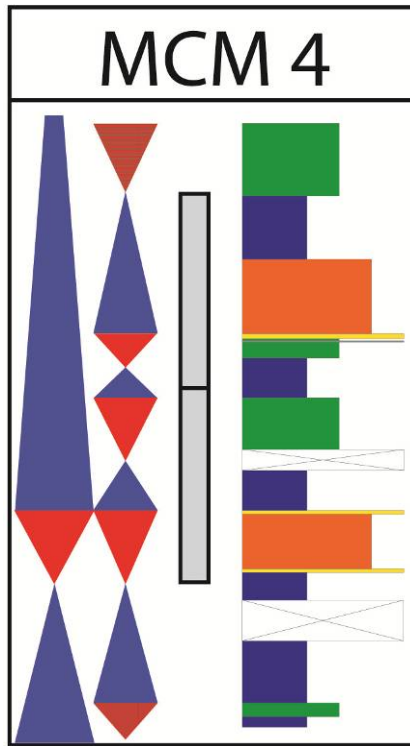
McMahon, J. & B. #4 – Marathon Oil Company

Permit #22460, Calhoun County, MI



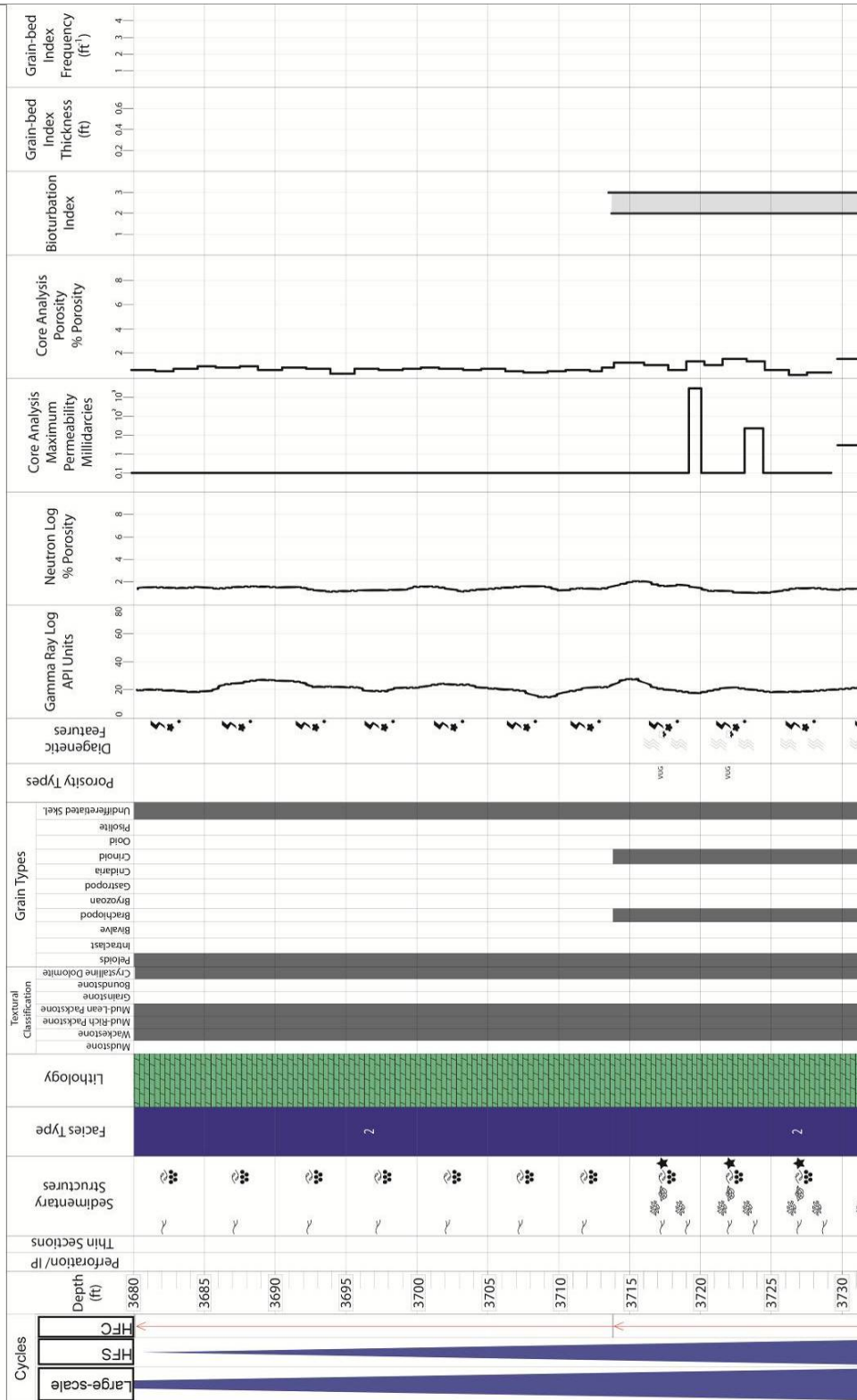


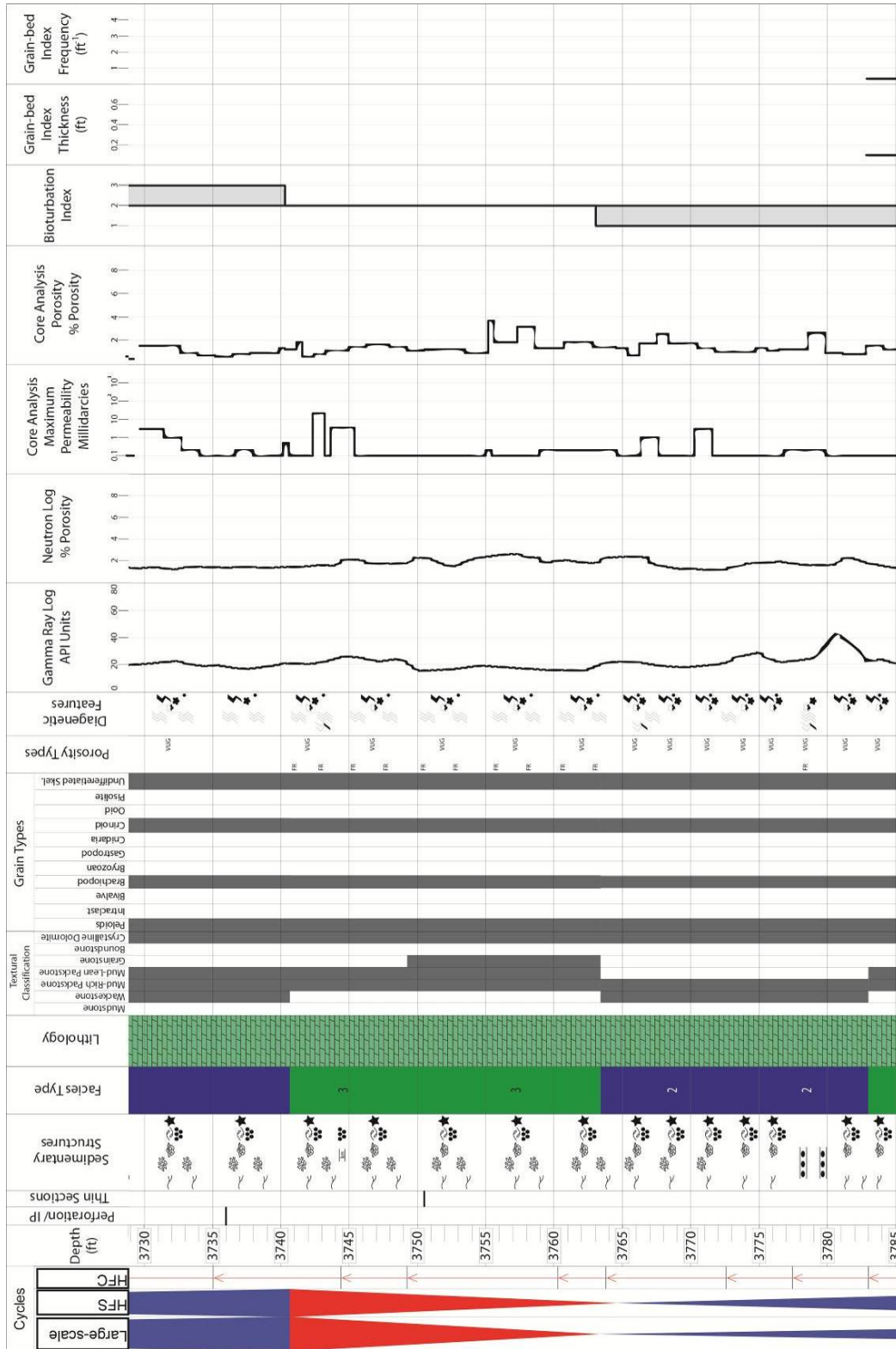


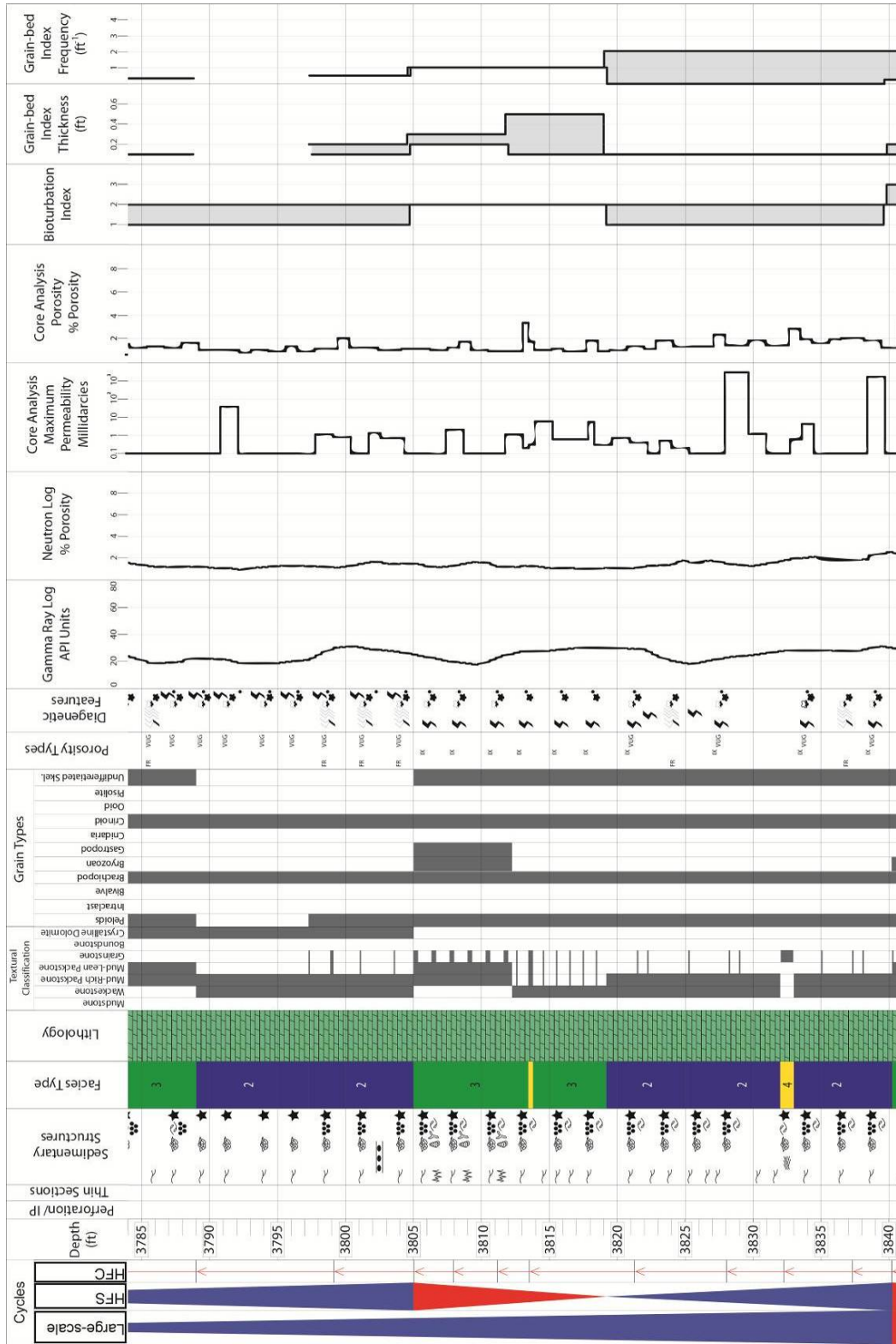


Rowe A-2 – McClure Oil Company  
Permit #37239, Hillsdale County, MI

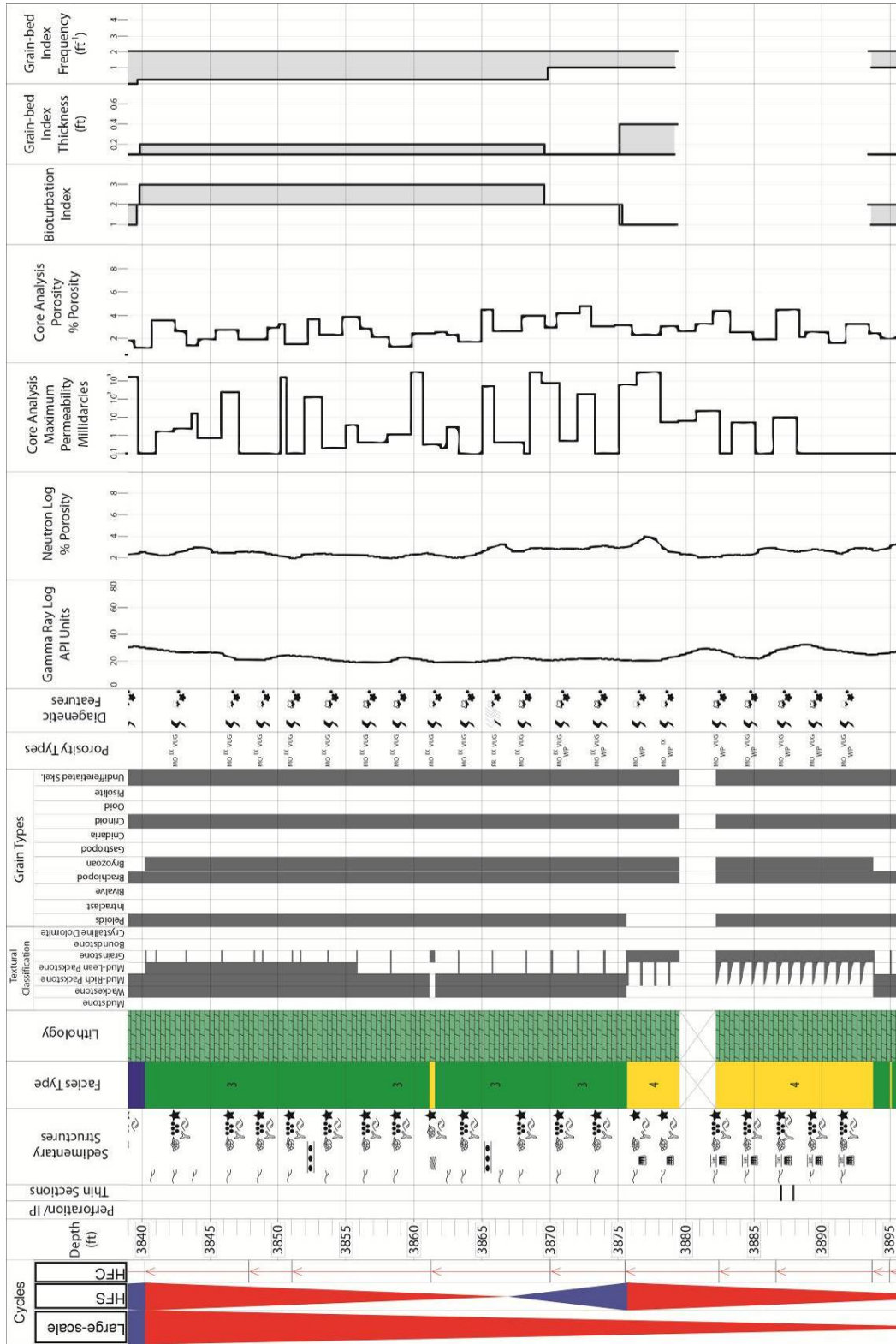
Rowe A-2 – McClure Oil Company, Hillsdale County, MI  
 Formation: Black River Gp., Black River Shale, Trenton Gp.  
 Cored Interval: 3680.0' – 4030.0' Examined Interval: 3680.0' – 4027.0'  
 Wire-line logs are shifted [-5'] in depth to match BKRYSH

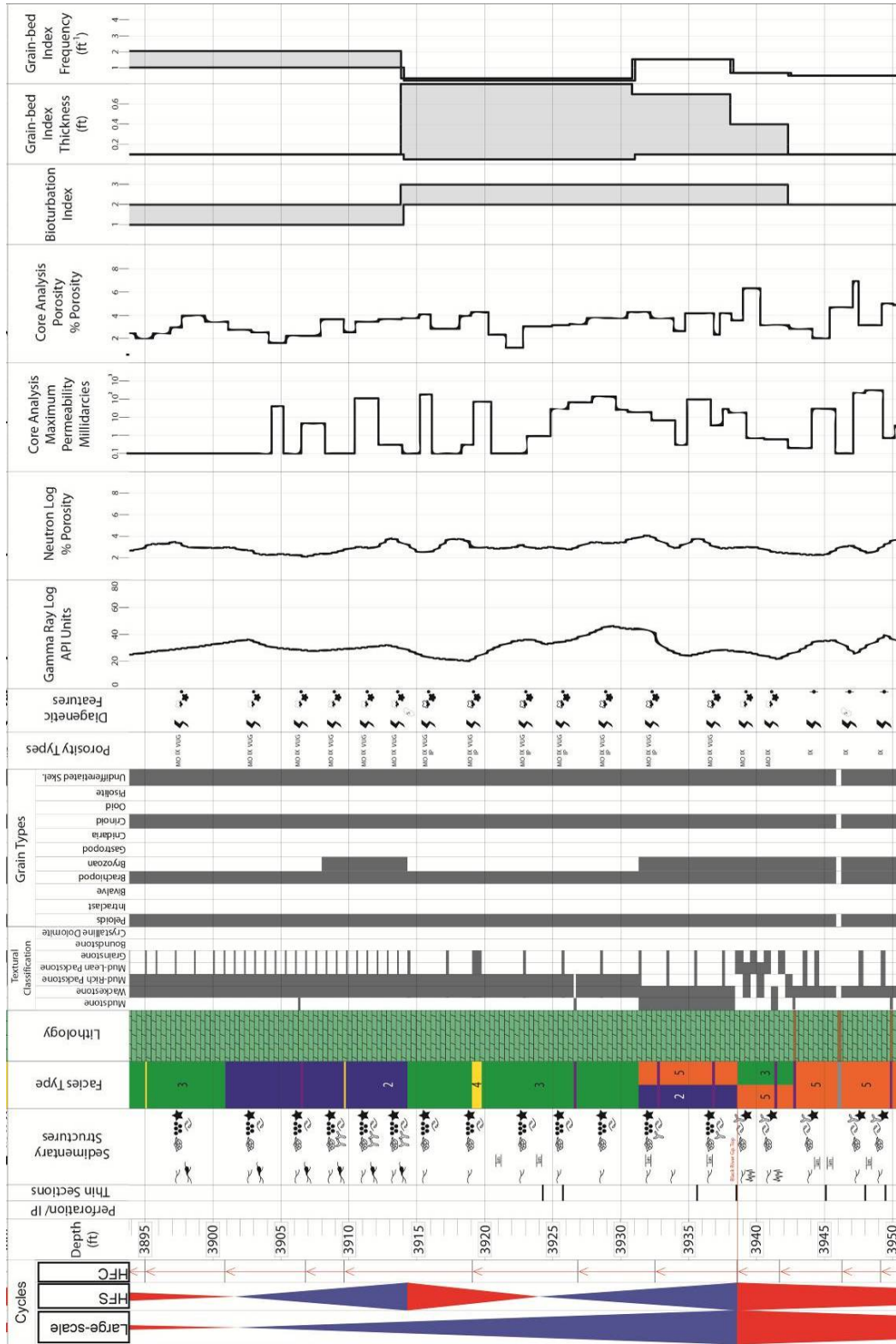


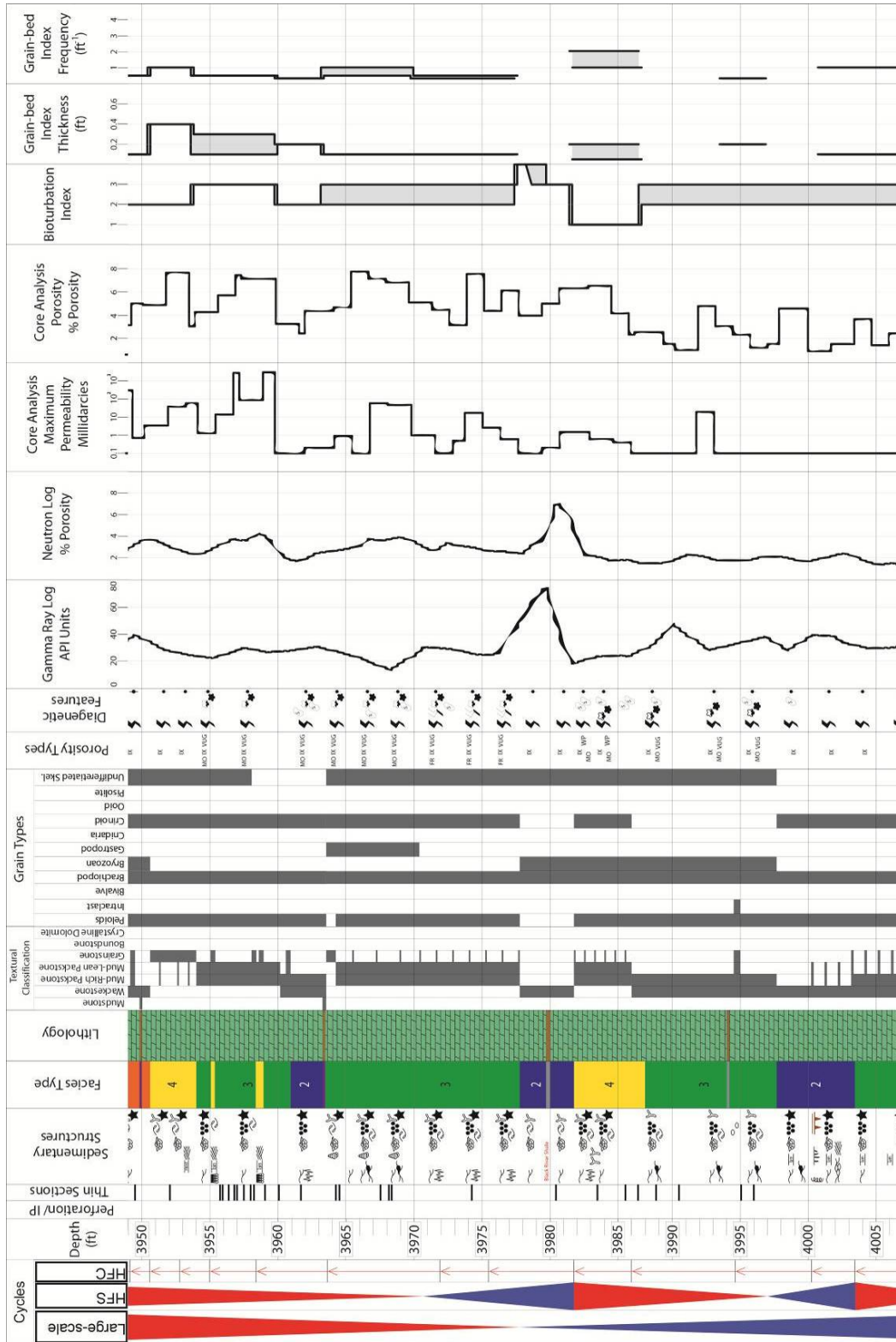


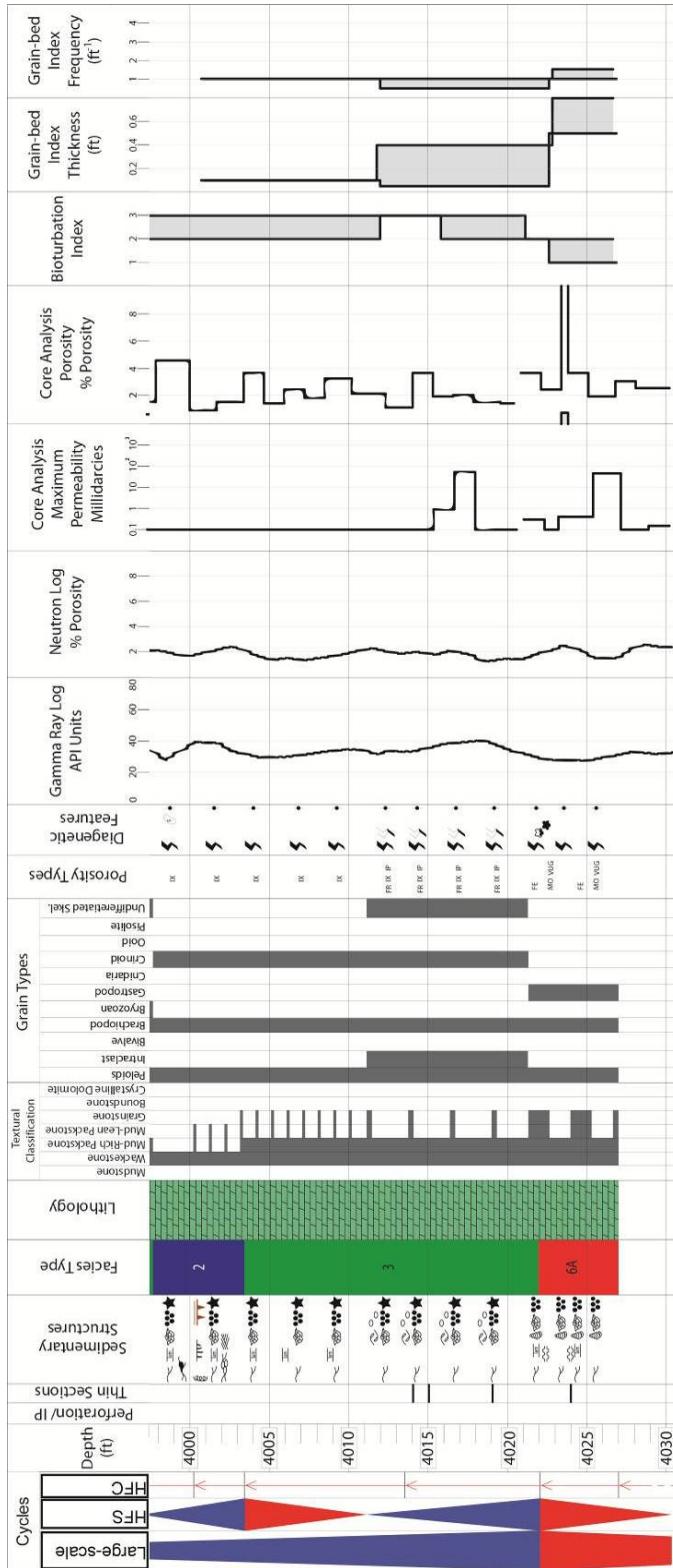


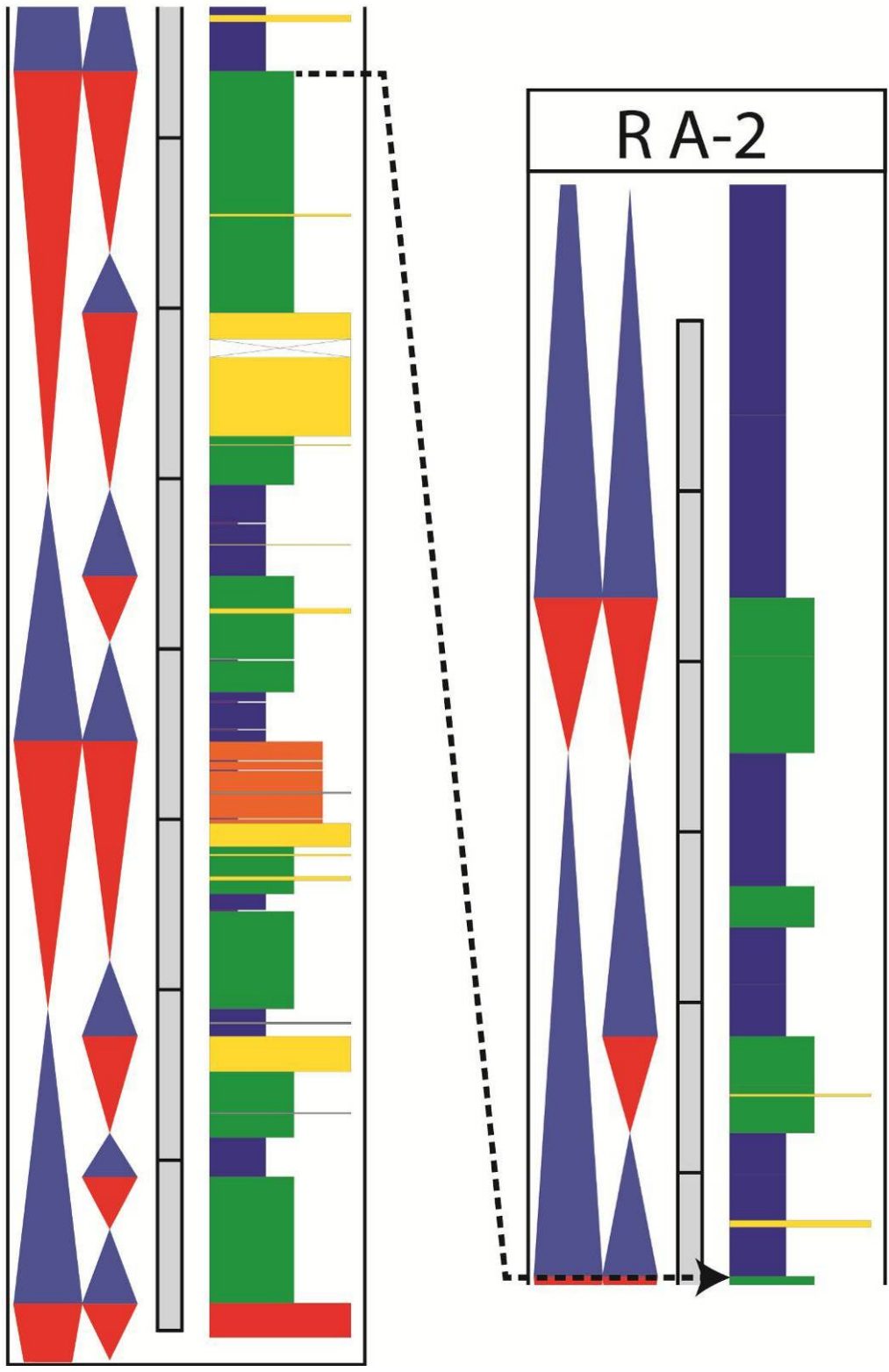












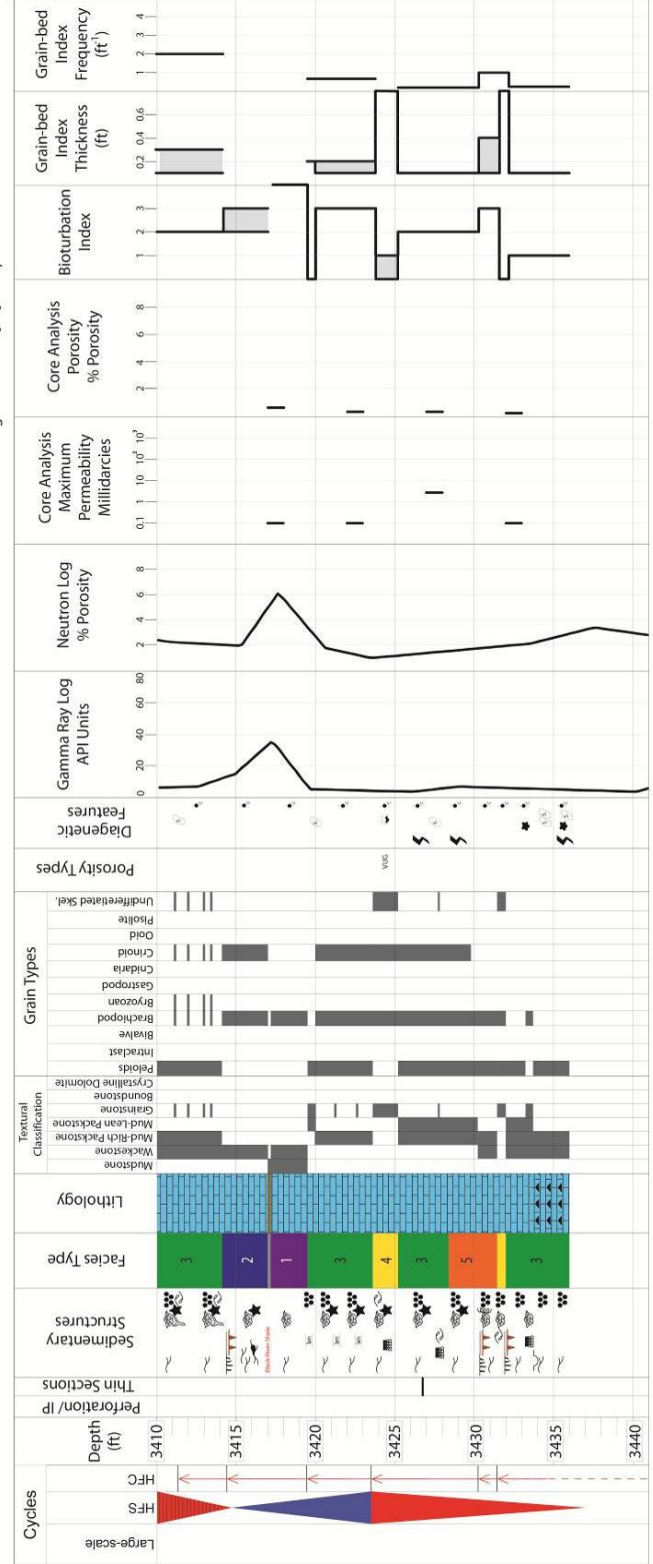
Rzepke 1-27 – Marathon Oil Company

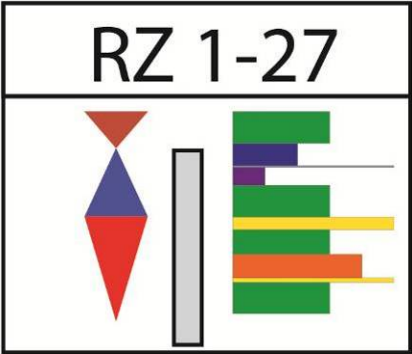
Permit #31253, Branch County, MI



### Rzepke 1-27 – Marathon Oil Company, Branch County, MI

Formation: Black River Gp., Black River Shale  
 Cored Interval: 3387.0' – 3345.0' Examined Interval: 3410.0' – 3436.0'  
 Wire-line logs are shifted [+5] in depth to match BKRVSJH

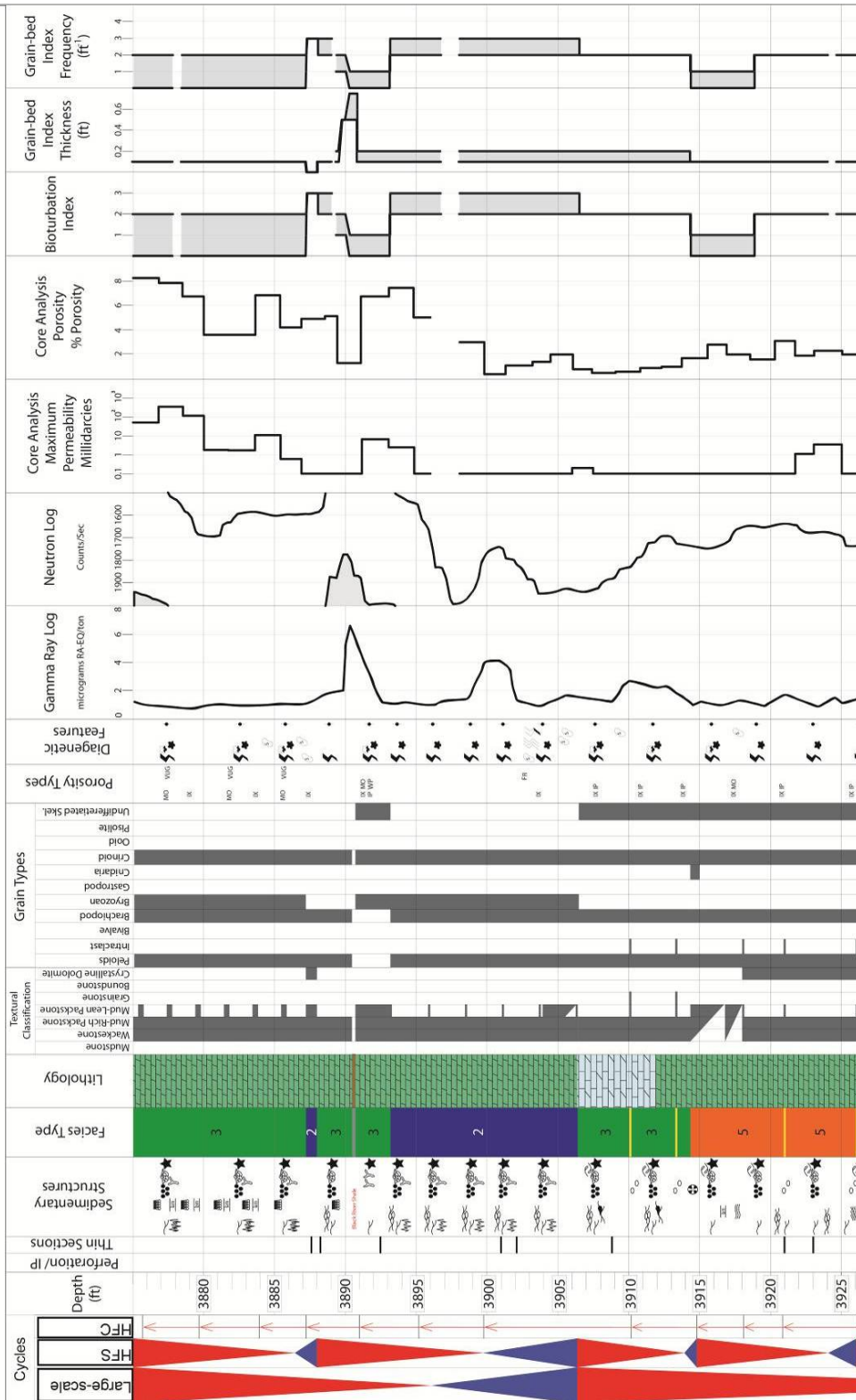


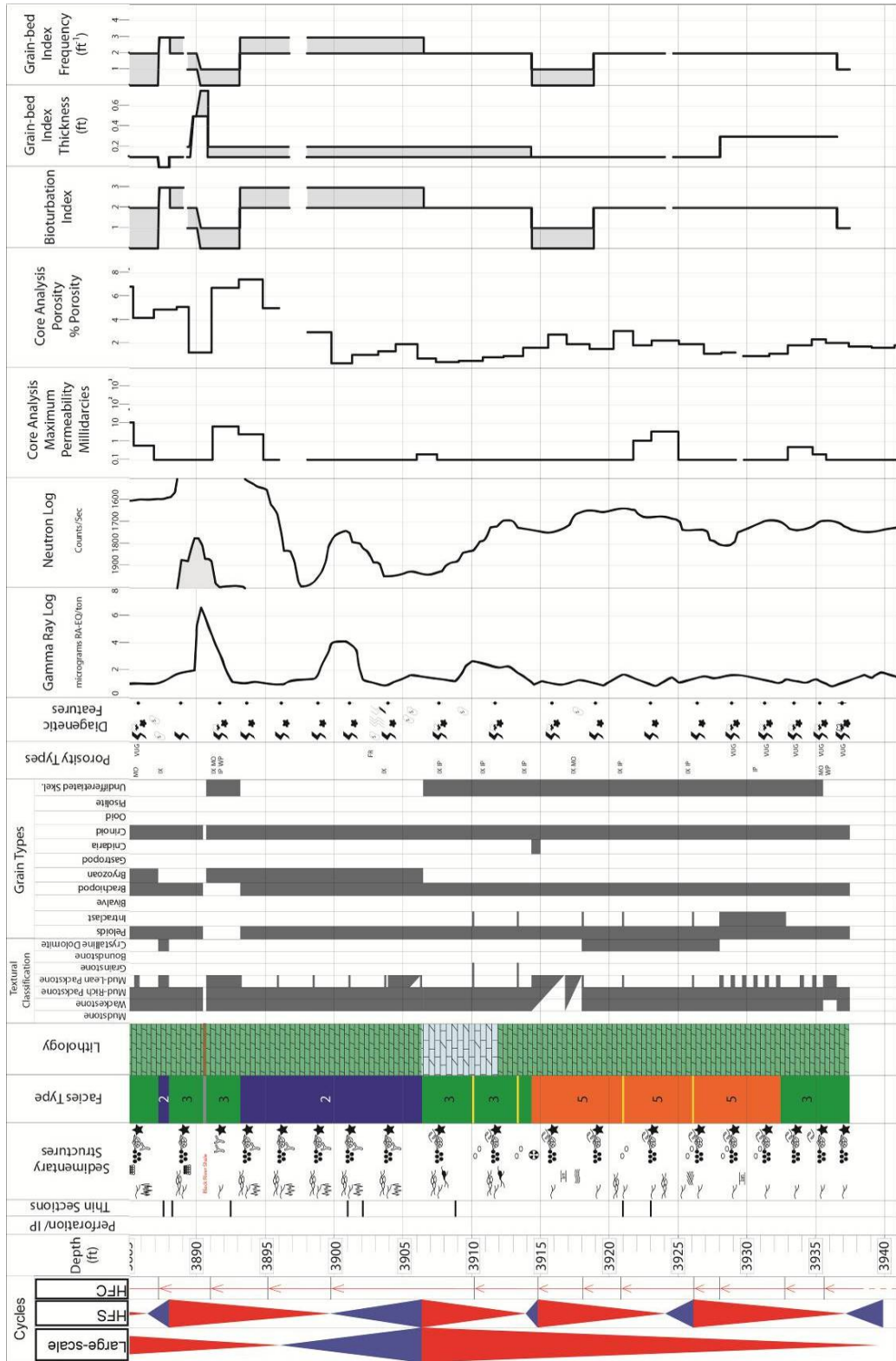


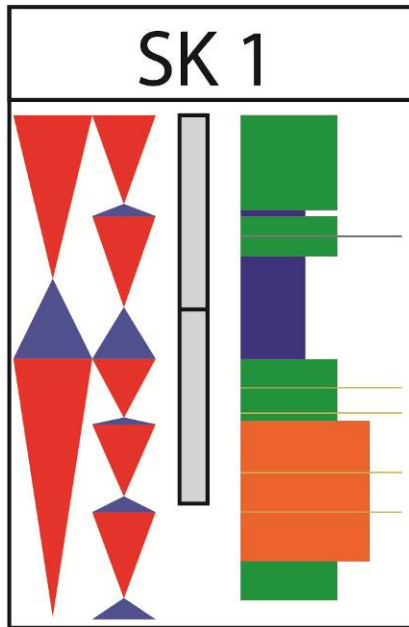
Skinner 1 – Marathon Oil Company  
Permit #21833, Hillsdale County, MI

# Skinner 1 – Marathon Oil Company, Hillsdale County, MI

Formation: Black River Gp., Black River Shale  
 Cored Interval: 3875.0' – 4000.0' Examined Interval: 3875.0' – 3937.4'  
 Wire-line logs are shifted [-1'] in depth to match BKRVSJH







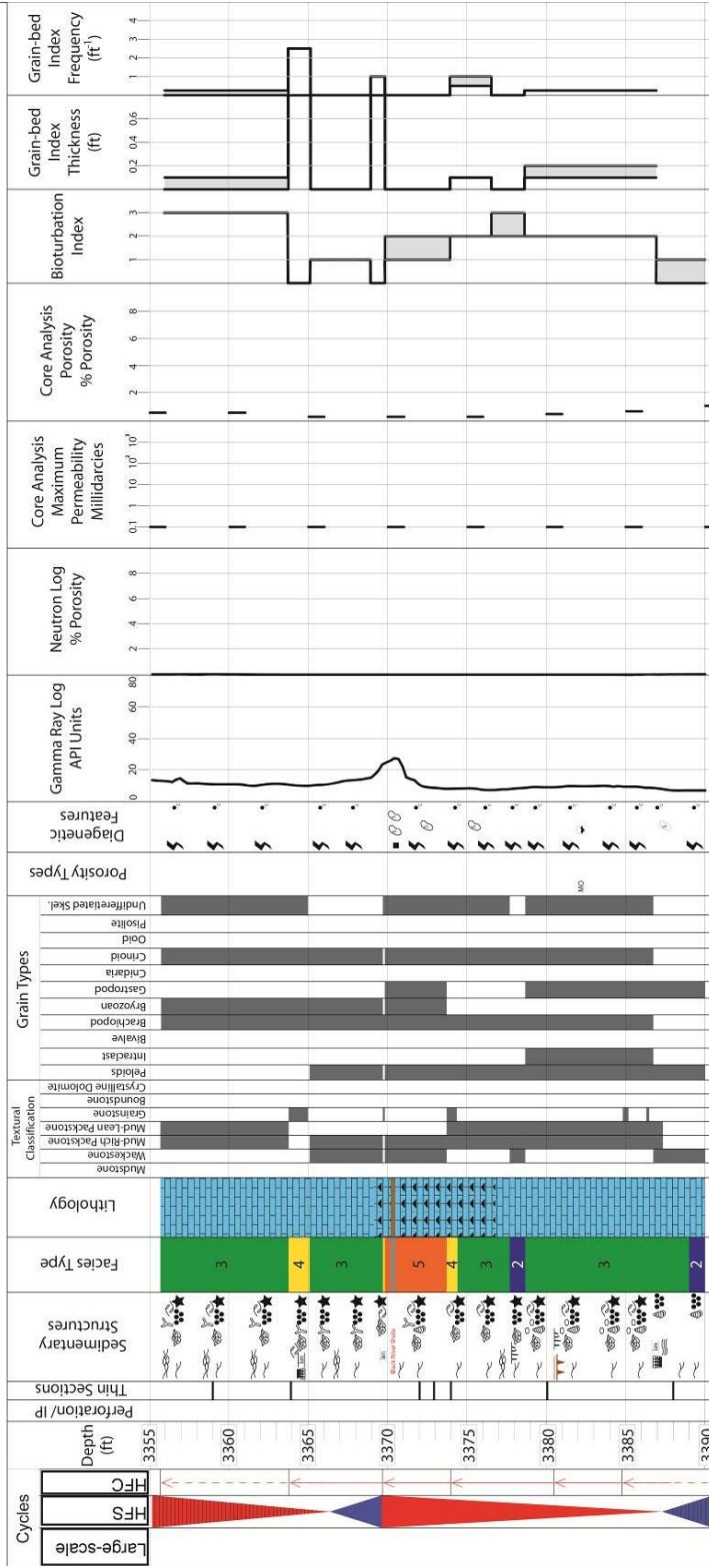


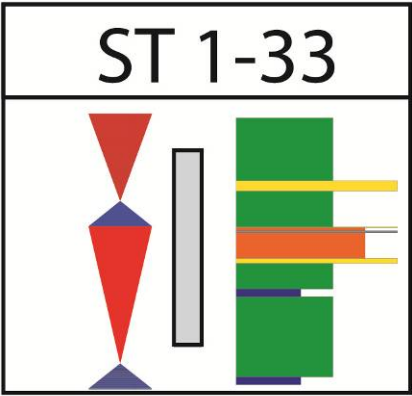
Stetler 1-33 – Marathon Oil Company

Permit #31407, Branch County, MI

### Stetler 1-33 – Marathon Oil Company, Branch County, MI

Formation: Black River Gp. Black River Shale  
 Cored Interval: 3350.0' – 3395.0' Examined Interval: 3355.9' – 3390.0'  
 Wire-line logs are shifted [-7'] in depth to match BKRVSJH





APPENDIX D – Photomicrographs and Descriptions

Abbreviations, definitions, and introduction

<b>Key to Common Core and Thin Section Image Labels</b>							
<b>Feature Key</b>		<b>Key (cont.)</b>		<b>Key (cont.)</b>		<b>Porosity Key</b>	
<b>Bo</b>	boring	<b>CG</b>	compound grain	<b>Ic</b>	intraclast	<b>IX</b>	intercrystalline
<b>Br</b>	brachiopod	<b>Cr</b>	crinoid	<b>M</b>	mud/mudstone	<b>IP</b>	interparticle
<b>BSN</b>	burrow-bounding stylonodular	<b>C</b>	calcite	<b>ME</b>	micritic envelope	<b>MO</b>	moldic
<b>Bu</b>	burrow	<b>D</b>	dolomite	<b>O</b>	ostracode	<b>FE</b>	fenestral
<b>Bu-Gr</b>	grain dominant burrow fill	<b>FR</b>	fracture	<b>P</b>	peloid	<b>FR</b>	fracture
<b>Bu-M</b>	mud dominant burrow fill	<b>G</b>	gastropod	<b>Py</b>	pelecypod	<b>VU</b>	vug
<b>Bu-Mx</b>	mud-grain mix burrow fill	<b>GB</b>	grain-bed	<b>S</b>	stylolite	<b>WX</b>	intracrystalline
<b>By</b>	bryozoan	<b>HG</b>	hardground	<b>Tr</b>	trilobite	<b>WP</b>	intraparticle
<b>Pg</b>	platy grain	<b>LC</b>	lithoclast	<b>Sk</b>	skeletal fragment	<b>zvu</b>	zebra-fabric vug
<b>Psi</b>	pressure solution	<b>N</b>	normal grading	<b>Cn</b>	coral		
<b>Ct</b>	chert	<b>L</b>	lamination				

Thin-section photomicrographs show magnified view of core samples. All samples are oriented with horizontal core axis parallel with long axis of images unless otherwise noted. Images are organized by well, and show samples from deepest to shallowest. Additional thin-section sample descriptions without accompanying photos are included at the end of each core sub-section to supplement images shown here.

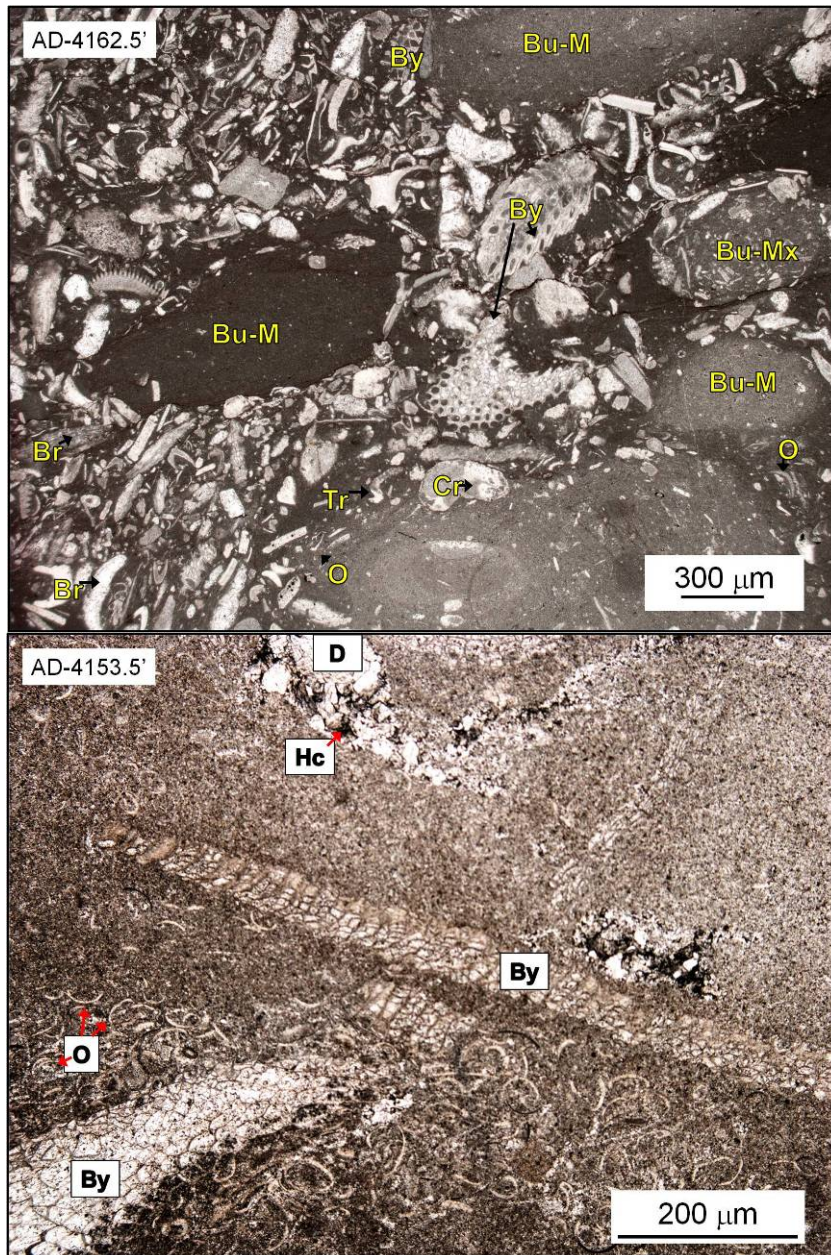
All samples are shown in plane polarized light and labeled with the above key, unless otherwise noted. Multiple photomicrographs are shown for some thin-

section samples (denoted by alphabetic code, i.e. A., B. C.), showing multiple scales, comparisons of samples in cross-polarized light (XPL) and with white-card viewing technique (WC).



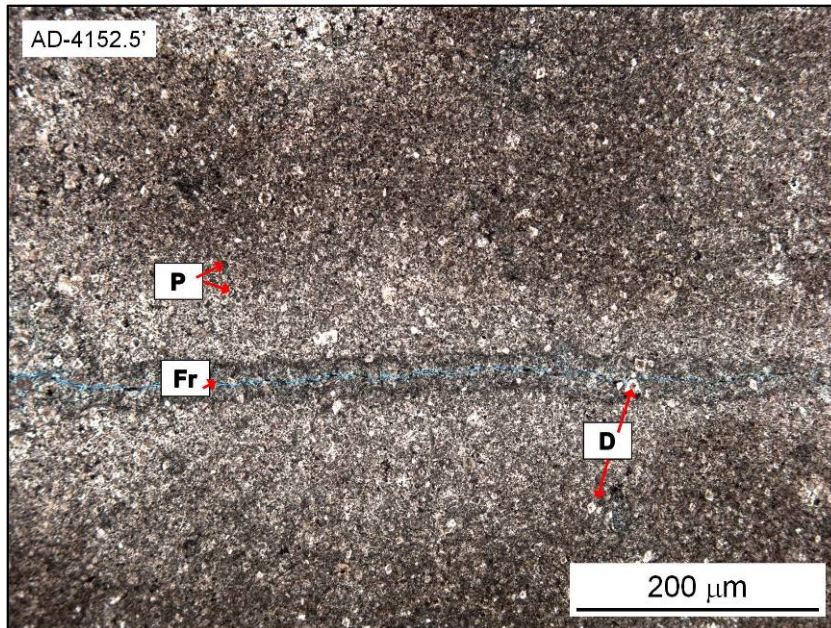
ARCO Dunn 1-14 – Atlantic Richfield Oil and Gas Company

Permit #37239, Calhoun County, MI



**AD – 4162.5' – Mud-rich skeletal packstone-to-wackestone with variable burrow fills.** Crinoid (30%), brachiopod (25%), bryozoan (15%), mollusc, ostracode, trilobite mud-rich packstone-to-wackestone, with mud dominated burrow fill and one (of five) skeletal grain-rich burrow fill. Skeletal grains are fragmented and abraded, with no dominant grain orientation. No visible porosity. **AD – 4153.5' – Bryozoan, ostracode wackestone-to-mud-rich packstone.** Bryozoan (50%), ostracode (40%)

wackestone-to-mud-rich-packstone (few bryozoan grains with dimensions >2.0 mm, ~floatstone-to-rudstone), with chert and few crinoid and trilobite fragments. No visible porosity. Residual hydrocarbon (Hc) remains in interparticle and intercrystalline locations.

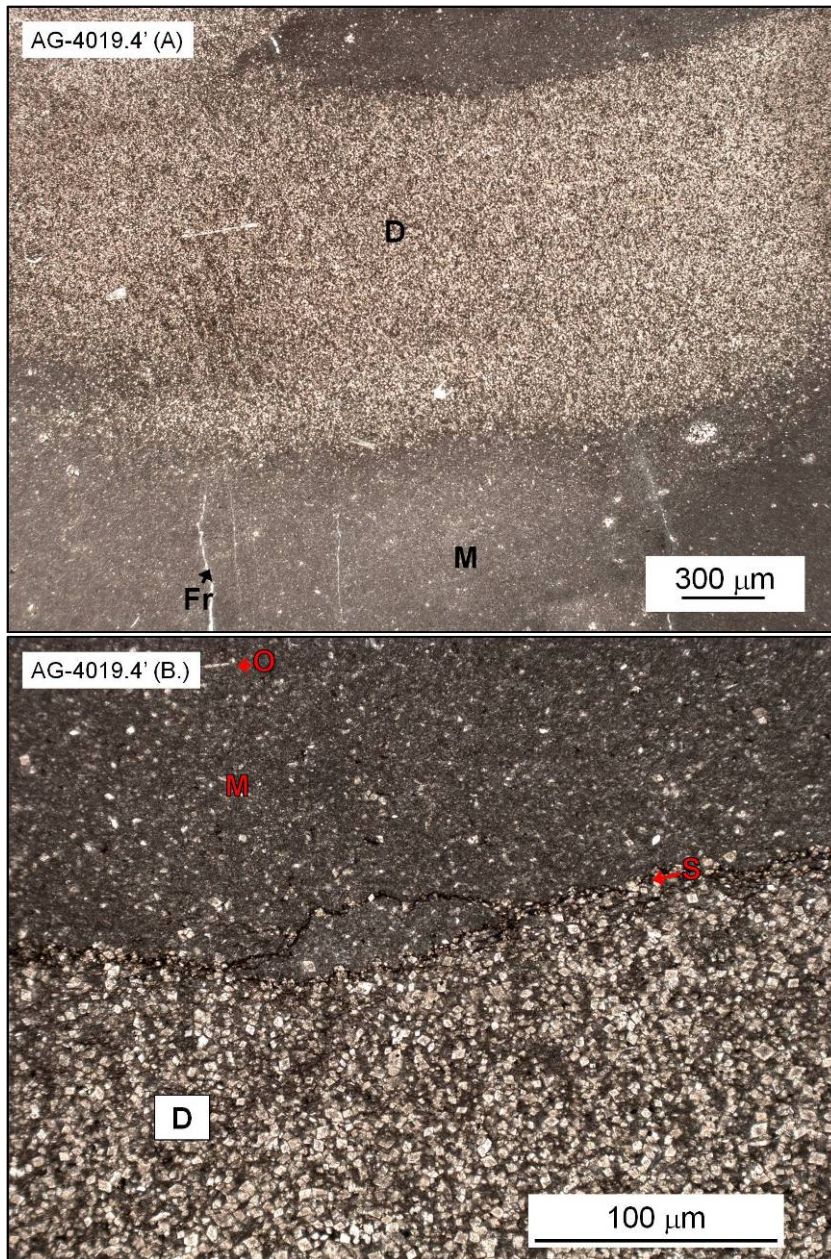


**AD – 4152.5' – Mudstone-to-ostracode wackestone.** The presence of peloids is indeterminable, however rock texture indicates silt/very fine sand sized particles. The origin of this texture may be attributed to depositional grains (peloid/fecal pellets) or diagenetic burial processes. Very minor FR visible (<2%), with alteration zones surrounding.

ARCO Gardner 1-16 – Atlantic Richfield Oil and Gas Company

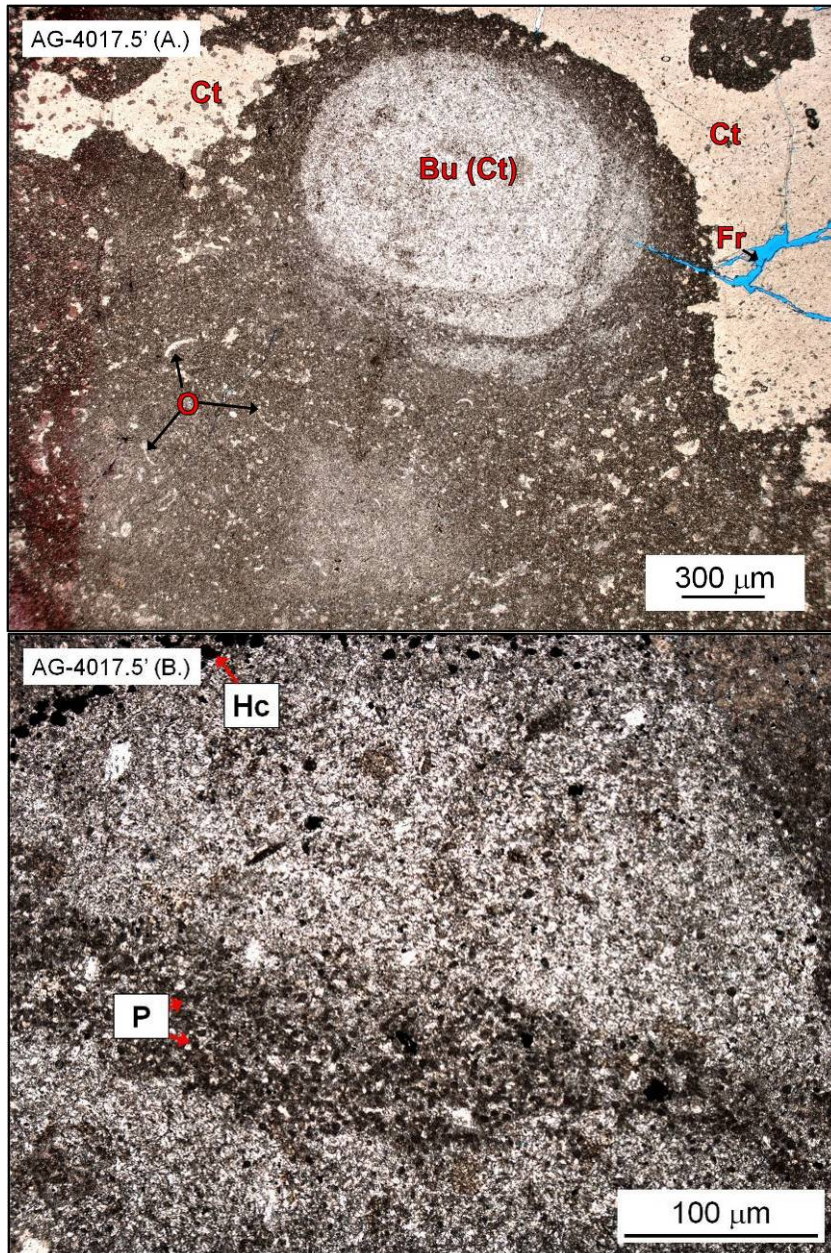
Permit #37838, Hillsdale County, MI





**AG – 4019.4' – Mudstone. (A. and B.)** Less than 1% of bioclasts (ostracode). Euhedral dolomite rhombs (burial) occur throughout, but are concentrated at likely pressure solution seam and minor dolomite filled fractures occur throughout. No visible porosity.

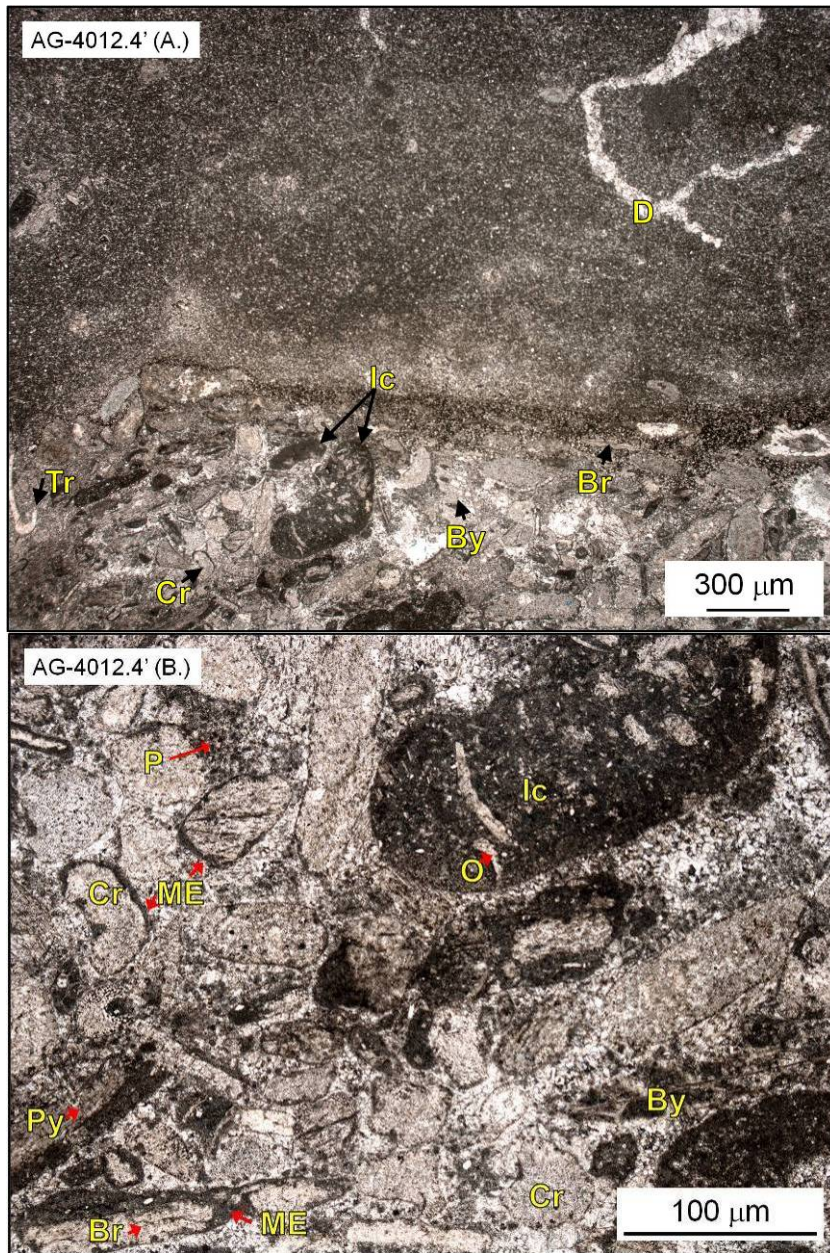




**AG - 4017.5' - Ostracode wackestone-mud-rich packstone. (A. and B.)**  
Dolomitization and certification have partially obscured depositional fabric. Minor burrow preservation (n=1, 0.5 mm). Commonly associated with chert are few fractures, constituting all minor visible porosity



(<3%). Residual hydrocarbon (Hc) remains in interparticle and intercrystalline locations.



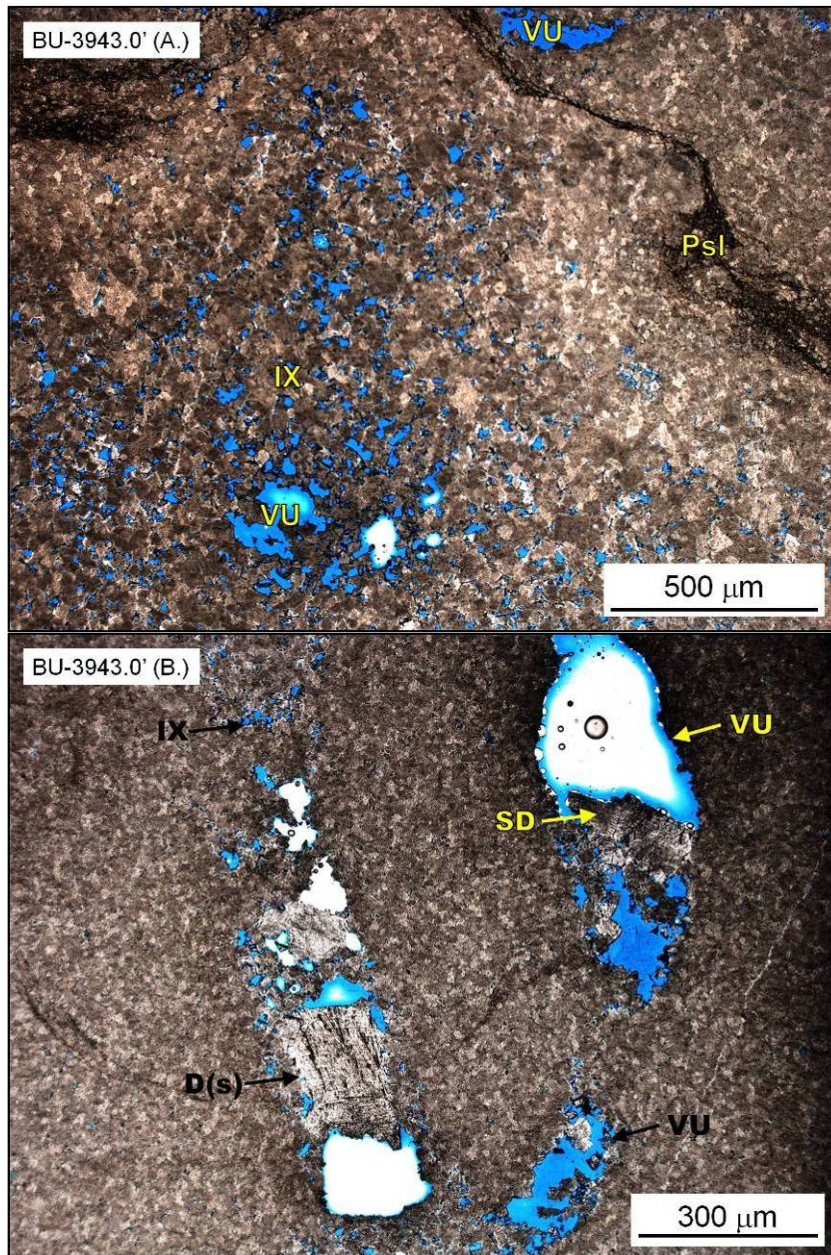
**AG – 4012.4 – Skeletal intraclastic grainstone interbedded with peloidal packstone.** Crinoid (60%), undifferentiated skeletal fragment (20%), brachiopod, intraclast, bryozoan, trilobite grainstone interbedded with mud-rich peloid packstone. Grainstone bioclasts consist of skeletal fragments that range from complete, to abraded, partially micritized. Grainstone intraclasts consist of rounded ostracode, pelecypod, undifferentiated skeletal fragment wackestone compound grains.

Euhedral dolomite rhombs (burial) are concentrated in a seam in the upper 2.0 mm of sample. Fractures/ veins are few (n=2) and completely filled. Very little WP porosity (>1%).

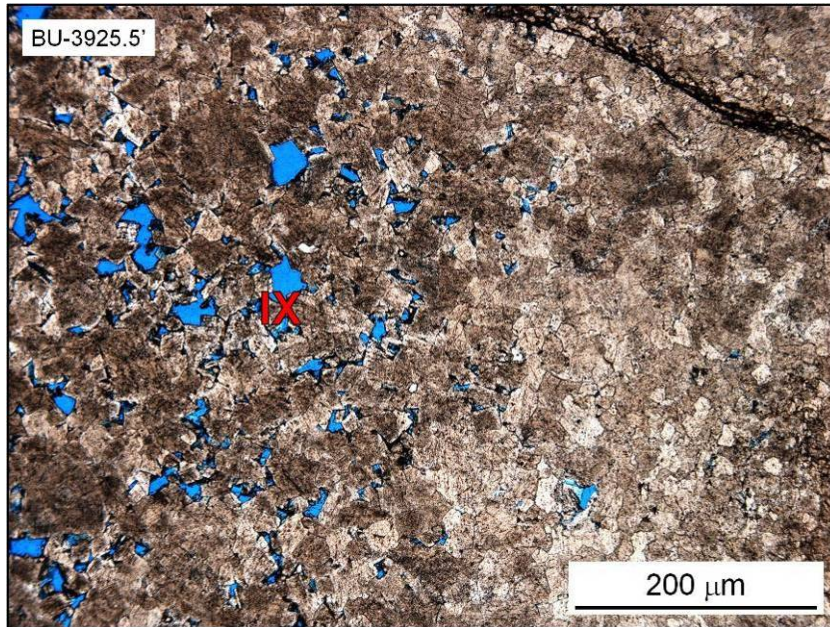
Buehrer 1 – Aurora Gasoline Company and McClure Oil Company

Permit #21064, Hillsdale County, MI



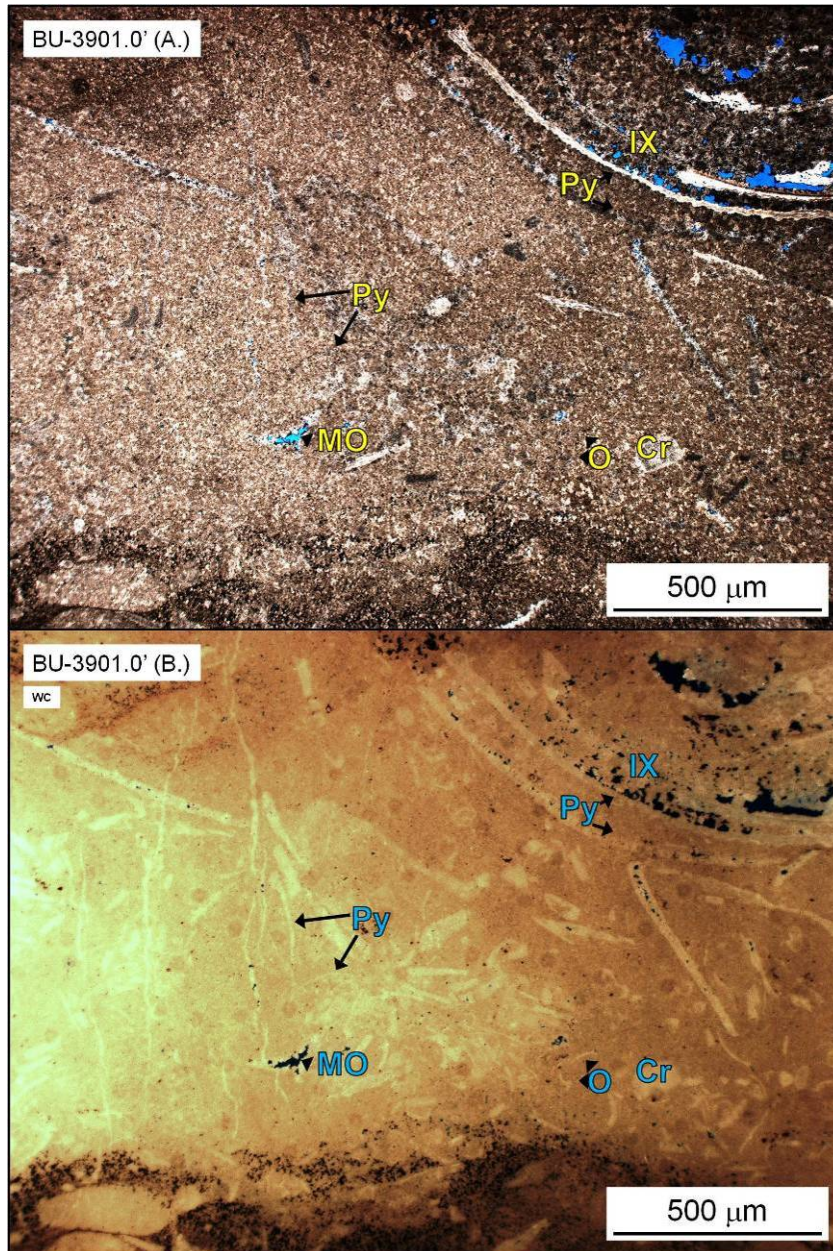


**BU – 3943.0' – Depositional fabric obscured by dolomitization.** Dolomite crystals are dominantly very fine sand sized (0.062 – 0.125 mm) with very minor IX porosity and well developed VU (5-6%) in locations with common occlusion by residual hydrocarbon in each pore type. Saddle dolomite (D(s)) (commonly 0.25 – 1.0 mm) also partially occludes VU porosity. Microfractures present are filled with dolomite.



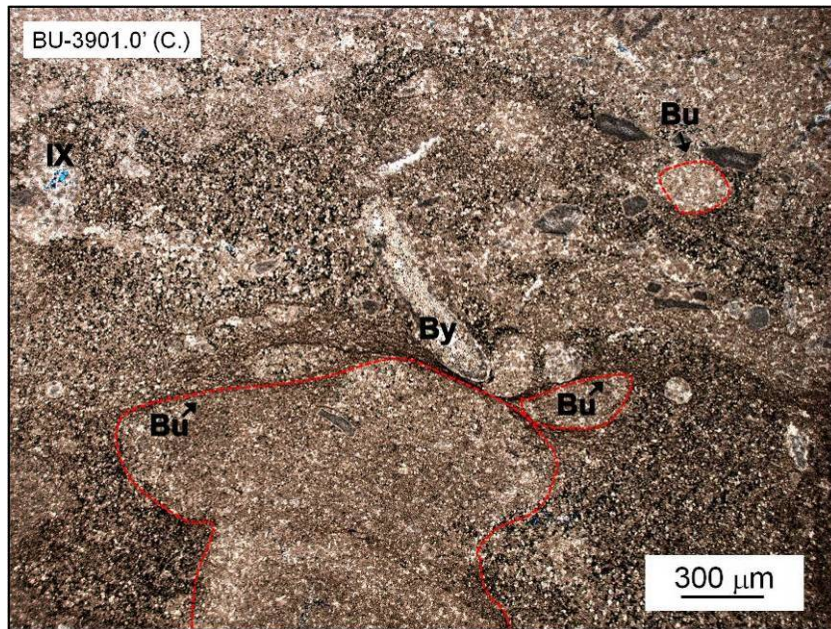
**BU – 3925.1’ – Depositional fabric obliterated by dolomitization.** Locally developed intercrystalline porosity (8%). Occlusion in each pore type by residual hydrocarbon is common.





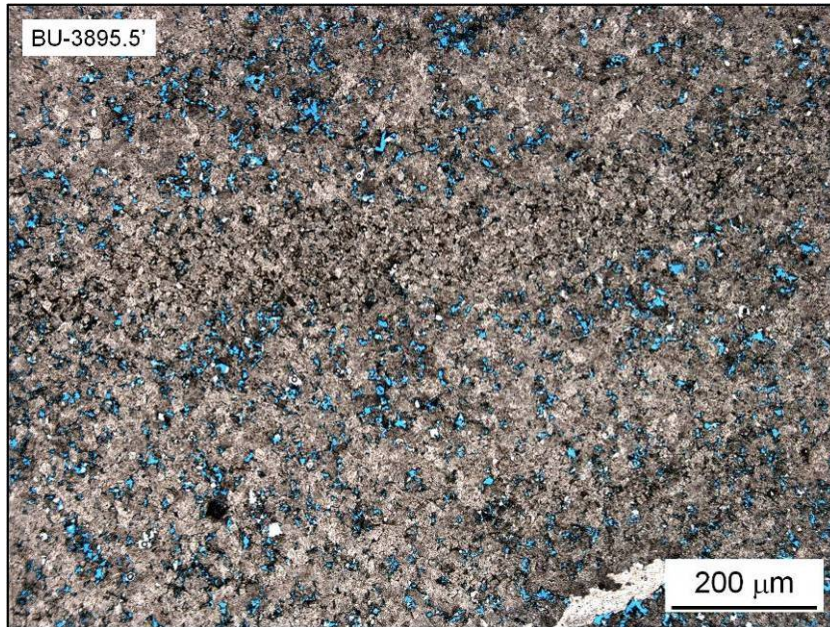
**BU – 3901.0' – Depositional fabric obscured by dolomitization. (A. and B.-WC)**

Likely brachiopod/pelecypod (40%), bryozoan, crinoid, ostracode wackestone/peloidal packstone with moderate bioturbation. Burrows contain no significant porosity development; however matrix surrounding is well developed IX and additional MO and WP (~5%). Few vertically oriented dolomite filled fractures occur. Occlusion in each pore type by residual hydrocarbon is common.

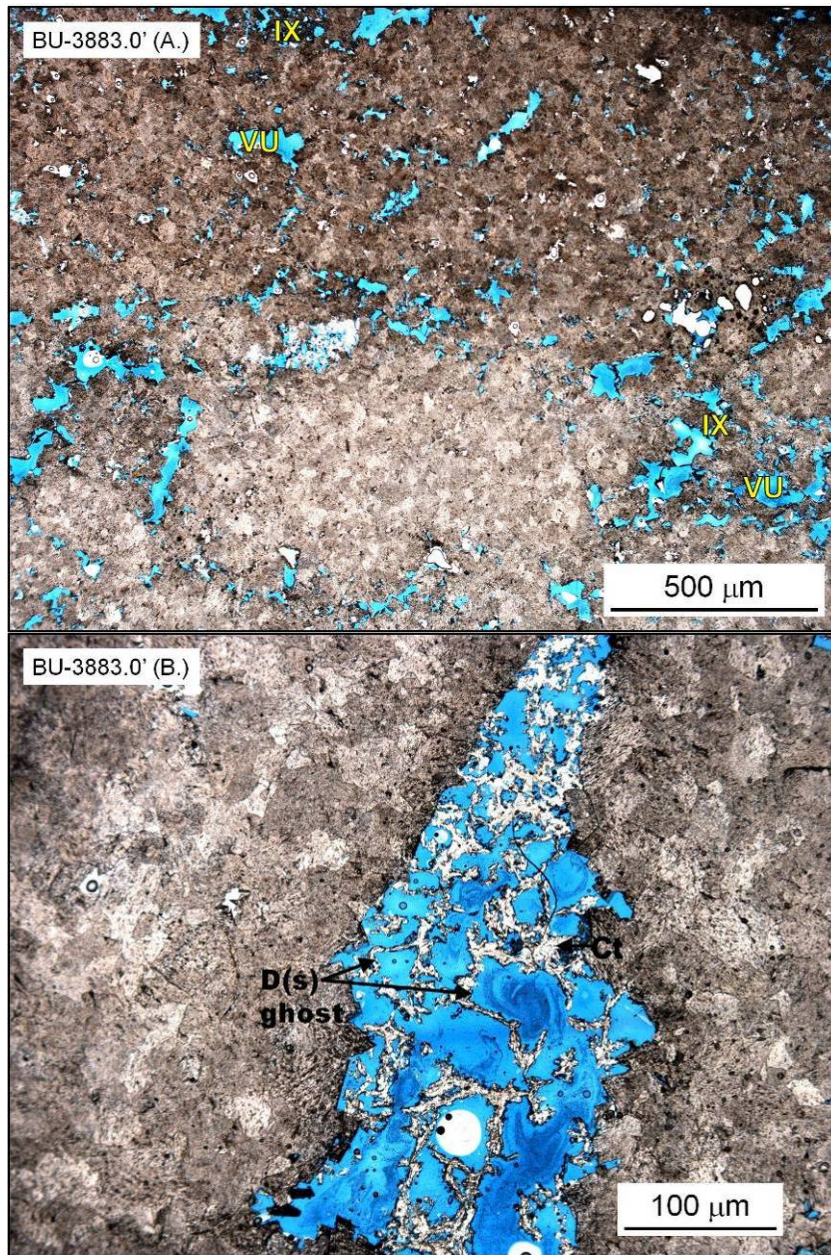


**BU – 3901.0' – Depositional fabric obscured by dolomitization. (C.)** Likely brachiopod/pelecypod (40%), bryozoan, crinoid, ostracode wackestone/peloidal packstone with moderate bioturbation. Burrows contain no significant porosity development; however matrix surrounding is well developed IX and additional MO and WP (~5%). Burrow fill is apparently grain-rich.



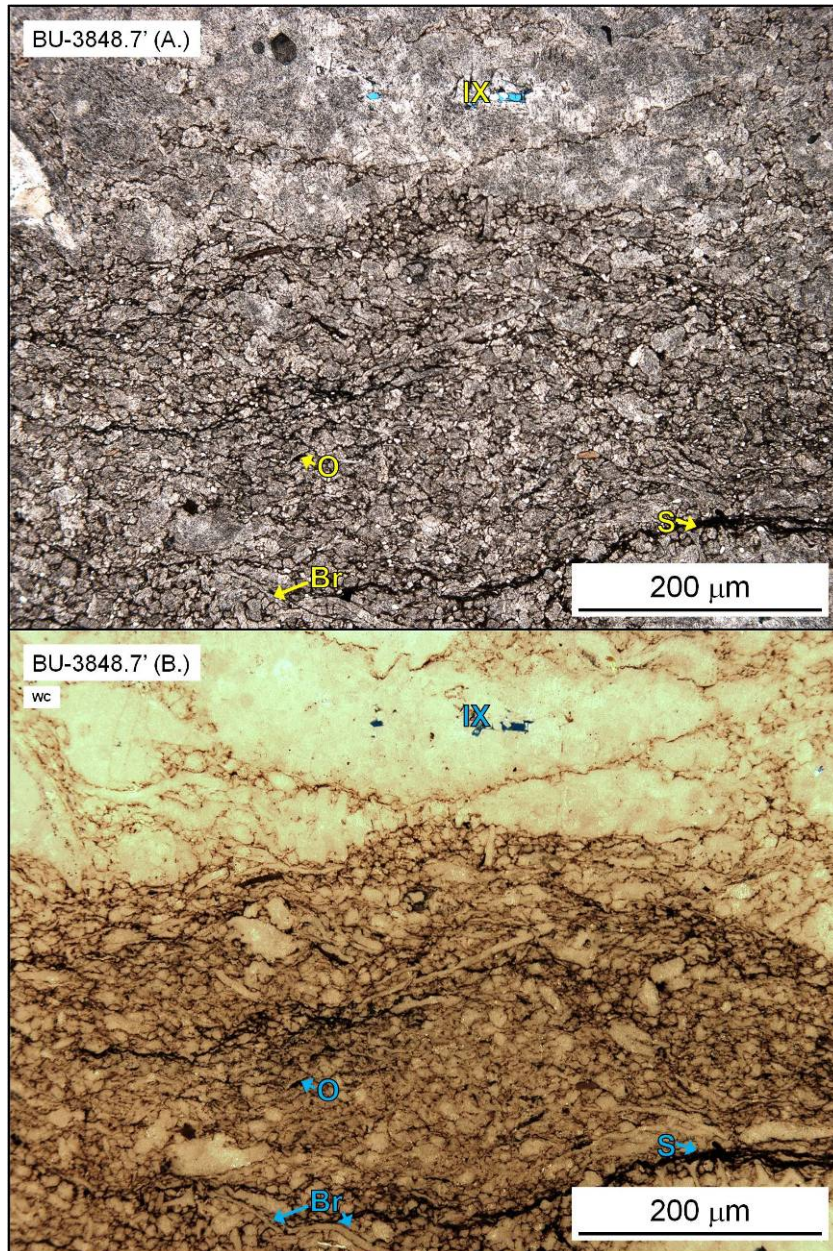


**BU – 3895.5’ – Depositional fabric obscured by dolomitization.** Few preserved skeletal fragments at the top of the sample indicate brachiopod wackestone (?), however matrix is unidentifiable. Porosity is well developed as IX throughout (10%), with zones/seams of residual hydrocarbon accumulations occluding IX porosity. A minor chert component is present in the sample (<3%).



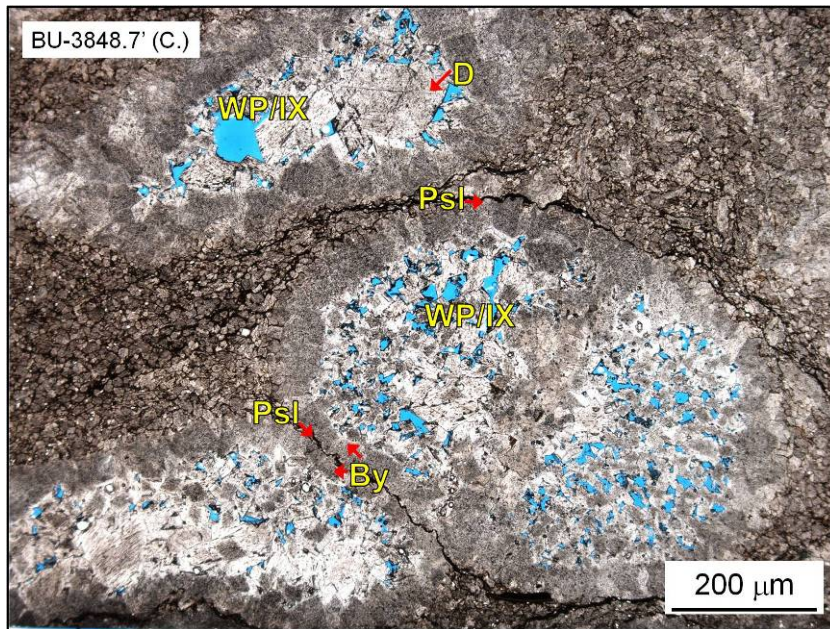
**BU – 3883.0' – Depositional fabric obscured by dolomitization. (A. and B.)**  
 Dolomite crystals are fine sand-sized (0.125 – 0.25 mm). Porosity is well developed as IX and VU (8-10%). Multiple generations of dolomite crystal growth and dissolution is shown by VU occluding chert (chalcedony) outlining removed dolomite rhombs (likely euhedral saddle dolomite) (D(s) ghost).





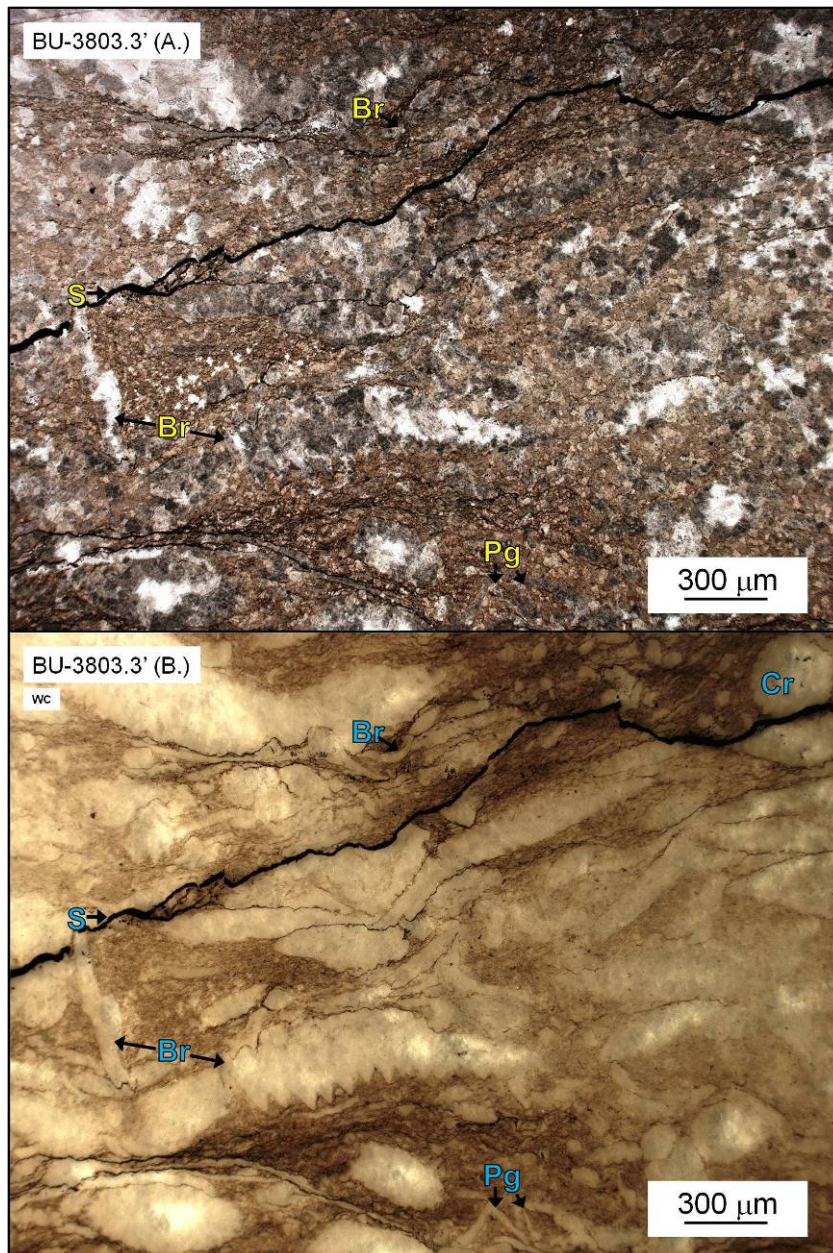
**BU – 3848.7' – Depositional fabric obscured by dolomitization. (A. and B.-WC)**

Identifiable fabric (white card technique) is interbedded well abraded brachiopod (40%), crinoid, bryozoan, trilobite packstone. Included in packstone textures are large (0.3 – 0.9 cm diameter, ~rudstone) (ramose) bryozoan fragments that are replaced by saddle dolomite with well developed IX (WP) porosity. Additional porosity is IX in unidentifiable sections of sample (5-8% total).



**BU – 3848.7' – Depositional fabric obscured by dolomitization. (C.)** Identifiable fabric (white card technique) is interbedded well abraded brachiopod (40%), crinoid, bryozoan, trilobite packstone. Included in packstone textures are large (0.3 – 0.9 cm diameter, ~rudstone) (ramose) bryozoan fragments that are replaced by saddle dolomite with well developed IX (WP) porosity. Additional porosity is IX in unidentifiable sections of sample (5-8% total).

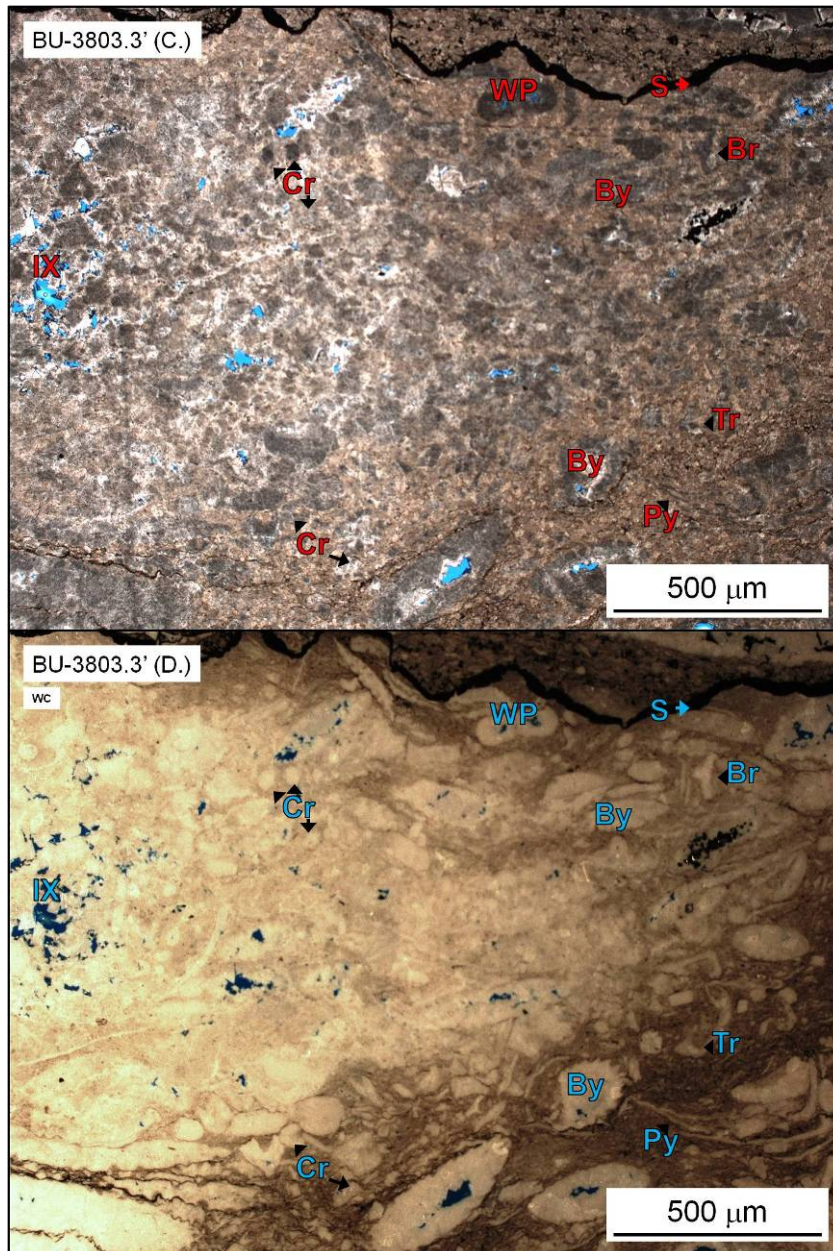




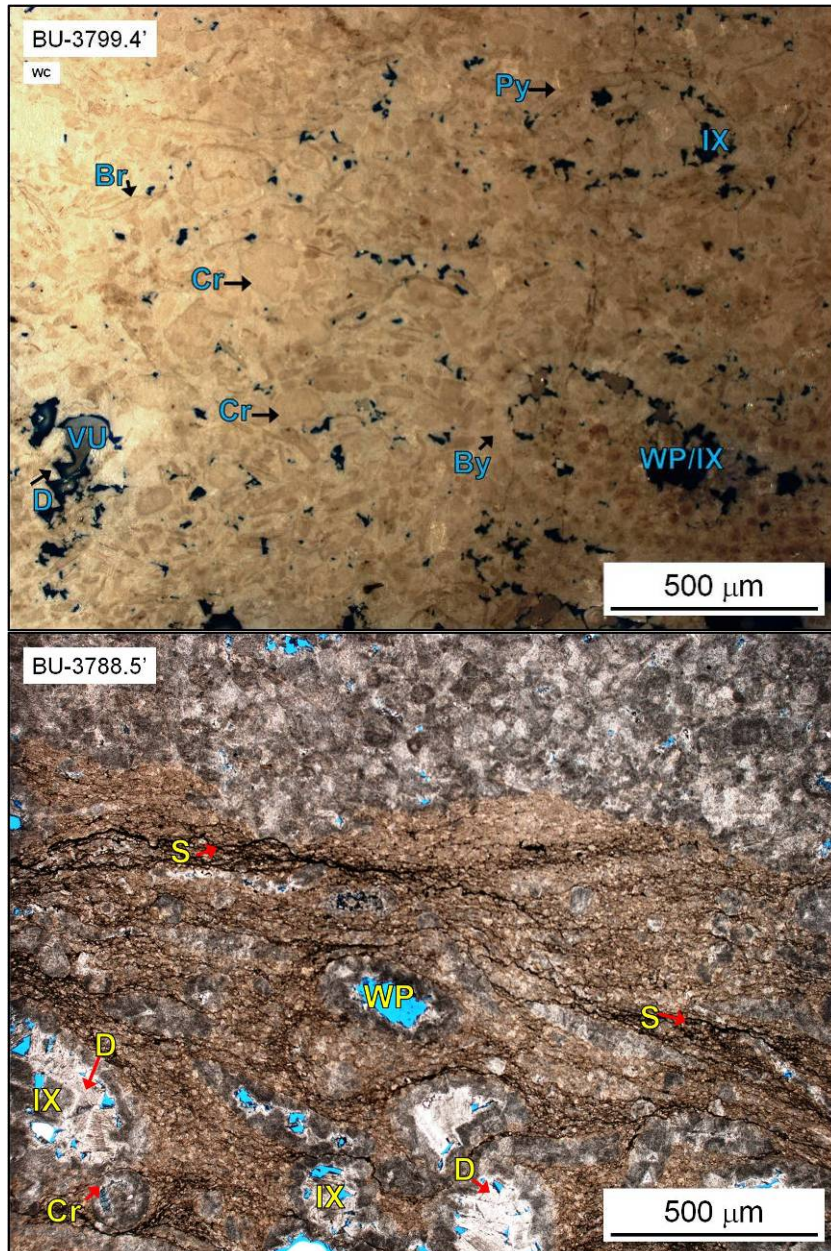
**BU – 3803.3' – Depositional fabric obscured by dolomitization. (A. and B.-WC)**

White card technique shows crinoid, brachiopod, pelecypod (platy-grains, Pg), bryozoan, and trilobite fragments with packstone-to-wackestone textures. Prominent stylolites (n=3) occupy the upper portions of the sample. Porosity is IX in areas of complete recrystallization, with additional IX (WP/MO) in bryozoan and crinoid fragments (<8%).





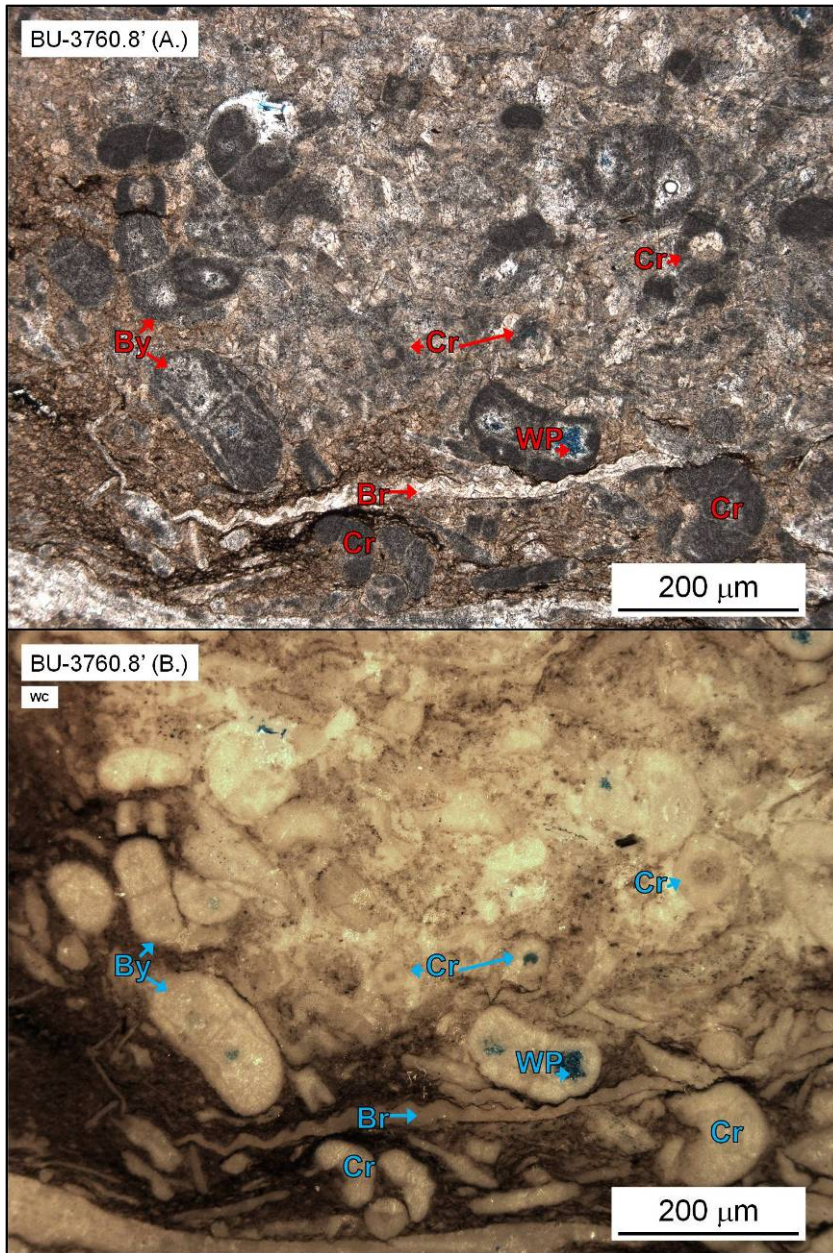
**BU – 3803.3' – Depositional fabric obscured by dolomitization. (C. and D.-WC)**  
 White card technique shows crinoid, brachiopod, pelecypod (platy-grains, Pg), bryozoan, and trilobite fragments with packstone-to-wackestone textures. Sample shows IX and WP (bryozoan) (<6%).



**BU – 3799.4' – Depositional fabric obscured by dolomitization. (WC)** White card technique shows undifferentiated skeletal (40%), crinoid (30%), brachiopod (20%), pelecypod, and bryozoan, fragments with packstone-to-grainstone (?) textures. Grains show no dominant orientation or sedimentary structures, however originally platy skeletal fragments are

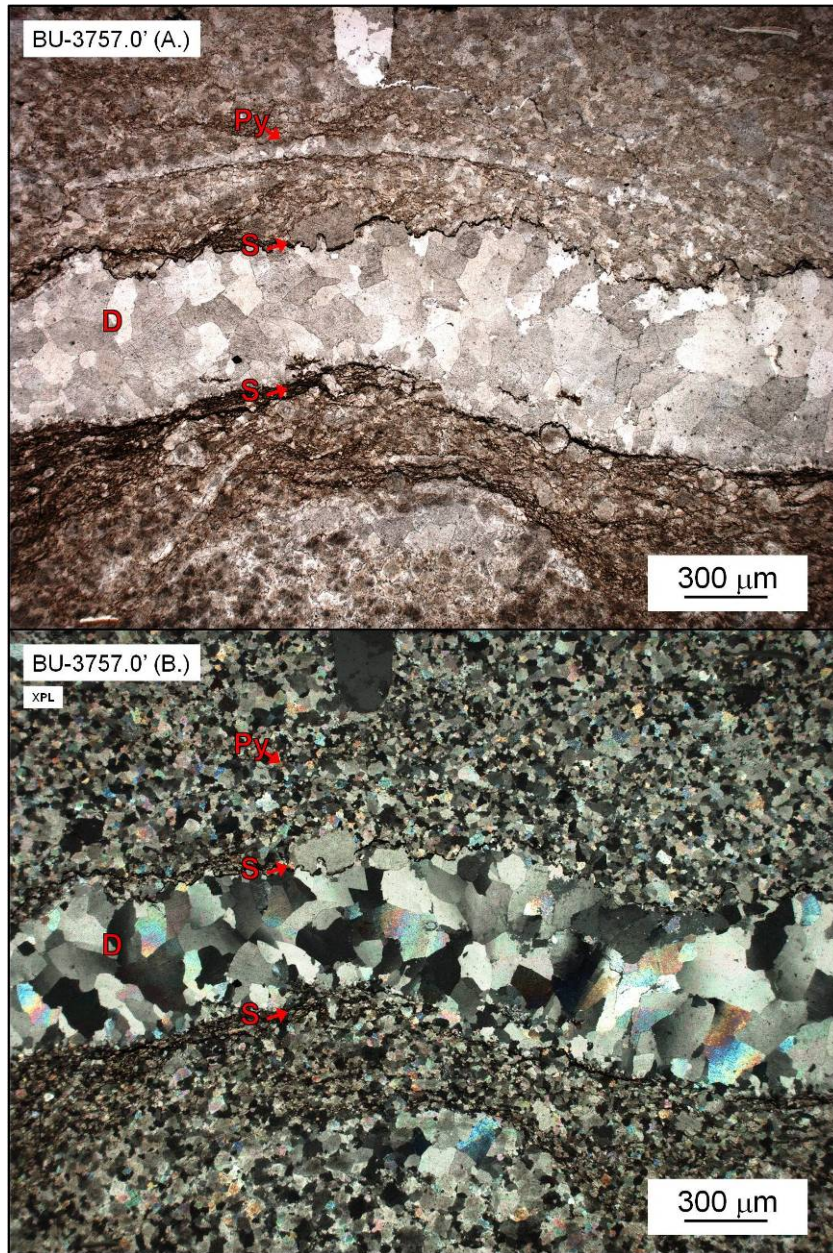


well fragmented and abraded. Porosity includes MO (brachiopod), IX, and VU, with saddle dolomite partially occluding VU pores (7-10%) in lower half, decreasing in percentage-up). **BU – 3788.5’ – Depositional fabric obscured by dolomitization.** Identifiable grains include crinoid and bryozoan fragments in likely packstone-wackestone textures. Local areas show complete dolomite recrystallization. Porosity includes IX and WP (crinoid, bryozoan) (~5%).



**BU – 3760.8' – Crinoid, bivalve packstone-to-wackestone. (A. and B.-WC)**  
 Depositional fabric obscured by dolomitization. Identifiable grains include pelecypod/ostracode (35%), crinoid (35%), brachiopod, bryozoan, trilobite, undifferentiated skeletal fragments with packstone-to-wackestone textures. No dominant grain orientation or sedimentary structures are present. Porosity is minor WP (IX) and FR (<5%).

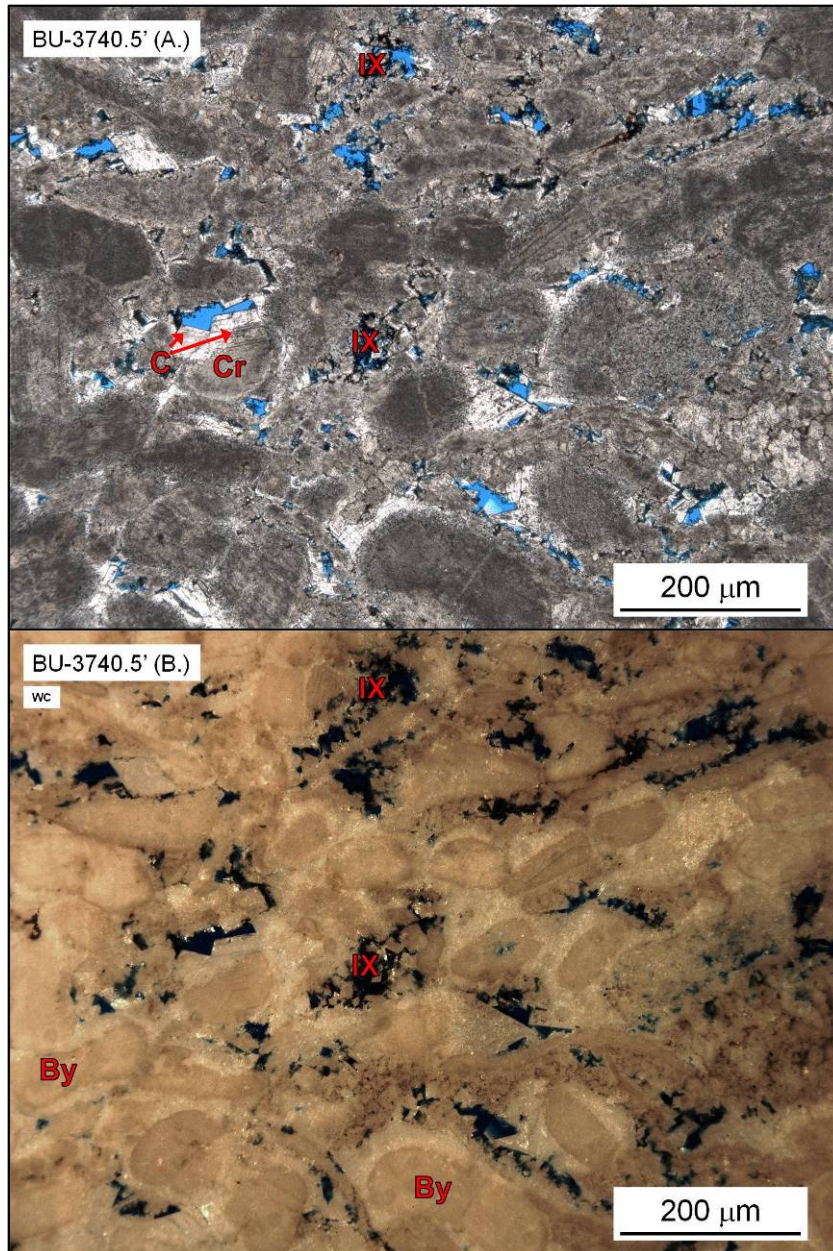




**BU – 3757.0' – Depositional fabric obscured by dolomitization. (A. and B.-XPL)**

Few identifiable grains show the primary fabric is likely brachiopod/pelecypod, crinoid wackestone/packstone. A prominent feature in the sample is a stylolite-bound dolomite vein that contains coarse (250 μm) crystals relative to surrounding matrix dolomite (50 - 100 μm). Minor porosity development is IX in matrix dolomite (<3%).

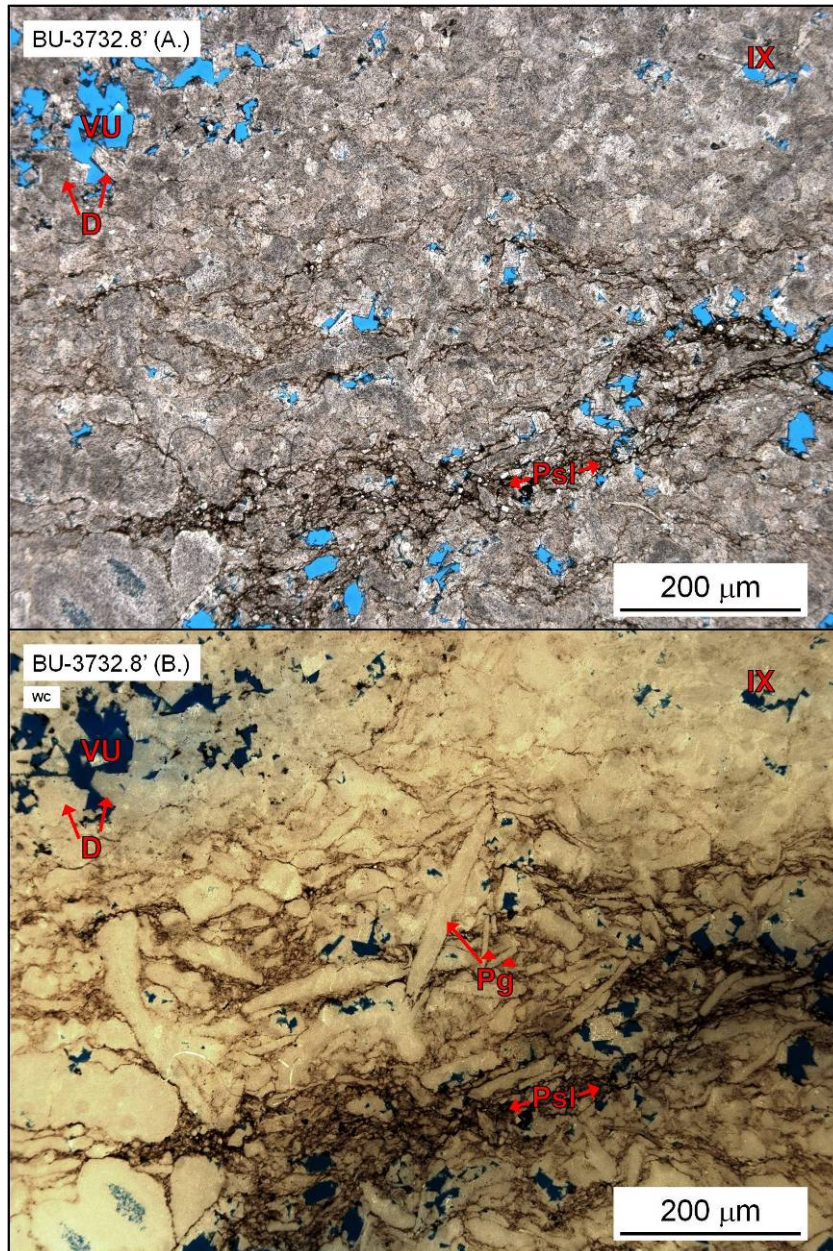




**BU – 3740.5' – Depositional fabric obscured by dolomitization. (A. and B.-WC)**

White card technique shows crinoid, bryozoan, brachiopod, wackestone/packstone (?). Grain components are relatively well preserved compared to matrix (?), which has been preferentially recrystallized developing porosity. Porosity is well developed as IX (IP) in matrix and minor WP (crinoid) (15-20%) with residual hydrocarbon partially occluding pore space.

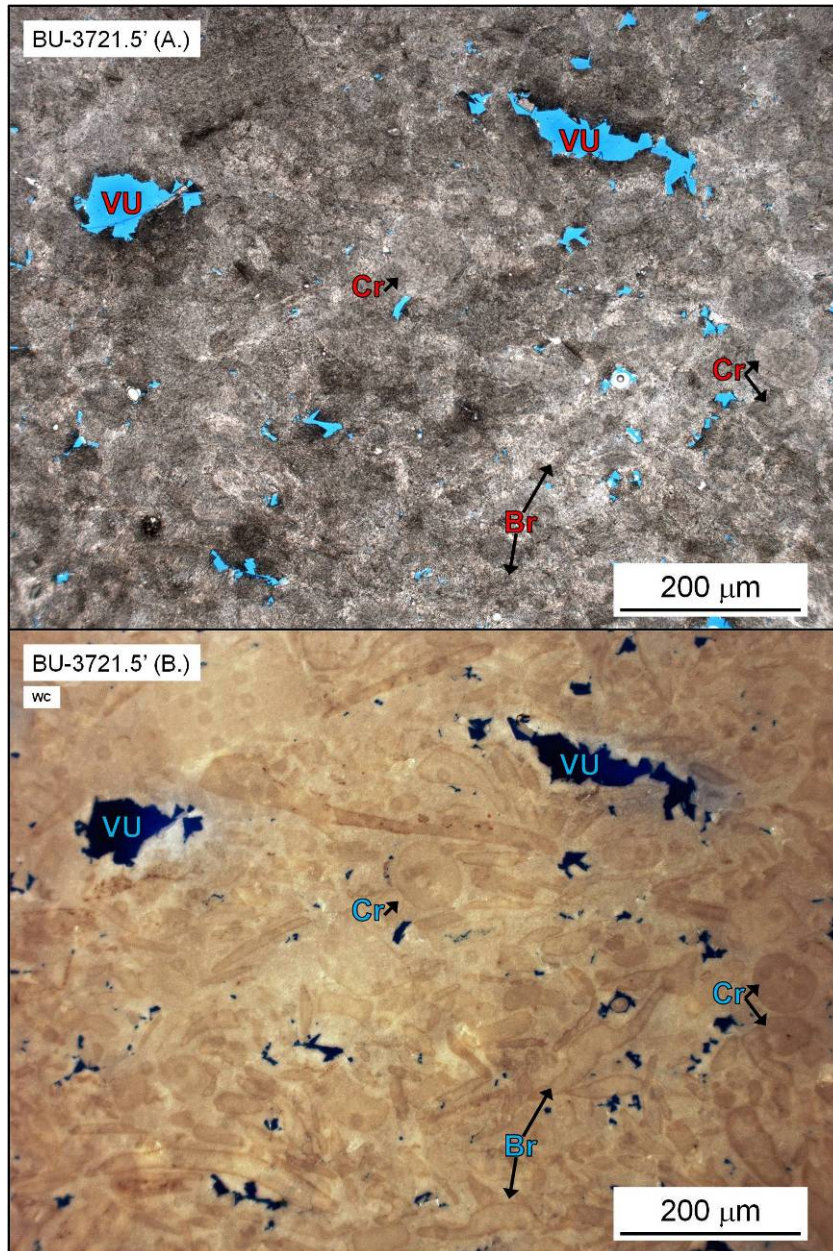




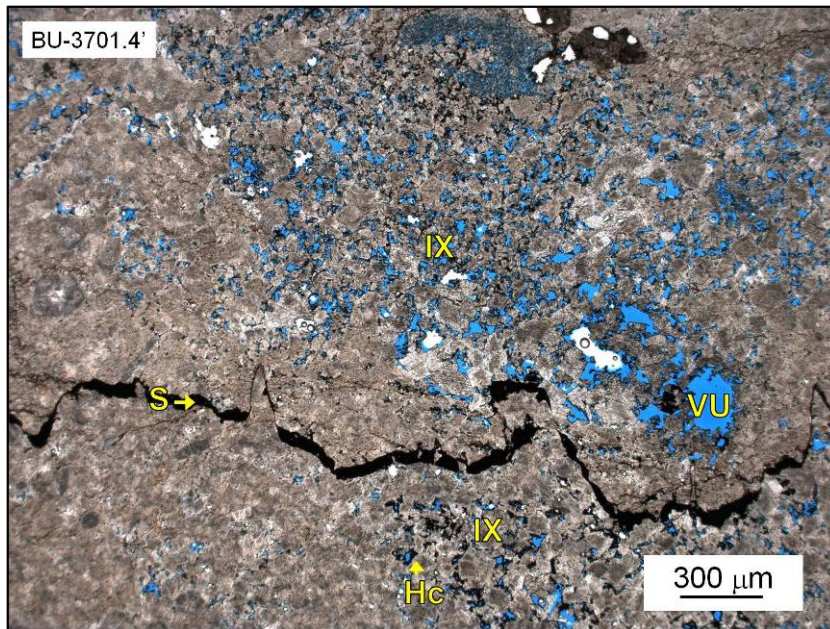
**BU – 3732.8' – Depositional fabric obscured by dolomitization. (A. and B.-WC)**

White card technique shows crinoid (40%), brachiopod (30%), bryozoan (30%), pelecypod, undifferentiated skeletal fragment packstone. Grains do not show a dominant orientation or sedimentary structures. Insoluble material is concentrated in pressure solution zones. Porosity is well developed as IX and VU in the sample (20%).



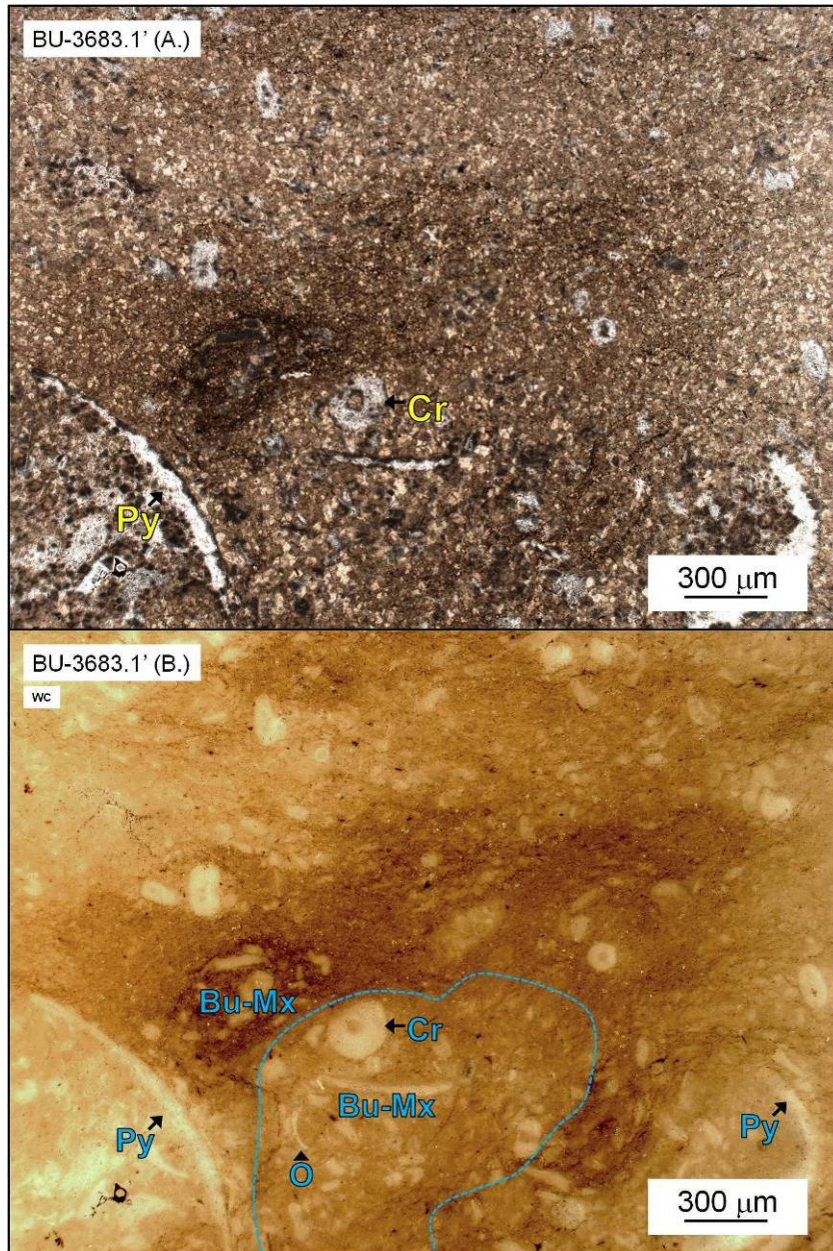


**BU – 3721.5' – Depositional fabric obscured by dolomitization and recrystallization. (A. and B.-WC)** White card technique shows brachiopod/pelecypod (40%), crinoid (20%), undifferentiated skeletal fragment, bryozoan grains in packstone/grainstone textures. Grains show no dominant orientation. Platy grains range from near complete, to fragmented and abraded. Porosity is IX and VU (5-8%), with saddle dolomite partially occluding VU porosity.



**BU – 3701.4' – Depositional fabric obscured by dolomitization and recrystallization.** Grains are obscured by recrystallization. Original texture was likely bioturbated peloid packstone-wackestone. Intercrystalline porosity is associated with burrows (35% in burrows, 9% total). Residual hydrocarbon (Hc) commonly occludes porosity.

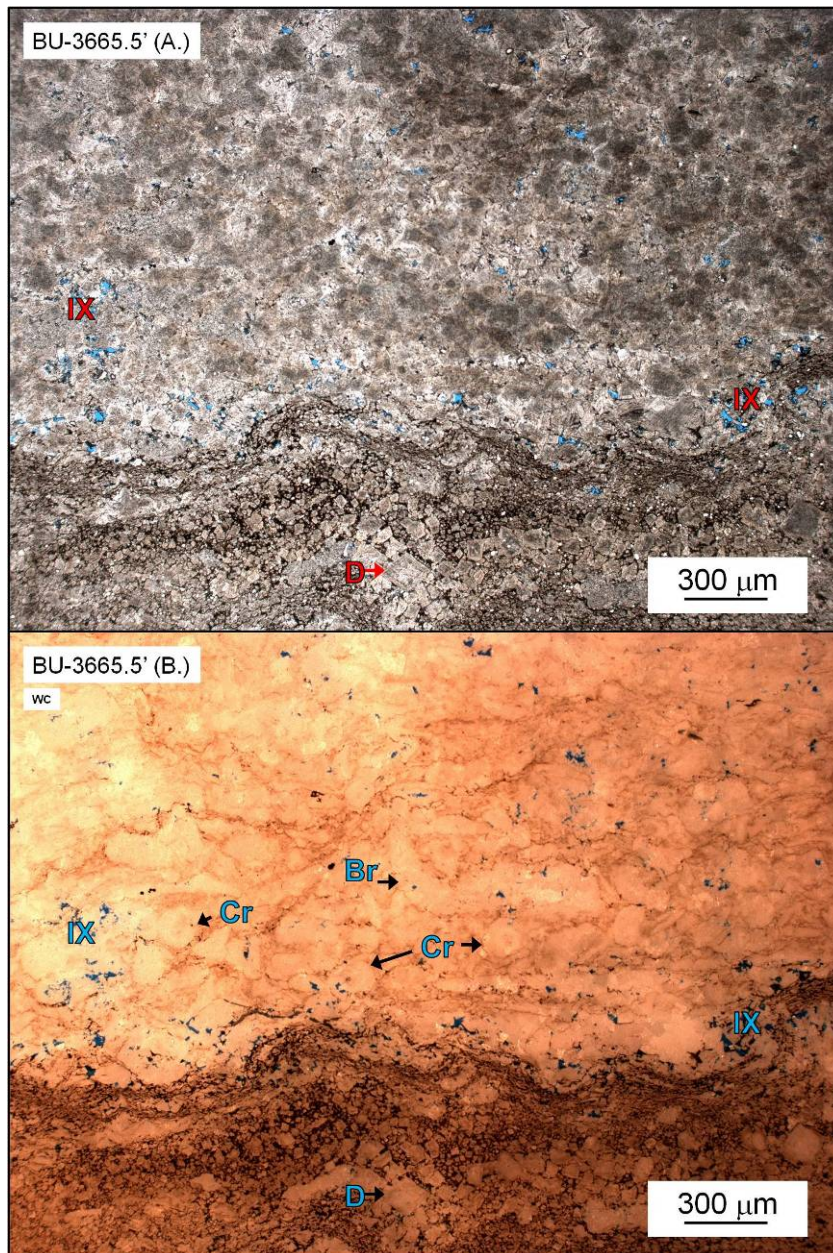




**BU – 3683.1' – Depositional fabric obscured by dolomitization. (A. and B.-WC)**

White card technique shows crinoid (50%), undifferentiated skeletal fragment (30%), brachiopod/pelecypod/ ostracode, trilobite wackestone with packstone-to-wackestone mud-grain mix burrow fill. Stylolites and insoluble seams distributed throughout. No visible porosity.





**BU – 3665.5' – Depositional fabric obscured by dolomitization.** White card technique shows crinoid (80%), undifferentiated skeletal fragment packstone (grainstone?) texture overlying a concentration of insoluble/seam with unidentifiable depositional fabric. The unidentifiable portion of the sample also contains a concentration of euhedral and sub-hedral dolomite crystals. Minor IX porosity is



developed, dominantly in the sample portion where grains are identifiable.

#### Additional thin section sample descriptions

**BU – 3897.1’ – Depositional fabric obscured by dolomitization.** Likely brachiopod/bivalve packstone-to-wackestone. Matrix is completely recrystallized and depositional texture is unidentifiable. Identifiable grains are pelecypod and brachiopod fragments (70%) with few crinoid and bryozoan fragments. Porosity is moderately developed as IX, WP, and VU (10-12%).

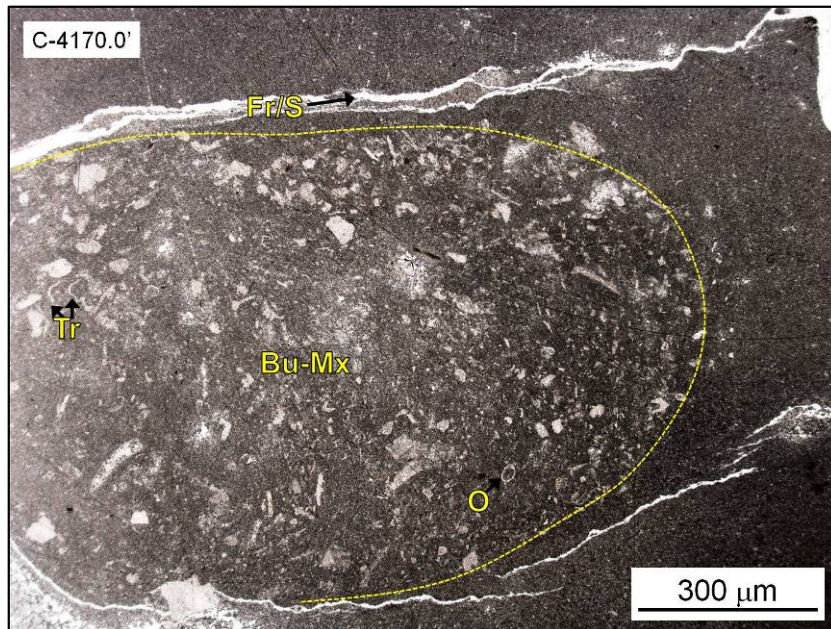
**BU – 3895.5’ – Depositional fabric obscured by dolomitization.** Few preserved skeletal fragments at the top of the sample indicate brachiopod wackestone (?), however matrix is unidentifiable. Porosity is well developed as IX throughout (10%), with zones/seams of residual hydrocarbon accumulations occluding IX porosity. A minor chert component is present in the sample (<3%).

**BU – 3802.3’ – Depositional fabric obscured by dolomitization.** White card technique shows brachiopod (30%), crinoid (25%), pelecypod, ostracode, undifferentiated skeletal fragment packstone. Larger platy skeletal fragments are near complete (halves) with a dominant horizontal grain orientation, constructing a lattice in which crinoid, ostracode, undifferentiated skeletal fragment packstone-to-wackestone fills interstitial spaces. Insoluble material (organic?) accumulates at grain contacts, likely as a result of pressure solution. Few well defined stylolites (n=4) occur throughout. Porosity is WP (MO/IX) and IX, totaling >5% of the gross sample.

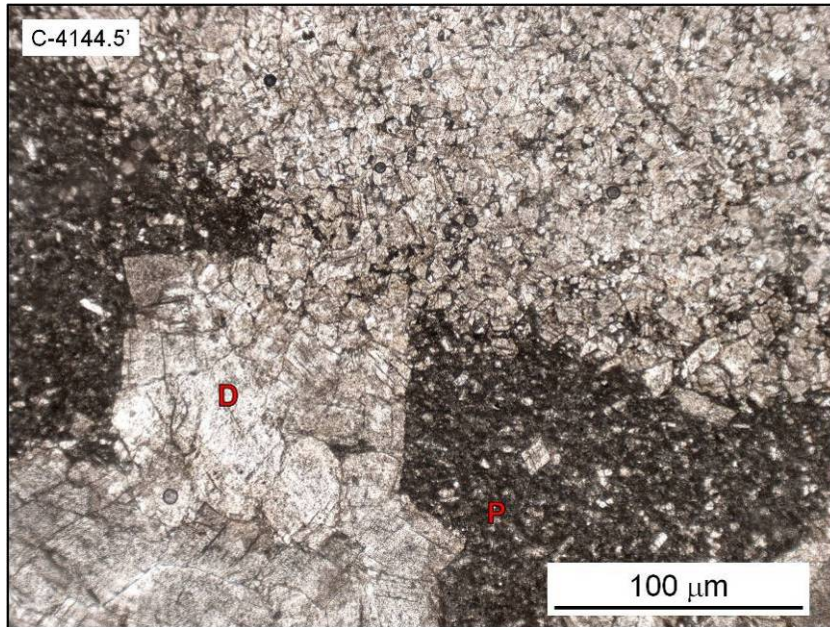
**BU – 3705.0’ – Depositional fabric obliterated by recrystallization.** Complete recrystallization. Dolomite crystals form interlocking mosaic with concentrations of insoluble material at crystal faces and face junctions. Crystal sizes range 88 – 125  $\mu\text{m}$ . No visible porosity.

Casler 5-30 – Whiting Oil and Gas Company

Permit #36587, Jackson County, MI

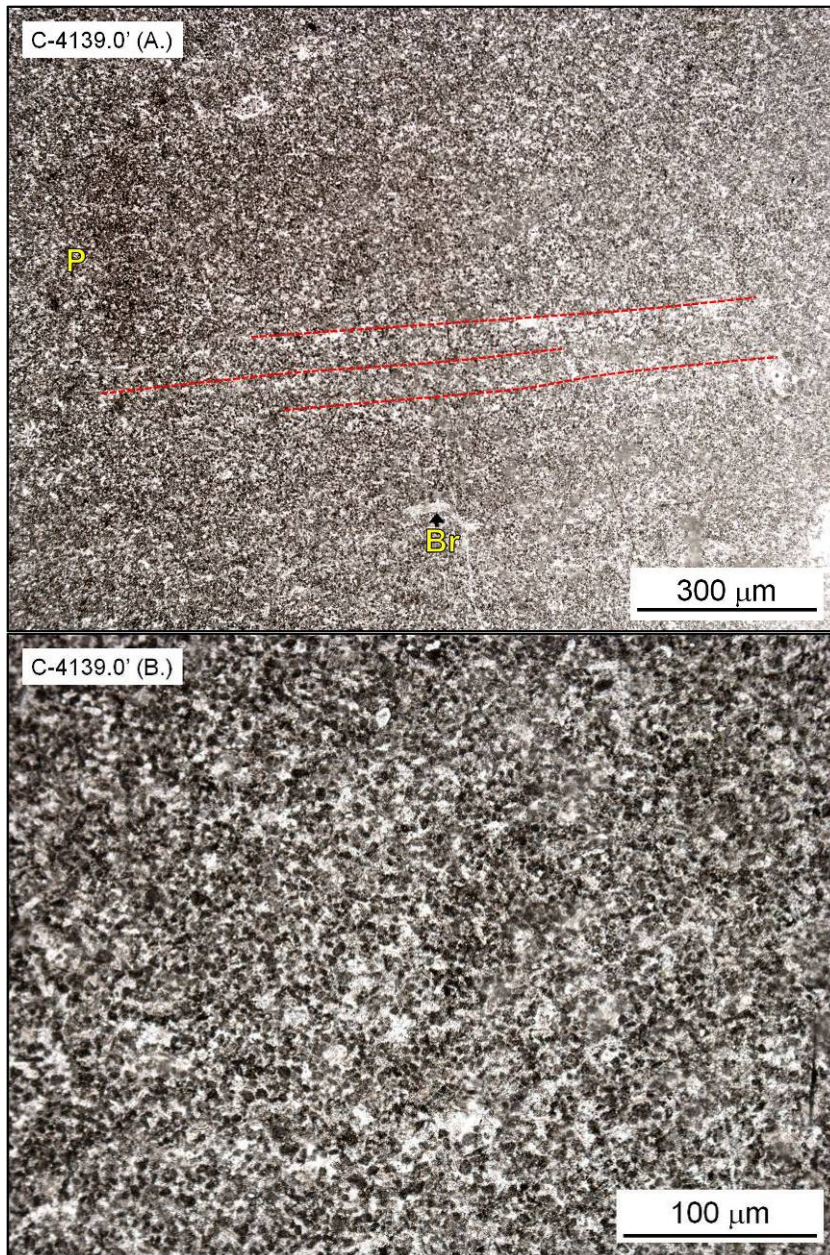


**C - 4170.0' - Mudstone with skeletal wackestone burrow fill.** Mudstone containing >5% ostracode and brachiopod skeletal fragments, with brachiopod, ostracode, crinoid, trilobite wackestone-to-mud-rich packstone burrow fill. Wispy occur throughout sample. Porosity consists of sub-horizontal FR, which sometimes are associated with stylolites (<5%).



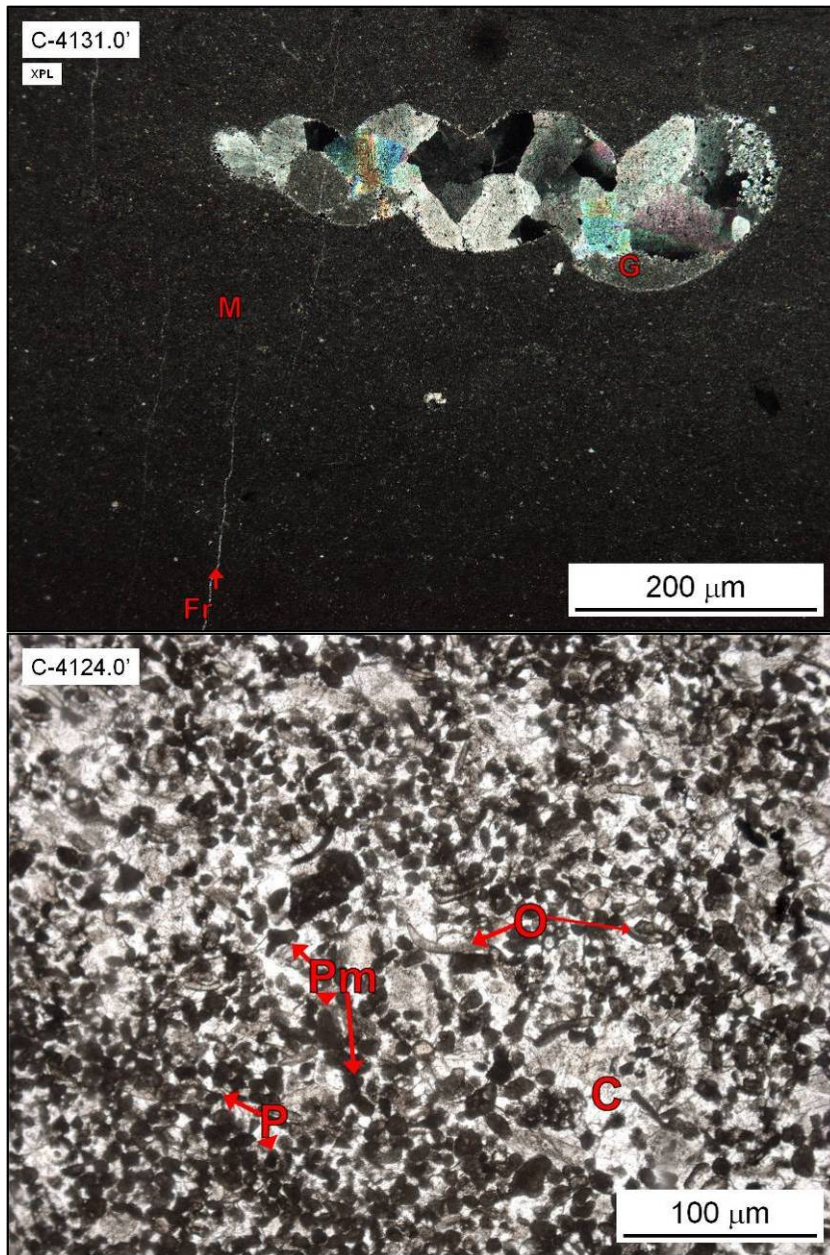
**C – 4144.5' – Peloidal, skeletal packstone.** Peloid (90%), brachiopod, pelecypod, crinoid mud-rich packstone with fine ( $\sim 15\ \mu\text{m}$ ) dolomite crystals replacing burrow sediments. Fine ( $15\ \mu\text{m}$ ) euhedral dolomite rhombs are distributed throughout sample, replacing peloidal matrix. Additional replacement by saddle dolomite is more localized into discrete zones, showing no dominant location of occurrence related to depositional fabric.





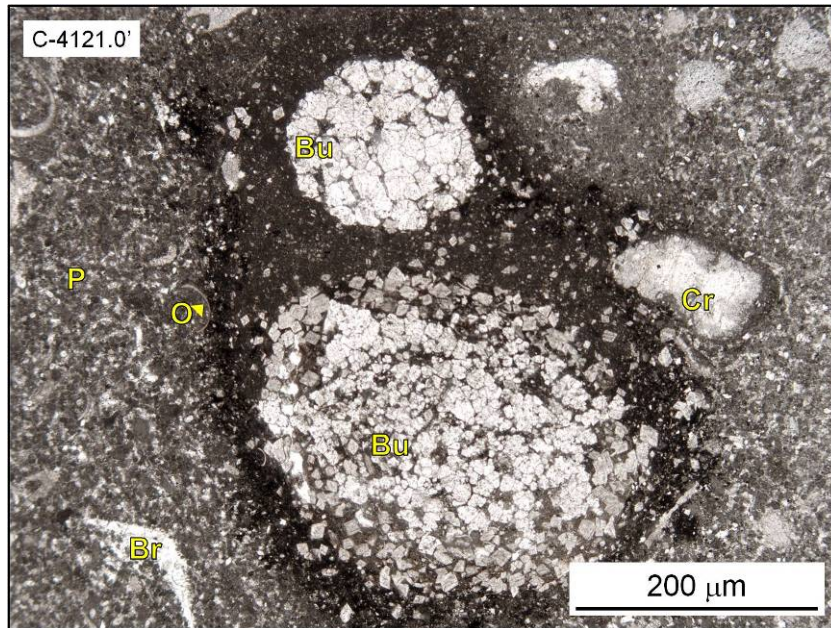
**C – 4139.0' – Peloidal grainstone-to-mud lean packstone. (A. and B.) Peloid (90%), ostracode, crinoid, brachiopod grainstone-to-mud-lean packstone with faint sediment laminations (dashed red lines). Included in the sample is a low-amplitude suture-stylolite. Porosity is minor FR and IX associated with stylolites and dolomite rhombs at pressure solution accumulations.**





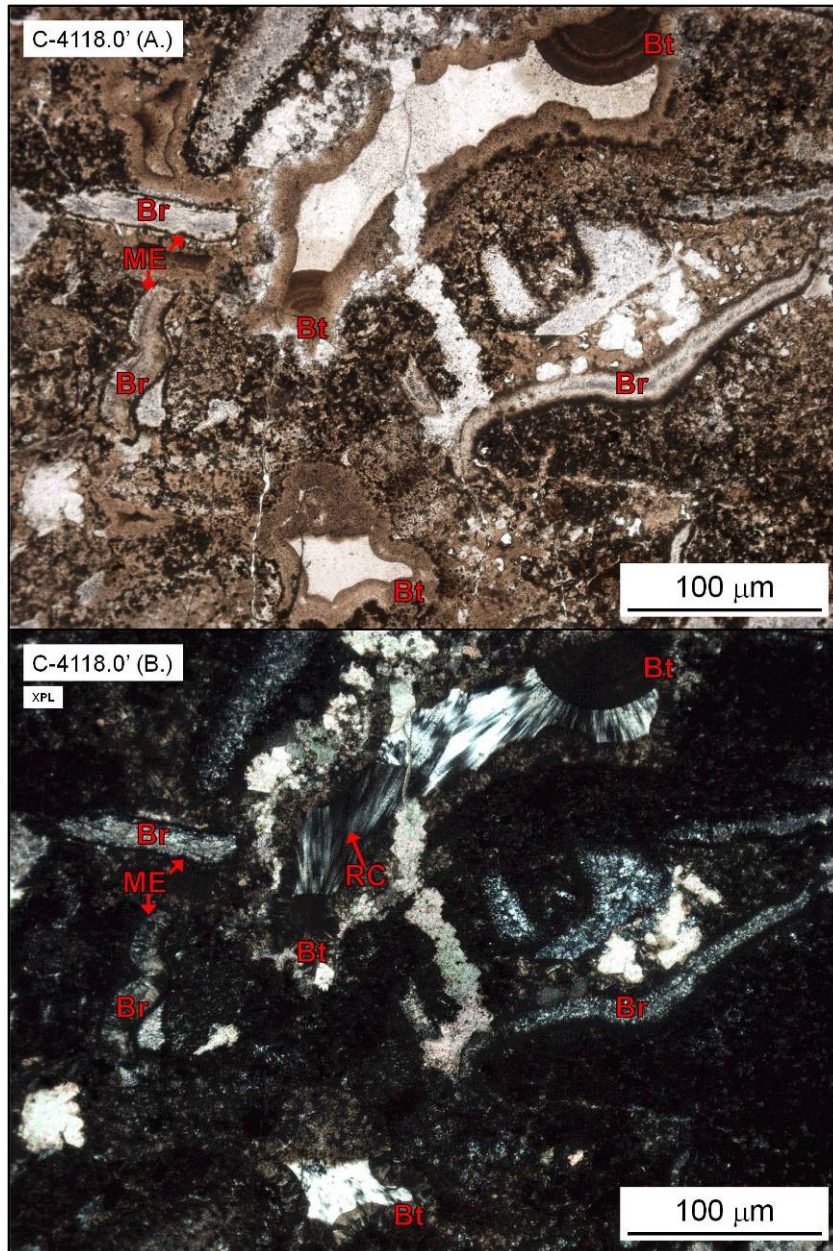
**C – 4131.0’ – Mudstone.** Mudstone with fine crystalline dolomite (15 – 30 μm) filling burrows. The single skeletal grain included in the sample is a complete gastropod fragment with geopetal structure, all replaced by crystalline dolomite. No visual porosity. **C – 4124.0’ – Peloidal grainstone.** Peloidal (80%), pelecypod, crinoid, brachiopod, grainstone with blocky (sometimes poikilotopic) calcite cement filling interstitial

grain space. The majority of identifiable skeletal fragments are fragmented and micritized. Porosity is very minor WP (<2%).

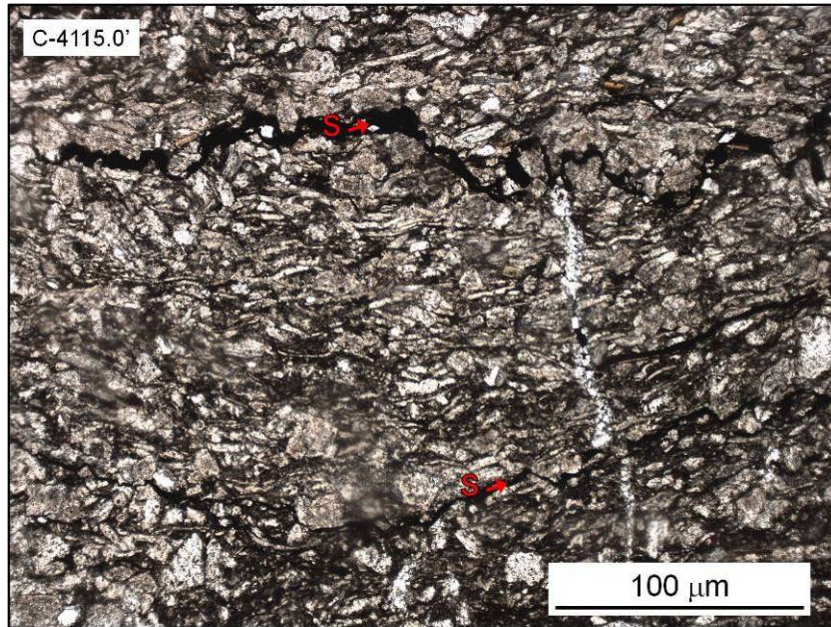


**C – 4121.0' – Peloidal packstone with dolomite replaced burrows.** Peloidal (65%), ostracode (25%), pelecypod, brachiopod, bryozoan, crinoid packstone, with replacement of burrow sediments by crystalline dolomite (25 - 40 μm). Porosity is FR and IX (dolomite), totaling >3% of the sample.



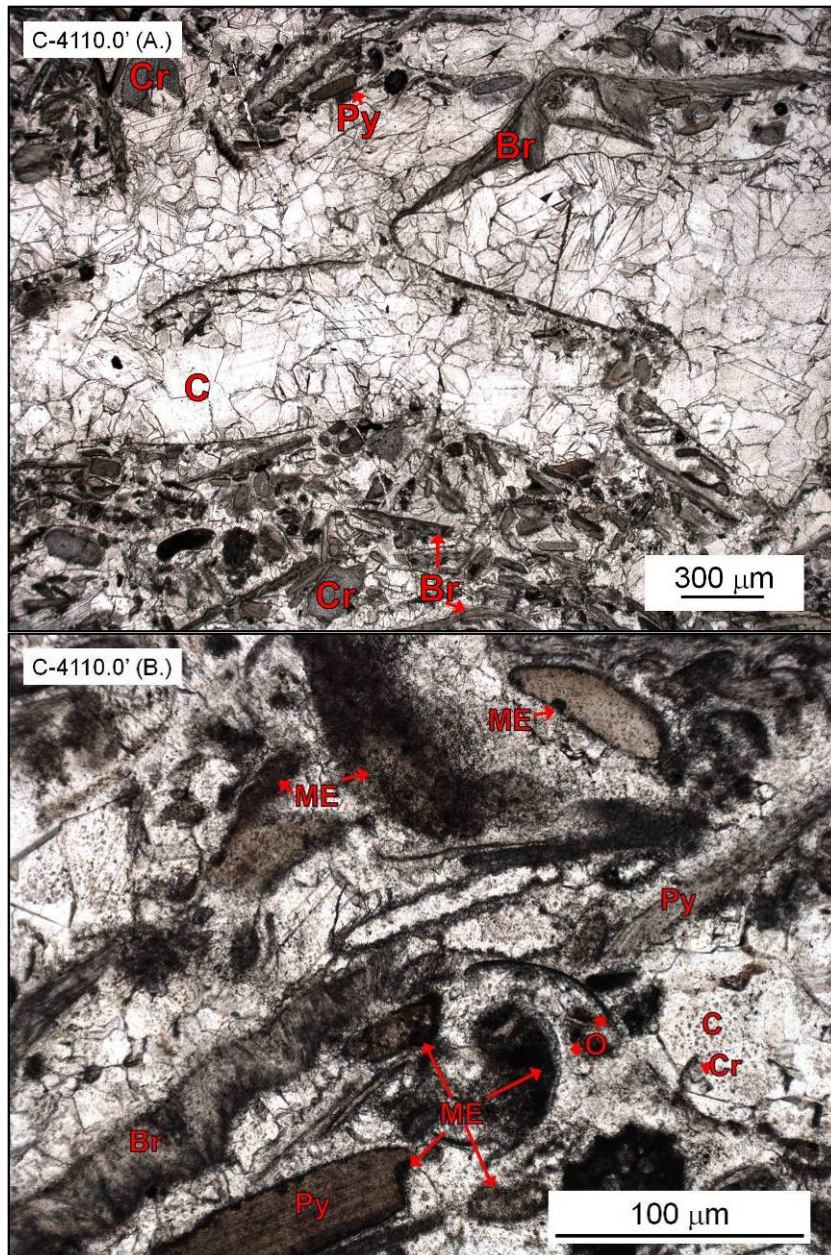


**C – 4118.0' – Peloidal, skeletal packstone with botryoidal cement. (A. and B.-XPL) Peloid (65%), brachiopod (15%), crinoid (10%), bryozoan, ostracode packstone-to-grainstone with botryoidal (Bt) and radial (RC) (calcite replacement of aragonite?) cement filling pores in the center of the sample. Skeletal grains are a composed of a combination of near complete skeletal fragments (half of platy skeletons) and highly fragmented and abraded grains. No visible porosity.**



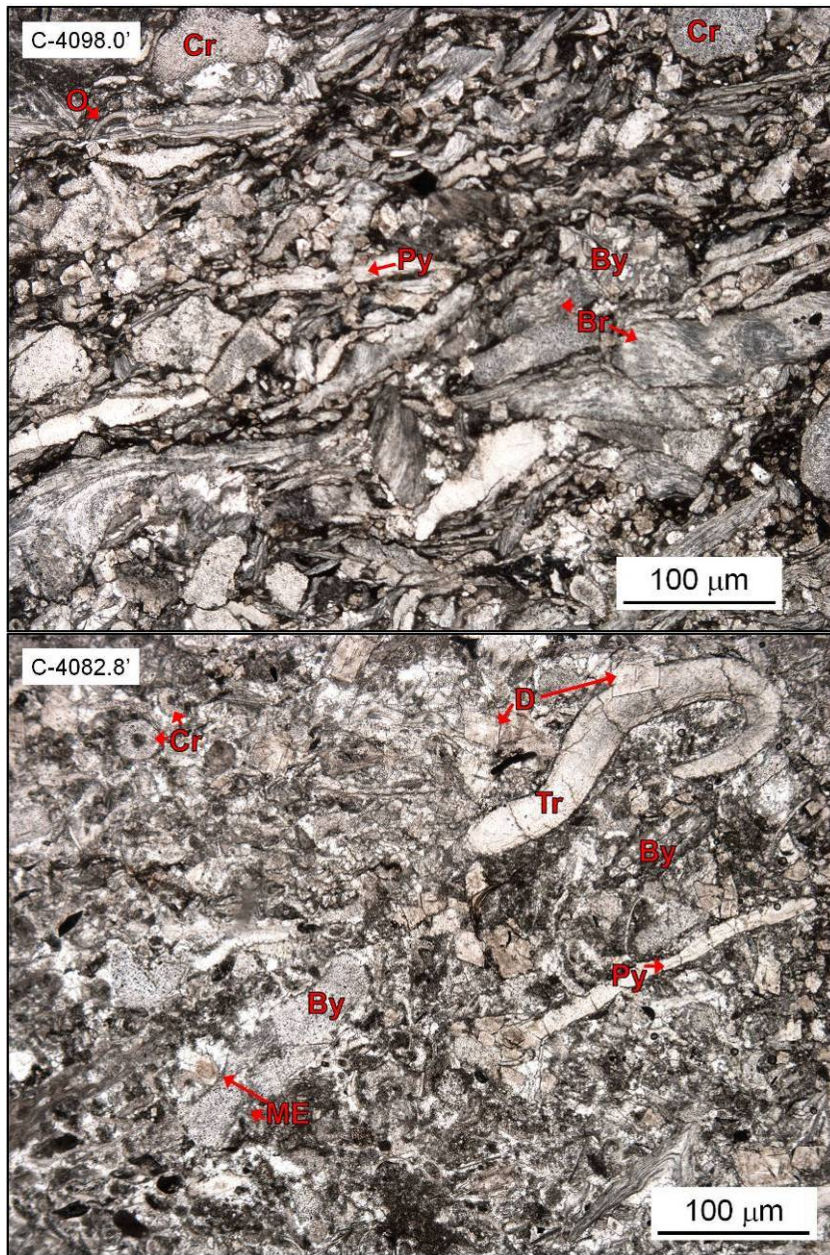
**C – 4115.0' – Skeletal packstone-to-grainstone.** Brachiopod (35%), pelecypod (30%), ostracode (20%), crinoid undifferentiated skeletal fragment packstone-to-grainstone. Grains are dominantly fragmented and abraded. Grains show various degrees of micritization. No visible porosity.





**C – 4110.0’ – Skeletal grainstone-to-packstone. (A. and B.)** Brachiopod (35%), pelecypod (30%), crinoid, trilobite, bryozoan, undifferentiated skeletal fragment grainstone-to-packstone with abundant (30% of sample) twinned blocky calcite cement. Grains are dominantly fragmented and abraded. Grains show various degrees of micritization, from surface envelopes and micrite filled borings, to complete obliteration of internal structure. No visible porosity.





**C – 4098.0' – Skeletal packstone to grainstone.** Brachiopod (20%), pelecypod (20%), ostracode (20%), crinoid (15%), trilobite, bryozoan, peloid undifferentiated skeletal fragment packstone-grainstone. Grains are dominantly fragmented and abraded. Platy grains show sub-horizontal orientation of elongate axis. No visible porosity. **C – 4082.8' – Skeletal packstone to grainstone.** Brachiopod (20%), pelecypod (20%), crinoid (15%), bryozoan (10%), trilobite, ostracode, undifferentiated skeletal

fragment packstone-grainstone. Grains are a mix of un-abraded and fragmented/abraded bioclasts. Stylolites and accumulations of non-soluble material at pressure solution zones are common. Minor FR porosity is associated with stylolites (< 3%). Dolomite crystal overgrowths in bioclasts are common.

#### Additional thin section sample descriptions

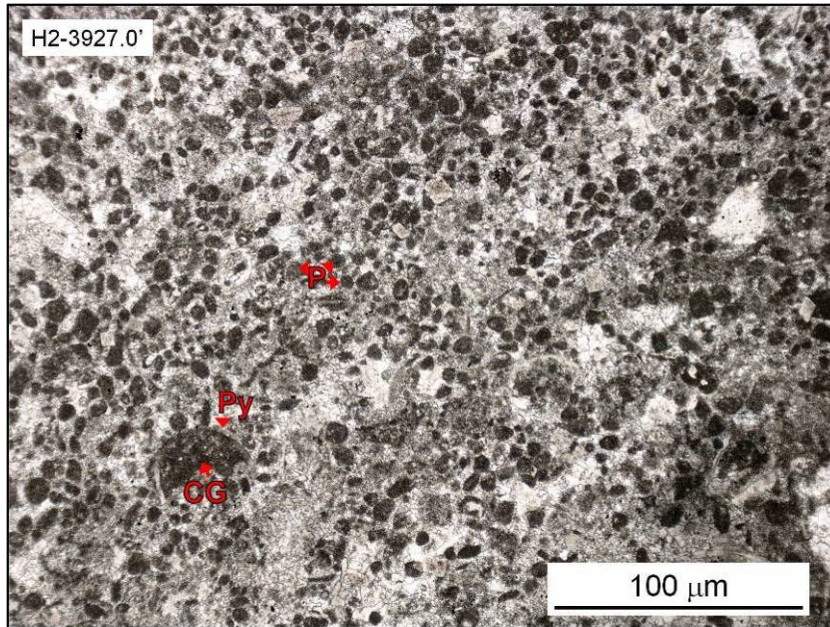
**C – 4164.5’ – Wackestone-to-mud-lean packstone.** Grains include brachiopod (30%), crinoid (30%), ostracode (10%), pelecypod, bryozoan, and gastropod fragments. The upper portion of the sample is mud dominated as the lower portions; however the upper portion is lighter in color, likely reflecting higher degree of oxidization. Grains are dominantly chaotically oriented with a zone of grain concentration/winnowing of mud at the contact between lighter and darker mud deposits. Porosity is FR associated with stylolite partings (<4%).

**C – 4156.0’ – Mudstone with skeletal wackestone pockets.** Dominantly mudstone with euhedral-to sub-hedral dolomite rhombs throughout, with large portions of the sample dominated by dolomite rhombs. Included are laterally discontinuous crinoid (60%), pelecypod, ostracode wackestone pockets (<0.3 mm thick, 2.0 mm horizontally). Porosity is minor FR (<4%).

**C – 4148.5’ – Mixed skeletal wackestone.** Crinoid, pelecypod, brachiopod wackestone with low-amplitude suture stylolites throughout. Porosity consists of dominantly sub-vertically oriented FR (5%).

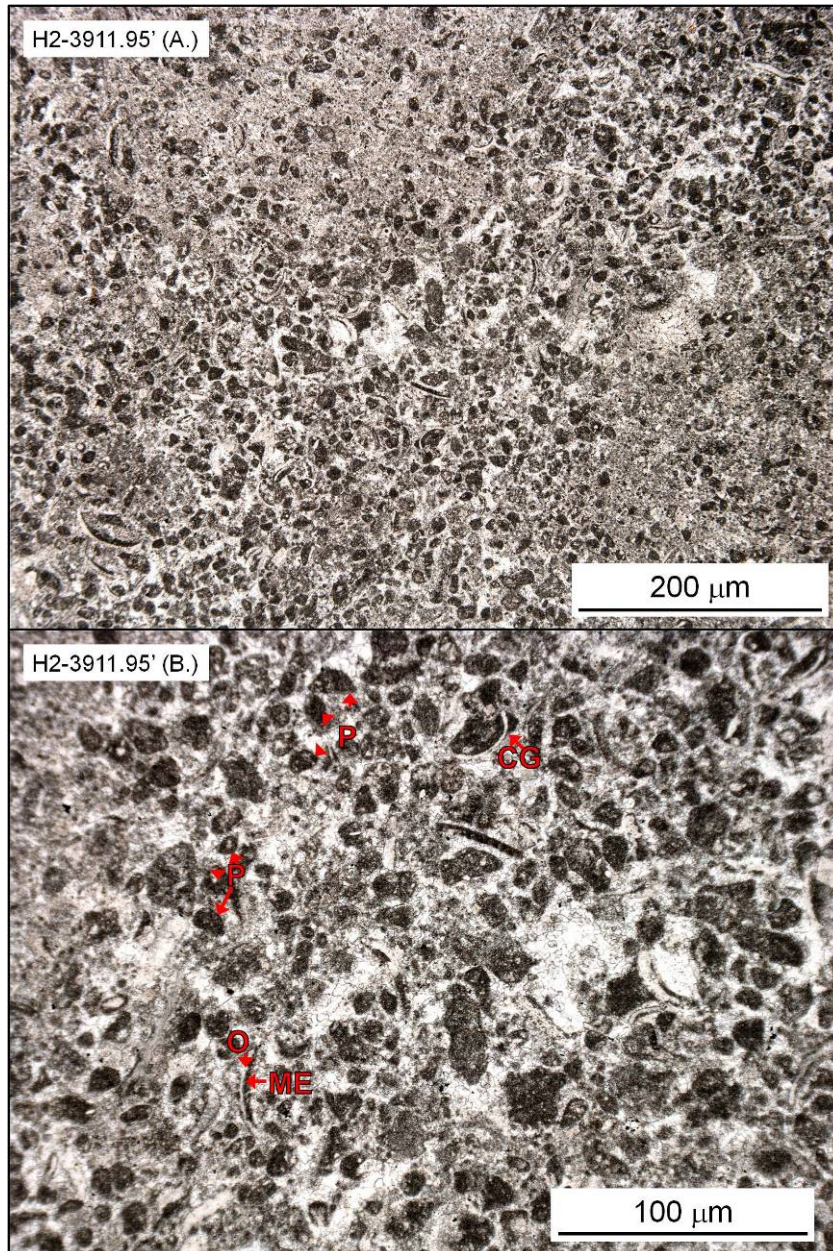
**C – 4087.0’ – Depositional fabric obscured by dolomitization.** Primary fabric likely brachiopod, crinoid, bryozoan, pelecypod packstone. Porosity is FR associated with partings at pressure solution seams.

Hergert 2 – McClure Oil Company  
Permit #22196, Hillsdale County, MI



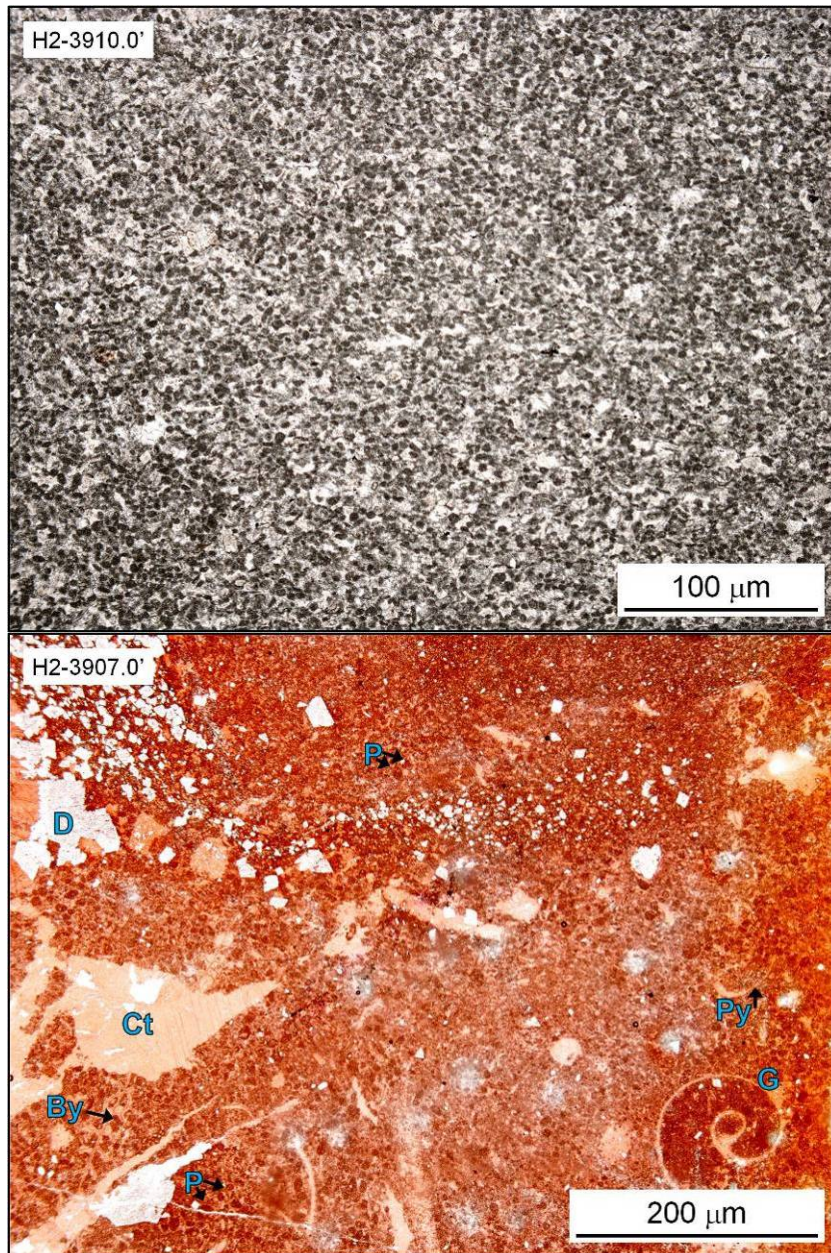
**H2 – 3927.0' – Peloidal packstone.** Peloid (80%), pelecypod/brachiopod, crinoid, ostracode, bryozoan packstone-to-grainstone. Grain micritization is a continuum from none, to total, with a dominant number totally micritized to peloids. No visual porosity.





**H2 – 3911.95' – Peloid intraclast packstone-to-grainstone. (A. and B.)** Peloid (75%), ostracode (10%), bryozoan, brachiopod, intraclast (CG) packstone-to-grainstone. Intraclast grains are commonly composed of one/two skeletal fragments and micrite (wackestone texture?) and are commonly rounded and sub-spherical. Identifiable skeletal grains show various degrees of micritization. Grain interstitial voids are filled with blocky calcite cement. No visible porosity.





**H2 – 3910.0’ – Peloid packstone-to-grainstone.** Peloids constitute nearly the entire sample’s grain component, with few ostracode fragments (<5%). Distributed throughout are euhedral dolomite rhombs (10 – 15 μm), composing 10% of the total sample. The sample contains few (n=6) calcite filled fractures/veins and low-amplitude suture-stylolites with accumulations of euhedral dolomite rhombs. No visual porosity. **H2 – 3907.0’ – Peloid, skeletal packstone.** Peloid (70%), ostracode (10%),

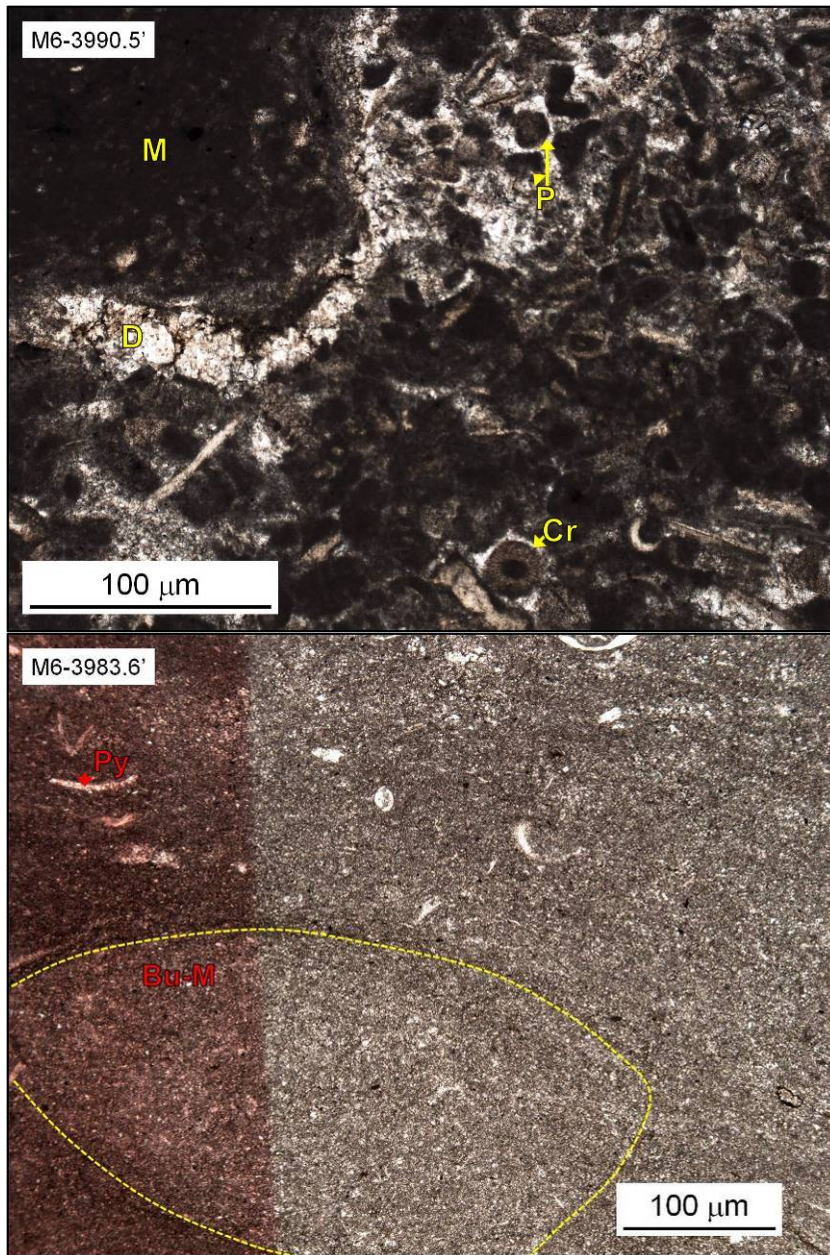
bryozoan, pelecypod, gastropod, crinoid packstone-to-grainstone with replacement of peloid matrix by euhedral dolomite rhombs (5 – 30  $\mu\text{m}$ ) and chert replacement. Dolomite rhombs concentrate at pressure solution seams. Included in the sample are a dolomite filled microfractures. No visible porosity. Red color of sample is staining by alizarin-red.

#### Additional thin section sample descriptions

**H2 – 3922.0' – Peloid, skeletal packstone.** Peloid (30%), crinoid (25%), ostracode (20%), pelecypod, brachiopod, trilobite, bryozoan mud-rich packstone-to-wackestone. Few identifiable skeletal grains (<10%) are micritized. Distributed throughout are euhedral dolomite rhombs (10 – 15  $\mu\text{m}$ ), which are accumulated at stylolites/pressure solution seams (<10% of sample). Porosity is FR and micro-WP (3%).

Mann, H 6 – Ohio Oil Company  
Permit #22381, Hillsdale County, MI

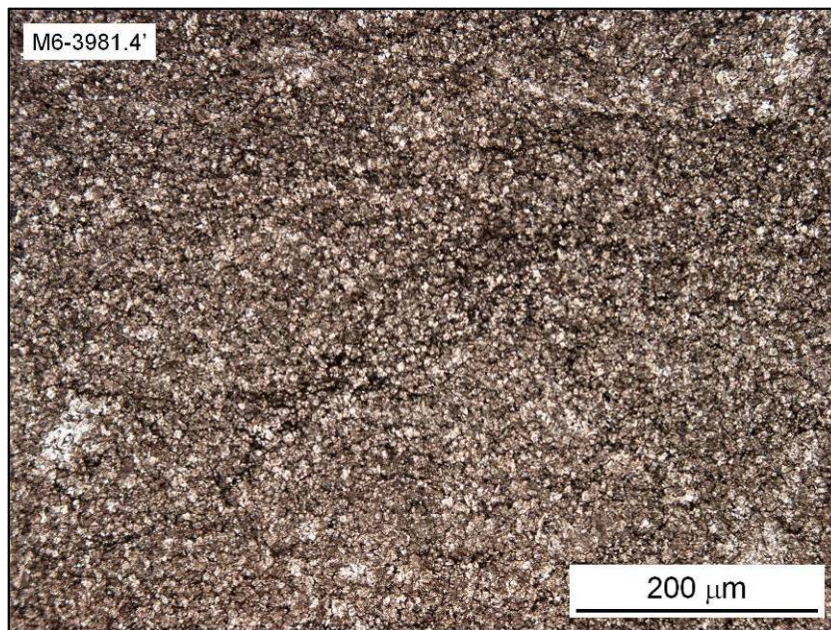




**M6 – 3990.5' – Peloid and micritized skeletal packstone.** Peloid (70%), crinoid, ostracode, brachiopod, intraclast, packstone-to-grainstone, with blocky calcite cement. Identifiable skeletal grains are heavily micritized, resulting in all grains altered to some degree. The sample is separated into the upper portions of fine silt-sized peloid packstone (likely pellet origin) and lower section of coarse silt-to-fine sand peloid (likely micritized bioclasts) by a prominent stylolite. The prominent stylolite is

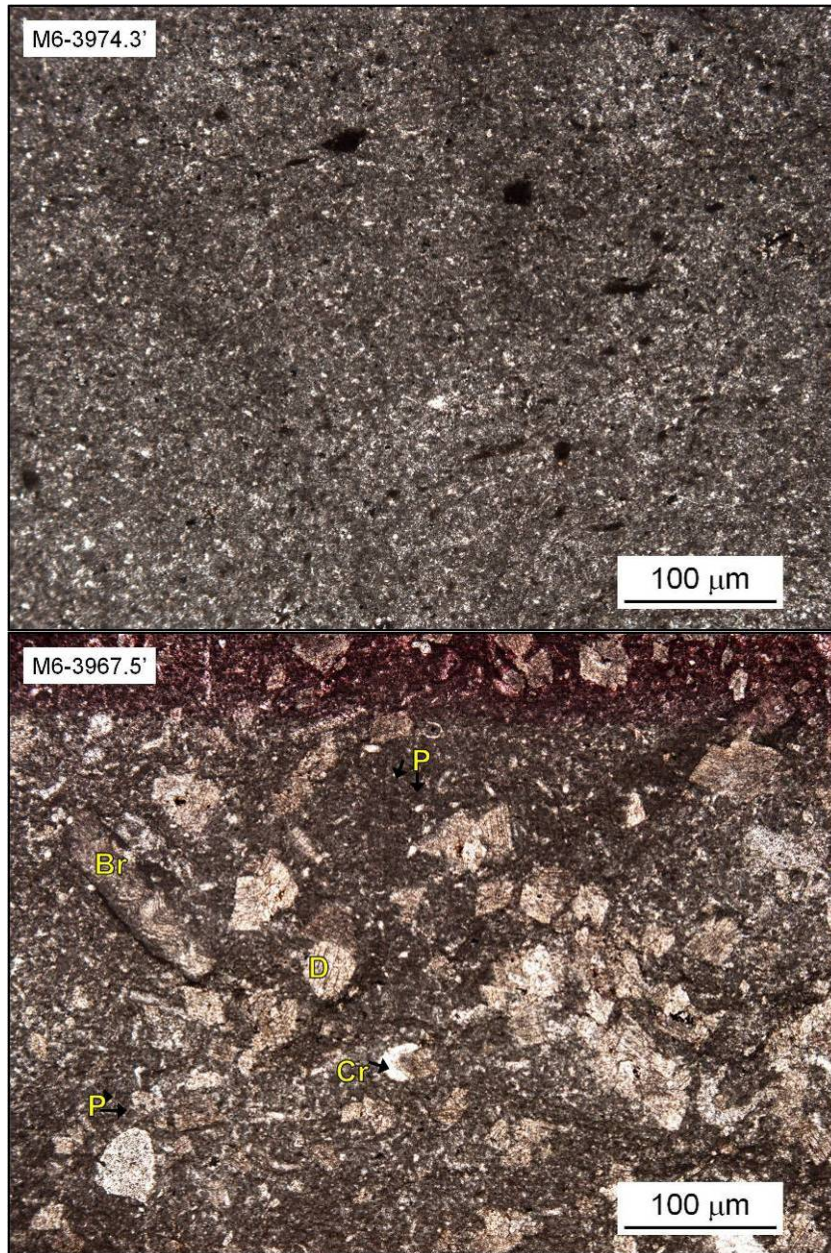
also a zone of stylocumulate euhedral dolomite rhombs (20  $\mu\text{m}$ ). Few (n=2) vertically oriented micro-fractures are filled with crystalline calcite. Porosity is IX (n=2, <1%).

**M6 – 3983.6' – Depositional fabric partially obscured by dolomitization. Likely peloid and micritized skeletal wackestone.** Original depositional fabric likely is a peloid (70%), crinoid, pelecypod, ostracode wackestone packstone. Stylolites commonly follow burrow boundaries (BSN-fabric). Red coloration is alizarin-red stain.



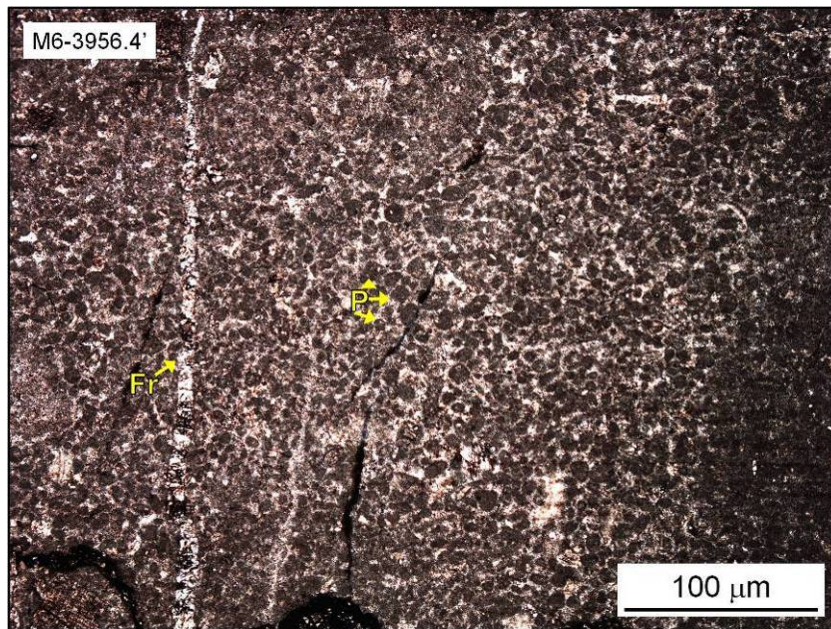
**M6 – 3981.4' – Primary fabric is obscured by dolomitization and recrystallization.** Primary fabric is likely wackestone, with faint recognizable pelecypod/brachiopod, and ostracode fragments. Dolomite crystals are interlocking and sub-hedral (5 – 15  $\mu\text{m}$ ). Porosity is a single MO (<1%).





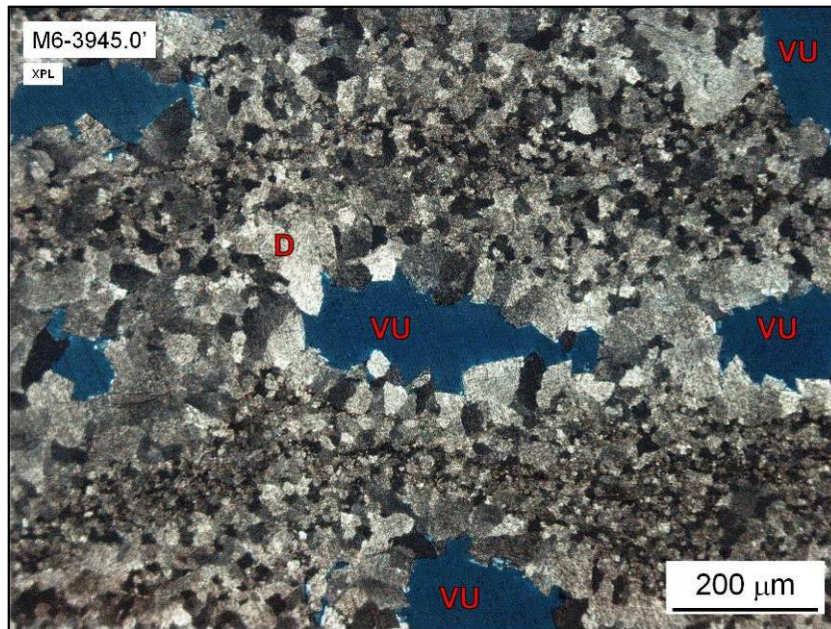
**M6 – 3974.3' – Peloidal wackestone-to-packstone.** Peloids likely did not act as grains resulting in muddy texture. Wispy stylolites are distributed throughout. Reddish-brown opaque mineral, commonly round and sub-horizontally oriented elongate ellipsoidal are also distributed throughout the sample (<10%). No visible porosity.

**M6 – 3967.5’ – Peloidal packstone.** Grains include peloids (75%), and fragments of crinoid, ostracode, and brachiopod bioclasts. Depositional texture is replaced (35%) by fine silt, to fine sand-sized euhedral dolomite rhombs, dominantly recrystallizing the peloid matrix. Grains and dolomite rhombs show no dominant orientation or structural organization. Red coloration is alizarin-red stain.



**M6 – 3956.4’ – Peloidal grainstone-to-packstone and ostracode wackestone.** Ostracode wackestone grading up-to peloid grainstone-to-mud-rich packstone. Peloid grains range fine-to-coarse silt-sized, showing no dominant grain orientation. Sub-vertical dolomite filled micro-fractures and euhedral dolomite rhombs (10 μm) are distributed throughout. Minor FR porosity occurs where complete mineral fill has not occurred (<3%).





**M6 – 3945.0’ – Primary fabric is obscured by dolomitization and recrystallization.** Complete recrystallization. Matrix dolomite crystals size ranges 15 – 30 μm, with very little IX porosity (<3%). Larger VU and ZVU pores (commonly 0.1 x 0.2 mm, horizontal elongate) are lined by coarse saddle dolomite (up to 150 μm in size). Total porosity is 10%.

Additional thin section sample descriptions

**M6 – 3998.3’ – Tabulate coral framestone.** Tabulate coral framestone (longitudinal section, *favosities* sp.?) in wackestone/packstone matrix (~floatstone). Coral cavities have been filled by calcite cement and tabulae are replaced by crystalline dolomite. Very minor WP porosity is developed in coral (<1%).

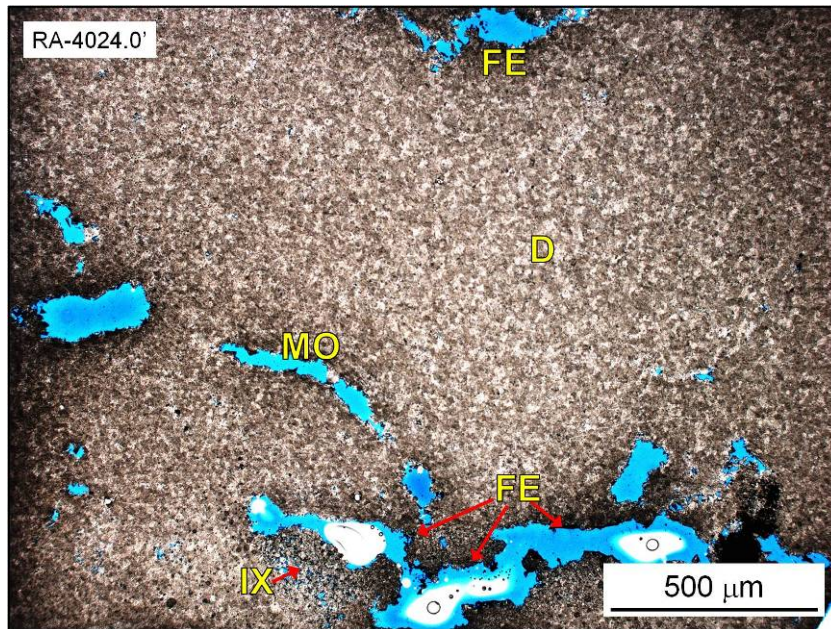
**M6 – 3987.5’ – Moderately bioturbated packstone-to-wackestone.** Primary fabric is obscured by dolomitization and recrystallization. Original texture is likely packstone-to-wackestone, with moderate bioturbation (0.2 – 1.0 mm). Matrix replacing dolomite crystal size ranges 8 -15 μm in size, with associated moderate development of IX porosity (5-6%). Burrow replacing dolomite crystals are coarse (50 – 125 μm) and interlocking (saddle), commonly surrounded at fringe by insoluble material, resulting in burrow-bounding stylonodular fabric. The dolomite crystal textures shows pore network inversion from original low porosity/ permeability matrix and relatively higher porosity/permeability burrow fill, and likely is the result of multiple dolomitization episodes.

**M6 – 3985.4’ – Primary fabric is obscured by dolomitization and recrystallization.** Likely sparse-moderately bioturbated wackestone-to-packstone with grain-dominated burrow fills. Burrow replacing dolomite is finely crystalline (8 – 15  $\mu\text{m}$ ), with moderate development of IX porosity (8 – 10% of burrow area) and occlusion of porosity by insoluble material/residual hydrocarbon. Matrix replacing dolomite crystals are relatively coarser than burrow replacing crystals (25  $\mu\text{m}$ ) and interlocking with very little IX porosity (<1%). Sub-vertical fractures are dominantly filled with crystalline dolomite, with little IX porosity in filling mineralization (>2%). Total porosity is ~5%.

Rowe A-2 – McClure Oil Company

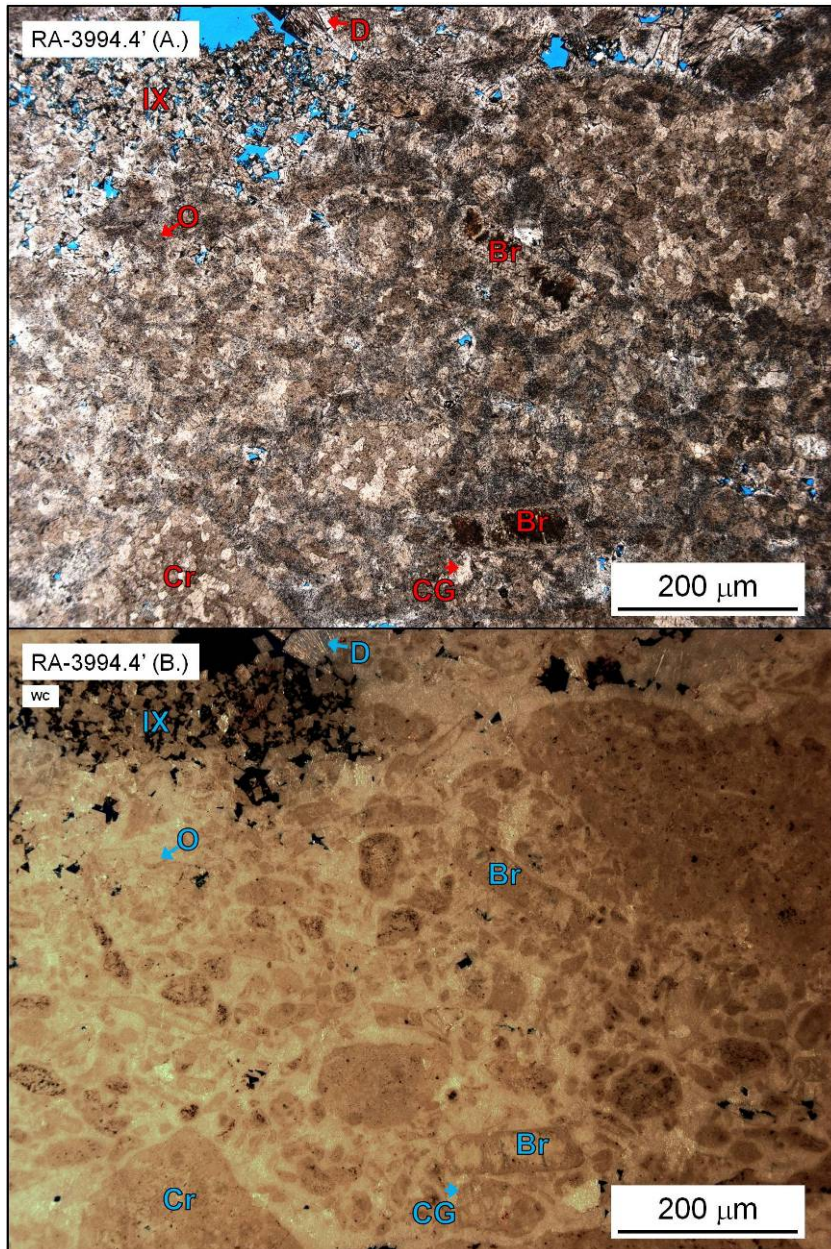
Permit #37239, Hillsdale County, MI





**RA – 4024.0' – Primary fabric obscured by dolomitization and recrystallization.**

Total recrystallization of depositional texture, however peloid ghosts suggest a peloidal packstone/grainstone. Few (n=3) platy skeletal fragment molds (brachiopod/pelecypod) show a bioclastic component to grains. In addition to MO and minor IX, solution enhanced FE and horizontal elongate (bird's eye geometry) pores are distributed throughout (totaling 9%). Saddle dolomite lines and partially occludes larger pores. Included in the sample are few (n=2) micro-fractures filled with crystalline dolomite.

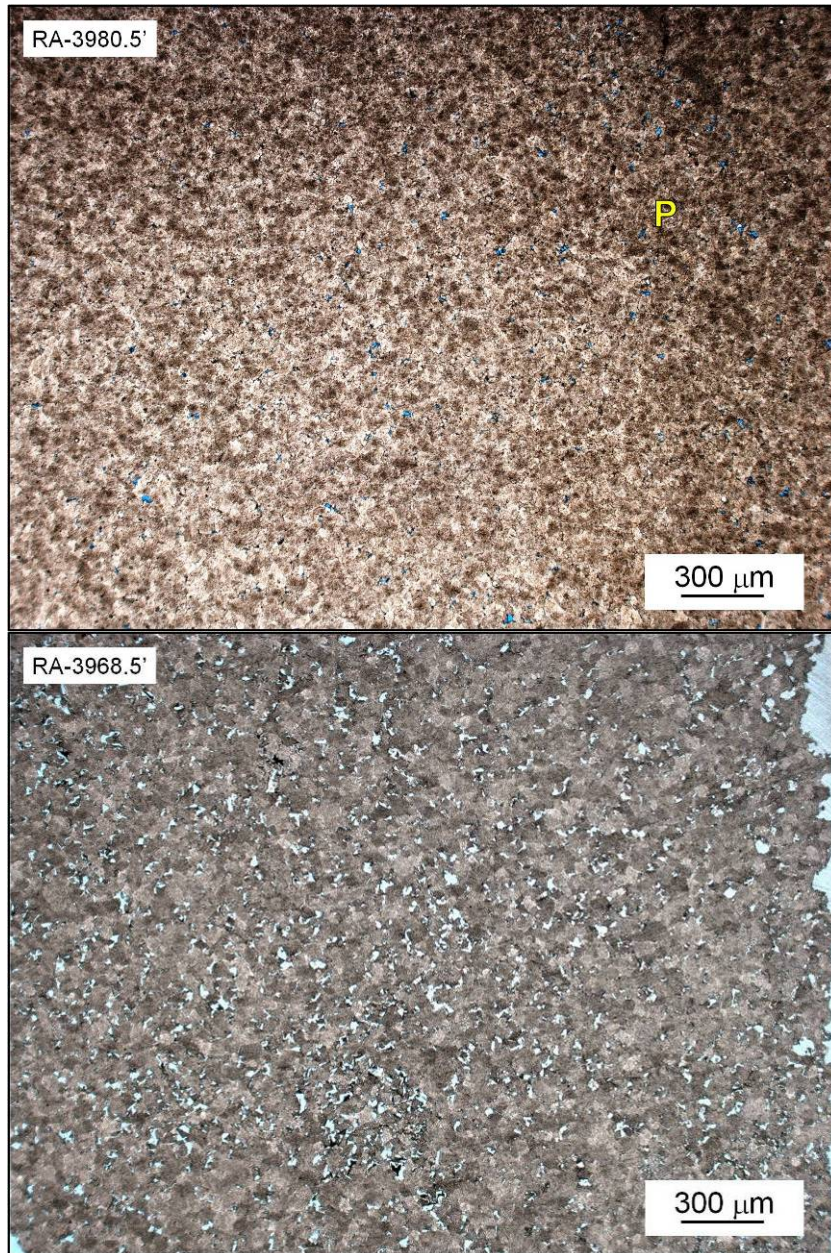


**RA – 3994.0' – Primary fabric obscured by dolomitization. (A. and B.-WC)**

White card technique shows crinoid (40%), undifferentiated skeletal fragment/peloid, brachiopod, pelecypod, bryozoan packstone, where bioclasts are well abraded and fragmented and likely micritized. Moderate development of VU and IX porosity is distributed throughout



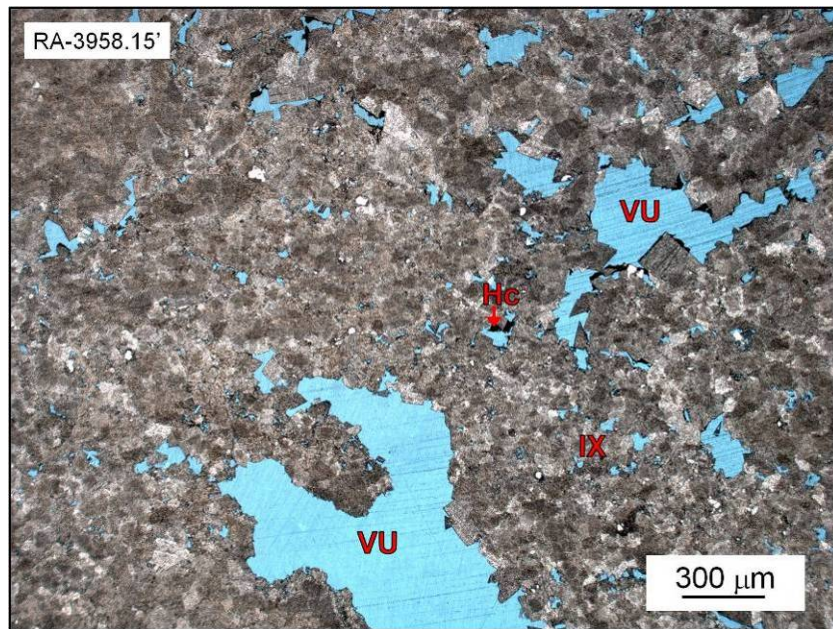
(8 – 10%), with common occlusion of VU pores by saddle dolomite (75 – 125  $\mu\text{m}$ ).



**RA – 3980.5' – Primary fabric obliterated by dolomitization.** Interlocking dolomite mosaic consists of medium silt-, to very fine sand-sized

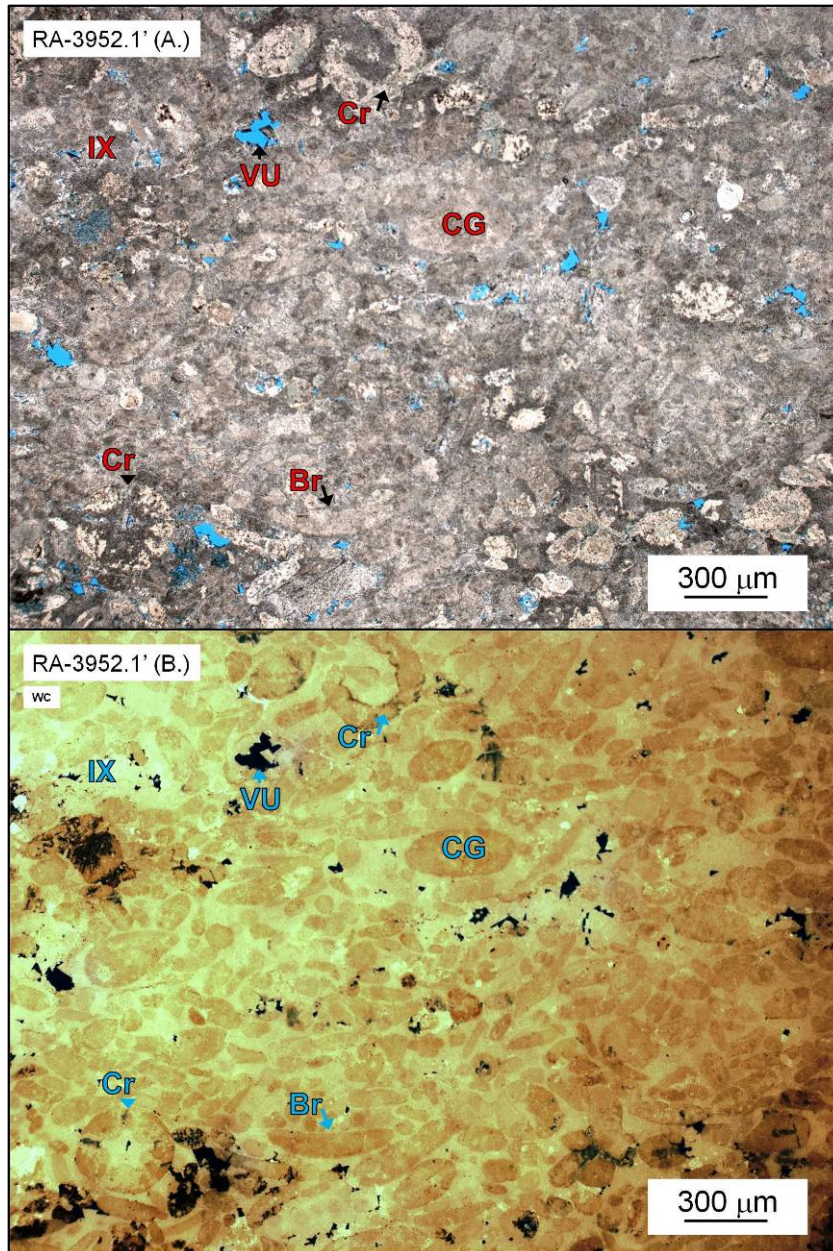
crystals. Dolomite crystals show ghosts of peloids in packstone-grainstone texture (?). One single brachiopod/pelecypod fragment is identifiable. Minor IX porosity is developed of in crystalline dolomite (<5%).

**RA – 3968.5’ – Primary fabric obliterated by dolomitization.** Interlocking dolomite mosaic consists of medium silt-, to very fine sand-sized crystals. Few stylolites are distributed throughout (n=4). Sample showing the crystalline dolomite IX porosity (6%) development associated with burrows (single burrow here).



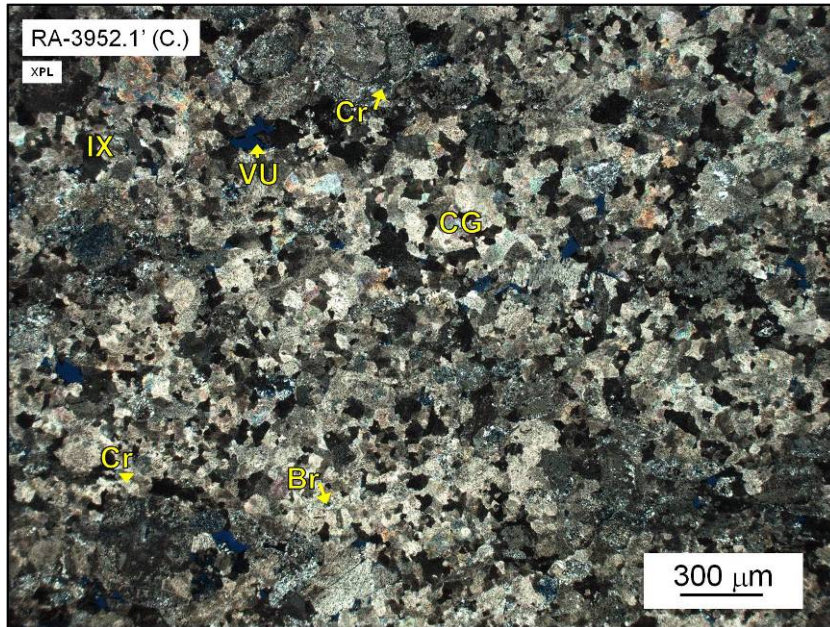
**RA – 3958.15’ – Primary fabric obscured by dolomitization.** Depositional texture is unrecognizable due to dolomitization/recrystallization. Dolomite crystals are dominantly 20 – 90  $\mu\text{m}$  in size, with larger saddle dolomite crystals lining pores (75 – 250  $\mu\text{m}$ ). Porosity is dominantly VU (up to 2.0 mm in diameter) with additional IX developed throughout (15 – 20%). Residual hydrocarbon line a number of pores in the sample.



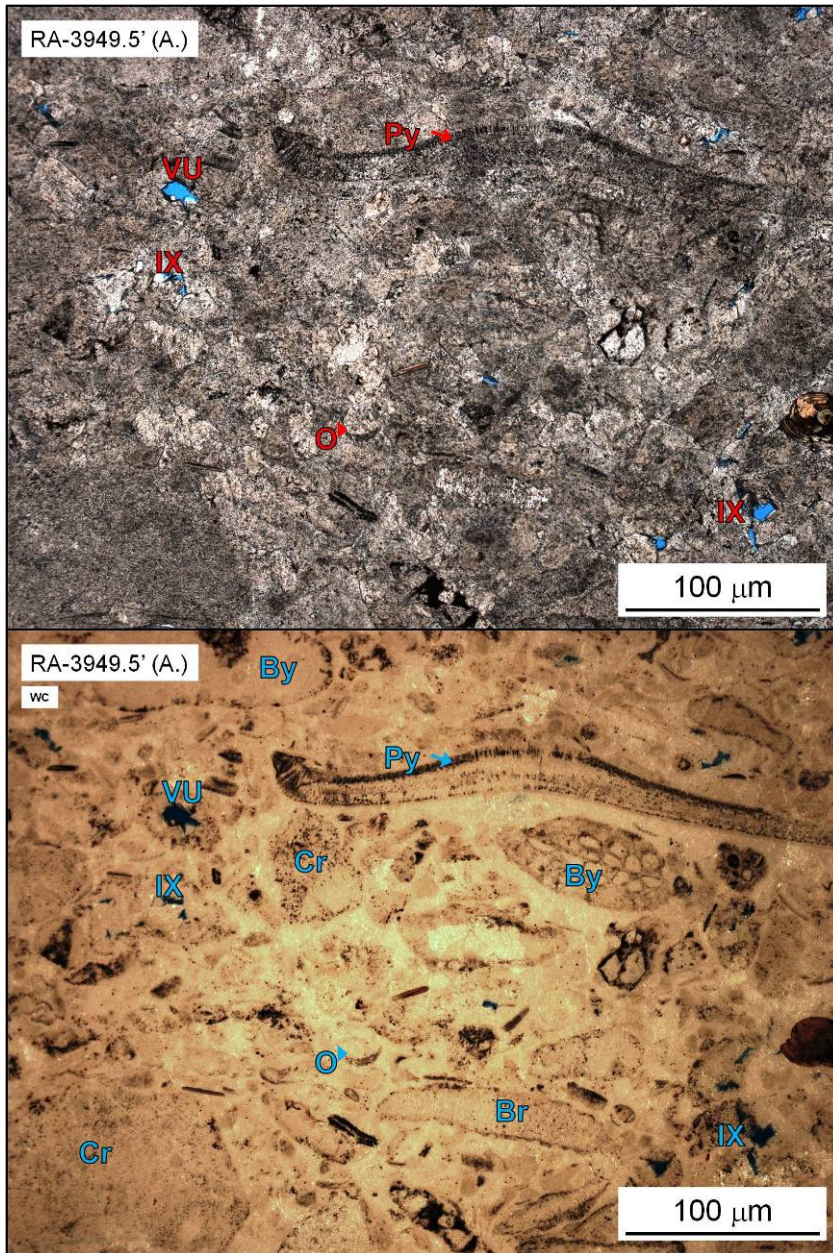


**RA – 3952.1' – Skeletal intraclastic grainstone. (A. and B.)** Primary fabric obscured by dolomitization. White card technique shows undifferentiated skeletal fragment/peloid (50%), brachiopod/pelecypod, crinoid and (likely) well rounded intraclastic grains in a grainstone texture with some primary IP porosity remaining. Elongate and platy grains are dominantly oriented 15-20° from horizontal. Additional porosity is IX, WP, and MO (totaling 8%).





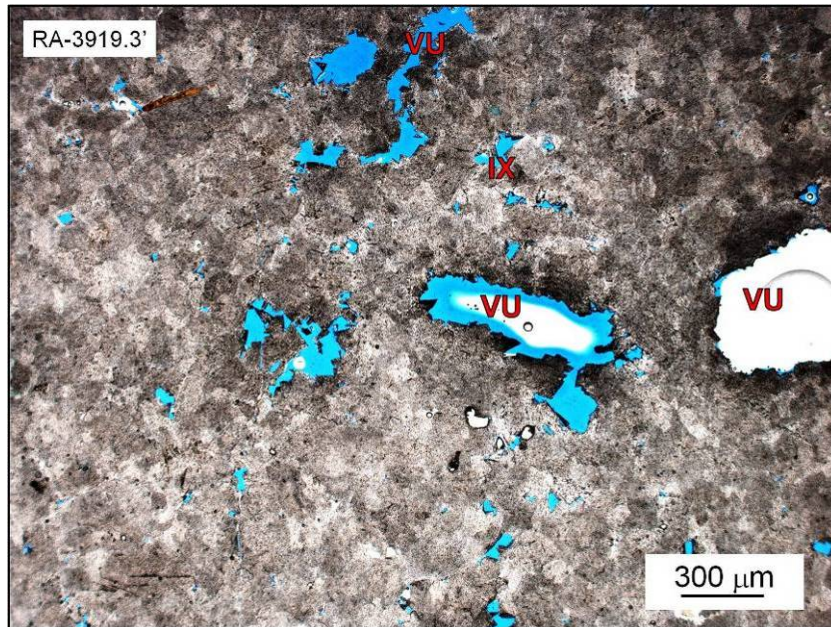
**RA – 3952.1' – Skeletal intraclastic grainstone. (C.-XPL)** Primary fabric obscured by dolomitization. Cross-polarization shows the pervasive recrystallization of sample during dolomitization.



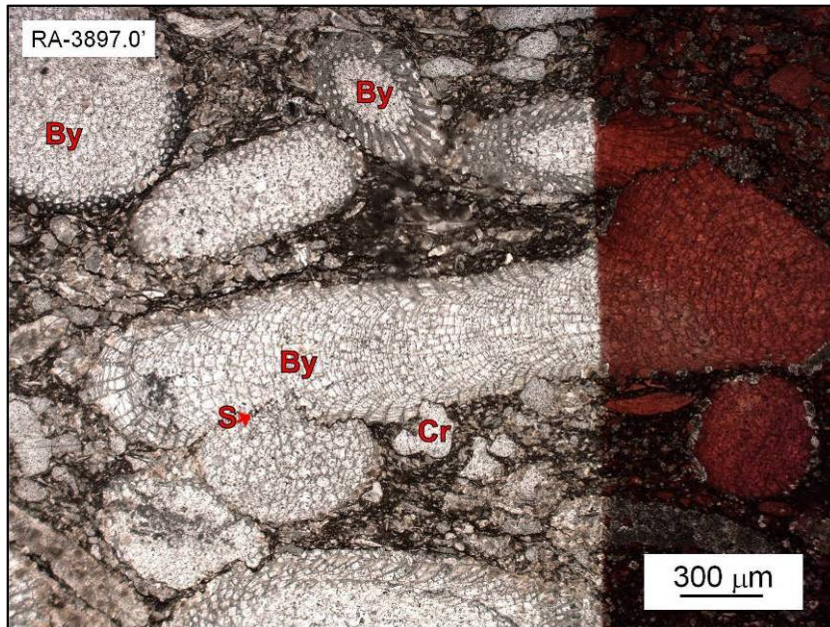
**RA – 3949.5' – Skeletal packstone/grainstone.** Primary fabric partially obscured by dolomitization. White card technique shows undifferentiated skeletal fragment (40%), crinoid (20%), brachiopod (15%), pelecypod (10%), bryozoan, trilobite grains in a (likely) packstone/grainstone overlaying a stylocumulate undifferentiated skeletal fragment, crinoid packstone/wackestone texture. Grains are dominantly horizontally oriented. Minor IX porosity development increases from 4% in lower



packstone/wackestone, up-to 10% in packstone/grainstone (totaling 6% porosity). Included in the sample is a dolomite filled fracture.

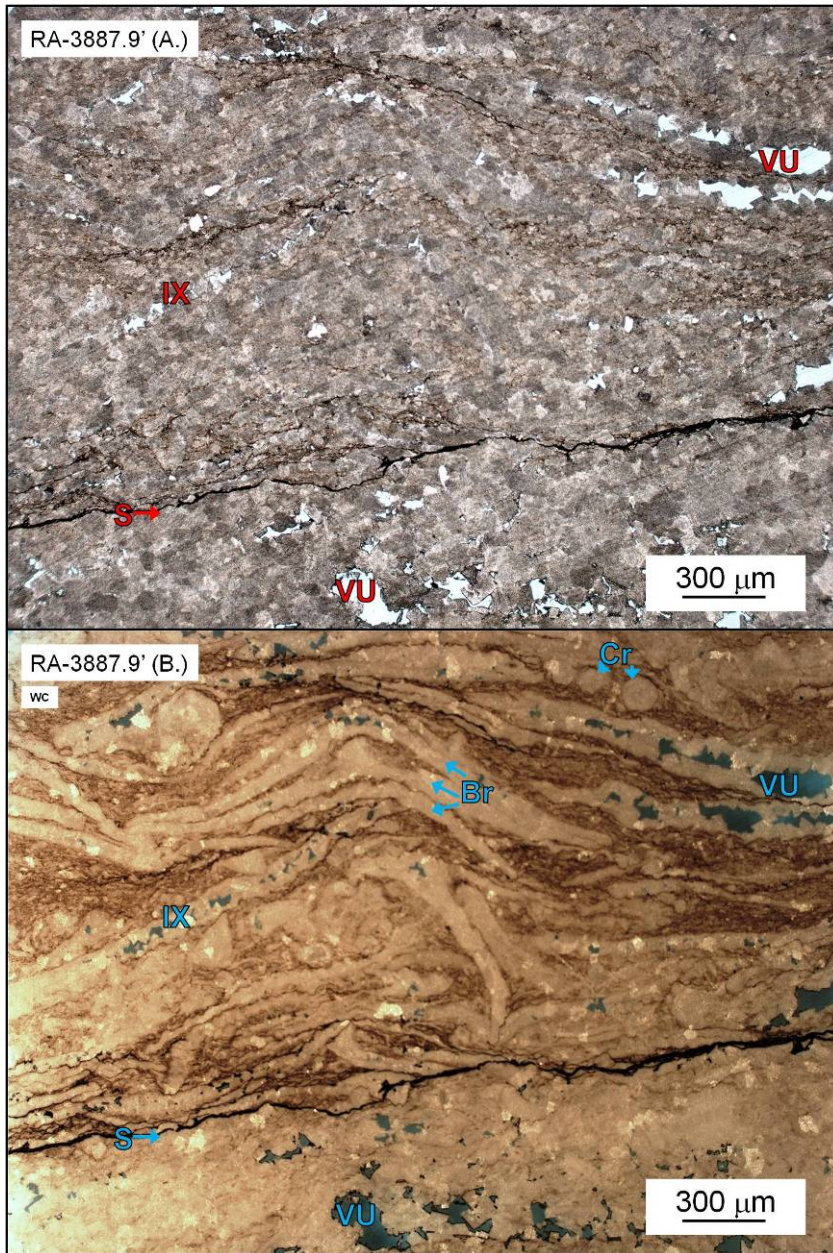


**RA – 3919.3' – Primary fabric obscured by dolomitization.** Sample obscured by recrystallization. Identifiable texture shows few crinoid, brachiopod, pelecypod, bryozoan fragment grains. Porosity is VU and IX with residual hydrocarbon lining many pores (8 – 10%).



**RA – 3897.0' – Bryozoan rudstone-to-floatstone.** Large bryozoan grains (branching morphology, up to 1.75 cm) are commonly in contact in an undifferentiated skeletal fragment, brachiopod, pelecypod, ostracode packstone texture. Euhedral dolomite rhombs cover 15% of the sample, with preferential formation at the rim of large bryozoan fragments. No visible porosity. Red coloration is alizarin-red stain.



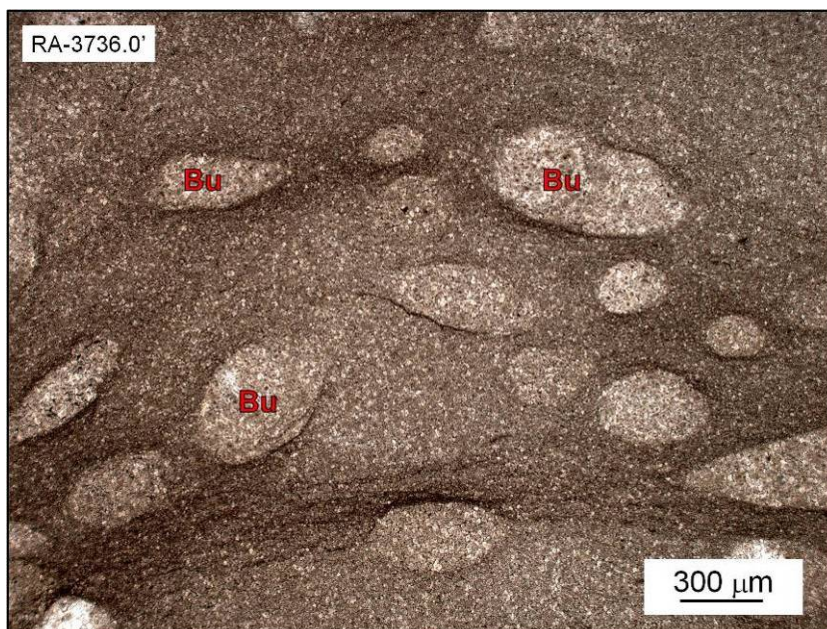


**RA – 3887.9' – Primary fabric obscured by dolomitization. (A. and B.-WC)**

White card technique shows pelecypod/brachiopod packstone that overlies a completely recrystallized portion of the sample. Separating the recognizable texture from obliterated portions is a prominent stylolite. Identifiable grains in packstone consist of pelecypod/brachiopod (60%), ostracode (20%) crinoid, undifferentiated skeletal fragments, with a dominant horizontal grain orientation. Platy



grains are “nested”, with efficient stacking patterns. Porosity is MO/IX developed in packstone texture, and well developed IX/VU in obliterated sections of the sample (6%) with residual hydrocarbon partially occluding pores. Dolomite grain size range 75 – 175  $\mu\text{m}$ .



**RA – 3836.0’ – Primary fabric obscured by dolomitization.** Identifiable sample texture is a moderately burrowed crinoid wackestone (peloidal packstone?), with concentrations of insoluble material/pressure solution seams around burrows (burrow bounding stylonodular fabric). Dolomite color contrast between burrows and matrix suggests burrow filling sediments was different than matrix textures and sediments. No visible porosity.

#### Additional thin section sample descriptions

**RA – 3964.3’ – Primary fabric obscured by dolomitization.** Interlocking dolomite mosaic consists of medium silt-, to very fine sand-sized crystals. One single brachiopod or pelecypod fragment is identifiable. Very minor development of IX porosity in crystalline dolomite (<3%).

**RA – 3935.6’ – Brachiopod packstone/wackestone.** Primary fabric partially obscured by dolomitization. Brachiopod grain size is bimodal, with complete (halves)

commonly 2.0 mm in length and very fine sand-sized fragments. Porosity is IX and IP (dominantly very fine sand-sized fragments) (3-5%).

**RA – 3925.7’ – Primary fabric obscured by dolomitization.** Sample mostly obscured by dolomitization, however white card technique shows the uppermost pelecypod/ostracode, brachiopod, undifferentiated skeletal fragment packstone stylocumulate texture. Packstone texture is in a zone of (likely) stylocumulate grain concentration, which is the result of insoluble material preserving grains from the texture obliteration observed above and below. Dolomite crystal size range 175 – 350  $\mu\text{m}$ . Porosity is well developed IX in completely recrystallized sections of the sample (10%).

**RA – 3911.0’ – Skeletal packstone-to-wackestone with horizontally oriented elongate grains.** Crinoid, brachiopod, ostracode, bryozoan, undifferentiated skeletal fragment, mud-rich packstone-to-wackestone with euhedral dolomite rhombs (10 – 30  $\mu\text{m}$ ) distributed throughout (20% of sample). Grains are dominantly intact, with little micritization of bioclasts. Elongate grains are horizontally oriented. Porosity is poorly developed as WP (2%).

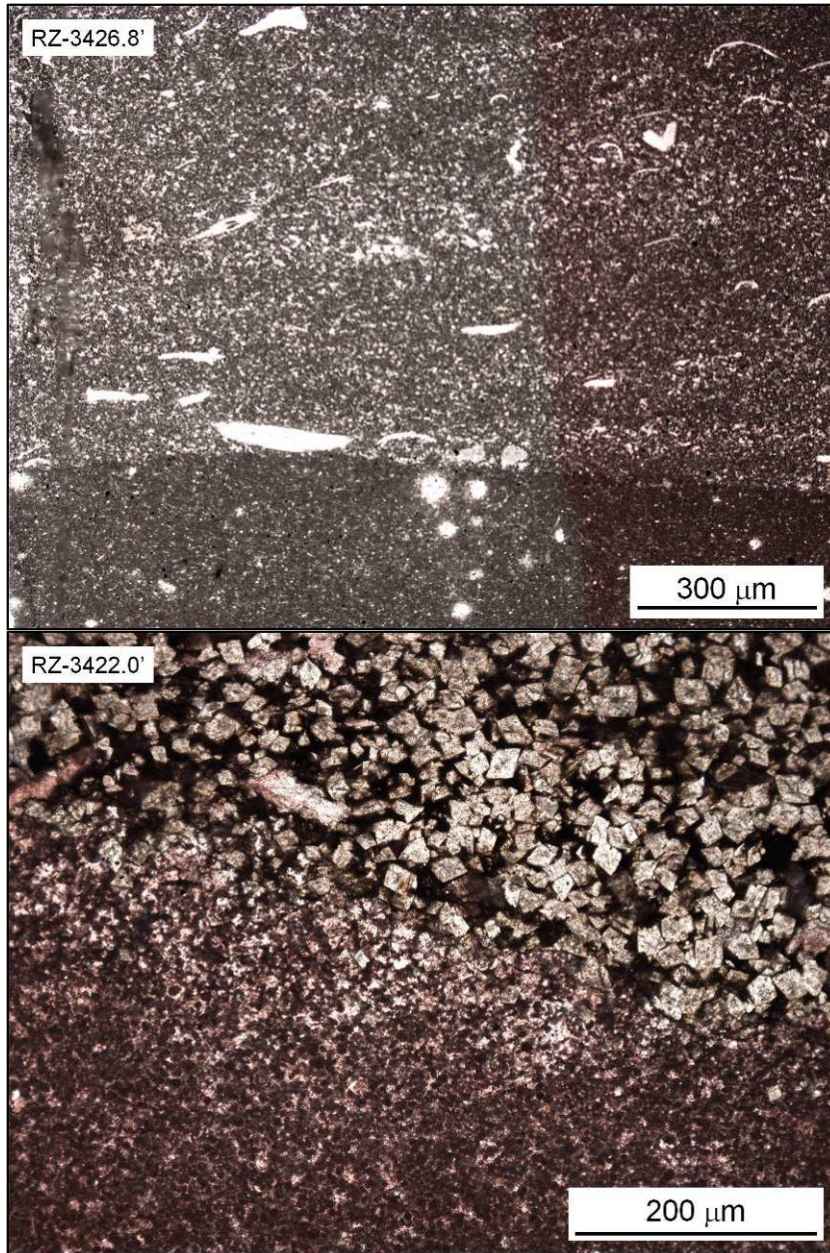
**RA – 3900.0’ – Primary fabric obscured by dolomitization.** White card technique shows crinoid (30%), brachiopod/pelecypod (30%), bryozoan, trilobite, undifferentiated skeletal fragment grains in a wackestone (or peloidal packstone) texture. Stylolites are prominent in distinct sections of the sample (n=2) with additional black opaque material accumulation at dolomite crystal faces (residual hydrocarbon). Dolomite crystal size ranges 75 – 175  $\mu\text{m}$ . No visible porosity.

**RA – 3888.9’ – Primary fabric obscured by dolomitization.** White card technique shows crinoid (40%), brachiopod/pelecypod (30%), bryozoan, and undifferentiated skeletal fragment grains in a packstone texture. Platy grains are horizontally and sub-horizontally oriented. Dolomite crystals are dominantly 125 – 175  $\mu\text{m}$  in size. Insoluble material accumulates at interpenetrating grain contacts. Porosity is IX, MO, and VU, with saddle dolomite partially occluding VU and MO (5%).

**RA – 3858.0’ – Primary fabric obscured by dolomitization.** White card technique shows brachiopod, pelecypod, packstone-to-wackestone (peloidal matrix?). Grains show no dominant grain orientation of larger (cm-scale, rudstone/ floatstone), near complete platy fragments. Included in the sample is a single bryozoan fragment. Dolomite crystal size ranges 75 -175  $\mu\text{m}$ . Porosity is minor VU and IX (<3%).

Rzepke 1-27 – Marathon Oil Company

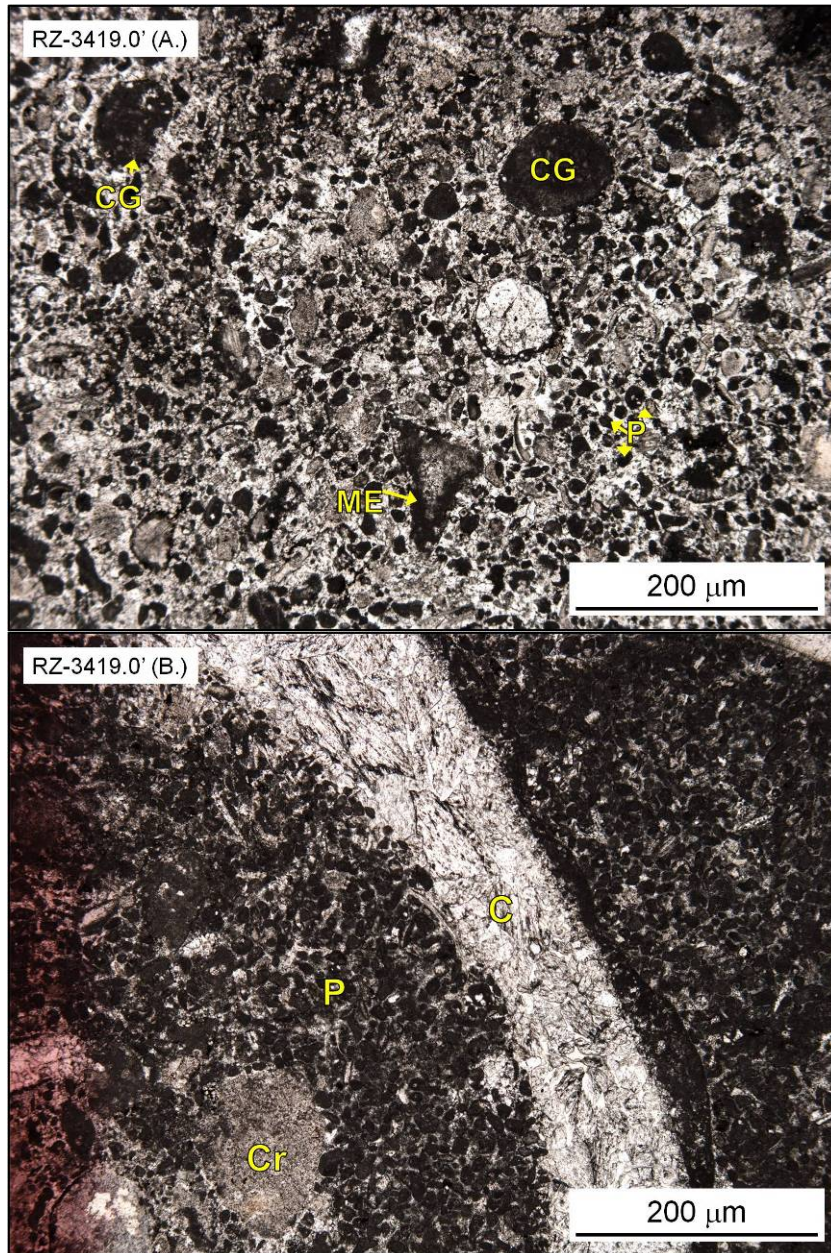
Permit #31253, Branch County, MI



**RZ – 3426.8' – Peloidal grainstone overlying a peloidal packstone.** Peloid (80%), ostracode (5%), brachiopod, crinoid, trilobite packstone overlying grainstone with the same grains and proportions. Distributed throughout are crystalline calcite crystals grouped in spheres (50 – 100 μm in diameter) and opaque material spheres (hydrocarbon?) (10 – 50 μm in diameter). Elongate grains are oriented horizontally. The clean grainstone contacts the packstone texture clearly and well defined,

suggesting that peloids (likely fecal origin) acted as individual depositional grains. No visible porosity. Red coloration is alizarin-red stain. **RZ – 3422.0’ – Peloidal packstone.** Peloid (85%), ostracode, crinoid packstone, with variability between mud-rich and mud-lean packstone-to-grainstone zones and mud lean burrow fill. Zones of clean peloids (grainstone) contain blocky calcite cement. Insoluble material/residual hydrocarbon accumulations commonly occur at calcite crystal faces. Included in the sample are numerous calcite filled fractures/veins. No visible porosity (note: only visible blue epoxy is an artifact of sample preparation). Red coloration is alizarin-red stain.

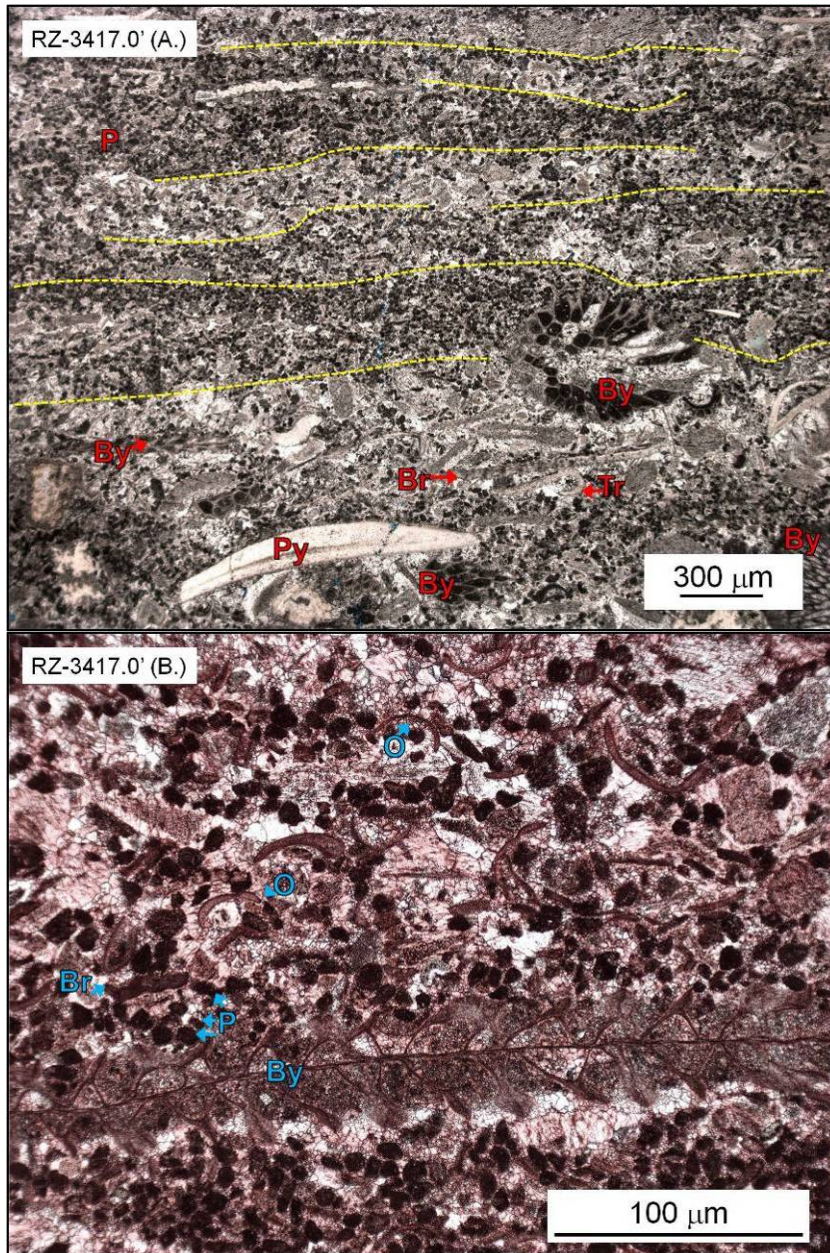




**RZ - 3419.0' - Peloidal, intraclastic grainstone-to-packstone. (A. and B.)**  
Undifferentiated skeletal fragment/peloidal (60%), crinoid (15%), brachiopod, bryozoan, pelecypod, intraclast grainstone-to-packstone. Grains show no dominant grain orientation. Bioclasts range from completely micritized, to unaltered fragments. Intraclasts are sub-

angular, rounded wackestone fragments. Blocky calcite cement fills primary porosity and few euhedral dolomite rhombs (burial?) are distributed throughout. Red coloration is alizarin-red stain (B.).



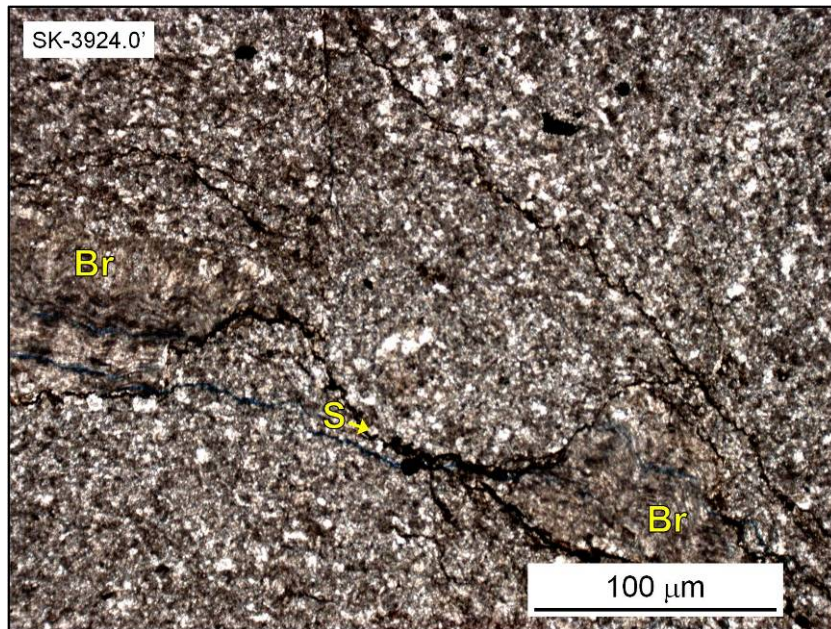


**RZ – 3417.0' –Laminated peloidal and skeletal grainstone. (A. and B.)** Laminated (dashed yellow lines) peloid (60%), brachiopod (15%), ostracode, bryozoan, pelecypod, crinoid, trilobite grainstone. Minor WP, IP, and MO porosity development (<1 – 2%). Red coloration is alizarin-red stain

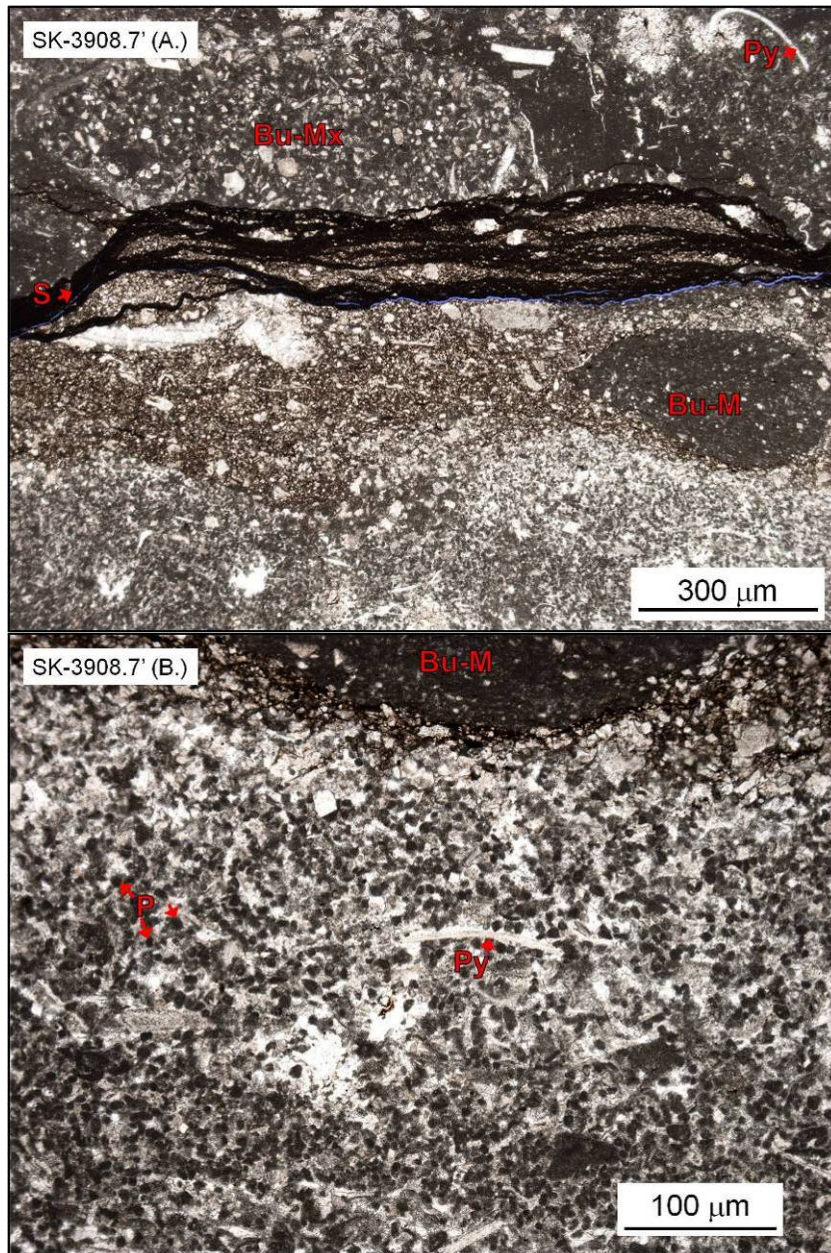
(B.).

Skinner 1 – Marathon Oil Company  
Permit #21833, Hillsdale County, MI



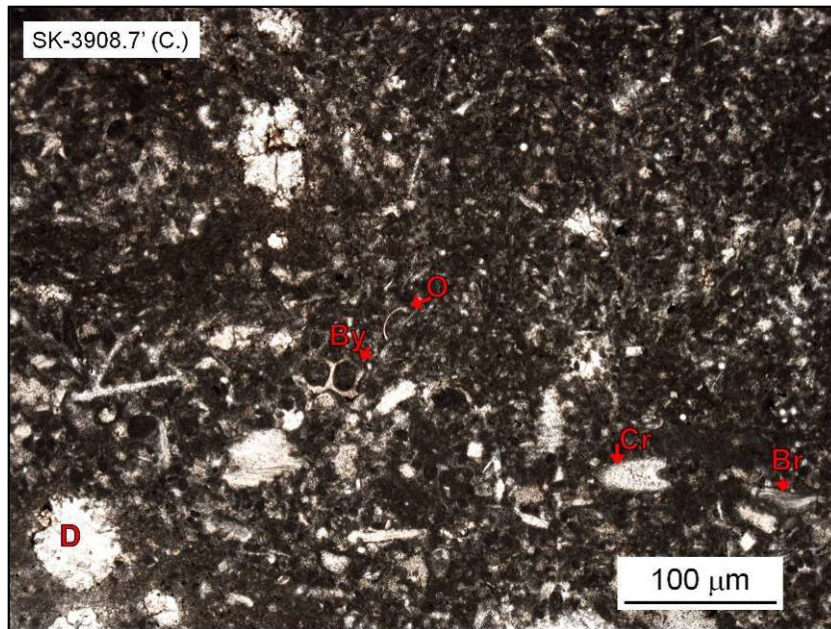


**SK – 3924.0' – Peloid mudstone to wackestone.** Peloidal (90%) brachiopod mudstone to wackestone with abundant anhedral dolomite crystals (~5 μm diameter, 40% of sample). Photomicrograph shows brachiopod fragment cut by stylolitization. Minor FR porosity associated with stylolites was likely induced during sample preparation. No visible porosity.

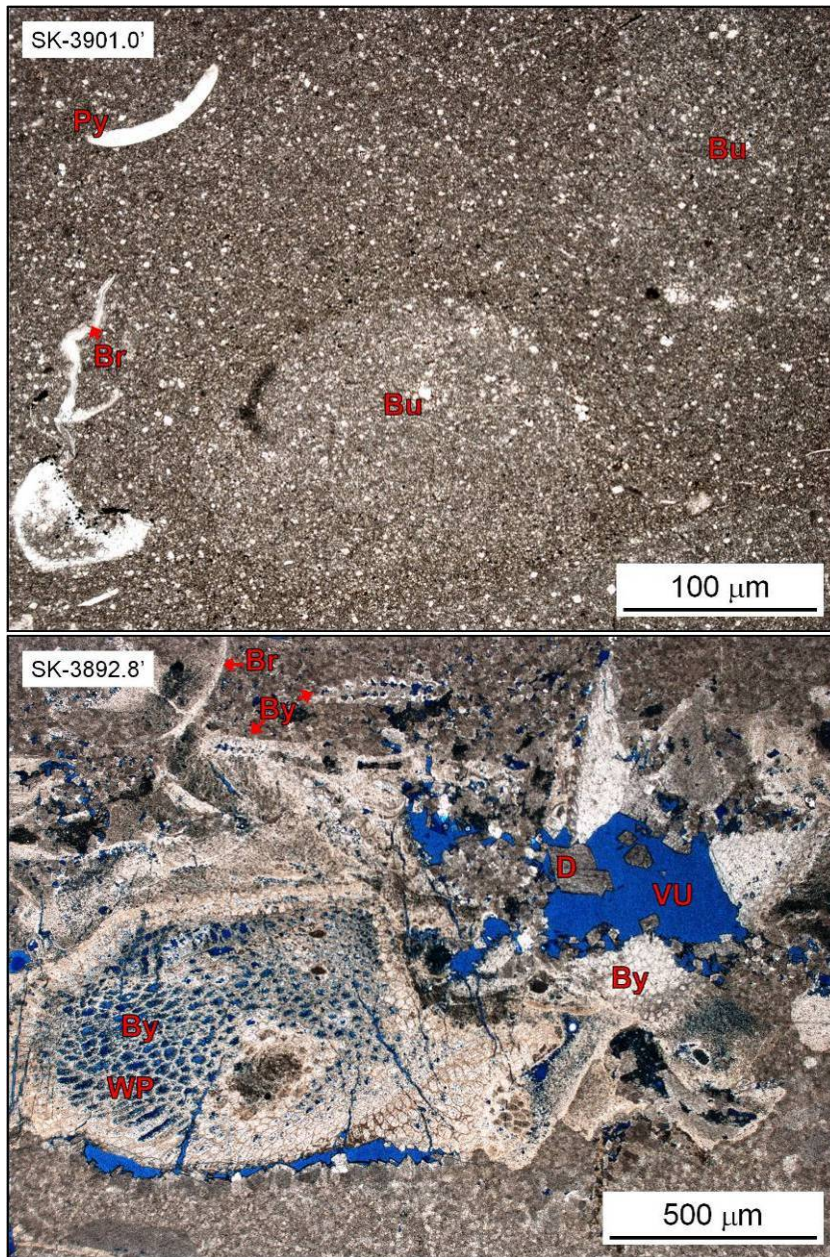


**SK – 3908.7' – (A. and B.) Peloidal skeletal fragment wackestone to packstone overlying peloidal grainstone.** Peloid (70%), ostracode, crinoid, bryozoan, brachiopod wackestone with mud-grain mixed burrow filling sediment overlying peloidal (80%), ostracode, pelecypod grainstone with mud rich burrow filling sediment. Crystalline calcite fills intergranular space in grainstone texture. Minor FR porosity (<2%) is associated with prominent stylolite in the center of (A.).





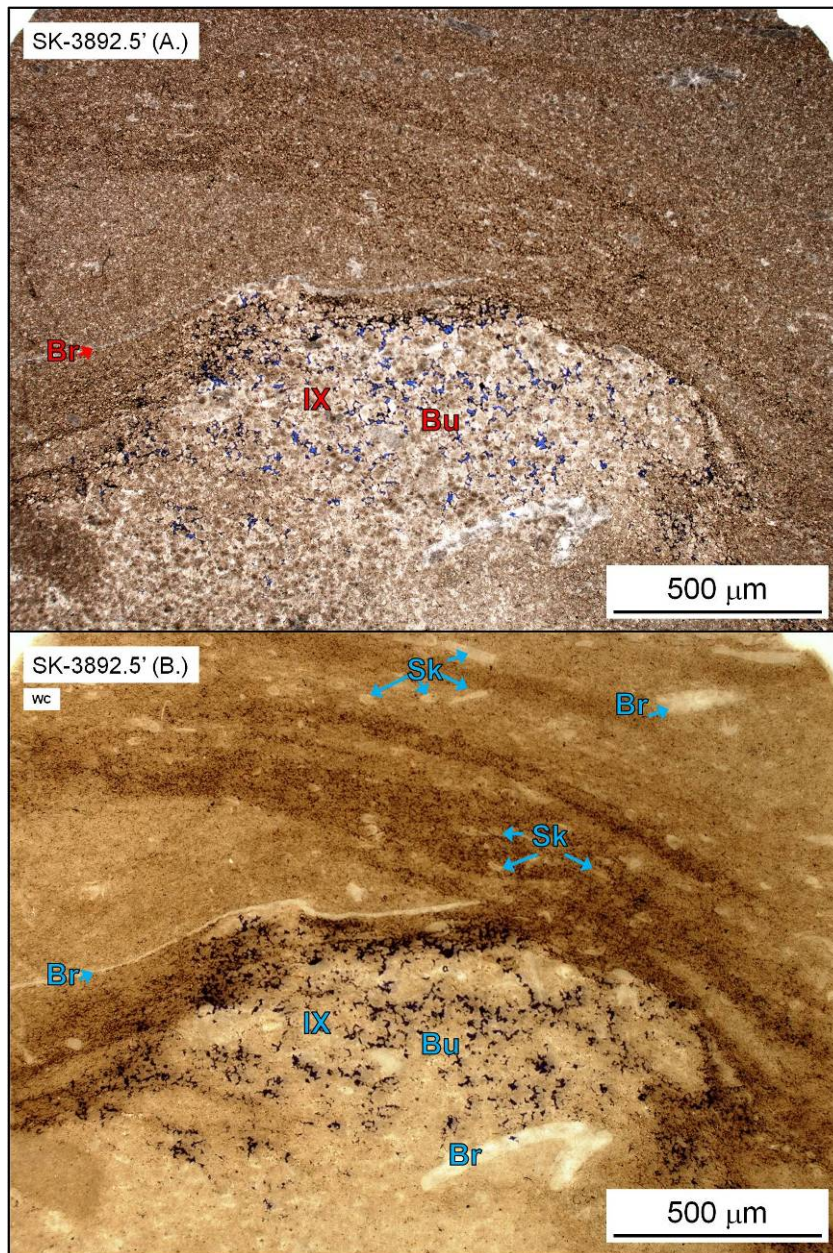
**SK – 3908.7' – (C.) Peloidal skeletal fragment wackestone to packstone.** Small scale view of wackestone textures (in SK – 3908.7-A. and B.) showing bryozoan, brachiopod, and ostracode bioclasts in a peloid-mud matrix. Additionally shown is round (spherical) accumulation of dolomite crystals. No visible porosity.



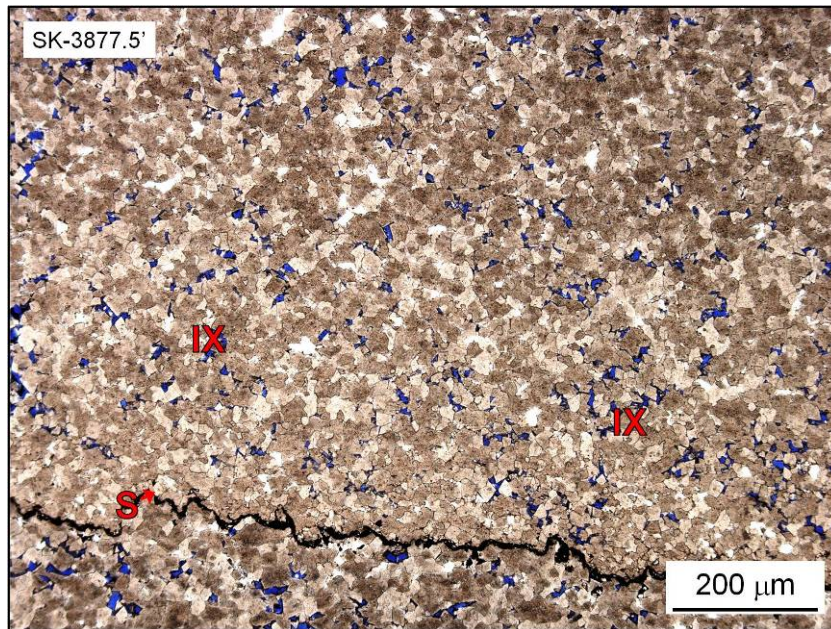
**SK – 3901.0' – Platy-bioclastic wackestone to mudstone.** Ostracode (40%), brachiopod, pelecypod, crinoid, wackestone and mudstone with mud filled burrows (0.2 – 0.4 cm in diameter). Sub-hedral dolomite rhombs (3 – 7 μm diameter) are distributed throughout sample (~10% of total).

**SK – 3892.8’ – Brachiopod, bryozoan wackestone to packstone.** Brachiopod (40%), bryozoan (40%) peloid (?), ostracode wackestone to packstone. Photomicrograph shows well developed WP, IP/IX porosity (3%) associated with bioclasts. Additional minor FR porosity is distributed throughout (~1%) (4% total pore-space).





**SK – 3892.5' – Bioclastic wackestone with intercrystalline burrow replacement.**  
 (A. and B.-WC) **Depositional** fabric is obscured by dolomitization, however white-card technique shows it to likely be undifferentiated skeletal fragment (Sk) (80%), brachiopod wackestone. Porosity is IX within burrow boundaries (15% burrow, 3% total).

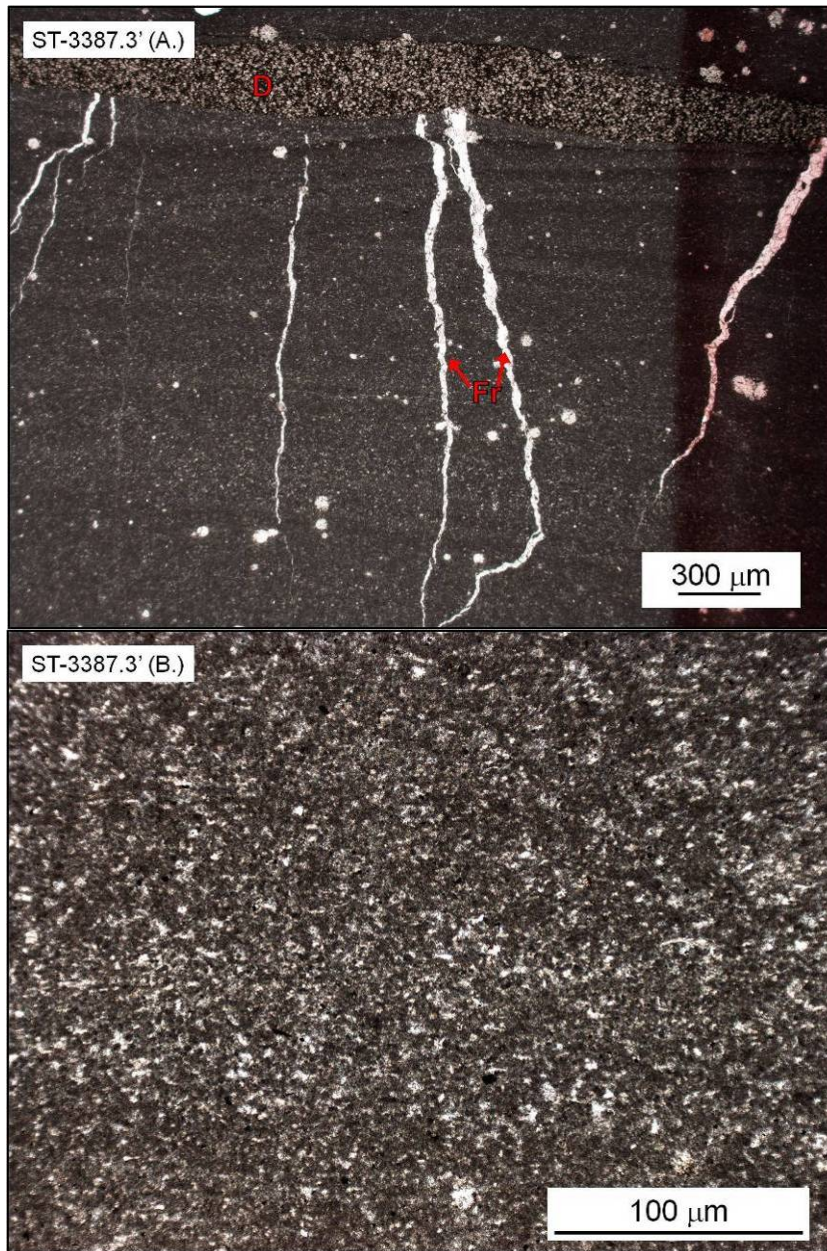


**SK – 3977.5’ – Depositional fabric obliterated by dolomitization and recrystallization.** Sample shows well developed IX porosity (9%) resulting from dolomitization of a grain-bed (apparent, as identified in core) and low-amplitude suture stylolites.

Stetler 1-33 – Marathon Oil Company

Permit #31407, Branch County, MI

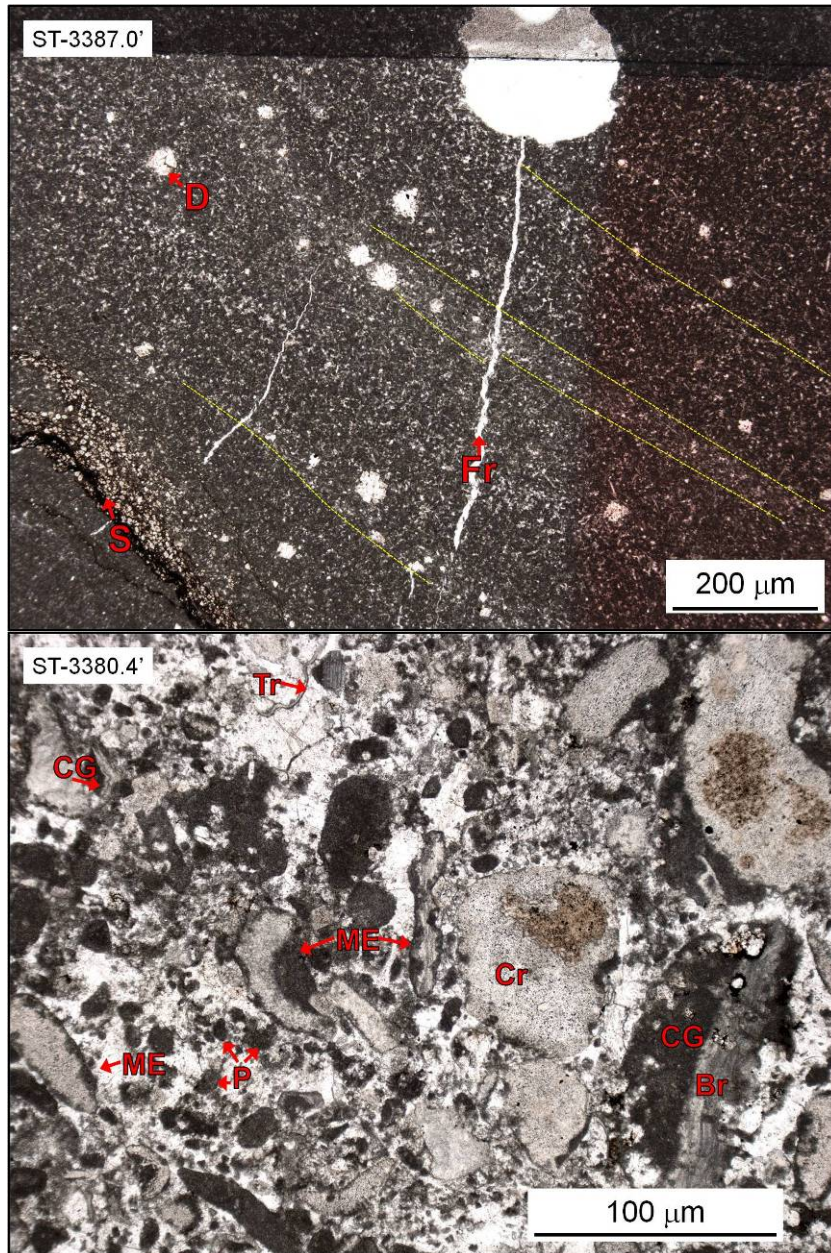




**ST – 3387.3' – (A. and B.) Laminated mudstone-peloid wackestone.** Mudstone and peloid (80%), ostracode (5%), crinoid wackestone with wavy cross-laminations (micro hummocky cross-lamination?). Very fine silt-sized dolomite rhombs are distributed throughout sample (~6%), and show preferential accumulation/formation (D) at prominent pressure solution seam. Dolomite also forms/accumulates in round (spherical) crystal



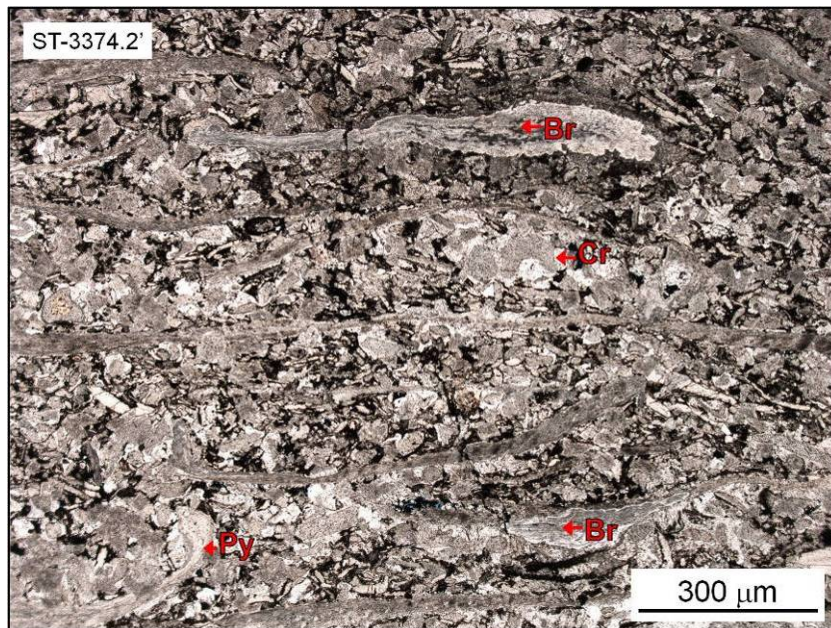
groups (10 – 30  $\mu\text{m}$  in diameter). Calcite fills sub-vertical fractures. No visible porosity.



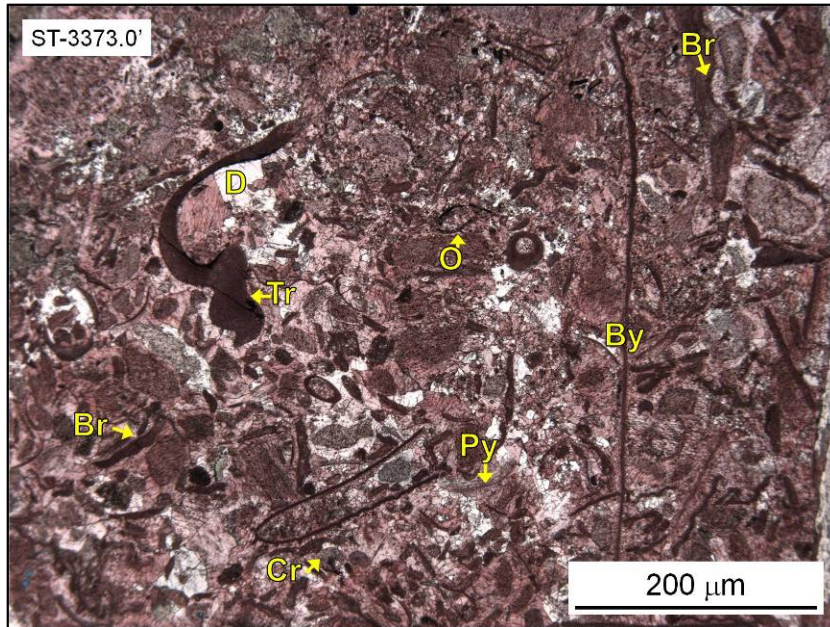
**ST – 3387.0' – Cross-bedded peloid packstone and wackestone.** Peloid (90%), pelecypod, ostracode, crinoid packstone to wackestone with inclined laminations. Very fine silt-sized dolomite rhombs are distributed throughout sample (~20%), and show preferential accumulation/formation (D) at pressure



solution zones and stylolitization. Dolomite also forms/accumulates in round (spherical) crystal groups (10 – 60  $\mu\text{m}$  in diameter). Calcite fills sub-vertical fractures. No visible porosity. **ST – 3380.4' – Bioclastic grainstone with variable grain micritization.** Peloid/undifferentiated micritized grain (40%), crinoid (30%), brachiopod, pelecypod, bryozoan, intraclast (CG), trilobite grainstone to packstone. Chaotic grain orientation shows that sample is likely intensely bioturbated. Calcite cement fills inter-grain space and fractures. Few very fine silt-sized dolomite rhombs (5-10%). No visible porosity.

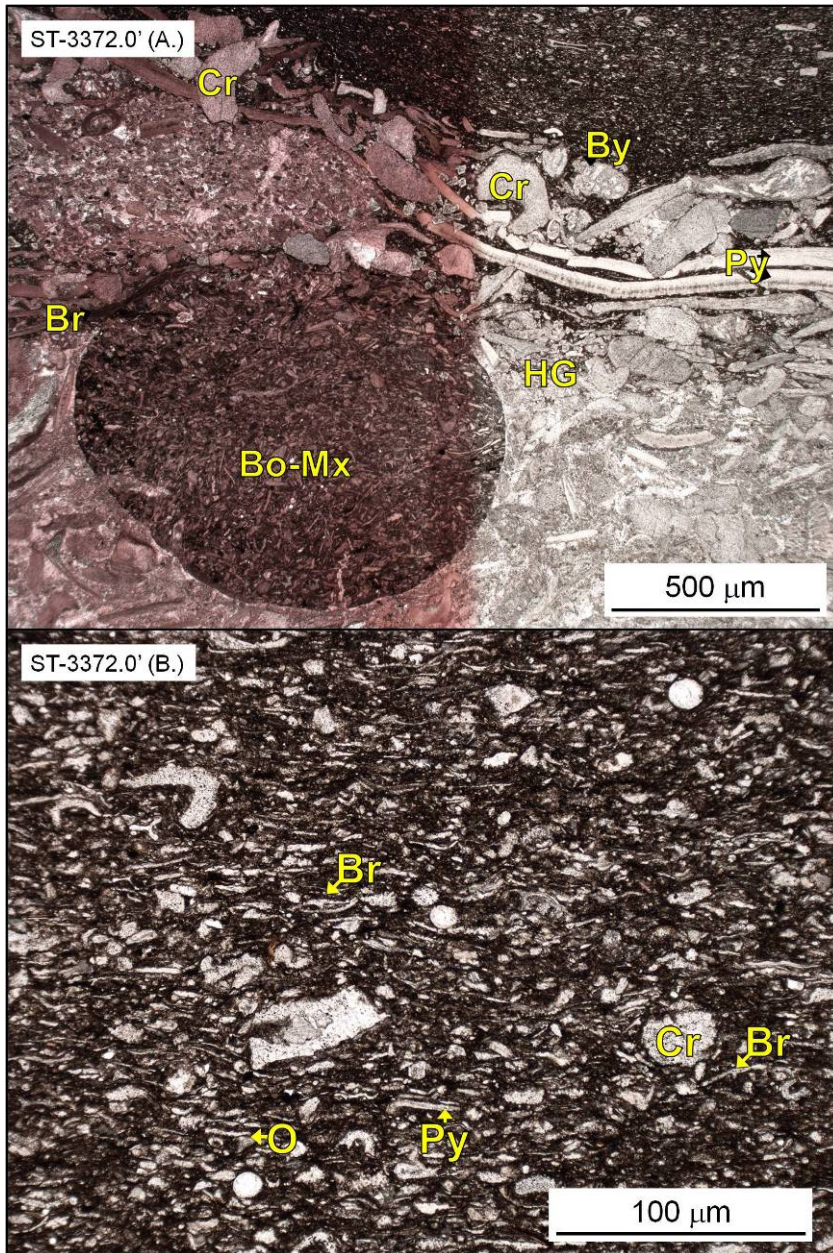


**ST – 3374.2' – Laminated platy-bioclastic packstone.** Brachiopod (40%), pelecypod (30%), crinoid, undifferentiated skeletal fragment packstone with a strong horizontal grain orientation (laminations?). Very fine silt-sized dolomite rhombs and organic-rich(?) insoluble material is distributed throughout (15-25%). Very minor IP/IX porosity (<1%).



**ST – 3373.0’ – Skeletal grainstone to packstone.** Pelecypod (30%), brachiopod (20%), undifferentiated skeletal fragment (20%), crinoid, ostracode, trilobite, bryozoan grainstone to packstone, with variable grain micritization and micrite envelope formation. Blocky calcite cement fills inter-grain space and dolomite locally replaces calcite. No visible porosity. Red coloration is alizarin-red stain.

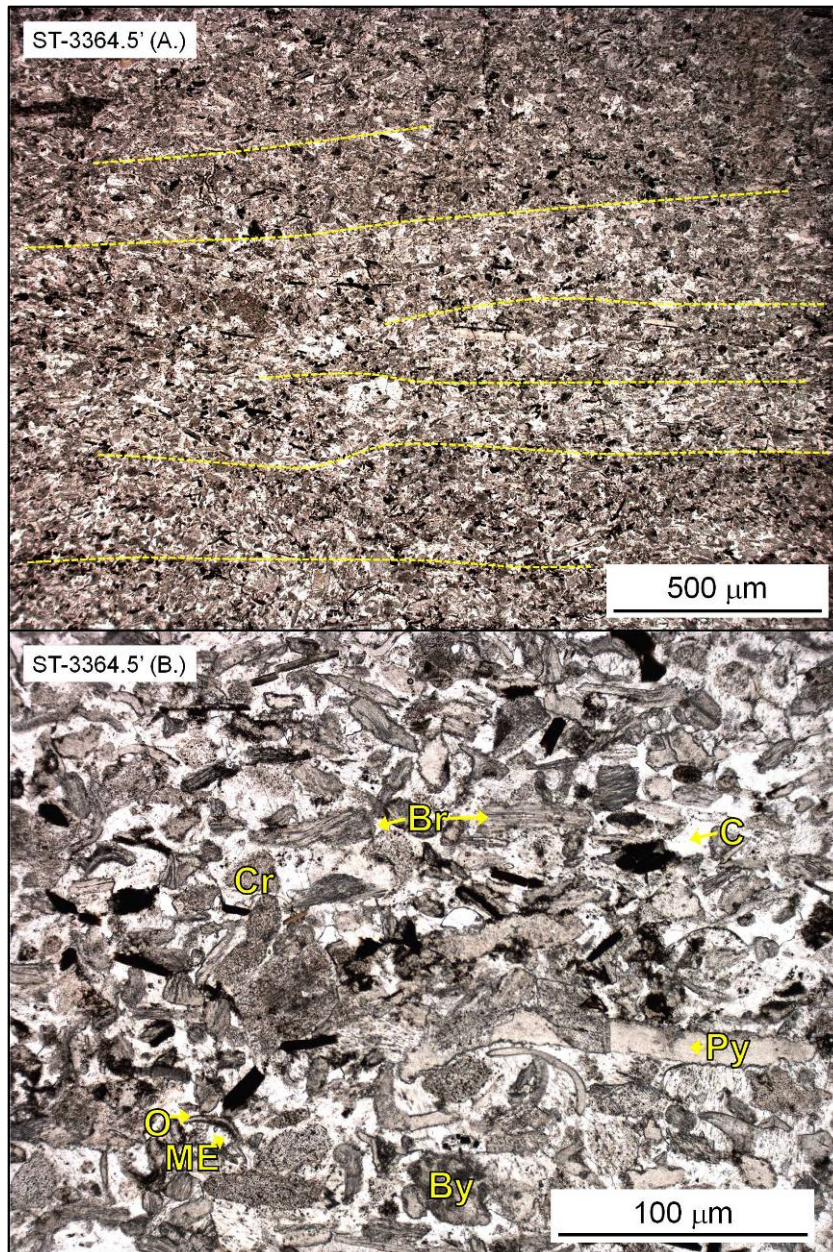




**ST – 3372.0' – (A. and B.) Skeletal grainstone-packstone overlain by fine-grain mud-rich skeletal wackestone-packstone.** Pelecypod (20%), brachiopod (15%), bryozoan (15%) crinoid grainstone to packstone with capping bored hardground, overlain by a normally graded ostracode (50%), pelecypod, brachiopod, crinoid, undifferentiated skeletal fragment wackestone to mud-rich packstone with dominant horizontal



grain orientations (shown in smaller scale in B.). No visible porosity. Red coloration is alizarin-red stain (A.).



**ST – 3364.5' – (A and B.) Laminated skeletal fragment grainstone.** Laminated (dashed yellow line) crinoid (40%), pelecypod (20%), brachiopod (15%), bryozoan, trilobite, ostracode grainstone. Calcite dominates inter-grain space, however dolomite replaces/porosity fill also occurs (5-








10%). Small scale view (B.) shows abundant opaque tabulate grains. Grain micritization is variable, showing some development of micrite envelopes. No visible porosity.



## APPENDIX E – Reservoir Aspects

Introduction

<u>Reservoir Types</u>	<u>Abbreviation</u>	<u>Lower K cut-off (mD)</u>	<u>Upper K cut-off (mD)</u>
<b>Gross</b>	<b>GR</b>	n-a	n-a
<b>Fractured</b>	<b>FR</b>	≥1,000	n-a
<b>Non-Fractured</b>	<b>NF</b>	n-a	<1,000
<b>Non-Producible</b>	<b>NP</b>	n-a	≤0.1
<b>Producible</b>	<b>PD</b>	>0.1	n-a
<b>High-Quality</b>	<b>HQ</b>	>0.1	<1,000

<b>Facies Symbol Key:</b>			
	 F1	 F2	 F3
	 F4	 F5	 F6

Whole core porosity and permeability data are plotted with different controlling variables in the following section. These plots use the reservoir-type definitions and abbreviations as outlined in the above figure. Also used in all plots is the above facies symbol key for depositional facies type (1:1 denotes line indicating an exact match for data point values between plotted axes).

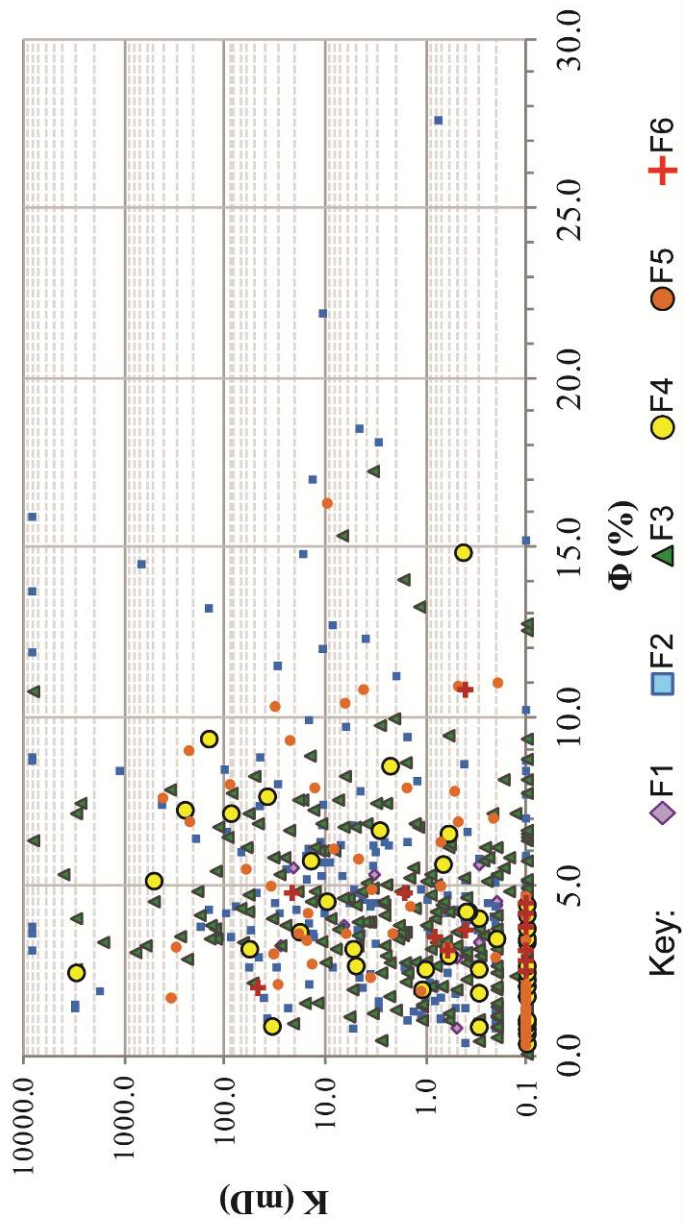
The plots are arranged as follows:

- All core data for GR reservoir-type plotted by facies, including core outside of Albion-Scipio and Stoney Point reservoirs.
- All core data for GR reservoir-type, plotted by facies for individual cores.
- All core data for NF reservoir-type in plots for each depositional facies

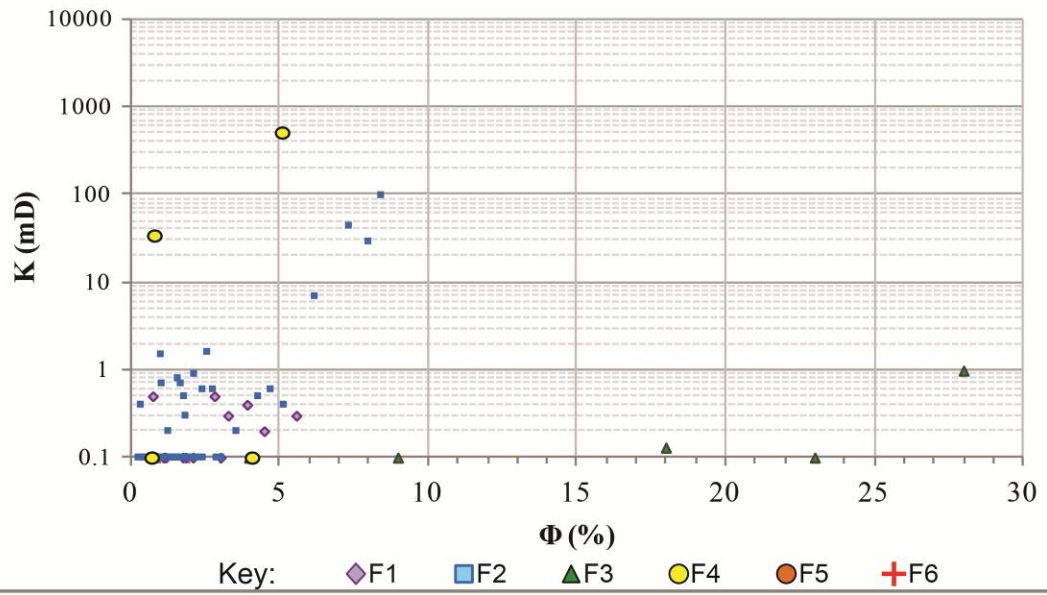
type.

- Average and median porosity for NF reservoir-type with variable T-R facies stacking pattern framework distributions.
- Average and median permeability for NF reservoir-type with variable T-R facies stacking pattern framework distributions.
- Average and median porosity for HQ reservoir-type with variable T-R facies stacking pattern framework distributions.
- Average and median permeability for HQ reservoir-type with variable T-R facies stacking pattern framework distributions.

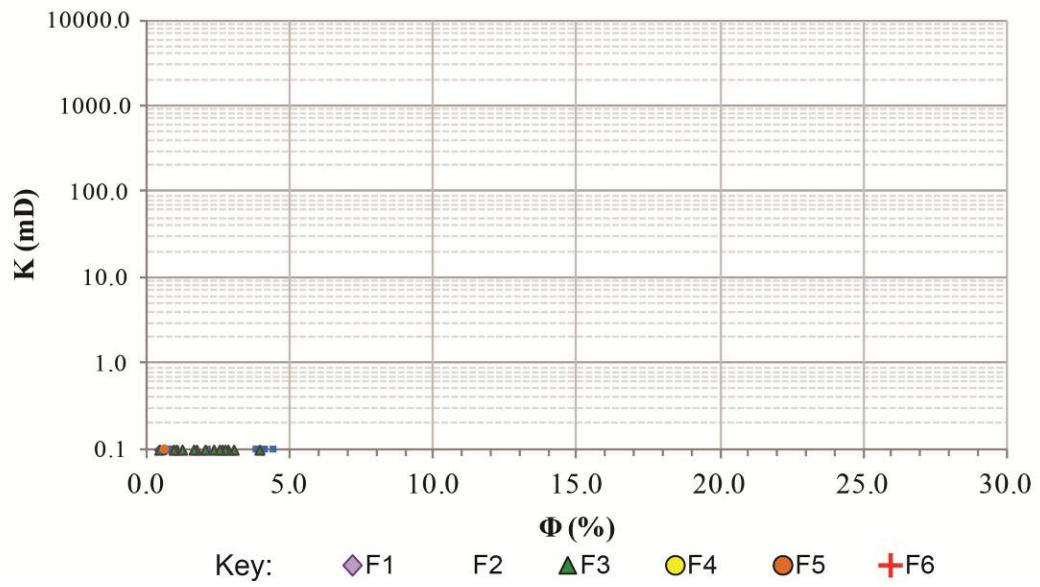
# GR Porosity-Permeability All Facies: All Core



### GR Porosity-Permeability All Facies: AC 1-31

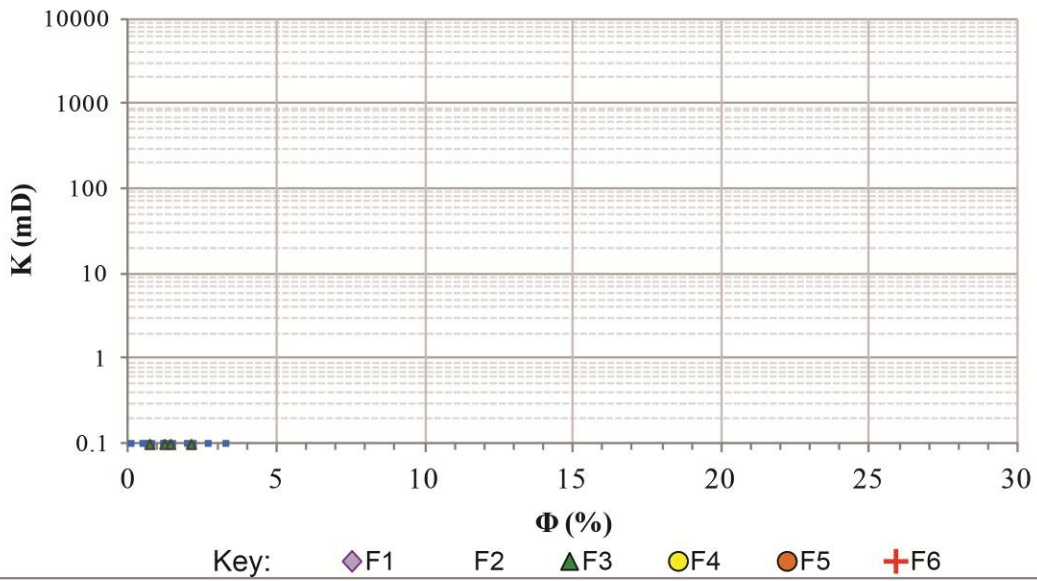


### GR Porosity-Permeability All Facies: AD 1-14

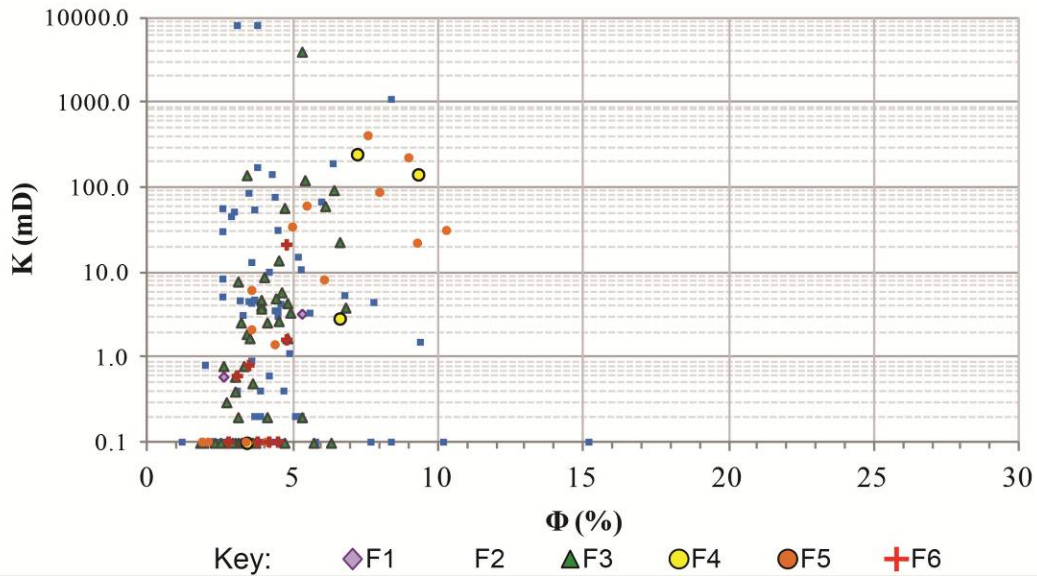




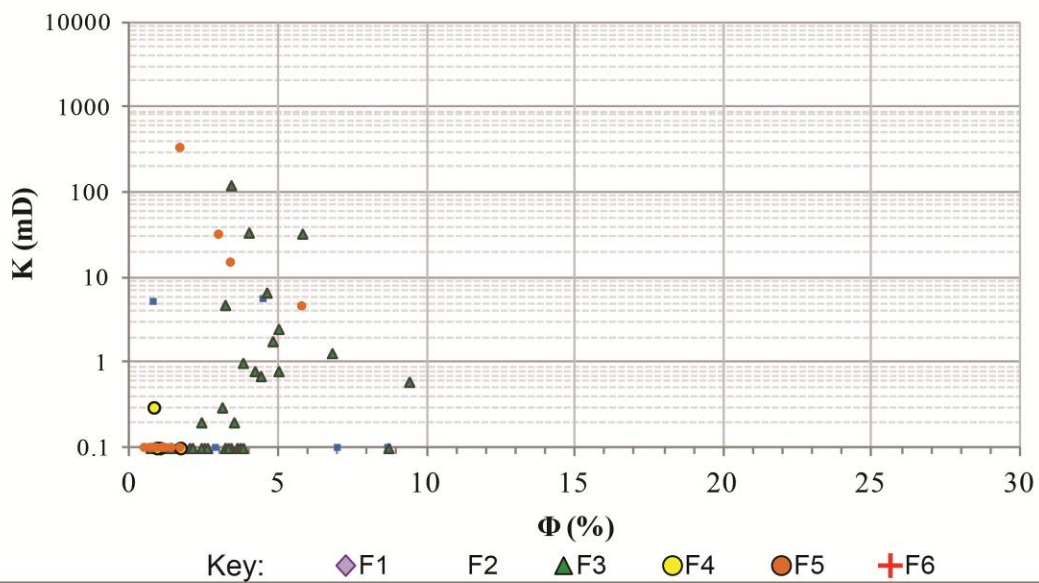
### GR Porosity-Permeability All Facies: AG 1-16



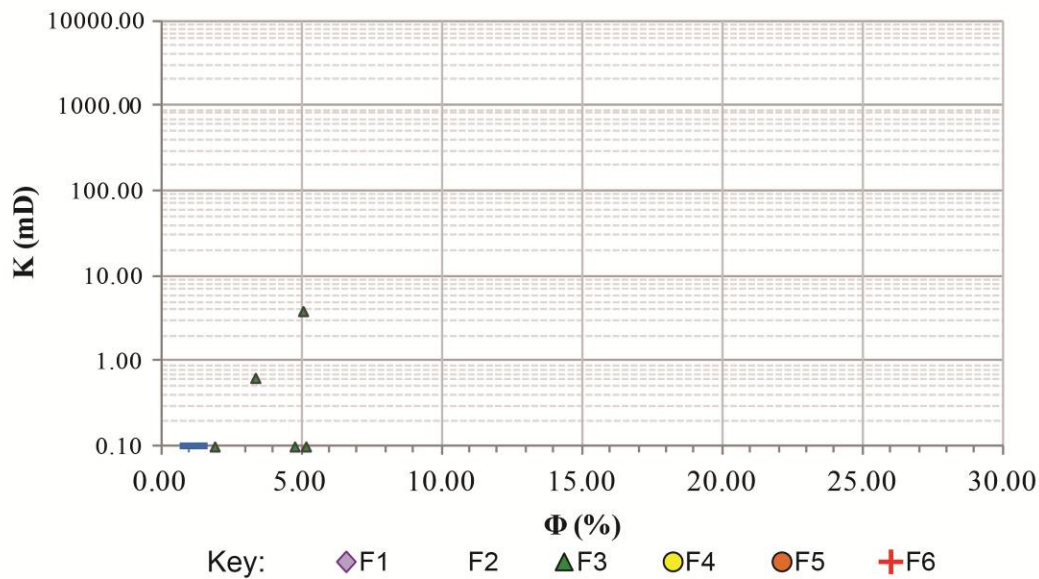
### GR Porosity-Permeability All Facies: BU 1



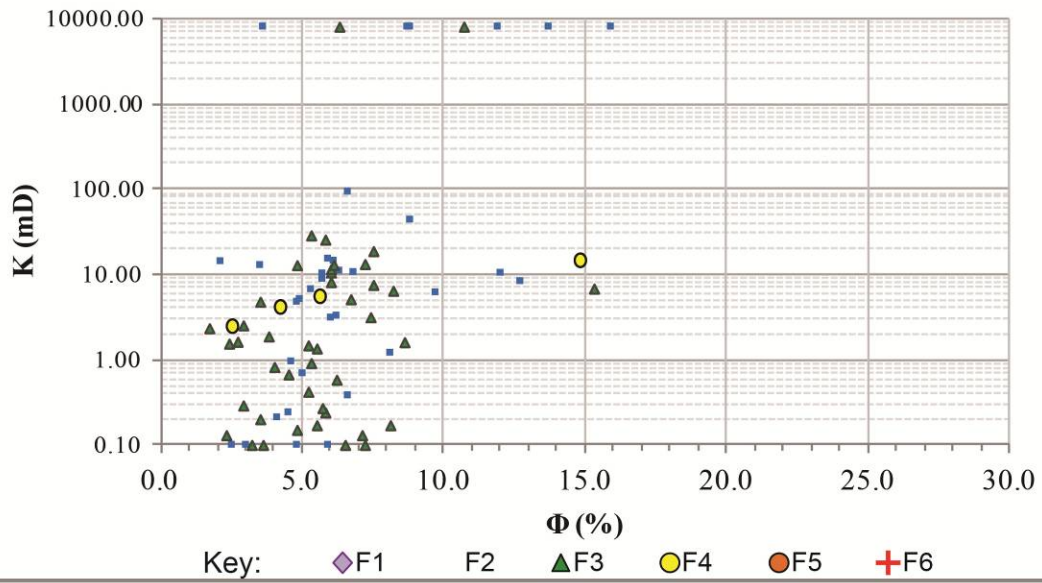
### GR Porosity-Permeability All Facies: C 5-30



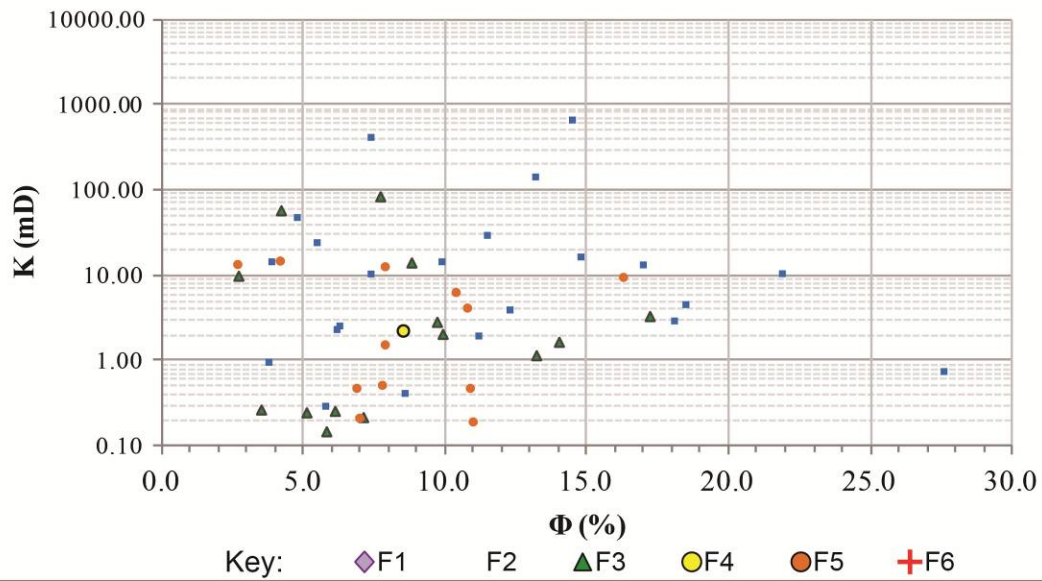
### GR Porosity-Permeability All Facies: M 6



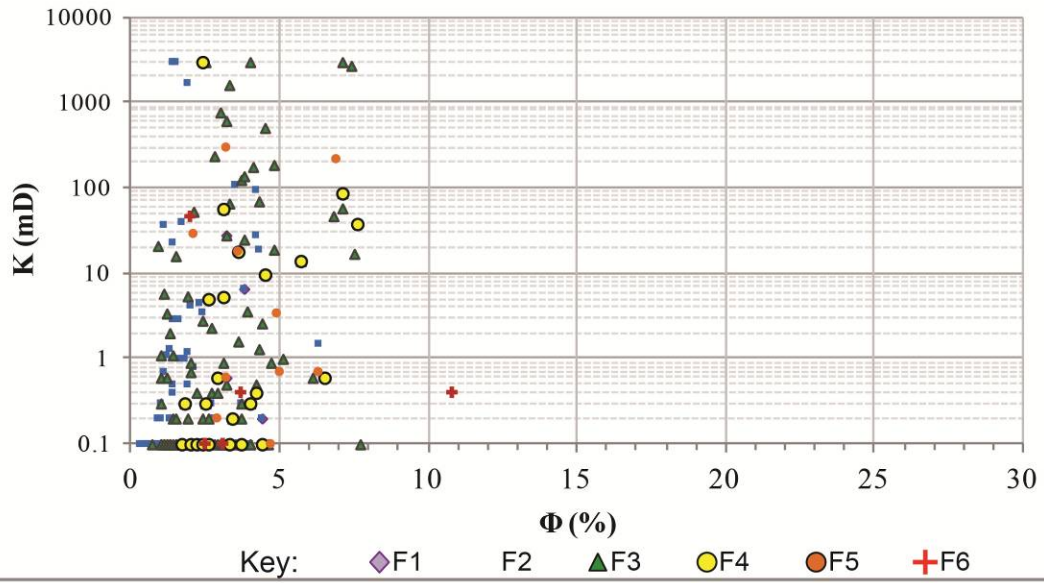
### GR Porosity-Permeability All Facies: M 2-A



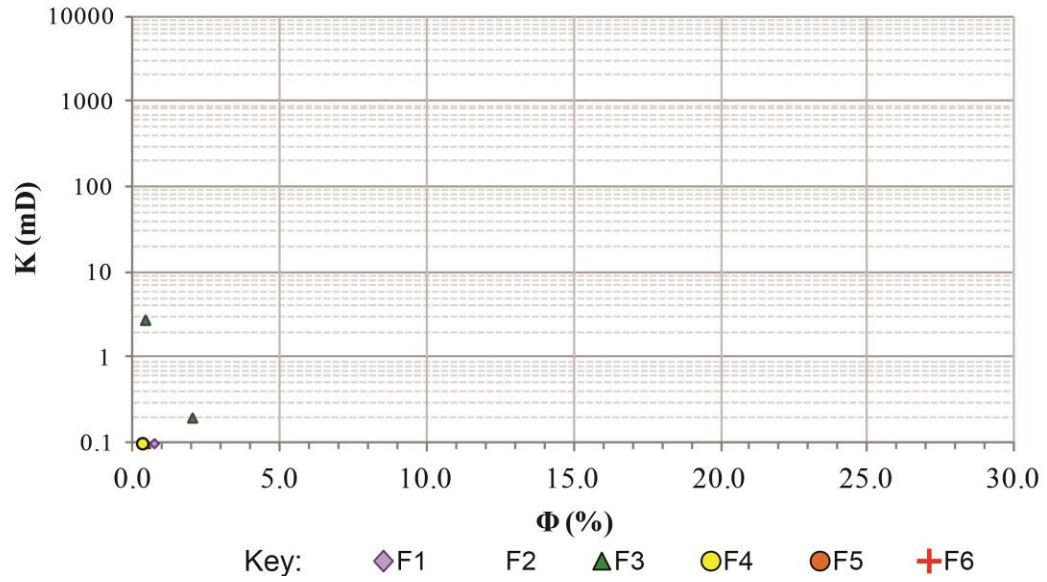
### GR Porosity-Permeability All Facies: MCM 4



### GR Porosity-Permeability All Facies: R A-2

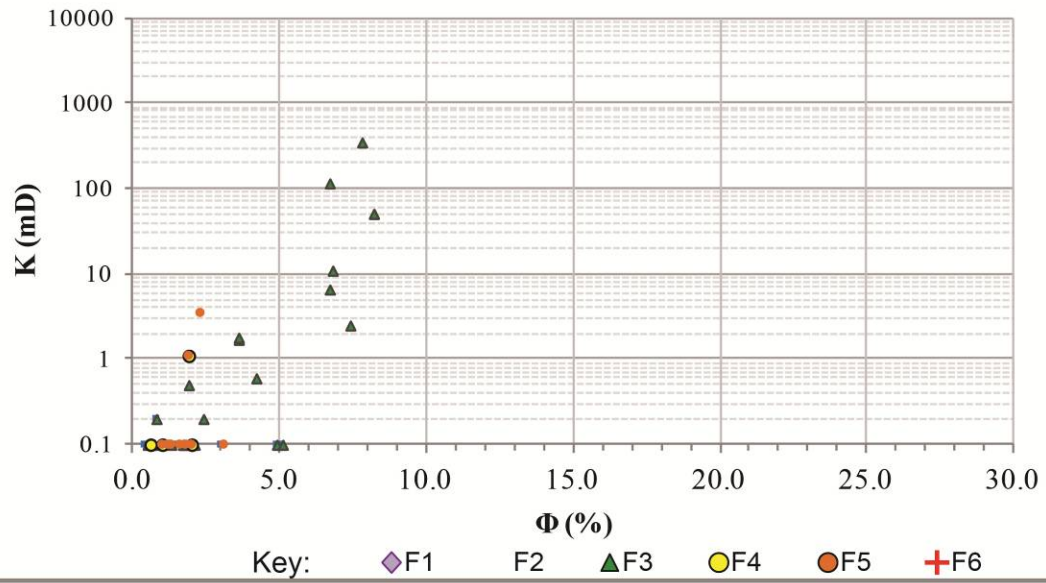


### GR Porosity-Permeability All Facies: RZ 1-27

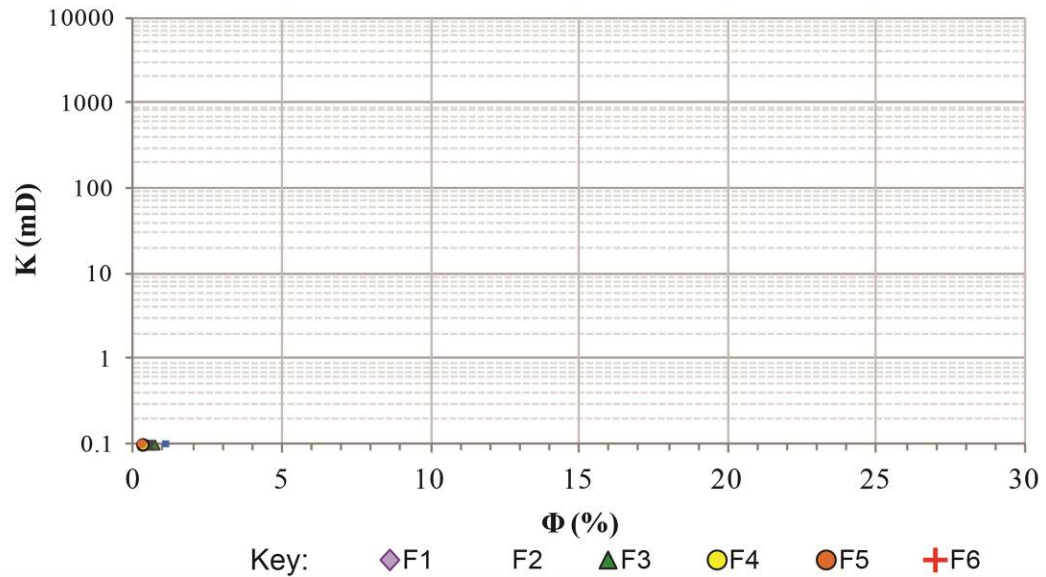




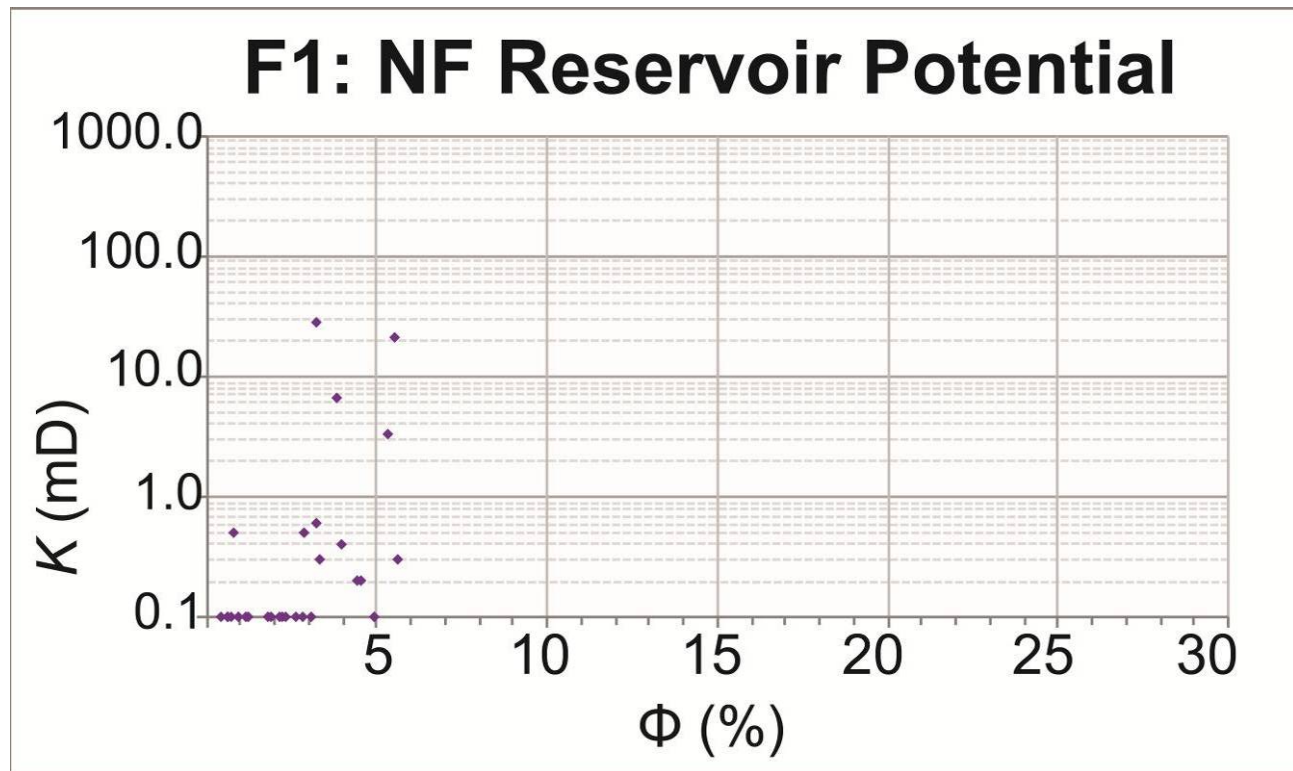
### GR Porosity-Permeability All Facies: SK 1

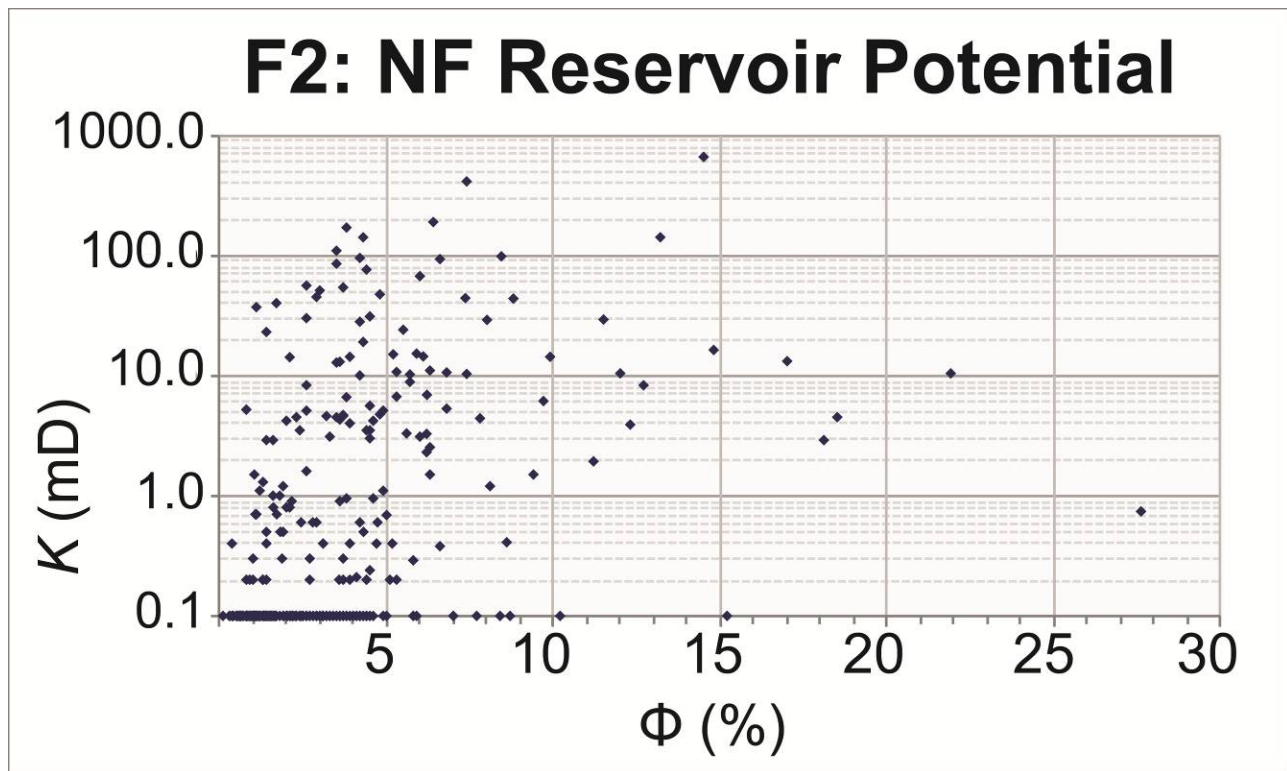


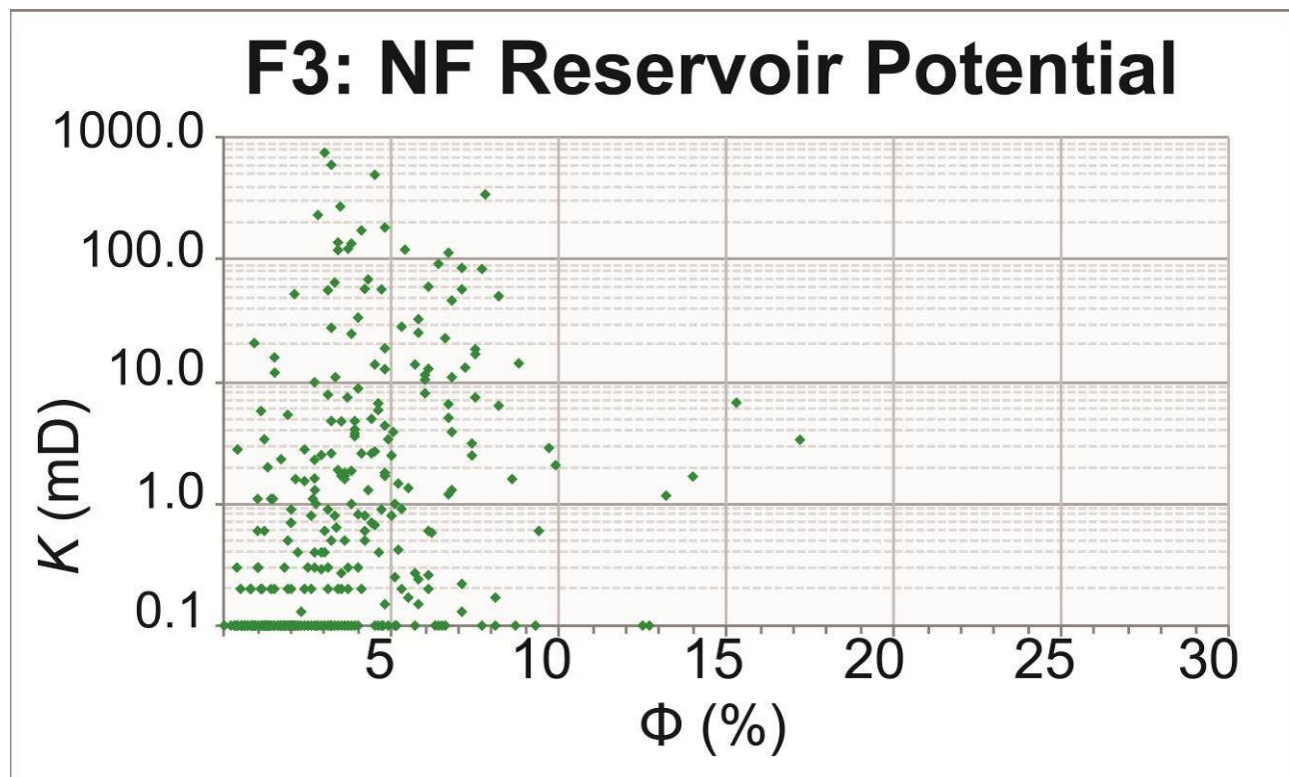
### GR Porosity-Permeability All Facies: ST 1-33

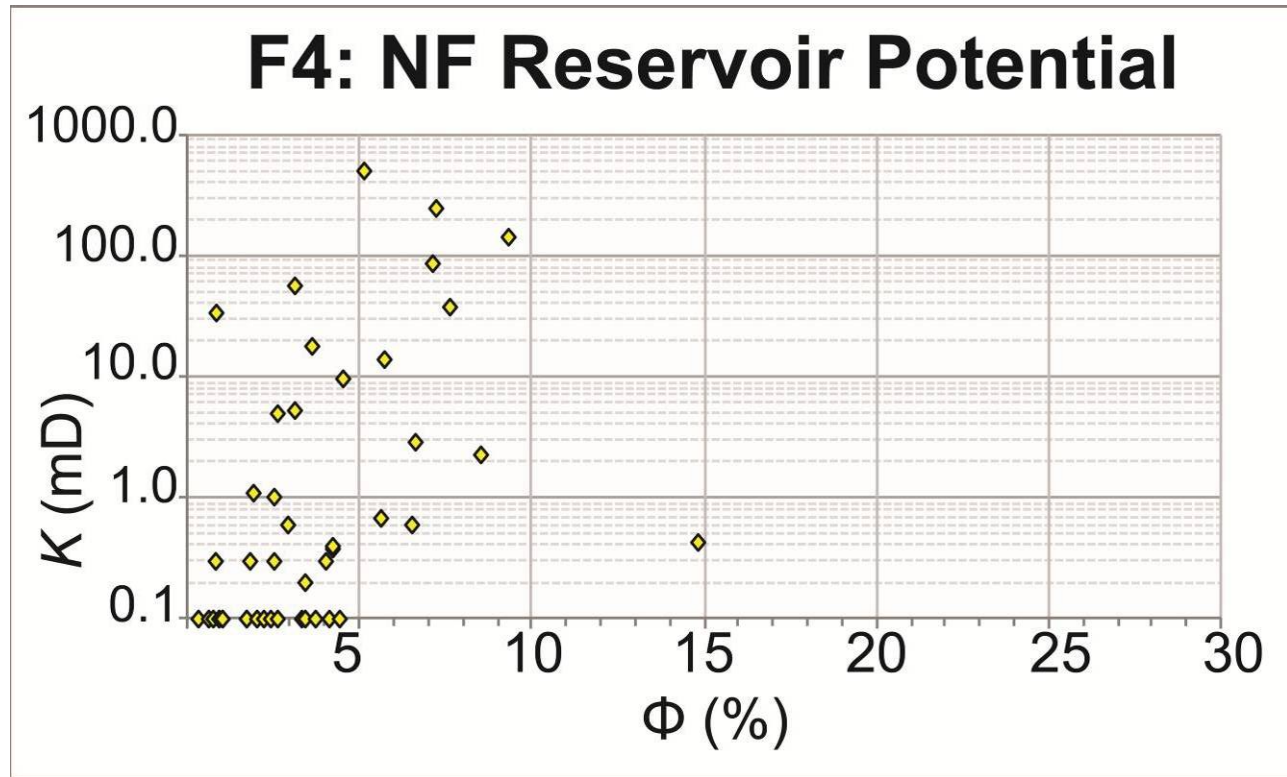


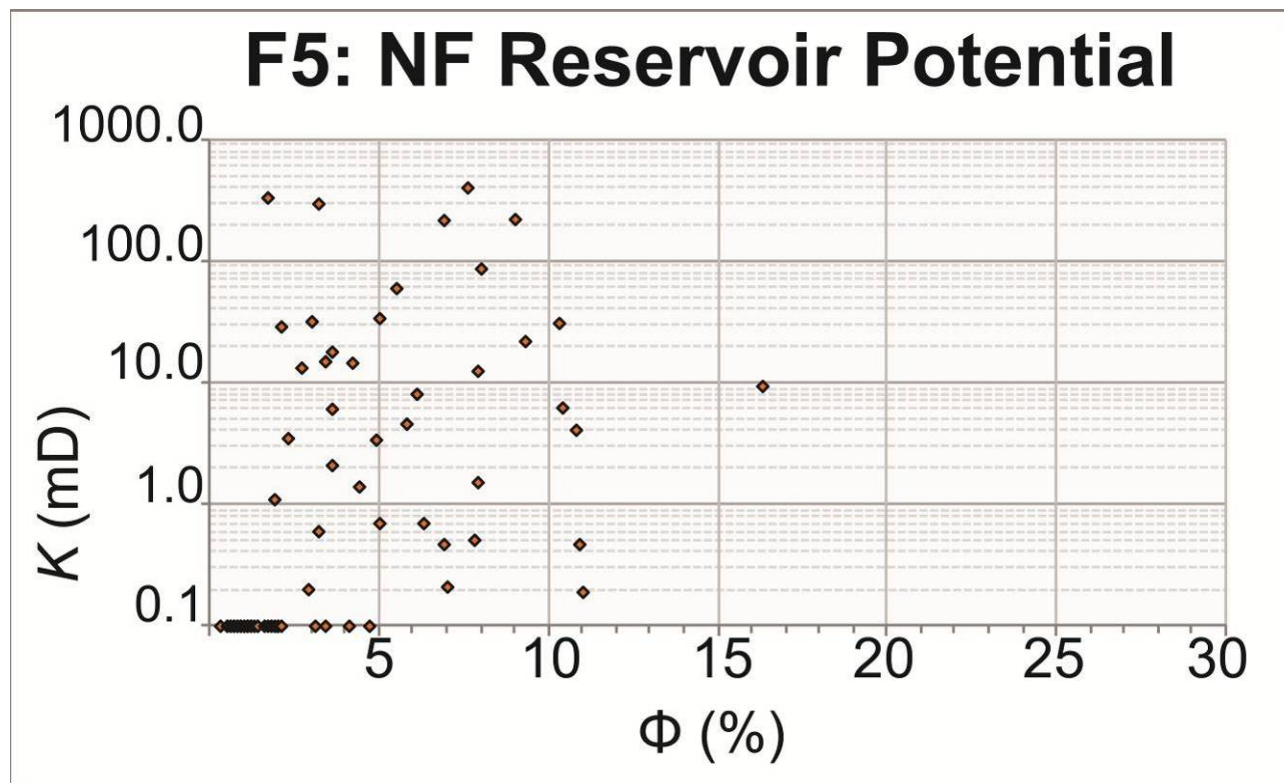




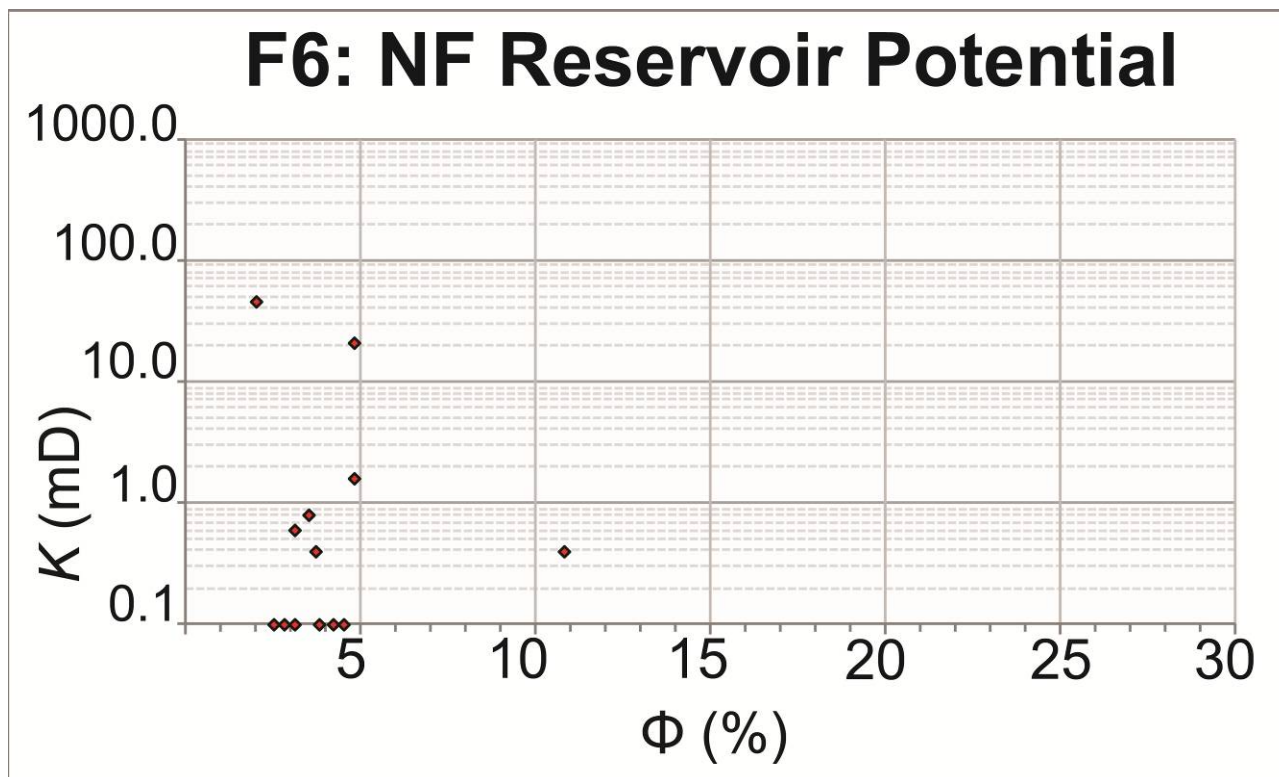


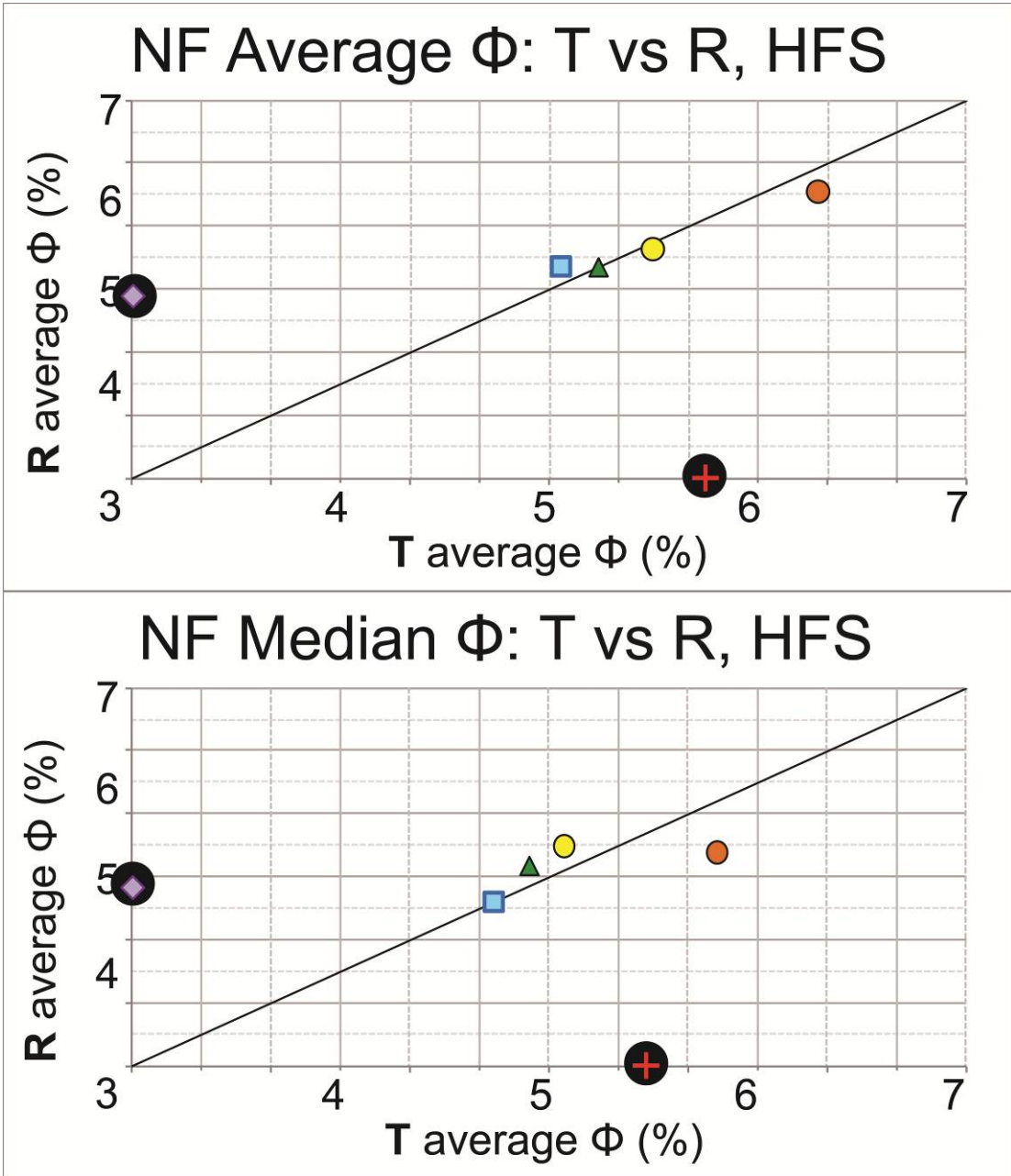




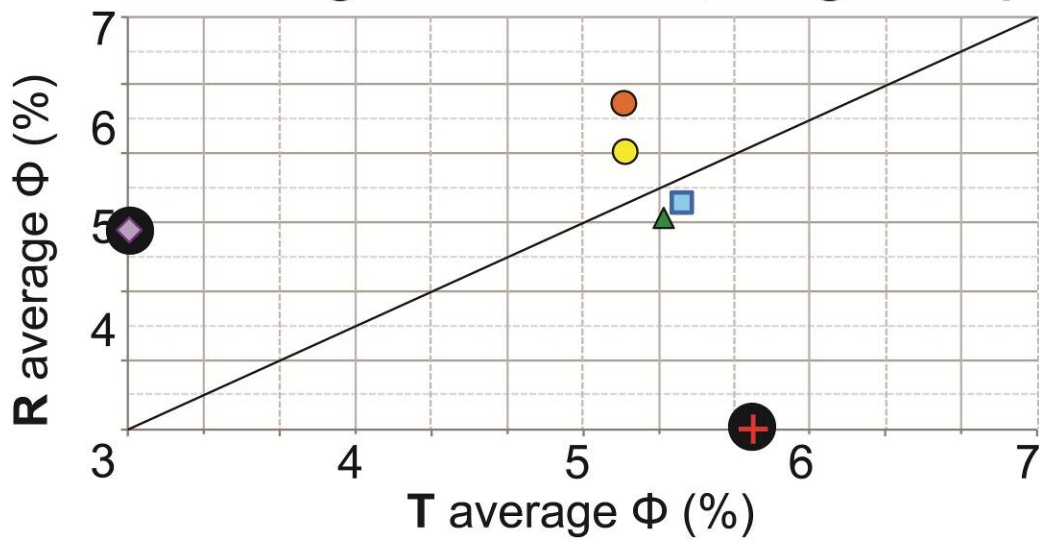




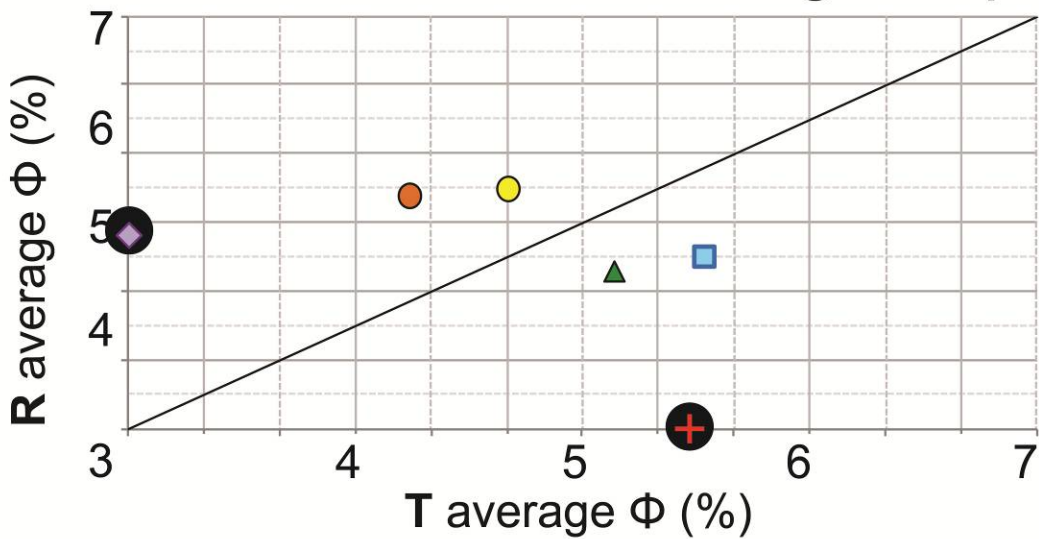


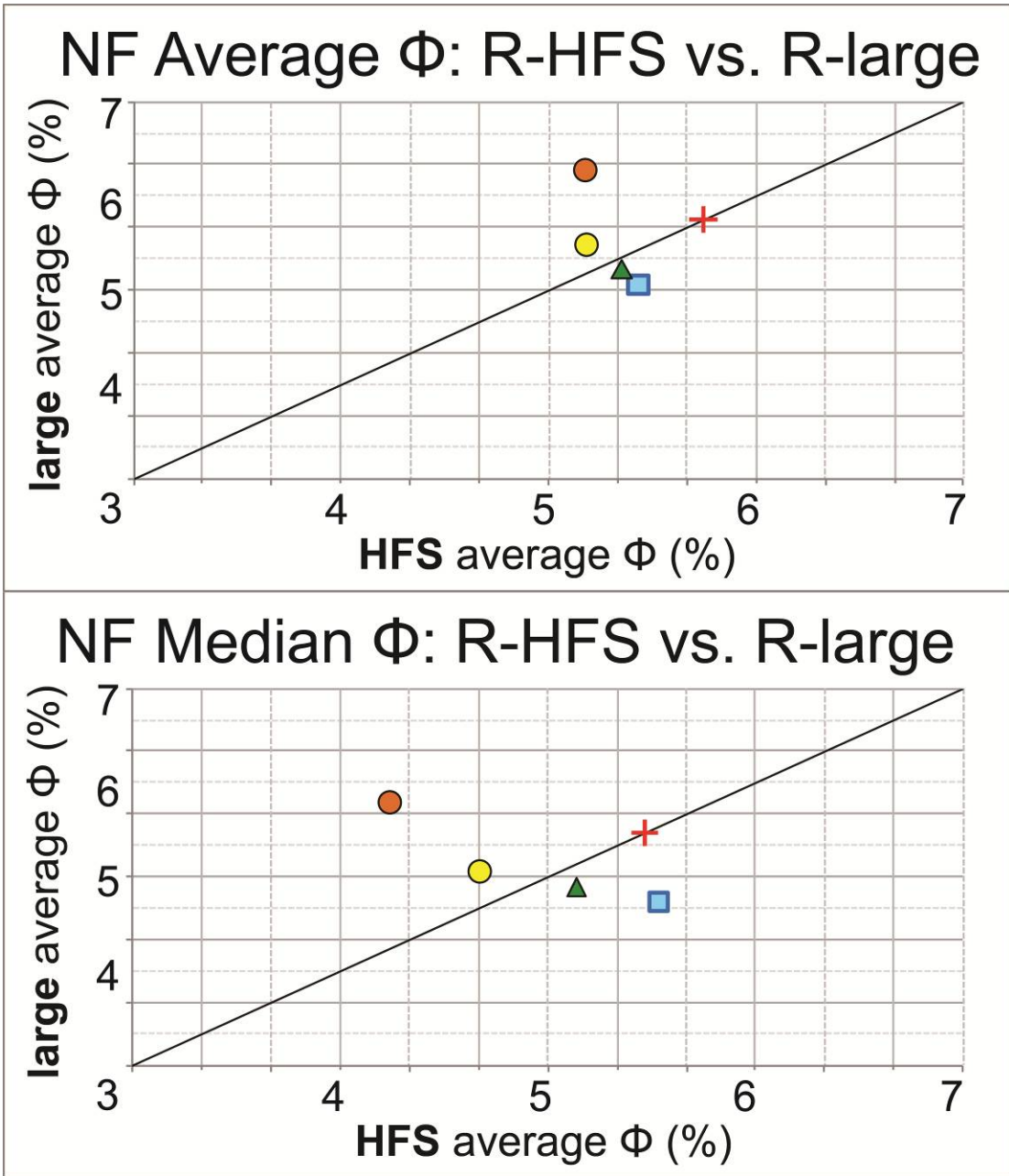


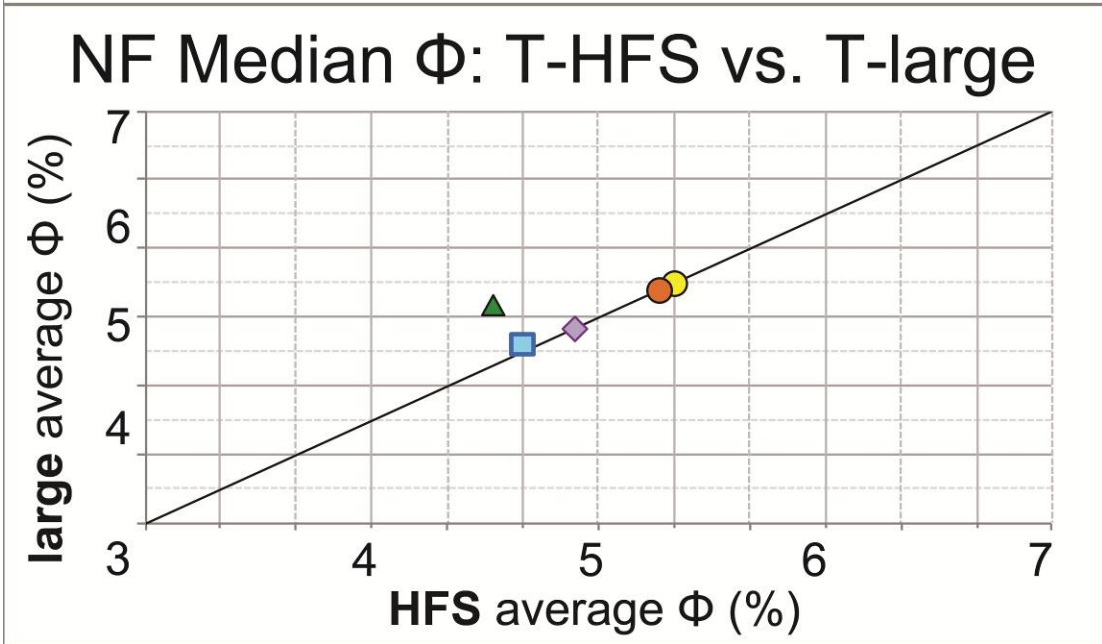
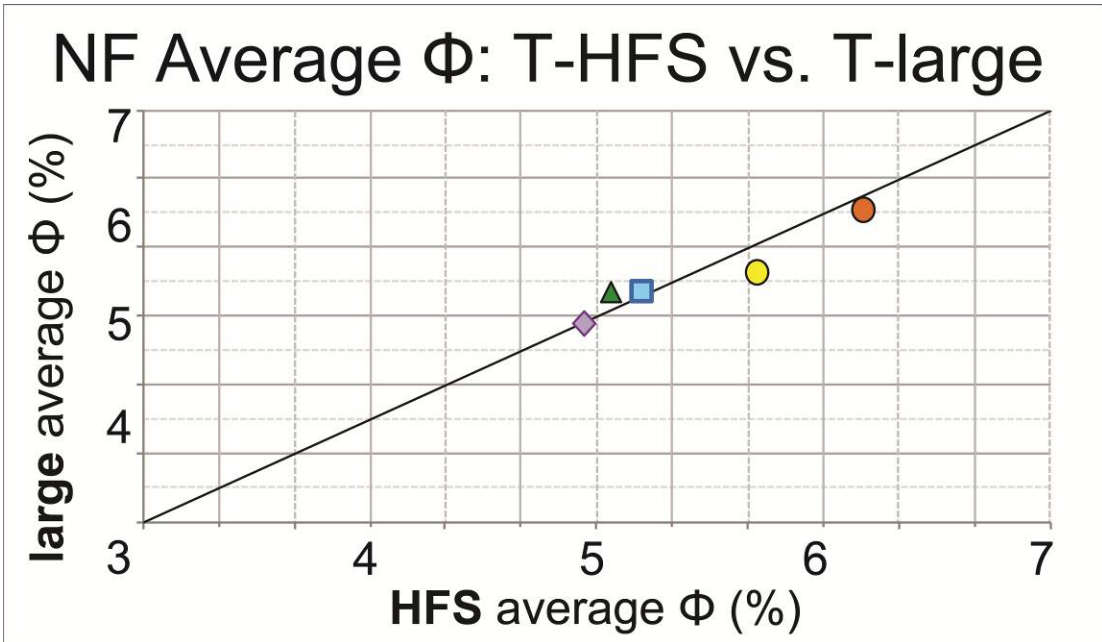
NF Average  $\Phi$ : T vs R, large seq.



NF Median  $\Phi$ : T vs R, large seq.

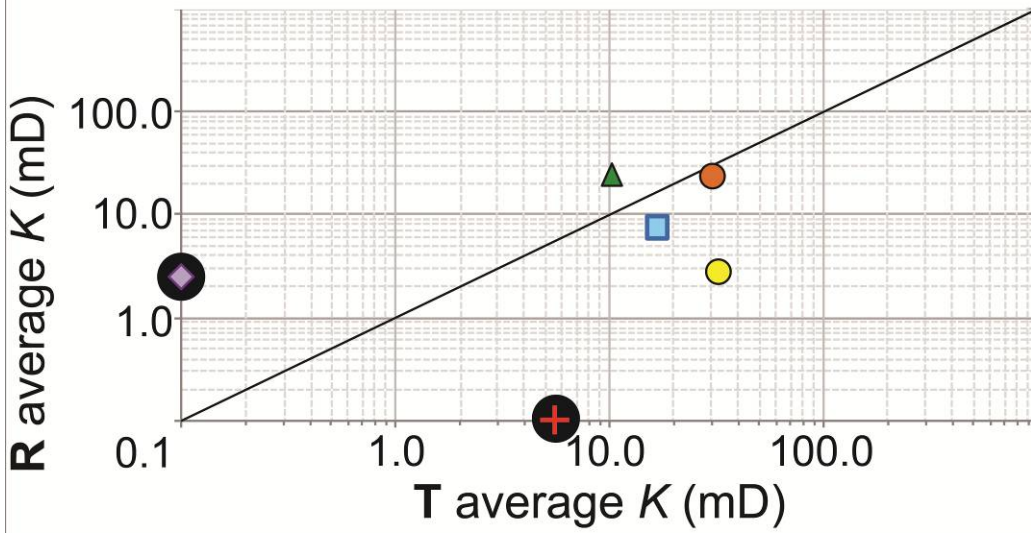




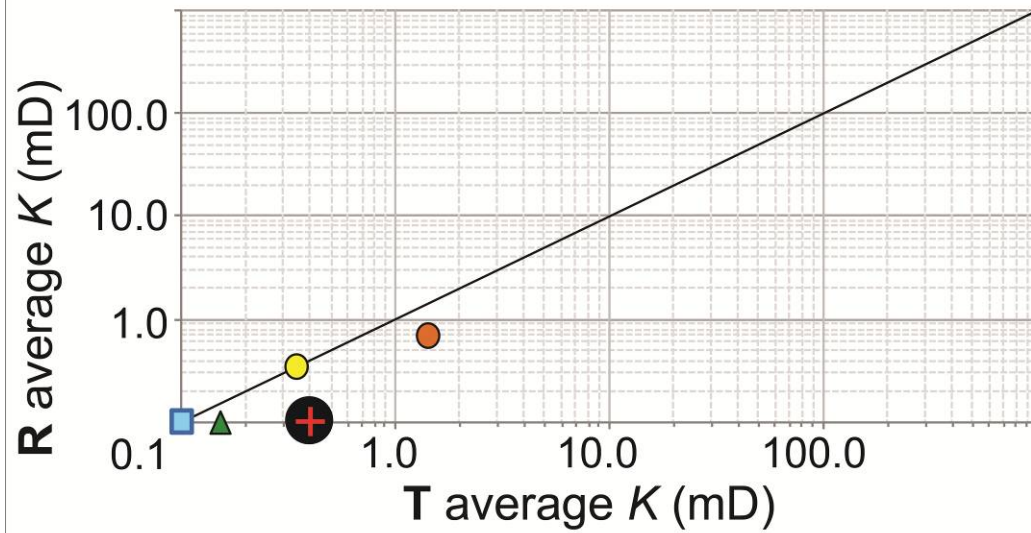




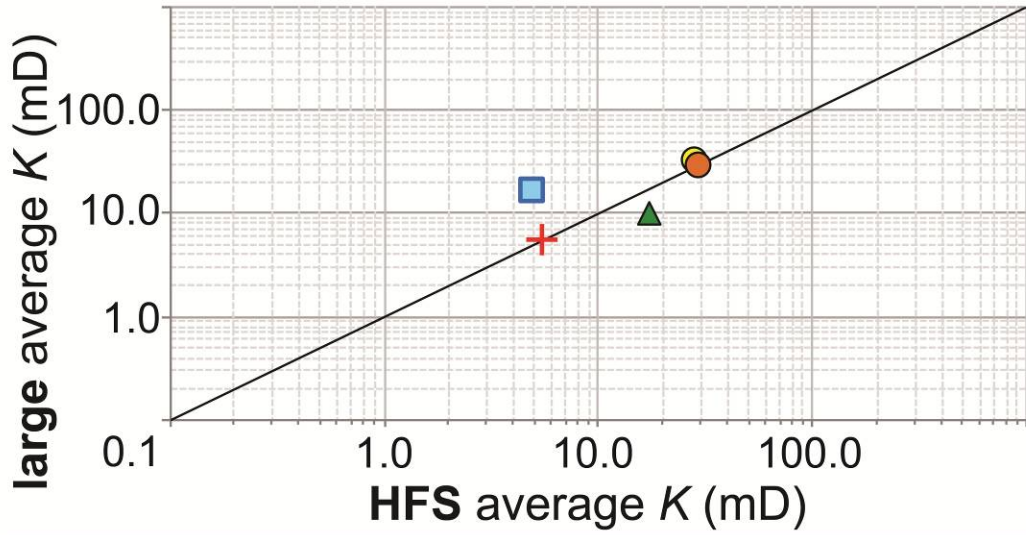
### NF Average $K$ : T vs R, HFS



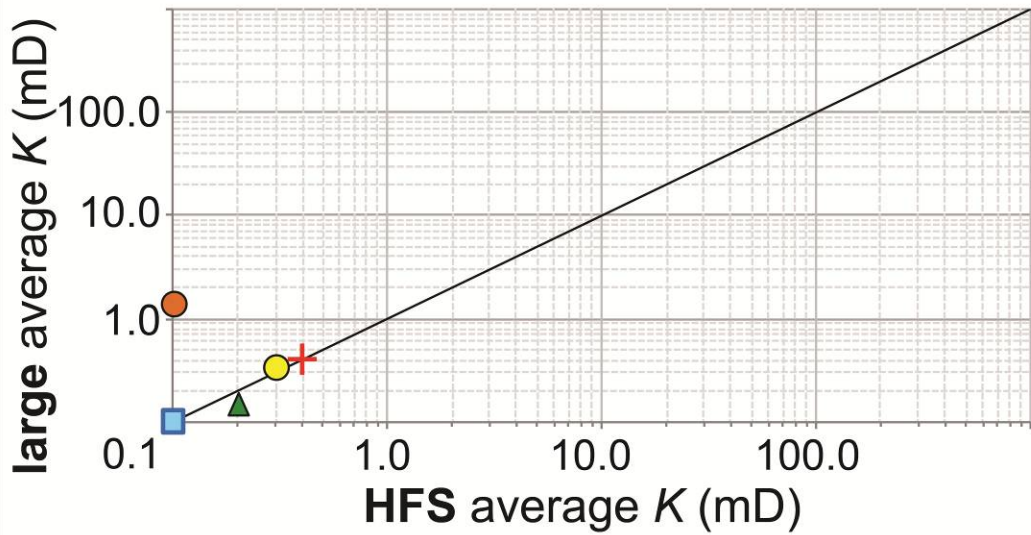
### NF Median $K$ : T vs R, HFS



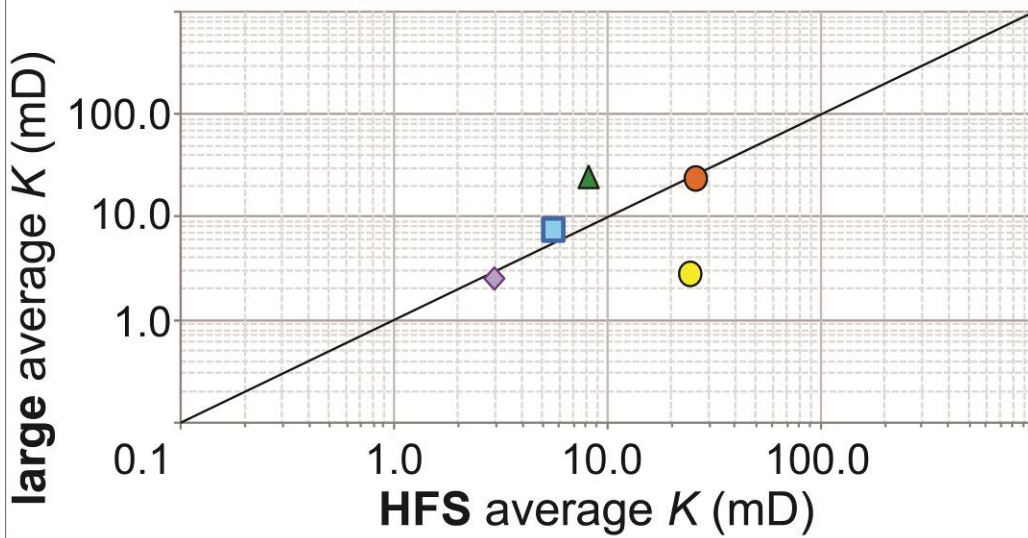
### NF Average $K$ : R-HFS vs. R-large



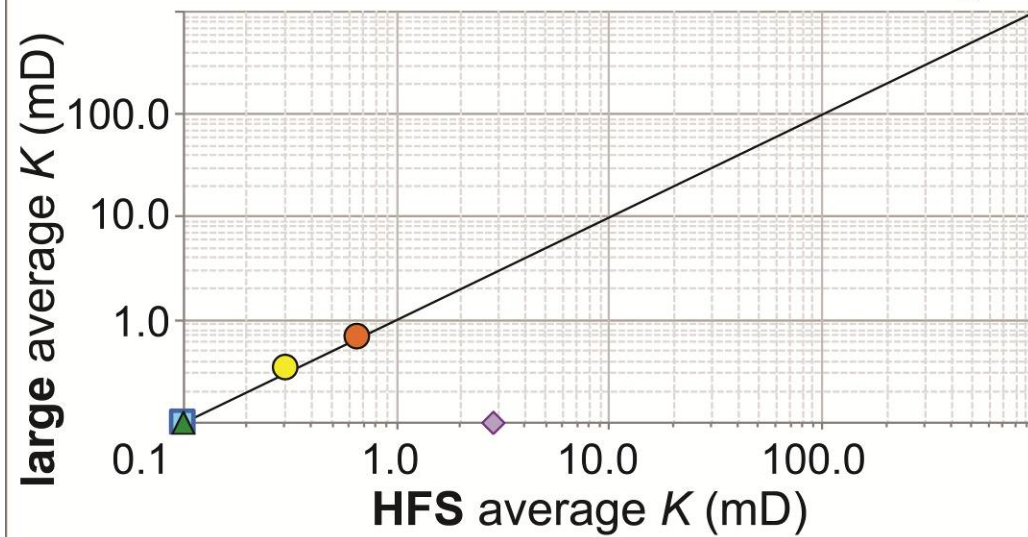
### NF Median $K$ : R-HFS vs. R-large



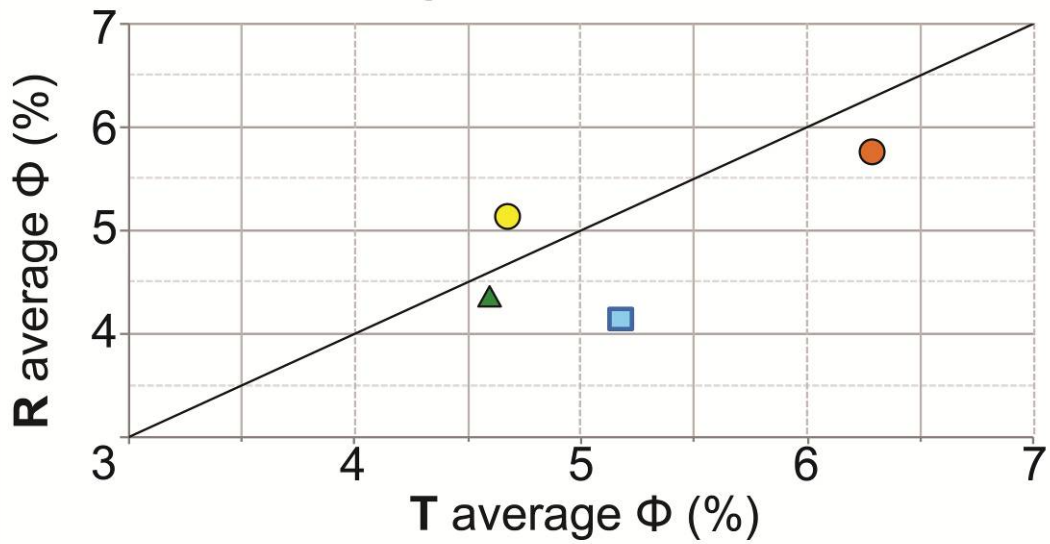
### NF Average $K$ : T-HFS vs. T-large



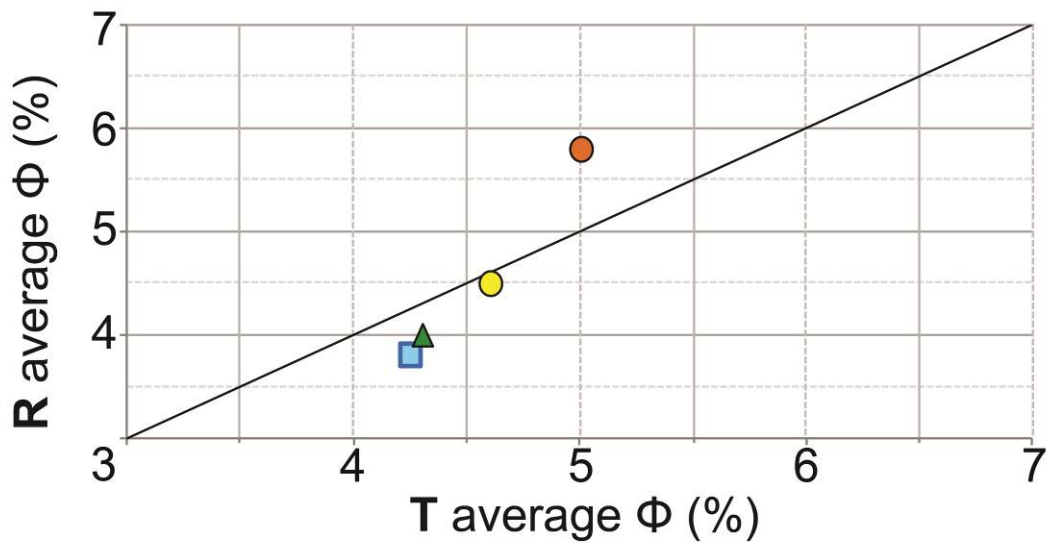
### NF Median $K$ : T-HFS vs. T-large



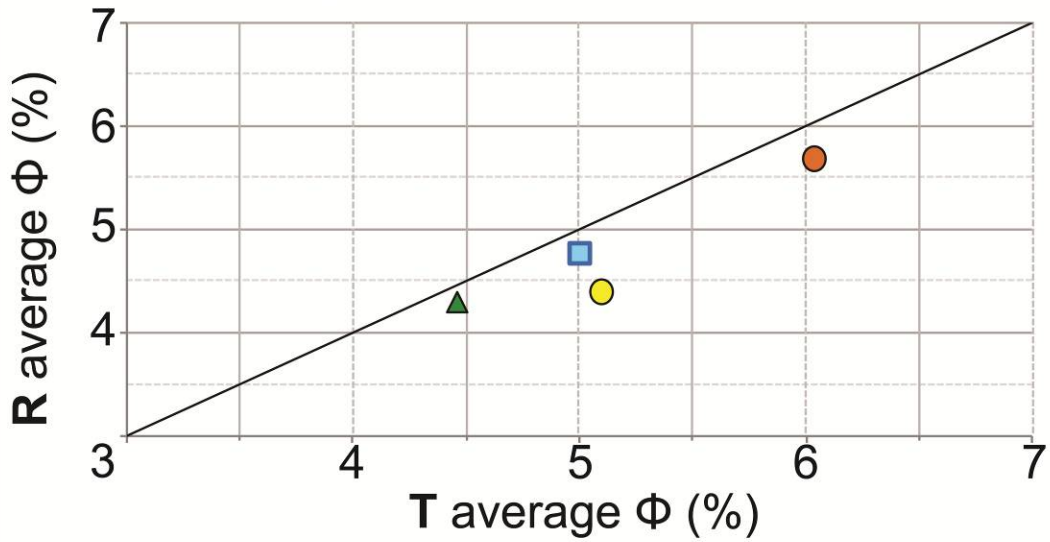
### HQ Average $\Phi$ : T vs R, HFS



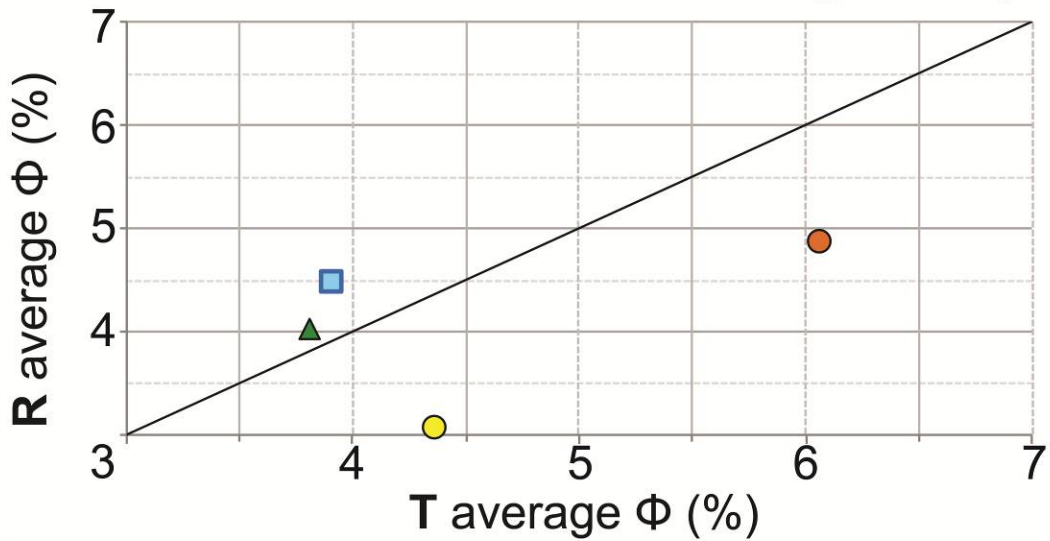
### HQ Median $\Phi$ : T vs R, HFS



HQ Average  $\Phi$ : T vs R, large seq.

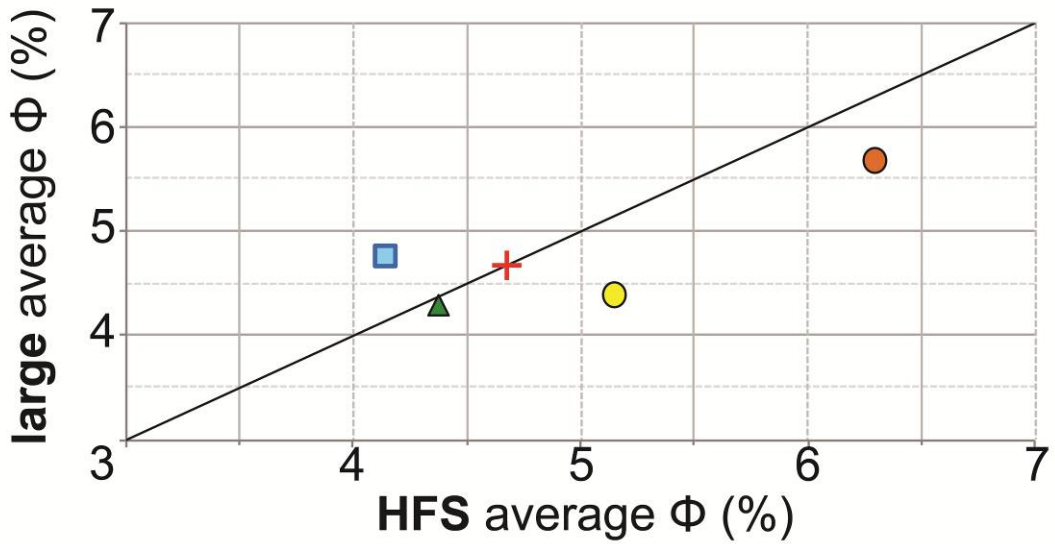


HQ Median  $\Phi$ : T vs R, large seq.

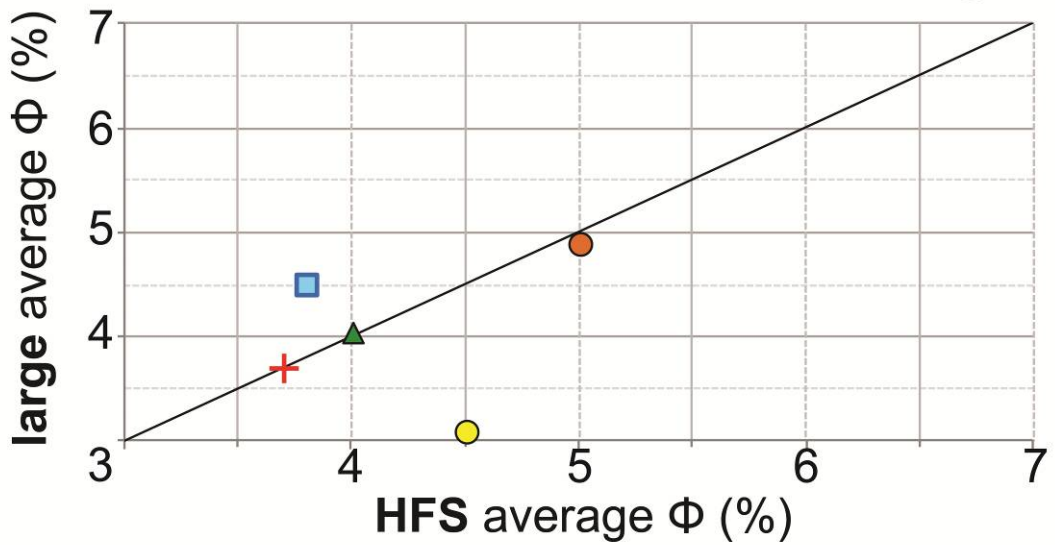




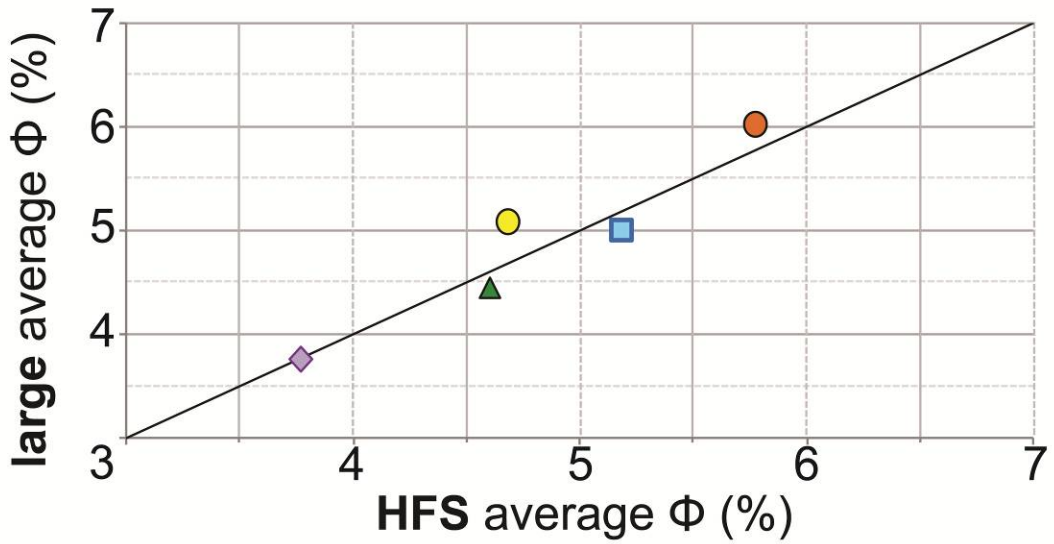
HQ Average  $\Phi$ : R-HFS vs. R-large



HQ Median  $\Phi$ : R-HFS vs. R-large



HQ Average  $\Phi$ : T-HFS vs. T-large



HQ Median  $\Phi$ : T-HFS vs. T-large

